NREL/TP-410-4724 • UC Category: 270 • DE92001248

Annual Report

Photovoltaic Subcontract Program FY 1991

K. A. Summers, Coordinator

National Renewable Energy Laboratory
(formerly the Solar Energy Research Institute)
1617 Cole Boulevard
Golden, Colorado 80401-3393
A Division of Midwest Research Institute
Operated for the U.S. Department of Energy
under Contract No. DE-AC02-83CH10093

Prepared under task No. PV211101

March 1992

NOTICE

Printed in the United States of America
Available from:
National Technical Information Service
U.S. Department of Commerce
5285 Port Royal Road
Springfield, VA 22161

Price: Microfiche A01
Printed Copy A14

Codes are used for pricing all publications. The code is determined by the number of pages in the publication. Information pertaining to the pricing codes can be found in the current issue of the following publications which are generally available in most libraries: *Energy Research Abstracts (ERA)*; *Government Reports Announcements and Index (GRA and I); Scientific and Technical Abstract Reports (STAR)*; and publication NTIS-PR-360 available from NTIS at the above address.

PREFACE

This report summarizes the fiscal year (FY) 1991 (October 1, 1990, through September 30, 1991) progress of the subcontracted photovoltaic (PV) research and development (R&D) performed under the Photovoltaic Advanced Research and Development Project at the National Renewable Energy Laboratory (NREL)—formerly the Solar Energy Research Institute (SERI). The NREL subcontracted PV R&D represents most of the subcontracted work that is funded by the U.S. Department of Energy (DOE) National Photovoltaics Program. The DOE National Photovoltaics Program is managed by the Photovoltaics Division under the Office of Solar Energy Conversion (which is under the Office of Utility Technologies within DOE's Conservation and Renewable Energy organization). Major program thrusts in FY 1991 continued to be implemented based on DOE's new *Photovoltaics Program Plan FY 1991—FY 1995*. The mission of the national PV program is to develop PV technology for large-scale generation of economically competitive electric power in the United States. The major challenge in fulfilling the mission is to assist industry in laying the foundation for installing at least 1000 MW of electrical capacity by the year 2000. The NREL PV subcontracts are managed under the following areas: Amorphous Silicon, Polycrystalline Thin Films, Crystalline Silicon Materials Research, High-Efficiency Concepts, New Ideas for Photovoltaic Conversion, University Participation, Photovoltaic Manufacturing Technology Project, and Module and System Performance and Engineering. In these areas, technical summaries of each of the subcontracted programs list approaches, major accomplishments, and future research directions. This document assists technology transfer of research results into commercial products and applications.

Approved for the NATIONAL RENEWABLE ENERGY LABORATORY

Thomas Surek, Manager
Photovoltaic Program

Robert Stokes, Acting Director
Photovoltaics Division

SUMMARY

The National Renewable Energy Laboratory (NREL)—formerly the Solar Energy Research Institute (SERI)—subcontracted photovoltaic (PV) research and development (R&D) represents most of the subcontracted work funded by the U.S. Department of Energy (DOE) National Photovoltaics Program. The DOE National Photovoltaics Program is managed by the Photovoltaics Division under the Office of Solar Energy Conversion (which is under the Office of Utility Technologies within DOE's Conservation and Renewable Energy organization). This report covers fiscal year (FY) 1991 (October 1, 1990, through September 30, 1991).

Major program thrusts in FY 1991 continued to be implemented based on DOE's new *Photovoltaics Program Plan FY 1991—FY 1995*. The mission of the national PV program is to develop PV technology for large-scale generation of economically competitive electric power in the United States. The major challenge in fulfilling the mission is to assist industry in laying the foundation for installing at least 1000 MW of electrical capacity by the year 2000.

The NREL PV subcontracts are managed under the following areas: Amorphous Silicon, Polycrystalline Thin Films, Crystalline Silicon Materials Research, High-Efficiency Concepts, New Ideas for PV Conversion, University Participation, PV Manufacturing Technology Project (PVMaT), and Module and System Performance and Engineering. The subsections that follow summarize the objectives and approaches for each area. Technology transfer activities are also summarized.

There were more than 80 subcontracts in FY 1991 with a total, planned annualized funding of over $19 million. Cost sharing by seven industry subcontractors added another $3.7 million to the NREL funding. Slightly over half of the subcontracts were with universities, at a total funding of about $5.4 million. We initiated all approved FY 1991 subcontract procurements, and we awarded approximately 75% of the planned $19 million. Procurement highlights included awards under the amorphous silicon government/industry and fundamental studies programs, the polycrystalline thin films government/industry and fundamental studies programs, the crystalline silicon materials research on impurities and defects, high-efficiency concepts Phase 1 of the PVMaT Project, and various module, system, and market development subcontracts. Highlights of initiated activities included Phase 2A of PVMaT, the amorphous silicon utility/industry PV power project, and the DOE collegiate Sunrayce 93 PV powered car competition.

Amorphous Silicon Research Project (ASRP)

The near-term objective is to achieve a 12% stable prototype module efficiency by 1994 in accordance with the goals in DOE's new *Photovoltaics Program Plan (FY 1991–FY 1995)* through better understanding and improvement of the optoelectronic properties of amorphous-silicon-based alloy materials. A transition in emphasis has occurred in FY 1990 from single-junction cell and submodule research to multijunction module research, and from initial efficiency to stabilized efficiency.

The ASRP consists of three tasks: (1) subcontracted research, (2) NREL amorphous silicon research, and (3) Surface and interface analysis. Within the subcontracted research there are two principal activities: subcontracted multidisciplinary research activities, and subcontracted fundamental research activities. The subcontracted multidisciplinary research activities are performed by broad-based research teams under cost-shared programs between government and industry. The teams are located at the individual industrial facilities that perform focused research ranging from feedstock materials through the development of modules. The subcontracted fundamental research activities involve basic and supporting research done by academia and research laboratories to aid the industry groups' advances of the technology base. The cost-shared subcontracted multidisciplinary research programs address issues related to all aspects of two-terminal amorphous silicon multijunction cells and modules using same-bandgap or different-bandgap device structures. Research was performed to advance the stabilized conversion efficiency of multijunction modules with areas of about 900 cm^2 that use glow discharge deposition as the primary method of fabricating the amorphous silicon films.

Polycrystalline Thin Films

The objective of the Polycrystalline Thin Films Program is to develop thin-film, flat-plate modules that meet DOE's long-term goals of reasonable efficiencies (15%–20%), very low cost (near $\$50/m^2$), and long-term reliability (30 years). The approach relies on developing solar cells based on highly light-absorbing, compound semiconductors such as $CuInSe_2$, CdTe, and thin-film crystalline silicon. These semiconductors are fabricated as thin films (1–3-μm thick) with minimal material and processing costs. Cell efficiencies greater than 10% have been achieved by 18 laboratories. Module efficiencies of 10%–11% have been reached by both CdTe and CIS at one square foot; 10% has been reached by CIS for a 4-ft^2 module.

Polycrystalline devices require continued development to achieve 15%–20% conversion efficiencies. The focus of our work is to develop single-junction cells. Improvement in the single-junction technologies has been steady and reliable. This strategy remains the major focus of the task. Potentially achievable module efficiencies exceed 15% at costs under $\$50/m^2$.

Developing scalable, low-cost fabrication methods is important in providing industry with a foundation for future large-area, high-throughput commercial processes. Within the NREL program, methods for fabricating polycrystalline cells include various selenization methods (for $CuInSe_2$), sputtering, close-spaced sublimation, evaporation, electrodeposition, metal-organic chemical vapor deposition, and spraying for CdTe.

Crystalline Silicon Materials Research

The emphasis of the NREL Crystalline Silicon Materials Research Program is to develop a coordinated effort between industry, university, and NREL to study basic mechanisms pertaining to the kinetics of defects and synergistic effects related to defect-impurity interactions. Of particular interest is the work to identify the effects of post-growth processing on the photovoltaic properties of low-cost silicon and methods for passivating electrically active defects in silicon.

Although silicon solar cells fabricated on low-cost substrates have already demonstrated efficiencies exceeding 15%, the technology to commercially produce cells of such high efficiency on low-cost substrates does not exist. Some of the reasons for the lack of such a technology are related to our inadequate understanding of the roles that many defects and impurities play in cell performance. Furthermore, it is not well understood how the characteristics of silicon, containing defects/impurities, change under various thermal processes; this lack of information makes it difficult to design cell fabrication processes that can ameliorate the deleterious effects of defects/impurities.

High-Efficiency Concepts

The objective of the High-Efficiency Concepts program area is to evaluate and develop advanced PV technologies capable of energy conversion efficiencies in excess of 20% for flat-plate configurations and 30% for concentrator systems. Because of the demonstrated performance of crystalline III-V semiconductors, the task has become synonymous with III-V compound semiconductor research.

NREL's program of research in High-Efficiency Concepts has approached the terrestrial PV goals from the direction of first demonstrating the feasibility of exceeding these efficiency targets to ensure that production engineering trade-offs between performance and cost can be accommodated. Recent advancements by the community researching high-efficiency technologies provide a high level of confidence that the efficiency goals can readily be met.

Research supported by this program benefits future development activities by strengthening the understanding of basic mechanisms that affect the uniformity of doping, composition, and thickness over large-area wafers, from wafer to wafer and from run to run. Efficiently utilizing source materials and evaluating potentially superior sources (cost, purity, control, safety, and other factors) are also important topics for research. Continued improvement in cell efficiency is also a critical factor in reaching cost-effectiveness for the technology.

The basic issues that form the focus of research supported under this program have been summarized. Clearly, the technology for deposition of III-V compound semiconductors by potentially low-cost processes that provide excellent uniformity, purity, and crystallographic quality is the key factor for achieving the near-term PV program goals through the high-efficiency path. Research on characterizing materials and cells, analyzing loss mechanisms in cells, demonstrating improved cell designs, and improving the monitoring, control, and safety of the processes also contribute greatly to the technology base.

New Ideas Program

The objectives of the New Ideas Program are to identify new PV materials, device configurations, and concepts, and to conduct preliminary R&D in the areas that show the most promise.

The program provides public solicitations for new and innovative research ideas that are relevant under the PV program guidelines. The responses to the solicitations are submitted by universities, businesses, and non-profit organizations. Subcontracts are awarded to study the most promising concepts. These subcontracts are reviewed, and successful concepts are selected for renewal with a second year of funding. Subcontracted New Ideas research that shows significant potential is transferred into the appropriate major task area within the DOE PV program for continued support.

University Participation Program

The objective of this program is to maximize the contribution of universities to the future of PV technology by focusing on the traditional needs and strengths of that community. Thus, it provides a forum in which the university researchers identify research topics critical to advancing the PV technology with minimal influence from the current programmatic interests. The selected participants are then permitted to pursue the proposed basic and applied research ideas in an environment designed to foster creativity both by limiting the requirements for delivering reports and samples and by achieving specific goals. Reporting is limited to annual reports and journal publications. Research symposia organized by the participants are held periodically and are open to all students, program participants, and outside researchers. The intent of the initiative is to provide continuity of funding over a minimum three-year period, which will allow universities to build and support interdisciplinary teams with specialized expertise that can be applied to furthering the technology base of PV. Such a program is expected to attract the most highly qualified university research teams to the national PV program. The University Participation Program also supports the PV industry through technology transfer; this occurs through publishing research results in the technical literature but also through enhanced student awareness of PV technology and educating future professionals.

PV Manufacturing and Technology (PVMaT) Project

The objective of the Photovoltaic Manufacturing Technology (PVMaT) Project is to assist the U.S. PV industry in improving manufacturing processes, accelerating manufacturing cost reductions for PV modules, increasing commercial product performance, and generally laying the groundwork for a substantial scale-up of U.S.-based PV manufacturing plant capabilities. This project is a government/industry PV manufacturing R&D effort composed of partnerships between the federal government (through the U.S. Department of Energy) and members of the U.S. PV industry.

Phase 1 of this project, the problem identification phase, was completed early in 1991. Phase 1 competitive bidding was open to any U.S. firm with existing manufacturing capabilities, regardless of material or module design. Twenty-two subcontracts of up to $50,000 each were

awarded. Phase 2 is now under way. This is the solution phase of the project and addresses problems of specific manufacturers. Subcontracts under the first Phase 2 solicitation, called Phase 2A, will be awarded in early FY 1992. This Phase 2A solicitation was only open to participants in the Phase 1 effort. The envisioned subcontracts under Phase 2 may be up to three years in duration and will be highly cost-shared between the U.S. government and U.S. industrial participants. A second, overlapping, and similar process-specific solicitation (Phase 2B) is planned to follow soon and will be open to all U.S. PV manufacturing companies. A third portion of the PVMaT project, called Phase 3, is also under way, although it is slightly behind Phase 2. In October 1991, a Phase 3A solicitation was released for subcontracted team research on module-related R&D problems common to several PV manufacturers. In Phase 3, because of the general interest to industry, some general issues related to PV module development will be studied through various teaming arrangements. The PVMaT project's ultimate goal is to ensure that U.S. industry retains and extends its world leadership role in the manufacture and commercial development of PV components and systems. Activities to date under PVMaT have received outstanding support, and the level of interest in participation is exceptional.

PV Module and System Performance and Engineering Project

The PV module and system performance and engineering project is structured to conduct state-of-the-art PV module, system, and application research; to perform engineering, testing, evaluation, and analysis tasks; to provide technical results and solutions to technical issues; to develop PV applications and application opportunities. The project is also designed to maintain and enhance supporting facilities and capabilities that are consistent with DOE's new *Photovoltaics Program Plan FY 1991—FY 1995*, are complementary to other DOE PV projects, and will ensure that project capabilities and facilities are available resources for cooperative research and utilization by the PV research and development community.

Project activities are managed through the module and systems performance and engineering project management task and are organized to address project objectives through the following five primary tasks: (1) Cell and Module Standardized Characterization Performance; (2) Module and System Performance Testing; (3) Module Reliability Research: (4) Solar Radiation Research; and (5) System and Utility Applications.

Subcontract activities represent support for industry/utility PV power projects, domestic and international standards development, PV systems applications including demand-side management, assessment of and effects on roof mounted modules, and solar resource utility load matching assessment.

Technology Transfer

Consistent with recent DOE policy, technology transfer is collaborative R&D with industry to aid industry in the commercialization of products or services. An underlying theme of NREL technology transfer activities is the joint work (focused on a common R&D objective) accomplished by industry researchers and NREL researchers. Among government laboratories, there are seven principal tools for effecting technology transfer: subcontracted R&D, cooperative

R&D, industry sponsored R&D, user facilities (at NREL), technology licenses, researcher exchanges, and information dissemination. NREL's PV program conducts its technology transfer primarily through three of the above: subcontracts, informal cooperative R&D, and information dissemination.

TABLE OF CONTENTS

TABLE OF CONTENTS (continued)

TABLE OF CONTENTS (continued)

TABLE OF CONTENTS (continued)

TABLE OF CONTENTS (continued)

TABLE OF CONTENTS (continued)

TABLE OF CONTENTS (continued)

1.0 INTRODUCTION

This report reviews subcontracted research and development (R&D) activities under the NREL Photovoltaic Program from October 1, 1990, through September 30, 1991.

1.1 Background

The National Renewable Energy Laboratory (NREL) — formerly the Solar Energy Research Institute (SERI) — subcontracted photovoltaic (PV) R&D represents most of the subcontracted work funded by the U.S. Department of Energy (DOE) National Photovoltaics Program. The DOE National Photovoltaics Program is managed by the Photovoltaics Division under the Office of Solar Energy Conversion (which is under the Office of Utility Technologies within DOE's Conservation and Renewable Energy organization.)

Major program thrusts in fiscal year (FY) 1991 continued to be implemented based on DOE's new *Photovoltaics Program Plan FY 1991—FY 1995*. The mission of the National Photovoltaics Program is to develop photovoltaic technology for large-scale generation of economically competitive electric power in the United States. The major challenge in fulfilling the mission is to assist industry in laying the foundation for the installation of at least 1000 MW of electrical capacity by the year 2000.

Under the DOE PV program, the NREL Photovoltaic Advanced Research and Development Project sponsors fundamental and applied R&D, manufacturing development, and systems and market development in PV energy technology. The project also provides services to industry and electric utilities or other users, and it provides the leading support for the national PV program. The NREL subcontract program is responsible for most of the R&D, manufacturing technology development, and some of the systems and market development task areas under the national PV program. The implementation of the subcontract program is based on competitive public solicitations. One of the most important mechanisms is in the form of government/industry partnerships, with industry frequently sharing the cost of research with DOE. We also work closely with both manufacturers and potential users to expand the market and foster a viable PV industry, and to hasten the acceptance of PV systems by utilities.

NREL's PV activities include managing subcontracted R&D projects as well as conducting research at the laboratory. The primary research activities are conducted in advanced PV material technologies, including amorphous-silicon thin-film materials; polycrystalline thin films, such as copper indium diselenide (CIS) and cadmium telluride and their alloys; and high-efficiency crystalline cells, including silicon and gallium arsenide and their alloys. Improving the way that PV devices are manufactured is vital. Two complementary approaches are pursued. One involves government/industry partnerships under the PV Manufacturing Technology (PVMaT) Project. That approach focuses on improving manufacturing processes and products, accelerating manufacturing cost reduction, and laying the foundation for increased production capacity. The second approach involves module development research to evaluate modules and module performance and to suggest solutions to common module problems. System and market development rounds out the balanced approach pursued. The objective is to create the environment whereby system technology, user acceptance, and the PV industry can accommodate the continued expansion of PV into larger applications and markets. NREL subcontracts also support the continued influx of new ideas and highly qualified university research teams to

expand the current limits of PV technology. And, transferring research results into commercial products and applications in a timely and effective manner is another major activity of NREL's PV project.

Subcontracted R&D is a significant part of the NREL PV project — more than 50% of the project's budget is allocated yearly to subcontracts. In FY 1991, we managed more than 80 subcontracts with a total planned annualized funding of better than $19 million. Cost-sharing by seven industry subcontractors added an additional $3.7 million to the NREL funding. Slightly over half of the subcontracts were with universities, at funding of $5.4 million. Table 1-1 shows how the subcontract budget was distributed. Figure 1-1 shows the distribution of subcontract funds by business category. Table 1-2 shows the NREL contacts for the PV subcontracts.

	Fiscal Year			
Task Area	**1978-1988 ($M)**	**1989 ($M)**	**1990 ($M)**	**1991 ($M)**
Research and Development				
Amorphous Silicon Thin Films	59.2	7.7	6.0	3.3
Polycrystalline Thin Films	37.1	3.7	4.6	4.5
High-Efficiency Concepts	30.6	2.0	1.9	1.3
Crystalline Silicon	22.1	0.6	0.5	0.9
New Ideas	17.6[b]	0.4	0.4	0.4
University Participation	4.8	0.9	0.4	0.8
Subtotal	171.4	15.3	13.8	11.2
Manufacturing Technology, and, System and Market Development				
PV Manufacturing Technology Project	N/A	N/A	1.7	6.7
Module and System Performance and Engineering Project[c]	N/A	N/A	N/A	2.0
Subtotal	N/A	N/A	1.7	8.7
Total	**171.4**	**15.3**	**15.5**	**19.9**

Table 1-1. Subcontract Budget History of the NREL Photovoltaic Program[a]

Notes: (a) Includes approximately 10–15% for program management; fees, etc.
(b) Includes $9 million for photoelectrochemical cell research.
(c) Significant effort initiated in FY 1991.

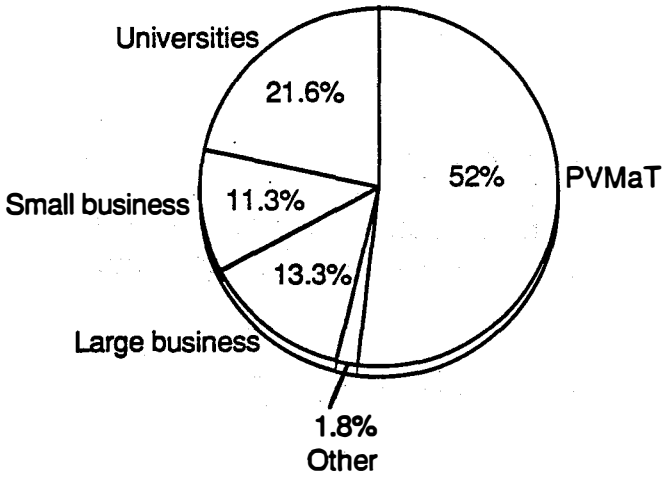

Total Subcontracts = $18.5 million
Cost-Share by industry = $9 million (est.)

Figure 1-1. Business category distribution of FY 1991 subcontract funds

Task Area	Contact Name	Telephone[a]
PV Program	Thomas Surek, Manager	231-1371
	Kathy Summers, Admin. Assist.	231-1395
	Thomas Basso	231-7035
Amorphous Silicon Research Project	Werner Luft, Manager	231-1452
	Byron Stafford	231-7126
	Bolko von Roedern	231-1380
High-Efficiency Concepts, Crystalline Silicon Materials, and University Project	John Benner, Manager	231-1396
	Bhushan Sopori	231-1383
Polycrystalline Thin Films	Kenneth Zweibel, Manager	231-7141
	Harin Ullal	231-1486
New Ideas Project	Thomas Basso	231-7035
PV Manufacturing Technology	Ed Witt, Manager	231-1402
	Rick Mitchell	231-1379
	Dave Mooney	231-7074
Module and System Performance and Engineering	Richard DeBlasio, Manager	231-1286

Table 1-2. NREL Photovoltaic Program Subcontract Personnel

Notes: (a) Area code (303), FTS number 327-xxxx.

1.2 Key Accomplishments

1.2.1 Amorphous Silicon Research Project

NREL implemented a transition to focus industrial subcontractors and university subcontractors on *stabilized* efficiencies, rather than to focus on maximizing initial performance and minimizing degradation.

- One contract to United Solar Systems Corporation was awarded under the third government/industry 50% cost-shared partnership for amorphous silicon research. This contract completed the awards under this competitive procurement. The principal objectives of this procurement are: (1) to conduct research on semiconductor materials and non-semiconductor materials to enhance two-terminal, multijunction, thin-film, large-area, all-amorphous-silicon-alloy device performance, (2) to develop high-efficiency, *stable, reproducible*, and *low-cost* multijunction photovoltaic modules based on all-amorphous materials, (3) to demonstrate stable 12% (AM 1.5) aperture-area solar conversion efficiency for different-bandgap modules, and (4) to demonstrate stable 10% (AM 1.5) aperture-area solar conversion efficiency for same-band-gap modules. The modules will be at least 900 cm^2 in area and will consist of at least two integrally stacked devices using all-amorphous-silicon alloy materials.

- The awards under the recompetition for amorphous silicon fundamental research were completed. Awards under the competitive procurement were made to Colorado School of Mines, Institute of Energy Conversion (IEC), Iowa State University, North Carolina State University, Pennsylvania State University, Syracuse University, University of Illinois, University of North Carolina, University of Oregon, and Xerox. Two additional non-competitive awards were made—one to the National Institute of Standards and Technology and one to the Jet Propulsion Laboratory.

- An extensive safety analysis review for resuming amorphous silicon operations in Building 16 was completed, and an off-site safety analysis review began for amorphous silicon deposition from concentrated silane.

- On 20–22 February 1991, an international conference convened jointly with NREL and the Electric Power Research Institute (EPRI) to review the status of understanding of the light-induced degradation of amorphous silicon and to refocus the research onto pertinent stability issues. The proceedings from the conference were published and distributed worldwide.

- On 29 August 1991, a DOE panel of selected experts evaluated the progress and future direction of the amorphous silicon research project and found the project well balanced and well managed.

- Improved *stabilized* efficiencies for amorphous silicon modules were measured by NREL: 7.2% efficiency for a Solarex triple-junction prototype module (962-cm^2 aperture area), and 6.3% efficiency for a United Solar Systems Corporation dual-junction module from their

production line (3676-cm^2 aperture area). These stabilized efficiencies of 6%–7% for commercial and prototype modules are a significant improvement from the 3%–5% efficiencies of such modules produced 3 or 4 years ago.

- The IEC at the University of Delaware developed, in collaboration with Pennsylvania State University, a charge-defect equilibrium model that concludes that the light-induced dangling bond defect is formed in an exothermic reaction with negative entropy and free energy changes. This model suggests that the annealed state is unstable and can only be maintained when there is a lack of free charge.

- Syracuse University reported changes in the drift mobilities measured at low temperatures in a high-quality p-i-n junction upon light-soaking. None of the present prevailing models for the Staebler-Wronski effect include the possibility of mobility changes.

- The University of North Carolina reported that the electroluminescence in thick p-i-n junctions, when normalized for the current density, does not degrade upon light-soaking. The radiative lifetime does not shorten with photo-degradation at a temperature below 200°K. An attempt was made to describe these phenomena using a hopping transport model that includes Coulomb interaction.

- The University of Oregon reported drive level photocapacitance results suggesting changes in the deep-tail-state region of a-Si:H upon light-soaking. In high-quality a-SiGe:H samples, these states may also be important. High midgap defect densities of states coexist in these a-SiGe:H alloys with sharp Urbach parameters. This questions the validity of certain defect equilibrium models (Stutzmann, Smith and Wagner).

- Xerox reported very strong field dependencies of the conductivity of doped layers below 100°K. The conductivities are virtually temperature-independent. An analysis of a compensated a-Si:H sample shows 6 orders of magnitude decrease of the carrier mobilities with increased compensation. These very large decreases in mobility cannot be rationalized in terms of gap states and are attributed to potential fluctuations of the band edges.

- A new model for light-induced degradation was proposed by B. von Roedern at NREL. The model combines the features of the "bond breaking" models and the "charge defect" models. The model suggests that solar cell degradation is mostly due to degraded mobility of electrons. Experiments carried out in collaboration with R. Braunstein (University of California-Los Angeles) have now experimentally confirmed the mobility decreases caused by light-soaking. We also showed that metastable defects are charge-trapping defects.

- A 1991 R&D-100 award was made for low-emissivity coated glass. The award is partially based on NREL-funded research on fluorine-doped tin-oxide films deposited on glass for amorphous silicon photovoltaic modules. The awards was made jointly to Libby-Owens-Ford (LOF) and inventor R. Gordon of Harvard University. LOF obtained a license for the basic patent (awarded to R. Gordon) that was based on NREL-funded subcontracted research. LOF scaled-up the process to deposit the film on 12-ft sheets of glass while the glass is still molten. The basic patent is also used by manufacturers of commercial amorphous silicon photovoltaic modules. Gordon is currently funded by NREL to develop a low-temperature

fluorine-doped zinc oxide coating to be used on the next generation thin-film photovoltaic modules.

1.2.2 Polycrystalline Thin Films

Significant progress was made in FY 1991 in the subcontracted research of polycrystalline thin films. The key accomplishments in both CdTe and $CuInSe_2$ solar cells and modules are listed below.

- A phased, two-year subcontract with Martin Marietta of Denver, Colorado, was signed. The purpose of the subcontract ("Innovative Sputtering Techniques for CIS and CdTe Submodule Fabrication") is to investigate the potential of rotating cylindrical magnetron sputter deposition of copper and indium for CIS modules; and of cadmium and tellurium for CdTe modules. If successful, the use of rotating cylindrical magnetrons would provide an attractive opportunity for cost reductions since such magnetrons have higher rates and better materials utilization than conventional planar magnetrons. The period of performance is from September 1, 1991 through November 30, 1993. The subcontract provides $396K for the first year and $596 for the second year. International Solar Electric Technology (ISET) is a sub-tier contractor of Martin Marietta, for whom they are providing selenization expertise. ISET is also providing the expertise needed to produce CdTe from a Cd/Te film. (ISET holds the patent for this approach, developed under a recent NREL New Ideas project.)

- Photon Energy reached a significant milestone by demonstrating an 8% aperture-area efficiency for an approximate 1 ft^2 CdTe module. The module was measured outdoors at NREL using a specially designed maximum power (P_{max}) tracking system. P_{max} was 6.82 W under 1018 W/m^2 sunlight at 32°C. The aperture area of the module is 831 cm^2, yielding an aperture-area efficiency of 8.1%. This is the highest efficiency for 1-ft^2 CdTe that we have measured at NREL, and it was measured at 7°C hotter than standard conditions (i.e., the efficiency at standard conditions would be slightly higher than 8.1%). British Petroleum (BP) Solar has reported reaching 10% efficiency on 1-ft^2 CdTe modules. Photon Energy is beginning the process of fabricating 4-ft^2 modules.

- The judges for the 1991 R&D 100 Awards competition for significant new technology have selected for recognition the thin-film cadmium telluride PV modules project. R. Mitchell and K. Zweibel, jointly with Photon Energy, received the award.

- Siemens Solar Industries delivered a 9.7% efficient (aperture area) 4-ft^2 module (fully encapsulated) to NREL. The achievement of this efficiency surpasses the first year milestone of its new subcontract (9.4%). The final goal of the subcontract is 12.5% at the end of the third year. The DOE's new *Photovoltaics Program Plan FY 1991—FY 1995* key thin-film goals are for stable, 4-ft^2 module efficiencies of 10% (1992), 11% (1993), and 12% (1993). All of these goals are within the scope of the Siemens effort.

- NREL representatives K. Zweibel, R. Noufi, and L. Kazmerski attended the kickoff meeting of the EPRI/NREL CIS Working Group (CISWG) in Denver on May 23, 1991. Sixteen invited attendees included representatives from EPRI, Siemens Solar, ISET, Solarex, American Physical Society, Boeing, Martin Marietta, University of Illinois, IEC, Colorado State University, University of South Florida (USF), and AT&T. A mission statement for

the CISWG was developed during the meeting. The group's purpose is to accelerate the availability of the CIS technology for significant energy contributions. Members will consist of CIS "stake holders" who are willing to work together on issues that will serve the group's purpose. The first two subcommittee topics were chosen: life-cycle environmental acceptability and modeling. The two chairmen for these subcommittees are K. Zweibel and J. Sites, respectively.

- We have further confirmation of the outstanding intrinsic stability of CIS modules. After almost three years (972 days) outdoors, the two ARCO Solar (now Siemens Solar) CIS modules delivered in October 1988 are within 97.5% and 99.8% of their original efficiencies as measured outdoors in Golden, Colorado. In fact, all the parameters on these 8% efficient (aperture area) modules are within experimental error of their original values. Although these tests are not yet adequate to predict a 30-year life for CIS modules, they provide a very strong indication that, with proper encapsulation, long outdoor life can be expected.

- T. Chu at USF has achieved a major advance in CdTe cell technology through a NREL-verified world record 13.4% efficiency for a 1.2-cm^2 CdTe cell (standard conditions). The cell structure is glass/tin oxide/cadmium sulfide/cadmium telluride/graphite. The device parameters were 840 mV, 21.9 mA/cm^2, and a 72.6% fill factor (FF). Four one-cm^2 cells were measured, and all were over 12% efficiency. Besides remarkable voltages (all 825-840 mV), cell FFs were as high or higher than any seen before. The highest FF was 74.6%, almost 2% higher than any previous FF. The improvement was achieved via progress in chemically dip-coated CdS. In fact, 840 mV was achieved several weeks ago when Photon Energy deposited its CdTe on a dip-coated CdS substrate made at USF. Thus, USF's high voltages are a result of improved CdS, not improved CdTe. (USF makes CdTe by close-spaced sublimation (CSS), and it is developing dip-coated CdS as a sub-tier contractor to Photon Energy.) An important aspect of the USF device is that the record efficiency was achieved despite very mediocre short-circuit current. We have previously reported currents over 26 mA/cm^2 made with thin CdS on CdTe (Photon Energy). The dip-coated CdS being developed by USF is designed to make thin layers that allow high currents. But USF has not yet optimized its dip-coating process for this advantage. Thus, it may be expected that within the next few months USF will be able to increase their currents substantially, i.e., to in excess of 25 mA/cm^2. Combining the existing parameters with a 25 mA/cm^2 current would allow USF to surpass 15% efficiency. Both Photon Energy and Solar Cells Inc. (which uses CSS to make their CdTe) have shown intense interest in the USF results.

- A major government/industry partnership subcontract with Siemens Solar Industries has been awarded by the Polycrystalline Thin Films Project. The goal of the three-year subcontract is to develop high efficiency CIS power modules (12.5%, 49 watt, 4-ft^2 modules). Achieving this goal is important to reaching the key thin-film milestones of the *Photovoltaics Program Plan FY 1991—FY 1995*. The three-year award is for $4.6 million, of which NREL's share is $2.4 million. With the award of this and the Boeing subcontract, we have accomplished a key annual operating plan milestone, completing the Polycrystalline Thin Films Module Development request for proposal (RFP). The purpose of the RFP was to bolster the infrastructure in CIS and CdTe, two very promising thin film materials. With the recent award of several subcontracts, we are now supporting Solarex, Siemens, ISET and Boeing in CIS, and Photon Energy and Solar Cells Inc. in CdTe. In addition, we have added support for Astropower in thin x-Si. The participation of these key companies meets the goals of the

RFP. They should provide the progress needed to bring the polycrystalline thin-films technologies to commercial success.

- Photon Energy, under its subcontract entitled "Module Process Optimization and Device Efficiency Improvement for Stable, Low-Cost, Large-Area, CdTe-Based Photovoltaic Module Production," has produced another record cell. Separate from its equally promising work on solution grown thin-CdS with Chu at the USF, Photon Energy has made additional advancements in the deposition of its CdS window layer. This has resulted in a significant improvement in the uniform thickness of the CdS layer allowing Photon Energy to reduce this layer to a few hundred angstroms. Results of this process improvement have been two record 0.3-cm^2 cells cut from 6" by 12" panels and tested at NREL. The device parameters of the cells were as follows: eff = 12.7%, V_{oc} = 0.7888 V, J_{sc} = 26.18 mA/cm^2, and FF = 61.40%; and Eff - 12.7%, V_{oc} = 0.7989 V, J_{sc} = 26.21 mAcm^2, and FF = 60.51%. These measurements have established record efficiencies and short-circuit currents. When measured in May 1991, efficiency equaled the highest efficiency polycrystalline thin-film cells measured at NREL.

- AstroPower has been awarded a multiyear phased subcontract for $2.6M. AstroPower will be cost sharing the subcontract at about 20%. The period of performance is from May 1, 1991, through February 28, 1994. The objective of the research is to fabricate, by the end of the third year, 12% efficient thin silicon-film submodules deposited on ceramic substrates that are monolithically integrated. The area of the submodule is 1200 cm^2. The film thickness of the silicon-film will be less that 50 microns (AstroPower will be using its proprietary method for depositing the thin silicon-film.)

- We met with G. Coors and B.L. Mornin of Adolph Coors Company to discuss the company's interest in PV. The Coors Company is considering PV as a possible technology for corporate development. NREL provided an overview and introduction to PV at the company in January.

- ISET has made further improvement to the metal organic chemical vapor deposition (MOCVD) ZnO films for ZnO/CdS/$CuInSe_2$/MO/glass devices under their Polycrystalline Thin Film subcontract, entitled "Process Development for High Efficiency, Low-Cost, Cu(In, Ga) Se_2 Module Fabrication." The result has been a new NREL-measured efficiency record for ISET. Two devices were measured at NREL with 11.4% and 11.5% efficiencies, improving ISET devices significantly over the 10.6% ISET record set recently. The best of these 1-cm^2 cells had the following parameters; η = 11.5%, V_{oc} = .483 V, J_{sc} = 35.60 mA/cm^2, and FF - 66.65%. The improvement in these devices has been attributed mainly to a reduction in ZnO layer sheet resistance from 35 ohms/square to 20 ohms/square, and a 10% increase in their transmission. These efforts have been supported by measurements by R. Matson, K. Emery, R. Dhere, and K. Ramanathan of NREL. Further reductions in sheet resistance and thinning of the ISET ZnO is expected to produce additional improvements in the next few months. Other areas of improvement being addressed at ISET include control and thinning of the CdS layer (now ranging from 800 Å to 1200 Å), and the addition of antireflection costing (MgF_2).

- The BP Solar unit has announced several important results in its thin film CdTe technology. We have known for about seven years that BP Solar has been developing CdTe, however, the company has never before made its results public. At the 5th International PVSEC, in Kyoto, Japan, it reported reaching 9.5% efficiency on a 706 cm^2 (aperture area) CdTe submodule made by electrodeposition. BP Solar also announced stability results from a CdTe module tested outdoors for more than year. There was no significant difference between the initial efficiency (6.4%) and the final one (6.2%). BP Solar stated that it expects to be able to reach about 12% efficiency on submodules with its existing CdTe capabilities. The BP Solar work is based on previous work funded through DOE/NREL at Monosolar. Monosolar was purchased by SOHIO and BP in 1983.

1.2.3 Crystalline Silicon Materials Research

NREL has actively worked with subcontractors in several research areas and facilitated interactions among subcontractors and with the industry. Development of a basic facility for optical processing and availability of NREL expertise for hydrogenation have led to formation of a nucleus for a collaborative program.

Major accomplishments of this project are:

- A method, based on optical processing, was developed to produce texturing on the back-side of a solar cell. This "dry texturing" technique works on all crystal orientations.

- Formation of hydrogen damage and the associated defect structure was identified. A back-side hydrogenation technique was developed for defect passivation of solar cells.

- Efficiency of dislocations as sinks for point defects was determined for commercial low-cost silicon.

- Diffusion of hydrogen in silicon was modelled using experimental data.

- Influence of dissolved oxygen on minority-carrier lifetime in silicon was studied.

- A technique for fabrication of optically reflecting low-resistivity ohmic contacts on silicon was developed.

1.2.4 High-Efficiency Concepts

The following is a list of FY 1991 key accomplishments for the high-efficiency project.

- Rensselaer Polytechnic has experimentally validated a new stagnation-point reactor configuration. The uniqueness of the design arises from the prediction that a water-cooled, source-gas design manifold can be located only 1 cm away from the 700° C susceptor and still be maintained at less than 150°C temperature. Initial growth runs yielded films with close to the predicted uniformity.

- Spire developed thin GaAs cells for enhanced efficiency using Bragg reflectors to double the optical path length. The Bragg reflector was tuned to have peak reflectivity in the range of 850–900 nm. Tests using a cell thickness of only 1 micrometer showed significantly improved red response. These cells have exceptionally high open-circuit voltages, at least 20 mV higher than Spire has ever achieved in traditional cells, due to the reduction in recombination attained by using only a 1 micron thick active layer.

- In a collaborative effort with the Massachusetts Institute of Technology and IBM, Spire has performed initial investigations of a silicon substrate patterning concept for reduced dislocation densities in heteroepitaxial GaAs. NREL's transmission electron microscopy (TEM) analysis of one sample revealed that some annihilation of dislocations resulted from the use of surface features.

- Kopin established operating parameters using diethylgallium chloride needed to attain lateral overgrowth capability in the MOCVD reactor. GaAs growth was demonstrated with good morphology and growth rates of up to 10 micrometers per hour. Little or no nucleation of polycrystalline material was observed on CLEFT masks. Tests to optimize the overgrowth will be performed. Successful development of this technology will cut epitaxy costs in half relative to the current process by elimination of the hydride chemical vapor deposition overgrowth prior to organometallic vapor deposition solar cell growth.

1.2.5 New Ideas for Photovoltaic Conversion

Competitive, public solicitations are periodically issued for new and innovative PV research ideas. In late FY 1991, a letter-of-interest (LOI) solicitation was issued and over one-hundred responses were received. The LOI responses will be reviewed during FY 1992 and the ones found to be in the competitive range will be invited to submit an expanded proposal for review. Based on FY 1992 funding and the availability of FY 1993 funds, it is likely that subcontract awards will start late in 1992.

Three ongoing subcontracts were renewed: novel ways of depositing ZnTe films by solution, researched by the IEC at the University of Delaware; development of an inverted AlGaAs/GaAs patterned tunnel junction cascade concentrator cell, at the Research Triangle Institute (RTI), and development of high efficiency epitaxial optical reflector cells, at USC. These awards started in FY 1990 based on the FY 1988 solicitation.

The following is a list of FY 1991 key technical accomplishments for the new ideas project.

- Researchers at IEC achieved Cu-doped ZnTe films, 50–300 nm thick, deposited directly by an electrochemical method for the first time. A CdTe/CdS solar cell using the ZnTe:Cu as the primary contact to the CdTe achieved an efficiency of 8.7% with a FF >65%. The optical transmission of cells using electrochemically deposited ZnTe:Cu is higher than for cells using evaporated ZnTe:Cu.

- Scientists at RTI have reported the first demonstration of an inverted-grown, thin-film, fully processed GaAs solar cell. This suggests that the inverted-growth approach to high efficiency AlGaAs/GaAs cascades is realistically feasible in the near term. Further, inverted growth can

offer a significant degree of freedom for the complete optimization of many multijunction cascade solar cells.

- Scientists at RTI developed an approach denoted as eutectic-metal-bonding (EMB) for providing PV-device-quality GaAs-AlGaAs thin films bonded onto Si substrates. The material quality is evidenced by the demonstration of a minority-carrier lifetime of 103 ns on an EMB GaAs-AlGaAs double heterostructure. Also, Raman spectroscopy indicates the EMB thin films on Si are free of strain.

1.2.6 University Participation Project

The following is a list of FY 1991 key accomplishments for the university participation project.

- North Carolina State University reported results of extended light soaking on "intrinsic" (lightly doped with boron) micro-crystalline silicon material. The measurements for more than 40 hours under 100 mW/cm^2 of white light can detect no degradation in the photoconductivity.

- C. Taylor at the University of Utah has been awarded a patent for doping amorphous silicon using tertiary butyl phosphine as the phosphorus source. Alternate sources may lead to a high ratio of electronic activity to chemical concentration. The university has chosen not to elect title to this invention. DOE may wish to take title on it.

1.2.7 PV Manufacturing Technology (PVMaT) Project

The PVMaT project is a government/industry PV manufacturing R&D project composed of partnerships between the federal government (through DOE) and members of the U.S. PV industry. It is designed to assist the U.S. PV industry in improving manufacturing processes, accelerating manufacturing cost reductions for PV modules, increasing commercial product performance, and generally laying the groundwork for a substantial scale-up of U.S.-based PV manufacturing plant capabilities.

Phase 1 activities under this project have been completed, with each company identifying and developing a specific set of R&D areas that address its specific process problems. In FY 1991, a competitive solicitation was directed to these Phase 1 participants to identify R&D efforts appropriate under Phase 2 of this project. Under Phase 2, selected companies will develop and implement solutions to their manufacturing problems. The final selection of successful bidders under this phase has been completed, negotiations are under way at this time, and the award of research subcontracts is expected to begin soon. It is anticipated that as many as six subcontracts will be awarded under this phase, in which successful bidders will be supported for as long as three years as they realize improvements to their manufacturing processes. As with most PVMaT projects, these companies will be expected to cost-share their work.

Future efforts in the PVMaT project are expected to include an additional Phase 2B solicitation focusing on company-specific problems (open to all U.S. firms, including those who weren't yet ready for the Phase 1 call for proposals). Additionally, in October 1991, a Phase 3A solicitation

was released for subcontracted team research on module-related R&D problems common to several PV manufacturers. The activities under PVMaT to date have received outstanding support, and the level of interest in participation is exceptional.

1.2.8. PV Module and System Performance and Engineering Project

The PV module and system performance and engineering project is structured to conduct state-of-the-art PV module, system, and application research, and engineering, testing, evaluation, and analysis tasks. The project also provides technical results and solutions to technical issues and develops PV applications and application opportunities. The project is designed to maintain and enhance supporting facilities and capabilities that are consistent with DOE's new *Photovoltaics Program Plan FY 1991—FY 1995*, are complementary to other DOE PV projects, and will ensure that project capabilities and facilities are available resources for cooperative research and utilization by the PV R&D community.

Overall project activities are managed through the module and systems performance and engineering project management task and organized to address project objectives through the following five primary tasks: (1) Cell and Module Standardized Characterization Performance; (2) Module and System Performance Testing; (3) Module Reliability Research: (4) Solar Radiation Research; and (5) System and Utility Applications.

Subcontract activities represent support for industry/utility PV power projects, domestic and international standards development, PV systems applications (including demand-side management), assessment of and effects on roof mounted modules, and solar resource utility load matching assessment. A solicitation entitled "Amorphous Silicon Utility/Industry Photovoltaic Power Project" was released to the general public in FY 1991.

1.3 Technology Transfer

Consistent with recent DOE policy, technology transfer is collaborative R&D with industry to aid industry in the commercialization of products or services. The industry and NREL joint work accomplished by researchers focused on a common R&D objective is an underlying theme of NREL technology transfer activities. Among government laboratories, there are seven principal tools for effecting technology transfer: subcontracted R&D, cooperative R&D, industry sponsored R&D, user facilities (at NREL), technology licenses, researcher exchanges, and information dissemination. NREL's PV program conducts its technology transfer primarily through three of the above: subcontracts, informal cooperative R&D, and information dissemination.

1.3.1 Subcontracts with Industry

In FY 1991, NREL had seven cost-shared subcontracts to industry totalling $7.8 million. The industry contribution to these research projects totals about $3.7 million. Technically knowledgeable NREL research managers participate in the definition, evaluation, award, and negotiation of statements of work submitted by industry researchers in R&D proposals. Following subcontract awards, NREL subcontract managers direct and evaluate research progress;

they made numerous site visits to subcontractor facilities in FY 1991 to review research progress. A fundamental assumption of NREL's PV Program is that technology development done by industry researchers circumvents the obstacles to technology transfer that are intrinsic in technology development done by NREL in-house research.

1.3.2 Informal Cooperative R&D

NREL in-house researchers frequently perform informal cooperative R&D with their industrial counterparts working under NREL subcontract. These interactions have been virtually ongoing since NREL (SERI) PV research started in 1977. The majority of these informal cooperative R&D activities involves performance measurements and materials analysis performed with NREL's large and unique set of capabilities for photovoltaic efficiency and materials analysis. Informal cooperative R&D, as distinguished from Cooperative Research and Development Agreements (CRADAs), is a natural complement to NREL's subcontracted PV program. CRADAs, as authorized by the National Competitiveness Technology Transfer Act of 1989, are formal agreements signed by the NREL Director and his industrial counterpart for the conduct of joint research projects involving both NREL and industrial researchers. No CRADAs were signed in FY 1991 although preliminary discussions were conducted on four potential CRADAs. Informal cooperative R&D in FY 1991 included the analysis of over 10,000 samples of materials, devices, or modules. Over 100 companies worked with NREL researchers in this fashion. The following list from one month's activities (not at all a complete listing for the year) illustrates the large, small, PV, and non-PV companies working with NREL researchers: Solarex Corporation, International Telephone and Telegraph, Photon Energy, Inc., Boeing Aerospace and Electronics, Siemens Solar Industries, Mobil Solar Corporation, Pacific Gas and Electric Company, Solec International, Inc., United Solar Systems Corporation, Tideland Signal Corporation, Italsolar, Carrizo Solar, Chronar Corporation, and Public Service Company of Colorado.

1.3.3 Information Dissemination

During FY 1991, there were various conferences, meetings, or workshops organized with the help of PV program staff members. These events include the 22nd IEEE PV Specialists Conference and the International Solar Energy Society Conference. Other activities in which NREL researchers and subcontracted researchers participated include an ad-hoc IEEE Standards Coordinating Committee and SOLTECH 91. These gatherings provide important opportunities for industry researchers to exchange technical information with NREL and NREL-subcontracted university researchers. These information dissemination activities do contribute to progress for industry researchers; one measure of progress is the joint publications of NREL and industry researchers that describe the outcome of their joint research endeavors. A small sampling taken from the conference proceedings of the 22nd IEEE Photovoltaic Specialists Conference showed NREL researchers publishing in conjunction with researchers from Spectrolab Inc., Boeing Aerospace and Electronics, International Solar Electric Technology, Photon Energy, Inc., AT&T Microelectronics, and Varian Research Center.

1.4 Conclusions

Major program thrusts in FY 1991 continued to be implemented based on DOE's new *Photovoltaics Program Plan FY 1991—FY 1995.* The mission of the National Photovoltaics Program is to develop PV technology for large-scale generation of economically competitive electric power in the United States. The major challenge in fulfilling the mission is to assist industry in laying the foundation for the installation of at least 1000 MW of electrical capacity by the year 2000. Under the DOE PV program, the NREL PV Advanced Research and Development Project sponsors fundamental and applied R&D, manufacturing development, and systems and market development in PV energy technology. The project also provides services to industry and electric utilities or other users, and it provides the leading support for the National Photovoltaics Program. The NREL subcontract program is responsible for most of the R&D, manufacturing technology development, and some of the systems and market development task areas under the National Photovoltaics Program.

The subcontract activities of the NREL PV project are summarized under the following sections: 2.0 Amorphous Silicon, 3.0 Polycrystalline Thin Films, 4.0 Crystalline Silicon Materials Research, 5.0 High-Efficiency Concepts, 6.0 New Ideas for Photovoltaic Conversion, 7.0 University Participation, 8.0 Photovoltaic Manufacturing Technology Project, and, 9.0 Module and System Performance and Engineering. The sections include a brief overview including the objectives, approaches, and some key developments. Following the overview are technical summaries of the subcontract activities in that area. The summary sections were provided by the subcontractors themselves or were compiled from various project reports submitted by the subcontractors. Section 10.0 lists FY 1991 subcontracts, and Section 11.0 lists subcontractor major reports.

2.0 AMORPHOUS SILICON RESEARCH PROJECT

Werner Luft (Manager), Byron Stafford, and Bolko von Roedern

The near-term objective of the Amorphous Silicon Research Project (ASRP) is to achieve 12% stable prototype module efficiency by 1994 in accordance with the goals in DOE's. new *Photovoltaics Program Plan FY 1991—FY 1995* through better understanding and improvement of the optoelectronic properties of amorphous-silicon-based alloy materials. A transition in emphasis did occur in FY 1990 from single-junction cell and submodule research to multijunction module research, and from initial efficiency to stabilized efficiency. NREL implemented the transition in FY 1991 to focus industrial subcontractors and university subcontractors on *stabilized* efficiencies, rather than to focus on maximizing initial performance and minimizing degradation.

The ASRP consists of three tasks: (1) subcontracted research, (2) NREL amorphous silicon research, and (3) surface and interface analysis. Within the subcontracted research there are two principal activities: subcontracted multi-disciplinary research activities, and subcontracted fundamental research activities. The subcontracted multi-disciplinary research activities are performed under cost-shared programs between government and industry by broad-based research teams located at the individual industrial facilities that perform focused research ranging from feedstock materials through the development of modules. The subcontracted fundamental research activities involve basic and supporting research done by academia and research laboratories to aid the industry groups' advances of the technology base. The cost-shared subcontracted multidisciplinary research programs address issues related to all aspects of two-terminal amorphous silicon multijunction cells and modules using same-bandgap or different-bandgap device structures. Research was performed to advance the stabilized conversion efficiency of multijunction modules having areas of at least 900 cm^2 using glow discharge deposition as the primary method of fabricating the amorphous silicon films. The stability of these devices was examined for fundamental changes in the bulk material properties, for temperature effects such as diffusion, for fabrication and area-related defects (interfaces), and for extrinsic degradation related to module encapsulation and framing issues. Transparent conductors were studied to improve the electrical conductivity while achieving optical transmissions greater than 85%. The quality and controlled texturing of ZnO transparent conductors based on low-cost processes were emphasized. The opto-electronic properties of a-SiGe:H and a-SiC:H alloy materials were investigated to determine the limits of these materials with regard to their use in practical multijunction devices. The interconnection of cells in a series-connected module configuration was a major issue studied since it impacts conversion efficiency through the inactive area losses, influences stability through changes over time in the contact resistance, and influences cost through its impact on yield and on the number and types of processing steps.

Multidisciplinary subcontracted research was initiated in FY 1990 to transfer the small-area technology developed under previous government/industry initiatives to large-area multijunction modules that are stable, reliable, reproducible, and have low cost. For this purpose, a new Government/Industry Program with 3-year subcontracts was started with three subcontract awards funded from the FY 1990 budget (Solarex, Glasstech Solar [GSI]), and United Solar Systems Corporation). One of these (GSI) was subsequently terminated after 6 months of work. The principal objectives of this research are: (1) to conduct research on semiconductor materials and non-semiconductor materials to enhance two-terminal, multijunction, thin-film, large-area, all-

amorphous-silicon-alloy device performance, (2) to develop high-efficiency, *stable, reproducible*, and *low-cost* multijunction photovoltaic modules based on all-amorphous materials, (3) to demonstrate in stable 12% (AM 1.5) aperture area solar conversion efficiency for different-bandgap modules, and (4) to demonstrate in stable 10% (AM 1.5) aperture area solar conversion efficiency for same-bandgap modules. The modules will be at least 900 cm^2 in area and consist of at least two integrally stacked devices using all-amorphous-silicon alloy materials. The Government/Industry Program has been highly successful and significant advances have been made in cell/submodule performance.

The total subcontracted fundamental research program (with the exception of ZnO transparent electrode development) was recompeted in FY 1990. Ten awards were made in FY 1991 under the competitive procurement to Colorado School of Mines, Institute of Energy Conversion, Iowa State University, North Carolina State University, Pennsylvania State University, Syracuse University, University of Illinois, University of North Carolina, University of Oregon, and Xerox. Two additional noncompetitive awards were made to the National Institute of Standards and Technology and the Jet Propulsion Laboratory. The following general areas are being addressed in support of the multidisciplinary activities: light-induced stability, alternative material deposition approaches, amorphous silicon alloy materials, and material characterization. Several models have been proposed to explain metastable effects observed in amorphous silicon films. More research was done to differentiate between the often subtle aspects and predictions of the models. More importantly, research was done on photovoltaic devices to correlate light-induced changes in the films with light-induced changes in the device performance. Continued research was done on both high- and low-bandgap alloys to determine the relationship of observed structural inhomogeneities to electrical transport properties. Research was done on high- and low-bandgap alloys in device structures and under measurement conditions which simulate the intended end-use environment of the materials. Alternative deposition methods are explored to improve or develop discrete component layers such as wide bandgap, high conductivity doped layers, or alloy films. As the amorphous silicon technology matures, more sophisticated measurement and characterization techniques are needed for studies from the atomic level to characterization of materials in efficient photovoltaic devices. Collaborations between the fundamental research groups, government/industry research groups, and the NREL internal research groups was maintained through sample exchanges, workshops, and copublications.

The NREL in-house research by the amorphous silicon group covered four investigations: (1) using alternate deposition methods such as hot-wire thermal decomposition deposition, hydrogen ion-implantation, and remote plasma hydrogen-radical chemical vapor deposition for improved material properties; (2) maintaining our ability to fabricate good quality p-i-n solar cells for device physics and photo-degradation studies; (3) maintaining state-of-the-art measurement facilities and developing new methods for material and device characterization; and (4) investigating and modeling photo-degradation phenomena with particular emphasis on correlating microstructure and defect properties with stability. Early in May 1991, deposition of a-Si:H using concentrated silane was stopped for safety reasons in the existing laboratories in Building 16 of NREL. To restart deposition from concentrated silane, the activity will have to be moved off-site. A new Safety Analysis Review was started for an off-site facility. Facility modifications and deposition equipment modifications are required to meet safety demands. Shake-down of the modified facility and equipment is expected to be completed by May 1992.

fabricating polycrystalline cells include, for $CuInSe_2$, sputtering (with selenization) (Siemens Solar, Martin Marietta, International Solar Electric Technology, and Solarex), a reactive-sputtering and hybrid sputtering/evaporation method (University of Illinois and Solarex), and evaporation (Boeing); for CdTe, close-spaced sublimation (Solar Cells Inc. and USF), evaporation (Institute of Energy Conversion), metal-organic chemical vapor deposition (Georgia Institute of Technology and USF), and spraying (Photon Energy). For $CuInSe_2$, we are also investigating non-H_2Se selenization methods at NREL and Institute of Energy Conversion. For CdTe, we plan work in sputtering and electrodeposition.

An initiative in the Polycrystalline Thin Film Program was begun with the release of a Request for Proposal (RFP) in FY 1989. The objective of the solicitation was to stimulate progress in $CuInSe_2$ and CdTe submodule development and to deepen the U.S. participation in these promising technologies. The research community responded favorably, as reflected in the many excellent technical proposals received in response to the solicitation. Several new cost-shared contracts have resulted from the RFP. In 1991, we completed our university program plan to add several new participants early in FY 1992.

Title: **Small Angle X-ray Scattering Studies of Amorphous Silicon-Based Semiconductors**

Organization: Department of Physics, Colorado School of Mines, Golden, Colorado

Contributors: D. L. Williamson, principal investigator, Y. Chen, S.J. Jones, and G. D. Mooney.

Objectives

In fiscal year 1991, Small Angle X-ray Scattering (SAXS) measurements were made on a host of amorphous semiconductor films in order to examine their microstructures on a scale of 1 to 25 nm. The objectives of this work are to determine whether the presence of microstructure as detected by SAXS 1) limits the photovoltaic properties of the present device-quality a-Si:H, 2) plays a role in determining the stability of the amorphous semiconductor materials, and 3) is responsible for the degradation of the photoelectronic properties upon alloying with germanium. Besides these studies, efforts are also being made towards improving the methods used in sample preparation for SAXS measurements and SAXS data analysis.

Approach

To address the above objectives, the following tasks have been completed:

1) A number of a-Si:H and silicon-based alloy films were measured and the results compared with the films' relative photoelectronic properties;

2) Several device-quality a-Si:H films were measured in both the light-soaked and annealed conditions to search for any light-induced effects (Staebler-Wronski effect) in the SAXS data;

3) A first round of measurements was made using the Brookhaven National Synchrotron Light Source (NSLS). The use of high x-ray intensities and a point focus geometry at this facility allows for quick data acquisition (30 minutes as compared to 15 hours using the system at CSM) and, in principle, a more straight-forward interpretation of the data;

4) Some initial steps were taken to model the SAXS data in order to extract microvoid shape information based on a recent paper by Shibiyama et al. [1].

Results

a-Si:H films

We have examined series of rf glow discharge-produced a-Si:H samples made using different applied powers (NREL) and substrate temperatures (Utrecht University). Increases in the microvoid volume fractions were found with increasing applied power and decreasing substrate temperature. In both cases, the increases in microstructure follow typically observed deteriorations in the photoelectronic properties.

A set of samples prepared in a rf sputtering system (J. Shinar's Group of Iowa State University) at various deposition powers was also measured. Contrary to what was found for the films produced by rf glow discharge, the smallest void fractions were found for the films produced at the highest powers. The low void volume fraction samples have

microvoids that are predominantly 0.8 to 1.0 nm in diameter, whereas the higher void fraction films have a significantly larger predominant size of 1.5 nm.

SAXS data obtained for six ECR-deposited films provided by Yu-Han Shing of JPL reveal microvoid volume fractions which are at least four times larger than those usually found for device quality, rf glow discharge produced a-Si:H.

a-$Si_{1-x}Ge_x$:H

a) The SAXS data for several a-$Si_{1-x}Ge_x$:H films produced by different groups are displayed in figure 1. In contrast to device quality a-Si:H, the SAXS signals for each of these films are more intense and the associated microvoid volume fractions at least four times larger. Results from tilting experiments suggest all but one of these films contain large ellipsoidal voids which are preferentially oriented parallel to the film surface normal. The exception contains the smallest amount of germanium (37%). Plans in the next year are to measure sets of alloy films produced under conditions where deposition parameters are systematically varied and representative opto-electronic properties are known.

Staebler-Wronski Effect and SAXS

Five device quality a-Si:H samples were measured in an annealed state (170°C for 20 hrs) and in an accelerated light-soaked state (20 Suns for 20 hrs). For each of the five films, the SAXS data taken in the two states are the same within experimental uncertainty (see figure 2). We note that these results *do not imply* that the microvoids play no role in the Staebler-Wronski effect.

SAXS Measurements at NSLS

Several of the SAXS data sets obtained from our initial visit to NSLS have now been analyzed and the results are qualitatively consistent with those obtained using the apparatus at the Colorado School of Mines. Quantitative comparisons will require corrections for differences in the slit geometries and in an apparently much larger background signal in the NSLS data.

Modeling

The developed software models the SAXS data based on a Gaussian size distribution of ellipsoids of revolution. The model used can qualitatively account for the hot wire a-Si:H film tilting effects [2] for ellipsoids with major-to-minor axis ratio much larger than unity and a preferred orientation of the major axes perpendicular to the film plane. The glow discharge a-Si:H film tilting effect can be modeled by an axis ratio less than unity (pancake shape) and a preferred orientation of the short axis perpendicular to the film plane [2].

References

1. Shibayama, M., Nomura, S., Hashimoto, T. and Thomas, E.L., J. Appl. Phys. 66 (1989) 4188.
2. Mahan, A.H., Chen, Y., Williamson, D.L. and Mooney, G.D., Proceedings of ICAS 1991 (Garmisch-Partenkirchen, Germany), to be published in J. Non-Cryst. Solids.

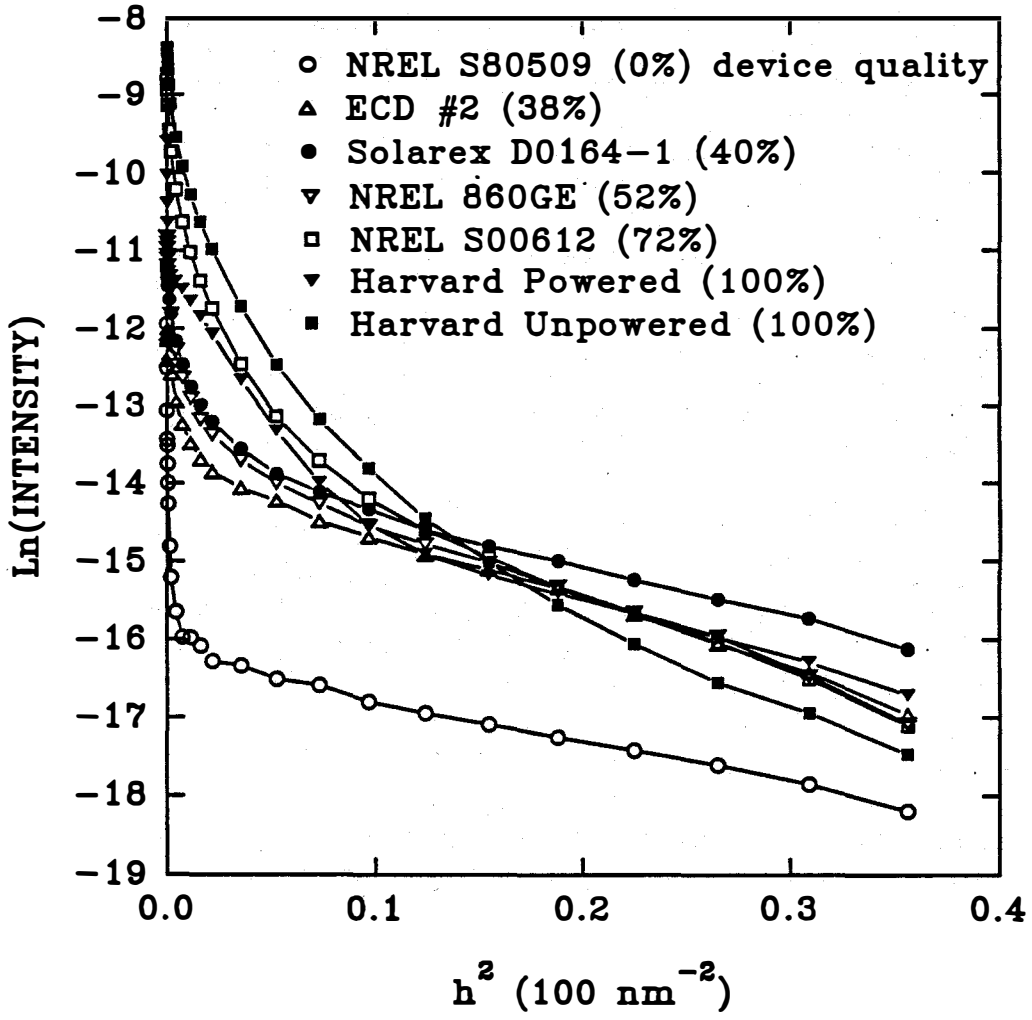

Figure 1. SAXS data for several a-SiGe:H films with the germanium contents in parentheses in the legend ($h=4\pi\theta/\lambda$ where 2θ and λ are the scattering angle and x-ray wavelength, respectively).

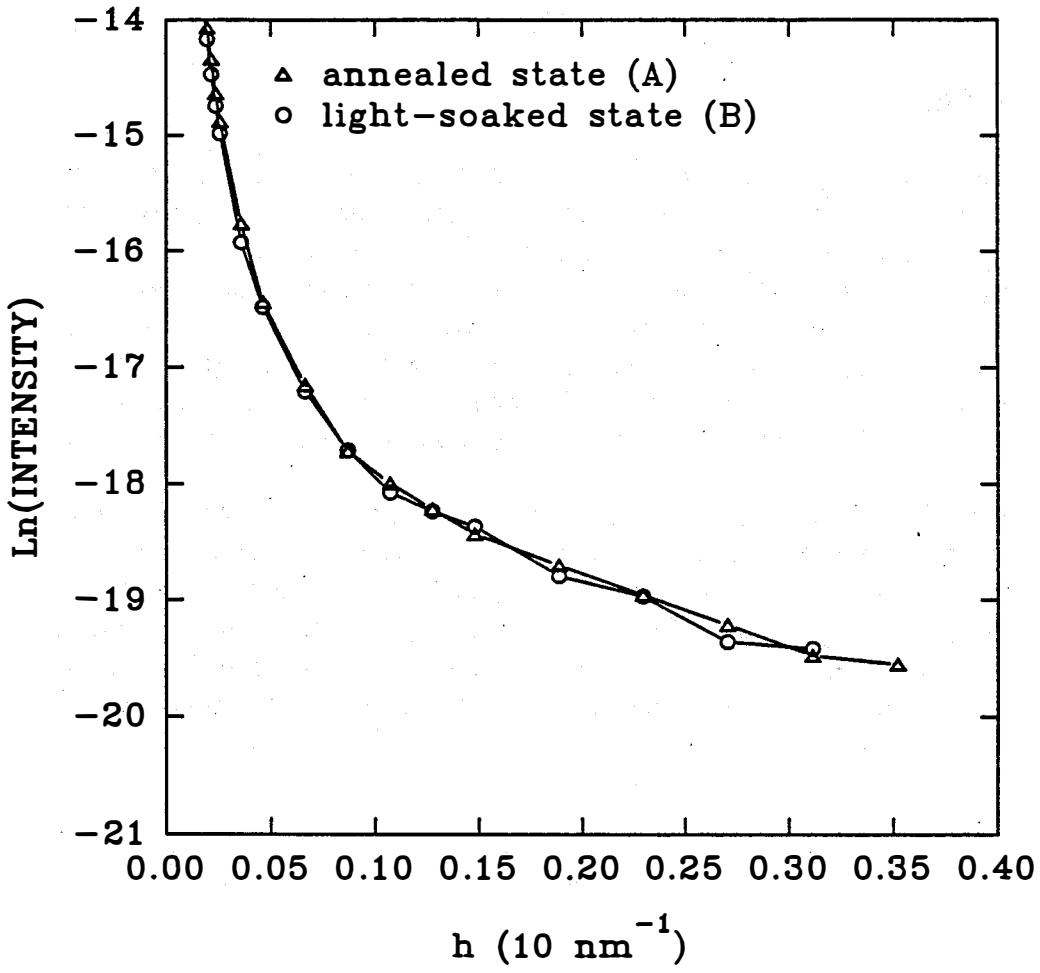

Figure 2. SAXS data for a device quality a-Si:H sample in the Staebler-Wronski states A and B.

Title: **Optimization of Transparent and Reflecting Electrodes for Amorphous Silicon Solar Cells**

Organization: Department of Chemistry,
Harvard University, Cambridge, MA

Contributors: R.G. Gordon, Principal Investigator;
J. Hu; J. Musher; H. Hummel; D. Lacks

SUMMARY

OBJECTIVES

Transparent conducting materials are essential components of many kinds of solar cells, in which they serve as front-surface electrodes. In tandem cells, back surface electrodes also need to be transparent. Finally, some designs for highly reflective back contacts also call for a transparent conducting layer. The compositions of these transparent conducting layers are usually based on oxides of tin, indium and/or zinc, and hence referred to as transparent conducting oxides (TCO). In addition to having low electrical resistance and low optical absorption, the structure of a TCO must minimize reflection losses. The TCO must also resist degradation during cell fabrication and use. Finally, the method for making the TCO must be inexpensive and safe.

Our general objectives are to improve the performance of TCO materials and the methods for their production. We aim to reduce their electrical resistance, optical absorption and refection losses, and to avoid degradation of the materials. For the production method, the prime consideration is to deposit the TCO layers at a high rate with relatively simple apparatus. The method chosen is chemical vapor deposition at atmospheric pressure (APCVD), since it has been demonstrated, in the glass-coating industry, to be the most cost-effective method for making large areas of TCO coatings.

RESULTS

Preparation and Characterization of Textured Zinc Oxide Films

Zinc oxide is a promising material for forming less expensive TCO layers, since zinc metal is much less expensive than tin or indium. Also, zinc is much more abundant in the earth's crust, than is tin or indium, so that even large-scale use of solar cells would not lead to any shortage of zinc.

Also, zinc is widely distributed on earth, and is mined in many countries, so continuity of supply is assured in any kind of political situation. In contrast, tin is mined in large quantities in only a few countries. Another advantage of zinc oxide is its greater stability toward hydrogen plasmas used to deposit amorphous silicon solar cells.

We discovered that fluorine can also be used to dope zinc oxide to high electrical conductivity. Fluorine is an ideal dopant for zinc oxide, since it is known to be electrically inactive, or even beneficial, in hydrogenated amorphous silicon. An additional benefit of the fluorine doped zinc oxide is its higher electron mobility, which results in greater transparency. The absorption loss in fluorine-doped zinc oxide is only about half of the loss in fluorine-doped tin oxide having the same sheet resistance.[1,2]

The fluorine-doped zinc oxide is produced by CVD from diethyl zinc, ethanol and hexafluoropropylene at atmospheric pressure, in the temperature range 375-450°C. Films deposited under these conditions show good adhesion to the glass substrates (Scotch tape test). The highest electrical conductivity and light transmission are found for films deposited at the highest temperatures (450°C), and containing about 0.5 atomic percent fluorine. With this material, we could produce a TCO with a sheet resistance of 5 ohms pr square and visible transmission of about 87%, at growth rates up to 250 nm/minute.

We discovered that the amount of texture (roughness) of the zinc oxide films depends dramatically on the amount of water vapor in the growth atmosphere. Small amounts of water vapor (about 1% of the ethanol concentration) produce smooth films, but decreasing the water content to less than 0.25% of the ethanol content produces textured (rough) zinc oxide films suitable for efficient light-trapping growth, so a small, controlled source of water vapor is essential to control of film texture[1].

Depositions of zinc oxide films were carried out using aluminum as a dopant instead of fluorine. Detailed optical, electrical and structural characterization of these films was done. The electrical conductivities achieved were comparable to those we found using fluorine as a dopant. Higher electron concentrations were achieved with aluminum, but the mobilities were lower than with fluorine. The higher electron concentrations might be helpful in producing lower contact resistances between the zinc oxide and other layers in a solar cell. The lower mobility for the aluminum-doped layers, however, also results in higher optical absorption and lower transparency than with fluorine. Therefore, an optimum transparent conductor for solar cells might consist mainly of fluorine-doped zinc oxide, covered by a thin surface layer of aluminum-doped zinc oxide. Such a multilayer coating could be produced practically in a multi-chamber CVD furnace.

Solar Cell Deposition on Zinc Oxide Films

Production of large area, uniform films has been delayed because of Watkins-Johnson's inability to deliver the belt furnace which it was contracted to produce. Although we still hope to take delivery of this machine, which will produce uniform coatings more than 12-inches wide, we have received a smaller 6-inch furnace from BTU Engineering. More work will be required to adapt this machine to our purposes, but we hope to have it operating in a few months.

Zinc Oxide Deposition for Applications as Final Contact for Solar Cells

The reaction of diethylzinc and ethyl alcohol is too slow to deposit zinc oxide at temperatures below 300°C. However, by switching to tertiary-butyl alcohol, we found that zinc oxide films could be deposited at these low temperatures. However, neither the aluminum nor the fluorine

dopant was found to be electrically active when the deposition temperature was below 300°C. therefore, these low-temperature films had very low electrical conductivity.

These layers can be used only for deposition before the amorphous silicon, as, for example, the layer between a glass superstrate and the amorphous silicon. Therefore, we are continuing our search for a suitable lower-temperature APCVD method for a conductive layer to be applied onto amorphous silicon, to be a diffusion barrier and reflection enhancer for the back metallization. Further work will attempt to remedy this problem by the use of boron, gallium or indium as dopants. Also, alternate transparent conductor materials will be considered for low-temperature deposition.

a) Boron doping using diborane is being investigated, since its use has been successful at low temperatures in low-pressure CVD. So far, our efforts at atmospheric pressure had only produced insulating films at low temperatures, although conductive boron-doped films have been produced at temperatures above 300°C.

b) Gallium doping experiments have been started. Conductive films have been produced at about 300°C, but the reaction has been difficult to control. The trimethylgallium dopant has a very strong inhibitory effect on the CVD reaction kinetics. We will try to put this effect to use, in order to reduce the reaction rate of diethylzinc and water vapor, which is normally too fast to produce uniform CVD films at temperatures above about 200°C.

c) Indium will be tried as a dopant for APCVD zinc oxide films.

Development of Zinc Oxide Layers which are Compatible with New Amorphous Silicon Processing Requirements

Progress in this area must await installation of the new equipment for large-area deposition, as discussed in paragraph 2, above.

Growth and Bonding Theory

Our density functional theory of chemical bonding has been developed further, and programs written to carry it out. The theoretical energy and structure are in good agreement with experiments on α-quartz. The new bonding theory has also been applied to another phase of silicon dioxide, stishovite, which is stable at high pressures. The structure and energy of this phase are in good agreement with calculations, and the pressure of the phase transition is also in agreement with experiment. Further tests of the bonding theory will be made on other phases of silica. Then the calculations will be extended to zinc oxide and tin oxide.

CONCLUSIONS

- Textured fluorine-doped tin oxide films with high electrical conductivity (5 ohms/square) and high transparency (87%) were produced by chemical vapor deposition at atmospheric

pressure (APCVD) on glass substrates at about 450°C, at moderate deposition rates (up to 250 nm per minute).

- Amorphous silicon solar cells grown on these textured films show very high quantum efficiencies which demonstrates the high light-trapping ability of this texture, and the high transparency of the zinc oxide film.

- Transparent, conductive aluminum-doped zinc oxide films were grown by APCVD at temperatures above 300°C. The electron concentrations are higher for fluorine-doped films, but their transparency is lower. These layers are suitable for low-resistance contact to p-type amorphous silicon on the front surface of a solar cell.

- Boron, aluminum and fluorine-doped zinc oxide films were grown at temperatures below 300°C, but they have low conductivity and are not suitable for back contacts to solar cells.

References

1. Jianhua Hu and Roy Gordon, Solar Cells **30**, 437(1991).

2. Jianhua Hu and Roy Gordon, Materials Research Society Symp. Proc. **202**, 457 (1991).

Title: **Structural and Electronic Studies of a-SiGe:H Alloys**

Organization: Division of Applied Sciences, Harvard University, Cambridge, MA

Contributors: William Paul, principal investigator;

Professor J.H. Chen, visiting professor; Mr. (now Dr.) S.J. Jones, Dr. E.Z. Liu, Dr. J. Lyou, Dr. F.C. Marques, Ms. Dawen Pang, Dr. W.A. Turner, Ms. Anna E. Wetsel and Mr. Paul Wickboldt

Objectives

The principal objectives of this research have been (1) to carry out a detailed study of the structural, electrical and optical properties of a-Ge:H, the end-component of the a-SiGe:H alloy series, in order to determine deposition conditions and paramater values that will optimize the properties relevant to photovoltaic devices, (2) to extend the work on pure a-Ge:H to alloys of a-Si_xGe_{1-x} of $x < 0.5$, so as to arrive at methods of deposition yielding films with comparable quality to the best a-Ge:H, (3) to continue a collaboration with Professor Richard Norberg of Washington University by preparing films of a-Si and a-Ge containing deuterium, so that the Norberg laboratory can study deuteron magnetic resonance (DMR), which may be interpreted to give information on the microstructure of films on a 100 Å scale, (4) to continue a collaboration with Dr. M.L. Theye of the Laboratoire d'Optique, University of Paris, to explore low photon energy absorption spectra determined by photothermal deflection spectroscopy or steady-state photoconductivity, (5) to continue a collaboration with Professor J. Chen of Boston College to study the electron spin resonance spectra of hydrogenated amorphous semiconductors, and (6) to carry out a collaboration with Professor J. Tauc of Brown University on the photomodulation spectra of high quality a-Ge:H films.

Approach

Our research has been guided by the philosophy that insight into the difficulties surrounding the preparation of acceptable low band-gap a-SiGe:H alloy material may be obtained through a detailed understanding of the deposition conditions necessary for the preparation of high-quality a-Ge:H and high quality a-Si_xGe_{1-x}:H of high Ge content. The typical experimental approach used in the production of such low band-gap alloy materials is to start from conditions which produce high-quality a-Si:H, add some form of germanium to the deposition plasma, and to then perturb the conditions of deposition slightly from those used to produce a-Si:H until the properties of the resulting material are empirically optimized. It is not unreasonable to suggest that the properties of such alloy materials should be at least as sensitive, if not more so, to conditions which produce high-quality germanium, as a-Ge:H is typically found to be notoriously bad. It is our contention that the conditions necessary for the preparation of high-quality a-Ge:H are significantly different from those used to produce high-quality a-Si:H.

The films required were prepared by r.f. glow discharge. These films were subjected to an extensive battery of structural, optical and electrical characterizations in our laboratory and, in some instances, those of our collaborators. The measurements made included

conductivity *versus* temperature, optical absorption in the sub-band-gap region of the spectrum, optical vibrational absorption in the infrared region, photoconductivity spectra, ambipolar diffusion length, Raman spectra, gas evolution, transmission and scanning electron microscopy, differential scanning calorimetry, isothermal calorimetry, and deuteron and electron magnetic resonance.

Discussion

Our research this year has concentrated first on consolidation of our successful production of high density, non-porous, highly photoconductive, environmentally-stable a-Ge:H under more precisely delineated production conditions, second on extension of our film production and characterization to a-Si_xGe_{1-x}:H alloys of low x, and third on initiation of studies of the PECVD plasma yielding different quality films of a-Ge:H and a-Si_xGe_{1-x}:H.

Sufficient detail on the structural, optical and electronic properties of the optimized films of a-Ge:H was included in the Branch Annual Report for 1990. During 1991 the range of parameter-space (substrate temperature T_s, r.f. power, GeH_4 flow rate, H_2 flow rate, total gas pressure) was extended, but without significant improvement in typical values of the $\eta\mu\tau$ product and photosensitivity ratio $\Delta\sigma/\sigma$. We continued to confirm that the properties of the samples obtained were sensitive to apparatus geometry and gas flow conditions to a greater extent than in the production of a-Si:H. It will be recalled that the principal significant contribution leading to better a-Ge:H was the realization of the efficacy of having a certain amount of ion bombardment of the growing films, a condition usually minimized for a-Si:H. The effect of ion bombardment was studied by arranging to prepare a-Ge:H simultaneously at the cathode and anode of r.f. glow discharge systems with asymmetric electrodes, which leads to higher electric fields and bombardment of the films growing at the smaller-area cathode, and probably to different plasma conditions in its vicinity. Anode-deposited films have optical absorption spectra and transport parameters which appear to be normal, but TEM micrographs show that they possess microstructural inhomogeneities, and their photoelectronic $\eta\mu\tau$ and $\Delta\sigma/\sigma$ are very poor. By contrast, cathode-deposited films have superior properties, orders-of-magnitude higher $\eta\mu\tau$ and $\Delta\sigma/\sigma$, and TEM micrographs resembling device-grade a-Si:H. This year we have completed a very instructive study of material deposited at the cathode at different values of the spacing (1.0 cm to 3.2 cm) between the parallel electrodes. At selected spacings, other deposition parameters such as total r.f. power, substrate temperature and gas flows were systematically varied, and a full series of structural, electrical and optical measurements made. The results demonstrate a consistent improvement in optimized film quality as the electrode separation is decreased. This improvement is apparently not related directly to increased energy of the bombarding ions, since the self-bias of the cathode hardly changes, but must be due instead either to an increased ion flux or to a more appropriate concentration and distribution of plasma radicals at the reduced electrode separation. This reduced electrode separation, it must also be noted, corresponds to higher local power density. The superiority of the films produced at small electrode separations has been confirmed in about 100 film depositions. These results demonstrate that the production of "good" a-Ge:H is very sensitive to the precise plasma conditions, and are a principal reason for our decision to explore, to the extent possible, the properties of the plasma corresponding to the optimum values of electrode separations, r.f. power, pressure, gas flows. etc. By distinguishing the properties of the islands and connecting tissue evident in the microstructure of these films, we have also given a self-consistent explanation of the

optical. transport, photoluminescent and photoelectronic properties of these two phases. This analysis suggests that the extended state and drift mobilities of cathode-deposited films are as high as those for a-Si:H, and that further improvement of $\eta\mu\tau$ must come from a decrease in the gap density of states. By contrast, the much reduced mobilities of anode-deposited films are linked to the observation of increased microstructure. Reduction of the microstructure is crucial for improvement of a-Ge:H and a-Si_xGe_{1-x}:H.

During this year we have extended our studies to the production and characterization of a-Si_xGe_{1-x}:H alloys of high Ge content, corresponding to E_{04} band gaps of 1.4 and 1.6 eV. Guided by our experience with Ge, we have deposited films under appropriate combinations of substrate temperatures, r.f. powers, gas pressures, gas flows, and electrode separations, and have carried out the full series reported above of structural, electrical and optical measurements. Such studies are painstaking, because every parameter variation is apt to lead to a different composition of alloy. The trends in measured properties with production conditions have been (not surprisingly, because x is small) very similar to those for a-Ge:H and, significantly, includes the microstructural characterization by TEM. We have been able to show that the mere introduction of SiH_4 into the GeH_4 plasma does not automatically lead to a degradation in photoelectronic properties, as has been the nearly-universal experience in the fabrication of these alloys. As an example of our success this far, we have been able to produce a-Si_xGe_{1-x}:H with the following characteristics: E_{04} optical gap 1.40; Urbach parameter 46 meV, sub-band gap α at 0.8 eV of 2.5 cm^{-1}; transport activation energy 0.62 eV; $\eta\mu\tau$ 3.1×10^{-7} cm^2/V, and ambipolar diffusion length 630 Å.

Toward the end of this report period, we have concentrated on examining the relative concentrations of the radicals GeH_x, Ge_2H_x, SiH_x, Si_2H_x and $SiGeH_x$ ($x = 0$ to 4) in the different plasmas responsible for yielding good quality films, and also on examining the radicals on systematic variation of one or other of the deposition parameters while the rest are maintained fixed. The radical content of the plasma is sampled by constructing a small orifice leading from the plasma to an RGA. By this means, for example, we have confirmed that conditions leading to good quality films of a-Ge:H also give a low concentration of Ge_2H_x radicals ($x > 1$) in the plasma. This result is significant in helping to explain large changes in film properties as the electrode spacing is varied in that no other measured deposition condition was observed to significantly change.

Simultaneous with these studies we have measured the self-bias potentials of the anode and cathode during deposition. These potentials give an indication of the ion bombardment energy. Our results suggest that the production of optimum films requires ion energies within a particular range of values.

We have also continued our several collaborations with considerable success. The DMR results establish a multiplicity of environments for D (and thus H) in a-Si:H, a-Ge:H and a-Si_xGe_{1-x}:H alloys with more specificity than in any other investigation of which we are aware. It has been established that the relative populations of tightly-bound D, weakly-bound D, molecular HD and D_2 in microvoids and trapped on internal surfaces correlate with photovoltaic quality measured by the quantity $\eta\mu\tau$. It has also been found that intense irradiation produces DMR-detected changes in the populations of the above-named entities, which may be the first direct structural demonstration of the involvement of D (H) in photo-induced degradation of the photoresponse. On another front, our samples of a-Ge:H, produced at both the anode and the cathode, were examined by steady-state and transient

photomodulation spectroscopy. The spectra of the anode-deposited material were found to be dominated by transitions between dangling bond states and the conduction and valence bands. By contrast. the spectra of the cathode-deposited material required contributions from the band-tail states, indicating that the reduced defect density has resulted in pump beam-induced quasi-Fermi levels reaching near the conduction and valence band edges. These measurements thus confirm the analysis carried out earlier using more conventional optical techniques of sub-band-gap absorption, electron spin resonance and photoelectronic response. The ultrafast dynamics of photocarriers studied in femtosecond pump and probe experiments with 2 eV photons on our cathode-deposited a-Ge:H have also been reported.

Conclusions

The superior quality of a-Ge:H produced under PECVD conditions very different from those optimizing a-Si:H has been confirmed in many different types of experiment. The experimental conditions yielding this good material have been extensively explored and reported. Correlation between good photoelectronic quality and minimal microstructure has been consistently confirmed. Moreover, a self-consistent explanation of the structural, electrical and optical properties of the island and tissue phases has been devised. These studies have been extended to the examination of a-Si_xGe_{1-x} alloys of small x, corresponding to E_{04} band gaps of 1.4 eV and 1.6 eV. It has been found that environmentally-stable films with $\eta\mu\tau$'s almost as high as those for optimized a-Ge:H can be produced by suitable combinations of substrate temperature, GeH_4/SiH_4 flow ratio, r.f. power and H_2 dilution. The constitution of the plasma corresponding to different deposition parameters, and also corresponding to conditions giving our best films, has been examined by a residual gas analyzer. It has been found that the relative proportions of GeH_x, Ge_2H_x, SiH_x and Si_2H_x radicals vary greatly with change in deposition conditions and that better films emerge from plasmas with fewer higher radicals ($x > 1$). Our in-house studies have been supplemented by very useful collaborations on structural determination using DMR spectroscopy, on optical spectra using photothermal deflection spectroscopy, and on carrier dynamics using femtosecond pump and probe techniques.

References

1. W.A. Turner, D. Pang, A.E. Wetsel, S.J. Jones, J.H. Chen, and W. Paul, Optimization of the properties of undoped a-Ge:H, Proceedings of the Materials Research Society, **192**, 493 (1990).

2. D. Fournier, J.P. Roger, A.C. Boccara, M.L. Theye, L. Chahed, W.A. Turner and W. Paul, Subgap amorphous silicon photothermal deflection spectroscopy; spatial absorption localization, in ***Photoacoustic and Photothermal Phenomena II***, Springer Series in Optical Sciences (J.C. Murphy, J.W. Maclachlan-Spicer, L. Aamodt and B.S.H. Royce, eds.), **62**, 156 (1990).

3. L. Chahed, M.L. Theye, D. Fournier, J.P. Roger, A.C. Boccara, Y.M. Li, W.A. Turner and W. Paul, Surface effects in hydrogenated amorphous silicon studied by photothermal deflection experiments, ***Phys. Rev.*** **B43**, 14488 (1991).

4. A.E. Wetsel, S.J. Jones, W.A. Turner, D. Pang, W. Paul, I. El Zawawi, Y. Bouizem, L. Chahed, M.L. Theye, F.C. Marques, and I. Chambouleyron, Comparison of the properties of sputtered and glow discharge a-Ge:H, Proceedings of the Materials Research Society, **192** 547 (1990).

5. S.J. Jones, W.A. Turner, D. Pang and W. Paul, The effect of sample substrate on the structural properties of co-deposited films of a-Ge:H, Proceedings of the Materials Research Society, **192** 553 (1990).

6. W. Paul, S.J. Jones, and W.A. Turner, Studies on the structure of a-Ge:H using DSC, GE and TEM techniques, ***Phil. Mag.*** **B63**, 247–268 (1991).

7. S.J. Jones, W.A. Turner, D. Pang, and W. Paul, An electron microscopy study of the effects of deposition conditions on the growth of glow discharge prepared a-Ge:H films, Materials Research Society Symposium Proceedings ***Evolution of Thin Films and Surface Microstructure*** (C.V. Thompson, J.Y. Tsao and D.J. Srolovitz, eds.), **202** 43 (1991).

8. M. Wraback, J. Tauc, D. Pang, W. Paul, and Z. Vardeny, Femtosecond dynamics of photo-generated carriers in amorphous hydrogenated germanium, in ***Ultrafast Phenomena VII***, (C.B. Harris ***et al.***, eds.) 306 (Springer. Berlin 1990).

9. M. Wraback, J. Tauc, D. Pang, W. Paul, J.-K. Lee, and E.A. Schiff, Femtosecond studies of photoinduced bleaching and surface effects in a-Si:H and a-Ge:H, Proceedings of the 14th ICAS, Garmisch, Germany (1991), accepted for publication.

10. W.A. Turner, S.J. Jones, Y.M. Li, D. Pang, A.E. Wetsel, and W. Paul, Structural, optical and electrical studies of amorphous hydrogenated germanium, ***Solar Cells*** **30**, 245 (1991).

11. L. Chen, J. Tauc, D. Pang, W.A. Turner, and W. Paul, States in the gap of improved a-Ge:H studied by photomodulation spectroscopy. Proceedings of the Materials Research Society, **219**, 575 (1991).

12. Y.M. Li and W. Paul, Comments on the determination of defect density in a-Si:H alloys

by sub-bandgap optical absorption, Proceedings of the Materials Research Society, **219**, 587 (1991).

13. W. Paul, Influence of deposition conditions on the optical and electronic properties of a-Ge:H, Proceedings of the Materials Research Society, **219**, 211 (1991).

14. R.E. Norberg, P.A. Fedders. J. Bodart, R. Corey, Y.W. Kim, W. Paul, and W. Turner, Correlation of structure and structural changes with photovoltaic quality of a-Si:D,H and a-Ge:D,H films, Proceedings of the Materials Research Society, **219**, 223 (1991).

15. W. Paul, S.J. Jones, W.A. Turner, and P. Wickboldt, Structural properties of amorphous hydrogenated germanium, ***J. Non-Cryst. Solids*** (1992), accepted for publication.

16. P. Wickboldt, S.J. Jones, F. Marques, D. Pang, W.A. Turner, A.E. Wetsel, W. Paul, and J.H. Chen, A study of the properties of a-Ge:H produced by RF glow-discharge as the electrode gap is varied: the link between microstructure and optoelectronic properties, ***Phil. Mag.*** (1991), accepted for publication.

17. W. Paul, A review of the structural, optical and photoelectronic properties of improved PECVD a-Ge:H, Proceedings of the 14th ICAS, Garmisch, Germany (1991), accepted for publication.

18. P. Wickboldt, F. Marques, S.J. Jones, D. Pang, W.A. Turner, and W. Paul, Stress measurement of glow-discharge produced a-Ge:H thin films and its relation to electronic and structural properties, Proceedings of the 14th ICAS, Garmisch, Germany (1991), accepted for publication.

19. R.E. Norberg, P.A. Fedders, J. Bodart, and R. Corey, Connections between photovoltaic quality and the structure of deuterated amorphous Si and Ge films, Proceedings of the 14th ICAS, Garmisch, Germany (1991), accepted for publication.

20. C. Lee, W.A. Turner, and W. Paul, True position of dangling bonds in the gap of undoped hydrogenated amorphous silicon, Proceedings of the 14th ICAS, Garmisch, Germany (1991), accepted for publication.

Title: **Stable, High Efficiency Amorphous Silicon Solar Cells with Low Hydrogen Content**

Organization: **Institute of Energy Conversion**
University of Delaware
Newark, De 19716-3820

Contributors: **B.N. Baron, project director;**
C.M. Fortmann, principal investigator;
S.S. Hegedus, principal investigator

Objectives

The current project is phase I of research on the development of amorphous silicon based solar cells that have a stabilized efficiency greater than 12%. The present objectives are to develop the most stable materials, understand the nature of the Staebler-Wronski effect in a-Si:H and the transport phenomena in the Si-Ge alloy system. Results from those studies will provide the later phases of this project with the materials and design parameters necessary to develop solar cells with greater stabilized efficiency.

Technical Approaches

Theoretical studies of multi-junction a-Si:H solar cells project efficiencies greater than 20%. This project addresses the material limitations and device design considerations that until now have limited demonstrated stabilized efficiencies to values less than 10%. Clearly multi-junction solar cells offer the greatest potential for increased solar cell performance with acceptable long term stability. Research indicates that multi-junction solar cell stability is apparently controlled by the stability of the middle solar cell which is typically made relatively thick to absorb a sufficient quantity of the solar spectrum. On the other hand the alloy back solar cell limits the performance of the annealed multi-junction solar cell and would also limit the performance of the degraded cells should more stable second cells be prepared. Low hydrogen materials address the performance and stability of multi-junction amorphous silicon based solar cells. Previously (1) we have reported that reduced hydrogen content improved the electronic transport properties of the silicon-germanium alloys while increased hydrogen content clearly reduces the stability of a-Si:H. Reduced hydrogen content may improve the stability of a-Si:H materials (this topic is currently being explored at the Institute of Energy Conversion under EPRI funding). Even if low hydrogen materials do not have increased stability the low hydrogen materials offer a means by which the middle solar cell could be made more stable. Reducing the hydrogen content (or perhaps just the di-hydride content) results in smaller band gaps permitting the use of thinner i-layers in the critical middle cell. These thinner i-layers enhance solar cell stability. Ultimately these elements of research will be combined to demonstrate amorphous silicon-based solar cells with greater stabilized efficiency.

Significant Results

Task 1 - Stabilized a-Si:H Materials and Devices

In Phase I research we attempted to prepare films and devices grown by new

deposition conditions thought to reduce the hydrogen content of the a-Si:H. These experiments employed our photo-CVD reactor using techniques which do not require high substrate temperatures (to be more compatible with solar cell processing). For example, light attenuation and helium dilution were used to reduce the possibility of gas phase polymerization which could be one of several sources of excess film hydrogen. Unfortunately the films grown by these new techniques tend to peel and flake from most substrates. These films peeled from glass and single crystal silicon substrates making standard photo conductivity and IR analysis impossible.

Since the preparation and testing of low hydrogen materials is integral to our research project, alternate tests and substrates were developed. Both of these problems were addressed during this part of our project. SnO_2 coated glass substrates did not produce the flaking problem found on the glass substrates. Therefore, we shifted our primary analysis away from film based measurements to device based measurements.

Previously we have published a number of papers on the use of device analysis for material and stability characterization (2,3). During Phase I these techniques were reviewed. The sub-band gap primary photo current technique was found to be flawed. Solar cells of similar thickness made with different hydrogen contents (7 and 11%) produced different degradation behavior (1,4). However, the primary photo currents increased with increasing light exposure at the same rate in both cells. Thus, the PPC signal during degradation did not depend on i-layer hydrogen content in contrast to cell results. Also the primary photo current is not a function of i-layer thickness suggesting PPC is not sensitive to bulk defects. These considerations were discussed in detail elsewhere (4).

The change in the short wavelength quantum efficiency (ΔSWQE) was also reviewed and no apparent inconsistencies were found. For example, ΔSWQE tracked with the relative solar cell conversion efficiency. More recently in a collaboration with Diego Fischer at IEC (visiting scholar on leave from the University of Neuchatel), we examined ΔSWQE by numerical techniques. The preliminary results of the numerical modeling agree (see Figure 1) with those of the earlier analytical investigation (3). The ΔSWQE scales with the bulk recombination which in turn is proportional (to first order) with the defect density. Unless the interface recombination velocity scales directly with solar cell thickness (very unlikely), ΔSWQE yields a reasonable measurement of the bulk density of Staebler-Wronski defects. The numerical modeling of p-i-n solar cells predicts the ΔSWQE vs i-layer thickness and bulk densities of S-W defects shown in Figure 1. The same results can be applied to Schottky barrier devices, however, a different interface recombination velocity is required.

The conductive SnO_2 substrates precluded transverse photo-conductivity measurement, however it was possible to use the SnO_2 as a back contact when Schottky barriers were formed by Ni deposition on the front surface. ΔSWQE was used as a measure of relative stability of these Schottky barriers.

During this portion of Phase 1 research, several methods of reducing hydrogen content (C_H) were attempted; two interrupted growth schemes and the light attenuation method. The first interrupted growth scheme involved a short

deposition cycle of 1 minute (~20-40Å growth) followed by exposure to excited mercury alone for 5 minutes (#3497) or 2 minutes (#3496). It was hoped that a surface collision by an excited mercury could abstract a surface hydrogen atom, thereby reducing the hydrogen content. In the second interrupted growth scheme, hydrogen radical etch cycles were used to attempt to abstract surface hydrogen (sample #3505). Finally, in a non-interrupted growth scheme light attenuation, low reactor pressure, and high helium dilution were used to lessen the density of gas phase silane radicals, thereby reducing the hydrogen that incorporates through $(SiH_2)_n$ molecules (sample #3482, 3492, 3494). Deposition conditions of select samples are shown in Table 1.

In a collaborative effort with C.R. Wronski at Penn State University Ni Schottky barrier devices were formed on our materials deposited under a range of conditions expected to have lower hydrogen content. Co-deposited samples were sent to Charles Evans East for determination of hydrogen content. The results of this study are shown in Table 2. Several of the results are encouraging. The photo-CVD materials appear to have hydrogen contents lower than the standard provided to us from Solarex. Also, the impurity contents are comparable to the industrial standard. However, our attempts to lower the hydrogen content by light attenuation, Hg annealing and H etching seem to have failed with the possible exception of sample 3492 (light attenuation) for which the SIMS measurement indicates a low hydrogen content (this value is consistent with a concentration of ~2-3 %). Previously IR measurements indicated that the hydrogen content of the light attenuated samples to be 5 to 6%. However, sample 3494 grown under similar conditions to 3492 had a larger hydrogen concentration. There are several possible explanations for this including an unintentional rise in chamber pressure during the deposition of 3494. Also, the accuracy of the SIMS technique could be questioned. More samples will be grown to answer these questions. We have begun efforts to drastically reduce hydrogen content by using higher deposition temperatures.

The relative stability of the Schottky barrier devices can be inferred from ΔSWQE (see Table 3). Based on the experience of the Penn State group it appears that both 3492 and 3497 have better stability than standard materials even though our reference device (3491) appears to exhibit similar stability. The apparent stability of the standard material is related to the ΔSWQE sensitivity to sample thickness (for example, see Figure 1), as this standard sample turned out to be thinner than expected. The i-layer of 3492 employed light attenuation, low pressure, and He dilution to reduce the possibility of gas phase polymerization (as discussed above). Mercury annealing was used in #3497. The sample prepared with alternating deposition and hydrogen etch cycles (#3505) was too thin (~2000Å) for stability analysis.

Several manuscripts were prepared describing a thermodynamic treatment of dangling bond defect formation at high temperatures (T>150°C) (for example, reference 5). These works describe the method and results leading to the establishment of the enthalpy and entropy of dangling bond formation. Results from this model will permit us to establish the maximum number of dangling bonds that would result from a given light flux. These values would then be used as inputs to our modelling efforts aimed at designing solar cells with improved end-of-life efficiency.

Task 2 - a-SiGe:H Materials and Devices

As in Task 1 our efforts during this phase of the project focused on materials and characterization on which future devices will be based. In a collaboration with J.David Cohen at the University of Oregon a-SiGe:H materials were investigated using charge release techniques (see reference 6 for details). Thus far we have found that the Urbach energy for our alloy with a band gap of ~1.3 eV grown by photo-CVD is similar to that of high quality a-Si:H (~50 meV). The deep defect density of states was found to be ~$2x10^{16}cm^{-3}$ (amongst the very lowest reported for an alloy of such a low band gap) and $8x10^{15}cm^{-3}$ for an alloy with a band gap of ~1.45 eV. The value of the hole $\mu\tau$ is relatively large compared to that of the electron ($\mu\tau_e$~3 $\mu\tau_n$) as previously found by solar cell analysis (2). While low number are encouraging, we believe the real value of these number are as inputs to the detailed models that we will use to guide device design.

In a collaborative effort with P.M. Fauchet at the University of Rochester the picosecond carrier dynamics of the alloys prepared by photo-CVD have been investigated (7). Interestingly it was found that the electron thermalizes with approximately the same time constant as electrons in high quality a-Si:H. It is of considerable interest to solar cell design that the electron could be collected prior to thermalization in thin solar cells. Our detailed modelling of a-SiGe:H solar cells will take this into account.

Recently we have prepared a front loaded a-SiGe:H solar cells using designs previously shown to yield good performance. A 400Å thick a-SiGe:H layer was used in an i-layer which had a total thickness of 1000 Å. Non-ideal abrupt transitions were used between the a-Si:H regions (150 Å p/i interface buffer and the back 450 Å of the i-layer) and the a-SiGe:H i-layer regions. Even with these abrupt transitions the performance of this solar cell (#3520.11-1) was good with an efficiency of 5.96% (V_{oc}=0.605V, J_{sc}=16.85 mA/cm^2, fill factor=58.54 QE_{800nm}=25%).

Conclusions

In conclusion there is some indication that C_H can be reduced without an increase in deposition substrate temperature. However, it appears necessary to pursue higher substrate temperatures to guarantee markedly lower C_H values. Lower C_H materials are necessary for the middle solar cell of a multijunction device where the smaller band gap would permit the use of a thinner i-layer for enhanced stability. Material characterization and theoretical modeling of defect formation carried out during this stage of research is expected to provide the input parameters necessary for the development (through solar cell modeling and experimentation) of amorphous silicon-based solar cells with improved end-of-life performance.

References

1. C.M. Fortmann, S.S. Hegedus, T.X. Zhou, and B.N. Baron, Solar Cells 30(1-4), 255 (1991).
2. C.M. Fortmann, S.S. Hegedus, and W.A. Buchanan, Journal of Non-Crystalline Solids 115, 21 (1989).

3. C.M. Fortmann, S. Lange, M. Hicks and C.R. Wronski, J. Appl. Phys. 64(8), 4219 (1988).
4. T.X. Zhou, S.S. Hegedus, and C.M. Fortmann, Mat. Res. Soc. Proc. 219, 415, (1991) Materials Research Society, Pittsburgh, PA.
5. C.M. Fortmann, R.M. Dawson, and C.R. Wronski, Mat. Res. Soc. Proc., 219, 63, (1991) Materials Research Society, Pittsburgh, PA.
6. T. Unold, J. D. Cohen, and C.M. Fortmann, presented at the International Conference on Amorphous Semiconductors 14, Garmisch-Partenkirchen, August 1991.
7. P.M. Fauchet, D.A. Young, W.L. Nighan Jr., and C.M. Fortmann, IEEE Journal of Quantum Electronics 27(12), 2714, December 1991.

Table 1 - Growth Conditions

Sample No.	Gas Flow	Time min	Cycles	T °C	P torr	SiH	He (SCCM)	H_2	d (μm)
3497	(growth)	1	51	205	5	2.0	8.0	0	0.37
	(anneal)	5	51	205	5	0	8.0	0	
3496	(growth)	1	78	205	5	2.0	8.0	0	0.55
	(anneal)	2	78	205	5	0	8.0	0	
3492	(growth)	375	1	230	1	2.8	2.8	0	0.60
3491*		335	1	205	5	2.0	8.0	0	0.37
3505	(growth)	1	20	230	2	2.2	0	20	0.2
	(etch)	0.5	20	230	0.5	0	0	20	

* This is our standard amorphous silicon recipe from which solar cells with 10% efficiency have been prepared.

Table 2 - Charles Evans East SIMS Determined H, C and O Concentrations

Sample No.	Comments	C_H	C_O $*10^{21}cm^{-3}$	C_C
3482	Light atten.*	3	0.03	0.015
3491	standard	2.5	0.03	0.005
3492	light atten.	1.0	0.009	0.007
3493	standard	2.6	0.017	0.005
3494	light atten.**	2.2	0.02	0.005
3496	2 min. Hg anneal	3.0	0.02	0.005
3497	5 min. Hg anneal	3.0	0.05	0.010
3505	H anneal	3.0-2	0.2-3	0.05
PB55	glow discharge***	4.0	0.009	0.01

* possible contamination from substrate cleaning process as C and O concentrations are higher near the substrate more O & C at back
** possible increase in H concentration due to an unintentional pressure rise during deposition
*** supplied by Solarex

Table 3

ΔSWQE of Samples as a Function of Deposition Technique

Sample	Dep. cond.	T_{dep} (°C)	QE_{450nm} (annealed)	(degraded 64 hrs. AM1.5)
3497	Hg anneal	205	0.4	0.35
3496	Hg anneal	205	0.55	0.38
3492	72%light	225	0.46	0.39
3491	standard	205	0.34	0.3
3505	H anneal	230		

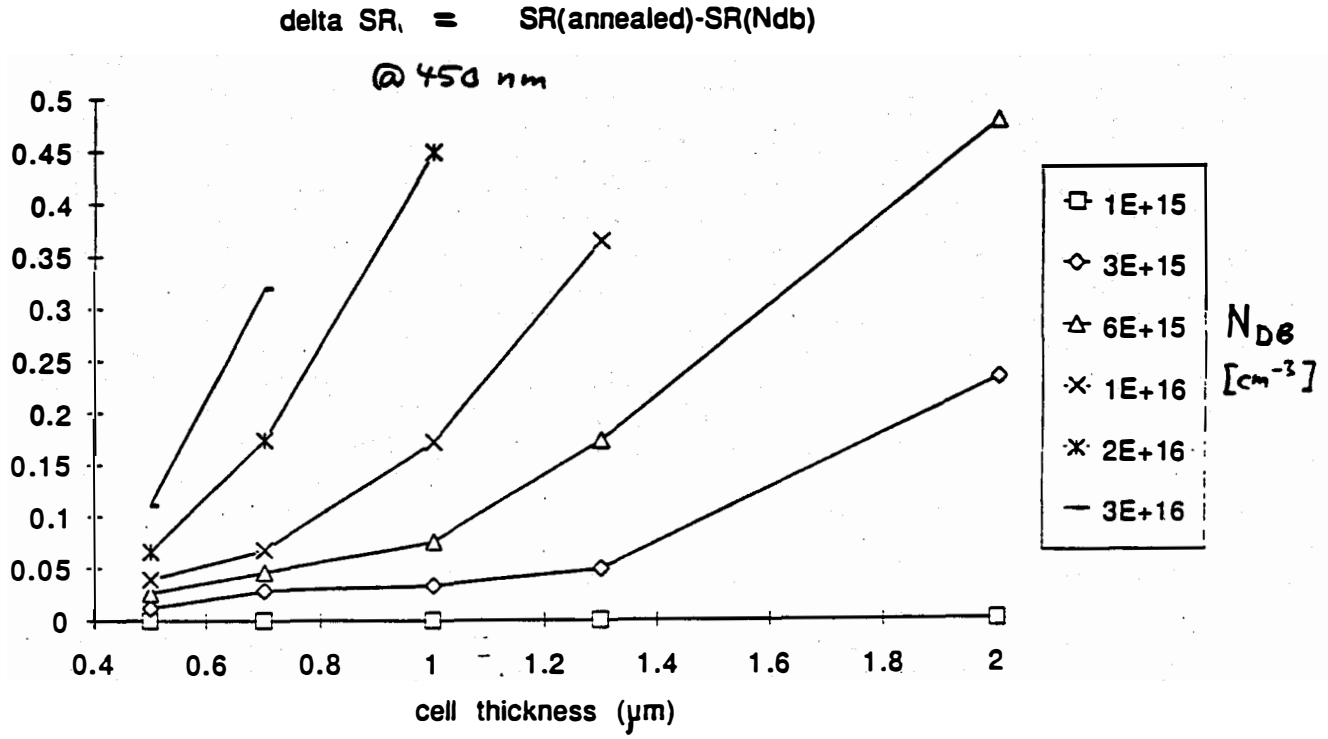

Figure 1 The ΔSWQE of a p-i-n solar cell vs i-layer thickness and dangling bond concentration

Title:	**Electron Cyclotron Resonance Deposition of Amorphous Silicon Alloy Films and Devices**
Organization:	Jet Propulsion Laboratory, California Institute of Technology, Pasadena, California
Contributors:	Y. H. Shing, Principal Investigator; F. S. Pool and J. M. Essick (Occidental College)

Objective

The objective of this research task is to obtain an understanding of amorphous silicon and amorphous silicon-germanium film deposition processes using electron cyclotron resonance (ECR) microwave plasmas, leading to improved optoelectronic film properties and resulting in improved stabilized device performance.

Approach

ECR microwave plasma deposition processes for a-Si:H, μc-Si:H, a-SiGe:H and μc-SiGe:H films will be developed using the JPL state-of-the-art ECR plasma enhanced chemical vapor deposition system[1]. Thin film material characterization, photovoltaic device performance and plasma diagnostics will be used to establish correlations between ECR deposition conditions and the resultant film properties and device performance. Material properties of ECR-deposited films will be characterized using light and dark conductivities, photodegradation studies, dark activation energy, hydrogen content, scanning electron microscopy and Raman spectroscopy. Additional measurements, such as minority carrier diffusion length, small-angle x-ray scattering, secondary ion mass spectroscopy, junction capacitance and constant photocurrent method, will be obtained through collaborative research. The gas phase species of ECR plasmas will be analyzed by appropriate plasma diagnostic techniques, such as mass spectrometry, Langmuir probe measurements, optical emission spectroscopy, and laser induced fluorescence. Diagnostic solar cells incorporating ECR-deposited films will be fabricated. Current-voltage characteristics will be studied on diagnostic p-i-n solar cells to evaluate the stability of ECR-deposited films.

ECR-Deposited a-Si:H Films Using Hydrogen Plasma Gas

The optimization of the ECR deposition process for photosensitive a-Si:H films has been systematically investigated in the parameter space of substrate temperature and mirror magnetic field profile. The material properties of ECR-deposited, photosensitive a-Si:H films have been characterized using constant photocurrent method (CPM) and junction capacitance measurements[2-3]. The total integrated density of filled deep defect states was obtained through drive-level-capacitance profiling. The Fermi level position was acquired from the complex AC admittance as a function of temperature. The substrate temperature dependent effect on material properties of ECR-deposited, photosensitive a-Si:H films was investigated in the temperature range of 100 to 300°C. The ECR plasmas were generated under identical conditions for all depositions using microwave power of 300 W and deposition pressure of 4 mTorr. Figure 1 shows the integrated density of filled deep defects as a function of substrate temperature. As can be seen, depositions from ECR plasmas at substrate temperature of 175-300°C resulted in high-quality a-Si:H films with $1\text{-}2\times10^{16}$ cm^{-3} deep defects. In

comparing the temperature dependence of the defect density for ECR-deposited a-Si:H to identical studies for RF-deposited a-Si:H, both systems are found to follow very much the same behavior.

The energy of ions in the plasma stream extracted from the ECR plasma chamber into the deposition chamber is dependent on the magnetic field profile. A systematic variation of the magnetic field profile can provide an additional control of the film quality in the ECR deposition process. The ion density of ECR microwave plasmas has been analyzed by using Langmuir probe measurements. The correlation between the defect density and the ion current as a function of the mirror magnetic field is shown in Figure 2 under the deposition pressure of 0.7 mTorr. The direct correlation shown in Figure 2 is consistent with the plasma etching or sputtering at low pressures, caused by high-energy ions which can also generate defects resulting in an increase of the defect density. An anti-correlation between the defect density and the ion density has been observed at low mirror magnetic fields under the deposition pressure of 5 mTorr. This anti-correlation indicates that there is a threshold in the ion density and the ion energy for producing an optimized defect density. The correlation studies on the defect density and ion density show that the ECR deposition process can be sensitively controlled by varying the ion density and energy.

The integrated defect density has also been determined for the initial and the light-soaked states. The light soaking was performed under concentrated AM 1.5 simulated solar illumination with a concentration ratio of 10 at 50 degrees C for 12 hours, which is equivalent to one sun, AM 1.5 illumination time of about 750 hours. The defect density of the light-soaked state is increased by a factor of about 3 to 3.5 as compared to the initial defect density. This factor of increase in the light-soaked defect density for ECR-deposited a-Si:H films is similar to that of RF-deposited, device-quality a-Si:H films.

Diagnostic Solar Cells to Evaluate ECR-Deposited Films

Diagnostic p-i-n a-Si:H solar cells have been fabricated by using ECR- and RF-deposited films[4]. The RF-deposited films are used as standard components to form the p-i-n device structure. For evaluating the ECR-deposited p-type a-SiC:H window layer, the RF-deposited i and n layers are employed to complete the solar cell structure. Likewise, the ECR-deposited intrinsic a-Si:H films are evaluated by forming the p-i-n diagnostic device using RF-deposited p and n layers. Owing to the transfer of samples between the ECR and RF deposition systems, the interface between p and i layers is exposed to air in the fabrication of diagnostic solar cells involving an ECR-deposited p-layer. The interfaces between p and i and between i and n layers are exposed to air in the fabrication of p-i-n devices containing an ECR-deposited i-layer. Air exposure of the interfaces in the fabrication of diagnostic solar cells is a major uncontrolled factor in comparing the performance between the diagnostic and the standard RF-deposited p-i-n solar cells. Table I lists the fabrication conditions and performances of diagnostic solar cells containing ECR-deposited p-type and intrinsic layers. Diagnostic solar cells incorporating an ECR-deposited p-type a-SiC:H window layer have shown an efficiency of 5.9%. Air exposure of the p/i interface in these diagnostic solar cells is probably the major cause of the reduction of the short-circuit current (Isc) from the standard 14.7 to 12.9 mA/cm^2. Diagnostic solar cells incorporating an ECR-deposited intrinsic a-Si:H layer have also been fabricated and have shown an efficiency of 2.9%. The I_{sc} and the fill factor (F.F.) of these diagnostic solar cells have shown a severe

degradation to the values of 7.45 mA/cm^2 and 46.4%, respectively. This severe degradation is most likely caused by the air exposure of both the p/i and i/n interfaces. The air exposure of the interfaces can be eliminated by a vacuum substrate transport system. The fabrication and the performance of these diagnostic solar cells are being improved by integrating the ECR and RF deposition processes to avoid interfacial air exposure.

TABLE I

Characteristics of Diagnostic Solar Cells Containing ECR-Deposited Layers

CELL AREA (cm^2)	SUBSTRATE	DEPOSITION METHOD p	i	n	INTERFACIAL CONDITION p/i	i/n	V_{oc} (mV)	I_{sc} (mA/cm^2)	F.F.	EFFICIENCY (%)
0.126	Textured SnO_2	ECR	RF	RF	Air	Vacuum	759	12.9	60.2	5.88
0.1	Specular SnO_2	ECR	RF	RF	Air	Vacuum	745	11.9	60.9	5.38
0.126	Textured SnO_2	RF	ECR	RF	Air	Air	841	7.45	46.6	2.92
0.1	Textured SnO_2	RF	ECR	RF	Air	Air	871	7.10	38.4	2.38
0.1	Textured SnO_2	RF	RF	RF	Vacuum	Vacuum	869	14.7	60.4	7.69
0.1	Specular SnO_2	RF	RF	RF	Vacuum	Vacuum	875	13.0	64.0	7.26

ECR-Deposited a-Si(Xe,H) Films Using Xenon Plasma Gas

Highly photosensitive a-Si(Xe,H) films with an improved stability have been produced by ECR plasmas using xenon (Xe) as a plasma gas [4]. The use of Xe plasma gas is an innovative approach for realizing the beneficial effect of low-energy ion bombardment in the ECR deposition process. The heavy mass of Xe produces a significant increase in the momentum of low-energy bombarding ions. ECR depositions of a-Si:H films were performed using pure Xe and mixed Xe/H_2 plasma gases and SiH_4 source gas. Figure 3 shows a typical infrared spectrum of a-Si(Xe,H) films deposited by ECR plasmas containing Xe. It is interesting to note that the silicon-hydrogen stretching and bending modes were not observed in the infrared spectrum of a-Si(Xe,H) films. The infrared detection limit for hydrogen bonded to silicon in a-Si:H films is known to be about 3% for a film with a thickness of 1 μm. These infrared spectral features indicate that a-Si(Xe,H) films are a new type of amorphous silicon material in which the content of hydrogen bonded to silicon is lower than the detection limit of the infrared spectroscopy.

Light and dark conductivity measurements of Xe plasma deposited a-Si(Xe,H) films show two kinds of behavior. One kind has a high photoconductivity of 5×10^{-5} $(\Omega\text{-cm})^{-1}$ and a high photosensitivity of 10^6; another kind has a high photoconductivity of 10^{-5}-$10^{-4}(\Omega\text{-cm})^{-1}$ and a moderate photosensitivity of 10^4. These two kinds of a-Si(Xe,H) films were deposited by varying the ECR microwave plasma modes using different mirror magnetic field profiles. Light soaking experiments on a-Si(Xe,H) films have been performed using concentrated AM 1.5 simulated solar illumination with a concentration ratio of about 7. We have shown that the equivalent, one sun, AM 1.5 illumination time of 80-100 hours is adequate for light soaking these films to reach a quasi stabilized state for conductivity measurements. Figure 4 shows light and dark conductivities of a-Si(Xe,H) films and a conventional RF-deposited a-Si:H film as a function of the illumination time. The light and dark conductivity of a-Si(Xe,H) films with a high photosensitivity of 10^6 have shown an improved photodegradation rate of

about 35% less than that of RF-deposited a-Si:H films. The light conductivity of a-Si(Xe,H) films with a moderate photosensitivity of 10^4 has shown photodegradation and self-recovery effects. However, the dark conductivity of these films tends to increase after light soaking and hence, the photosensitivity degrades. The self-recovery effect in the light conductivity of a-Si(Xe,H) films with a moderate photosensitivity can apparently maintain their light conductivities at relatively stable values. The material properties of ECR-deposited a-Si(Xe,H), a-Si:H and RF-deposited a-Si:H films are summarized in Table II to show that they have comparable material qualities suitable for photovoltaic device applications. However, there is a significant improvement in photodegradation for ECR-deposited a-Si(Xe,H) films, as shown by the initial-to-degraded light conductivity ratio. In addition, the low, stable dark conductivity of 10^{-11} $(\Omega\text{-cm})^{-1}$ for a-Si(Xe,H) films with a high photosensitivity of 10^6 is another indication of improved stability for device-quality materials.

TABLE II

Material Properties of ECR-Deposited a-Si(Xe,H), a-Si:H and RF-Deposited a-Si:H Films

	ECR-Deposited a-Si(Xe,H)	ECR-Deposited a-Si:H	RF-Deposited a-Si:H
Initial Light Conductivity at 100 mW/cm^2 after 10 min. illumination: σ_L(10 min) $(\Omega\text{-cm})^{-1}$	2.9×10^{-5}	4.8×10^{-5}	6.0×10^{-5}
Degraded Light conductivity at 100 mW/cm^2 after 80 hours illumination: σ_L(80 hrs) $(\Omega\text{-cm})^{-1}$	1.1×10^{-5}	1.5×10^{-5}	1.4×10^{-5}
Dark Conductivity: σ_D $(\Omega\text{-cm})^{-1}$	1.2×10^{-11}	3.5×10^{-10}	1.2×10^{-10}
Initial Light-to Dark Ratio: σ_L(10 min)/σ_D	2.4×10^6	1.4×10^5	5.0×10^5
Initial-to-Degraded Light Conductivity Ratio: σ_L (10 min)/σ_L (80 hrs)	2.6	3.2	4.3
Urbach Slope: (meV)	48	50-60	55
Optical Gap: (eV)	1.72	1.80	1.73

The lack of infrared detected silicon-hydrogen bonding in a-Si(Xe,H) films is a quite intriguing result. The photo-degradation of light and dark conductivities of a-Si(Xe,H) films has shown promising results to achieve improved stability in these films. ECR plasmas containing Xe certainly offer a new approach for modifying the material properties of a-Si:H films and for achieving stable photovoltaic device performance. The integration of ECR-deposited a-Si(Xe,H) films into diagnostic p-i-n solar cells is being pursued for demonstrating the device applications.

Conclusions and Future Plans

Device-quality a-Si:H films have been deposited using ECR plasmas of SiH_4 and H_2 gas mixtures. The ECR deposition process has a complex, interacting deposition

parameter space, and is sensitive to the microwave mode variations. The ion density and energy in the ECR plasma can be controlled by the mirror magnetic profile. The device evaluations of these films are performed by fabricating diagnostic p-i-n solar cells incorporating ECR- and RF-deposited a-Si:H and a-SiC:H films. Initial results show that the air exposure of the interfaces in the diagnostic solar cells has degraded its performance. Xenon has been employed as an ECR plasma gas to deposit a new type of a-Si(Xe,H) film in which hydrogen-silicon bonds have not been detected by infrared spectroscopy. However, Xe plasma deposited a-Si(Xe,H) films have shown high photoconductivity of 10^{-5} to 10^{-4} $(\Omega\text{-cm})^{-1}$ and improved stability which are promising material properties for solar cell applications.

In our future research, the performance of diagnostic solar cells will be improved by eliminating the air exposure of the interfaces. The stability of ECR-deposited a-Si:H and a-Si(Xe,H) films will be systematically evaluated using the diagnostic solar cells. The improved stability in material properties and device performance will be demonstrated using accelerated light-soaking under concentrated, simulated solar illumination. The low-energy ion bombardment effect in the ECR deposition process will be further optimized by applying RF bias to the substrate. The ECR deposition of a-SiGe:H alloy films will be developed to achieve stable, low-bandgap materials for tandem solar cell applications.

Reference

1. Y.H. Shing and F.S. Pool, Solar Cells, 30, 391 (1991).
2. J.M. Essick, F.S. Pool, Y.H. Shing and M.J. Holboke, Mat. Res. Soc. Symp. Proc., 219, 679 (1991).
3. J.M. Essick, F.S. Pool and Y.H. Shing, J. Vac. Sci. Technol. (submitted).
4. Y.H. Shing, F.S. Pool and J.M. Essick, 22nd IEEE PVSC (1991) (in press).

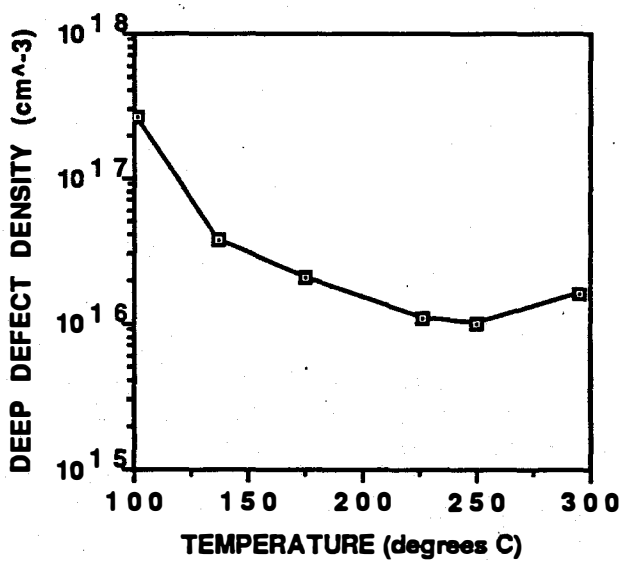

Figure 1. Integrated defect density of ECR- deposited a-Si:H films as a function of substrate temperature.

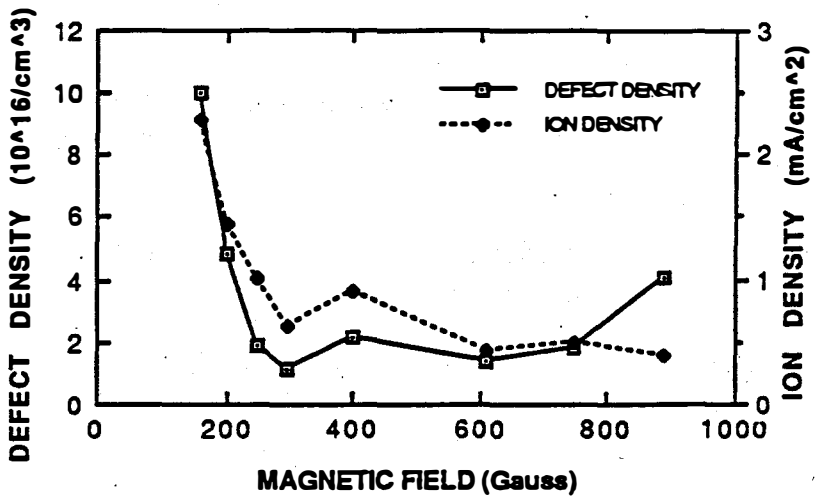

Figure 2. Defect density and ion density as a function of mirror magnetic field for ECR deposition under 0.7 mTorr pressure.

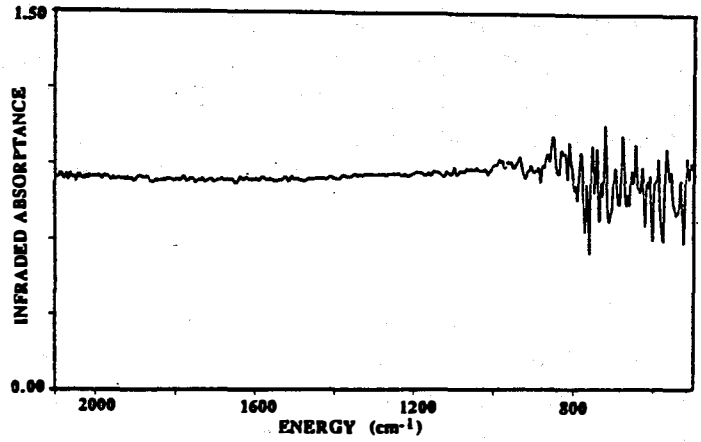

Figure 3. Typical infrared spectrum of ECR-deposited a-Si(Xe,H) films.

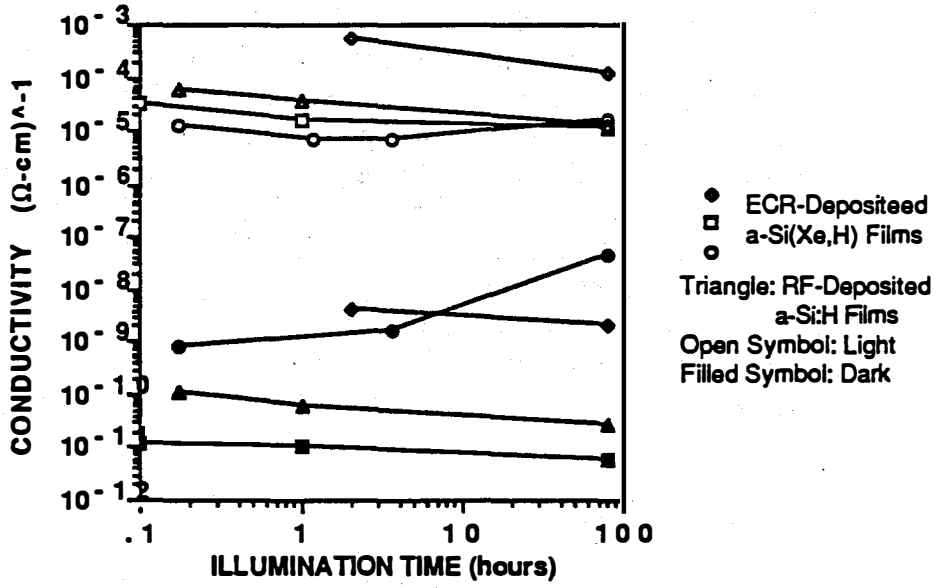

Figure 4. Light and dark conductivities of a-Si(Xe,H) films as a function of AM 1.5, 100 mW/cm^2 illumination time.

Title:	**Growth Mechanisms and Characterization of Hydrogenated Amorphous Silicon Alloy Films**
Organization:	National Institute of Standards and Technology (NIST) Boulder, Colorado
Contributors:	A. Gallagher, R. Ostrom, G. Stutsin

Objective

The overall objective of this work is to explain causes of glow-discharge produced a-Si:H, a-Ge:H and a-Si:Ge:H film quality, and its dependence on deposition discharge conditions. A secondary objective is to establish a definitive, in situ diagnostic of film quality that could be used to efficiently optimize process parameters in photovoltaic production systems. The approach taken is to measure the morphology and chemical characteristics of the as-grown film surface with atomic scale resolution using a scanning tunneling microscope (STM). Many of the limitations of a-Si:H based photovoltaics are attributed to micro voids, boundary defects, and microparticulate incorporation, and all of these should be visible to the STM.

Technical Approach

We expect the initial atomic-scale morphology of C, Si, Ge and H deposition from a glow discharge into a-Si:H and alloy films to depend strongly on the atomic-scale roughness and chemical composition of the substrate. To minimize the effect of such uncontrolled parameters in our initial studies, and to optimize the connection to a large body of surface-science knowledge, we are initially studying a-Si:H and alloy film deposition onto oriented atomically smooth and clean surfaces of crystal Si and GaAs. This requires ultra high vacuum (UHV) operation of the STM and other surface diagnostic equipment, and exacting sample preparation. The film deposition is done in an attached, turbomolecular pumped chamber and film-coated substrates are transferred through a gate valve into the UHV chamber after termination of the glow discharge and deposition-gas flows. This pump down, sample cooling and sample transfer into the STM typically requires ~ 15 minutes, during which time the sample is exposed briefly to $\sim 10^{-8}$ and thereafter to $< 10^{-10}$ Torr of impurities (primarily CO and CH_4) in the two chambers. Due to the well known, exceptionally low surface reactivity of A-Si:H films and this very low impurity pressure this is not expected to significantly alter the as-deposited film. Due to the high dark resistivity of high-quality a-Si:H films, films thicker than ~ 300 Å are generally illuminated during STM scanning to control voltage drop in the film. Repeated and varied depositions on a single sample can easily be studied in this experimental arrangement, without exposure to air.

Morphology of a-Si:H film surfaces.

We have so far studied intrinsic a-Si:H film growth or crystal Si and GaAs, concentrating on atomic-scale irregularities and smoothness of the initial film growth. The film is deposited at T_s = 25 or 230°C on the grounded electrode of a rf silane discharge. The electrodes are 5 cm

square with 2 cm gap, placed in a 5.5 cm diameter stainless steel tube. The gas flow is 10-20 sccm and the entire tube and electrodes are heated. The silane pressure, at 230°C, is typically 0.4 Torr and the film deposition rate on the substrate is 1-3 Å/s. No particulates are visible on electrode or downstream surfaces for these conditions, but they do appear at the throttle valve when the power/flow is increased a factor of ~5.

The atomic-scale morphology of the surface of a 100 Å layer of a-Si:H film on an atomically flat Si (111) crystal is shown in Figs. 1-4 for T_s = 25°C. Figures 1-3 are typical of many different regions of the surface that were scanned with similar resolution. In essence, most 100 Å square regions of the surface are flat within one atomic layer (3 Å), but occasional protrusions or troughs of several Å height are seen, as in Fig. 3. The larger-scale topology contains gradual undulations, as seen in Fig. 1. There is no indication of incipient voids as might have been expected on the basis of reports of voids measured in bulk films. Also, although a limited number of ~1,000 Å square surface regions have been studied so far, no micro or nano particulates have been observed on this as-grown surface. Very occasionally, a severe flaw in the surface flatness is detected, but is attributed to a flaw in the crystal Si surface polish which propagates into the film structure. Surface flaws are very dense on most substrates, and this implies that these may propagate considerable distances into the film, in addition to introducing many surface states.

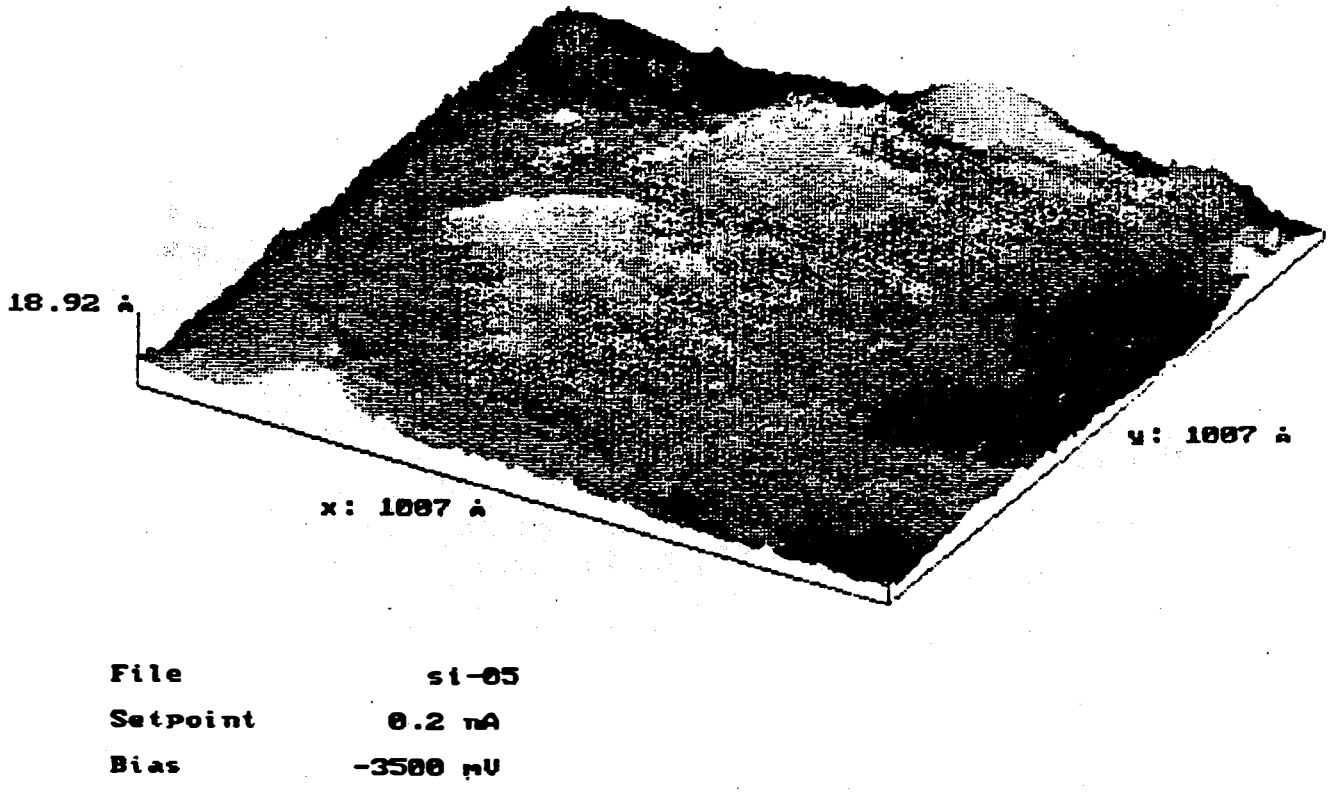

Fig. 1. STM image of a 100 Å thick, T_s=20°C, a-Si:H film deposited on a Si(111) crystal surface.

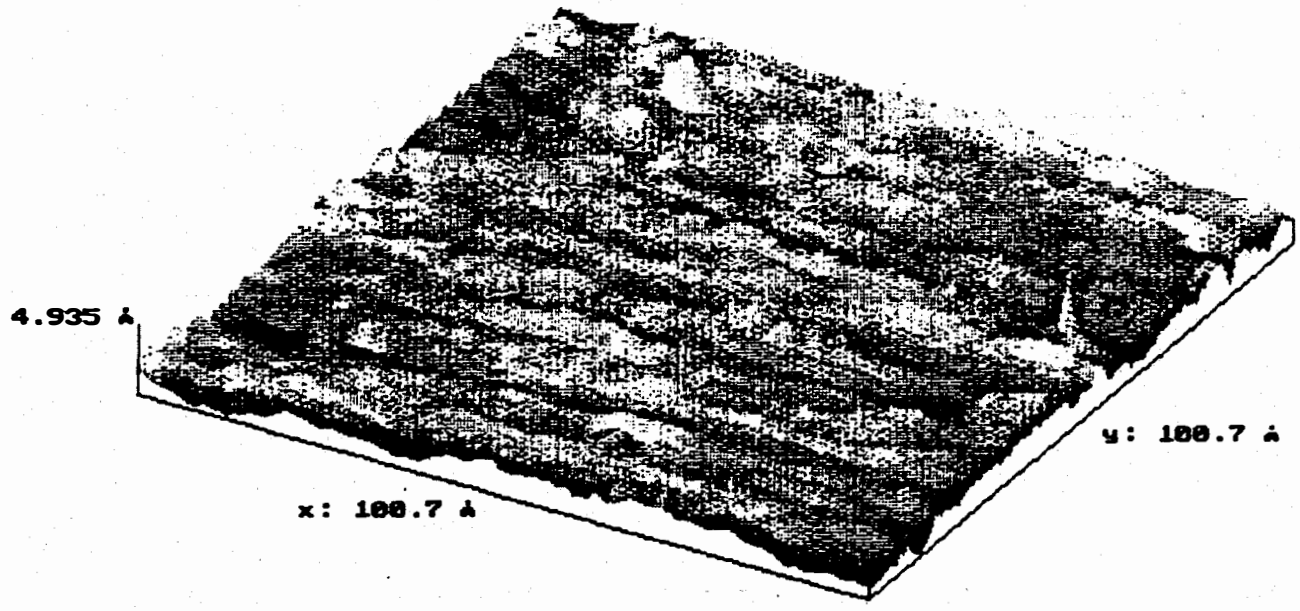

File si-06
Setpoint 0.2 nA
Bias -3500 mV

Fig. 2. STM image of a different region of the a-Si:H film in Fig. 1.

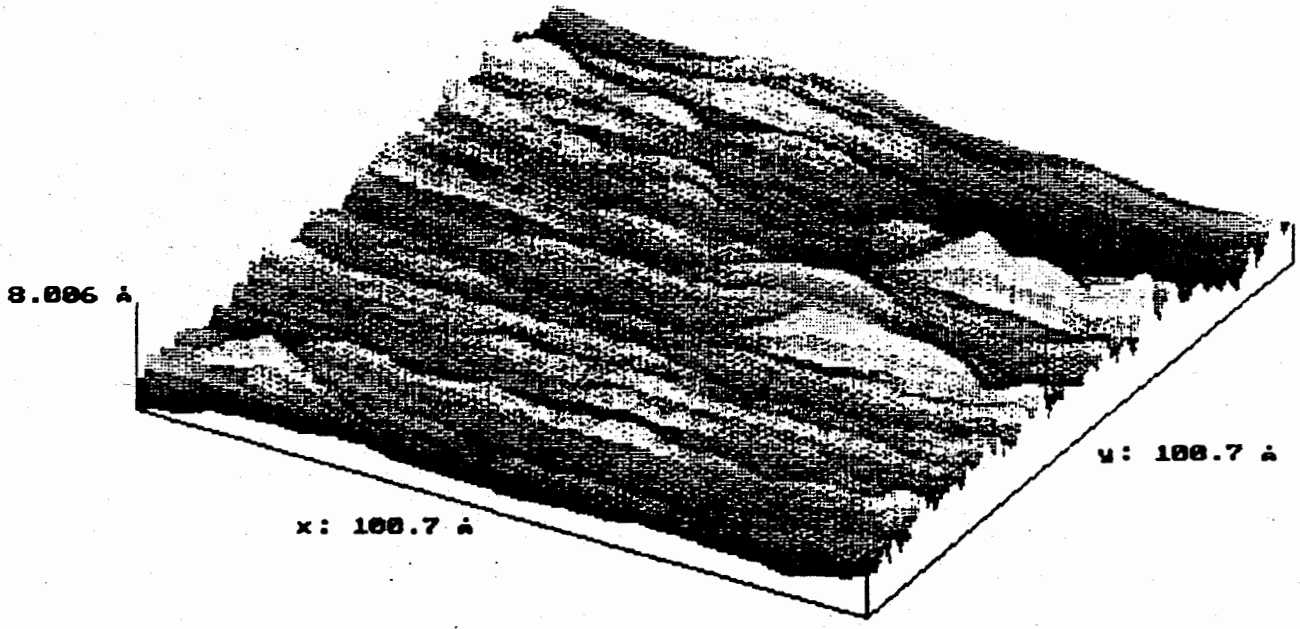

File si-07
Setpoint 0.2 nA
Bias -3000 mV

Fig. 3 STM image of another region of the a-Si:H film shown in Fig. 1.

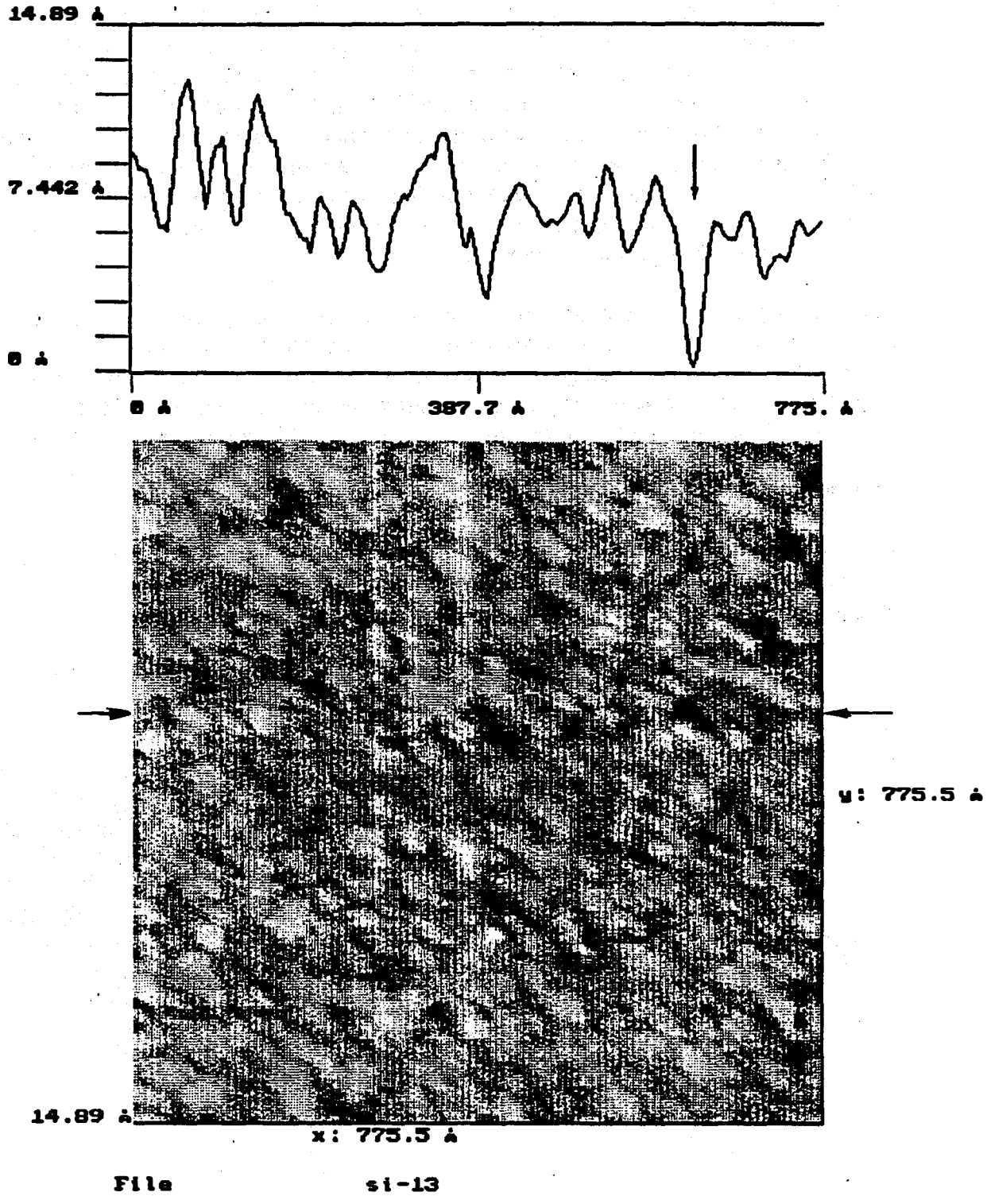

Fig. 4 STM image of a 100 Å thick a-Si:H film grown on crystal GaAs at T_s 250°C. The dark to white shading scale represents a 14 Å height range. A single scan line across the image, at the location indicated, is shown at the top of the figure.

Figures 4 and 5 show the typical surface topology of a 100 Å layer of a-Si:H grown at 2.4 Å/s on a GaAs crystal at T_s = 250°C. The vacuum-cleaved crystal surface is atomically flat and clean, while the a-Si:H surface typically has ~10 Å height variations, as seen in the figures. At the top of Fig. 4 a single scan line is shown with a highly expanded vertical scale. This scan line passes through the sharpest depression in this particular image, seen as a dark spot in the image. This depression , marked by an arrow, is 6 Å deep and ~35 Å wide at the top; the sides slope ~20° to the horizontal. Thus, even this depression is a very open trough, far from that which might be expected to initiate a void with further film growth. This region is representative of many scanned regions of the film surface.

These STM images are a convolution of the shapes of the probe tip and of the substrate, hence steep-sided surface troughs (incipient voids) might not be visible if the probe-tip is blunt. For this reason we have independently measured the shape of our probe tip, by scanning steep nanostructures we have created in other surface regions using strong pulsing. These observations have established that the tungsten probe tip tapers at 45° and larger angles to a sharp (< 15 Å) end. This is sharper than any surface features in the above figures, so those images represent the substrate shape without significant distortion.

These preliminary studies have shown that intrinsic a-Si:H film grows very homogeneously and smoothly on a flat substrate under typical "optimum" deposition conditions. No indications of particulate deposition, of > 10 Å diameter nanoparticles, have yet been seen.

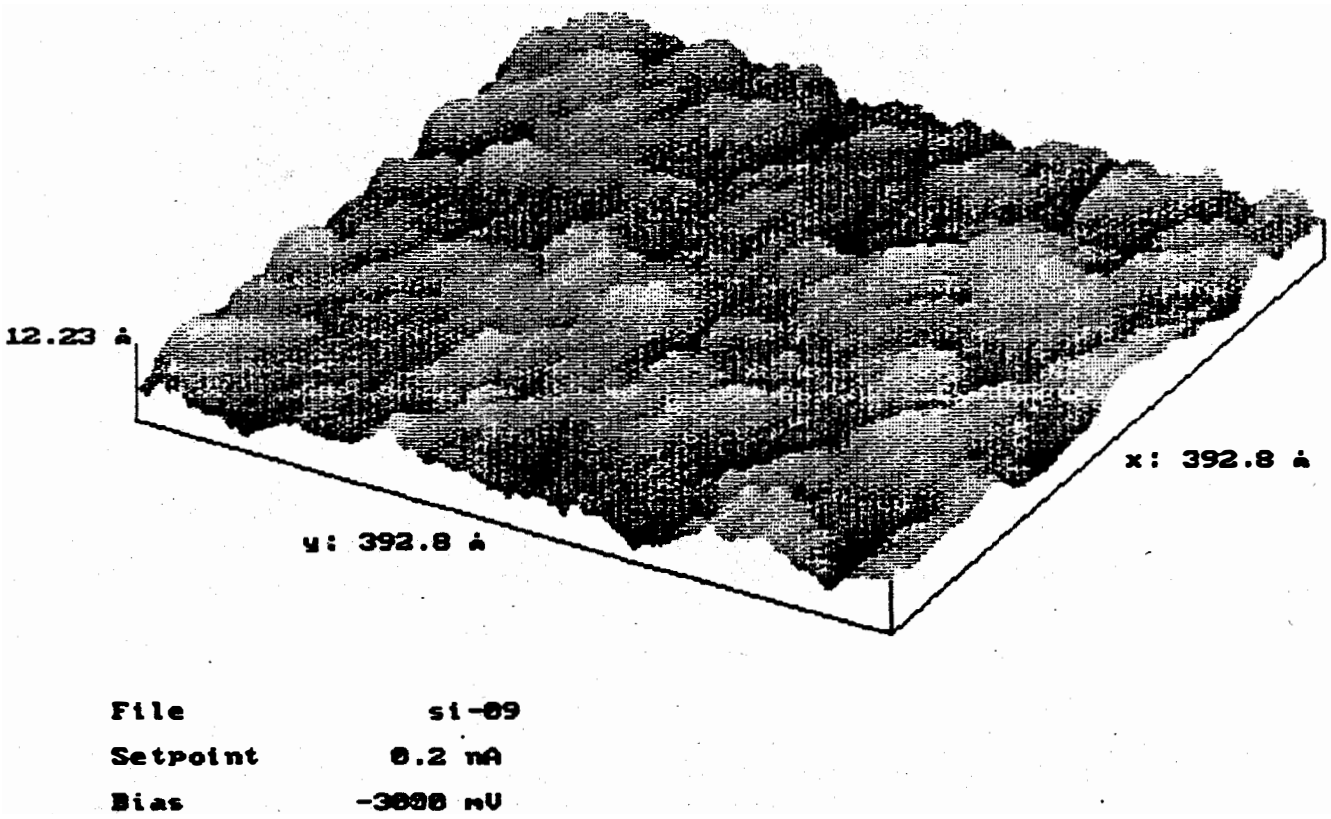

Fig. 5 STM image of another surface region of the a-Si:H film in Fig. 4.

Title: **Fundamental Studies of Defect Generation in Amorphous Silicon Alloys[a], and Transport in Microcrystalline Si[b], both Grown by Remote Plasma-Enhanced Chemical-Vapor Deposition (Remote PECVD)**

Organization: Departments of Physics, and Materials Science and Engineering,
North Carolina State University
Raleigh, North Carolina 27695-8202

Contributors: Professor Gerald Lucovsky: Principal Investigator;
Professors Robert J Nemanich and Jerzy Bernholc: Faculty Contributors;
Cheng Wang, Brian Davidson, Meredeth Williams, Seon-Mee Cho, David Lee and Claes Bjorkman: Graduate Students;
Warren Turner and Ze Jing: Post Doctoral Fellows

Introduction

The report describes research performed under two SERI sub-contracts, XM-9-18141-2[a] and XG-1-10063-1[b].

1. Deposition of Doped Microcrystalline Si (μc-Si) by Remote PECVD

We have identified conditions for deposition of undoped, near-intrinsic and heavily-doped thin films of μc-Si by Remote PECVD. This is achieved at substrate temperature of 250°C, with an H_2/SiH_4 flow rate ratio of 30:1, and with the H_2, and the Si-atom and dopant-atom source gases injected downstream from the plasma generation region. Conductivities of 50-100 S/cm for n-type material, and 6-10 S/cm for p-type μc-Si, with activation energies of 0.02 eV and 0.040 eV respectively, have been achieved for source gas mixtures of 10^{-2} PH_3/SiH_4 and 10^{-3} B_2H_6/SiH_4, respectively. Gas mixtures greater than 10^{-3} B_2H_6/SiH_4 result in p-type a-Si:H films with properties similar to films grown without downstream injection of H_2.

2. Deposition of a-Si,C:H and μc-Si,C Alloys by Remote PECVD

The Remote PECVD process has been used to deposit undoped and doped a-Si,C:H and μc-Si,C alloy films. This was accomplished by adding the C-atom source gas, CH_4, downstream, along with the Si- and dopant-atom source gases, and for the case of μc-Si,C, with downstream injection of H_2. We have compared dark conductivities of a-Si,C:H and μc-Si,C alloy films, respectively, with those of a-Si:H and μc-Si, and have demonstrated that the decreased conductivity of the Si,C alloy films is due to the wider bandgaps of the Si,C alloys. For the μc-Si,C film, the dark conductivities are limited by thermal emission of carriers from the Si crystallites into the a-Si,C:H material that separates the Si crystallites, and as such the dark conductivities in films with bandgaps of ~2 eV or more are limited to values less than ~0.1 S/cm.

The formation of μc-Si,C films is reduced with increasing concentration of C, and with increasing concentration of dopant atoms. Most of our studies have been conducted with a source gas ratio of $SiH_4/(SiH_4 + CH_4) = 0.67$. For undoped films and for dopant atom to Si + C atom source ratios to 10^{-3}, the films obtained are μc-Si,C. For higher C-atom concentrations in undoped

films, $SiH_4/(SiH_4 + CH_4) = 0.50$ and 0.33, the films are found to be amorphous, and for $SiH_4/(SiH_4 + CH_4) = 0.67$, and doping gas to ratios $>10^{-3}$, the films are also amorphous.

3. TEM studies of μc-Si and μc-Si,C Alloy Films

We have performed extensive studies of the deposited μc-Si and μc-Si,C films by TEM techniques, including: i) bright-field and dark-field contrast imaging; ii) lattice imaging in cross-sectional and plan-view modes; and iii) selected area diffraction. These studies, combined with IR and Raman measurements, have demonstrated that: i) crystallites in μc-Si and μc-Si,C alloys are silicon; ii) the crystallites have dimensions of ~50-200Å; and iii) the crystallites are encapsulated by amorphous material; a-Si:H for μc-Si and a-Si,C:H alloys for μc-Si,C. μc-Si and μc-Si,C alloys have been deposited on relatively thick, ~1000Å, thermally grown SiO_2 on Si substrates, and on native oxides, ~20Å thick, on Si substrates. In both instances nucleation of μc-Si and μc-Si,C alloys occurs at the onset of film deposition by remote PECVD. Deposition of either μc-Si or μc-Si,C alloys on cleaned Si substrates results in the epitaxial growth of Si layers on the Si substrates.

4. Transport Mechanisms in Si and Si,C Amorphous and Microcrystalline Films

We have analyzed dark conductivity data for a-Si:H, a-Si,C:H, μc-Si and μc-Si,C films and have concluded that transport in the heavily-doped microcrystalline films is limited by either of two mechanisms: i) thermionic emission over band offset barriers at boundaries between crystalline and amorphous regions; or ii) by thermal assisted tunnelling from Si crystallites into band tail states of the amorphous component. A combination of three plots: σ_{rt} versus E*, σ^* versus E*, and E*(Si,C) versus E*(Si), was used to establish the mechanisms limiting carrier transport. These studies have shown that for Si,C alloys with optical bandgaps of the order of 2.1 eV and above, carrier transport of both holes and electrons is limited by thermionic emission over potential barriers at the interfaces between doped Si crystallites, and the encapsulating and doped a-Si,C:H alloy. For C-atom concentrations of the order of 10-15 at.% C and greater, these band offsets are ~0.2-0.3 eV, so that dark conductivities of these materials are at most of the order of $5x10^{-2}$ S/cm, and comparable to those of heavily doped a-Si:H, for the same values of the doping gas ratios.

5. Formation of Device Structures using Doped a-Si:H and μc-Si

We have studied the properties of doped a-Si:H and μc-Si in MOS capacitors using ~10 Ω-cm p-type crystalline substrates and thermally grown SiO_2 dielectric layers. These studies have provided information about the relative electron affinities of a-Si:H and μc-Si, and the effective Debye lengths in μc-Si films with different levels of p-type and n-type doping. This information is important in the design of solar cell structures that utilize the doped a-Si:H or doped μc-Si in the p- and n-layers of p-i-n structures.

We have expanded these studies of μc-Si as a gate electrode material, and have compared the properties of n^+ and p^+ μc-Si, with respective conductivities of ~50-100 S/cm and 6-10 S/cm, onto thermally-grown and remote PECVD SiO_2 films. The remote PECVD SiO_2 films were subjected to a post-deposition anneal prior to μc-Si depositions. C-V measurements established that changing from n^+ to p^+ μc-Si electrodes produced a 0.8 eV shift of the flatband voltage for both types of oxides. This provides a measure of the Fermi level difference between the n^+ and p^+ μc-Si, and has implications for the maximum values of the open circuit voltages using μc-Si materials as the n^+ to p^+ layers in p-i-n photovoltaic devices.

6. Defect States in a-Si:H by Sub-Pico-Second Spectroscopies

We have collaborated with Professor Heinz Kurz's group at RWTH in Aachen, Germany, and have studied the contributions of process induced defect states to recombination of photogenerated electron-pairs. We find that process induced defect states that contribute to the sub-bandgap absorption to levels of ~100 cm^{-}, as determined by CPM, also serve as recombination centers for an Auger type recombination process for electron-hole pairs that dominates in the sub-picosecond time regime.

The transient change of absorption, Δa, obtained from an a-Si:H film deposited at 40°C and annealed at 200°C, and with $N_d \triangleq 10^{16}$ cm^{-3} is the same as for a film deposited at 250°C with the same [H] and N_d. Since the photon energy of the probe pulses (E_{pr} = 1.48 eV) is below the optical bandgap in a-Si:H, the change in absorption is entirely due to the optical response of photoexcited free carriers. Contributions to Δa due to changes of lattice temperature can be neglected. During the excitation pulse, Δa rises and reaches a maximum of Δa_{max} at the end of the excitation pulse. It has been found that Δa_{max} is linearly proportional to the density of photoexcited free e-h pairs, N_{ex}: $\Delta a_{max} = a_c \times N_{ex}$, where a_c is the absorption cross section for e-h pairs at the probe photon energy: for E_{pr} = 1.48 eV, $a_c = 6.6*10^{-17}$ cm^2. After the end of the excitation pulse, Δa starts to recover on a picosecond time scale. This recovery can be due to either trapping, or recombination. If we assume a_c to be constant on the time scale we have explored, then the time evolution of Δa is consistent with a bimolecular recombination process previously reported for higher excitation densities: $dN/dt = -\gamma \times N^2$. For this mechanism, the decrease in Δa results from a disappearance of photo-generated free carriers, rather than from any change in a_c. A model calculation provides a satisfactory fit to the experimental data, with a constant of proportionality, $\gamma = 6*10^{-9}$ s/cm^3, very close to the value of $\gamma = 7*10^{-9}$ s/cm^3 obtained in previous studies. This demonstrates that for the low defect density a-Si:H, the picosecond recovery of photoinduced absorption is dominated by an intrinsic bimolecular recombination process. For this material, any changes of a_c due bandtail state trapping or deep defect state trapping can then be neglected.

The transient changes in absorption obtained for the a-Si:H film deposited at 40°C before and after annealing are are consistent with a reduction in the defect state density. The sub-bandgap absorption indicates a defect density in the as-deposited state of $N_d \triangleq 10^{18}$ cm^{-3}, and defect density of $N_d \triangleq 10^{16}$ cm^{-3} after annealing at 200°C. In the unannealed state, there is a substantial increase of the recovery rate on both psec and sub-psec time scales. Since the density of photogenerated electron-hole pairs is essentially the same as in the annealed sample discussed above, the bimolecular mechanism cannot apply since this would require a significant increase in γ, which is neither consistent with previous studies, nor with the results reported above for annealed samples.

The recovery of absorption in a-Si:H with a defect density, $N_d \triangleq 10^{18}$ cm^{-3}, is consistent with an ultrafast recombination process, rather than a deep trapping process. We propose an Auger-mechanism where recombining e-h pairs can ionize a dangling bond state (D^o). The ionized dangling bond state (D^+) is then neutralized by the capture of free electrons, also on a psec time scale.

7. Modelling of Bond and Dihedral Angle Disorder in a-Si:H

We have applied a tight-binding model to Si-Bethe lattice structures in order to investigate the effects of bond-angle, and/or dihedral angle disorder. We have used a Hamiltonian with nearest and second-nearest neighbor interactions, and have been able to identify and separate the effects

bond angle disorder and dihedral angle disorder on the states at the states at the conduction and valence band edges. We have systematically investigated the formation of electronic states in the region of the conduction and valence band edges of a-Si as functions of variations in the bond and dihedral angle distributions. Local Density of States (LDOS) for Si atoms in disordered environments have been calculated using the cluster Bethe lattice method with a tight-binding Hamiltonian containing both first and second nearest neighbor interaction terms. We conclude that the change in orbital overlap, incurred from rotations about the axes defining the dihedral angle distortions, is the origin of the effect of dihedral angle disorder on the electronic states near the band gap.

Short range disorder in a-Si can effect the electronic density of states (DOS) near the band edges, shift the band edges or create discrete states in the band gap. We have made a study of short range disorder arising from bond angle distortions on the DOS of a-Si near the band edges. Raman scattering studies of a-Si and a-Ge by Lannin have related the bond angle disorder to a shift in the optical energy gap. Previous studies using a tight-binding approach have shown valence band states for individual atoms in distorted tetrahedral environments, or have estimated the bounds for band tailing due to bond and dihedral angle distortions. The Hamiltonians in these studies were restricted to nearest neighbor interactions, whereas our calculations have been performed with a tight-binding Hamiltonian that includes both first and second neighbor interaction terms.

Bond angle distortions and dihedral angle variations in clusters embedded in a Bethe lattice show effects on the LDOS at the top of the valence and at the bottom of the conduction band. Both E and F mode distortions increase the states at the edge of the conduction and valence band for the staggered configurations. Rotation of the dihedral angles to the eclipsed configurations can reduce the magnitude of states at the band edges by pushing these states farther into the band. This effect cannot be seen with a nearest neighbor Hamiltonian, which can model the bond angle distortions adequately, but cannot account for changes in distance and symmetry of the outer shells of atoms due to intermediate range disorder such as the dihedral angle variations. A key component of modeling the dihedral angle distortion are the 2nd neighbor interaction terms and the distance scaling law used with them. We are currently investigating other tight-binding parameters to determine the sensitivity of these results to the empirical fit of the terms and their relationship to neighbor distance on the band structure of Si.

8. Chemical Effects in Local Bonding Arrangements in a-Si:H: Ab Initio and Empirical Calculations

We have used ab initio and empirical calculations to study non-random bonding arrangements in a-Si,O:H and doped a-Si:H films. The two approaches give comparable results for the bond energies of SiH groups that are near-neighbors to the oxygen and dopant atoms. The calculations have been used to develop a model for the way in which these bonding arrangements are created in thin film deposition processes in which surface, rather than gas phase reactions dominate for the range of deposition parameters used to produce electronic or device grade materials.

We have identified several important *non-statistical* bonding environments in alloyed and doped a-Si:H. These include O-Si-H *linkages* in a-Si,O:H alloys, and P^+-Si-H and Si-B^--H *linkages* that play a significant role in the doping processes in a-Si:H. We present the experimental evidence for these bonding arrangements, and a model that accounts for their creation during film deposition.

Bond energies have been determined in two ways for 3 bonding configurations that include Si, O and H: 3Si-SiH, 2Si,O-SiH and 3O-SiH. This was done: i) using empirical relationships based on differences in electronegativities; and ii) by ab-initio calculations applied to hydrogen-terminated clusters that contain the SiH group, but with different numbers of Si- and O-atoms back-bonded to the Si-atom of that group.

The calculated Si-H energies are given below:

Group	Bond Energy (eV) Ab-initio Calculation		(Relative Energy) Empirical Calculation	
3Si-SiH	4.06	(1.00)	3.92	(1.00)
2Si,O-SiH	4.21	(1.04)	4.14	(1.06)
3O-SiH	4.66	(1.15)	4.64	(1.18)

The bond-energies, normalized to 3Si-SiH, demonstrate that both approaches yield similar relative bond-energies for the three groups.

Ab-initio calculations have not as yet been performed on clusters that include the charged and electrically active P^+ and B^- dopant atoms. We have estimated bond energies for these configurations using the empirical approach based on electronegativities. We first compute bond energies for some of the probable bonding arrangements involving H-atoms, and then for the case of the P-atom bonding environments establish a *chemical equivalence* between the O-Si-H and P^+-Si-H *linkages* through a calculation of the *partial charge* on the Si and H atoms. The empirically determined bond energies are given below:

Group	Bond Energy (eV)	Relative Energy
2Si,P^+-SiH	4.37	1.00
2Si-PH	4.18	0.96
3Si,B^--H	4.56	1.00
2Si-BH	4.99	1.09

The calculation of partial charges below establishes a *linkage* between these empirical bond energy calculations, and the ab-initio and empirical calculations presented above:

Bonding Group	Si Charge	H Charge
3Si-SiH	+ 0.04 e	- 0.15 e
2Si,O-SiH	+ 0.15 e	- 0.05 e
2Si,P^+-SiH	+ 0.19 e	- 0.02 e

Partial charges obtained from ab-initio calculations give equivalent trends for the first two groups. The partial charges on the Si- and H-atoms for the 2Si,O-SiH and 2Si,P^+-SiH groups are similar, and therefore exhibit *equivalent* differences with respect to the corresponding partial charges of the 3Si-SiH group. In the spirit of the empirical models, this implies comparable bond energies for these SiH groups, and therefore similar differences with respect to bond energy of the SiH group in the 3Si-SiH cluster. This is supported by the bond energies calculations that we have presented above.

a-Si,O:H alloys are typically deposited at temperatures between 225 and 300°C. Film growth proceeds from a heavily hydrogenated surface, so that differences in the bonded H-concentrations derive from the rate at which H atoms are thermally *removed* from that growth surface. Since bond energies of all relevant SiH groups are of the order of 4 eV, the relatively

small differences between these bond-energies, ~0.2 eV, for SiH in 3Si-SiH, and in 2Si,O-SiH clusters cannot completely account for the preferential retention of H in 2Si,O-SiH arrangements.

It has been shown that H-atoms initially bonded to a crystalline Si surface, can be removed from that surface at low temperatures by exposure to atomic hydrogen. This is followed by some type of surface reconstruction, as in the transition from a dihydride H-terminated Si(100) surface with 1x1 symmetry to an SiH-terminated surface with a 2x1 symmetry: surface dihydride groups are converted to monohydride groups, and a Si-Si dimer bond is formed.

We propose that plasma generated H-atoms (or protons) play a similar role in H-removal from hydrogen-terminated a-Si surfaces during film deposition. The rate limiting step for a surface reaction is often through the creation of an intermediate arrangement in which the Si surface atom is over-coordinated as in 3Si-Si-2H. This surface structure is energetically unstable with respect to interaction with an SiH_3 group. The rate of attachment of H, that creates the over-coordination will depend on the partial charge on the Si atom, and whether the H that is to be attached is an atom or a proton. If we assume that protons are the active species, then the rate of attachment is expected to decrease as the partial charge on the Si atom of the surface bonding group increases and becomes more positive. This factor could account for the increased stability of the bonding arrangements involving O and P^+ atoms.

Based on the experimental studies of a-Si,O:H, and P and B-doped a-Si:H, there are local bonding environments involving Si and H atoms with either O, P or B atoms that are non-statistical in the sense that they would not be anticipated solely by the relative concentrations of these atoms in the films. This infers that there are chemical driving forces for their creation in the deposited films. Since SiH groups, as well as OH, PH and BH groups all have bonding energies of about 4 eV, small differences in these energies by themselves cannot account for preferential formation of SiH or B^-H bonding groups for films deposited at 200-300°C. This leads us to propose a mechanism for the occurrence of the non-statistical bonding arrangements that is related to surface reaction chemistry. The model includes three steps: i) the formation of an intermediate structure in which the Si, and/or B or P atoms are over-coordinated by additional H-atoms; ii) the break-up of these surface intermediates through the release of molecular H - H_2; and iii) the attachment of an SiH_n group that continues the film growth process. In addition to these bonding sites involving H atoms and the dopant atoms P and B, there are other bonding groups in which P and B are threefold-coordinated and inactive with respect to doping. In this context, the calculated relative bonding energies for the *doping and inactive groups* are in accord the observation that the doping efficiency for P-atoms is significantly higher than for B-atoms.

9. Model Calculations Dangling Bond Energies in a-Si,Ge Alloys

We have used an empirical tight-binding approach to determine the relative energies of Si and Ge dangling bonds in a-Si. These calculations use a Bethe lattice structural model, and an sp^3s^* Hamiltonian, with only nearest We maintain perfect tetrahedral geometry at the dangling bond sites, and within the Bethe lattice as well. The self-energies of the Si and Ge atoms have been adjusted to give the experimentally determined valence band offset energy of ~0.2 eV. We find that a Ge-atom dangling bond, with three back-bonded Si-atoms, is about 0.1 eV lower in energy that a Si-atom dangling bond, also back-bonded to three Si-atoms. These calculations are being extended: i) to Si and Ge atoms with different number of Si and Ge atoms as their immediate neighbors, and with Bethe lattice terminations to these local clusters that are appropriate to a-Si,Ge alloys; and ii) to include bond and dihedral angle distortions at the dangling bond sites.

Title: **In Situ Characterization of Growth and Interfaces in a-Si:H Devices**

Organization: Materials Research Laboratory, Department of Physics, and Department of Electrical and Computer Engineering, The Pennsylvania State University, University Park, PA.

Contributors: R.W. Collins and C.R. Wronski, principal investigators; Ilsin An and Youming Li, graduate students.

Objective

Because of the complexity of the atomic structure of amorphous semiconductor devices and the stringent demands on their specifications, techniques for real time monitoring of bulk material and interface characteristics during preparation and processing are desirable. Optical probes are among the few techniques that can be applied in real time to monitor plasma-enhanced chemical vapor deposition (PECVD) processes. Such probes are monolayer-sensitive and non-invasive; they require optical access to the sample surface through windows, as well as an optical alignment capability. A disadvantage of the optical probes is that they are indirect, and considerable analysis is required to extract useful information. Ellipsometry is the most powerful and reliable real time optical measurement because it simultaneously provides changes in both amplitude and phase of the light wave when it reflects from a surface.

Previous real time ellipsometry studies have involved probing a-Si:H materials during growth or modification at a single photon energy.[1] Although this approach has provided useful information, the technique is limited in two ways. First, one of the most important material parameters, the optical band gap, cannot be determined and, second, it is often difficult to separate surface and bulk effects from data collected during film growth or surface modification. These limitations have been overcome with the recent development of real time spectroscopic ellipsometry in our laboratory.[2] With the complete spectroscopic capability over the range from 1.5 to 4.0 eV, the dielectric function and band gap can be determined; furthermore, detailed quantification of the microstructural evolution is now possible.[3] The use of a multichannel detection system provides ~50 point spectra in the ellipsometric amplitude and phase parameters [(ψ,Δ)] with monolayer thickness sensitivity in 64 milliseconds.[4]

The following problems have been the focus of research in FY 1991: (1) quantification of the microstructural evolution of PECVD a-Si:H versus deposition conditions and (2) real time characterization of Si-Si bond breaking and H-diffusion during post-hydrogenation of a-Si:H. The results will be described in turn in the first two sections of this Report.

Research Results: a-Si:H Nucleation and Coalescence

We have found that a two-layer optical model with three free microstructural parameters at each time characterizes the dynamic processes of thin film nucleation and coalescence. Such a model cannot be verified on the basis of single wavelength ellipsometry, which returns two parameters [(ψ,Δ)] at any given time. The real time spectroscopic capability, which returns more than one-hundred experimental parameters, is needed to verify the validity of the model and deduce the three parameters.[5] These parameters are as follows: (1) d_s, the thickness of a surface layer of low bond-packing density; (2) d_b, the thickness of an underlying layer of bulk density; and (3) f_v, the surface layer bond-packing density, expressed in terms of a void volume fraction. The surface layer simulates either the nuclei in the earliest stages of growth or the residual surface roughness layer after the nuclei make contact to form the first bulk density monolayer.

Figure 1 shows d_s and d_b, obtained as a function of time during the growth of a-Si:H onto c-Si by rf PECVD in the parallel-plate configuration. Conditions were set for optimum material:

250°C substrate temperature, 0.2 Torr pressure, and 2 W rf power (52 mW/cm^2 at sample). When the plasma is struck, the bulk layer remains near 0 Å in thickness, but the surface layer (simulating the initial nuclei) grows rapidly. The growth rate of the nuclei begins to saturate near t=10 s as nuclei make contact. The first bulk monolayer (d_b=2.5 Å) is formed at t=t_b=13 s, and at this point, a surface roughness layer 19.5 Å thick remains from the initial nucleation process. The most interesting aspect of the growth process is the evolution of this surface layer in the bulk film growth regime. The results of Fig. 1 show that the surface smoothens with subsequent deposition -- by about 8 Å in the first 50 Å of bulk film growth.

In continuum models of film growth,[6] the stability of one dimensional surface profiles have been studied in response to sinusoidal perturbations of spatial wavelength λ_r. Effects of finite atomic size and shadowing are proposed to enhance the perturbations, whereas adatom surface diffusion smoothens them. Basically, one expects to regain a smooth profile for $\lambda_r<\lambda_o$, the surface adatom diffusion length; however when $\lambda_r>\lambda_o$, the surface roughens, eventually stabilizing with features that appear analogous to columnar microstructure. These theories make direct contact to our experimental situation. If the nucleation-induced roughness present at time t=t_b in Fig. 1 is assumed to exhibit a hemispherical geometry, then a dominant roughness wavelength of λ_r~2d_s(t=t_b)~40 Å is predicted. Thus, in order for this profile to smoothen, as is observed experimentally, then the precursor diffusion length must be greater than 40 Å under optimum PECVD conditions.

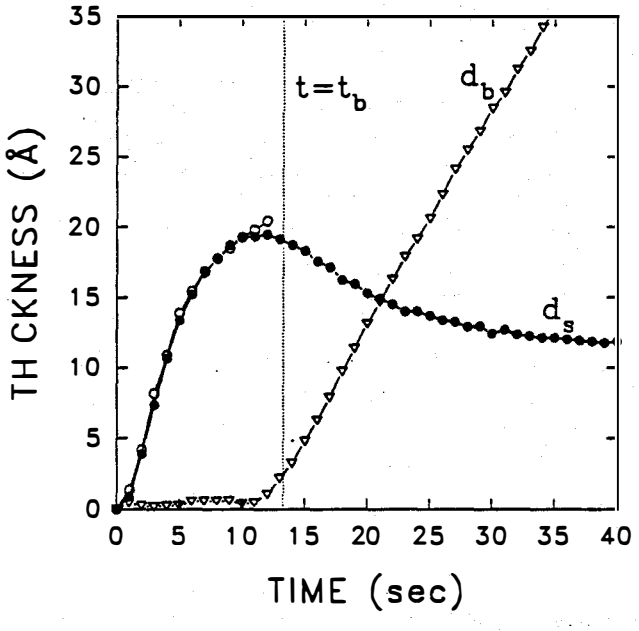

FIG. 1 Thicknesses of the surface layer (solid points) and the bulk layer (triangles) deduced in an analysis of real time spectroscopic ellipsometry data collected during the nucleation and growth of optimum PECVD a-Si:H on a c-Si substrate. The open circles were obtained using a one-layer model in the nucleation regime.

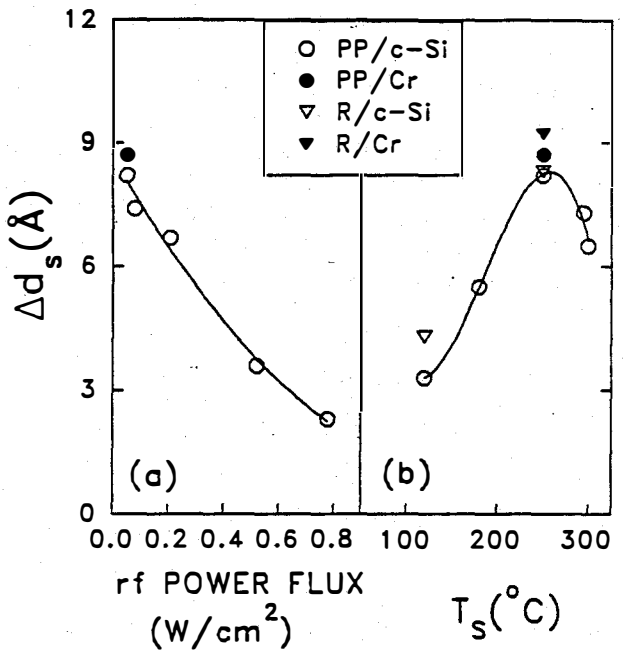

FIG. 2 Surface smoothening in the first 50 Å of bulk film growth for PECVD a-Si:H plotted vs. (a) rf plasma power at the substrate surface and (b) substrate temperature. The key is as follows PP: parallel-plate PECVD; R: remote He PECVD; Cr: Cr substrate; c-Si: silicon wafer substrate. The solid lines are guides to the eye for the PP/c-Si depositions.

Figure 2 shows the magnitude of the smoothening effect in the first 50 Å of bulk film growth plotted vs. substrate temperature and plasma power flux at the sample surface for both remote-He and parallel-plate a-Si:H PECVD.[7] In most cases the substrate was c-Si. It is noteworthy that the films prepared under conditions known to be optimum for parallel-plate rf PECVD, i.e. low power and T_s~250°C, exhibit the greatest effect. The clear trends to weaker surface relaxation at higher power and both higher and lower T_s, appear to reflect trends in precursor surface diffusion length. Specifically, as the diffusion length decreases the Fourier components in the surface roughness with $\lambda_r > \lambda_o$ tend to stabilize, leading to the weaker relaxation effect. The lower λ_o for T_s<250°C arises from a thermally-assisted diffusion process. The lower λ_o for T_s>250°C probably arises because the H-coverage of the surface is reduced, and this provides reactive sites for precursor attachment. The effect of high power is more complex. With a greater ionic flux, an effect similar to that at high T_s is possible, i.e. a greater number of sites for surface bonding. Alternatively a higher concentration of SiH and SiH_2 may be generated in the plasma, and these are more reactive at the surface.[8] In either case, λ_o is expected to decrease.

Research Results: H-Modification of a-Si:H Thin Films

Real time spectroscopic ellipsometry has also been applied to characterize the changes in the distribution of Si-Si and Si-H bonding in conventional parallel-plate PECVD a-Si:H when it is exposed to a H_2 atmosphere enriched with atomic species generated by a filament heated to ~2000K. The exposures are performed in situ just after a-Si:H preparation with the film held at the deposition temperature (250°C). In effect, the chemical potential in the gas phase is raised well above that in the film, and H diffuses into the film in order to equalize the potentials. We anticipated that this may convert weak Si-Si bonds to Si-H bonds without changing the overall Si network connectivity. There are a few important differences between this study and previous post-hydogenation studies. (1) A hot filament is an effective way of generating large quantities of low energy atomic H. (2) We avoid the high energy ion bombardment associated with plasma hydrogenation methods. (3) We apply a real time probe that is sensitive to the depth profile of the Si-Si bond-packing density in the top 600 Å of the film. From the latter capability, we have the first real time probe of bonded H-diffusion.

To provide an overview of the phenomena involved in H-modification, we find that the treatments generate additional Si-H bonds in the film, as indicated by a preferential increase in the integrated absorption for the 2000 cm^{-1} mode in the infrared spectrum. Furthermore, as described below, subgap photoconductivity measurements suggest that no additional midgap states are generated in this process. This would seem to suggest that two H atoms completely passivate the defect generated by breaking a Si-Si bond. In any event, we require an optical model for the conversion of Si-Si bonds to Si-H bonds so that the spectroscopic ellipsometry data collected during H-treatment can be simulated with changes in the bonded H profiles. The simplest such model assumes that some fraction of the volume occupied by Si-Si bonds is converted to Si-H bonds which exhibit the optical response of voids. The next best model is to extract the dielectric response of the Si:H component itself, rather than simulating it with voids. Such an analysis has been performed, and an excellent fit is obtained to spectra collected in real time. For the purposes of this discussion we assume that the Si:H component dielectric function is correct; however, the conclusions below are insensitive to potential errors.

The conventional method for measuring H-diffusion involves preparing layered structures of hydrogenated and deuterated materials, annealing the structures for a given duration, and then analyzing the deuterium profiles with SIMS. Such results have yielded diffusion coefficients in the range of 10^{-16}-10^{-17} cm^2/s for intrinsic a-Si:H at 250°C when a time scale of several hours (corresponding to a ~1000 Å diffusion depth) is utilized.[9,10] A model of dispersive diffusion has been developed to explain a decrease in the diffusion coefficient by a factor of 5 for annealing times from 10 min to 100 hrs, observed in doped materials.[10]

In an attempt to make connection with the literature results, we present simulated ellipsometric spectra from 2.5 to 4.0 eV in Fig. 3, assuming a diffusion coefficient for intrinsic a-Si:H of 10^{-16} cm^2/s at 250°C. The a-Si:H is assumed to be opaque at 2.5 eV; thus the substrate does not need to be included in the optical model. In this calculation we used a multilayer film to simulate the diffusion profile, and the optical response of each sub-layer was determined as a mixture of bulk material and Si:H bonding components. Corresponding data appear in Fig. 4, obtained during H-treatment of 2500 Å thick, intrinsic a-Si:H at 250°C. Clearly the data cannot be understood in terms of the diffusion model. In effect, the time-independence of Δ in Fig. 4 shows that the new Si:H volume generated has a constant profile throughout the penetration depth of the light (~600 Å), and increases with time. This suggests that the breaking of Si-Si bonds to form stable Si-H bonds is limited by reaction with H, not by H diffusion. Figure 5 shows a calculation that verifies this behavior; to obtain it we simply assume that Si-Si volume is converted to Si:H volume uniformly throughout the penetration depth of the sample.

We find that the volume fraction of the Si:H component increases at the expense of Si-Si bonding according to an exponential relationship, i.e. $f=f_0(1-e^{-kt})$. Although a closer inspection of the results over a very wide time range suggests a distribution of rate coefficients k, a value of 0.001 s^{-1} provides a reasonably good fit for the time scale of ~10 min. The saturation value of the Si:H volume fraction, f_0~0.24 is approached after about an hour; however, this value is quite sensitive to filament conditions. We estimate that ~5-10 at.% Si-Si bonds are actually broken under the filament conditions used here. The larger affected vol.% arises from the fact that the fundamental optical unit of polarizability is not a single Si-Si bond, but more likely a tetrahedron. The value

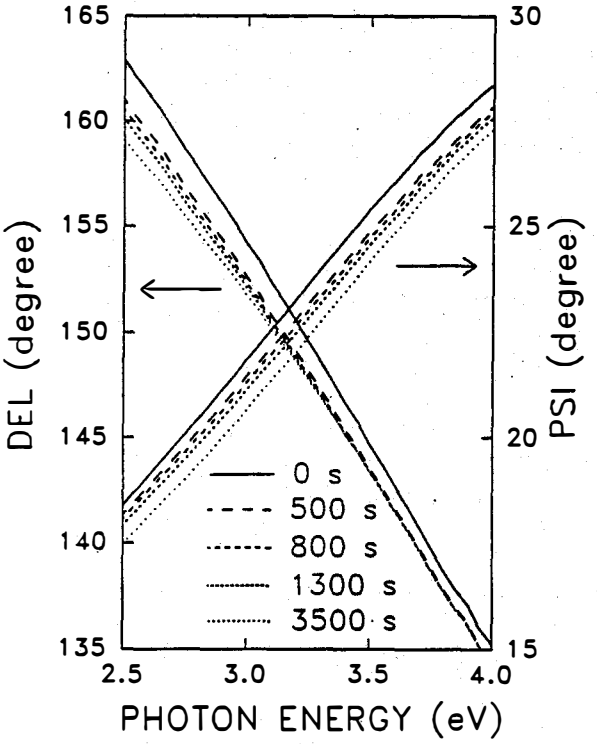

FIG. 3 Simulation of ellipsometric spectra for the diffusion of H into an opaque film of a-Si:H, assuming a diffusion coefficient of 10^{-16} cm^2/s. The ultimate equilibrium volume fraction of Si:H is taken to match the experimental result of 0.24.

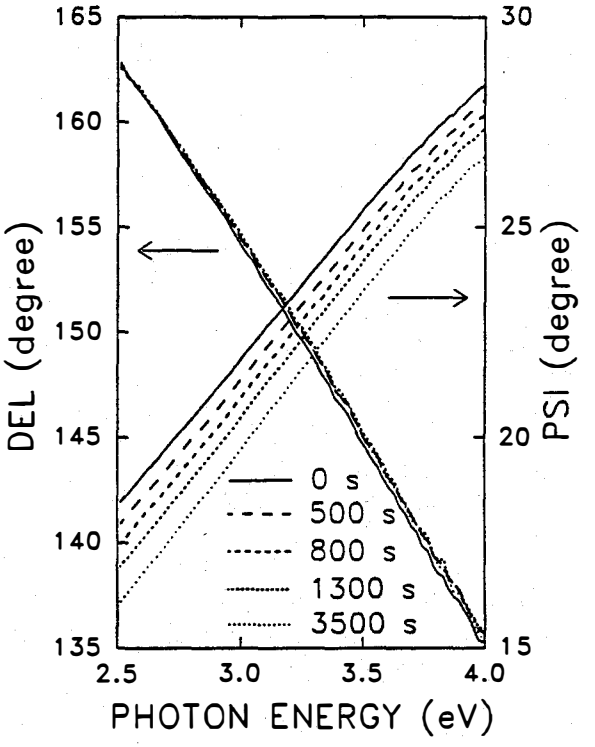

FIG. 4 Experimental ellipsometric spectra collected during a one hour H-treatment of intrinsic a-Si:H at 250°C. The film was 2500 Å thick, and thus opaque over the full photon energy range.

of the rate coefficient, along with the optical probing depth, can be used to place a lower limit on the diffusion coefficient D_H. A conservative estimate shows that in order to observe reaction-limited behavior to a depth of 600 Å, $D_H > 4 \times 10^{-14}$ cm^2/s, a value 100x higher than that obtained by the multilayer approach.

When the filament is extinguished, the volume fraction of Si:H decreases by ~0.08, indicating that some fraction of the broken Si-Si bonds reform as the gas phase chemical potential is reduced; however, the remainder are irreversibly broken and remain so upon returning the sample to room temperature. Furthermore, we find that surface oxides at the near monolayer level prevent equilibration of gas phase and thin film H chemical potentials. This in turn suggests that the rapid diffusion driven by the imbalance in the gas phase and solid state chemical potentials involves bonded H and not interstitials, and the strong Si-O bonds at the surface prevent H from entering the network. The H-bonding configuration that provides the diffusive pathway is unclear at present, but must be distinct from the stable configuration observed optically. The oxide barrier results also show that the H-treatment must be performed in situ in order to observe the process of reaction-limited bond-breaking.

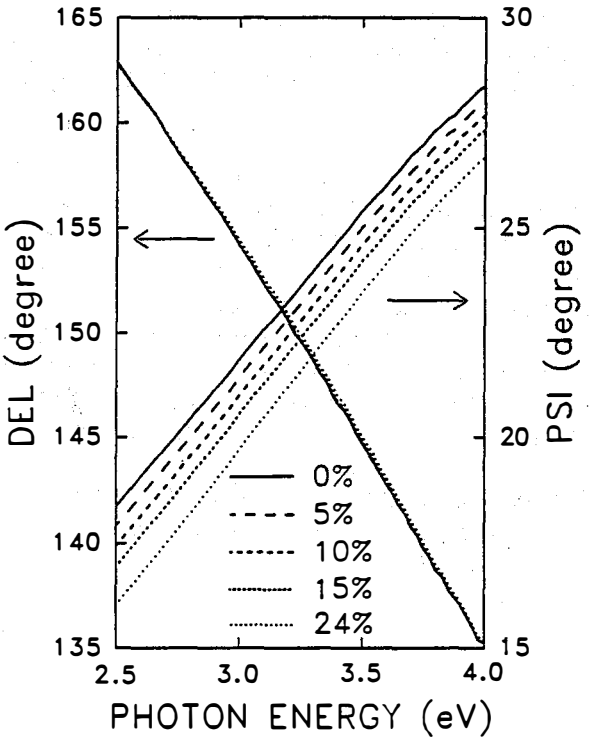

FIG. 5 Simulation of ellipsometric spectra as in Fig. 3, except that the conversion of Si-Si bonding to Si-H bonding is assumed to occur uniformly throughout the bulk of the material.

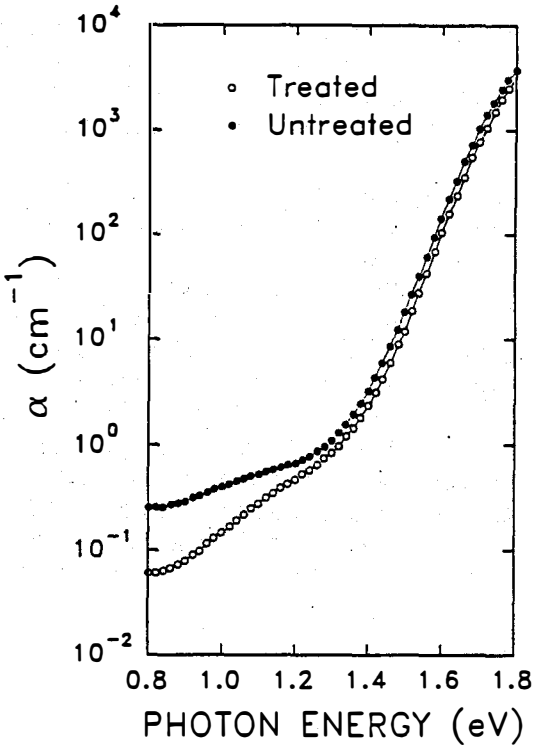

FIG. 6 Optical absorption coefficient obtained from photoconductivity and optical transmittance-reflectance measurements for a 0.85 μm thick a-Si:H film prepared by alternating growth and H-treatment (open points). Corresponding data for a control sample prepared without the H-treatment is also provided (solid points). Both samples were in the annealed state.

Thick films were prepared by alternating 800 Å of intrinsic a-Si:H growth with 20 min of H-treatment, a procedure expected to provide relatively uniform films with more than 2 at.% broken bonds. Figure 6 shows the absorption coefficient from photoconductivity and transmittance-reflectance measurements for such a film 8500 Å thick, in comparison to a control sample prepared without the H-treatment steps. Both samples were measured in the annealed state. There is an overall uniform shift in the absorption edge consistent with an optical gap increase of 0.04 eV and bonded H content increase of 4 at.%. It is clear that, even though $>10^{21}$ Si-Si bonds were broken, no excess defect states were generated. In fact, there is a reduction in the integrated absorption attributed to dangling bonds. Thus, as occurs in the a-Si:H growth process, H effectively passivates broken bonds, leaving no more than 1 defect per 10^6 broken bonds. Finally, the band tail states remain rigid with only a very slight decrease in slope (0.047 vs. 0.049 eV) upon H-treatment. Thus, we do not detect any significant tendency for H to break Si-Si bonds associated with the band tail electronic states in preference to those associated with the band edge states.

Conclusions

Real time spectroscopic ellipsometry has been applied to characterize microstructural evolution in the early stages of a-Si:H growth by PECVD in greater detail than was possible in previous single wavelength studies. The data exhibit monolayer-sensitivity to coalescence, i.e. the decay of nucleation-generated surface morphology, after nuclei make contact to form the first bulk monolayer. We offer clear evidence of the dependence of precursor surface diffusion on substrate temperature and plasma power, thus identifying the role it plays in determining the ultimate properties of the bulk material.

Similar experiments have been used to investigate the conversion of Si-Si bonds to Si-H bonds in PECVD a-Si:H upon exposure to a H_2 atmosphere enriched with atomic H from a heated filament. In effect, we monitor the modification that the a-Si:H network undergoes as its H chemical potential equilibrates with that of the gas phase. For optical penetration depths of 600 Å and treatment temperatures of 250°C, Si-Si bond-breaking is reaction-limited. As a result, we find a lower limit for the H-diffusion coefficient that is at least 2 orders of magnitude higher than that typically obtained by conventional deuterium profiling. In a H-treatment of about 1 hour, we find that as much as 5-10 at.% of the Si-Si bonds in the network are irreversibly broken. Future research will concentrate on studying the mechanism of H-diffusion and determining the kinetics of the formation of stable Si-H bonds. In addition, the optoelectronic properties of H-modified materials will be studied in greater detail, along with assessment of their stability, for comparison with unmodified control materials. In the long term, we expect to apply real time spectroscopic ellipsometry in order to characterize interfaces in electronic device structures.

References

[1] R.W. Collins in Amorphous Silicon and Related Materials, edited by H. Fritzsche (World Scientific, Singapore, 1988) p. 1003.
[2] I. An and R.W. Collins, Rev. Sci. Instrum. 62, 1904 (1991).
[3] Y.M. Li, I. An, H. Nguyen, C.R. Wronski, and R.W. Collins, J. Non-Cryst. Solids 137&138, 787 (1991).
[4] I. An, Y.M. Li, H. Nguyen, and R.W. Collins, Rev. Sci. Instrum. (submitted, 1992).
[5] I. An, H. Nguyen, N. Nguyen, and R.W. Collins, Phys. Rev. Lett. 65, 2274 (1990).
[6] A. Mazor, D.J. Srolovitz, P.S. Hagan, and B.G. Bukiet, Phys. Rev. Lett. 60, 424 (1988); R. Karunasiri, R. Bruinsma, and J. Rudnick, Phys. Rev. Lett. 62, 788 (1989).
[7] Y.M. Li, I. An, H. Ngyuen, C.R. Wronski, and R.W. Collins, Phys. Rev. Lett. (submitted, 1992).
[8] A. Gallagher, Mater. Res. Soc. Symp. Proc. 70, 3 (1986).
[9] D.E. Carlson and C.W. Magee, Appl. Phys. Lett. 33, 81 (1978).
[10] W.B. Jackson and J. Kakalios, in Ref. 1, p. 207.

Title:	**Research on Defects and Transport in Amorphous Silicon-Based Semiconductors**
Organization:	Department of Physics, Syracuse University, Syracuse, New York
Contributors:	Eric A. Schiff, principal investigator; Homer Antoniadis, Jung-Keun Lee, and Qi Wang.

Projects and Research Approaches

In this report we describe our recent results on two research topics:

Effects of Light Soaking on the Electron Drift Mobility in a-Si:H. For many years it has been known that light-soaking modifies the drift of carriers in a-Si:H by changing direct trapping and recombination events involving deep levels. It has been presumed that light-soaking does not affect the fundamental transport mechanism, which is usually accepted to involve bandtail states. However, the measurements indicating that light-soaking does not affect bandtail transport are inconclusive. Since the performance of a-Si:H solar cells is determined by the light-soaked state, a clear understanding of this issue is crucial to understanding operating solar cells. A convincing demonstration of an effect of light-soaking on bandtail transport would also significantly change our views of the mechanisms limiting mobilities in a-Si:H.

We have performed studies of the electron drift mobility using photocarrer "time-of-flight" techniques for optimized, undoped a-Si:H specimen from three different laboratories; these observations will be described in some detail here. We found no significant effects of light-soaking upon the electron transport mechanism at room temperature; below 200 K two of the specimens showed no significant effect, but we found a sizable effect in a third. Part of this work is published [1].

Modulated Electron Spin Resonance Measurements and Defect Correlation Energies in a-Si:H. The "standard model" for deep levels in a-Si:H is that they represent transitions between three charge states of a single defect observed by electron spin resonance, the D-center. In this view the effective correlation energy describing the D-center is substantially positive, so that most D-centers are electrically neutral in the dark. However, many researchers have invoked models with small or negative correlation energies and relatively large densities of charged defects to account for their measurements. The most explicit way to address this issue is by modulating the specimen's charge or temperature and observing the effect upon the D-center spin density. We have measured thermal modulation effects in a large number of undoped a-Si:H specimens, and have examined models for both thermal and charge depletion measurements. We have concluded that these measurements can be interpreted satisfactorily using the standard model. Some of this work is published [2].

Effects of Light-Soaking on the Electron Drift Mobility in a-Si:H

We have examined electron transport in conventional diode structures prepared by Energy Conversion Devices, Inc., by Chronar, Inc., and by ourselves. We present our measurements here as *mobility normalized transient photocurrents:* $i(t)(d^2/Q_0V)$. The photocurrent $i(t)$ is the response to a short laser pulse absorbed near an interface of the diode. V is the reverse bias voltage applied to the diode shortly before the laser pulse. d is the thickness of the undoped layer of the diode. Q_0 is the charge of mobile electrons in the diode determined by integrating the photocurrent to times well past the electron transit time. We have established elsewhere [3] that this representation is fully equivalent to estimating an average drift-mobility from the transit time.

We discuss first the left side of Fig. 1, which shows the transient photocurrents measured for a very thick specimen prepared by Chronar, Inc.. These transients were measured with bias voltages chosen so that both internal field effects and also the effects of electron transit across the specimen are not apparent. The curves illustrated with open symbols are for the specimen in an annealed state obtained by heating the diode for one hour at 160° C; the closed symbols represent a state obtained after sustained light-soaking.

At 300 K in the annealed state the initial electron mobility is just below 1 cm^2/Vs. The rather slow rise time for this specimen is due to diode series resistance effects; the specimen was not specifically deposited for use in time-of-flight measurements. The decline after about 100 ns is due to deep-trapping. In the light-soaked state deep-trapping occurred much earlier; the initial mobilities were probably comparable at 300 K, but these data are inconclusive.

At lower temperatures the electron mobility declines with time as a power-law because of the onset of bandtail trapping effects. The light-soaked and annealed states converge at earlier times. The maximum effect of light-soaking on the bandtail dominated mobility compatible with these data is about 20%. We again attribute the divergence of the curves at longer times to deep-trapping.

Our measurements on a 5μm diode prepared at Syracuse were very similar to those just presented for the Chronar specimen, and will not be discussed separately here. We found somewhat different effects on a specimen prepared at Energy Conversion Devices, Inc.. The ECD specimen was clearly different than either the Chronar or Syracuse specimens. In the annealed state the electron deep-trapping mobility lifetime product $\mu\tau_{e,t}$ was smaller, and the hole deep-trapping $\mu\tau_{h,t}$ was larger.

The transient measurements are presented to the right of Fig. 1. At 300 K the initial electron mobility is 1 cm^2/Vs in the annealed state. The deep-trapping in this specimen is remarkably pronounced, which we attribute to a very narrow conduction bandtail for this specimen. The rise-time in these data is due to the 5 ns pulsewidth of our laser, which precludes quantitative estimates of the drift mobility prior to about 10 ns without use of deconvolution techniques. However, the current in this rise-time regime is nonetheless proportional to the actual drift-mobility. The convergence of the curves precludes a drift mobility difference between the annealed and light-soaked states larger than about 10%

prior to deep-trapping.

At low temperatures there is a marked difference in the transients measured before and after light soaking ("VLS" state) which we could not attribute to deep-trapping; the room-temperature drift mobility was not measured for the VLS state. The intermediate state ("LS") did not show a pronounced effect. There is an oddity about these states which may be important. Although the low-temperature drift mobility is clearly lower for the VLS state than for the VS state, the deep-trapping mobility-lifetime product $\mu\tau_{e,t}$ barely changed between the two states. The effects in Fig. 2 were reproduced several times by two different workers, and are very unlikely to be simple computational error. We consider them as preliminary evidence for an effect of light-soaking on bandtail transport in a-Si:H which sets in following saturation of deep-level generation.

A clear conclusion about the existence of light-soaking effects on electron transport involving the conduction bandtail is not possible at this stage. Although such effects are small in most cases, we have examined one specimen where the effect is significant.

Modulated Electron Spin Resonance Measurements and Defect Correlation Energies in a-Si:H.

Changing the temperature of an a-Si:H specimen or depleting an interfacial region of charge modifies the spin density. For a system with a single defect level in the midgap region, removal of an electron will usually destroy a single spin; changing the temperature will not affect the spin density. However, if the defect has two or more levels (cf. the $D^{+/0}$ and $D^{0/-}$ levels of a-Si:H) the situation is more interesting; if the correlation energy separating the two levels is comparable to the site-to-site variation in the level position or to the specimen temperature, the simple results for a single level described above are substantially changed.

We have performed calculations of modulation effects as well as measurements of temperature dependent electron spin resonance to further explore these issues; some of the work is published [2], and a manuscript including all work discussed here has been submitted for publication [4].

In Fig. 2 we show the correlation of depletion and temperature modulation for a simple model in which every defect has some definite correlation energy U, and the inhomogeneous width of the level position (the site-to-site variation noted above) is set to 0.3 eV. We define the depletion modulation of the spin density $DM \equiv \partial N_s/\partial n$, where N_s is the spin density and n is the density of electrons occupying the defect system. The thermal modulation is defined as $TM \equiv \partial(\ln N_s)/\partial T$, where T is the specimen temperature. Both TM and DM depend upon the particular values of U and n. The dependence on temperature for the conditions of the figure are weak.

The contours shown as solid lines were generated by selecting the indicated value for U_{eff} and varying the density of electrons n. The dashed curves are the contours generated by varying U_{eff} for a given density n. These latter curves are labeled using a dimensionless electron density $(n - N_D)/N_D$, where N_D is the density of defects. A value of

0 corresponds to one electron per defect in the system. These contours indicate that the thermal modulation TM determines U_{eff} nearly uniquely; TM is remarkably insensitive to $(n - N_D)/N_D$. Depletion modulation DM is not simply related either to U_{eff} or to $(n - N_D)/N_D$.

We performed temperature dependent ESR measurements from which we estimated the parameter TM from Fig. 2. In Fig. 3 we show the correlation of TM with the bulk spin density N_B; the error bars indicate the statistical uncertainties in the slope estimates. We estimate that "bulk spins" in a-Si:H of typical device quality exhibit a thermal modulation of $1 - 2 \times 10^{-4}$ K^{-1}, which corresponds to a deviation from Curie-dependence of 2 - 4% between 100 and 300 K. Poorer specimens exhibit a thermal modulation of nearly 4×10^{-4} K^{-1}. It surprised us that interfacial spins gave no detectible Curie-law deviation, since we might assume that these spins should be characteristic of "poor" a-Si:H; we have no explanation for this effect.

If we accept the model of Fig. 2, then we estimate from the data of Fig. 3 that U_{eff} for "device-grade" a-Si:H is about 0.3 eV, with "poor-quality" a-Si:H yielding a lower value. A better way to describe the implications of the TM data is to estimate the ratio N_s/N_D of the spin density to the total defect density N_D. This ratio depends less strongly on the particular parameters of $g(E)$; we obtained $N_s/N_D \sim 0.75$. Thus these temperature dependent ESR data agree broadly with earlier estimates of U_{eff} based on interpretations of infrared absorption measurements, and they support the widespread use of the spin density N_s as an estimate for the total density of deep levels in a-Si:H.

We now discuss the consistency of our TM measurements and the earlier depletion width modulated ESR work. Essick and Cohen [5] reported a depletion effect $\Delta N_s/\Delta n$ of 0.14 for each of five different "light-soaking" states in the one specimen which was studied; these results are based on their calibrations of the depletion-width modulation technique. These values cannot be immediately equated with the parameter DM of Fig. 2, since the depletion modulation Δn was nearly 25% of the spin density in some states. For the $U_{eff} = 0.3$eV contour in Fig. 2, the "operating point" of their experiment would actually have moved well down the contour as the sample was depleted. We previously estimated the value of U_{eff} which best accounts for the DWM-ESR based on "self-depletion" of the specimen starting from $(n - N_D)/N_D = 0.0$ and integrating the depletion effect down the various contours. We obtained a best fit for $U \sim 0.2 - 0.3$ eV [2].

In their original work Essick and Cohen did not have access to definitive temperature dependence data. They proposed that $U_{eff} \sim 0.0$ eV, which is self-consistent with their published data. However, for the models used both by Essick and Cohen and by ourselves, a zero correlation energy is incompatible with the temperature dependent measurements. The *simplest* model of which we are aware which rationalizes both the temperature and depletion modulation measurements is the "standard" view that the D-center in undoped a-Si:H has a reasonably large positive correlation energy, and that most of these defects are neutral and are detected by ESR. Models with additional assumptions can be advanced to account for our temperature dependence measurements in terms of a zero correlation energy, but we are unaware of any compelling reason to do this.

References

1. Homer Antoniadis, Qi Wang, E. A. Schiff, and S. Guha, in *Amorphous Silicon Technology - 1991*, edited by A. Madan, *et al* (Materials Research Society, Pittsburgh, 1991), p..
2. J.-K. Lee and E. A. Schiff, in *Amorphous Silicon Technology - 1991*, edited by A. Madan, *et al* (Materials Research Society, Pittsburgh, 1991), p.605.
3. Qi Wang, Homer Antoniadis, S. Guha, and E. A. Schiff, *unpublished.*
4. J.-K. Lee and E. A. Schiff, submitted for publication.
5. J. M. Essick and J. D. Cohen, *Phys. Rev. Lett.* **64**, 3062 (1990).

Figures

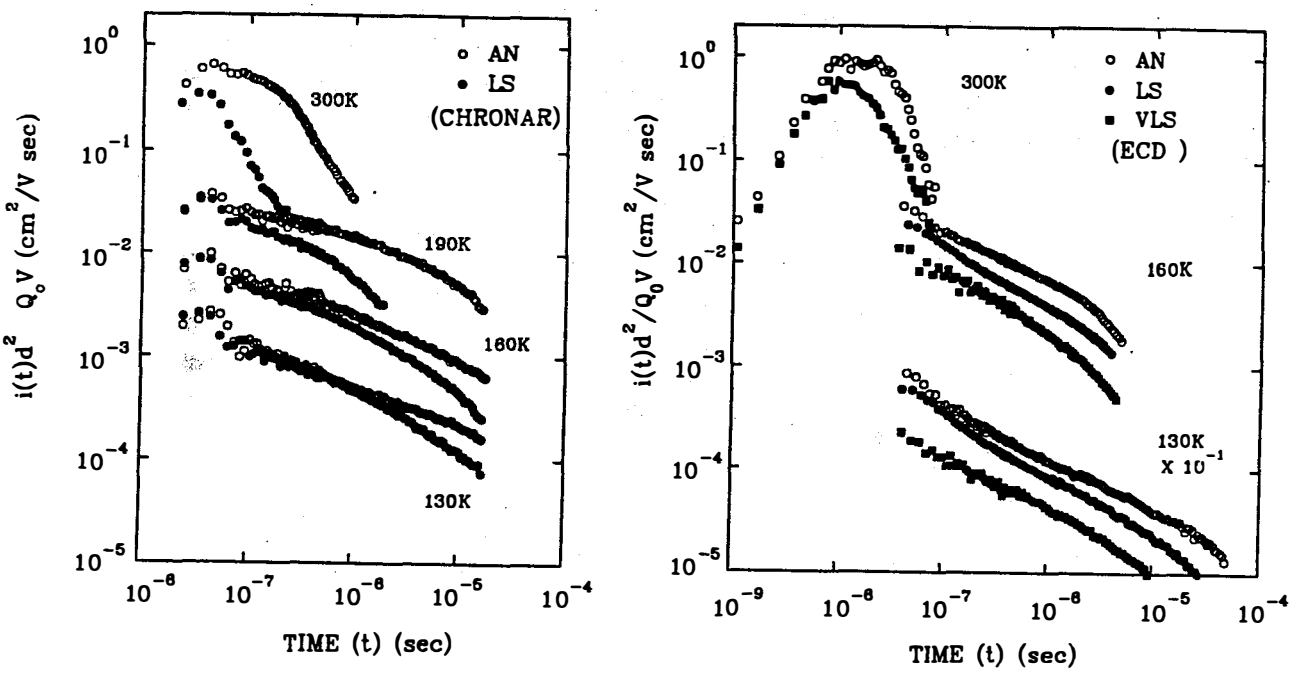

Fig. 1: (*left*) Mobility-normalized transient photocurrents for a 10 μm thick a-Si:H p-i-n diode prepared at Chronar, Inc.. Two specimen states are illustrated: AN - annealed, $\mu\tau_{e,t} = 4.4 \times 10^{-7}$ cm^2/V. LS - light-soaked, $\mu\tau_{e,t} = 4.2 \times 10^{-8}$ cm^2/V. (*right*) Mobility-normalized transient photocurrents for a 2.65 μm thick a-Si:H p-i-n diode prepared at Energy Conversion Devices, Inc.. Three specimen states are illustrated: AN - annealed, $\mu\tau_{e,t} = 6.6 \times 10^{-8}$ cm^2/V. LS - light soaked, $\mu\tau_{e,t} = 2.5 \times 10^{-8}$ cm^2/V. VLS - very light-soaked, $\mu\tau_{e,t} = 1.8 \times 10^{-8}$ cm^2/V.

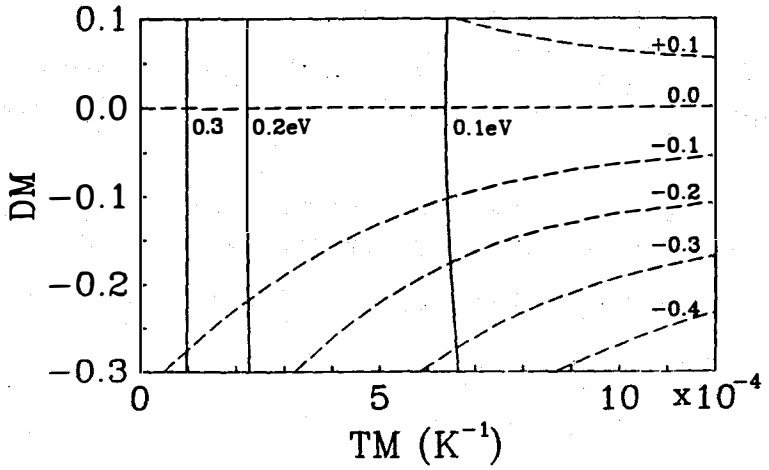

Fig. 2: Relationship of depletion-modulation $DM \equiv \partial N_s/\partial n$ and thermal modulation $TM \equiv (\partial(\ln N_s)/\partial T)$ for a simple model of defects incorporating a correlation energy U_{eff}. The dashed curves are contours generated assuming a constant electron density $(n - N_D)/N_D$ and varying the correlation energy U_{eff}. The solid curves are contours of constant correlation energy generated by varying the electron density.

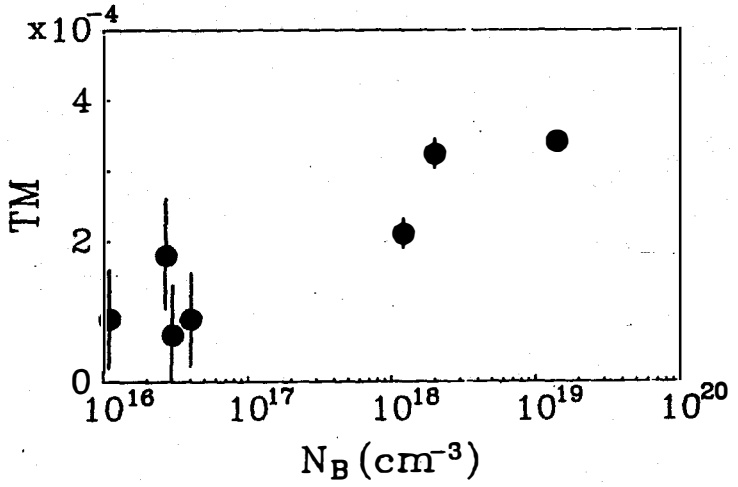

Fig. 3: Correlation of the thermal modulation of the spin density TM with the bulk spin density N_B for seven specimens of a-Si:H. High spin densities specimens were dominated by bulk behavior; a correction for the effects of interfacial spins was applied to the lower spin density temperature-dependence data.

Title: **Research on Amorphous-Silicon-Based Thin Film Photovoltaic Devices****

Organization: Solarex Corporation, Thin Film Division
826 Newtown-Yardley Rd., Newtown, PA 18940

Contributors: A. Catalano, Program Manager; L. Yang, Task I Project Leader; R.V. D'Aiello, Task II Project Leader; J. Newton, Task III Project Leader; M. Bennett, L. Chen, B. Fieselmann, Y.-M. Li, R. Podlesny, C. Poplawski, K. Rajan, S. Wiedeman, G. Wood

Introduction

Multijunction cells and modules offer the potential for achieving high conversion efficiency while overcoming the principal shortcoming of a-Si:H, namely the light-induced degradation. Amorphous silicon based devices are attractive because they are simply fabricated at low temperature from abundant non-toxic, low cost materials, have very high absorption coefficients which permit useful devices of submicron thickness, and the processes are environmentally responsible in keeping with the spirit of renewable energy.

In order to achieve the goal of developing low cost, stable, high efficiency modules, we have undertaken a program consisting of three tasks that address the important technological issues required to meet the program's second year (FY92) goal of obtaining 10.5% efficient, stable modules*. These tasks are 1) semiconductor materials research, 2) non-semiconductor materials research, and 3) module research.

Notable accomplishments within these tasks are:

- The demonstration of aperture area conversion efficiencies of 9.89% in modules with an area > 900 cm^2, and 98% area utilization.
- The demonstration of only 10% - 15% degradation in triple junction cells and modules.
- The development of a quantitative model based on the stretched exponential model that relates the time dependent performance of triple junction devices to device design, and operating parameters.
- A major improvement in the transport properties of a-SiC:H using novel feedstocks that will permit the fabrication of high efficiency a-SiC:H/a-Si:H/a-SiGe:H.

---

* 600 hrs., AM1.5 exposure, 50°C; area ≥ 900 cm^2.

** This work was supported under National Energy Renewable Laboratory ZM-19033-1.

- The development of improved front and rear ZnO contacts.

The following is a review of progress on a task-by-task basis.

Task I: Semiconductor Materials Research

An initial small area cell conversion efficiency of 12.5% is desirable, given an anticipated degradation of 15% in a triple junction device and the other losses associated with module design (loss of active area, etc.). In order to achieve this goal, we require a higher open circuit voltage, in the range of 2.5V, than is now obtained in state-of-the-art a-Si:H/a-Si:H/a-SiGe:H devices. Hence, we have begun an aggressive campaign to develop a-SiC:H alloys with acceptable transport properties and stability. This program has already yielded films and devices with excellent properties.

We have sought to develop improved a-SiC:H alloys by employing the paradigm that feedstock gases which incorporate the requisite Si-C bonds will give rise to such desirable bonding in the solid and hence improved transport properties. We have employed in-house synthesized tri- and di- silylmethanes (TSM, DSM) and conventional hydrogen diluted methane in order to develop the necessary film deposition processes, and fabricate the first devices whose performance and stability have been evaluated. The latter issue, stability, is of principal concern with a-SiC:H since previous experience has shown them to be less stable than a-Si:H. Experiments on films have now shown conclusively that the novel feedstocks, particularly TSM, give rise to 1.9 - 2.0 eV with excellent transport and optical properties (1). Figure 1 plots the ambipolar diffusion length of a-SiC:H films prepared from these new feedstocks as well as those prepared from the conventional source, methane.

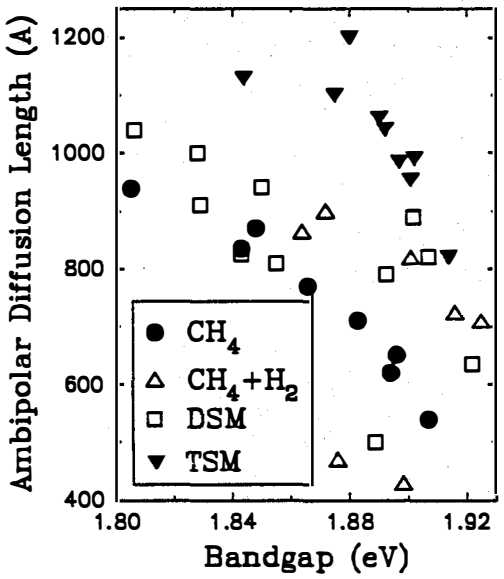

Figure 1. Ambipolar diffusion length for a-SiC:H films prepared from methane and DSM and TSM feedstocks.

Substrate temperature has been found to have a strong influence on film properties. The usual measure of electro-optic properties, e.g., diffusion length, photoconductivity, etc., are found to improve at low substrate temperature in contrast with reports of the opposite effect in the literature. This careful study has been done on material of the ***constant 1.96 + 01 eV bandgap.*** The measured properties of the best quality undoped films were found to depend strongly on thickness suggesting a strong influence of surface effects.

The first devices fabricated show that the improved transport properties of the films, translate into better device performance. a-SiC:H devices prepared from DSM proves even better than expected based on film properties. Most importantly, the devices prepared from TSM and hydrogen diluted methane show very good stability compared to conventional a-SiC:H devices. The stability of the devices appears to be comparable to a-Si:H.

In order to design the highest efficiency, stable devices it would be useful to have a quantitative, predictive model for the degradation process. We have succeeded in transforming the stretched exponential model developed by Redfield and Bube (2) which predicts the effect of light exposure on defect density to devices, and confirmed its quantitative, predictive nature by experiment. The model has also been expanded to include the effect of i-layer thickness. High intensity illumination has been used to degrade cells to saturation, confirming that the degradation process does indeed level-off after prolonged illumination. Figure 2 illustrates this behavior for a 4000Å thick device degraded at 100°C at several intensities. The high intensity degradation process can be used to rapidly assess the stability of devices and anticipate AM1.5 performance. The extension of this model to the alloys should enable a quantitative prediction of multijunction efficiency.

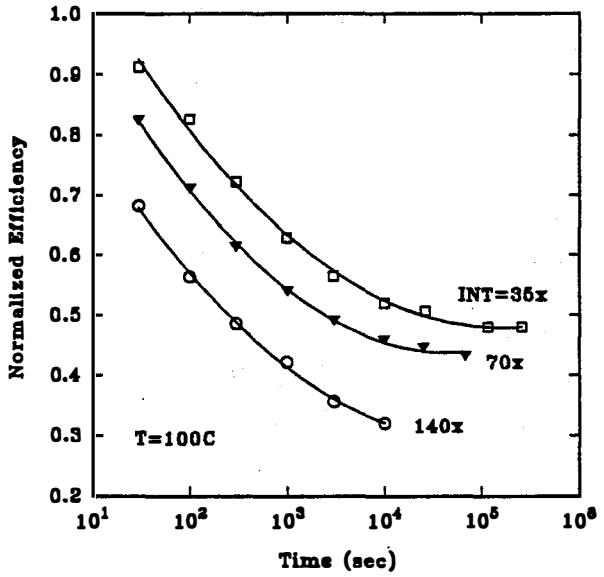

Figure 2. Normalized efficiency vs. time for devices subject to accelerated degradation.

The performance of a-SiGe:H devices has been improved and stability further quantified confirming earlier reports of better stability for this alloy. Optimization of the grading of the p/i and the i/n interfaces has occurred leading to devices with ~ 9% conversion efficiency for 1.48 eV bandgap cells with i-layers only 1200Å thick! Moreover, the stability of a-SiGe:H devices is clearly superior to conventional a-Si:H devices. Since the degradation process is recombination-driven, comparison of devices on the basis of short-circuit current is appropriate. The short-circuit current determines the maximum recombination rate for a given device. Furthermore, in a two-terminal multijunction cell, the short-circuit currents (hence, recombination rates at V_{OC}) are identical in each junction adding to the value of this comparison. Viewed in such a manner, a-SiGe:H alloy devices are more stable than a-Si:H and the stability improves with Ge addition. The data shown in Figure 3(a) plots the absolute and Figure 3(b) normalized efficiency after 1000 hours obtained from light-soaked cells prepared with various i-layer thicknesses. It can be seen that a-SiGe:H achieves a stabilized efficiency greater than at high generation-recombination levels (J_{SC}). The same trend is evident in the normalized data of Figure 3(b). At low current, the superior transport properties and V_{OC} of a-Si:H yield a higher efficiency.

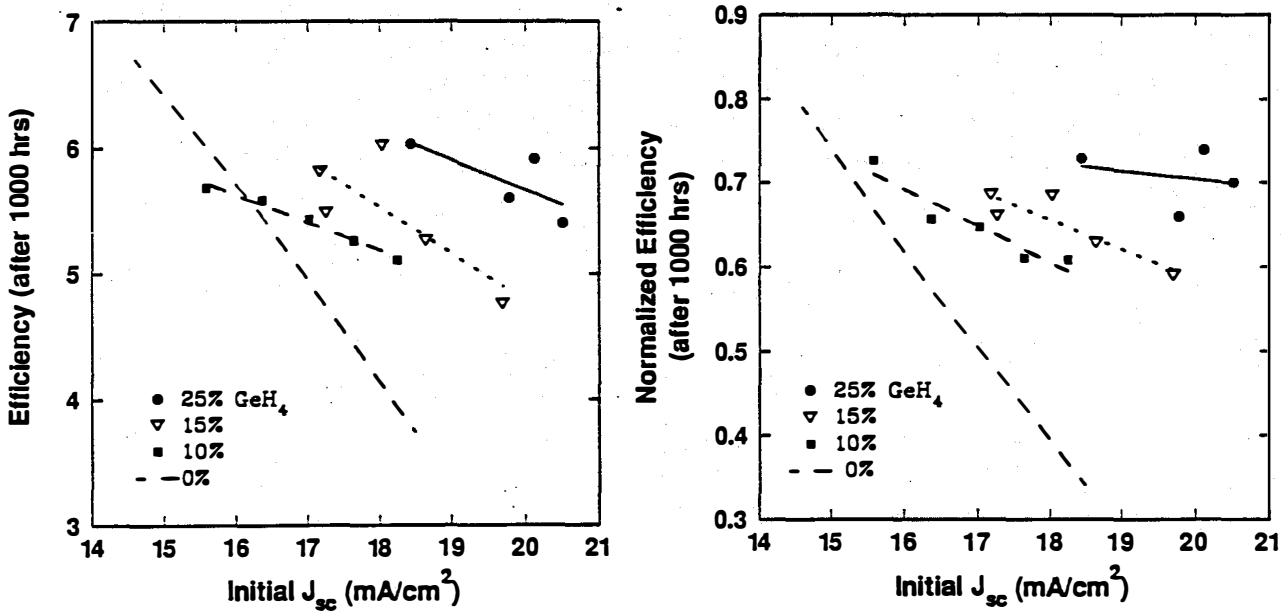

Figure 3. a) Absolute and b) normalized efficiency vs. initial J_{SC} for a-Si:H and a-SiGe:H devices prepared over a wide range of i-layer thickness.

Task II: Non Semiconductor Materials

Development of an atmospheric pressure chemical vapor deposition (APCVD) process of textured ZnO has begun in a newly constructed belt furnace. Diethylzinc, ethanol, and water are used as the reactants while both hydrogen fluoride and hexafluoropropylene (HFP) have been employed as dopants. Process development has proceeded by exploring the range of reactant flows, dopant concentrations and substrate temperature on growth rate, haze (texture), resistivity and

transmission. The films grown by APCVD appear to be comprised of spherical nodules compared to films grown by low pressure CVD which have well-defined crystal faces. Device quality films have been prepared which have a higher optical transmission compared to the present APCVD tin oxide of the same sheet resistance. Devices fabricated on the films confirm the higher optical transmission and have exhibited quantum efficiencies as high as 90% without anti-reflecting coating, indicating a net film absorption of about 5%. Further work, however, is necessary to optimize both the device fabrication process on ZnO and obtain better control of the APCVD process.

Low iron glass has been evaluated as a substrate material to replace the Corning 7059 glass generally used. Optical absorption measurements indicate, and device preparation and measurement confirm that the low iron glass is an effective, low cost substitute.

Task III: Submodule Research

Solarex has demonstrated close to 10% conversion efficiency using a 936.3 cm^2 triple junction device structure. This is the highest conversion efficiency measured to date for a device of this size. Table 1 summarizes the parameter for this module.

Table 1

V_{oc}, Volts	I_{sc}, mA	Fill Factor, %	Power, W	Aperture Efficiency, AM1.5	Aperture Area cm^2
56.7	243	67	9.23	9.82	936.3

Shunting defects in both cells and modules give rise to an anomalous light-induced degradation. The degradation takes place at a higher rate than in samples exhibiting few shunts and frequently gives rise to an increasing rate of degradation at long times. Although the mechanism is unclear, the origin of the defects appears to be large asperities in the tin oxide film formed by ~ 5 μm chunks of the oxide that have spalled off the APCVD furnace or belt. Because these particles are located at the periphery of the substrate, they can be minimized by laser scribing the module to confine the active area of the module away from the edges. Doing so results in a substantial improvement in not only stability, but also the distribution of initial cell and module efficiencies. The relationship between the extent of the leakage current and performance has been quantified. Light soaking studies have shown that the degradation of the module, after 600 hours, can be reduced from in the range of over 30% to 17% - 20% by minimizing the shunt current.

The extent of the leakage current appears to depend on the thickness of the junctions of the device including the doped layers, with the greatest thickness giving rise to the lowest shunt currents.

NREL has completed light-soaking studies of some of the Solarex first generation triple junction modules. After 600 hours of exposure at AM1.5, the modules have exhibited 17% - 22%

degradation from initial efficiencies in the range of 8.6% to 9.05%. These modules were fabricated before the importance of shunts was recognized.

There has been some suggestion that the rear contact might be involved in the anomalous degradation of modules since shunting defects reappear after curing in modules with ZnO/Ag rear contacts unlike modules with Al rear contacts. In fact, triple junction modules with Al rear contacts exhibit far lower degradation (~10%) than their ZnO/Ag backed counterparts. This may be due to the imbalance in the triple junction device. Thin device (2000Å middle junction) modules, without this imbalance, exhibit degradation at a rate similar to ZnO/Ag.

References

1. Y.M. Li and B. Fieselmann, Appl. Phys. Lett. **59** (14), 1720 (1991).

2. D. Redfield and R.H. Bube, Appl. Phys. Lett. 54, 1037 (1989).

Major Project Reports

"Research on Stable, High-Efficiency, Amorphous Silicon Multijunction Modules", A. Catalano, Program Manager, M. Bennett, L. Chen, B. Fieselmann, Y. Li, J. Newton, R. Podlesny, S. Wiedeman, L. Yang, Annual Technical Progress Report for the Period 1 May 1990 to 30 April 1991, April 1991, Prepared Under Subcontract No. ZM-0-19033-1.

Title: **Research on Stable, High-Efficiency Amorphous Silicon Multijunction Modules**

Organization: United Solar Systems Corp.
1100 West Maple Road
Troy, Michigan 48084

Contributors: S. Guha, principal investigator, A. Banerjee, E. Chen, T. Glatfelter, G. Hammond, M. Hopson, N. Jackett, M. Lycette, T. Palmer, A. Pawlikiewicz, I. Rosenstein, R. Ross, D. Wolf, J. Yang and K. Younan.

Objective

The principal objective of the program is to conduct research on semiconductor materials and non-semiconductor materials to enhance the performance of multi-bandgap, multijunction, large-area amorphous silicon-based alloy modules. The goal is to demonstrate stabilized module efficiency of 8% for multijunction panel of area greater than 900 cm^2.

Approach

Double-junction and triple-junction cells are made on Ag/ZnO_x back reflector deposited on stainless steel substrates. a-SiGe alloy is used for the *i*-layer in the bottom cell; the other cells use a-Si alloy. After evaporation of antireflection coating, silver grids and bus bars are put on the top surface, and the panel is encapsulated in a EVA/Tefzel structure to make a one-square-foot monolithic module.

Status/Accomplishments

- Uniform deposition of back reflector, a-Si alloy layers and transparent conducting oxide was achieved over one-square-foot area. The uniformity was checked by making an array of 16 x 5 subcells of 7.4 cm^2 area over the entire surface. The variation in subcell short-circuit density was within ± 5%.

- High quality a-SiGe alloys were deposited over large area, and single-junction cells were fabricated with an output of 3.2 mW/cm^2 under global AM1.5 illumination with a 630 nm red cut-on filter. These cells were used as the bottom cell of double-junction and triple-junction structures.

- A new method was developed [1] by which the performance of single-junction cells after long-term, one-sun exposure at 50°C can be predicted by exposing cells to short-term intense light at different temperatures. Using this method, we found that single-junction cells show the highest stabilized efficiency when the thickness of the intrinsic layer is about 2000 Å.

- Our numerical model for solar cells [2] was used to explain the light-induced degradation behavior of single-junction cells [3]. The experimental data on thick cells, both in the undegraded and degraded states, could be explained by assuming that the only effect of prolonged light illumination is an increase in the gap state density. In order to obtain quantitative agreement with the data for cells with different thicknesses, we had to assume that the optical absorption (or number of reflections) increases with cell thickness. The problem is being further investigated.

- We have fabricated a series of double-junction and triple-junction modules in which the grid loss is about 4%. The following table summarizes results of three double-junction and two triple-junction fully encapsulated modules as measured under USSC SPIRE simulator.

Table I. Performance of multijunction panels.

Sample No.	Aperture Area	V_{oc} (V)	I_{sc} (A)	FF (%)	η (%)
588	919.3	1.60	8.70	65	9.90
597	918.1	1.60	8.09	68	9.57
598	912.0	2.45	5.37	67	9.59
602	919.9	1.60	8.07	68	9.60
603	905.4	2.45	4.80	70	9.15

The same modules, however, show 15 to 18% lower efficiencies when measured under NREL SPIRE simulator. The major discrepancy is in the fill factor and short-circuit current density. The discrepancy in the measurements is now being investigated.

References

1. Semi-Annual Report on NREL Subcontract No. ZM-1-19033-2, July 1991.

2. A. Pawlikiewicz and S. Guha, IEEE ED-37, 403, 1990.

3. A. Banerjee, S. Guha, A. Pawlikiewicz, D. Wolf and J. Yang, in Amorphous Silicon Materials and Solar Cells, AIP Conf. Proc. 234, ed. B. L. Stafford, American Institute of Physics, p. 268.

Title: **Research on Silicon-Carbon Alloys and Interfaces**

Organization: Coordinated Science Laboratory
University of Illinois, Urbana Illinois

Contributors: J. R. Abelson and N. Maley, co-principal investigators;
S. Yang and J. R. Doyle

Objective

We focus on the fabrication of the "top junction" formed by transparent conductive oxide (TCO) on p-type Si,C:H on undoped a-Si:H. Our deposition tool is magnetron reactive sputtering of the Si,C:H and a-Si:H layers because this method: (i) provides independent control of hydrogen incorporation via the pressure of H_2 injected in the sputtering gas; (ii) has been used in our labs to deposit device quality a-Si:H layers [1]; (iii) can make films with a slower rate of metastable defect formation [2]; (iv) produces a-Si,C:H with better microstructure than typical PACVD films [3]; and (v) is an industrially mature process for the mass production of thin film coatings.

We use in-situ techniques to analyze films and interfaces. Si-H and C-H bonding in films $\geq$ 5Å thick are measured by reflection–absorption infrared spectroscopy (RAIRS) [4]. The electrostatic potential profile across the different layers of the top junction is measured by a Kelvin probe (KP). The combination of RAIRS and KP is intended to elucidate the fundamental relationships between deposition conditions, bonding, and electronic performance.

Approach

a-Si,C:H Growth

We are investigating two methods to introduce carbon into a-Si:H: (i) co-sputtering independent targets of Si and C, and (ii) introducing methane into the (Ar + H_2) working gas of Si sputtering.

Co-sputtered a-Si,C:H films have been deposited to investigate the variables of carbon content (0 - 30 at. %), hydrogen partial pressure (0.2 - 2.5 mTorr) and substrate temperature (170 - 330°C). We find that the hydrogen partial pressure must always be kept high ($\geq$ 0.8 mTorr) to attain a high energy gap when carbon is added. At smaller hydrogen pressures, C actually reduces the energy gap below that of standard a-Si:H: for example, at 0.2 mTorr H_2, the addition of ~20 at. % C drops E_g from 1.7 to ~1.6 eV! This indicates a tendency to form sp^2 bonded C. The AM1 photo- to dark-conductivity ratios have consistently been $\geq 10^4$, and the absolute value of photoconductivity is $\leq 4 \times 10^{-7}/\Omega$-cm.

However, co-sputtered a-Si,C:H films have proven inferior to those produced by reactive sputtering in methane (see below). The former exhibit lower temperature thermal evolution peaks, more SiH_2 or clustered SiH in IR absorption at 2100 cm^{-1}, and inferior photoconductivity. In addition, considerable oxygen content is detected beneath the surface by XPS, suggesting that oxygen permeates through a porous microstructure upon exposure to atmosphere.

The poor quality of these films likely results from inherent difficulties in sputtering a carbon (graphite) target: after some use, "soft" C deposits are found on the target and neighboring shields. These probably sputter as small clusters rather than individual atoms, and thus spoil the a-Si,C:H microstructure. However, this phenomenon should not occur with a SiC target, so the dual target technique may merit future investigation with Si and SiC as the two solid sources.

Methane sputtered a-Si,C:H films have been deposited by sputtering a single Si target (5 cm diameter) in (Ar + H_2 + CH_4), denoted hereafter as Si/CH_4 sputtering. By varying the partial pressure of hydrogen (0 - 1.0 mT) and methane (0 - 0.10 mT), the substrate temperature (200 - 400 °C), and the target current (50 - 100 mA), we have grown alloy films with Tauc energy gaps ranging from 1.70 to 2.45 eV. Infrared and thermal evolution spectra reveal interesting differences between SiH_4/CH_4 PACVD and Si/CH_4 sputtering. For comparable Tauc gaps, the latter are denser and show considerably less C-H bonding. The carbon content in these films, measured by sputtered neutral mass spectroscopy, is ~15-20% for films with a Tauc gap of 2.0 eV.

The electrical properties of the Si/CH_4 sputtered films have been evaluated by photo (AM1) and dark conductivity and sub-gap absorption (CPM, dual beam photoconductivity, and PDS at Solarex). Photoconductivity decreases gradually from mid 10^{-5} S/cm to mid 10^{-7} S/cm as the band gap is increased from 1.7 to 2.1 eV, and more rapidly thereafter (see Figure 1). The ratio of photo to dark conductivity is between 10^4 and 10^5 for E_g up to 2.1 eV. Sub-gap photoconductivity spectra yield defect densities in the mid 10^{16} /cc range and band tail slopes between 70 and 80 meV.

The IR spectra show interesting features, most notably a low intensity of C-H modes (see Figure 2). In films grown from SiH_4/CH_4 PACVD there is a strong tendency for C-H clustering and the C-H stretching (~2900 cm^{-1}) and wagging (~1400 cm^{-1}) modes are strong. For a comparable Tauc gap, the C-H stretching mode is 2-3 times weaker in the Si/CH_4 sputtered films, and the C-H wagging mode is small enough that it is difficult to observe above the background atmospheric absorption. Figure 2 also shows that the Si-H stretching mode is predominantly at 2000 cm^{-1} in these films.

In general, the Tauc gaps of the Si/CH_4 sputtered films increase with hydrogen and carbon content. However, the correlation between the band gap and film composition is not very strong (see the variation of the C-H stretching mode with E_g in Figure 2, for example). We thus believe that the band gap is also sensitive to the details of local ordering such as bond length and bond angle distortions and sp^2 vs sp^3 bonding of carbon.

Thermal evolution spectra show that the hydrogen content of the Si/CH_4 sputtered films is ~1.0 - 1.5×10^{22} atoms/cc for Tauc gaps up to 2.1 eV. The spectra typically consist of two overlapping peaks at 600 and 700 °C, a narrow peak ~950 °C (possibly due to crystallization), and a broad peak ~1050 °C. Most of the H_2 release occurs in the 700 °C peak, in contrast to PACVD material where there is considerable release of H_2 in the low temperature peak. This is consistent with IR observations that the microstructure is denser for the Si/CH_4 sputtered material.

In-Situ Kelvin Probe

A Kelvin probe, suitable for in-situ studies of a-Si:H growth, was constructed and installed in an environmental chamber for "shakedown" trials. Our first experiments concerned the influence of water vapor adsorption on the surface potential in a co-planar conductivity geometry [5]. Water chemisorbs as a donor, i.e., the surface accumulates positive charge, the semiconductor bands bend "down", and an n-type conductivity channel forms beneath the surface. Figure 3 shows the effect of water vapor adsorption on an a-Si:H film of bandgap 1.75 eV. The conductivity increases monotonically with surface potential. The slow initial increase in conductivity followed by the more rapid rise indicates that the dry, annealed surface is close to the flat-band condition.

In a second set of trials, we studied the effect of surface potential on the power law exponent of photoconductivity ($I \sim G^{\gamma}$). Figure 4 shows the difference in the apparent γ between a dry,

annealed surface and one with ~0.3 eV n-type surface band-bending. These results explicitly demonstrate the influence of band-bending on photoconductivity and are being further analyzed.

Future Work

Gas handling equipment for p-type doping and hardware for in-situ Kelvin probe studies are under construction. Evaluation of the long term stability of the carbon alloys is also underway as we now have a set up for accelerated light soaking which provides 1 W/cm^2 of red light or 3 W/cm^2 of heat-filtered white light. Special substrates allowing RAIRS analyses of a-Si:H and a-Si,C:H growth over TCO are being prepared. These developments will pave the way for our examinations of the solar cell "top junction."

References

1. M. Pinarbasi, N. Maley, A. Myers and J. R. Abelson, "Hydrogenated Amorphous Silicon Deposited by Reactive Sputtering - the Electronic Properties, Hydrogen Bonding and Microstructure," Thin Solid Films 171, 217 (1989).

2. M. Pinarbasi, M. J. Kushner, and J. R. Abelson, "Effect of Hydrogen Content on the Light Induced Defect Generation in DC Magnetron Reactively Sputtered a-Si:H," JAP 68(5), 2255 (1990).

3. N. Maley, to be published.

4. M. Katiyar, G. Feng, J. R. Abelson and N. Maley, "Real-Time, Infrared Reflectance Studies of the Growth of Hydrogenated Amorphous Silicon by Reactive Magnetron Sputtering," to be published in JVST (1991).

5. J. Abelson and G. deRosny, "The Relation Between Planar Conduction and Contact Potential as a-Si:H Films Undergo Gas Adsorption or Temperature Changes," Journal de Physique 44 , 993 (1983).

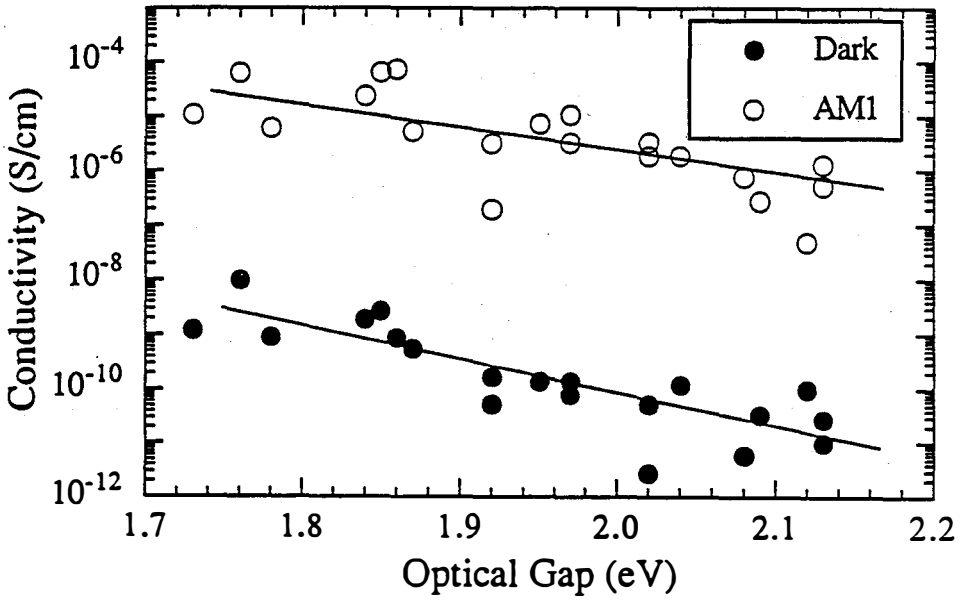

Figure 1
Photo and dark conductivity as a function of optical gap for a-SiC:H films grown by sputtering Si in ($Ar+H_2+CH_4$).

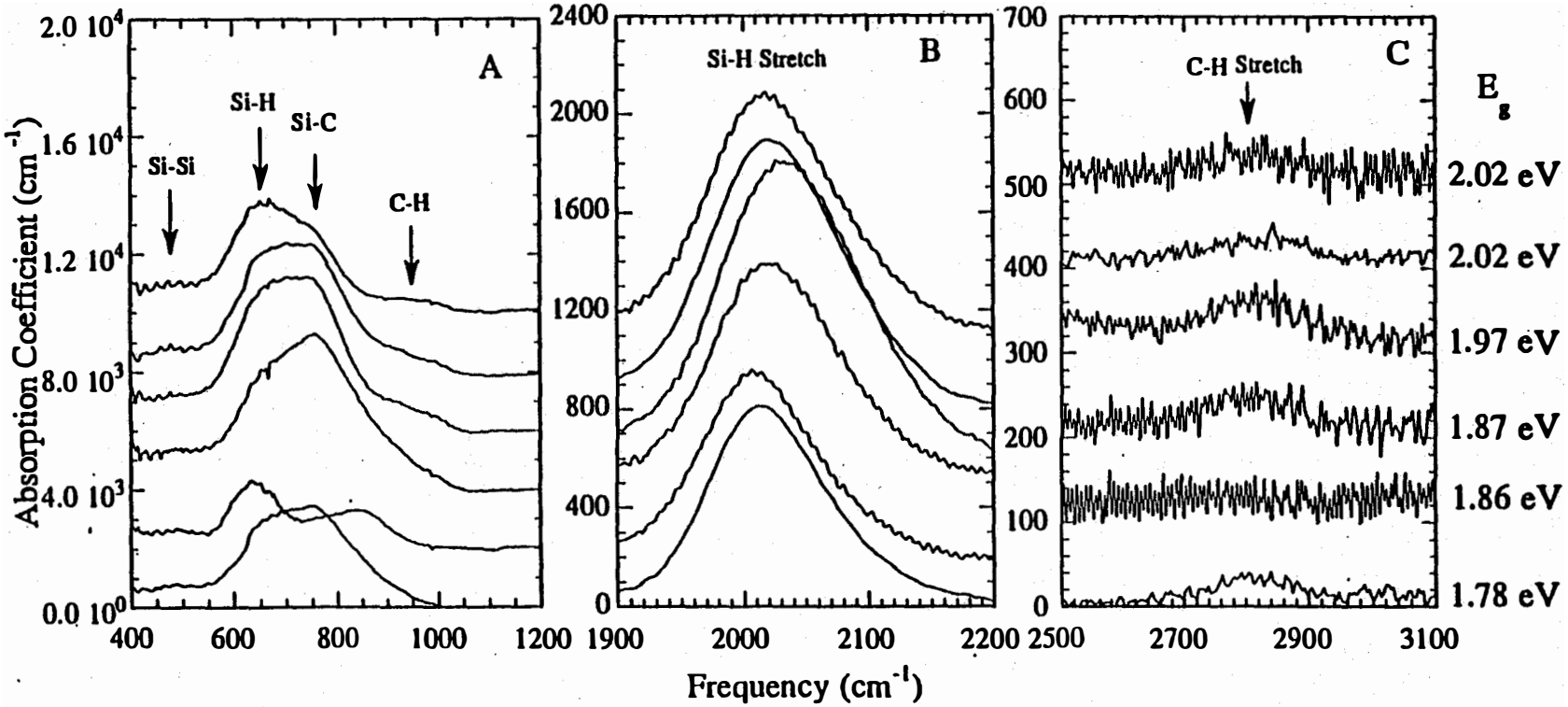

Figure 2
IR spectra of a-SiC:H samples grown by sputtering Si in ($Ar+H_2+CH_4$).
Spectra have been offset vertically for calrity.

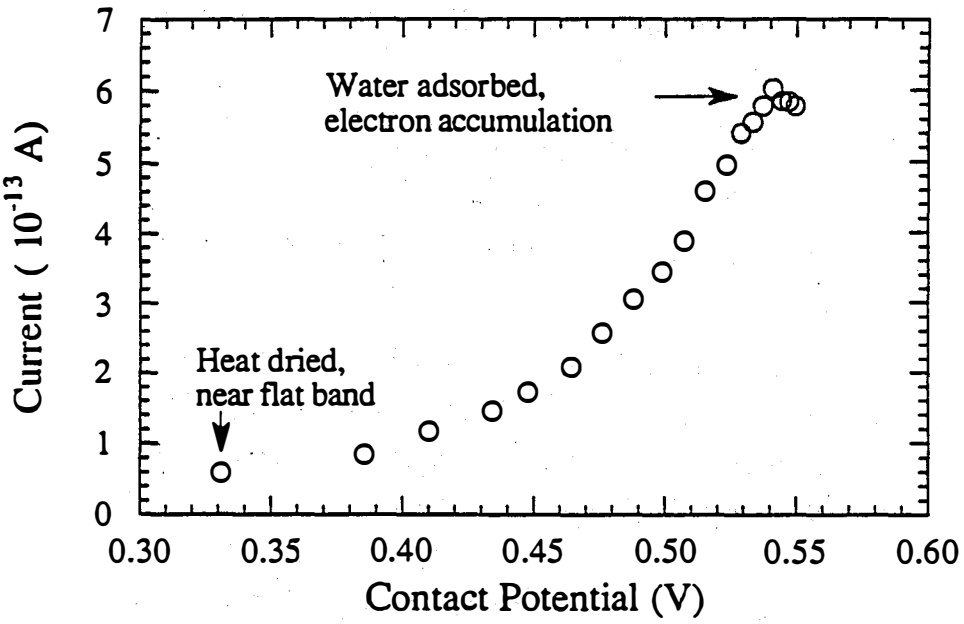

Figure 3
Effect of water vapor adsorption on the surface potential and co-planar dark conductivity of an a-Si:H film.

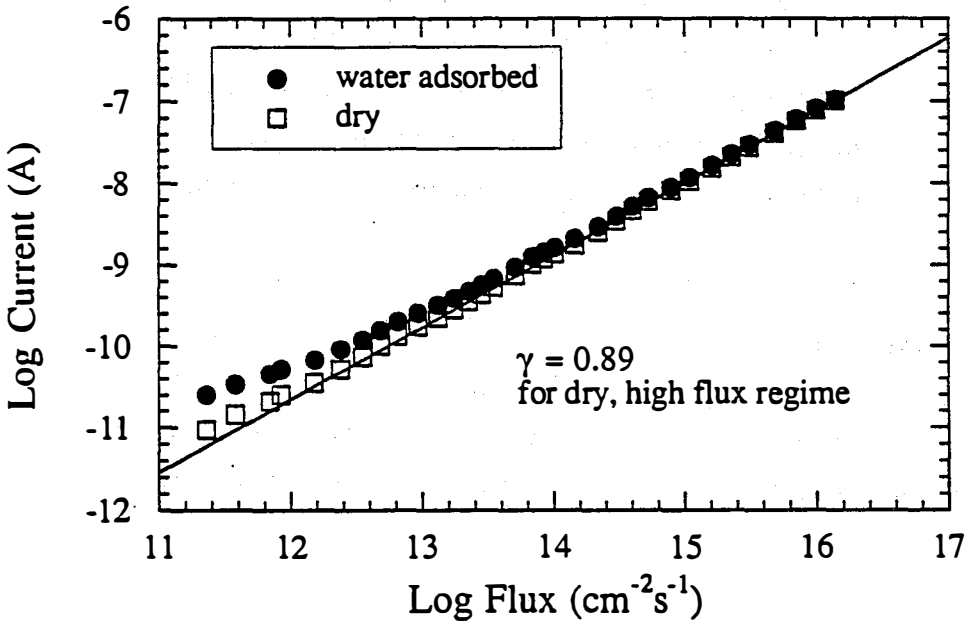

Figure 4
Effect of water vapor adsorption on the photoconductivity γ factor of an a-Si:H film.

Title: **RECOMBINATION AND METASTABILITY IN AMORPHOUS SILICON AND SILICON GERMANIUM ALLOYS**

Organization: Department of Physics and Astronomy
University of North Carolina
Chapel Hill, NC 27599-3255

Contributors: M. Silver, Daxing Han, Keda Wang and M. Kemp

The objectives of our research were (1) to determine how recombination, trapping and band mobility modifications affecting the electronic properties of amorphous semiconductors can be characterized and described by an appropriate spectrum of defect states and (2) how light induced defects (SWE) in a-Si:H and native defects in a-Si Ge:H affect the transport properties in these materials.

Experimentally we continued our studies on transient space charge limited current in a-Si:H n-i-n structures, on forward bias current and on electroluminescence in a-Si-:H p-i-n structures before and after photodegradation. The most interesting part of our data shows that while the steady state value of the forward bias current does not change much with SWE, the transient current is significantly altered. We tentatively assume the response-time governing the transient rising and the lifetime governing the steady state current result from different mechanism Theoretically, we have shown that in recombination, the coulomb interaction gives rise to two radiative lifetimes; one due to nearest neighbor recombination and the other due to a transport-controlled lifetime. We have calculated the relative contribution of geminate recombination at low temperature as a function of excitation density. Further, we have also calculated how the magnitude of the radiative lifetime varies with excitation.

Experimental Research

In figure 1 we show the transient double injection current vs voltage for an annealed sample. It is clear that the time for the current to rise depends upon the applied voltage. In fact, the product of the rise time and the maximum current is nearly constant. On the other hand, it was found that after photodegradation (SWE) the steady state current didn't change significantly at room temperature but the rise time was delayed by decades in some cases (see figure 2). Consequently, the simple relationship seen in annealed samples that the current-rise time product equals a constant does not hold. One possible explanation is that the deep recombination centers produced by the SWE are hole traps and control the rise-time (if the rise time is controlled by hole migration) while the final current at above 200K

is controlled by deep band tail states which are not significantly altered by the SWE. But at low T below 200K, the deep gap states including SW defects may again control the lifetime governing the steady state current. Figure 3 shows the change in the steady state current vs T before and after SWE. Notice, that at below 200K the steady state current drops a factor of 2-60 after light -soaking, while at above 250K it almost has no change.

Theoretical Research

Low temperature luminescence may have a geminate or non-geminate origin. We have shown that the coulomb interaction between electron and hole can play a crucial role providing that the width of the energy distribution of tail states is not too large, e.g. $kT_o < e^2/4\pi\varepsilon a$ where a is the mean distance between localized tail states. Further investigation of this problem showed that there were two dominant lifetimes (1) recombination controlled by the final jump between pairs located at nearest neighbor distances and (2) a transport determined lifetime which is controlled by a long jump between pairs.

Using these simple ideas we can calculate the relative contribution of geminate and non-geminate recombination and also the change in the radiative lifetime vs excitation density. These results are shown in figure 4. An interesting conclusion is that the transport-controlled geminate recombination is slower than the non-geminate process.

Publications:

1. "Comment on Theoretical Investigation of Transient Space-charge-limited Currents for Dispersive Transport in Amorphous Silicon", M. Silver, Daxing Han, Keda Wang and M. Kemp, Phil. Mag. Letts. 64 (1991) 379.

2. "Origin of the Low-temperature Drift Mobility Increase in a-Si:H", M. Kemp and M. Silver, Phil. Mag B63 (1991) 437.

3. "Influence of the Coulomb Potential on Photoluminescence", an invited talk in the 4th international conference on hopping and related phenomena, (Marburg, Germany, Aug 26-29, 1991).

4. "What Electroluminescence and Transient Space Charge Limited Currents Tell Us about Steabler-Wronski Effects", K. Wang, D. Han and M. Silver, Amorphous Silicon Materials and Solar Cells." AIP Conference Proc. 234, ed. by Byron L. Stafford, (New York, 1991), 162.

5. "Metastability in Hydrogenated Amorphous Silicon: the Adler Model Revised", H. M. Branz, R. S. Crandall and M. Silver, AIP Conf. Proc. 234, Amorphous silicon materials and solar cells, (AIP, New York, 1991) 29.

6. "Electroluminescence Studies of Recombination in Hydrogenated Amorphous Silicon p-i-n Devices", K. Wang, D. Han, M. Silver and H. Branz, Solar Cells, 30, (1991), 219.

7. "Temperature and Current Dependence of Electroluminescence in a-Si:H", Keda. Wang, Daxing. Han, M. E. Zvanut and M. Silver, Phil. Mag. B63, (1991) 175.

8. "Electroluminescence: a Study of Non-geminate Radiative and Non-radiative Bulk Recombination", K. Wang, D. Han, M. Kemp and M. Silver, 14th International Conference on Amorphous Semiconductors, Aug. 19-23, 1991,Garmisch, Germany, to be published in J. Non-Cryst. Sol. (1991).

9. "Light Induced Metastable Defects in a-Si:H Studied by Transient Space Charge Perturbed Currents", Daxing. Han, Keda. Wang and M. Silver, 14th International Conference on Amorphous Semiconductors, Aug. 19-23, 1991, Garmisch, Germany,to be published in J. Non-Cryst. Sol. (1991).

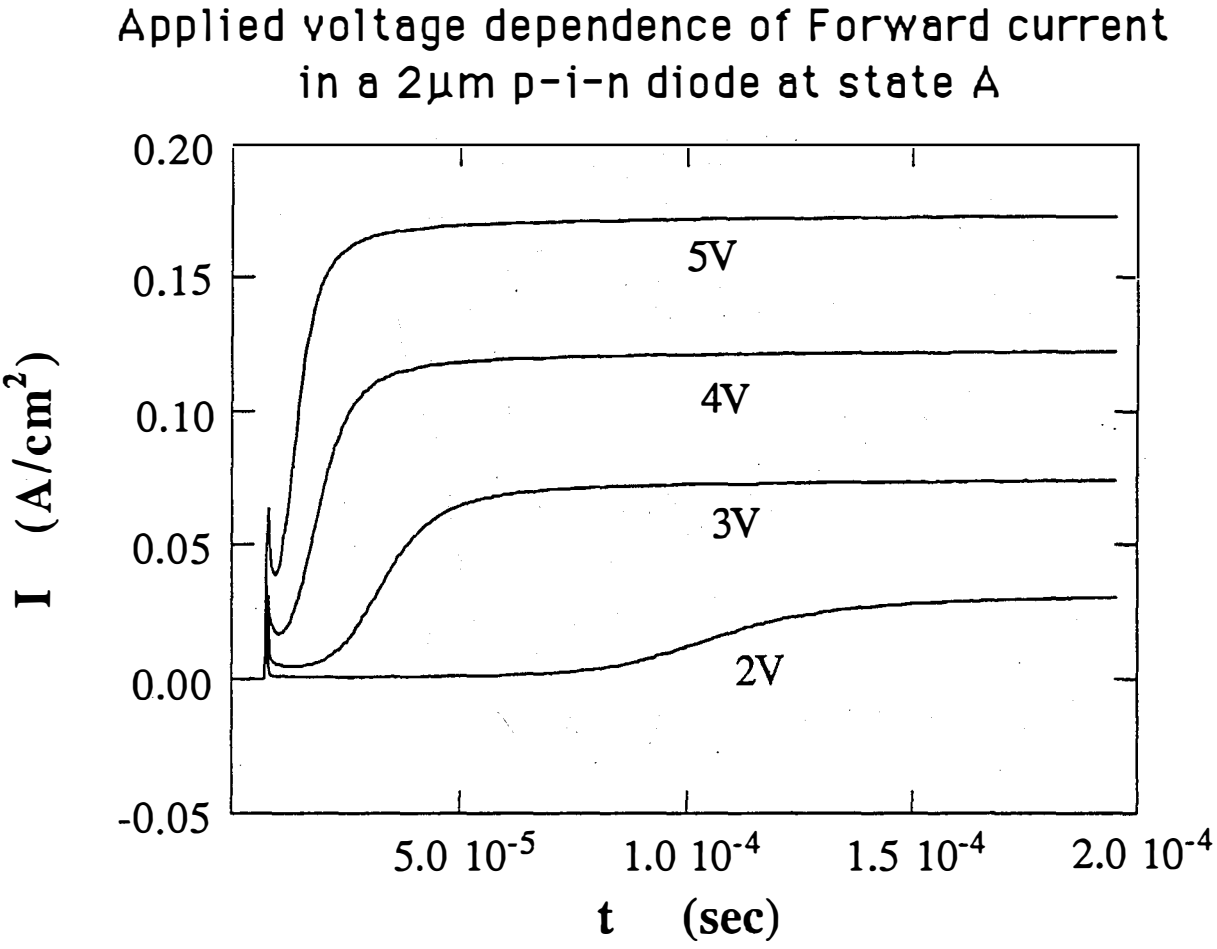
Applied voltage dependence of Forward current
in a 2µm p-i-n diode at state A
0.20
0.15
0.10
0.05
0.00
-0.05
I (A/cm²)
5V
4V
3V
2V
5.0 10⁻⁵
1.0 10⁻⁴
1.5 10⁻⁴
2.0 10⁻⁴
t (sec)

Fig. 1

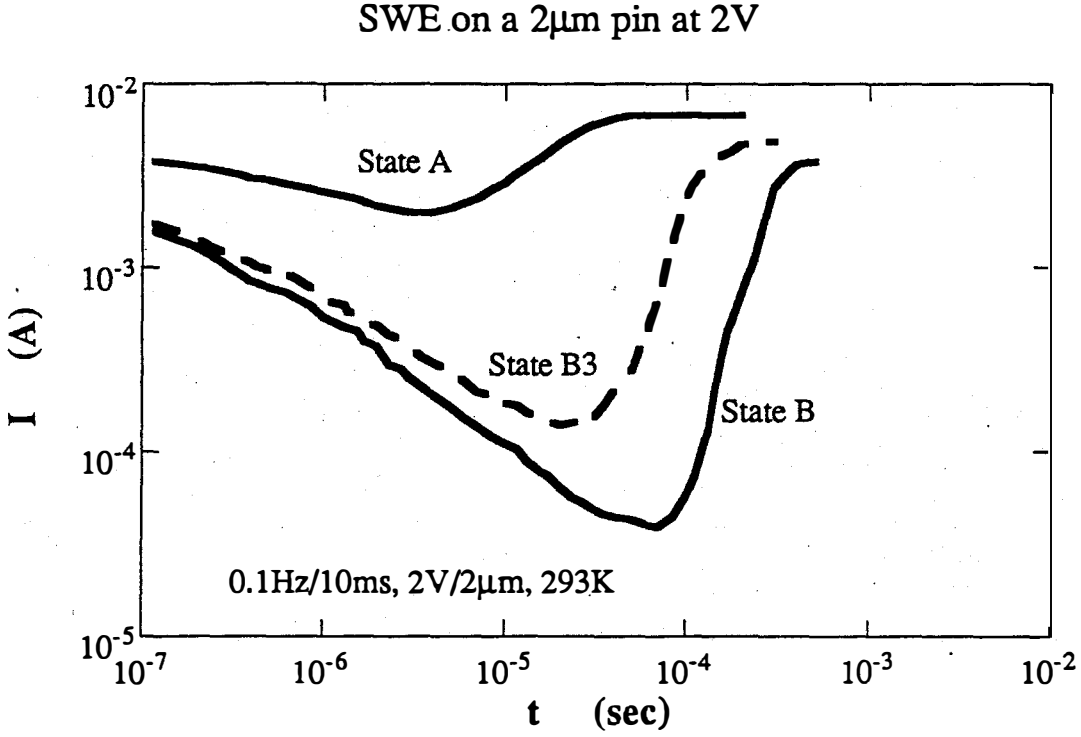
SWE on a 2μm pin at 2V
State A
State B3
State B
0.1Hz/10ms, 2V/2μm, 293K
I (A)
t (sec)
10-2
10-3
10-4
10-5
10-7
10-6
10-5
10-4
10-3
10-2

Fig. 2

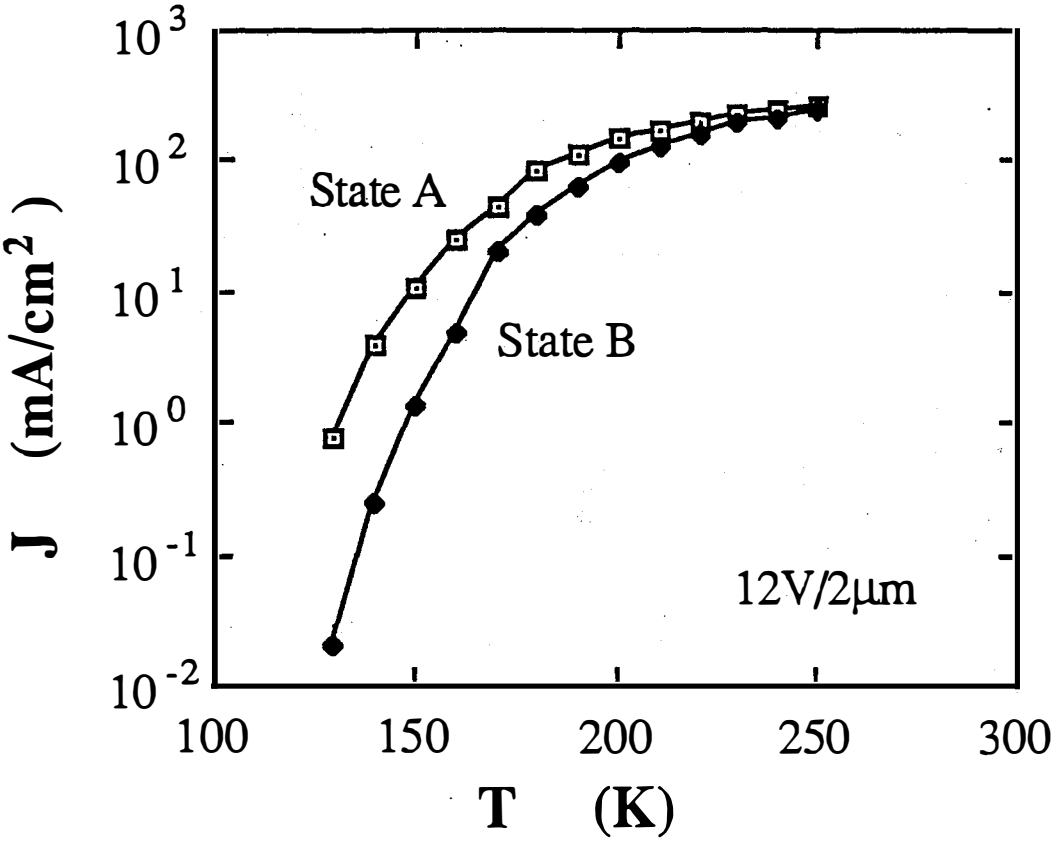
10^3
10^2
10^1
10^0
10^{-1}
10^{-2}
J (mA/cm^2)
State A
State B
12V/2μm
100
150
200
250
300
T (K)

Fig. 3

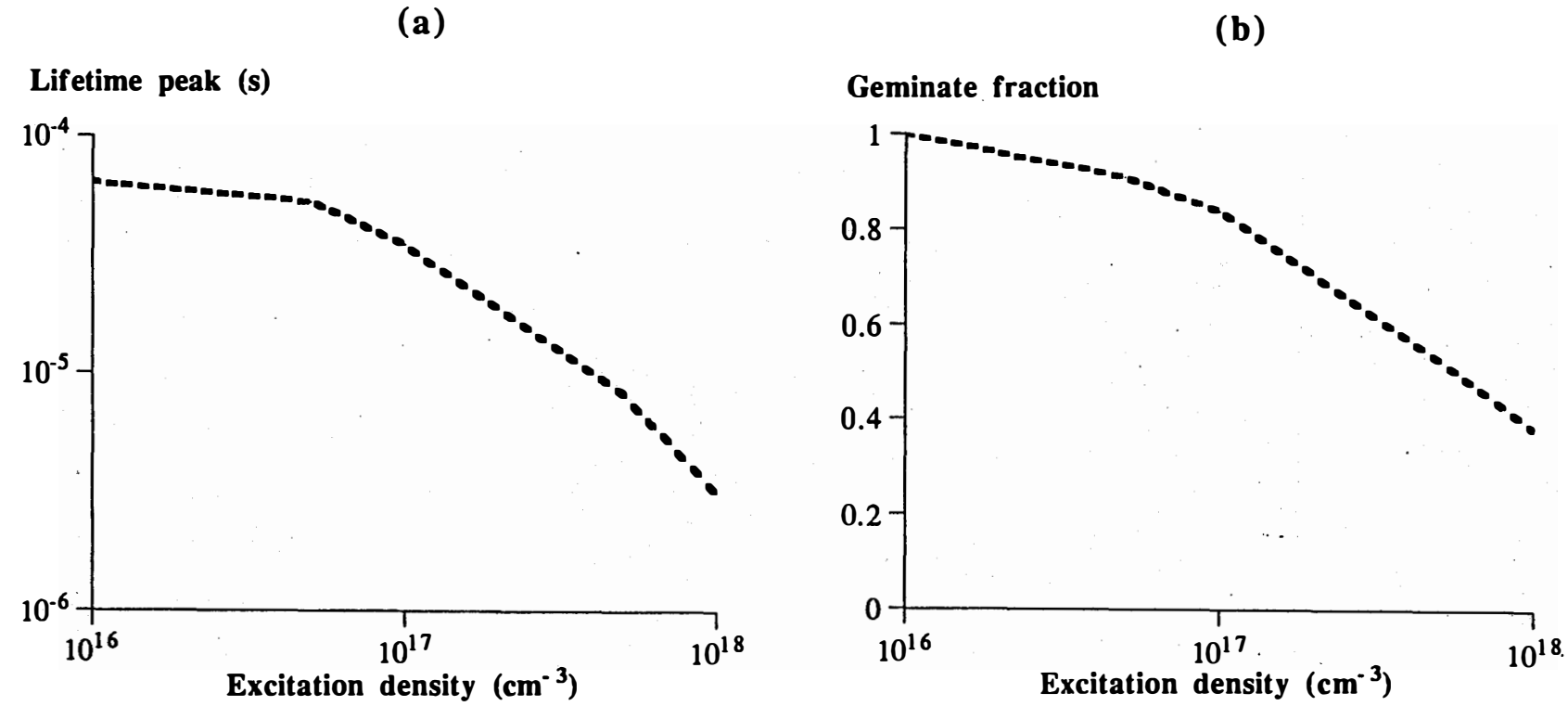
(a)
Lifetime peak (s)
10-4
10-5
10-6
10^16
10^17
10^18
Excitation density (cm-3)
(b)
Geminate fraction
1
0.8
0.6
0.4
0.2
0
10^16
10^17
10^18
Excitation density (cm-3)

Fig. 4

Title:	**Microscopic Origins of Metastable Effects in a-Si:H and Deep Defect Characterization in a-Si,Ge:H Alloys**
Organization:	University of Oregon, Eugene, Oregon
Contributors:	J. David Cohen, principal investigator; Randy Rasmusssen and Thomas Unold

The primary research goals of this program are to elucidate the basic mechanisms by which a-Si:H degrades with light exposure, and to study the defect structure in low bandgap a-Si,Ge:H alloys. During the past year we have concentrated our efforts on a determination of the basic defect properties of the low bandgap alloys.

Approach

We obtained several a-Si,Ge:H alloy samples of different compositions through a collaboration with C.M. Fortmann at the University of Delaware. These samples were grown on p^+ doped crystalline silicon substrates by the photo-CVD growth method, by decomposing a mixture of SiH_4 , GeH_4, and H_2 with UV radiation from a mercury vapor light source. A detailed account on the deposition method and the growth parameters has been published elsewhere[1]. Semi-transparent palladium contacts were deposited on the surface of our samples to serve as Schottky barriers for our junction capacitance measurements.

The experimental techniques employed to characterize the electronic properties of these samples included drive-level capacitance profiling[2] to deduce the midgap deep defect densities, and capacitance vs. temperature and frequency measurements to provide a cross check on the midgap defect densities and also to determine the activation energy of conductivity. We also employed two sub-band-gap optical spectroscopic methods: transient photocapacitance and junction photocurrent measurements. These latter methods, like other sub-band-gap optical methods, disclose the energy distribution of deep defects within the mobility gap and also the Urbach energy of the bandtail distribution of states. In addition, by comparing the photocapacitance and photocurrent spectra in detail, we are able to separate majority and minority carrier processes induced by the optical transitions. In particular, we are able to estimate a value of $(\mu\tau)_h$ for these samples. A more detailed discussion of how these data are analyzed in this fashion has been given previously.[3,4]

We will report results obtained on three of these samples: two with optical gaps near 1.3eV (implying a germanium fraction, x, of 0.6) and one pure a-Ge:H sample (with an optical gap near 1.07eV).

Results for a-Si,Ge:H Samples

In Fig. 1 we display transient photocapacitance and photocurrent spectra for one of our a-SiGe:H films. We have aligned the photocurrent and photocapacitance spectra in the low optical energy region, where only *electron* transitions from states in the gap to the conduction band occur. The fact that both spectra match almost perfectly over our range of optical energies is due to the lack of a hole contribution to the transient signal at this temperature. That is, this indicates that all of the photo-excited holes are re-trapped into gap states and are unable to escape the depletion region within the 0.4s time-window of the measurement.

Figure 2 shows spectra taken at the increased temperature T=330K. The obvious difference in current and capacitance signal for the higher optical energies is caused by the increased contribution of minority carriers to the transient signal. We have analyzed the spectra in Fig. 1 and Fig. 2 by considering the possible electron and hole transitions as depicted in Fig. 3. For low optical energies we expect only electrons to be excited to the conduction band (transition type 1) so that the spectra should match in this optical energy range. For optical energies approaching the gap electrons and holes will be excited into the conduction/valence band in equal numbers (transition type 3). We observe that for hν>1.2eV the two spectra do maintain a nearly constant ratio, R. This value of R can be directly related to the mobility lifetime product for holes, $(\mu\tau)_h$, and gives the value of 5×10^{-10} cm^2/V, in good agreement to values obtained for high quality glow discharge samples in this alloy range.[5]

For intermediate energies both electron excitation from the valence band into the gap (transition type 2), and from the gap into the conduction band (transition type 2') are possible. Within this regime our spectra show a somewhat unusual behavior not observed in our previous studies of a-Si:H[3]; namely, that the signal ratio R actually increases for values between 1.1eV<hν<1.2eV before it decreases monotonically to zero for hν<1.1eV. We interpret this as indicating a decreased contribution of the electronic part of the signal compared to the hole part in this intermediate energy range. This seems to indicate that electrons which are optically excited into an unoccupied defect band above E_F are not subsequently easily thermally emitted to the conduction band. This suppression of electron emission indicates that a large lattice relaxation is associated with this defect state. A similar conclusion has recently been obtained in some photo-induced absorption studies of a-Si,Ge:H alloys.[6]

A deep defect density was estimated by comparing these optical spectra with the drive-level profiling data and indicates a defect density of about 2 to 3×10^{16} cm^{-3} in a broad band located roughly mid-gap. A more pronounced narrow defect band exhibiting the lattice relaxation effects appears to be located roughly 1.1 eV above E_V. The Urbach energy, E_0, for this sample was determined to be 52 meV, indicating a fairly low level of intrinsic disorder for an a-Si,Ge:H sample in this alloy range.

The second a-Si,Ge:H sample studied indicated somewhat poorer qualities: a midgap defect density about 5 times higher, a value of E_0 near 57meV, and a value of $(\mu\tau)_h$ of only 3×10^{-11} cm^2/V. The results for both these samples are summarized in Table I.

Results for a-Ge:H Sample

We carried out similar junction-capacitance measurements on intrinsic a-Ge:H samples but were limited by the large defect density present in those samples. In particular, the small photoresponse prohibited sufficient signal strength for the photocapacitance measurement in the low energy regime. Thus, we were not able to deduce $(\mu\tau)_h$ products for our present samples.

The capacitance versus temperature measurements for our a-Ge:H samples clearly indicated the presence of a large defect band close to the Fermi level. By fitting our data to the capacitance response of a density of states composed of a gaussian-shaped defect band below E_c we deduced a defect density of $N_d \cong 9 \times 10^{17} cm^{-3}$ located in a defect band at approximately 0.5eV below the conduction band edge E_c. Despite the large defect density we determined an Urbach energy of 50meV which is comparable to values found for a-$Si_{1-x}Ge_x$ and a-Si:H samples with much lower defect densities.

Summary

Table I summarizes the key results determined for the three samples studied. These results indicate that a detailed comparison between transient junction photocurrent and photocapacitance spectra can yield detailed information not only about the deep defect distributions and transition energies in amorphous semiconductors, but also about the carrier mobilities. This comes from the unique aspect of capacitance measurements to distinguish between minority and majority carrier processes.

The results also indicate that such alloy samples grown by the photo-CVD method are of quite good quality when compared to similar optical gap alloys produced by the glow discharge method. During the upcoming year we will be extending our studies to a series of such samples that cover the complete range of germanium compositions.

References

1. Albright, D.E., Saxena, N., Fortmann, C.M., Rocheleau, R.E., Russell, T.W.F., AIChE Journal 36, 1555 (1990).

2. Michelson, C.E., Gelatos, A.V., and Cohen, J.D., Appl. Phys. Lett. 47, 397 (1985).

3. Gelatos, A.V., Mahavadi, K.K., Cohen, J.D., and Harbison, J.P., Appl. Phys. Lett. 53, 403 (1988).

4. J.D. Cohen, T. Unold, A.V. Gelatos, and C.M. Fortmann, J. Non-Cryst. Solids, in press.

5. See, for example, Aljishi, S., Smith, Z E., and Wagner, S., in Amorphous Silicon and Related Materials, ed. by H. Fritzsche (World Scientific, Singapore, 1989), p. 887.

6. Chen, L., Tauc, J., Lee, J.-K., and Schiff, E.A., Phys. Rev. B43, 11694 (1991).

TABLE I. Sample parameters deduced for our two a-Si,Ge:H samples and our a-Ge:H sample by the methods described in the text.

Sample	E_g (eV)	Urbach Energy (eV)	Defect Density (cm^{-3})	$(\mu\tau)_h$ (cm^2/V)
3481	1.33	52	2×10^{16}	5×10^{-10}
3421	1.27	57	1×10^{17}	3×10^{-11}
3422	1.07	50	9×10^{17}	---

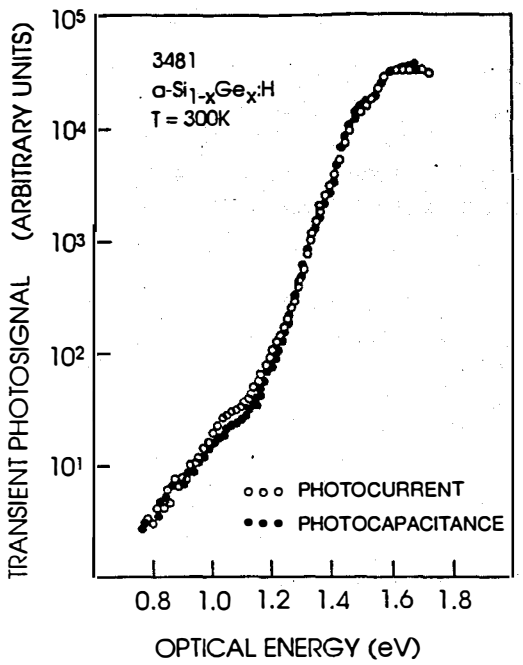

FIG. 1. Comparison of transient photocapacitance (solid circles) and junction photocurrent spectra (open circles) for a-Si,Ge:H at temperature 300K. The two types of spectra have been overlapped in the low energy regime and generally show the same specral dependence over the entire range of optical energies.

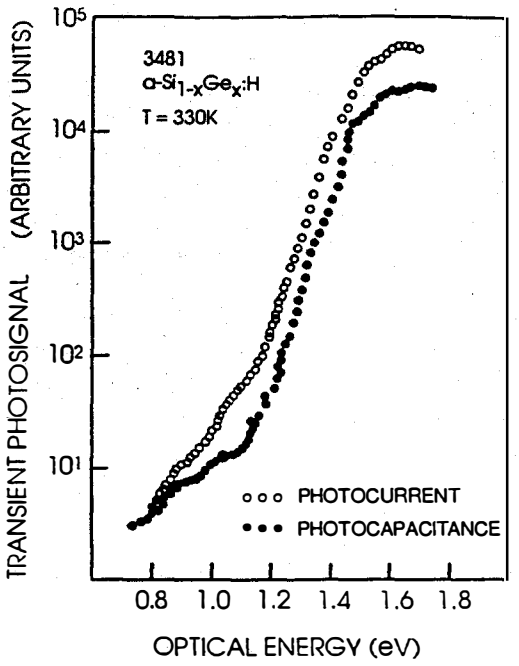

FIG. 2. Photocapacitance and photocurrent spectra for the same sample as in Fig. 1 but at the elevated temperature of 330K. The two curves are again overlapped in the low energy regime but now deviate at larger optical energies. This deviation is due to hole emission and transport processes as discussed in the text.

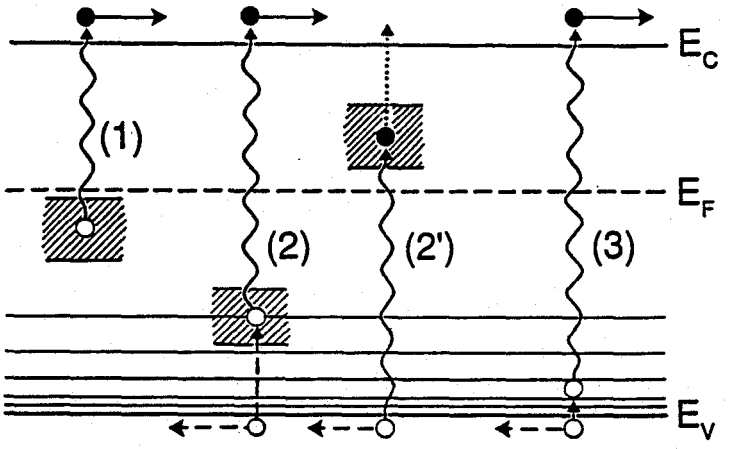

FIG. 3. Schematic of possible optical and thermal transistions for understanding the spectra in Figures 1 and 2. The wavy lines depict *optical* transitions and the other vertical lines represent *thermal* transitions. Horizontal arrows indicate electron and hole transport out of the depletion region. For the a-Si,Ge:H samples we found that electrons which are optically excited by a transition of type 2' undergo lattice relaxation so that they are not readily thermally emitted into the conduction band. (This is represented as a dotted line on the diagram).

Title: **Stability, Electronic Properties and Structure of a-Si:H and its Alloys**

Organization: Xerox Palo Alto Research Center, Palo Alto, CA 94304

Contributors: W. B. Jackson, N. M. Johnson, C. Nebel, P. Santos, R. A. Street (Principal Investigator), R. Thompson, C. C. Tsai.

The aim of this research project is to improve the performance of a-Si:H-based solar cells through the understanding of metastability, doping and growth.

Light Induced Hydrogen Diffusion

It has been suggested that the defect metastability in a-Si:H is caused by the motion of bonded hydrogen, which is released from a Si-H bond by the electron-hole recombination energy. It follows that an enhancement of the hydrogen diffusion would be expected under strong illumination. We have now observed this effect in undoped a-Si:H. Figure 1 indicates that that the diffusion coefficient can be measured above about 200°C and is about an order of magnitude larger under illumination compared to the value in the dark. The light-induced diffusion has a thermal activation energy of about 1 eV compared to about 1.5 eV in the dark. Great care was taken to eliminate sample heating by the light and to confirm that the effect is due to illumination. The results provide very strong support for the model of

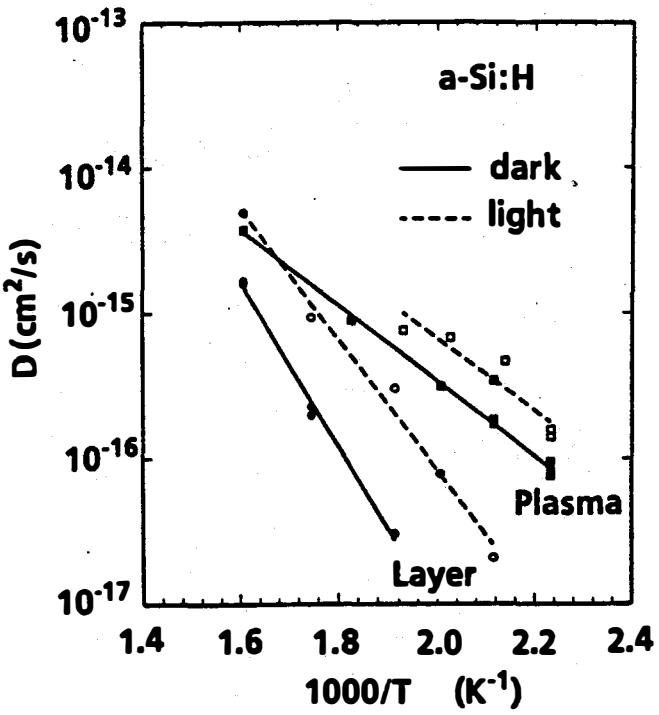

FIG. 1. Temperature dependence of the deuterium diffusion in the dark (solid symbols) and under illumination (open symbols) for diffusion from a deuterated layer(dots) and from a deuterium plasma (squares).

hydrogen induced metastability, because they show that illumination does indeed cause Si-H bond breaking.

Hydrogen diffusion under illumination was also investigated in doped and in compensated amorphous silicon films. The dark diffusion coefficient of compensated and phosphorus doped samples is approximately a factor of 10 larger than undoped material, and the boron doped material is a factor of 100 larger. Under illumination, small changes were observed in the concentration profiles of doped samples. The diffusion coefficient increased by less than a factor of 2, which is much smaller that the increase in undoped samples. These results provide further comfirmation that the results on undoped samples are not due to sample heating.

High field electron and hole transport

Measurements of high field electron and hole transport over a wide temperature range hhelp to clarified the transport mechanisms in a-Si:H. The conductivity of n-type and p-type material was obtained from room temperature down to 10K and at applied electric fields of up to $5x10^5$ V/cm and some of the results are shown in Figure 2. The conductivity activation energy decreases as the field is raised and above about 10^5 V/cm, the conductivity is virtually independent of temperature below about 100K.

The conductivity, σ, can be transformed into an effective drift mobility of the band tail carriers by assuming,

$$\sigma = n_{BT}\, e\, \mu_D \qquad (1)$$

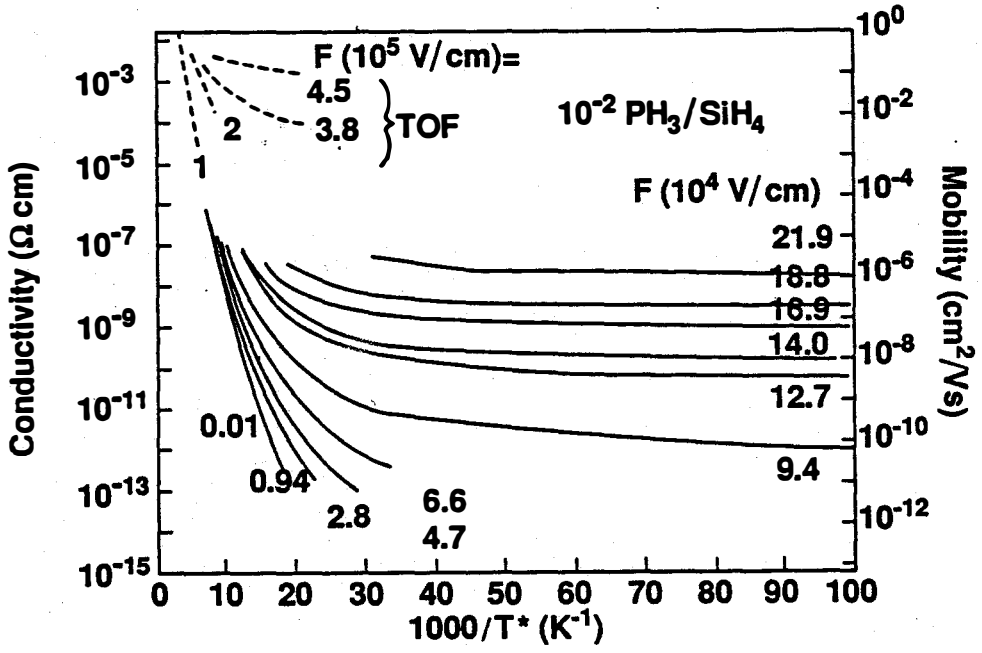

FIG. 2. Temperature- and field-dependent dark conductivity and mobility of phosphorus doped a-Si:H. Dashed lines are the mobilities of undoped material measured by time-of-flight.

where n_{BT} is the measured density of band tail cariers, and μ_D is their effective drift mobility. The temperature and field dependence of the electron drift mobility so obtained in n-type samples is found to very similar to the time-of flight results obtained in undoped a-Si:H under comparable high field conditions, showing that the same conduction mechanism applies in both cases.

The field (F) dependence is extremely strong effect at low temperature, with the effective mobility increasing as a power law F^n, with $n \simeq 10\text{-}12$. The absence of a temperature dependence at low T and high F indicates that transport is by hopping. Carriers can tunnel to states near the mobility edge because the energy gained by the carrier is eFr, where r is the tunnelling distance along the field. The transport path is determined by a balance between the energy gained by tunnelling and the loss of energy by thermalization.

Current induced defects in p-i-n devices

The density of light-induced metastable defects in a-Si:H saturates at about 10^{17} cm^{-3} after sufficiently long illumination times. It is controversial whether the saturation occurs because most defect creation sites are depleted, or whether it represents a steady state balance between creation and annihilation within a much larger density of possible creation sites. Our research has explored the defect generation mechanism through studies of metastable defects induced by a forward bias current. The measurements were performed on p-i-n structures and the defect density was measured from the reverse bias thermal generation current, which is proportional to the mid-gap density of states. The defect creation mechanism is

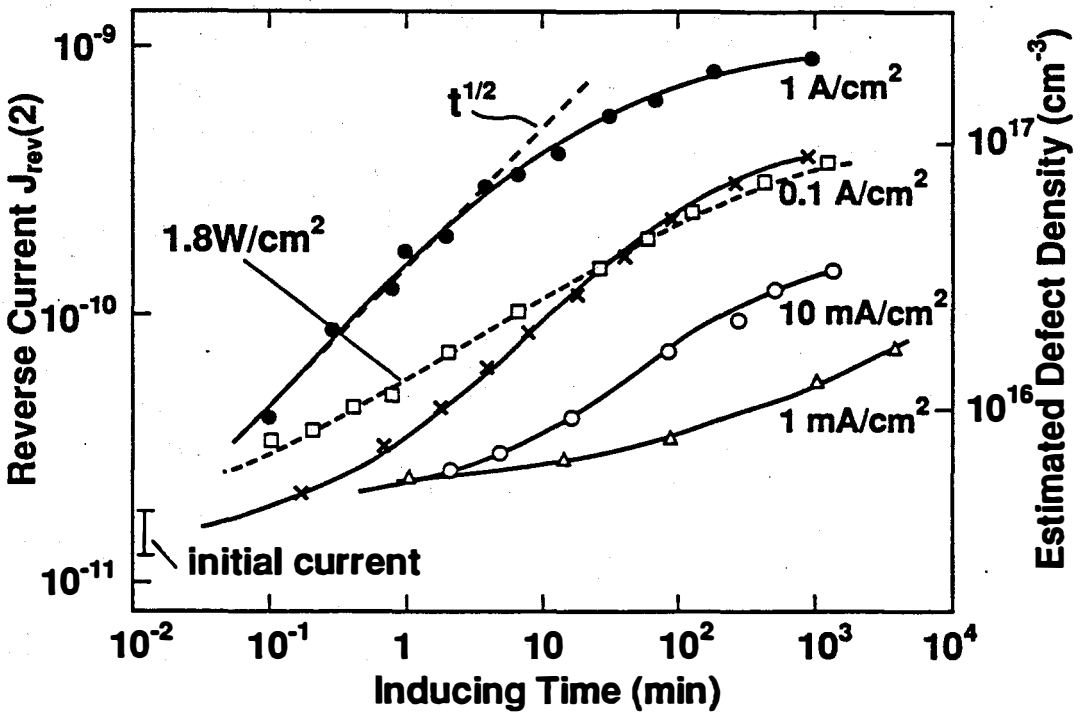

FIG. 3. Time dependence of the current-induced and light-induced defect density for different generation conditions. The left axis is the reverse curent at 2V and the right axis is the estimated defect density.

expected to be the same as for light-induced defects, arising from the recombination of electrons and holes. Figure 3 shows that the forward current induces up to about $3x10^{17}$ cm^{-3} defects. The creation kinetics measured at constant inducing current has a time dependence approximately $t^{1/2}$, reaching saturation at sufficiently long inducing times. The saturated defect density increases with the inducing current by about a factor 2 for each order of magnitude increase in current. The defect creation rate has a weak temperature dependence with an activation energy of about 0.2 eV. The creation kinetics of light-induced defects are shown for comparison

Current-induced defect recovery is also observed. In this measurement, more than 10^{17} cm^{-3} defects are induced by passing a large current for an extended time. When the forward current is reduced by a factor 10-100, the defect density is found to decrease. The much smaller decrease in the absence of a current clearly demonstrates that the recovery is induced by the current. The results show that the saturated defect density around room temperature is a balance between current-induced defect creation and recovery. Thermal annealing of the defects is important only at elevated temperatures (above about 340°C). The saturation level depends on the generation current and there is no sign of an upper limit to the defect density which would be expected if there was a limited density of defect creation sites.

High substrate temperature a-Si:H made by remote plasma deposition

The electronic properties of a-Si:H films deposited in our remote hydrogen plasma (RHP) reactor are found to differ in some interesting ways from those of optimized glow discharge (GD) films. Firstly, the optimum growth temperature (T_D) is about 400°C compared to 200-250°C for GD films. The defect density of undoped RHP films decreases monotonically as the T_D increases, reaching $\sim 3\times10^{15}$ cm^{-3} at 400°C. Secondly, the a-Si:H films deposited at this high temperatures display a greater

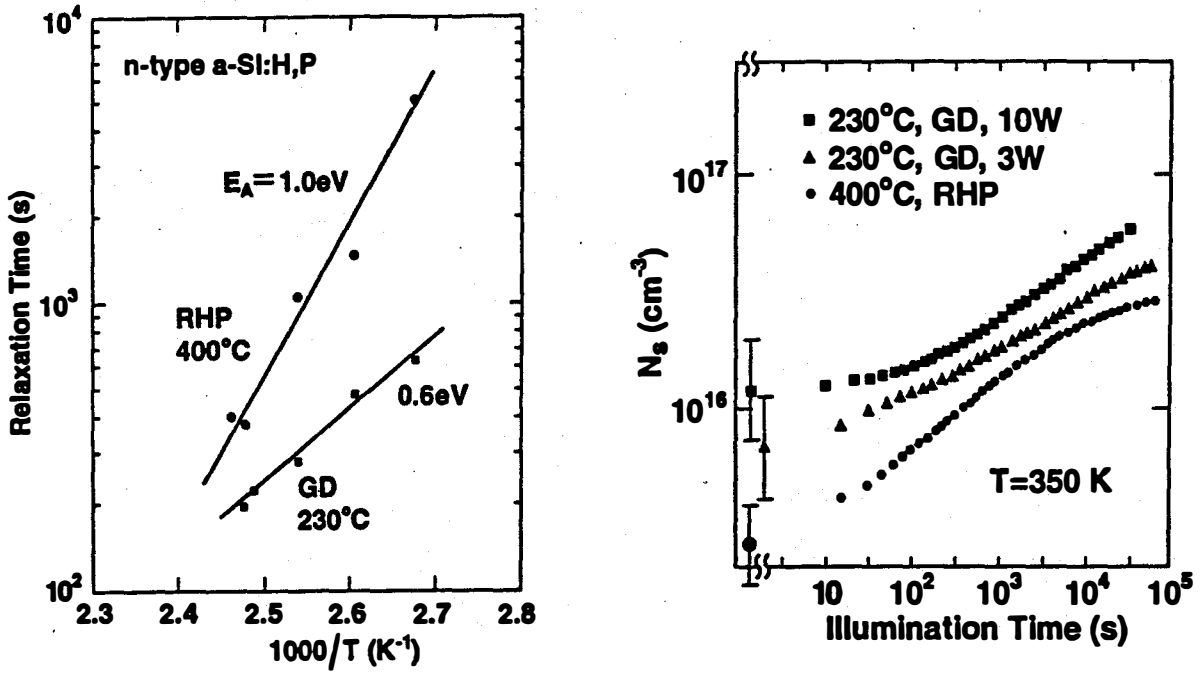

FIG. 4. (a) Comparison of the relaxation times of the dc conductivity of remote hydrogen plasma (RHP) films deposited at 673K and glow discharge (GD) films deposited at 503K. (b) Defect creation rates of undoped GD and RHP films

stability to reversible metastable effects than optimized GD films. The data in Figure 4 show a comparison of doped and undoped RHP and optimized GD material. In comparably n-type (phosphorus-doped) material, the dark dc conductivity in RHP films displays a higher equilibration temperature and, at a given measurement temperature, a longer stretched-exponential relaxation time than the GD films. Also, undoped material RHP films possess a lower saturated density of light-induced defects. Features of RHP deposition that may relate to these improved properties include: (1) the inherent use of hydrogen dilution which maintains the hydrogen concentration in the films at $\geq$ 10 at. % even at 400°C and (2) the high T_D's may permit a more stable incorporation of hydrogen in the random network and/or reduce the density of weak Si-Si bonds.

Hydrogen bonding and diffusion

We have proposed that the hydrogen bonding structure may be described in terms of the hydrogen density of states distribution, (HDOS), which is illustrated in Figure 5. The features of the HDOS are the Si-H bonds at E_H, the distribution of weak and

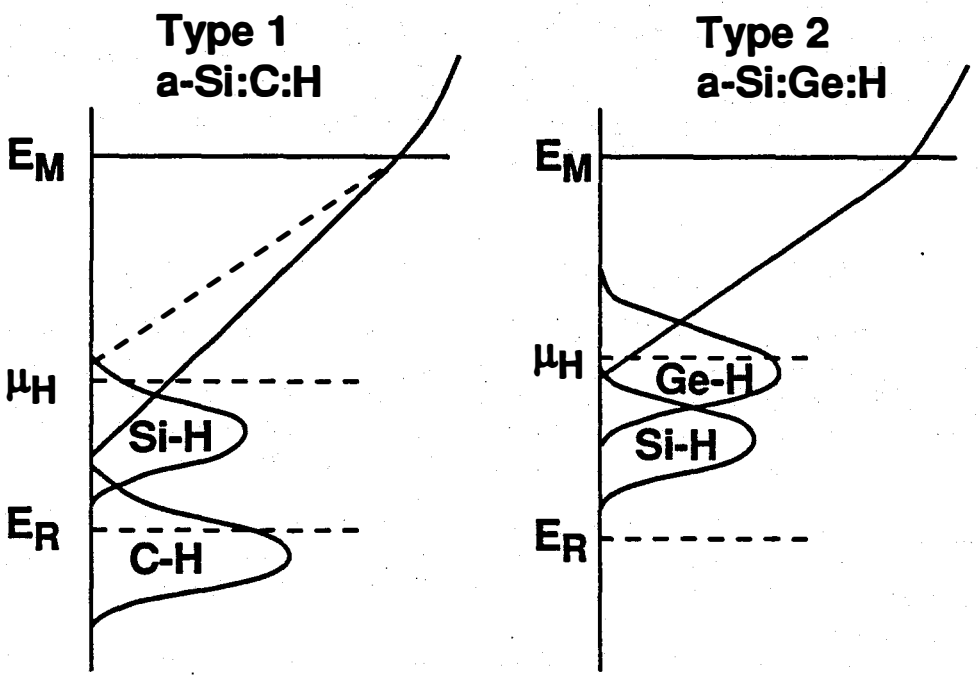

FIG. 5. The hydrogen density of states distribution for a-Si:C:H and a-Si:Ge:H alloys, showing the different H bonding states.

normal Si-Si bonds, of which the weakest are the lowest energy bonding sites for hydrogen, the energy E_M where hydrogen migrates, and the chemical potential, μ_H. In the ideal material, the distribution of bonds is as close as possible to equilibrium, with minimum disorder constrained by the amorphous network. Defects form at states near the chemical potential, so that μ_H of optimum films lies in a minimum of the HDOS.

Measurements of the diffusive transport of hydrogen are used to determine a rough H density of states. The diffusion profiles show clear evidence of deep traps separated from shallow traps, and the results are well explained by a simple division

of the H states into deep traps, shallow traps and transport states. The concentration of deep traps is about 0.8-2$\times 10^{20}$ cm^{-3} of which about 30% can be identified with dangling bonds. The energy of the deep traps is at least 1.9 eV below the transport states. The diffusion is dispersive with a power law time dependence and can be characterized by an exponential distribution of hopping barriers with a width of roughly 0.09 eV. The shallow traps are identified with clustered H pairs which determine the H chemical potential at high H concentrations. The results are consistent with a range of possibilities. One extreme is that H is predominately bonded on void surfaces and the transport energy is substantially different in a-Si than in crystalline Si (c-Si). The other extreme is the H predominately resides in platelet structures and the transport energy is roughly the same in as in c-Si.

Alloys of a-Si:H with Ge, C, N, O etc., have higher defect densities and poorer electronic properties than a-Si:H. The idea of hydrogen equilibration during growth can explain the structural trends in the alloys responsible for the different electronic properties. The analysis finds two characteristically different types of behavior, distinguished by the hydrogen bond strengths of the alloy elements. Type 1 alloys have predominately silicon dangling bonds and a large disorder broadening of the valence band tail, while type 2 alloys have dangling defects on the non-silicon element and low disorder. Examples are a-Si:C:H and a-Si:Ge:H respectively. The same approach to understanding the electronic structure is applied to alloys with halogens such as fluorine, to the different elemental hydrogenated amorphous semiconductors, and to microcrystalline thin films.

Bibliography

W. B. Jackson and C. C. Tsai, *Hydrogen transport in amorphous silicon,* Phys. Rev. B, in press

W. B. Jackson, C. C. Tsai and P. V. Santos, *Dependence of hydrogen trapping densities on hydrogen concentration,* Proc. Int. Conf on Amorphous Semiconductors, in press.

N. M. Johnson, C. E. Nebel, P. V. Santos, W. B. Jackson, R. A. Street, K. S. Stevens, and J. Walker, *Stability of hydrogenated amorphous silicon deposited at high temperature with a remote hydrohen plasma reactor*, Appl. Phys. Lett., 59, 1433 (1991).

N. M. Johnson, P. V. Santos, C. E. Nebel, W. B. Jackson, R. A. Street, K. S. Stevens, and J. Walker, *Stability of a-Si:H deposited at high temperature and hydrogen dilution in a remote hydrohen plasma reactor*, Proc. Int. Conf on Amorphous Semiconductors, in press.

C. E. Nebel, *Transport in amorphpous silicon*, Proc. Int. Conf on Amorphous Semiconductors, in press.

P. V. Santos, N. M. Johnson and R. A. Street, *Light-enhanced hydrogen motion in a-Si:H*, Phys. Rev. Lett.,

P. V. Santos, C. Doland, N. M. Johnson and R. A. Street, *Light-induced hydrogen diffusion in a-Si:H*, Proc. Int. Conf on Amorphous Semiconductors, in press.

R. A. Street and M. Hack, *Saturation and recovery kinetics of current-induced defects in a-Si:H*, Proc. Int. Conf on Amorphous Semiconductors, in press.

R. A. Street, *Model for growth of plasma-deposited a-Si:H and related materials*, Proc. Int. Conf on Amorphous Semiconductors, in press.

R. A. Street, *Hydrogen density of states model for amorphous silicon and alloys*, Proc. MRS Symp. 219, 253 (1991).

R. A. Street, *Model for growth of a-Si:H and its alloys*, Phys. Rev. B. in press.

R. A. Street, Current induced defect creation and recovery in hydrogenated amorphous silicon, Appl. Phys. Lett., 59, 1084, (1991).

3.0 POLYCRYSTALLINE THIN FILMS

Kenneth Zweibel (Manager), Harin Ullal, and Bolko von Roedem

The objective of the Polycrystalline Thin Film Project is to develop thin-film, flat-plate modules that meet DOE's long-term goals of reasonable efficiencies (15%–20%), very low cost (near $\$50/m^2$), and long-term reliability (30 years). The approach relies on developing PV devices based on highly light-absorbing compound semiconductors such as $CuInSe_2$, CdTe, and thin film crystalline silicon. These semiconductors are fabricated as thin films with minimal material and processing costs.

Very high efficiencies have been achieved by these promising materials. $CuInSe_2$ cells made by Siemens Solar Industries and by Boeing were measured at NREL at 13.1% and 12.9% efficiency (active area: 11.3% and 12.5% total area), respectively. Others surpassing 10% efficiency in $CuInSe_2$ are NREL, University of Stuttgart, Fuji, International Solar Electric Technology, and Institute of Energy Conversion. Larger area $CuInSe_2$ devices have also been fabricated with very high efficiencies. Siemens Solar has made a 938-cm^2 (aperture area) $CuInSe_2$ module with 11.1% efficiency (10.4 W), and a 9.7% (4-ft^2) module, both measured at NREL. Siemens Solar reported achievement of a 14.1% cell efficiency (active area).

$CuInSe_2$ shows good proven stability under controlled conditions (9000 hours of illumination), and outdoor tests (Siemens) are also promising. We have conducted three years of outdoor testing on two Siemens Solar $CuInSe_2$ panels with very little change in their efficiencies (under 4%). These are the first such tests on $CuInSe_2$ by an independent agency and show the great potential stability of $CuInSe_2$ panels.

Four U.S. laboratories (University of South Florida (USF), Institute of Energy Conversion, Georgia Institute of Technology, and Photon Energy) have achieved CdTe cell efficiencies between 10.5% and 12.5%. Photon Energy has fabricated near-square-foot CdTe submodules measured outdoors at NREL at 8.1% efficiency (aperture area). British Petroleum (BP) Solar has reported 10% efficient square-foot CdTe submodules (not NREL measured). Others who are making cells of 10% or more efficiency are Matsushita, Microchemistry, University of Queensland, and Battelle Europe. Innovative designs are now addressing past difficulties in contacting CdTe. We are testing encapsulated CdTe submodules provided by Photon Energy. Several show no degradation after two years. As with the $CuInSe_2$, these are the first independent tests of encapsulated devices made from this material. Both Matsushita and BP Solar have reported similar stability for their own CdTe modules. Since stability has been an identified issue with CdTe, these initial results are considered very favorable.

The improved efficiencies and larger areas of $CuInSe_2$ and CdTe devices, and their apparent stability, are the major recent advances in these technologies. But polycrystalline thin film cells require continued development to achieve 15%–20% conversion efficiencies. The major strategy is development of improved single-junction cells. Improvement of the single-junction technologies has been steady and reliable. Potentially achievable cell efficiencies approach 20%, and projections indicate the likelihood of fabricating modules of more than 15% efficiency.

Developing scalable, low-cost fabrication methods is important in providing industry with a foundation for future large-area, high-throughput commercial processes. Research methods for

Title: **Development of Large-Area Monolithically Integrated Silicon-Film Photovoltaic Modules**

Organization: AstroPower, Inc.
Solar Park
Newark, DE 19716-2000

Contributors: J.A. Rand, Principal Investigator, C. Bacon, J.E. Cotter, T.H. Lampros, A.E.Ingram, T.R. Ruffins, R.B. Hall, A.M. Barnett

Objective

The objective is to develop Silicon-Film Product III into a low cost, stable device for large scale terrestrial power applications. The Product III structure is a thin (<100 μm) polycrystalline silicon layer on a non-conductive supporting ceramic substrate (see Figure 1). The presence of the substrate allows cells to be isolated and interconnected monolithically. The long term goal for the product is efficiencies over 18% on areas greater than 1200 cm^2. The high efficiency will be based on polycrystalline thin silicon incorporated into a light trapping structure with a passivated back surface. Short term goals are focused on the development of large area ceramics, a monolithic interconnection process, and fabricating 100 cm^2 solar cells.

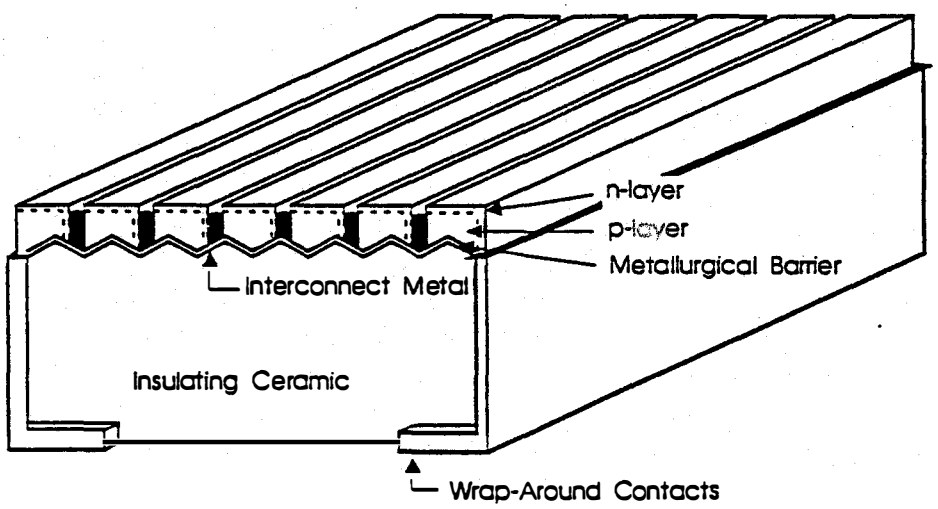

Figure 1. Silicon-Film Product III.

Technical Approach

Issues for large area ceramic development are: 1) the formulation of non-conducting materials, and 2) processing improvements to fabricate uniform, flat ceramics 500 cm^2 in size. Only production based processes (low cost) were utilized for the formation and firing of the ceramic.

Issues for the monolithic integration process are: 1) developing an isolation process to define cell areas, and 2) developing a diffusion and metallization scheme that allows for interconnection. The process must be done on a low cost, production basis. The limited conduction of crystalline silicon may have an impact on cell area. Without a back plane conductor at the silicon - ceramic interface, the base layer resistance limits the cell size by introducing efficiency limiting series resistance. The incorporation of a back plane conductor to alleviate this limitation must be done in such a way as not to introduce significant back surface recombination.

Significant Results - Materials

An insulating ceramic has been developed that has a resistivity higher than the 500 Ω-cm required of the Product III device design. The areal generation capabilities of ceramic substrates have been increased to generate samples greater than 500 cm^2. All ceramics are fabricated in-house at AstroPower and utilize low-cost materials and processing. Ceramic fabrication capabilities were demonstrated by delivering ceramics greater than 500 cm^2 to NREL.

The metallurgical barrier deposition process has been developed to uniformly cover areas over 500 cm^2. The silicon deposition equipment has also been altered to uniformly deposit silicon over areas greater than 400 cm^2. Light trapping structures require one or more surfaces to be textured. Random texturing has been incorporated into the ceramic-metallurgical barrier surface. An investigation of light trapping on the similar Product II Silicon-Film structure (planar junction, conducting ceramic) indicated high levels of light trapping from similar random texturing [1].

Significant Results - Process

A process has been developed that is capable of interconnecting isolated devices on a monolithic substrate. For the critical step of device isolation, dicing, laser ablation, and chemical etching were investigated. Dicing was chosen as the best alternative to meet the short term goals. To demonstrate both the isolating properties of the substrate and the isolation process, a test structure was developed. The test structure consisted of p-type silicon on an insulating substrate with an Al paste ohmic contact covering the front surface. Isolation cuts were then made to define cell area. Resistance measurements were made between adjacent cells as a function of isolation trench depth. As the trench depth exceeded the silicon layer thickness, the resistance increased as expected. The magnitude of the inter-cell resistance increased 4 orders of magnitude as the trench depth increased 25 μm past the layer depth. The resistivity target of 500 Ω-cm for the ceramic was obtained. These test structures were fabricated without a metallurgical barrier.

A metallization scheme has been developed that allows for front surface interconnection of cells. A schematic of the process is shown in Figure 2.

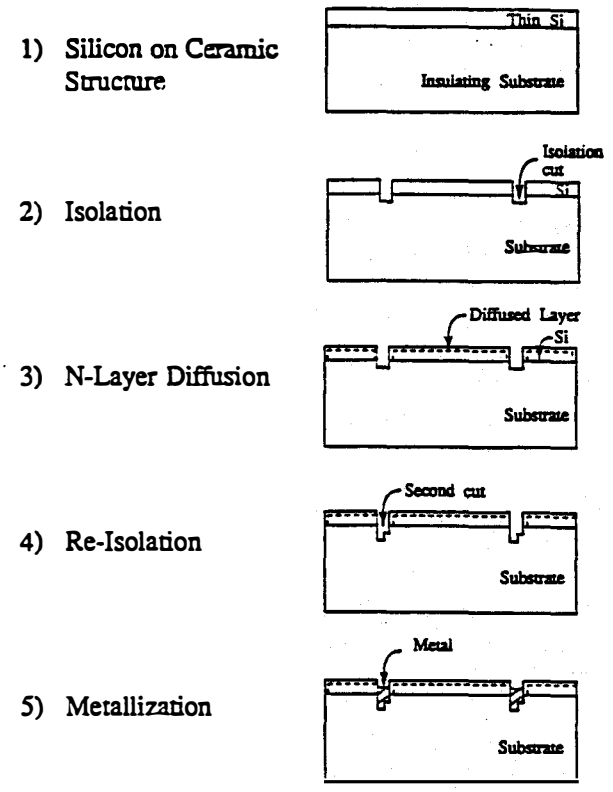

Figure 2. Silicon-Film Product III process sequence.

The Product III process begins with a wafer of p-type silicon on ceramic. A metallurgical barrier may or may not be included. As discussed above, an isolation cut is first made to define cell area. A phosphine or $POCl_3$ based diffusion is then performed to create a phosphorus doped n-type layer on the device surface, as well as line the interior of the trenches. A second isolation cut is then performed to remove the n-type lining from one side of the trench. Finally, the trench is filled with metal to interconnect the n-type region of one cell to the p-type region of the neighbor cell. A photograph of an isolated cell is shown in Figure 3.

A series of test structures has been fabricated to verify the processing steps. To adequately interconnect isolated cells, a two part metallization system had to be developed. High temperature metallization is used to make ohmic contact to the silicon, and a low temperature metal to fill the trench.

The process sequence in Figure 2 has been further developed to allow for the incorporation of a back plane conductor. Such a process eliminates any series resistance limitation to cell size. Front surface conduction can be assisted by placing grid lines perpendicular to the metallized trench for wide cells.

Solar cells have been fabricated on a regular basis to assess material quality. Impurity problems have been encountered with both in-coming feedstock, and with handling procedures. A second silicon feedstock source has been developed. Handling procedures have been improved to minimize contamination. Recent results indicate that the levels of impurities have been significantly reduced from the baseline level. The baseline level has been shown to generate low diffusion length material with overall conversion efficiencies of 6%.

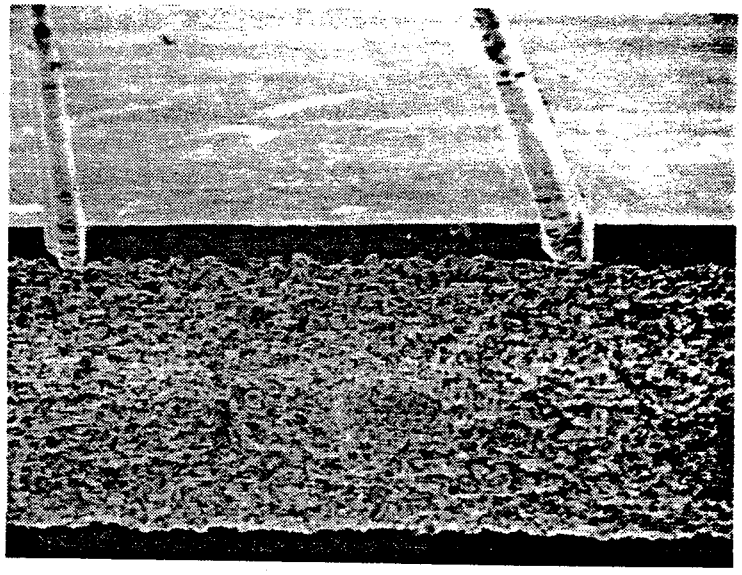

Figure 3. Cross section of silicon on ceramic structure showing isolation trenches (50X magnification).

To demonstrate the process sequence, free-standing silicon wafers were utilized as test structures. A process was developed that supported these wafers on a temporary substrate so that a monolithic processing sequence could be performed. Seventeen isolated cells were interconnected to generate a V_{oc} of 8.25V, measured under AM1.5 illumination.

Conclusions

Critical elements of the monolithically integrated device have been developed. An insulating ceramic substrate has been developed and tested. Ceramic areal generation capabilities have been expanded to 500 cm^2. A monolithic interconnection process has been developed that will isolate and interconnect individual cells on the ceramic surface. Production based, low cost process steps are utilized. The process was verified using free-standing silicon wafers to achieve a V_{oc} of 8.25 volts over a 17 element string. Overall efficiency of the Silicon-Film material has been limited to 6% due to impurities. Improved processing and feedstock materials are now under investigation.

[1] J.A. Rand and P.A. Basore, "Light-Trapping Silicon Solar Cells, Experimental Results and Analysis", presented at the 22nd IEEE Photovoltaics Specialists Conference, Las Vegas, Nevada, October 1991.

Title: **Research on Polycrystalline Thin Film $CuInGaSe_2$ Solar Cells**

Organization: Boeing Defense & Space Group, Seattle, WA

Contributors: B. J. Stanbery, program manager; W. S. Chen and J. M. Stewart, co-principal investigators; W. E. Devaney and R. A. Murray

Objectives

The objectives of this research effort are to fabricate high efficiency $CdZnS/CuInGaSe_2$ thin film solar cells, and to develop improved transparent conductor window layers such as ZnO.

Approach

Analysis of the properties of the best $ZnO/CdZnS/CuInGaSe_2$ cells developed by Boeing for SERI under a prior subcontract suggested that significant performance improvements could be realized by further optimization of the thin CdZnS layer to reduce shunt currents while maintaining subbandgap transparency, the ZnO layer to reduce IR absorption while maintaining adequate lateral conductivity, and the CIGS layer to optimize gallium content and gradients along with minority carrier transport properties.

Results and Discussion of FY '91 Activities

During the first five months of this contract our activities have been focussed on two areas. First, our CIGS deposition system was modified to quadruple its substrate capacity. This increased throughput is considered critical to speeding the pace of process development by providing multiple substrates from the same CIGS run which can be used to reduce uncertainty in the cause of differences resulting from the intentional variation of other process parameters. Second, new tooling was developed to enable investigation of a modified aqueous CdZnS process whose goal is to improve the yield of this critical step in the device fabrication process.

Characterization of the new CIGS deposition system substrate fixturing was completed. After some troubleshooting and modification, good thermal uniformity and adequately high temperatures for device-quality CIGS deposition were achieved. Optimization of the modified aqueous $Cd_{1-Y}Zn_YS$ process has enabled us to reproducibly deposit adherent, pinhole free films over a 2"x2" substrate for zinc fractions in the range $0 \leq Y \leq 0.20$.

Combining the new CdZnS process with CIGS from the newly fixtured deposition system has enabled us to fabricate (figure 1) an 11.5% efficient, 4 cm^2, $CuIn_{1-X}Ga_XSe_2/Cd_{1-Y}Zn_YS/ZnO$ cell with $X=0.29$ and $Y=0.19$. Though not as efficient as our best 12.5% CIGS cell, further process refinements should enable us to better that.

Conclusions

Significant improvement has been made in the repeatability of the aqueous deposition process for CdZnS, and the continuity of those films. Combined with a major laboratory upgrade and equipment modifications conducted during this period, the foundation has been laid for an accelerated process optimization program during the balance of this contract phase.

Figure 1: Performance of best CIGS cell fabricated to date in Phase I of this contract

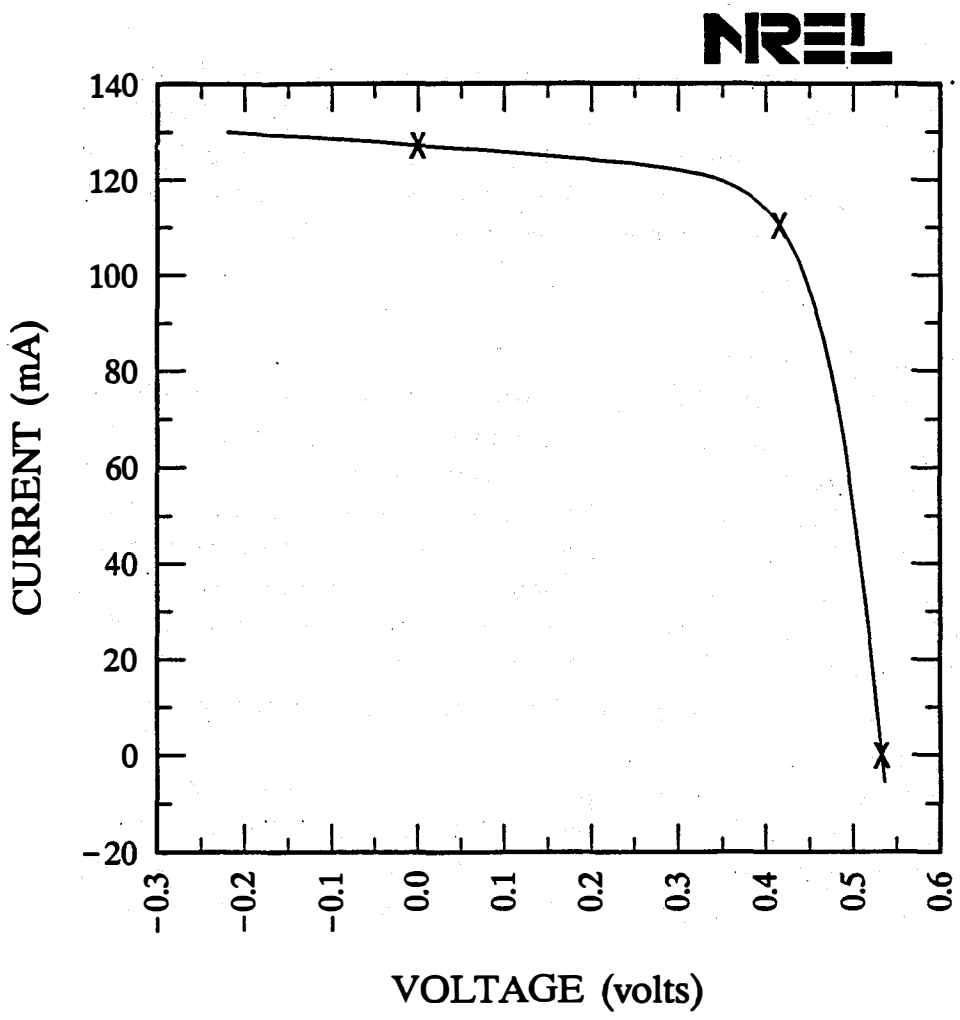

V_{oc} = 0.5324 volts	I_{sc} = 127.2 mA
J_{sc} = 31.88 mA/cm²	P_{max} = 46.0 mW
Fill factor = 67.89 %	I_{max} = 110.5 mA
Efficiency = 11.5 %	V_{max} = 0.4160 V

Title: **Investigations of $CuInSe_2$ Thin Films and Contacts**

Organization: California Institute of Technology
Applied Physics and Electrical Engineering
Pasadena, CA 91125

Contributors: J. S. Chen and M-A. Nicolet

I. Objectives

The major objective of this project is to characterize the crystallography and defect structure of $CuInSe_2$/CdS heterojunction solar cells and relate the results to their deposition process and their corollary device performance. Deposition of indium thin films by rf-sputtering for the Cu-In bilayer as precursor for the selenization process and a preliminary study to apply amorphous Ta-Si-N films as a diffusion barrier between the $CuInSe_2$ and the back contact layer were also investigated during this year.

II. Technical Approach

The microstructure of $CuInSe_2$/Cd(Zn)S solar cells is characterized by scanning electron microscopy (SEM) and cross-sectional transmission electron microscopy (XTEM). Three groups of cells fabricated at the Institute of Energy Conversion (IEC) of the University of Delaware were used for this study. The cross-sectional cell configuration and deposition conditions are shown in Fig. 1 and Table I. All samples were made by similar procedures except that cell groups #1 and #2 (IEC No.32065.21 and 32230.22) were deposited on Corning 7059 glass while group #3 (IEC No.32230.23) was deposited on soda lime glass. (#2 and #3 were fabricate in the same run, side by side.) The $CuInSe_2$ layers were grown by three-source thermal evaporation which is one of the most successful methods for depositing thin $CuInSe_2$ films for high-efficiency solar cells [1].

Samples for XTEM were prepared in a way similar to that followed for metallized semiconductor materials: two pieces of solar cell samples (2mm by 3mm) were cut from the glass substrate. The two samples were glued face-to-face, mechanically thinned down to about 20 μm, and finally milled by a 5-kV Ar^+ ion beam to electron transparency. All the XTEM analyses of this work were made with a Philips EM430 transmission electron microscope operating at 300 keV.

To study the reaction kinetics of Cu-In bilayers during the selenization process, it is necessary to have a smooth, unreacted In thin film on top of Cu. We have built a cold stage in our rf-sputtering system which can reach 4°C by ice water circulation, and -40°C by ethanol circulation combined with external dry ice cooling around the circulation pipe. A specially designed shutter was also set up in the same system to increased the number of possible depositions per pump down and expedite the experimental program to figure out the changes of the indium surface morphology during the sequential sputtering period.

It has been well established that conductive amorphous Ta-Si-N films are effective diffusion barrier in a number of VLSI metallization schemes [2,3]. To evaluate the applicability this film as a diffusion barrier between the $CuInSe_2$ layer and the back contact, a stability test

was carried out in collaboration with IEC and Siemens Solar where Ta-Si-N films were exposed to H_2Se. $CuInSe_2$/CdS devices were made on the Si/SiO_2/Ta-Si-N and Corning 7059 glass/Mo/Ta-Si-N samples by IEC.

III. Results

A. Microstructure of $CuInSe_2$/Cd(Zn)S Solar Cells

Figure 2(a) and (b) show the scanning electron micrographs of the surface morphologies of the $CuInSe_2$ layer (after removing the overlayers by etching) and Cd(Zn)S layer (with 0.2 μm ITO on top) for cell group #1 (deposited on Corning 7059 glass). Both of the $CuInSe_2$ and Cd(Zn)S surfaces are rough. The grains protrude up to 0.5-1 μm above the average level of the $CuInSe_2$ surface and about 1-2 μm above that of the average Cd(Zn)S surface. From the surface morphology of the $CuInSe_2$ layer, it is evident that the $CuInSe_2$/Cd(Zn)S interface will not be laterally uniform.

A cross-sectional scanning electron micrograph of sample #1 is shown in Fig. 2(c). One sees that has a columnar structure of Cd(Zn)S with a column diameter of about 1 μm. As shown below, the actual grains of the Cd(Zn)S have diameters that are two or three times smaller than that of the columns seen in this micrograph. The interface between the Cd(Zn)S and the $CuInSe_2$ is not visible in this figure, but must be located approximately midway between the sample surface and the Mo interface according to the deposition parameters in Table I. The $CuInSe_2$ region has a very irregular appearance. A distinguishing feature is the presence of holes (dark contrast) in that region, although it is unclear if some voids project into the Cd(Zn)S or not. The Mo layer again has a very pronounced columnar structure. Similar surface and cross-section morphologies were obtained by SEM for samples #2 (on Corning 7059 glass) and #3 (on soda lime glass).

Figure 3(a), (b) and (c) are the cross-sectional transmission electron micrographs of the $CuInSe_2$/Cd(Zn)S solar cells of samples #1 and #2 (both deposited on Corning 7059 glass)and #3(on soda lime glass), respectively. The Mo layers of samples #1 and #3 were separated from the upper layers during the TEM sample preparation and are absent in the micrographs (Fig. 3(a) and (c)) . The dark uppermost layers in the three cross-sections is ITO, as was established by EDAX. The thickness of that layer agrees roughly with the nominal value of Table I. The white dashed line in the figures indicates the location of the $CuInSe_2$/Cd(Zn)S interface. In agreement with the SEM results, the heterojunction interface is laterally nonuniform. The two semiconductors are intimately bonded to each other. the microstructure of the individual layers are described as follows:

a. Cd(Zn)S

The Cd(Zn)S layers have the same morphology in all three samples (compare the Cd(Zn)S layer in Fig. 3(a), (b) and (c)). The layers are dense, continuous, and vary in thickness from point to point by as much as 30%. The grains are elongated, separated by low angle boundaries. They are about 0.5 μm wide and about 1-2 μm long. It is easily to see in the transmission electron micrographs that several elongated grains are contained in one surface hillock. One thus cannot estimate the grain size of the Cd(Zn)S layer from the surface topology of SEM micrographs.

By electron diffraction, the Cd(Zn)S shows hexagonal wurtzite crystal structure. The main defects in this layer are stacking faults on {0001} basal planes. However, the stacking faults in Cd(Zn)S could be artificial defects due to the Ar^+ ion sputtering for TEM sample preparation [4]

b. $CuInSe_2$

Compare the $CuInSe_2$ layer in Fig. 3(a), (b) and (c), one sees that voids exist in the $CuInSe_2$ layer for all three samples. The same result has been reported for $CuInSe_2$ films without CdS overlayer by Talieh and Rockett for films deposited directly on Corning 7059 glass [5] and by Raud and Nicolet for the films made by ARCO on Mo-coated glass [6]. A survey of the cross-sectional samples investigated in the present study clearly established that the size and number of the voids is larger in samples #1 and #2 than in #3. This fact is also noticeable in Fig. 3(a), (b) and (c) even though the latter two samples were actually processed simultaneously. These two samples differ by their glass substrate. It has previously been proposed that the thermal expansion and contraction of the substrate has an effect on the structure of the $CuInSe_2$ film [7]. The differences in the $CuInSe_2$ structure may result from the different thermal expansion coefficients for the different glasses.

In all samples, the grain size of $CuInSe_2$ is about 1 μm in diameter. By electron diffraction, the crystal structure of $CuInSe_2$ is chalcopyrite. Because the diffraction rings of the sphalerite structure are included in those of the chalcopyrite structure, we cannot rule out the existence of sphalerite phase.

By high-resolution TEM images in conjunction with electron diffraction, we found the principal defects in $CuInSe_2$ films are twins and stacking faults on $\{112\}_{chalcopyrite}$ planes. The present defects identified here are consistent with the results of other TEM studies of physical-vapor-deposited $CuInSe_2$ thin films [6,8,9].

c. $CuInSe_2$/Cd(Zn)S heterojunction interfaces

Figure 4 shows the interface of $CuInSe_2$/Cd(Zn)S heterojunction, one can see that most of the stacking-fault line contrast in the Cd(Zn)S grains is parallel to the contrast of twin bands in the $CuInSe_2$ grain. This shows that the {0001} basal planes of the Cd(Zn)S grain tend to be parallel to the {112} planes of $CuInSe_2$ grains. So the growth orientation of Cd(Zn)S grains in this micrograph clearly depends on the crystal orientation of the $CuInSe_2$ grains. Assuming that this picture is typical for the junction everywhere, one concludes that in spite of its very nonplanar shape, the $CuInSe_2$/Cd(Zn)S interface is structurally a heterojunction.

For the microstructure study, the principal observations one draws from the cross sections are (i) the laterally rough and uneven morphology of the Cd(Zn)S and $CuInSe_2$ layers, (ii) the very intimate bonding between these two layers, and (iii) the numerous voids and fractures that are present in the $CuInSe_2$. The main difference between the samples #1 and #3 is the $CuInSe_2$ layer, where voids and cracks are clearly more numerous in sample #1 than in sample #3 (compare Fig. 3(a) and (c)). The presence of the voids and cracks in CuInSe2 layer is attributed to the thermal contraction of the substrate/film assembly upon cooling after the film deposited at 450°C [10].

B. Deposition of Indium Thin films by Sputtering

Systematic tests have resulted that smooth, shiny In thin films can be obtained by sputtering only with very low sputtering power (30W) and rotating the thermally floating substrate table. At the resulting very low deposition rate, impurities are incorporated into the films. For a 250Å thick In film, the oxygen concentration can be as high as 25% (by RBS), even though the x-ray diffraction of the film shows the In body-centered-tetragonal structure. To reduce the impurity content would request base pressure much below that of our vacuum system. The shiny film will turn rough when it becomes thicker than a certain thickness (about 500Å).

Not much improvement on surface morphology is accomplished by decreasing the substrate temperature from room temperature to 4°C and -40°C. Shiny, smooth In films are only obtained with low deposition rate. Oxygen contamination and thickness limitation are also present in the In films deposited at low temperature.

C. Ta-Si-N Diffusion Barrier

The stability of TaSiN films exposed to H_2Se was tested in collaborating with IEC and Siemens Solar. Amorphous Ta-Si-N layers do not react when exposed to H_2Se gas at 400°C. In this respect, this ternary layer is a very promising diffusion barrier for the back contact of $CuInSe_2$ cells. However, when the $CuInSe_2$/CdS cells were deposited on a Si/SiO_2/Ta-Si-N substrate at IEC, the adhesion between the Ta-Si-N film and the $CuInSe_2$ is poor. This is also true for the cells deposited on the Corning 7059 glass/Mo/Ta-Si-N subatrates. The bad adhesion is consistent with the inertness of Ta-Si-N to the H_2Se exposure. Improved adhesion can be obtained by tailoring the composition profile of the amorphous film. Experiments addressing that issue are the next step to pursue in this project to develop the stable contact to $CuInSe_2$ cells.

IV. Summary

This year, clear advances in insight and understanding of crystallography and defect microstructure of $CuInSe_2$/CdS heterojunction solar cells have been made by XTEM studies. Significant mechanical damage (voids, cracks) is observed in all $CuInSe_2$ films. The differential thermal contraction of the substrate/film assembly during processing is identified as a likely cause for this mechanical damage. Cracks and voids in the $CuInSe_2$ film create internal surfaces that certainly do not improve the lifetime of electrons and holes and the cell efficiency. Although difficult, the preparation of XTEM samples for a XTEM analysis is shown to be feasible by our present method of sample preparation. Future work based on this method and focussed on developing a deposition process for $CuInSe_2$ films that have few or no mechanical defects such as voids and cracks could lead to a major advantage in polycrystalline $CuInSe_2$ cells. The technique can also be used to support efforts aimed at enhancing the grain size of $CuInSe_2$ cells without introducing voids and cracks.

V. References

1. A. Rockett and R. W. Birkmire, J. Appl. Phys., 70(1991), R81.
2. E. Kolawa, J. M. Molarius, C. W. Nieh, and M-A. Nicolet, J. Vac. Sci. Tech. A8(1990), 3006.
3. E. Kolawa, J. S. Chen, J. S. Reid, P. J. Pokela, and M-A. Nicolet, J. Appl. Phys., 70(1991), 1369.
4. A. G. Cullis, N. G. Chew and J. L. Hutchison, Mat. Res. Soc. Symp. Proc. Vol. 62(1986), p. 83.
5. H. Talieh, and A. Rockett, Solar Cells, 27(1989), 321.

6. S. Raud and M-A. Nicolet, Annual Report, Photovoltaic Program, FY 1989 (March 1990), SERI/TP-211-3643, p. 85.
7. L. Margulis, G. Hodes, A. Jakubowicz, and D. Cahen, J. Appl. Phys., 68(1989), 3554.
8. B.-H. Tseng, A. Rockett, T. C. Lommasson, Y. C. Yang, C. A. Wert, and J. A. Thornton, J. Appl. Phys. 67(1990), 2673.
9. C. J. Kiely, R. C. Pond, G. Kenshole, and A. Rockett, Phil. Mag. A 63(1991), 1249.
10. J. S. Chen, E. Kolawa, C. M. Garland, M-A. Nicolet, and R.P. Ruiz, MRS 1991 Spring Meeting (submitted).

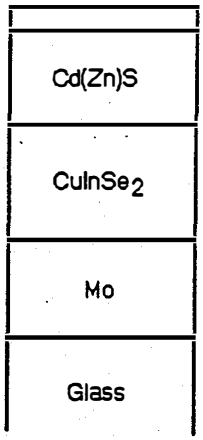

Table I

Sample	#1	#2	#3
ITO	0.2 μm	0.2 μm	0.2 μm
Cd(Zn)S	1.7 μm	1.5 μm	1.5 μm
$CuInSe_2$	2.0 μm	2.1 μm	2.1 μm
%Cu	26.0	24.7	25.1
%In	26.3	25.7	25.6
%Se	47.7	49.6	49.3
Mo	2 μm	2 μm	2 μm
substrate glass	Corning 7059	Corning 7059	soda lime

Fig. 1 Schematic cross-sectional configuration and deposition conditions of the $CuInSe_2$/Cd(Zn)S solar cells supplied by IEC.

Table I Thickness of the individual layer and composition of $CuInSe_2$ layer in each sample given by IEC:

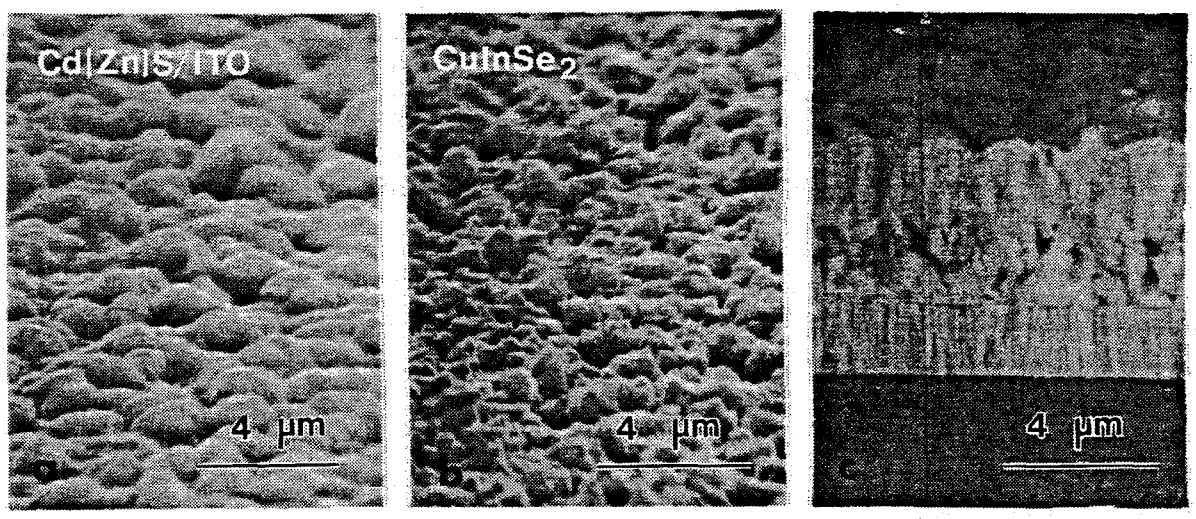

Fig. 2 Scanning electron micrographs of sample #1 (deposited on Corning 7059 glass) showing (a) Cd(Zn)S surface morphology(with 0.2 μm ITO on top); (b) $CuInSe_2$ surface morphology (after removing the ITO and Cd(Zn)S by a HCl etch); (c) cross-sectional morphology.

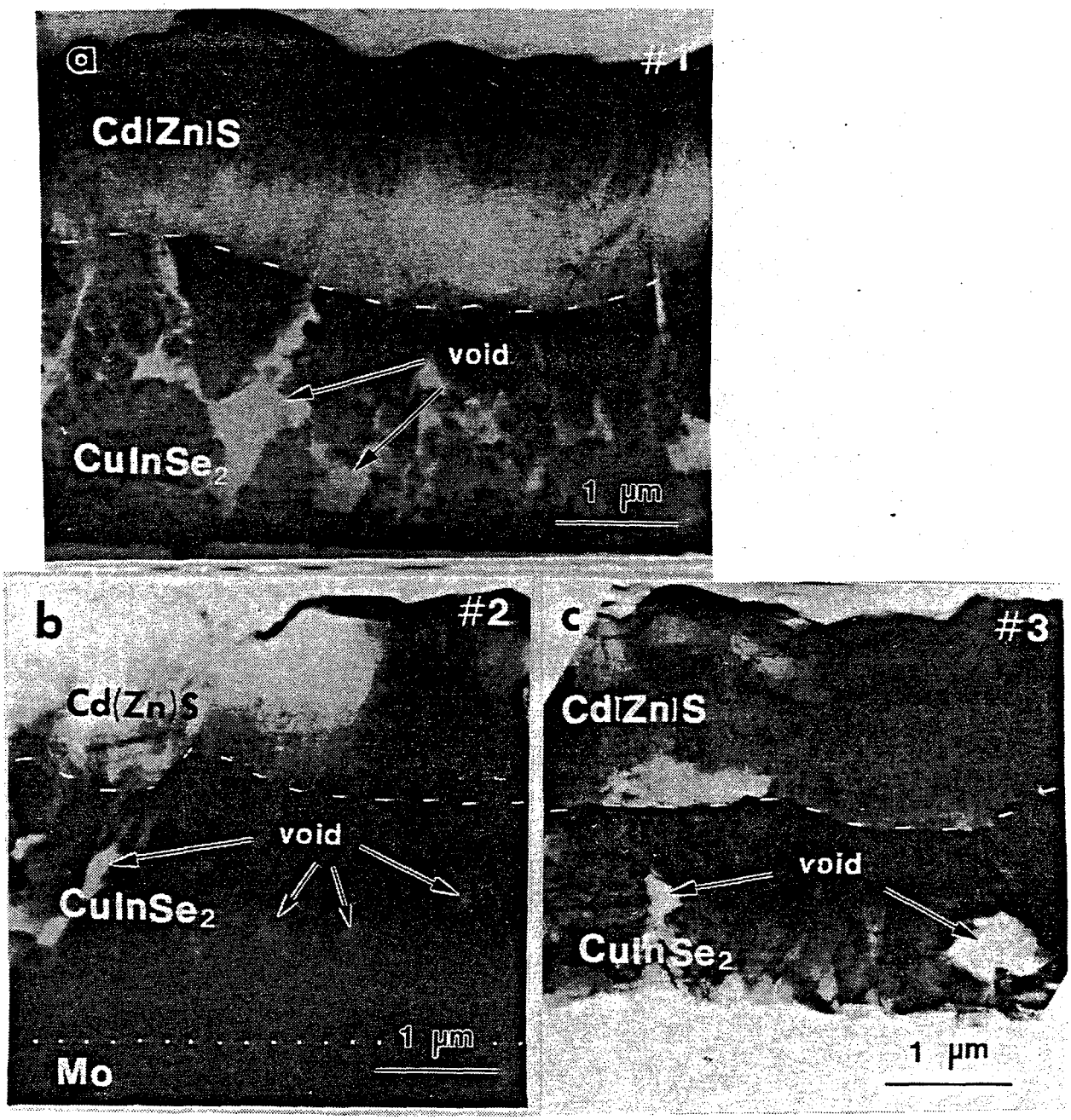

Fig. 3 Bright-field transmission electron micrographs of the cross-sectional structures of the $CuInSe_2$/Cd(Zn)S heterojunctions from sample (a) #1 (deposited on Corning 7059 glass); (b) #2 (deposited on Corning 7059 glass); (c) #3 (deposited on soda lime glass).

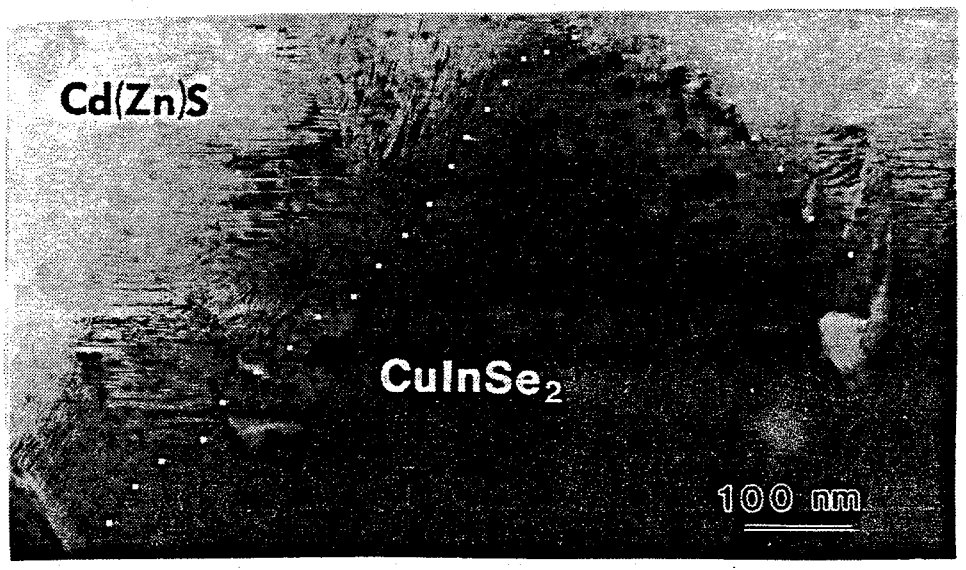

Fig. 4 A bright-field transmission electron micrograph of the $CuInSe_2$/Cd(Zn)S heterojunction interface (from sample #1, deposited on Corning 7059 glass).

Title:	**Role of Polycrystallinity in CdTe and $CuInSe_2$ Photovoltaics**
Organization:	Department of Physics, Colorado State University, Fort Collins, Colorado
Contributors:	J. R. Sites, Principal Investigator; R. A. Sasala, X. X. Liu, I. L. Eisgruber

Objectives

The objectives of this program are quantitative separation of individual loss mechanisms and characterization of extraneous electron states responsible for excessive forward recombination current in polycrystalline thin-film cells.

CdTe Cells

There has been considerable progress with CdTe solar cells during the past year [1]. Table I shows comparative parameters derived by us from cells made at the University of South Florida (USF), Photon Energy (PE), Microchemistry, Ltd., (MC) in Finland, Ametek, and Georgia Institute of Technology. Much of the data used came from SERI measurements, but some is from our laboratory and some was taken from the manufacturers' reports. Not shown in the table are cells made by British Petroleum, the Institute of Energy Conversion, and Queensland University, all of which are in the same efficacy range as those shown.

A photocurrent comparison of the cells from Table I is given in Fig. 1. The AM 1.5 spectrum in current units is at the top, and the lost photon fraction, or one minus quantum efficiency, is at the bottom. For several cells, the photocurrent losses approach the reflection limit over much of the visible spectrum. The long-wavelength bandgap cutoffs are all similar, but the short-wavelength window losses vary markedly according to the thickness of CdS used.

The forward current comparison (Fig. 2) gives a measure of junction quality, as well as resistive and shunting effects [2]. Smaller forward current means larger V_{OC}, and more importantly, larger V_{MP}. Junctions from cells made at USF, MC, and BP have achieved voltages above the hypothetical 15% target cell we have used in recent years. In fact, the best junctions produced at the University of South Florida, combined with the photocurrent achieved at Photon Energy, would yield an efficiency above 16%.

$CuInSe_2$ Cells

There has also been progress with $CuInSe_2$ junctions, although the efficiencies still fall short of that achieved by ARCD Solar in 1988 [3]. The primary progress reported was from International Solar Electric Technology (ISET)[4]. Fig. 3 shows the forward current, which is quite low due to a combination of low diode quality factor A, low series resistance R, reasonably high shunting resistance r, and modest changes between light and dark [5]. This cell also had a hole density of $7 \times 10^{16} cm^{-3}$, significantly larger than seen previously, suggesting that the density of compensating states has been reduced.

Table I. CdTe Cell Comparison

	USF	Photon Energy	Micro-Chemistry	Ametek	GIT
Cell Number	5-16-8-1	3	published	91A6-2	C224
Technique	CSS	Spray	ALE	Electrodep.	MOCVD
Efficiency (%)	13.4	12.7	11.5*	11.0	10.3
V_{OC} (mV)	840	790	810	765	715
A-value	2.5	3.6	2.2	2.25	3.9
R (Ω-cm^2)	0.4	0.7	0.8	0.6	0.2
r (Ω-cm^2)	1500	600	1800	1400	700
V_{MP} (mV)	675	585	665	615	530
Fill Factor	0.725	0.615	0.73	0.715	0.60
J_L (mA/cm^2)	21.9	26.2	19.5*	20.9	24.2
Reflection Loss (mA/cm^2)	2	2	2	2	2
Window Loss (mA/cm^2)	2½	1	8	5	2½
Deep Loss (mA/cm^2)	1	1	1	1½	1
Unknown Loss (mA/cm^2)	3	½		1	½

*Adjusted to SERI measurement.

NOTE: J_L plus losses equals 30½ mA/cm^2.

Time Dependence

There seems to be a general feature of thin-film polycrystalline cells that voltage continues to increase somewhat following the onset of illumination. The effect is primarily driven by the large step in voltage rather than the illumination itself. The voltage increase covers a time range from 10^{-4} to 10^{+2} sec, and has a magnitude of 20-50 mV, depending on the cell used. A practical consequence is that voltages measured with a pulse simulator will very likely underestimate the voltage for normal solar cell operation at the same temperature.

References

1. Sites, J. R. "Role of Polycrystallinity in CdTe and $CuInSe_2$ Photovoltaic Cells", SERI Annual Report, July 1991.

2. Tavakolian, H., and J. R. Sites, "Individual Losses in Thin-Film CdTe Solar Cells", Proc. 21st IEEE Photovoltaics Specialists Conf., (1990), p. 556.

3. Mitchell, K. W., C. Eberspacher, J. Ermer, and D. Pier, "Single and Tandem Junction $CuInSe_2$ Cell and Module Technology", Proc. 20th IEEE Photovoltaics Specialists Conf., (1988), p. 1604.

4. Basol, B. M., V. K. Kapur, and A. Halani, "Advances in High Efficiency $CuInSe_2$ Solar Cells Prepared by the Selenization Technique", Proc. 22nd IEEE Photovoltaics Specialists Conf., (1991).

5. Liu, X. X., R. A. Sasala, and J. R. Sites, "Junction Analysis of Selenized $CuInSe_2$ Solar Cells", Proc. 22nd IEEE Photovoltaics Specialists Conf. (1991).

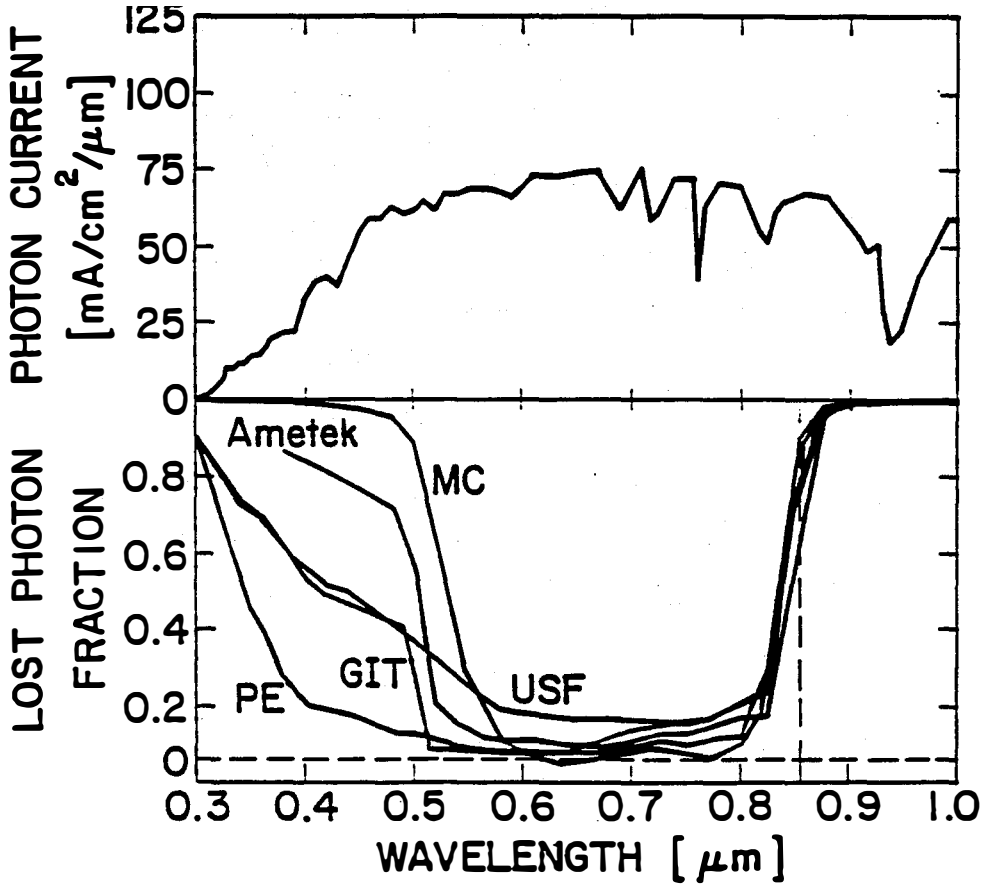

Fig. 1 Comparison of CdTe photocurrent losses.

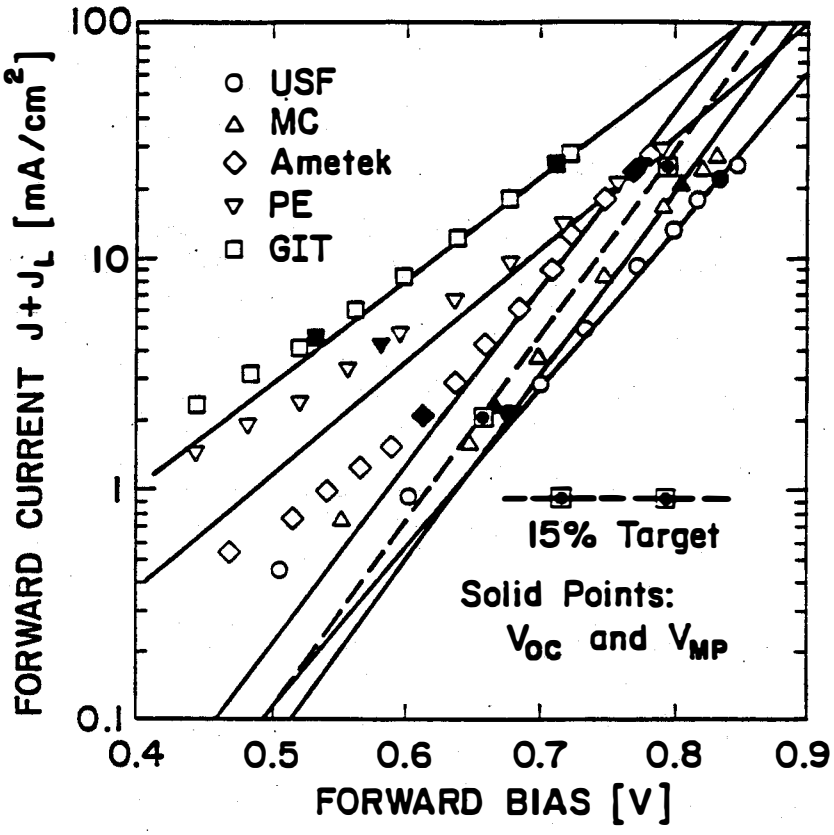

Fig. 2 Comparison of CdTe Junctions.

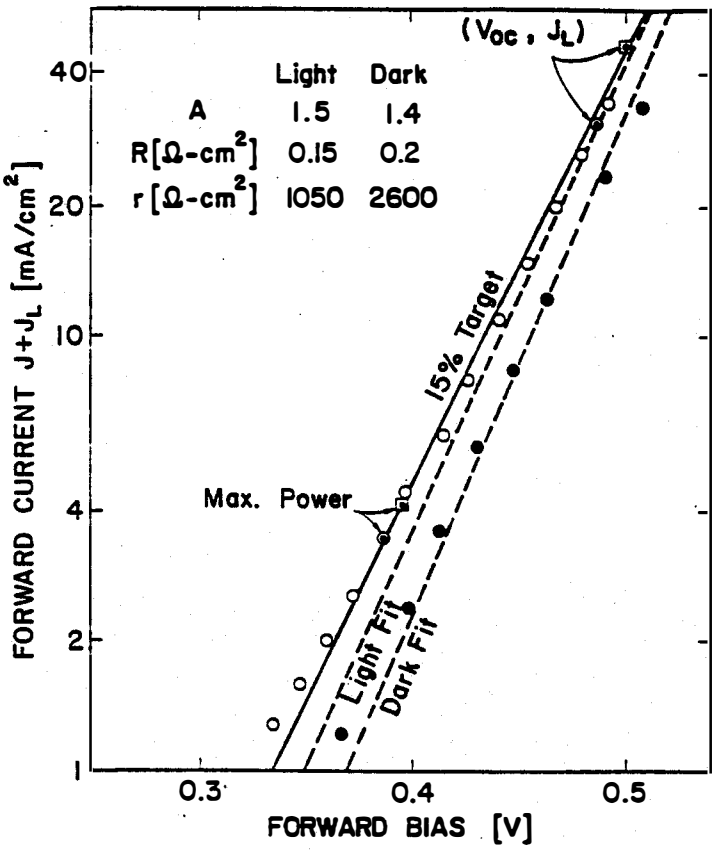

Fig. 3. Light and dark forward currents from best ISET junction.

Title: **Development of High Efficiency CdTe and CdZnTe Solar Cells**

Organization: School of Electrical Engineering, Georgia Institute of Technology, Atlanta, Georgia.

Contributors: A. Rohatgi, R. Sudharsanan, S. A. Ringel, and M. H. MacDougal

Objective:

The objective of this program is to improve the basic understanding of efficiency limiting mechanisms in the polycrystalline CdTe cell, fabricate high efficiency CdTe and CdZnTe cells, and provide guidelines for achieving CdTe cell efficiency of ~15% and wide bandgap (1.7 eV) CdZnTe cell efficiency of ~10%.

Film Growth:

CdTe films were grown on CdS/SnO_2/glass substrates by MOCVD and MBE. The Cd/Te ratio in the growth ambient was varied from 0.4 to 4.0. MBE CdTe and CdZnTe films were grown using a Varian Gen II MBE system [1].

Cell Fabrication:

P-i-n front-wall solar cells were fabricated at AMETEK applied materials laboratory. P-n CdTe cells were fabricated by treating the CdTe films with $CdCl_2$ followed by an air anneal at 400°C for 30 minutes. Contact to the p-CdTe was made by a sequential evaporation of 100 Å Cu and 400 Å Au followed by an anneal at 150°C in argon atmosphere for 90 minutes. Finally, bromine-methanol etch was performed on the entire structure to etch off any residual Cd and Te oxides.

Material and device characterization:

Electrochemical surface photovoltage (SPV) measurement, and photoluminescence (PL) measurements were used for optical, physical and chemical characterization of the films. J-V-T and Deep level transient spectroscopy (DLTS) measurements were used to characterize device properties.

Results and Discussion:

In the past we reported 9.7% cell with V_{oc}=726mV and J_{sc}=22.47 mA/cm^2 on a 2000 Å thick CdS. An attempt was made to improve the J_{sc} by using thinner CdS films. Figure 1 shows a comparison of the light I-V data for the two CdTe/CdS cells fabricated with thick (3000 Å) and thin (1000 Å) CdS films. As expected, the thinner CdS film (1000 Å) increased the efficiency to 10.3% from 9.7% by increasing the J_{sc} to 24.19 mA/cm^2. Further reduction in the thickness of the CdS films to 600 Å resulted in a net decrease in the efficiency (8.9%) primarily due to the reduction in V_{oc} (680 mV) and fill factor (0.55) along with some decrease in J_{sc} (23.47 mA/cm^2). Pin-holes in the CdS films can cause low shunt resistance which will reduce V_{oc} and

fill factor. In addition, CdS films were deposited on the textured SnO_2 films which can aggravate the pin hole problem in the CdS films. On the other hand, increasing the CdS thickness to 3000 Å increased the V_{oc} to 740 mV and, as expected, reduced the J_{sc} to 22.10 mA/cm^2. However, the cell efficiency increased to 10.9% which happens to be the highest efficiency for MOCVD-grown CdTe/CdS solar cell to date. Further, spectral response data showed that the short wavelength response is higher for the cell with thinner CdS films because more high energy photons are able to reach the CdTe film. These results suggest that to improve the CdTe cell efficiency further, the CdS layer thickness should be optimized or replaced by a combination of thin CdS and wider bandgap material such as ZnO [2].

Significant improvement in CdTe/CdS solar cell efficiency is commonly observed as a result of a post deposition $CdCl_2$ dip followed by a 400°C heat treatment. It is also known that the $CdCl_2$ treatment increases the grain size. However, exact physical mechanism for this improvement is not well understood. A study was conducted using DLTS, I-V-T and PL measurements to understand these beneficial effects and to investigate potential efficiency limiting mechanism due to $CdCl_2$ treatment. I-V-T measurements showed that this process changes the dominant current transport mechanism from interface recombination/tunneling to depletion region recombination, suggesting a decrease in the density or dominance of interface states due to the $CdCl_2$ treatment (Figure 2). The change in transport mechanism results in an increase in barrier height and reduction in leakage current, supporting the increase in cell efficiency. However, the DLTS measurements showed that depletion region recombination probably occurs through a large density of deep acceptor-like states at E_v + 0.64 eV which could result from the formation of Cd-vacancy related defects during the $CdCl_2$ dip and heat treatment. Traps in the vicinity of E_v + 0.6 eV have been attributed to V_{cd} and V_{cd} -Cl related complexes. The presence of the acceptor-like traps within the CdTe depletion region was found to affect the CdTe/CdS solar cell characteristics. Figure 3 shows the direct consequence of the density of this defect on the measured V_{oc} and J_{sc} of the CdTe/CdS cells that have undergone this treatment. It is clear from the figure that the V_{oc} and J_{sc} is inversely proportional to the trap density while there is no apparent correlation between the J_{sc} and the trap density. This shows that the $CdCl_2$ treatment is indeed important for improving the CdTe/CdS cell performance, however it appears to introduce a V_{oc} and efficiency-limiting defect whose role must be studied in more detail. It is important to note that in this experiment different trap density was measured on different small area cells fabricated in an identical manner and no controlled attempts were made to vary N_T [3].

In order to understand systematically the role of chlorine-related defects in CdTe/CdS cells, the concentration of $CdCl_2$ was varied in the range of 0.25 to 1 (saturated). PL measurements were performed on finished devices to investigate the defects produced by different $CdCl_2$ concentrations, because the DLTS measurements were not successful in some cells due to high leakage current near the DLTS peak temperature. Light I-V measurements were performed on the finished devices to monitor the device performance and correlate it with the defects. Figure 4 shows the PL spectra of CdTe/CdS devices treated with different $CdCl_2$ concentration. PL spectra showed two common features, a peak around 7900 A and a broad band centered around 8400 Å. In CdTe, the broad band centered around 8400 Å is generally attributed to structural defects, native defects or V_{cd}-Cl defect complexes. The peak at 7900 Å is attributed to Cd vacancies. The intensity or the peak amplitude of the broad band at 8400 Å is directly proportional to the defect concentration in the sample. Several investigators have studied the

effects of chlorine in single crystal CdTe by PL and DLTS measurements. Chlorine is a donor in CdTe and is also known to form defect complexes with Cd vacancies, which are produced during the heat treatment. Chlorine-cadmium vacancy complexes are acceptor type and give rise to shallow and deep energy levels depending on the type of defect complex. According to the literature the chlorine-cadmium defect complexes have energies in the range $E_v + 0.15$ - $E_v + 0.9$ eV. Generally, PL measurements give information about shallow levels and DLTS gives information about deep levels. The fact that the PL broad band around 8400 Å has been attributed to V_{cd}-Cl complex in the literature, and the intensity of the PL band and the density of $E_v + 0.64$ eV DLTS peak both are inversely proportional to V_{oc}, suggests that both the defects are probably chlorine related complexes formed during the $CdCl_2$ treatment. Thus, on one hand $CdCl_2$ treatment is critical to high efficiency CdTe cells but on the other hand it could place an upper limit on the practically achievable efficiency unless the $CdCl_2$ process is modified or optimized [2].

CONCLUSIONS:

We have made an attempt to reveal and understand the efficiency limiting mechanisms in CdS and CdTe films that constitute most of the polycrystalline CdTe cells today. Thickness of CdS limits the cell efficiency due to high energy photon absorption in the CdS layer. It was shown that reducing the CdS thickness first improves the cell performance by increasing the Jsc, but very thin CdS films tend to limit the cell performance due to pin holes which may reduce Voc and FF. It was found that even though $CdCl_2$ treatment is crucial for improving the CdTe cell performance today, it tends to introduce efficiency or V_{oc} limiting defects related to V_{cd}-Cl complexes. The above efficiency loss mechanisms indicate that in spite of the recent success in the CdTe cells, there is a considerable scope for further improvement provided the above efficiency limiting mechanisms can be eliminated by process modification and optimization.

REFERENCES:

1. A. Rohatgi, R. Sudharsanan, S. A. Ringel, and M. H. MacDougal, Solar Cells, 30 (1991) 109.
2. A. Rohatgi, S. A. Ringel, R. Sudharsanan, and H. C. Chou, Proc. 22nd IEEE Photovoltaic Specialists Conference, Las Vegas, Oct. 7-11, (1991).
3. S. A. Ringel, A. W. Smith, M. H. MacDougal, and A. Rohatgi, J. Appl. Phys., 70 (1991) 881.

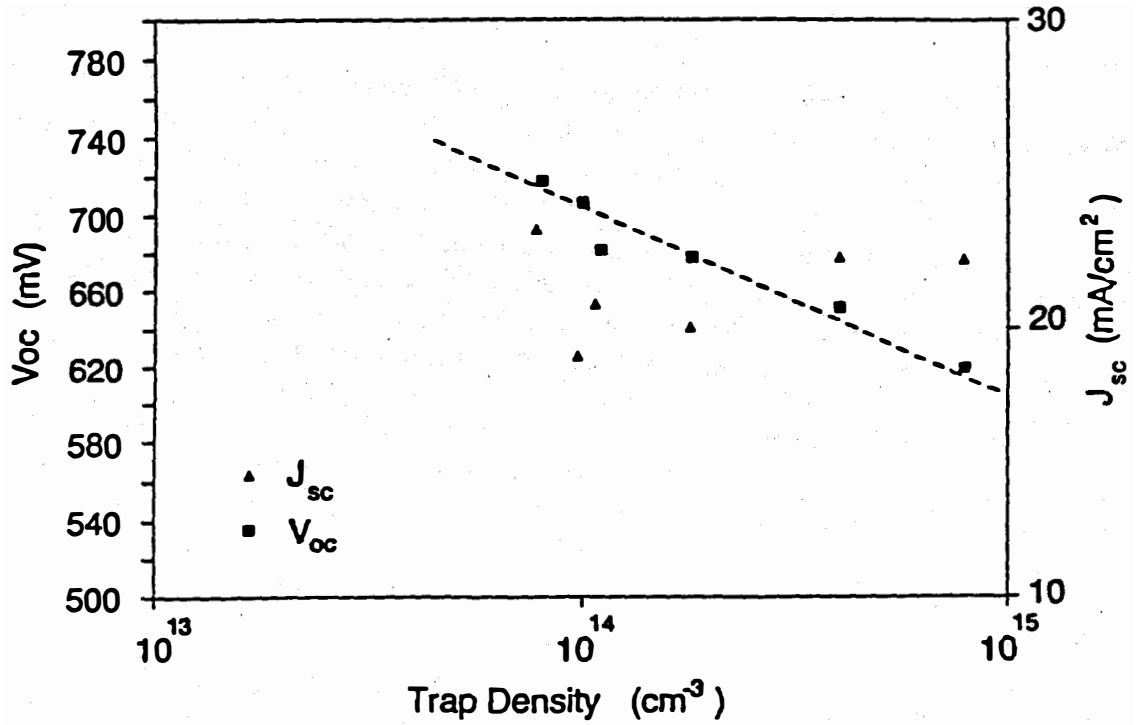

Figure 3. Measured cell V_{oc} and J_{sc} as a function of 0.64 eV trap concentration as determined from the DLTS data.

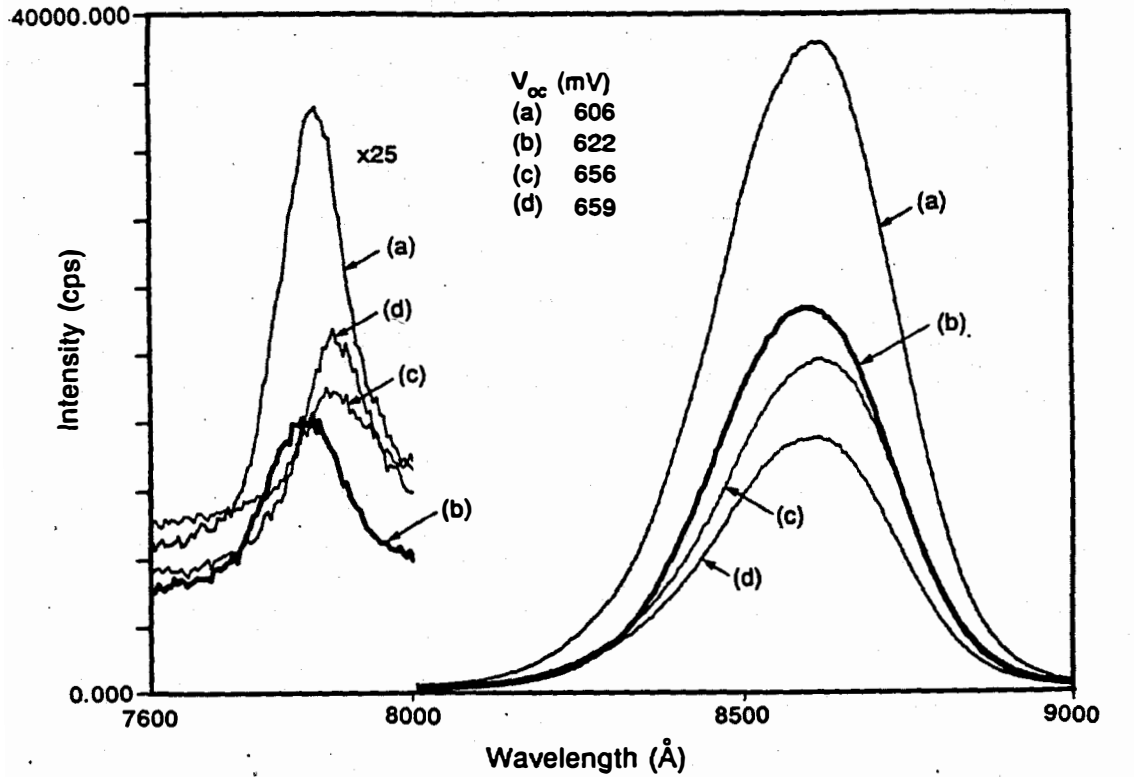

Figure 4. PL spectra of CdTe/CdS structures treated with different $CdCl_2$ concentrations, (a) 100% (saturated), (b) 50%, (c) 25%, and (d) 75%. The corresponding measured V_{oc} on these structures are also shown.

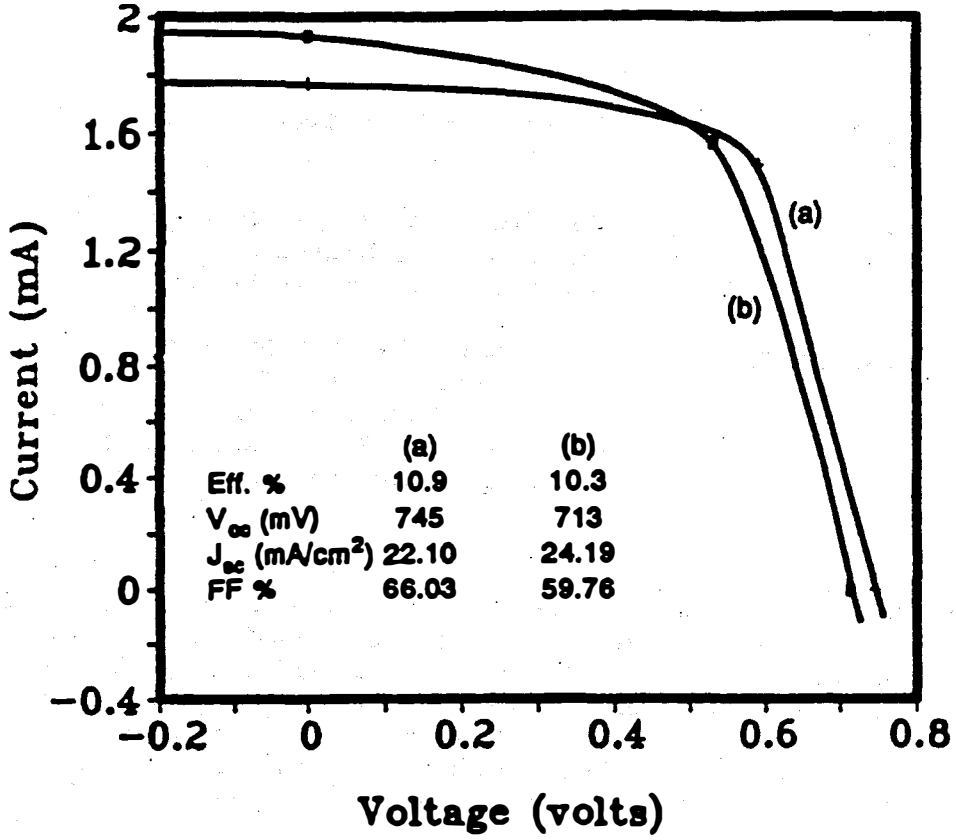

Figure 1. Comparison of light I-V data of MOCVD-grown CdTe/CdS cells fabricated on, (a) 3000 Å and (b) 1000 Å thick CdS films.

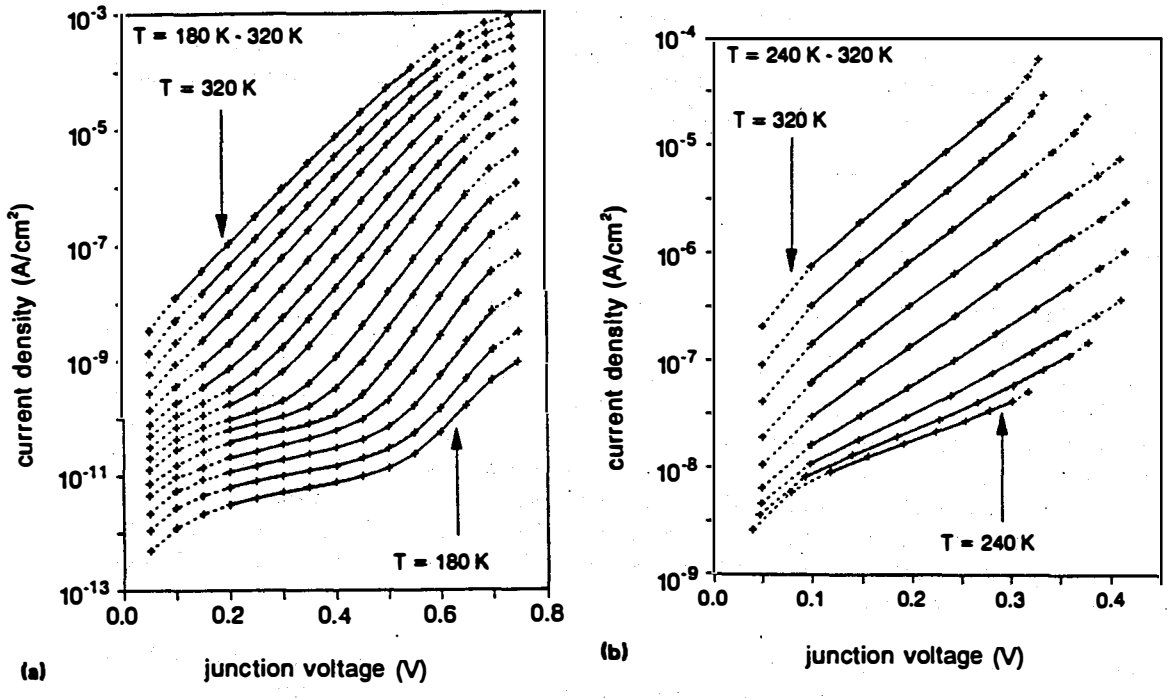

Figure 2. Measured (symbols) and modeled (lines) J-V-T data for (a) $CdCl_2$ + air annealed and (b) air annealed without $CdCl_2$ Ni/ZnTe/CdTe/CdS/SnO_2/glass solar cells. Shown is the current behavior as a function of junction voltage (V-JR*). The average error of each fit is less than 5%.

Title:	**Polycrystalline Thin-Film Materials and Devices**
Organization:	**Institute of Energy Conversion University of Delaware Newark, Delaware 19716-3820**
Contributors:	**B.N. Baron, Project Director; R.W. Birkmire and J.E. Phillips, Principal Investigators; B.E. McCandless, S.S. Hegedus, W.N. Shafarman, T.I. Yokimcus, Research Contributors**

Objectives

The objectives of this research are to obtain the understanding of the materials processing, properties and performance of polycrystalline $CuInSe_2$ and CdTe thin-film solar cells needed to achieve the goals for efficiency, reliability and cost for flat plate thin-film photovoltaic systems set by DOE for the National Photovoltaics Program. A further objective of this program is to support the development of a competitive U.S. photovoltaic industry through collaboration with other research groups and the training of photovoltaic engineers and scientists.

Technical Approach

Issues for $CuInSe_2$ addressed in this work are development of a process for forming $CuInSe_2$ films by the selenization of Cu and In layers with Se and understanding the mechanisms that limit V_{oc} in $CuInSe_2$/CdS solar cells. Research on CdTe is concerned with processing used to fabricate high efficiency CdTe/CdS solar cells with evaporated CdTe.

Results

$CuInSe_2$ by Selenization

An alternative to H_2Se for forming $CuInSe_2$ by selenization is the direct reaction of layers of Cu/In/Se. The Cu and In layers are sequentially deposited by electron beam evaporation with Cu/In atomic ratios of 0.85 to 0.95. The layers are then coated with Se by thermal evaporation. The amounts of Cu, In, and Se are adjusted to produce a 2 μm thick $CuInSe_2$ film. The layers are then heated under a background of Se vapor for about 1 hour at a temperature of 400 or 450°C. Several of the cells made had efficiencies > 9%. The results are summarized in Table 1. All of the devices required a 16 hour, 200°C heat treatment in air to optimize cell performance. This is similar to cells made from $CuInSe_2$ deposited by elemental evaporation.

To evaluate the reaction chemistry leading to the formation of $CuInSe_2$ using H_2Se as the source of Se, thermodynamic and kinetic calculations for H_2Se dissociation were performed. At 400°C, the typical reaction temperature for selenization, the gas phase contains about 50% Se_2 and Se_6 and 50% H_2Se. Kinetic experiments on

pyrolysis of H_2Se show that a reasonable fit to the data can be obtained by assuming Se_6 as the decomposition product (1).

V_{oc} Limits in $CuInSe_2$ Devices

Analysis of the J-V characteristics of $CuInSe_2$/(CdZn)S solar cells measured at various temperatures and light intensities have been used to examine the role of different mechanisms in the device that limit V_{oc}. Previous analysis of illuminated cells has shown that V_{oc} is primarily limited by Shockley-Read-Hall recombination in the $CuInSe_2$ (2) with the diode quality factor near 2. Recent analysis of $CuInSe_2$ cells has indicated that a tunneling mechanism might also be needed to describe the temperature dependence of the dark J-V data (3).

The analysis as a function of light intensity has shown that V_{oc} is controlled by a single current mechanism (Shockley-Read-Hall recombination) with no evidence for interface recombination, tunneling, or other mechanisms (4). Superposition of the dark and light J-V characteristics do not hold due to a light intensity dependent diode quality factor (1.5 to 2). Further comparisons of $CuInSe_2$ cells only differing in V_{oc} indicate that the difference is due to changes in barrier height as shown in Table 2. These results suggest that increasing V_{oc} will require reducing the density of recombination centers (some of which are photo-activated) and increasing the bandgap of the $CuInSe_2$ near the interface.

CdTe Cell Processing

Recent efforts have focussed on the post deposition $CdCl_2$ treatment and its effect on device performance (5,6). After the CdTe deposition, a 0.5 μm $CdCl_2$ coating is applied and the sample heat treated in dry air at 400°C for 30 minutes and rinsed in DI water. Auger and SIMS depth profiles show interdiffusion of Te and S. Also, a 30 meV red shift in the CdTe optical absorption and spectral response is observed. These results suggest the formation of a $Cd(S_xTe_{1-x})$ layer which would result in a narrower bandgap compared to the CdTe. There is also a decrease in the short wavelength response between 520 and 620 nm. This also suggests the formation of a $Cd(Te_xS_{1-x})$ window layer which increases optical absorption.

It has been possible to reduce the formation of the narrower bandgap window layer by applying the $CdCl_2$ treatment to the CdS prior to the CdTe deposition. This helps restructure the CdS and reduce the interdiffusion of S and Te.

Table 3 shows a comparison of device results measured at NREL with and without the $CdCl_2$ restructure treatment on 0.2 μm CdS layers. Restructuring the CdS improves J_{sc} due to improved collection, but has little effect on V_{oc} and FF. This has resulted in 11% efficient solar cells. The spectral responses are shown in Figure 1.

CdTe Device Analysis

J-V measurements as a function of temperature and illumination were made on high efficiency CdTe/CdS thin film solar cells (7). Meaningful analysis of light and dark I-V data could be performed only in the temperature range from 300 K to

345 K due to hysterisis in the I-V measurements at low temperature and irreversible heat treatment effects at high temperature. The analysis indicated that the light generated current varies with the applied voltage as seen in Figure 2 for spectral response ratios at three different bias voltages. If the voltage dependent current collection is included in the analysis of the J-V measurements made under illumination, then both the dark and light analysis give a barrier height near 1.3 eV with a diode quality factor of about 1.8. The barrier height of ~1.3 eV could be due to the narrowing of the CdTe bandgap discussed earlier, which indicates that the CdTe solar cell device operation is also controlled by Shockley-Read-Hall recombination via midgap states.

Conclusions

A process for fabricating $CuInSe_2$/CdS thin-film cells by the selenization of Cu/In/Se layers has been developed. Present device efficiencies exceed 9%. Future research is aimed at continued optimization and analysis of the growth process.

Equilibrium thermodynamic and kinetic calculations for H_2Se dissociation indicate that both Se_x species and H_2Se must be considered in evaluating the $CuInSe_2$ film growth. These results are being used to determine the chemical reactions to forming $CuInSe_2$ using H_2Se.

J-V analysis of $CuInSe_2$/CdS thin film cells as a function of illumination intensity has shown that the dominant V_{oc} limiting mechanism is Shockley-Read-Hall recombination in the $CuInSe_2$. Work is underway to reduce the amount of recombination by grading the bandgap of the $CuInSe_2$.

The post deposition heat treatment with $CdCl_2$ at 400°C has been shown to cause interdiffusion of the S and Te resulting in the formation of a $Cd(Te_xS_{1-x})$ layer which reduces J_{sc} but has no effect on FF or V_{oc}. Steps are being taken to minimize the interdiffusion and improve the optical transmission of the window layers. Progress so far has led to CdTe solar cells with 11% efficiency.

Preliminary J-V analysis of CdTe/CdS thin film cells indicates that there is a voltage dependent current collection which will reduce fill factor. Otherwise, the cells operate much like their $CuInSe_2$/CdS counterparts. Future analysis is aimed at pinpointing the cause of the fill factor problem.

References

1. T.W.F. Russell, R.W. Birkmire, S. Verma, and R.D. Varrin, "Critical Process Issues in Selenization", Proc. of 22nd IEEE PVSC, (1991), to be published.
2. M. Roy, S. Damaskinos, and J. Phillips, Proc. of 20th IEEE PVSC, 1618 (1988).
3. J.B. Yoo, A. Fahrenbruch and R. Bube, J. Appl. Phys. 68, 4694 (1990).
4. W.N. Shafarman and J.E. Phillips, "Diode Analysis of $CuInSe_2$/(CdZn)S Solar Cells", Proc. of 22nd IEEE PVSC, (1991), to be published.
5. B. McCandless and R. Birkmire, "Analysis of Post Deposition Processing for CdTe/CdS Solar Cells", Solar Cells 34 (1991), to be published.

6. B.E. McCandless and S.S. Hegedus, "Influence of CdS Window Layers on Thin Film CdS/CdTe Solar Cell Performance", Proc. of 22nd IEEE PVSC, (1991), to be published.
7. D.A. Fardig and J.E. Phillips, "Characterization of CdTe/CdS Solar Cells", Proc. of 22nd IEEE PVSC, (1991), to be published.

Table 1
J-V Characteristics of Cells Formed from Cu/In/Se

Device #	Cu/In ratio	$T_{substrate}$ (°C)	V_{oc} (V)	J_{sc} (mA/cm^2)	FF (%)	Eff (%)
61066-12	0.85	400	0.420	36.8	59.6	9.2
61066-11	0.90	400	0.426	31.9	60.7	8.3
61067-12	0.85	450	0.403	35.4	62.9	9.0
61067-11	0.90	450	0.395	37.9	61.5	9.2
61067-13	0.95	450	0.278	32.9	53.3	4.9

Table 2
J-V Characteristics of Cells with Differing V_{oc}

	Cell #1	Cell #2
V_{oc}	0.440V	0.417V
J_{sc}	33.8 mA/cm^2	33.8 mA/cm^2
FF	67.6%	67.2%
Eff.	10.1%	9.3%
ϕ (eV)	0.99eV	0.91eV
A [dark]	1.6	1.5
A [dark]	1.75	1.75

Table 3

NREL J-V Data Comparing 0.2 μm Evaporated CdS with and without $CdCl_2$ Recrystallization Process

Device #	Recrystallized CdS	V_{oc} (V)	J_{sc} (mA/cm^2)	FF (%)	η (%)
40723-11-3	yes	0.789	20.1	69.4	11.0
40723-12-1	no	0.799	18.4	72.0	10.6

EFFECT OF CDS/CDTE INTERDIFFUSION

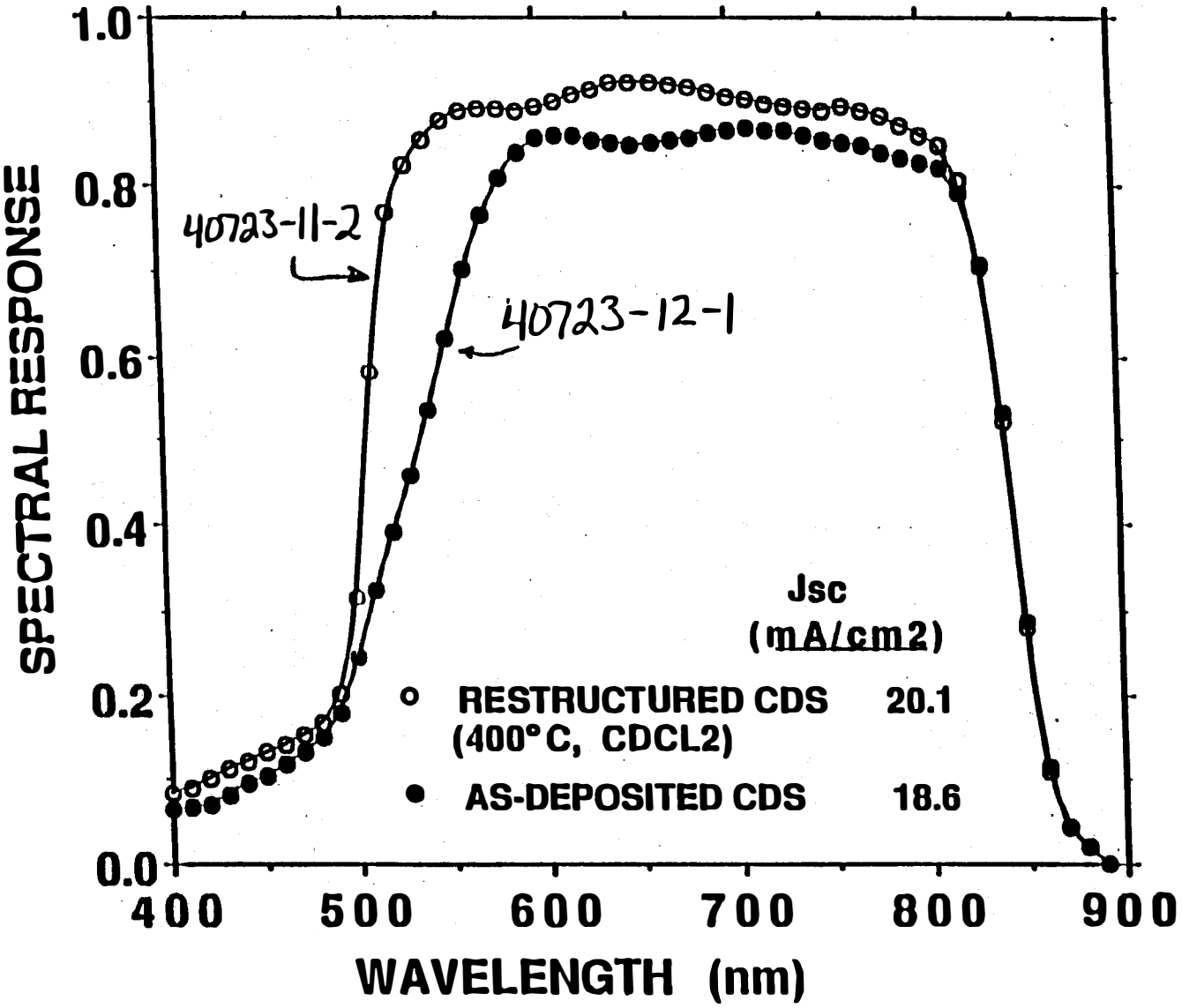

Figure 1

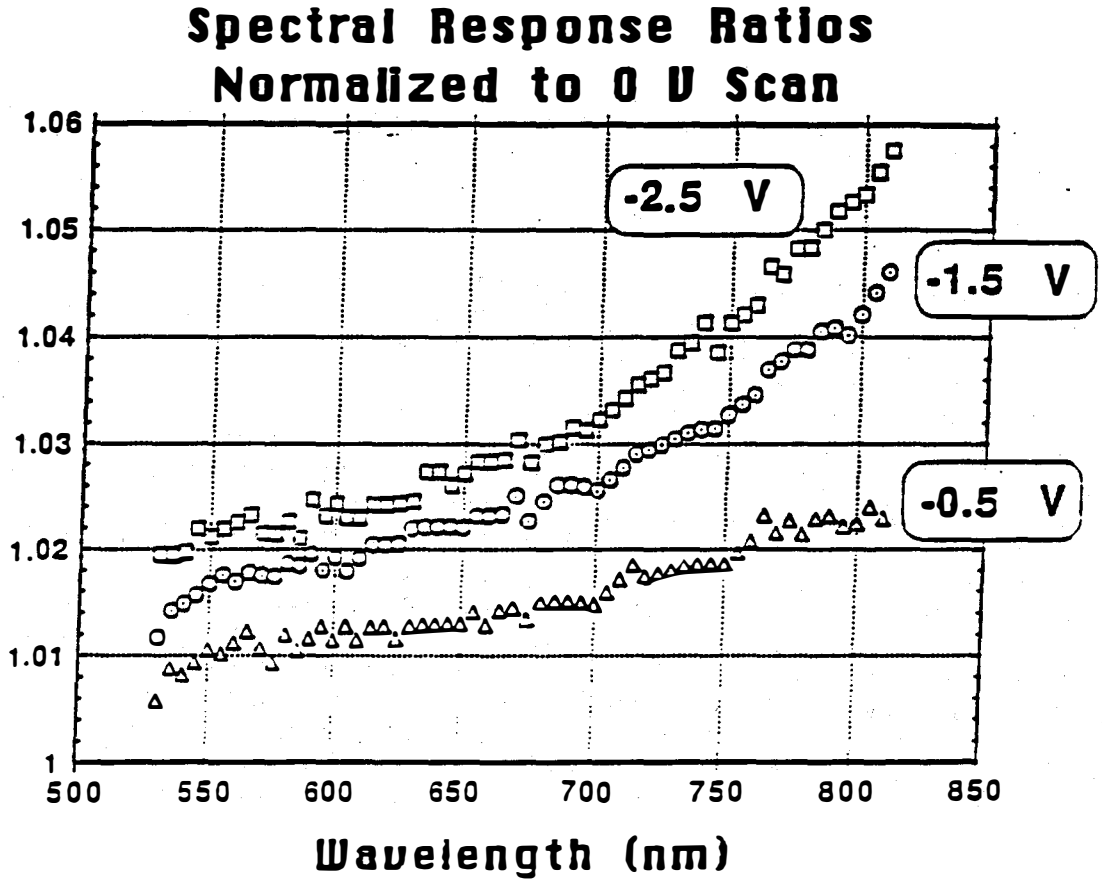

Figure 2. Spectral Response in Reverse Bias Normalized to Zero Bias for CdTe Solar Cell

Title: Low Cost $CuInSe_2$ Submodule Development

Organization: International Solar Electric Technology (ISET), 8635 Aviation Blvd., Inglewood, CA 90301

Contributors: Bülent M. Başol and Vijay K. Kapur, principal investigators, A. Halani and C. Leidholm

The objective of this program is to develop high efficiency thin film $CuInSe_2$ solar cells and 1 ft^2 modules using a two-stage process. The processing technique involves selenization of evaporated or sputtered Cu-In precursor layers. In our FY 1990 report, we had pointed out the influence of the nature of the Cu-In precursors on the resulting $CuInSe_2$ films and solar cells. During this period we continued our studies on Cu-In precursors. As a result, we developed a novel approach to the preparation of high-quality Cu-In films. We have improved the active area efficiency of our cells to the 12.4% range and we set up facilities to process 1 ft^2 $CuInSe_2$ modules.

Cu-In Precursor Preparation

The commonly used process for the preparation of a Cu-In precursor for selenization involves depositing a thin Cu layer on a glass/Mo substrate and then following this step with the deposition of an In film. The most important reason for the wide usage of the glass/Mo/Cu/In structure for selenization is related to the morphological and mechanical properties of the precursor films. Cu layers evaporated onto Mo coated glass substrates at room temperature form smooth and continuous layers with adequate adhesion to the Mo surface. After the indium deposition step these precursors are partially alloyed (1) and they still adhere reasonably well to their Mo coated glass substrates. The properties of Cu/In layers strongly depend on the deposition parameters of their elemental components. In the case of evaporation, low In deposition rates and fine-grain copper layers enhance the degree of alloying between the Cu and In films. Intermixing between Cu and In may also take place during the selenization step which involves high temperatures. Such variations can cause poor repeatability of the $CuInSe_2$ film characteristics which are affected by the nature of the precursors. The purpose of our work was to develop a new approach to Cu-In film preparation, where an extensively alloyed layer could be obtained within a reasonably wide range of deposition parameters.

In our previous reports we pointed out that the degree of alloying between the evaporated Cu and In films depend, among other factors, on the sequence of deposition (1). Specifically, we indicated that evaporating Cu over an In layer which has a low melting temperature, gave rise to more complete intermixing between the two

elements. Recognizing that a completely alloyed precursor which could be prepared in a repeatable manner would offer advantages over those whose properties change from batch to batch, we initiated work on developing In/Cu precursors where the In layer was deposited first on the Mo surface. However, when In is deposited on a Mo surface, it forms isolated droplets which grow and for a film thickness of >2000 Å, melt together to form a continuous film. The bond of the resulting layer with the underlying Mo layer is poor and failure of this weak bond often causes film peeling after the Cu evaporation step. Even if they do not peel off their substrates, Cu-In precursors prepared by this approach are highly non-uniform and they yield low-efficiency solar cells.

Characteristics of thin films, among other factors, depend on the nature of the interfacial region at the substrate/film interface . The nature of this region, on the other hand, is determined by the chemical interactions between the depositing species and the substrate material which can be altered by modifying the substrate surface. In our two-stage process, this can be achieved by interjecting a thin inter-facial layer between the depositing In film and the Mo coated substrate. In doing so, however, it is important to assure that the elements included in this inter-facial layer do not adversely affect the electrical properties of the $CuInSe_2$. Te is a group VI material like Se. It can be deposited by a variety of methods such as evaporation, sputtering and electrodeposition. Diffusion of Te has been shown to enhance the p-type character of $CuInSe_2$ crystals. Furthermore, Te reacts with In, forming various compounds. Therefore, a thin Te layer deposited on the Mo surface is expected to influence the nucleation characteristics of a subsequently evaporated In film. In our experiments we have successfully used 20-200 Å thick Te interfacial films to improve the quality of the evaporated In/Cu precursors and to optimize the structural, mechanical and electrical properties of the $CuInSe_2$ layers obtained utilizing these precursors (2). Results of such an experiment is shown in Figures 1a and 1b. Introduction of a thin Te layer at the substrate/film interface has provided a precursor film with smaller grain structure, better coverage and better adhesion to the substrate (Fig.1b).

Effect of CdS Deposition Processes on Cell Characteristics

The solar cell structure evaluated in this work was the ZnO/CdS/CIS/Mo/glass structure. ZnO films were grown by MOCVD. CdS layers were either evaporated or dip-coated. Evaporated and chemically grown CdS layers deposited on glass substrates were evaluated in terms of their optical properties. It was observed that the optical transmission of the chemically grown CdS layers was relatively high even at energies greater than the absorption edge which is at around λ=0.52 μm. This was the result of low reflectance and low absorption displayed by these films. One other difference between the evaporated and chemically coated CdS films was their resistivity values. The in-plane resistivity of the dip coated layers was $>10^5$ Ω-cm, whereas, this value was in the 100-500

Ω-cm range for the evaporated films.

Fig. 2 shows the lost photon fraction of a set of devices with evaporated and chemically grown CdS windows. The wavelength independent losses in the 0.6 μm<λ<1.0 μm range are due partly to reflection and partly to absorption in the ZnO layers. These losses do not show any clear relation to the method of CdS deposition. The short wavelength response, on the other hand, correlates well with the technique used to coat the CdS windows. Fig. 3 plots the short wavelength window losses for a group of ZnO/CdS/$CuInSe_2$ cells. It is observed that the devices with chemically grown CdS films generate about 2 mA/cm^2 more photocurrent than the evaporated CdS films even for CdS thicknesses of around 0.5 μm. This is consistent with the optical data we presented in the previous section.

CdS film properties are not the only factors affecting the characteristics of the ZnO/CdS/$CuInSe_2$ solar cells. The processes used in the deposition of the CdS and ZnO films are also expected to influence the quality of these junctions. For example, the chemical growth method allows the deposition of extremely thin (<0.05 μm) CdS films on rough $CuInSe_2$ surfaces in a conformal manner. In the evaporation approach, discontinuities in such thin layers and their thickness control present practical problems. Furthermore, evaporation requires heating the $CuInSe_2$ films to around 200 °C in vacuum. During the early phases of deposition the $CuInSe_2$ surface is exposed to the incoming elemental Cd and S vapors which react to form the compound. Chemical method is a low-temperature approach that allows the growth of a stoichiometric compound film on the $CuInSe_2$ surface at temperatures <80 °C. We have studied the possible influence of the CdS deposition techniques on the junction quality of ZnO/CdS/$CuInSe_2$ structures. For this purpose, we have carried out controlled experiments in which the same $CuInSe_2$ film was used in the fabrication of solar cells employing either a chemically coated or an evaporated CdS window layer. We have consistently measured lower diode factors, better fill factors (after taking out the series resistance effect) and higher open-circuit-voltages for the dip coated samples. Capacitance measurements showed that the dip coated $CuInSe_2$ films displayed higher hole density values than those coated with evaporated CdS windows. This observation points to a significantly reduced compensation in the junction areas of cells using the dip coated CdS layers. A list of the relevant parameters for a group of devices and their structures are given in Table 1. The observed correlation between the CdS deposition technique and these parameters is very good. The increased degree of compensation in the films with evaporated window layers may be due to their exposure to the elemental Cd vapor at relatively high temperatures in the vacuum chamber.

High Efficiency Cells and Large-Area Depositions

Fig. 4 is the illuminated I-V characteristics of a 1 cm^2 area device with 11.5 % total area efficiency measured at SERI under AM1.5 global spectra (3). The solar cell parameters of this device

are; V_{oc}= 0.4832 V, J_{sc}=35.60 mA/cm^2 and FF=66.65 %. The active area efficiency is 12.4 %. The J_{sc} value of this cell was limited by the reflection losses (about 5%),absorption in the ZnO and CdS layers (around 10%) and both ZnO absorption and carrier collection losses at longer wavelengths. The diode quality factors in the dark and under illumination are 1.6 and 1.8 respectively. The capacitance measurements made on this device yielded a carrier density of around $2x10^{16}$ cm^{-3} and very small frequency dispersion, again indicating good junction quality. The best diode quality factor and the highest hole density measured for our devices were 1.50 and $7x10^{16}$ cm^{-3}, respectively.

During this period we have also built facilities to process 1 ft^2 size $CuInSe_2$ modules. We have demonstrated monolithic integration on 6"x6" substrates and Cu and In deposition and selenization on 1 ft^2 substrates.

Conclusions

We have developed a new approach for the preparation of Cu-In precursor layers to be used in the selenization technique. In this approach, the surface of the Mo coated substrate was chemically modified to improve the growth characteristics of the precursors. Selenization of improved precursors yielded stoichiometrically, morphologically and mechanically superior $CuInSe_2$ films which were used to fabricate high efficiency solar cells. We have demonstrated that the nature of the CdS window layers as well as their processing approaches significantly affect the performance of the ZnO/CdS/$CuInSe_2$ solar cells. Chemical deposition of CdS gives devices with lower diode factors and better junction qualities compared to those using evaporated CdS windows. The high efficiency cells reported in this paper used chemically coated CdS layers and they have displayed good voltage and fill factor values. The current densities can be further improved to the 37-40 mA/cm2 level by optimizing the ZnO/CdS window layer. During this period, we have also started processing 1 ft^2 devices. We have demonstrated Cu and In depositions on 1 ft^2 substrates. We have carried out selenizations on these samples. We deposited CdS and ZnO layers on such substrates. Future work will concentrate on the optimization of the ZnO films and fabrication of monolithically integrated 1 ft^2 modules.

References

1. B. M. Başol and V. K. Kapur, Proc. 21st IEEE PVSC, 1990, IEEE, New York, p. 546.
2. B. M. Başol, V. K. Kapur and R. Matson, Proc. 22nd IEEE PVSC, 1991, IEEE, New York, in press.
3. B. M. Başol, V. K. Kapur and A. Halani, Proc. 22nd IEEE PVSC, 1991, IEEE, New York, in press.

(a)

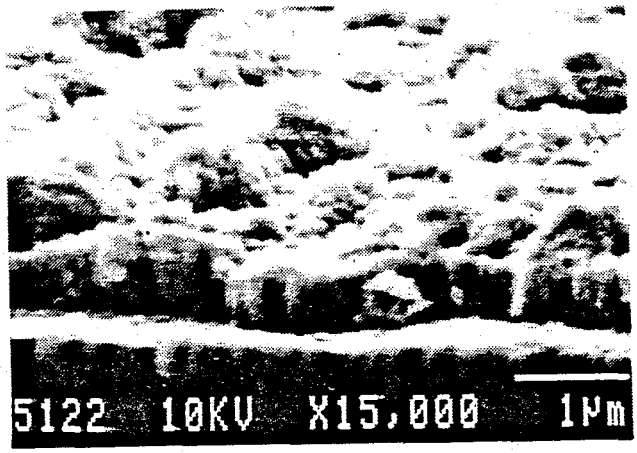

(b)

Fig. 1. SEMs of (a) Mo/In/Cu, and (b)Mo/Te/In/Cu structures demonstrating the effect of a 20 A thick Te layer.

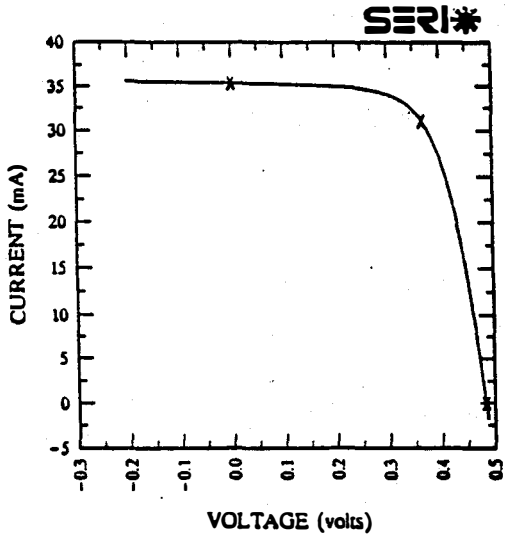

Fig. 4. Illuminated I-V characteristics of a 1 cm^2 device.

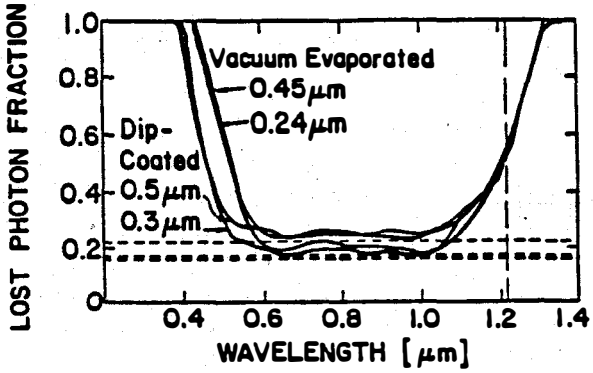

Fig. 2. Lost photon fraction for a group of cells.

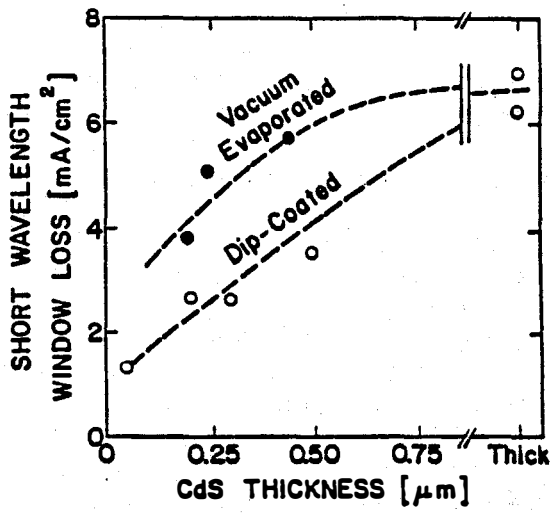

Fig. 3. Window loss vs CdS thickness.

Cell #	Window	A	FF	p(cm^{-3})	Eff.(%)
629-1	0.20 μm evap.	1.95	0.56	$1.3x10^{16}$	5.6
629-2	0.20μmdip	1.60	0.70	$3.0x10^{16}$	10.4
673-1	0.24 μm evap.	1.90	0.56	$1.0x10^{16}$	7.4
673-2	0.45 μm evap.	1.75	0.63	$1.2x10^{16}$	8.6
673-3	0.50 μm dip	1.70	0.68	$3.0x10^{16}$	10.4

Table I. Parameters of cells with evaporated or dip-coated CdS window layers.

Title: Innovative Sputtering Techniques for CIS and CdTe Submodule Fabrication

Organization: Martin Marietta Defense Space and Communications

Contributors: J.H. Armstrong, Principal Investigator, B.R. Lanning, R.G. Wendt, J.L. Draper, M.S. Misra

OBJECTIVES

This project, Innovative Sputtering Techniques for CIS and CdTe Submodule Fabrication, consists of two sequential 12-month phases. Objectives of this project are the following:

(1) To develop large-area deposition technology using rotating cylindrical magnetron sputtering for polycrystalline thin-film CdTe and CIS photovoltaics, and

(2) To produce CIS modules up to 930 cm^2 (1 ft^2) using state-of-the-art deposition and cell definition technologies with potential for production scaleup and low fabrication cost.

APPROACH

This project, initiated in September of 1991, utilizes a dual rotating cylindrical magnetron (C-Mag™) from AIRCO, Inc. to sputter thin films to fabricate copper-indium-diselenide (CIS) and cadmium-telluride (CdTe) photovoltaic devices over large areas (Fig. 1). Key advantages to this approach are (1) higher deposition rates, (2) efficient material utilization, and (3) potential for unique codeposition techniques as compared to planar sputtering [Ref 1, 2]. Maximum substrate size will be least 30.5 cm x 30.5 cm, although this technology can be scaled-up to production status; substrates larger than 250 cm x 360 cm in architectural glass coatings have already been demonstrated.

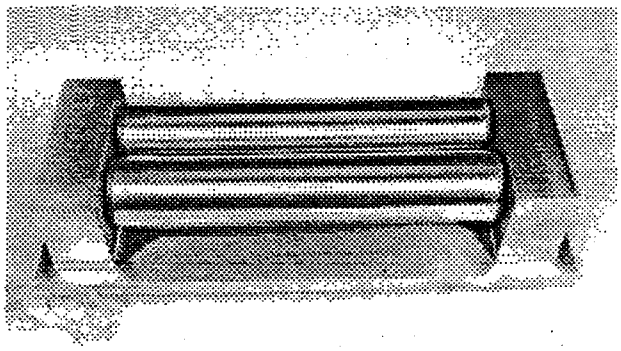

Figure 1
Photograph of AIRCO Dual Rotating Cylindrical Magnetron.

Three tasks are identified in this project, namely:

Task 1: Thin-film Deposition

Task 2: Device Manufacture and Scaleup

Task 3: Monolithic Integration of 930 cm^2 Submodules

Task 1 begins at the initiation of the program and continues for 12 months. Task 2 begins six (6) months into Phase 1 of the program and continues for 18 months. Task 3, which lasts for 12 months, begins in the second phase of the program. Below is a description of these tasks.

Task 1 — Thin-Film Deposition

A key issue of this project is the ability to develop large-area deposition techniques capable of low-cost submodule fabrication and scaleup potential. In all cases, soda lime glass will serve as the substrate (superstrate) for the CIS (CdTe) devices. C-Mag™ sputtering will be used to produce the absorber layers ($CuInSe_2$, CdTe), transparent conductive oxide (ZnO, ITO), and the back contacts with baseline parameters being established by planar magnetron. The absorber layer will be produced by sputtering of elemental targets (Cu and In, Cd and Te) using a two-step process [Ref 3,4]. Cosputtering of elemental and alloyed targets by C-Mag™ also will be attempted to minimize hazardous chemical environments and waste and to reduce the overall cost of production. Chemical immersion will be used to deposit the window layer (CdS). Details on both sputtering and chemical immersion are given below.

Large-Area Sputtering — To facilitate this program, requirements for a custom in-line sputtering system incorporating an AIRCO Model 940 C-Mag™ were identified and Denton Vacuum, Inc. was selected to fabricate the system. The system was designed to allow for simultaneous sputtering of a variety of target materials, including alloyed targets, over a vertically-mounted 40 cm x 40 cm substrate (Fig. 2). Cathodes are mounted to a large hinged plate attached to the main chamber via a swing arm, thereby allowing for easy access to targets for cleaning, inspecting, and changing. Calrods placed on both sides of the carrier in the pre-sputter position and behind the carrier during deposition allows for substrate temperatures up to 300°C. Aluminum foil barriers will be installed to accommodate easier cleanup after cadmium, tellurium, and selenium deposition. Viewports and inspection covers are included to enhance operation and cleanup. Standard operating procedures are being established in conjunction with Martin Marietta safety and hazardous waste disposal guidelines.

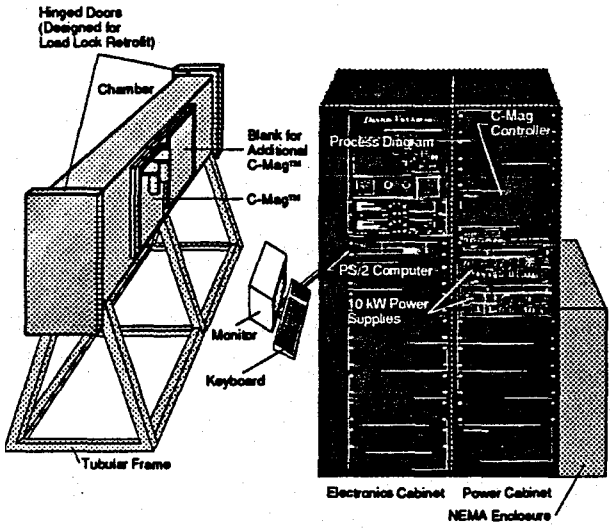

Figure 2
Schematic of Vertical Sputtering System Incorporating AIRCO Dual C-Mag™ Cathodes.

A key issue with regard to film uniformity is the precision of the substrate transport. Details on the substrate transport mechanism are shown in Figure 3. Vertical substrate transportation was selected to minimize contamination of the large-area substrates by debris and to accommodate changes and upgrades more easily. Multiple drive wheels are spaced 13.3 cm apart to ensure at least three wheels in contact with the substrate carrier at all times. Furthermore, the carrier is suspended only by the drive wheels, allowing for differential thermal expansion between the chamber(s) and the carrier.

Chemical Immersion Deposition — An inexpensive method for preparing thin films of CdS is by a chemical immersion deposition. In this method, CdS can be prepared by decomposition of

thiourea (or thioacetamide) in an alkaline solution of cadmium salts where the salt can be $Cd(CH_3COO)_2$, $CdSO_4$, $Cd(NO_3)_2$, or $CdCl_2$. Substrates are immersed in a pH-adjusted salt solution below 90°C, and CdS indiscriminately deposits on properly activated surfaces upon addition of thiourea.

Quality, deposit morphology, and deposition rate of CdS films are intimately related to the solubility equilibria in the salt solutions. Solutions containing suspended precipitates (cloudy appearance) yield surface coatings which are thin and tightly adherent. Good coatings can also obtained from solutions which are clear and do not contain suspended precipitates. To understand observed CdS film growth behavior, it is necessary to address the solubility equilibria for CdCl salts in NaOH, NH_4Cl, and NH_4OH solutions.

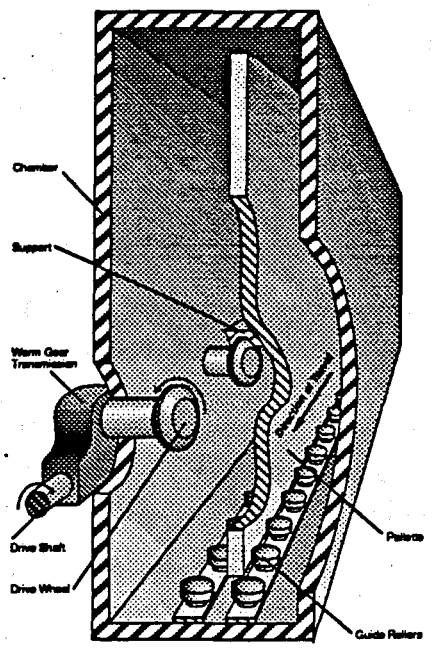

Figure 3
Schematic of Vertical Substrate Drive Mechanism.

To determine the distribution of all constituents present in the cadmium salt solution prior to addition of thiourea, mass and charge balances, as well as solubility equilibria, were determined for all cadmium and ammonium species and simplified to generate equations which relate total cadmium to total ammonium. For $CdCl_2$ in NH_4OH, a plot of (–)log C versus (–) log N is shown in Figure 4 ('C' refers to the total cadmium concentration and 'N' refers to the total ammonium concentration). The shaded portion of this curve is where $Cd(OH)_2$ will precipitate (turbid solution) and the numbers on the curve refer to the pH at the point of precipitation. Because $Cd(OH)_2$ precipitate is required in order to activate the decomposition of thiourea (i.e. formation of CdS), solution compositions should be contained within this shaded region. Although $Cd(OH)_2$ is required for activation, unassociated, free cadmium ion concentration is also a major factor in controlling the rate and morphology of the film growth process.

Testing and Evaluation — Once films have been deposited, extensive material testing will be conducted to quantify and correlate fabrication and performance parameters. Material testing such as glancing incidence X-ray diffractometry (GID), fast Fourier transform infrared spectrometry (FTIR), atomic absorption (AA), Auger electron spectroscopy (AES), scanning electron microscopy/energy dispersive X-ray spectroscopy

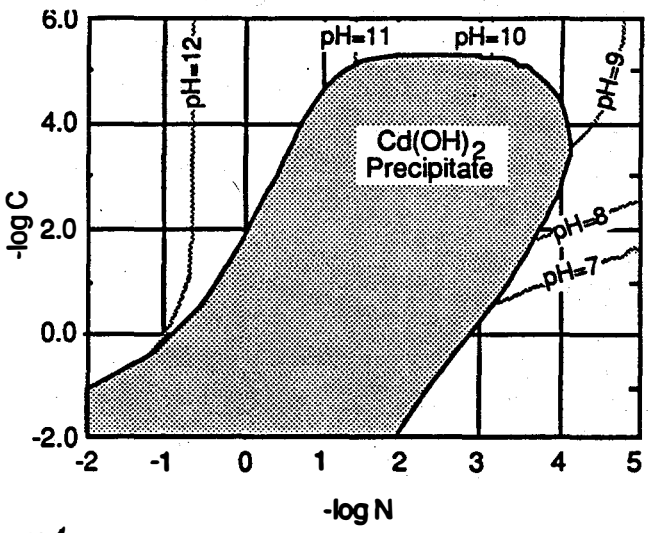

Figure 4
Plot of Total Cadmium Concentration versus Total Ammonium Concentration for $CdCl_2$ in NH_4OH.

(SEM/EDX), spectrophotometry, and reflection measurements shall be performed. Adhesion and electrical conductivity measurements will also be conducted to optimize performance of these films.

Task 2 — Cell Fabrication and Scaleup

Once baseline parameters are transferred to C-Mag™ sputtering system and chemical immersion deposition techniques, and quality films are demonstrated, both TCO/CdS/CIS/Mo/Glass and Glass/TCO/CdS/CdTe/Ni cells will be fabricated. Initial cells will be nominally 1 cm^2, although other specific geometries may be necessary for certain testing and evaluation. Although the absorber films will be made by two-step processing, devices will be fabricated with cosputtered absorber layers in Task 2, depending upon the quality of these films in Task 1.

In addition to the thin-film testing and evaluation noted above, capacitance and light/dark I-V response will be measured and the quantum efficiency of the device will be determined. Thermal dependence on cell output will be measured, and loss mechanism analysis will be performed to establish guidelines for improved performance.

Task 3 — Fabrication of Monolithically-Integrated Submodules — Data obtained in Tasks 2 and 3 with techniques in monolithic integration developed by Martin Marietta IR&D project D–17R, Photovoltaic Technologies in 1991 will be assimilated to demonstrate monolithically-integrated devices in either CIS or CdTe. Both photolithography and laser scribing will be investigated for scribing the back contact, CdS/absorber layer stack and the TCO. Width of the individual cells will be 1 cm or less, while the cell will run the length of the module.

Early demonstrations of monolithic integration will be performed on small-area devices (< 4 cm^2), and scaleup of all processes will ultimately lead to a 930 cm^2 submodule. Particular care will be taken in testing and evaluation of the interconnect region. The large-area pulsed solar simulator (LAPSS) facility at Martin Marietta will be used to analyze the performance of entire active area of each submodule, with special care taken to quantify differences in performance of polycrystalline devices due to time-dependent effects [Ref 5].

RESULTS

Thin-film Deposition — Preliminary films are being fabricated by planar magnetron to serve as baseline for the C-Mag™. Development efforts at Martin Marietta in chemical immersion deposition of CdS have been in the scale-up to larger surface areas required of this contract. Although there is currently a limitation on the size of the immersion bath for the batch process, CdS was deposited onto 20 cm x 20 cm ITO coated glass plates. The conditions of the bath were 0.1 M $Cd(CH_3COO)_2$, 1 M NH_4OH and 0.2 M Thiourea. CdS film thickness was ≈500 Å as confirmed by a DekTak II A Surface Profile Measuring system (Fig. 5).

Absorption measurements were made on 2.5 cm x 5 cm CdS films with the light incident from the glass side and the spatial uniformity was on the order of 3% (Fig. 6). Uniformity in the larger, 20 cm x 20 cm area coatings appears even better than the small, 2.5 cm x 5 cm glass slides and based on these results, there appears to be no fundamental limitation to scaling up the coating process to even larger areas. We are currently in the process of measuring the optical uniformity of the CdS coating on ITO/glass substrates for the larger 20 cm x 20 cm areas. Efforts to coat sputtered CIS films with CdS using the cadmium iodide system for improved interfacial properties are in progress.

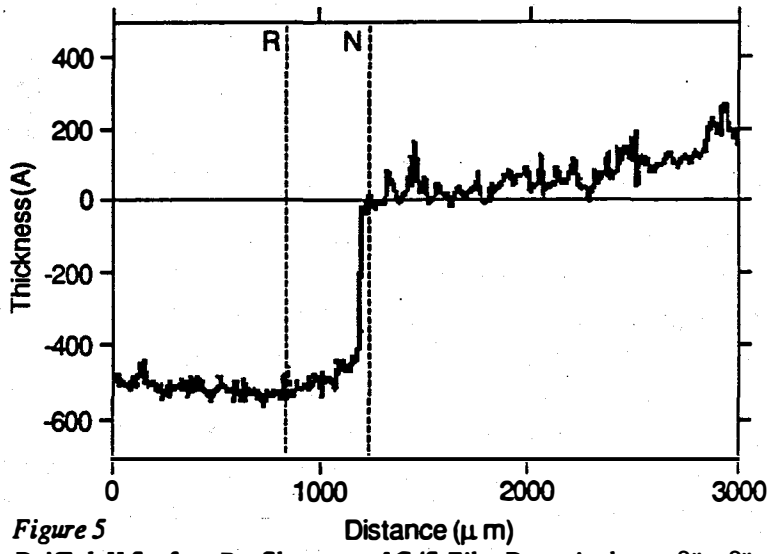

Figure 5
DekTak II Surface Profilometry of CdS Film Deposited onto 8" x 8" ITO-coated Glass.

C-Mag™ Target — One of the most important aspects to this program is the potential for cost reduction, both in terms of fabrication speed and efficient material utilization. Presently, nonstandard targets for the C-Mag™ system are very expensive (>$9K for molybdenum and indium) or difficult to obtain (high-purity Cu, Se, Cd, Te and alloys of the above). Consequently, two approaches are being pursued to manufacture C-Mag™ targets at Martin Marietta for polycrystalline thin-film PV, namely (1) electrodeposition of Cd, Te, and CdTe onto AIRCO stainless steel sleeves, and (2) target foil rolled onto the stainless steel sleeve. Using pulsed electrodeposition technology developed at Martin Marietta, films of Cd, Te, CdTe, and possibly In and Se will be placed on the AIRCO stainless steel sleeves (Fig. 7). While this process would not necessarily be economical for production, electrodeposition would allow for significant flexibility in producing sputtering targets for this investigation. Another economical way of producing these targets is the use of metallic foils bonded to the stainless steel sleeve with conductive epoxy (Fig. 8) While this technique has not been tried for C-Mag™ technology, careful bonding of target foils to the AIRCO cylinder would allow for easy elemental depositions, as well as cus-

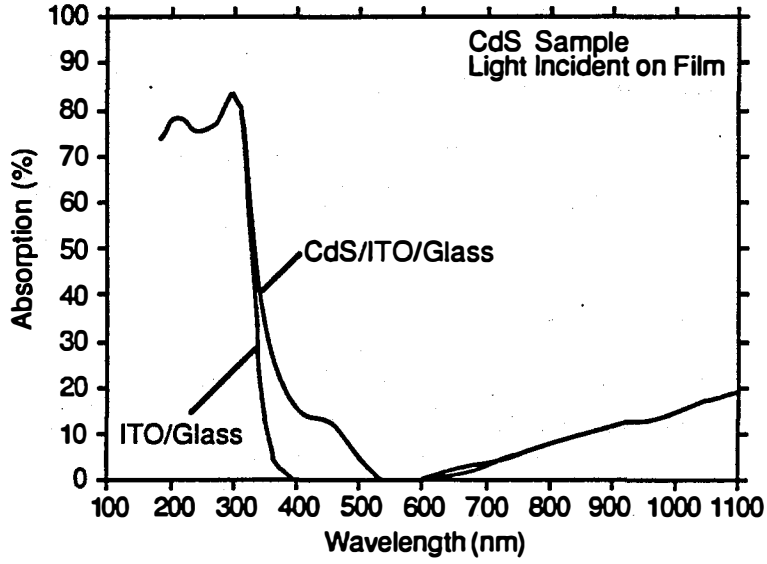

Figure 6
Absorption Measurements of 500 Å CdS Film Deposited onto 8" x 8" ITO-coated Glass.

tom-made alloy foils. Other techniques, such as plasma spraying are under investigation, although cleanliness of target material is an issue.

SUMMARY

A dual rotating cylindrical magnetron is being utilized to reduce the cost and increase the throughput of CIS and CdTe photovoltaic modules. Key issues with this project include (1) C-Mag™ target cost, (2) uniformity of films over large areas, (3) increase of deposition rate, (4) efficient material utilization, and (5) the abilitiy to perform cosputtering for reduced processing cost and minimization of hazardous waste.

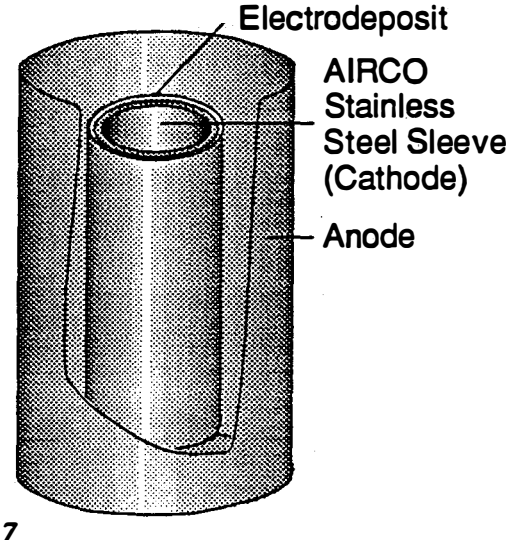

Figure 7
Schematic of C-Mag Targets Manufactured by Electrodeposition.

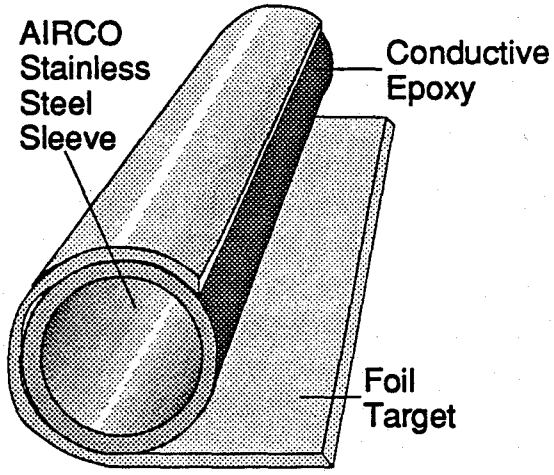

Figure 8
Schematic of C-Mag Targets Manufactured by Foil Bonding.

ACKNOWLEDGEMENTS

International Solar Electric Technologies, Inc. (ISET) is a major subtier contractor in this effort.

REFERENCES

1. V.K. Kapur and B.M. Basol: "Key Issues and Cost Estimates for the Fabrication of $CuInSe_2$ (CIS) PV Modules by the Two-Stage Process," Proc. 21th IEEE Photovoltaic Specialists Conf., IEEE, New York, 1990, p. 467

2. B.M. Basol and V.K. Kapur: "$CuInSe_2$ Thin-Films and High-Efficiency Solar Cells Obtained by Selenization," Proc. 21th IEEE Photovoltaic Specialists Conf., IEEE, New York, 1990, p. 458

3. D. Griffin: "The New C-Mag™ Dual Rotatable Sputtering Cathode: Present Status and Future Considerations," proceedings of the Third International Conference on Vacuum Web Coating, San Antonio, TX, 12-14 November, 1989.

4. C. Boehmler: "Film Properties of Coatings Deposited by C-Mag™ Rotatable Sputtering Cathode," AIRCO Technical Report, AIRCO Coating Technology, Concordia, CA.

5. J. Sites: Private Communications.

Title: **High-Efficiency, Large-Area CdTe Panels**

Organization: Photon Energy, Inc., El Paso, Texas

Contributors: S.P. Albright, R.R. Chamberlin, J.F. Jordan

Introduction and Objectives

Photon Energy Inc.(PEI) has been involved with the development of CdS/CdTe devices and modules since 1984. Starting in 1987, a three(3) year subcontract under SERI contributed to progress toward the common objectives between PEI and the Department of Energy(DOE). In mid 1990, a second three(3) year subcontract was begun in order to further improve the technology base at PEI in order to better address the objectives of the PEI and DOE photovoltaic goals.

The PEI objectives in Photovoltaics are covered through continuing advancement in four(4) major areas:

* Modules efficiency
* Module size
* Module reliability
* Module cost

Specific Goals For The Present Subcontract

The specific objectives of this three year program are:

* To achieve active area efficiencies of greater than 14% on small cells,

* To achieve aperture area efficiencies of greater than 13% on 1 ft^2 modules,

* To achieve aperture area efficiencies of greater than 12.5% on 4 ft^2 modules,

* To achieve greater than 20-year module life (based on life testing extrapolations) with no greater than 10% efficiency degradation.

Experimental

In order to meet the goals and milestones within this project at least five(5) basic tasks have been specified. They include:

TASK I: Windows, Contacts and Substrates (external device optimization)

* Improved CdS window layers using various methods of deposition, including deposition from solution,

* The tin oxide window layer-electrode resistivity and uniformity,

* Improved electroding techniques,

* Reduction of optical losses due to module division.

TASK II: Absorber Material (Internal device optimization)

* The deposition, characterization and evaluation of CdTe alloys,

* The characterization, evaluation, and improvement of morphology effects of the CdTe,

TASK III: Optimization of Device Structure

* Electronic characterization and modeling of the device,

* The development of improved device structures where appicable.

TASK IV: Encapsulation

* Analysis and optimization of present methods,

* Hermetic sealing techniques,

* Isolation and concentration on long term corrosion issues.

TASK V: Process Optimization

* The diffusions and reaction kinetics involved during the process,

* Exploration and improvement of heat transfer issues.

TASK VI: Employee Safety Evaluation and Improvement

* Evaluation and improvement (where necessary) of monitoring program for Cd in the workplace,

* Evaluation and improvement (where necessary) of policies and practices affecting worker safety in the workplace,

Results and Projections

Following are a review of the most important achievements during the first phase of this subcontract.

Small Device Efficiency

A device with an area of 0.302 cm^2 was delivered to SERI and was measured on May 3, 1991 with 12.7% efficiency. The open circuit voltage was measured as 799 mV and the short circuit current density was measured as 26.21 mA/cm^2 for this device. A current on another device measured by SERI in the same time frame measured 26.23 mA/cm^2, and this current is believed to be a record for high efficiency CdTe devices. These high currents (and the associated high quantum efficiencies at higher than CdS bandgap energies have become the norm at PEI. The fill factor was low at 60.5%. If the fill factor can be raised to 70%, the corresponding efficiency will be ~14.7%. Efforts in this direction continue.

Dr. T.L.Chu and his group at the University of South Florida are on a lower-tier subcontract under our subcontract through SERI. Part of his efforts under this subcontract are to help develop solution grown CdS for use as our thin CdS layer. One of the iterations resulted in devices which produced over 840mV. It was measured at SERI as 842mV. This is, to date, the highest voltage

device observed at PEI. Such trends are expected to continue as this development proceeds. Dr. Chu is able to achieve voltages that are typically higher than the best results at PEI. Dr.T.L.Chu has achieved 14.6% efficiency in recent weeks. Combining the high voltages and fill factors on his devices with the high quantum efficiencies and short circuit currents on PEI devices should result in 15-17% efficient devices in future developments.

1 ft² Module Efficiency

PEI modules have proven to be difficult to measure accurately. For module sizes larger than ~4" x 6", that due to their size cannot be tested on the continuous Xenon artificial sunlight source at NREL, there has been considerable question regarding accurate measurement of PEI module output. The pulse simulator typically utilized for large area module testing does not appear to be a satisfactory means of testing modules such as ours which have a testing sensitivity related to the prior biasing condition of the module and slow response times. However, it is believed that the methodology planned to be implemented at NREL will be quite satisfactory. This methodology includes maximum power point tracking to determine the maximum power point directly avoiding any significant pre-bias effects.

Two 1 ft² modules were sent to NREL in September 1991. The following table presents a comparison of the test results at NREL on 9/17/91 and at PEI earlier. Aperture area on both panels is 825 cm².

	PEI	NREL
AAB885B		
P_{max} (un-normalized)	6.4W	6.80W
P_{max} (normalized)	6.4W	6.54W
V_{oc}	21.1V	21.1V
I_{sc} (normalized)	0.590A	0.601A
FF	52%	51.6%
Aperture Area Efficiency	7.8%	7.9%
AAC024B		
P_{max} (un-normalized)	6.87W	6.59W
P_{max} (normalized)	6.84W	6.30W
V_{oc}	21.5V	21.3V
I_{sc} (normalized)	0.605A	0.597A
FF	52%	49.5%
Aperture Area Efficiency	8.3%	7.6%

It is concluded that PEI has attained aperture area efficiencies on modules between 7.6% and 8.3% on 1 ft² modules. The active area efficiency (due to non-optimized division losses) were ~9.5-10%. Uniformity across the modules and improvement of the fill factor (through improvement of the diode ideality factor) should result in significant improvements in the reasonably near future.

A 4 ft^2 module was tested at NREL in early November. The uncorrected outdoor value was 23.06 W. The corrected output (to 1000 watts/m^2 using a pyranometer reading) was 21.3 W.

Reliability Testing

The life testing data from NREL forms a significant part in the determination of the reliability objective under this program. In order to be able to extrapolate life testing data accurately, one must start with very narrow measurement error bars. As mentioned above, the difficulties associated with the accurate measurement of large area CdS/CdTe modules has resulted in a considerable amount of effort being expended at PEI and at NREL in order to accomplish this error minimization goal.

There have been a number of sets of modules in various stages of development delivered to SERI and NREL by PEI in the past several years. A number of the early sets were meant to serve as "proof-of-concept" indications that no initial degradation occurs and that CdTe, properly encapsulated, can be a stable and reliable photovoltaic system.

A number of these early attempts were presented for life testing without sufficient weatherproofing. The result has been that after several years the encapsulation system on a number of these modules has failed. As the encapsulation system and weatherproofing has advanced, these types of failures have been reduced as well.

Due to a combination of sample variations and measurement error bars, the life testing results have not been homogeneous. Some have failed dramatically (due to insufficient encapsulation design); few have appeared to degrade slightly; several have shown no signs of degradation.

The fact that several modules have shown no significant degradation indicates that there is no inherent degradation problem associated with CdTe modules. As further improvements to the encapsulation system and module measurement techniques are made, reliable module lifetimes are expected to become more homogeneous and are expected to show excellent reliability on both real time and accelerated life tests.

Summary and Conclusions

The efficiency and stability objectives at PEI on CdS/CdTe modules are being addressed. To summarize:

* Efficiencies of 12.7% have been achieved on small area devices.

* One square foot modules have achieved over 8% aperture area efficiency (active area efficiency up to ~10%)

* Four square foot modules have been tested at NREL at 21.3 watts.

* Life testing at NREL (and PEI) shows no inherent stability problems with the CdTe technology.

Progress has been made and advancement is expected to continue in a steady fashion in Phase 2 and Phase 3 of this subcontract. The results should approach or exceed the proposed objectives.

Publications

1. S.P.Albright, R.R.Chamberlin, J.F.Jordan, "Cadmium Telluride Module Development", Presented at PVAR&D meeting in Lakewood,CO, October 1990. (To be Published in *Solar Cells*).

Title: **Development of a Computer Model for Polycrystalline Thin-Film $CuInSe_2$ and CdTe Solar Cells**

Organization: School of Electrical Engineering
Purdue University
West Lafayette, IN 47907

Contributors: R. J. Schwartz and J. L. Gray, principal investigators; Y. J. Lee, graduate student

Objective

The purpose of this research program is to develop an accurate numerical model for $CuInSe_2$ (CIS) and CdTe based solar cells. This code will be used to analyze and aid in the design of CIS and CdTe based solar cells.

Approach

An accurate numerical model depends on precise knowledge of a variety of material and device parameters. The first phase of this research was to obtain published values for materials parameters and state-of-the-art CIS and CdTe solar cells. Initial models for absorption, recombination, carrier transport, band structure, and carrier profiles suitable for implementation in the code were then developed based on this information.

The numerical code developed for this program was based on a general purpose code, ADEPT (A Device Emulation Program and Toolbox). Customized versions of this code designed specifically for the simulation of CIS and CdTe based solar cells capable of running on a IBM compatible personal computers will be released to NREL.

Results

Results of this research are discussed in references [1-5]. Some results are summarized below.

A numerical computer model for $CuInSe_2$ and CdTe based solar cells has been developed which will run on IBM PC-AT or compatibles and Sun workstations. Features of this computer model are discussed in [2].

The initial effort of the program, besides development of the computer model, was devoted to a survey of cell performance characteristics and to a survey of relavent material parameters. Some of these results, taken from [5], appear below in Table 1.

In addition, the computer model has been used to analyze basic structures and develop design guidelines as described in [1,3,4].

Conclusions

Numerical simulation has already proved its usefulness in analyzing and designing a variety of semiconductor devices, including solar cells. Initial modeling of CIS cells has already improved the understanding of the performance of these cells. As the specific models relevant to absorption, recombination, transport, etc. are improved, the ability of the code to analyze and design CIS and CdTe based solar cells is expected to be an invaluable tool for PV researchers.

References

1. R. J. Schwartz and J. L. Gray, "The use of $CuIn_{1-x}Ga_xSe_2$ Layers to Improve the performance of $CuInSe_2$ Cells," Conference Record of the Twenty-First IEEE Photovoltaic Specialists Conference, Kissimmee, Florida, May 1990, pp. 570-574.
2. J. L. Gray, "ADEPT: A General Purpose Numerical Device Simulator for Modeling Solar Cells in One-, Two-, and Three-Dimensions," presented at and to appear in the Conference Record of the Twenty-Second IEEE Photovoltaic Specialists Conference, Las Vegas, Nevada, October 1991.
3. J. L. Gray and Y. J. Lee, "Numerical Modeling of CdS/CdTe Solar Cells: A Parameter Study," presented at and to appear in the Conference Record of the Twenty-Second IEEE Photovoltaic Specialists Conference, Las Vegas, Nevada, October 1991.
4. R. J. Schwartz, J. L. Gray, and Y. J. Lee, "Design Considerations for Thin Film CIS and Other Polycrystalline Heterojunction Solar Cells," presented at and to appear in the Conference Record of the Twenty-Second IEEE Photovoltaic Specialists Conference, Las Vegas, Nevada, October 1991.
5. J. L. Gray, R. J. Schwartz, and Y. J. Lee, "Annual Report on the Development of a Computer Model for Polycrystalline Thin-Film $CuInSe_2$ and CdTe Solar Cells," Purdue University Technical Report TR-EE-91-49, West Lafayette, Indiana, December 1991.

Table 1 - Survey of CuInSe2 Solar Cells

window layer	Voc Volts	J_{sc} mA/cm^2	FF	Efficiency. %	Illumination
CdS	0.396	35	0.64	8.72	AM1
	0.396	39	0.63	9.53*	ELH
	0.380	35	0.63	(10.01**)	sun 93.9
				8.95	mW/cm^2
	0.3	34	0.44	6.9	ELH 60 mW/cm^2
	0.470	30.50	0.715	10.26* (10.8**)	
	0.42	35 - 40	0.66		
bi - layer	0.370	35	0.64	8.5	
	0.395	38	0.67	10.1	
	0.397	36	0.53	7.7/9.9	
	0.44	34		9.9	
single-layer	0.278	36	0.55	5.5	
	0.44	35.6	0.62	9.7	100 mW/cm^2
	0.35	31.7	0.38	4.2	AM1.5
	0.396	39	0.63	9.53	AM1 101.5 mW/cm^2

** active area efficiencies.

* total areaefficiencies.

All the others were unspecified.

Title: **Research on High Efficiency, Large Area $CuInSe_2$-Based Thin Film Modules**

Organization: Siemens Solar Industries
Camarillo, California

Contributors: Kim W. Mitchell, Project Director; C. Eberspacher, J. Ermer, C. Fredric, R. Gay

Introduction

Siemens Solar Industries (SSI) began a 3-year, 3-phase cost shared contract on May 1, 1991 to demonstrate 12.5% aperture efficient, large area (3900 cm^2) encapsulated thin film $CuInSe_2$ (CIS) modules. Prior to the contract, SSI demonstrated a 14.1% active-area efficient, 3.4 cm^2 ZnO/thin CdS/CIS/Mo/glass cell and fabricated monolithic integrated submodules with unencapsulated aperture efficiencies of 11.2% on 940 cm^2 and 9.1% on 3900 cm^2 [1]. The best encapsulated large area CIS module power output prior to the contract was 33.7 W, 8.7% aperture efficiency (verified at NREL) over a 3883 cm^2 aperture area [2].

The key contract milestones are:

Table 1: CIS Module Performance Milestones

Parameter	Start 5/1/91	16 month 8/31/92	27 month 7/31/93	36 month 4/30/94
I_{sc} (A)	2.43	2.57	2.71	2.78
J_{sc} (mA/cm^2)	35.7	37.0	39.0	40.0
V_{oc} (V)	23.6	24.4	25.3	26.5
V_{oc}/cell (mV)	445	460	478	500
FF	0.59	0.62	0.65	0.66
P_{max} (W)	33.7	38.8	44.6	48.5
Eff (%)	8.7	10.0	11.5	12.5

Approach

The module design, illustrated in Fig. 1, consists of 53 series-connected ZnO/CdS/CIS/Mo/glass cells fabricated on a 4141 cm^2 (128.6 x 32.2 cm) glass substrate with a nominal aperture area of 3895 cm^2 (127.3 x 30.6 cm). The module interconnect region is portrayed in the expanded cross section. Module performance strongly depends on the spatial uniformity of cell and interconnect performance, which in turn depend on the properties of the constituent layers. Initial contract emphasis has been on module

diagnostics using improved techniques to characterize the cells and interconnects. V_{oc} maps provide information on the junction quality. Resistance losses due to individual interconnects or ZnO sheet resistance can be determined by mapping the cell voltage drops at a fixed forward bias current. In addition, individual cell I-V curves can be evaluated by measuring the dependence of the voltage drop of each cell on the applied module current. The physical nature of the defects is then correlated using optical beam induced current (OBIC), electron beam induced current (EBIC), scanning electron microscopy (SEM), and other techniques such as tape adhesion testing. The preliminary results of this studies are described in the next section.

Results

During FY 1991 (5/1/91 - 9/30/91), a new world record of 37.7W and 9.7% aperture efficiency for a 3883 cm^2 (126.9 x 30.6 cm) encapsulated CIS module was demonstrated and verified at NREL. The corresponding photovoltaic parameters are 2.44 A I_{sc} (36.5 mA/cm^2 J_{sc}), 24.0 V V_{oc} (453 mV cell V_{oc}), and 0.644 fill factor. Excellent measurement agreement was verified between SSI and NREL.

The V_{oc} maps for a 39W (10.0% efficient) and a 32W (8.2% efficient) module are compared in Fig. 2. The voltage is very uniform for the higher power module. In contrast, the cell voltages for the lower power module are both suppressed overall and non-uniform. OBIC studies indicate that the reduced V_{oc} cells have localized areas of low response. One source of low response identified by SEM and EBIC are areas of abnormal ZnO growth associated with "dust" contamination of the surface before the ZnO. Other areas do not correlate with surface features but have reduced adhesion between the CIS and Mo. Interconnect problems can substantially reduce the module fill factor (FF) as evidenced in Fig. 3. The 0.53 module FF (Fig. 3a) results from the poor FF of individual module slices (see Fig. 3b). Comparison of the V_{oc} and forward bias maps in Fig. 3c show the junctions are fairly uniform but some cells have high voltage drops associated with poor quality interconnects [3]. Research is focusing on improved materials and processing quality. Two papers have been presented resulting from this contract [3,4].

References

1. K. Mitchell, C. Eberspacher, J. Ermer, K. Pauls, D. Pier, D. Tanner. Proc. 4th International PV Science and Engineering Conf., Sydney, Australia, Feb. 14-17, 1989, pp. 889-896.

2. K. W. Mitchell, W. Chesarek, D. R. Willett, C. Eberspacher, J. H. Ermer, R. R. Gay. Solar Cells 30, 131-136 (1991).

3. R. Gay, J. Ermer, C. Fredric, K. Knapp, D. Pier, C. Jensen, D. Willett. Prcc. 22nd IEEE PV Specialists Conf., Las Vegas, NV, Oct. 7-11, 1991.

4. D. Tarrant, A. Ramos, D. Willett, R. Gay. See Ref. 3.

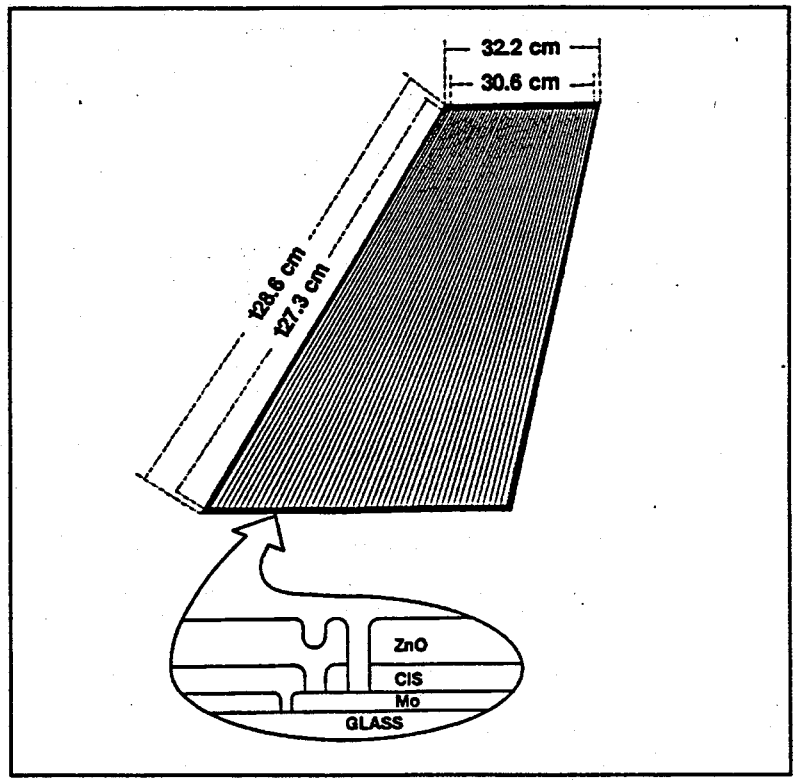

Fig. 1. Basic design of 0.4 m^2 CIS module. The details of the integrated interconnect are shown in the inset.

360 380 400 420 440 460 480

Fig. 2. Voltage maps comparing higher and lower power CIS modules.

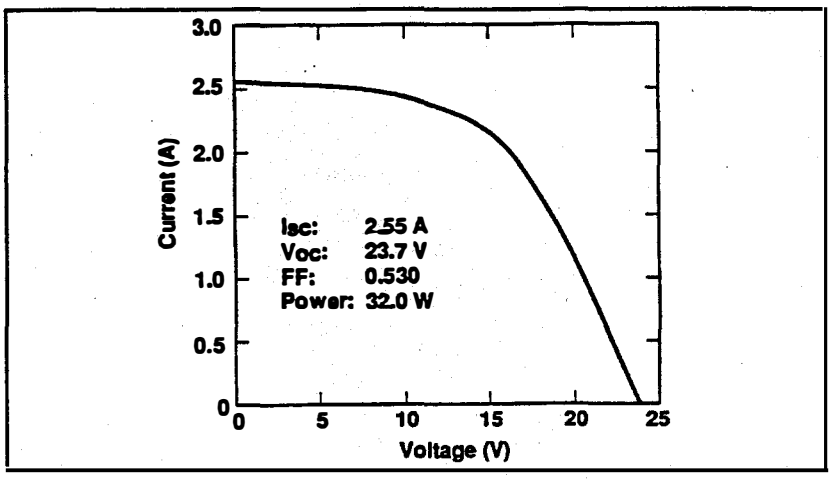

Fig. 3a. I-V curve of an unencapsulated 0.4 m^2 CIS module.

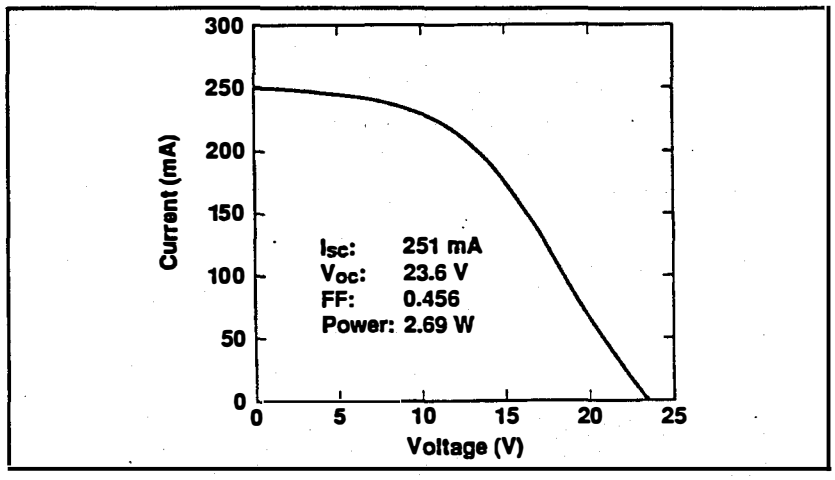

Fig. 3b. I-V curve of one slice of the module of Fig. 3a.

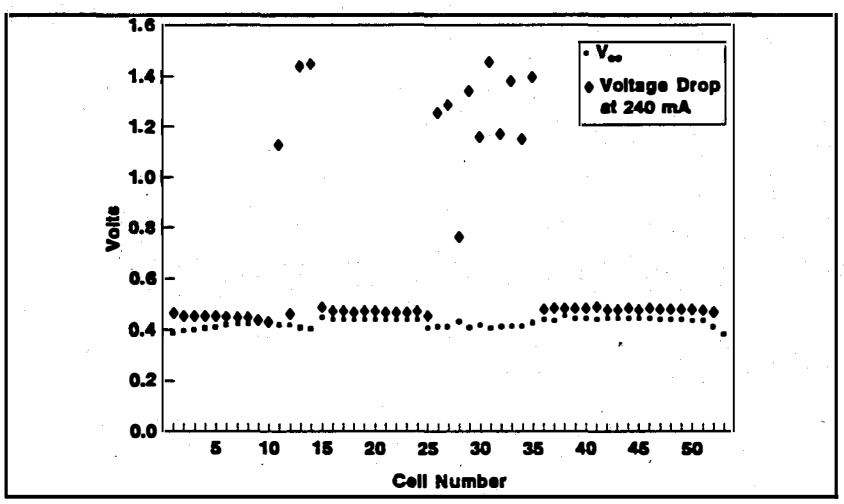

Fig. 3c. V_{pc} and dark forward bias voltage measurements of the slice of Fig. 3b.

Title: Fabrication of Stable Large Area Thin Film Cadmium Telluride Photovoltaic Modules

Organization: Solar Cells, Inc., Toledo, Ohio

Contributors: J.F. Nolan, Program Manager, P.V. Meyers, Principal Investigator, T. Zhou, N. Reiter

The overall objective is the demonstration of large area thin film CdTe photovoltaic modules fabricated using methods consistent with high throughput manufacturing. Specific goals for the three year program include producing 15% efficient 1cm^2 solar cells, 12% efficient 8cm x 8cm submodules, and 10% efficient 60cm x 120cm modules.

SCI has selected close spaced sublimation (CSS) as the primary method for deposition of the thin films. The most significant reasons for this choice are that CSS deposited CdTe has been used by several groups to produce >10% efficient small area solar cells and that CSS deposition rates are in excess of 4μm per minute - a rate which is very attractive from a manufacturing point of view. On the other hand, CSS has not yet been demonstrated to produce uniform films over substrates of this size. The process requires the precise control of elevated temperature over large areas. Typical source temperatures are in the 600-800°C range and typical substrate temperatures are in the 400-600°C range. SCI's present strategy is to deposit all semiconductor films using CSS, but the contract also includes investigation of films deposited from elemental sources.

The initial tasks of the contract involve the design, fabrication and testing of two pieces of apparatus - one each for deposition of 10cm x 10cm and of 60cm x 120cm films. The smaller system, consisting of four deposition zones within a single chamber, has been completed. A SnO_2:F coated glass substrate on a carrier can be placed into separate zones for preheating, for CdS deposition, for CdTe deposition, and for ZnTe deposition. Thin films of all three materials have been produced as well as a few cells. The most efficient cell had an efficiency of 8% over 0.25 cm^2. SCI has also produced a few submodules using a combination of laser and mechanical scribing to define and interconnect the individual cells. Efficiency was limited by interconnect related losses and active area efficiency was about 2.5%.

At the end of the contract fiscal year, work continued on the large area deposition apparatus, and on the optimization of cell deposition and module fabrication parameters. At this point - which is only four months into the program - the program is on schedule and is expected to achieve the contract goals.

Title: **Research on Polycrystalline Thin Film Submodules Based on $CuInSe_2$ Materials**

Organization: Solarex Corporation, Thin Film Division
826 Newtown-Yardley Rd., Newtown, PA 18940

Contributors: A. Catalano, Program Manager; R.R. Arya, Principal Investigator; T. Lommasson, B. Fieselmann, L. Russell, L. Carr and S. Skibo

Task 1: Windows, Contacts, Substrates

The window layer under development consists of two thin films, cadmium sulphide (CdS) and zinc oxide (ZnO). The CdS thin film is deposited by chemical solution growth from a mixture of $CdCl_2$, NH_4Cl, NaOH and Thiourea. At low temperature (< 90°C), the self-limiting reaction deposits approximately 1200Å thick CdS film on glass substrates. The films are stoichiometric and uniform over 3" x 3" substrates. The dark conductivity is high, in the range of 10^8 to 1 Ω-cm. Films with thicknesses varying from 500Å to 1 μm have been deposited, the thicker films being deposited by successive depositions. The transmission of light for wavelengths below the CdS cut-off (~500 nm) occurs for film thicknesses less than approximately 4000Å. Figure 1 shows the effect of CdS film thickness on transmission of light as a function of wavelength. CdZnS films have also been deposited by the same process. These films show an increase in bandgap as demonstrated by a shift in the transmission towards shorter wavelengths.

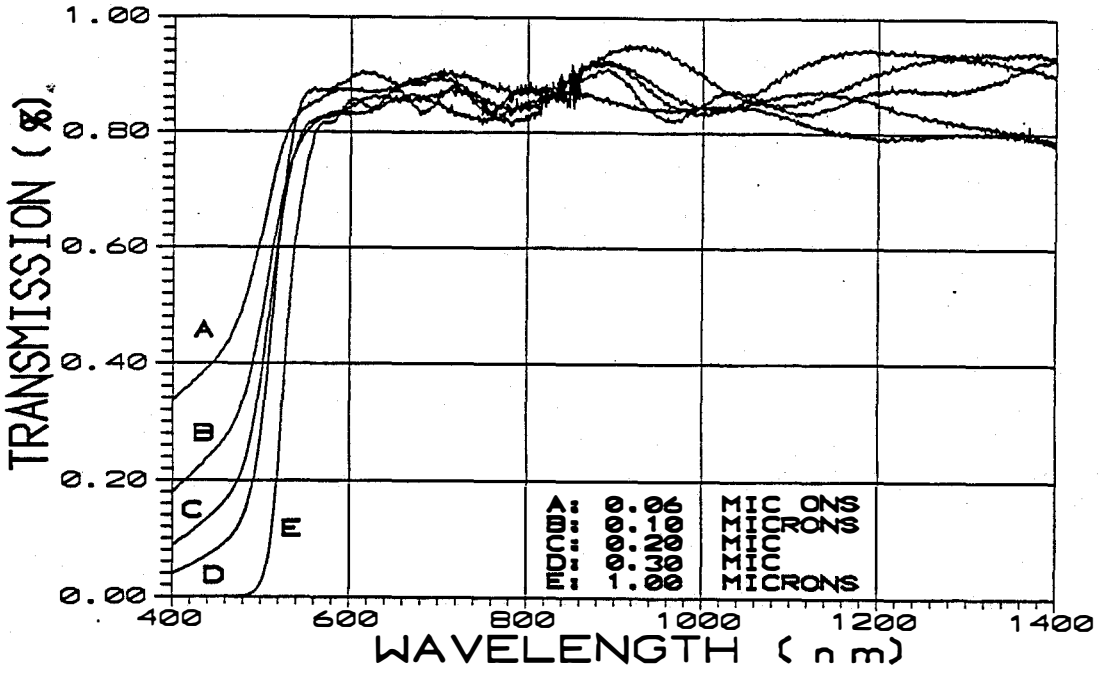

Figure 1. Optical transmission of CdS films as a function of film thickness.

A process has been developed to deposit ZnO films by low-pressure chemical vapor deposition (LPCVD). The deposition is carried out at low temperature (< 200°C) with feedstock or diethyl zinc (DEZ), water and diborane gas. The two main properties required in a good window layer - high optical transmission (in the wavelength range of 400 nm - 1400 nm) and low electrical resistivity (< 10 Ω/□) are interdependent. The transmission of ZnO films, particularly at long wavelengths (> 1000 nm) is found to be a strong function of the dopant gas concentration and film thickness at a given deposition temperature. Hence, a compromise has to be made between these two properties. The third necessity for these films is thermal stability of optical and electrical properties because often a completed CIS device is subjected to post-fabrication heat treatments up to several hours at ~200°C. The properties are found to be stable if the deposition is carried out at temperatures > 180°C. For film thickness of about 1.5 μm, the optical transmission at 1200 nm increases from approximately 65% to 95% as the dopant flow is decreased from 50 sccm to 0 sccm. The corresponding change in sheet resistance of the film decreases from 7 Ω/□ to 50 Ω/□. An optimum performance was achieved using films prepared with a dopant flow of about 10 sccm which led to films with transmission at 1200 nm of 90% and sheet resistance of 9 Ω/□. Further reduction in film thickness from 1.5 μm to 0.8 μm led to an increase in transmission to about 95% with a decrease in sheet resistance to 12 Ω/□. The short circuit current of a CIS device was increased by 5 mA/cm^2 by changing in the window layer thickness from CdS = 1200Å and ZnO = 1.5 μm to CdS = 500Å and ZnO = 0.8 μm. This is shown in Figure 2.

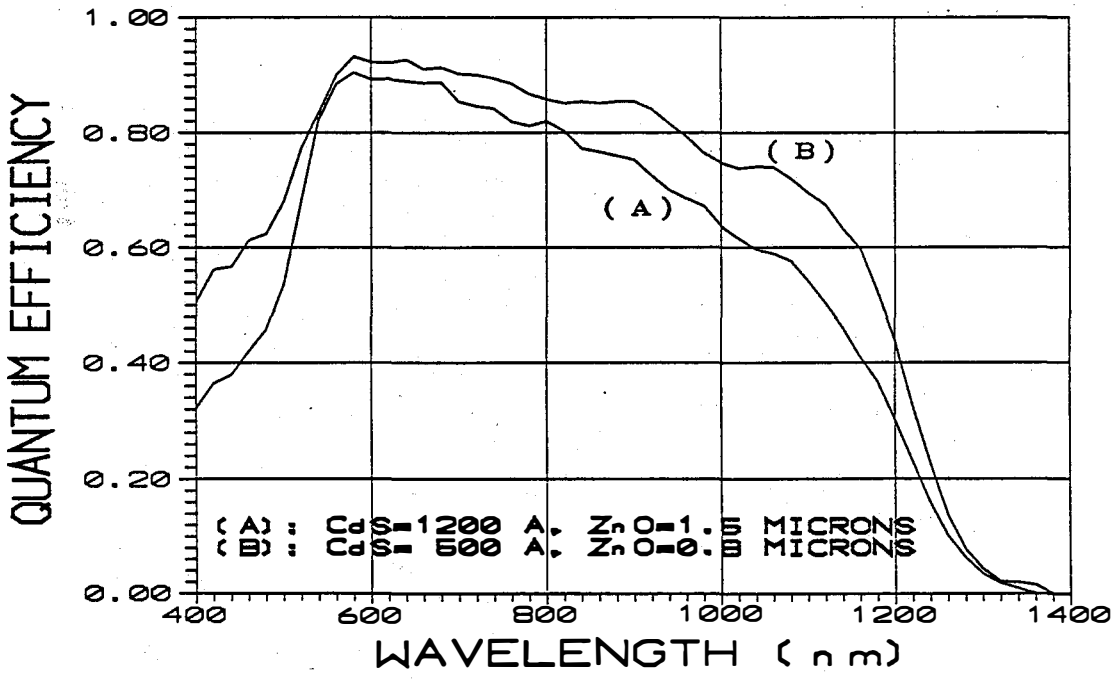

Figure 2. Effect of window layer on quantum efficiency of CIS devices.

The molybdenum (Mo) back contact has been deposited on glass both by sputtering from metal target and by e-beam evaporation. In both cases, 1-2 μm thick films exhibit good adhesion and sheet resistance of about 30 - 50 μΩ/□. The front contact consists of a bi-layer of aluminum and nickel, both evaporated by e-beam through a metal mask. Corning 7059 glass and soda-lime glass has been used as substrates.

Task 2: Absorber Layer

The absorber layer under development is copper indium diselenide (CIS) thin film deposited by magnetron sputtering from elemental targets onto Mo coated glass substrates held at elevated temperatures. The Se S-gun target has been fabricated in-house by a proprietary process. The three targets are mounted on the same plane such that the fluxes are parallel to each other. The substrates are mounted on a holder which is shrouded in an enclosure with openings above the three targets. Circular motion of the substrate holder allows sequential deposition of the Cu, In and Se layers and ensures spatial uniformity. Parametric studies of deposition parameters such as substrate temperature, deposition pressure and deposition power have resulted in development of p-type CIS films with composition (measured by EDAX) in the ranges of Cu = 22% - 24%, In = 24% - 26% and Se = 50% - 54%. The best films have been deposited at temperatures between 400°C - 450°C, sputtering pressure between 1.5-2.0 mTorr and at deposition rates between 3 - 4Å/sec. The surface morphology in these films is found to be a strong function of film composition and is not very dependent on other deposition parameters in these ranges. The composition of some typical CIS films is tabulated in Table 1. Figure 3 shows an SEM picture

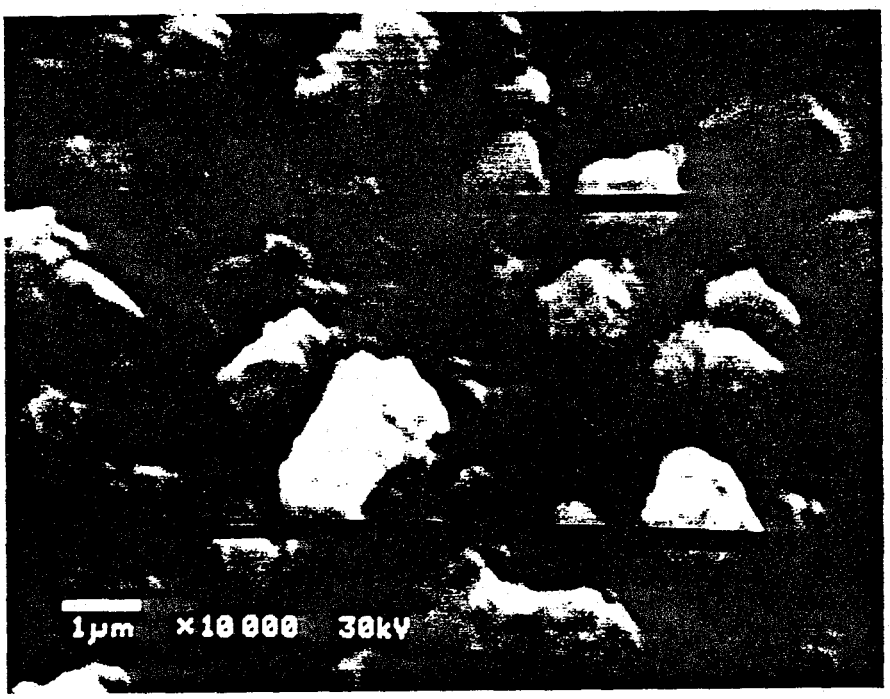

Figure 3. SEM picture of Cu-deficient sputtered CIS film (#S166-1-2).

Table I
Composition of Some Sputtered CIS Films

Sample #	% Cu	% In	% Se
S132-1	19.4	25.8	54.8
S132-4	20.6	24.9	54.5
S136-1	21.2	25.2	53.6
S136-4	22.3	24.5	53.2
S140-1	23.0	24.6	52.4
S140-4	23.6	24.0	52.5
S156-1	26.3	22.1	51.6
S156-4	25.1	22.8	52.1

of a typical CIS film. Two major problems have been encountered in the deposition of CIS films by sputtering from elemental targets. Both these problems are related to sputtering of Se. Due to the low thermal conductivity of Se, hotspots can develop in the Se target which result in non-uniform sputtering. Non-uniform sputtering perturbs the spatial and temporal uniformity of the Se flux. Furthermore, due to the proximity of the targets in our deposition system, the Cu and In targets are contaminated by the Se flux. The selenide layers that form on top of the Cu and the In targets can reduce the specific Cu and In flux by as much as 50% and 20%, respectively. This has led to poor run-to-run reproducibility. Two approaches are underway to overcome this problem. First, Cu and In films have been sputtered and the stack selenized in a Se vapour with an inert carrier gas in a tube furnace at temperatures between 400°C - 450°C. Second, the Se target has been replaced by a resistive heated evaporation source. This has resulted in films in which the composition was Cu = 22.8%, In = 23.7% and Se = 53.5%. This hybrid arrangement of sputtered Cu and In and evaporated Se has successfully solved the problem of target cross-contamination. Good CIS film composition has been achieved with this process but the surface morphology of the films are still poor. Both these approaches are at an early stage of development.

Task 3: Device Structure

Solar cells have been fabricated with two device structures:

(i) Light = > Ni-Al grid / ZnO / thin CdS / CIS / Mo / Glass
(ii) Light = > Ni-Al grid / ITO / thick CdS / CIS / Mo / Glass

The device structure (i) has been employed with all layers deposited at Solarex whereas the device structure (ii) has been employed by IEC on CIS deposited at Solarex. Several devices

with either device structure have resulted in conversion efficiencies about 5% [1]. The best device fabricated on sputtered CIS had a conversion efficiency of 6.2% with the following photovoltaic parameters: V_{oc} = 0.343 V, J_{sc} = 31.9 mA/cm^2 and FF = 0.562. The best device fabricated on hybrid CIS films had a conversion efficiency also of 6.2% but with the following device parameters: V_{oc} = 0.373 V, J_{sc} = 35.5 mA/cm^2 and FF = 0.474. The I-V characteristics of this device is shown in Figure 4.

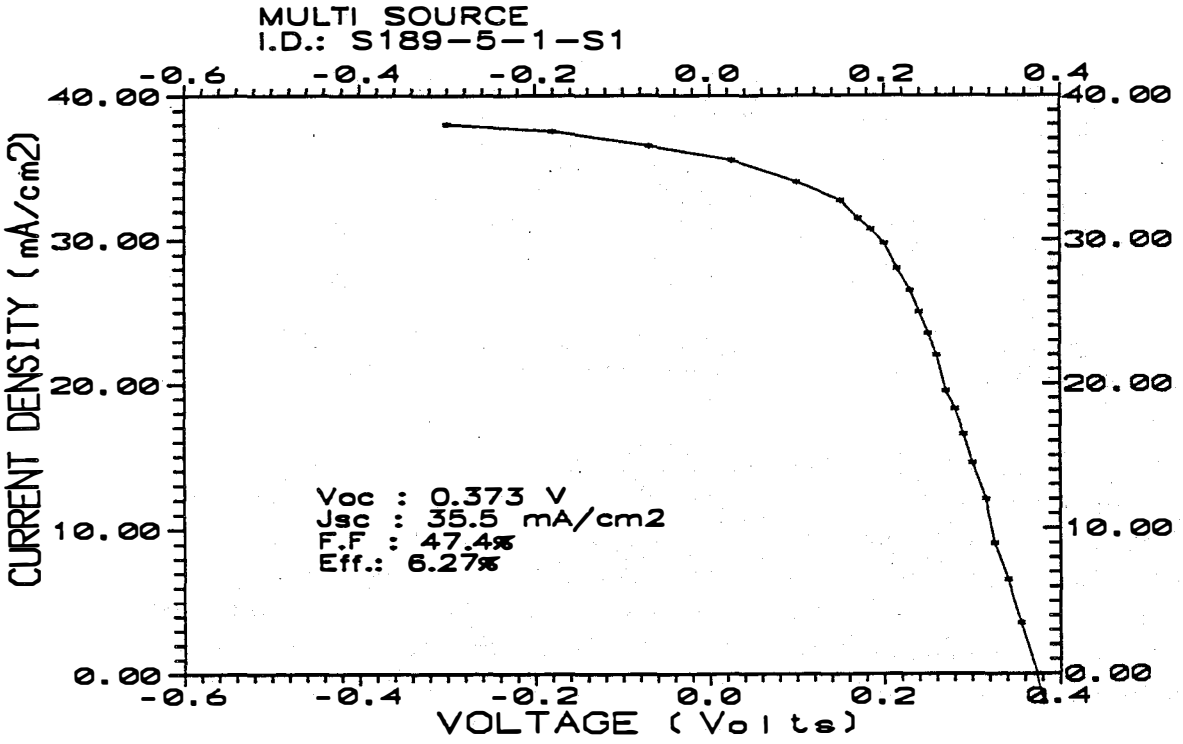

Figure 4. J-V characteristics of solar cell on sputtered/evaporated CIS with conversion efficiency of 6.2%.

Device Modeling (Drexel University)

The modeling effort at Drexel University has involved a number of analytic and simulation tasks:

1) Analytic calculations of the light generated current in CIS layer as a function of voltage, with doping density and diffusion length as parameters have been carried out. This involves calculating the current collected in the space-charge region as well as that in the neutral region. The collection of electron-hole pairs generated in the space charge region, depends upon the applied voltage through two aspects. First, the collection depends on the electric field which changes with applied voltage. Second, the width of the space-charge region depends upon the doping density N_A in the CIS. The effectiveness of the field in collecting the carriers depends upon the electron diffusion length, L, through the parameter of a critical field $F_C = kT/qL$. The collection beyond the space-charge region also depends on L. The consequences of the voltage dependence of light-generated

current density are that the collection efficiency versus wavelength, $\eta(\lambda)$, will be voltage dependent, and there will be a loss in fill-factor due to this cause.

Calculated results show the interplay of N_A and L, $\eta(\lambda)$, and the loss in fill factor Δ FF as:

$$\Delta FF = (J_\lambda(O)-J_L(O))\ V_{mp}/V_{oc}$$

The value of V_{mp} can be obtained by assuming an expression for the dark diode current and combining it with J_L (V) through the equation:

$$j = j_{diode}(V) - J_L(V)$$

2) The calculations under 1) above treated the CIS as though it were a single crystal, neglecting any grain boundary effects. To include grain boundary effects an analytic expression has been used which calculates the reduction in $\eta(\lambda)$ due to the size of the grains, assuming a large value for the grain boundary recombination velocity. The calculated $\eta(\lambda)$ as a function of the radius of the grains has been carried out by simply multiplying the results of 1) by a function of $\eta(R,\lambda,d)$ where d is the thickness of the absorbing region (either the space-charge region, or the neutral region, since η has two components [2].

Summary

The window layer, both CdS and ZnO, has been optimized to minimize optical absorption losses. CIS films prepared by sputtering from elemental targets looks promising because it allows the deposition of CIS films without any H_2Se post-selenization or heat-treatments. Problems associated with uniformity of Se flux can be successfully addressed by evaporation of Se. We continue to optimize deposition conditions to achieve better surface morphology in these films.

References

1. R.R. Arya, T. Lommasson, B. Fieselmann, L. Russell, L. Carr and A. Catalano, Proceedings of the 22nd IEEE Photovoltaic Specialists Conference (IEEE, N.Y., 1991).

2. A. Rothwarf, I. Gonchar, Y. Melnikova, F. Shapiro, T. Lommasson and R.R. Arya, Proceedings of the 22nd IEEE Photovoltaic Specialists Conference (IEEE, N.Y., 1991).

Title: **Alternative Fabrication Techniques for High-efficiency $CuInSe_2$ and $CuInSe_2$-alloy Films and Cells**

Organization: University of Illinois

Contributors: A. Rockett (principal investigator), L. Chung Yang, G. Kenshole, L.-J. Chou, and A. Feen.

Objectives

The objective of this project is to demonstrate a scalable $CuInSe_2$ thin film deposition technique capable of producing material suitable for solar cell applications. To achieve efficient use and scale up of any such technology it is essential to understand the fundamental behavior of the principal materials involved.[1] Hence, the program seeks to characterize the structure/processing/cell-performance relationships for $CuInSe_2$. This will serve to improve the processes under development, optimize deposition conditions, and ultimately to accelerate the return of large deposition facilities to service after periods of maintenance.

Technical Approach

The $CuInSe_2$ deposition method considered by this project is a hybrid of sputtering and evaporation. Cu and In are sputtered with Ar gas while Se is supplied to the growing film by a conventional effusion cell.[2] The substrate temperature is controlled between room temperature and 550°C. The process has been shown to be straightforward to control with a linear relationship between the ion current ratio at the targets and the film composition established by previous results.[3] The experiments underway focus development of a reasonably high efficiency $CuInSe_2$/CdS heterojunction solar cell, and on understanding the fundamental properties of $CuInSe_2$.[4,5] The materials characterization involves $CuInSe_2$ single crystal and polycrystalline thin films deposited by the hybrid process by various chemical and structural analysis techniques.

Results for FY 91

Hybrid Process $CuInSe_2$ for Devices

Heterojunction solar cells were fabricated by the Institute of Energy Conversion at the University of Delaware (IEC) using several of the deposited polycrystalline $CuInSe_2$ films. Test cells were produced by evaporation of 1.7 μm of $Cd_{0.9}Zn_{0.1}S$ with a sheet resistance of 50 Ω/˙. This was coated with 180 nm of sputtered ITO and finished with Ni buss bar contacts. The active areas were 0.08 cm^2. All active devices were tested at IEC under an 87.5 mW cm^{-2} simulated solar spectrum. The results were then normalized to 100 mW cm^{-2} flux values. Samples on which solar cells were fabricated ranged from Cu-rich to In-rich, although successful devices were only produced on In-rich material. All layers used for devices were deposited as bilayers on Mo-coated glass substrates. The initial layers were Cu-rich followed by a strongly In-rich deposition. Both layers were deposited at 400°C and were completely intermixed after deposition as determined by energy-dispersive X-ray analysis (EDX) in the transmission electron microscope (TEM) and by secondary ion mass spectrometry (SIMS). Optimal performance was obtained from a sample with a composition measured near the center by EDX of 26% In, 24% Cu, and 50% Se. The maximum conversion efficiency recorded was 8.4% with V_{OC}=392mV, J_{SC}=33.9 mA, and a fill factor of 63.1% after normalization to 100 mW cm^{-2} flux. The current/voltage (i/v) curves for this cell with and without illumination are shown in Figure 1. The performances measured at IEC were not verified at the Solar Energy Research Institute (SERI) as the cells were destroyed in the mail.

Single Crystals

During this contract period single crystals of $CuInSe_2$ have been grown on GaAs. There were two major reasons for doing this. First, to understand why some devices based on $CuInSe_2$ work well while others do not it is essential to understand the dynamics of $CuInSe_2$ crystal growth. This is best carried out on single crystals. In addition, $CuInSe_2$ devices in conjunction with GaAs-based cells have been considered as potential candidates in tandem structures. To produce a two-terminal $CuInSe_2$/GaAs tandem device it would be desirable to grow $CuInSe_2$ directly on GaAs. A number of results have been obtained from the single crystal studies. Space permits only two of these to be described in any detail. Discussion of other results can be found in reference 6.

Single crystals of $CuInSe_2$ were successfully deposited on GaAs substrates as shown by electron channelling patterns obtained from the layers. A number of growth defects were observed which, while a potential problem for device applications, provide important insights into growth mechanisms and are directly relevant to polycrystalline film growth. The principal defects were pits in the surface of Cu-rich layers and small islands or ripples on the surface of In-rich films. Voids formed and interdiffusion occurred at the interface between the $CuInSe_2$ and the GaAs substrate after deposition began. The structure of pits on the (002)- and (112)-oriented $CuInSe_2$ surfaces suggest that the low energy $CuInSe_2$ faces are (112)-type and that a strong preference for either the metal-terminated or Se-terminated facet exists. A scanning electron micrograph image of one such pitted single crystal surface is shown in Figure 2. Which facet face is preferred will be determined in angle-resolved X-ray photoelectron spectroscopy experiments now in progress.

It is evident that $CuInSe_2$ can affect the GaAs substrate based on fracture cross sections. These show pyramidal pits in the GaAs near the interface although the lower $CuInSe_2$ surface is flat! This can only occur if the GaAs surface on which the $CuInSe_2$ originally nucleates is flat and if the voids form during growth. Figure 3 shows a SIMS profile along with a fracture cross section of the substrate and epitaxial layer. Substantial interdiffusion has occurred with Ga found in the $CuInSe_2$ epitaxial layer and Cu, In, and Se all found in the substrate. Relatively little As outdiffusion was observed by SIMS indicating that the observed mixing is not a SIMS artifact.

Conclusions and Future Research

The improvement in device performance relative to previous results[4] shows continued progress toward matching devices based on evaporated $CuInSe_2$. Microanalysis results show no significant differences between hybrid-process $CuInSe_2$ and evaporated material suggesting that continued progress may be expected. However, devices based on single crystal epitaxial $CuInSe_2$ would probably not produce good results. Cu is a deep trap in GaAs and would create an intrinsic layer even in the presence of In and Se impurities. This would create a large series resistance reducing the fill factor and short-circuit current of the resulting cell. In addition, pits in the surface layers would lead to shorting of devices when overcoated with a highly conductive window layer. The results are consistent with growth of polycrystals in which voids, analogous to the pits, form spontaneously in vapor-deposited material.

Relationship to Other Contracts

The research program described above is funded by SERI for development of high-performance photovoltaic devices based on $CuInSe_2$ deposited by sputtering-based techniques. The development of the hybrid sputtering and evaporation process itself is funded by the Electric Power Research Institute. Both agencies fund the materials characterization with additional direct support from the Department of Energy.

References

[1] A. Rockett and R.W. Birkmire, "$CuInSe_2$ for Photovoltaic Applications", Applied Physics Reviews, in J. Appl. Phys. **70(7)**, R81 (1991).

[2] A. Rockett, T.C. Lommasson, P. Campos, L.C. Yang, and H. Talieh, "Growth of $CuInSe_2$ by Two Magnetron Sputtering Techniques", Thin Solid Films **171**, 109 (1989).

[3] A. Rockett, T.C. Lommasson, L.C. Yang, H. Talieh, P. Campos, and John A. Thornton, "Deposition of $CuInSe_2$ by the Hybrid Sputtering and Evaporation Method", Proceedings of the 20th IEEE Photovoltaic Specialists Conference, Las Vegas, September 26-30, 1988 (Institute of Electrical and Electronics Engineers, New York, 1988), p. 1505.

[4] H. Talieh and A. Rockett, "Device-Quality $CuInSe_2$ Produced by the Hybrid Process," Solar Cells **27**, 321 (1989).

[5] A. Rockett, G. Kenshole, L. Chung Yang, H. Talieh, L.C. Yang, P. Campos, E. Banda and A. Agarwal, "Characterization of CuInSe2 Deposited by the Hybrid Sputtering and Evaporation Method and Heterojunction Solar Cell Performance", 21st IEEE Photovoltaic Specialists Conference, Orlando, May 21-25, 1990 (Institute of Electrical and Electronics Engineers, New York, 1990), p. 764.

[6] L. Chung Yang, L.J. Chou, A. Agarwal, and A. Rockett, "Single Crystal and Polycrystalline $CuInSe_2$ by the Hybrid Sputtering and Evaporation Method," 22nd IEEE Photovoltaic Specialists Conference, Las Vegas, October 7-11, 1991 (Institute of Electrical and Electronics Engineers, New York, 1990), in press.

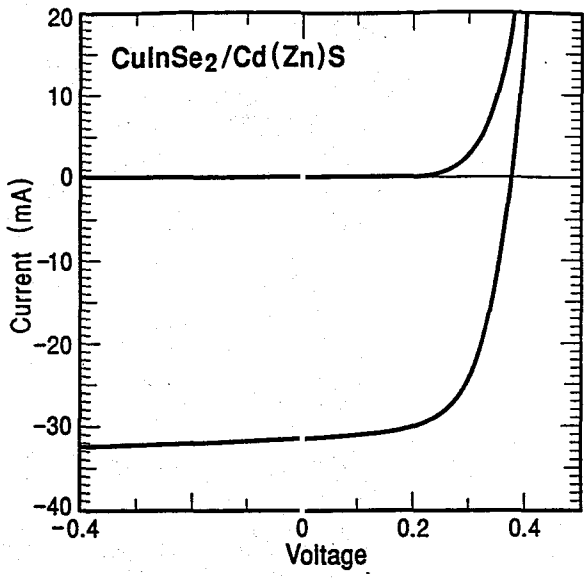

Figure 1. Light and dark current/voltage curves recorded at IEC for the best solar cell produced from $CuInSe_2$ deposited by the hybrid process.[6]

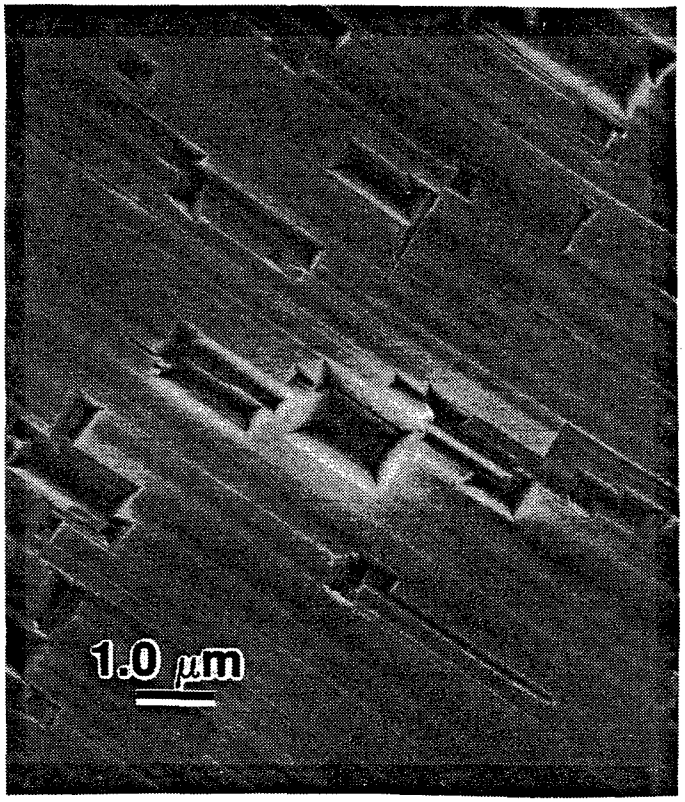

Figure 2. A SEM micrograph of the surface of an In-rich (002)-oriented $CuInSe_2$ single crystal grown on GaAs (001). Pits in the surface of this film resulted from the GaAs surface preparation[6] and consist of (112) facets. No pits occur when surface preparation is optimal.

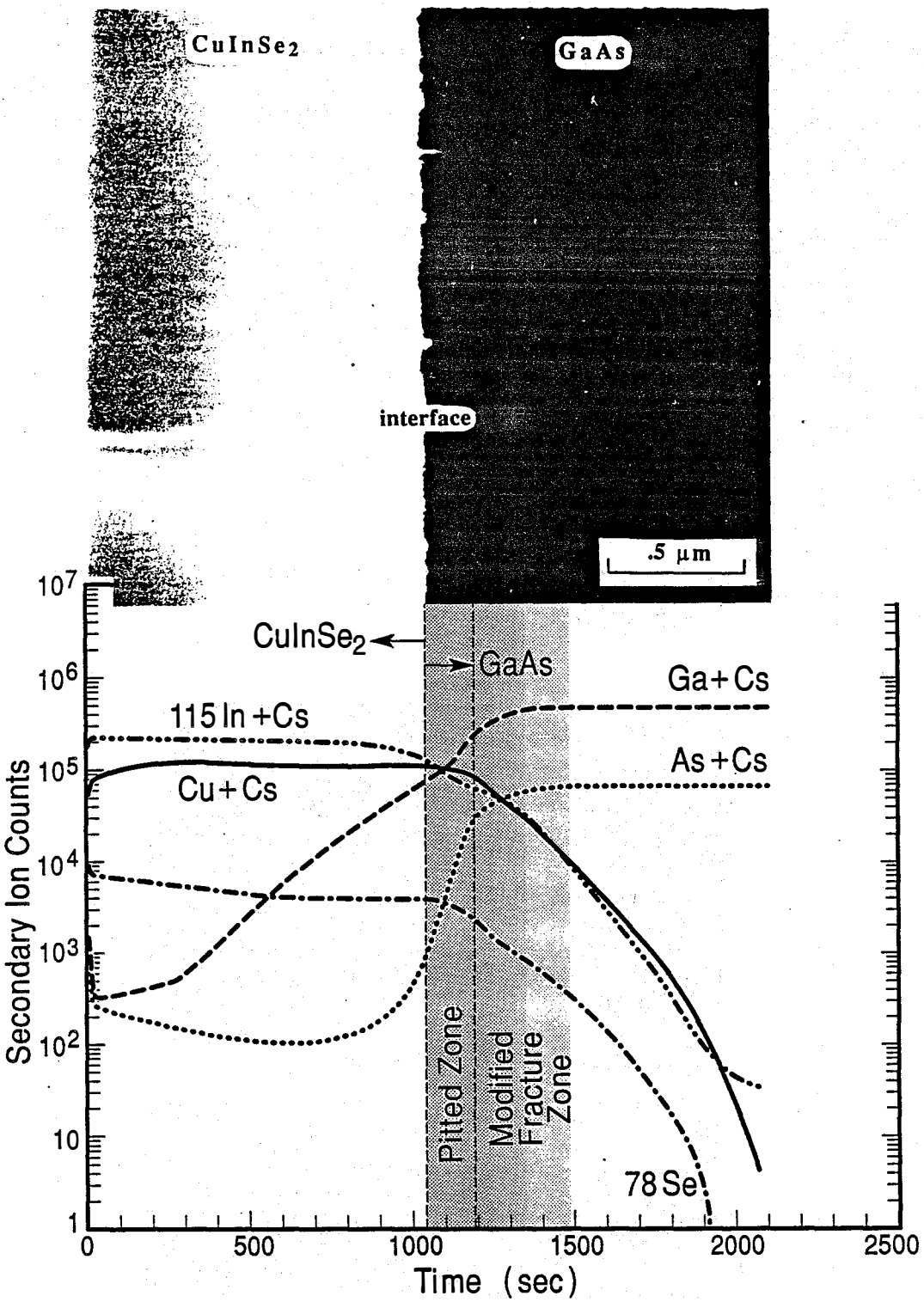

Figure 3. A SIMS profile (lower section) of a (112)-oriented slightly In-rich $CuInSe_2$ film deposited on GaAs (111). A fracture cross section SEM image of a corresponding area of the sample is also shown (upper portion). Interdiffusion has resulted in void formation at the interface during growth. Impurities in the GaAs modify the fracture characteristics of the GaAs where their concentration is significant.

Title: **Thin Film Cadmium Telluride, Zinc Telluride, and Mercury Zinc Telluride Solar Cells**

Organization: University of South Florida, Tampa, Florida

Contributors: T. L. Chu and S. S. Chu, Principal Investigators; J. Britt, G. Chen, C. Ferekides, N. Schultz, C. H. Wang, and C. Q. Wu.

The major objective of this program is to investigate the preparation, characterization, and optimization of thin-film solar cells of II-VI compounds and alloys with emphasis on cadmium telluride (CdTe), cadmium zinc telluride ($Cd_xZn_{1-x}Te$), and mercury zinc telluride ($Hg_xZn_{1-x}Te$). Thin film CdTe solar cells are of the homojunction and heterojunction configurations in order to demonstrate a quantum efficiency of 75% at 0.44 μm and a photovoltaic conversion efficiency of 11.5% or greater. Thin film $Cd_{1-x}Zn_xTe$ and $Hg_{1-x}Zn_xTe$ with bandgap energy of 1.65-1.75 eV are suitable as the top members in two-cell cascade structures. The solar cells are of the heterojunction configuration in order to demonstrate a transparency to sub-bandgap radiation of 65% and a photovoltaic conversion efficiency of 8% or greater. The technical approach consists of (1) the deposition of transparent conducting semiconductor (TCS) films from aqueous solutions and by metalorganic chemical vapor deposition (MOCVD), (2) the deposition of CdTe films by close-spaced sublimination (CSS), (3) the deposition of CdTe films by MOCVD with emphasis on doping and the characterization and processing of these films with emphasis on contact formation, (4) the deposition and characterization of $Cd_{1-x}Zn_xTe$ and $Hg_{1-x}Zn_xTe$ films, and (5) the formation and characterization of thin film junctions and solar cells.

Transparent Conducting Semiconductors (TCS)

Thin films of cadmium sulfide (CdS), cadmium zinc sulfide ($Cd_{1-x}Zn_xS$), and zinc selenide (ZnSe) have been deposited and characterized. CdS films were deposited on glass and SnO_2:F/glass substrates from an ammonical solution of a cadmium salt, an ammonium salt, and thiourea at 70°-90°C. The important process parameters, the composition and temperature of the solution, have been optimized to promote the heterogeneous reaction on the substrate surface and to minimize the homogeneous reaction in solution. The crystallographic, optical, and electrical properties of solution-grown CdS films have been investigated. The typical lateral resistivity of CdS films on glass substrates is 10^5-10^6 ohm-cm in the dark and is 50-300 ohm-cm under illumination with ELH lamps at 100 mW/cm^2. The use of solution-grown CdS films has produced high efficiency CdS/CdTe solar cells with the CdTe films deposited by CSS and spraying techniques.

$Cd_{1-x}Zn_xS$ films have been deposited by MOCVD using dimethylcadmium (DMCd), diethylzinc (DEZn), and propylmercaptan (C_3H_8S) in a hydrogen atmosphere with trimethylaluminum (TMAl) as a dopant. The composition of $Cd_{1-x}Zn_xS$ films has been controlled by optimizing the DMCd/DEZn and (DMCd + DEZn)/C_3H_8S molar ratios in the reaction mixture. The crystallographic, optical, and electrical properties of $Cd_{1-x}Zn_xS$

films with Eg < 3 eV have been investigated. The incorporation of Al into $Cd_{1-x}Zn_xS$ films becomes difficult at bandgap energies higher than about 2.8 eV (Fig. 1). Thin film II-VI heterojunctions have been prepared by the in-situ deposition of Al-doped $Cd_{0.7}Zn_{0.3}S$ (Eg~ 2.8 eV), an absorber, and the ohmic contact on an n^+-ZnO/glass substrate. The n^+-ZnO films were deposited by MOCVD using DEZn and ethanol in an He atmosphere with C_3F_6 or TMAl as a dopant; the resistivity of F-doped ZnO films were found to increase more than one thousand folds after heating at 600°C, while that of Al-doped ZnO films showed essentially no change after heating.

ZnSe with a bandgap energy of 2.67 eV is a potentially useful TCS for thin film II-VI heterojunction solar cells. Polycrystalline ZnSe films have been deposited on glass and ZnO:F/glass substrates at 400°-500°C by MOCVD using DEZn and DESe in a H_2 atmosphere. Films deposited under a wide range of conditions all have high resistivity, about 10^5 ohm-cm, and negative photoconductivity. The resistivity can be reduced and photoconductivity significantly improved by the incorporation of a group VI (Cl or Br) or a group III (Al) dopant. The use of TMAl as a dopant is considerably more effective than that of Cl or Br compounds. The resistivity of Al-doped ZnSe films depends strongly on the DESe/DEZn and TMAl/DEZn molar ratios in the reaction mixture (Fig. 2). Photoconductivity ratios as high as 10^4 have been observed in Al-doped ZnSe films. ZnTe/ZnSe and CdTe/ZnSe junctions have been prepared by depositing the absorber films on ZnSe/ZnO glass substrates.

CdTe Junctions by MOCVD

Intrinsic CdTe films deposited by MOCVD from DMCd and DIPTe can be n-type (Te vacancies) or p-type (Cd vacancies), depending on the composition of the reaction mixture. Extrinsic CdTe films have been deposited by using group III and group V compounds as dopants during the MOCVD process. Gallium can be readily incorporated into CdTe films to yield a dark resistivity of about 1000 ohm-cm and a carrier concentration of about 2 x 10^{17} cm^{-3}; however, the incorporation of As or Sb is considerably more difficult, and low resistivity p-CdTe films have not been obtained (Figures 3 and 4). Intrinsic and extrinsic CdTe films of the same conductivity type show significantly different photoluminescence spectra. Heterojunctions have been prepared by depositing p-CdTe on CdS/SnO_2:F/glass substrates. The as-deposited structures show poor electrical and photovoltaic characteristics which are dramatically improved by the $CdCl_2$ treatment. The saturation current density and diode quality factor of $CdCl_2$ treated CdS/CdTe junctions are typically 1.5 x 10^{-10} A/cm^2 and 1.7, respectively. Solar cells of larger than 1 cm^2 area show near 10% efficiency under AM 1.5 conditions (Fig. 5).

The effect of the $CdCl_2$ treatment has been investigated using photoluminescence measurements by illuminating the CdTe surface and the glass surface of the $CdTe/CdS/SnO_2$:F/glass structure with the 484 nm radiation from an argon ion laser (Fig. 6). When the CdTe surface is illuminated, essentially all laser radiation is absorbed by CdTe. The CdS/CdTe interface region contributes to the PL spectrum only when the glass surface is illuminated. The analysis of the PL spectra suggests the incorporation of Cd into

the CdTe film during $CdCl_2$ treatment and the shifting of the heterojunction from the metallurgical interface into CdTe.

Thin film CdTe homojunctions were prepared by the successive in-situ deposition of Ga-doped and As-doped CdTe films on SnO_2:F/glass substrates. The as-deposited structures have been found to have a high saturation current density, about 4×10^{-8} A/cm^2, similar to the as-deposited heterojunctions, and poor photovoltaic characteristics. This is presumably related to the poor microstructure of MOCVD CdTe films. Attempts to improve the junction characteristics by $CdCl_2$ treatment were not successful due to the disturbance of the homojunction structure.

CdTe Heterojunctions by CSS

The process parameters for the deposition of CdTe films by CSS have been optimized for the deposition of dense films at a rate of about 1 μm/min. Thin film cells were prepared by the deposition of 4-5 μm of CdTe onto CdS/SnO_2:F/glass substrates at 600°C. Heterojunctions prepared from CSS CdTe films show considerably better characteristics than those from MOCVD CdTe films due mainly to the better microstructure of CSS CdTe films. Typical saturation current density and diode quality factor deduced from the dark characteristics are 6×10^{-11} A/cm^2 and 1.65, respectively. Solar cells of larger than 1 cm^2 area with a conversion efficiency of 13.4% under global AM 1.5 conditions have been prepared (Fig. 7).

The CdTe/CdS heterojunction structures were used to determine deep energy states in CdTe films. Six states with activation energies of 0.85, 0.79, 0.51, 0.63, 0.46, and 0.37 eV have been observed in samples prepared under various conditions and post-deposition treatment (Fig. 8). These states have all been observed in single crystalline CdTe, although their nature has not been identified. The density of these states in CdTe films is relatively low, on the order of 10^{13} cm^{-3}.

$Cd_{1-x}Zn_xTe$ Films and Junctions

Thin films of $Cd_{1-x}Zn_xTe$ with bandgap energy over a wide range have been deposited by MOCVD, and their crystallographic, optical, and electrical properties characterized. Thin film heterojunctions have been prepared by the successive in-situ deposition of $Cd_{0.7}Zn_{0.3}S$ (Eg~ 2.8 eV), $Cd_{0.7}Zn_{0.3}Te$ (Eg~ 1.7 eV), and p^+-ZnTe ohmic contact on ZnO:F/glass substrates. The as-deposited structures show low photocurrent due to poor grain structure of $Cd_{0.7}Zn_{0.3}Te$. By using a thin $Cd_{0.7}Zn_{0.3}Te$ layer (0.1-0.2 μm) in combination with a 2-3 μm CdTe layer as the absorber, the photovoltaic characteristics are greatly improved. A conversion efficiency of about 7.5% has been measured.

References

1. "MOCVD Cadmium Telluride and Zinc Telluride Films for Photovoltaic Devices," presented at the 2nd International Conference on Electronic Materials, Materials Research Society, Newark, NJ, September 17-19, 1990.

2. "Films and Junctions of Cadmium Zinc Telluride and Mercury Zinc Telluride by MOCVD," presented at the 5th Biennial Workshop on Organometallic Vapor Phase Epitaxy, Panama City Beach, FL, April 14-17, 1991.

3. "Cadmium Zinc Telluride Films by Metalorganic Chemical Vapor Deposition," presented at the 5th International SAMPE Electronic Materials and Processes Conference, Los Angeles, CA, Jun 18-20, 1991.

4. "High Efficiency Thin Film CdS/CdTe Heterojunction Solar Cells," presented at the 5th International Conference on II-VI Compounds, Okayama, Japan, September 8-13, 1991.

5. "High Efficiency CdS/CdTe Solar Cells from Solution-Grown CdS Films," presented at the 22nd IEEE Photovoltaic Specialists Conference, Las Vegas, NV, October 7 - 11, 1991.

6. "Cadmium Zinc Sulfide Films for Heterojunction Devices," presented at the 22nd IEEE Photovoltaic Specialists Conference, Las Vegas, NV, October 7 - 11, 1991.

7. T.L. Chu, Shirley S. Chu, C. Ferekides, J. Britt, C.Q. Wu, G. Chen, and N. Schultz, "Thin Films of II-VI Compounds and Alloys," Solar Cells, 30, 123 (1991).

8. T.L. Chu, Shirley S. Chu, J. Britt, C. Ferekides, and C.Q. Wu, "Zinc Telluride Films by Photoenhanced Metalorganic Chemical Vapor Deposition," J. Electronic Mater., 20, 483 (1991).

9. T.L. Chu, Shirley S. Chu, C. Ferekides, J. Britt, and C.Q. Wu, "Cadmium Telluride Films by Metalorganic Chemical Vapor Deposition," J. Appl. Phys., 69, 7651 (1991).

10. T.L. Chu, Shirley S. Chu, J. Britt, and C. Ferekides, "Cadmium Zinc Sulfide Films and Heterojunctions," J. Appl. Phys., 70, 2688 (1991).

11. T.L. Chu, Shirley S. Chu, C. Ferekides, C.Q. Wu, J. Britt, and C. Wang, "13.4% Efficient Thin Film CdS/CdTe Solar Cells," J. Appl. Phys., Dec. 1991.

12. T.L. Chu, Shirley S. Chu, G. Chen, J. Britt, C. Ferekides, and C.Q. Wu, "Zinc Selenide Films and Heterojunctions," J. Appl. Phys., submitted for publication.

13. T.L. Chu, Shirley S. Chu, C. Ferekides, J. Britt, and C.Q. Wu, "Thin Film Junctions of Cadmium Telluride by Metalorganic Chemical Vapor Deposition," J. Appl. Phys., submitted for publication.

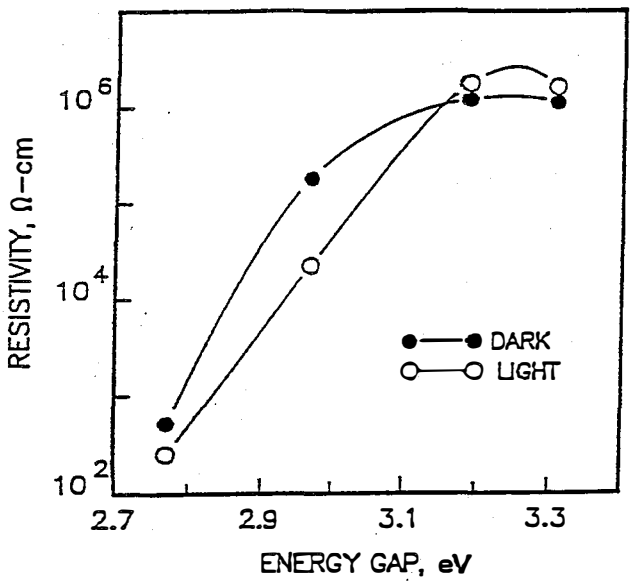

Fig. 1 Resistivity of Al-doped $Cd_{1-x}Zn_xS$ films versus bandgap energy

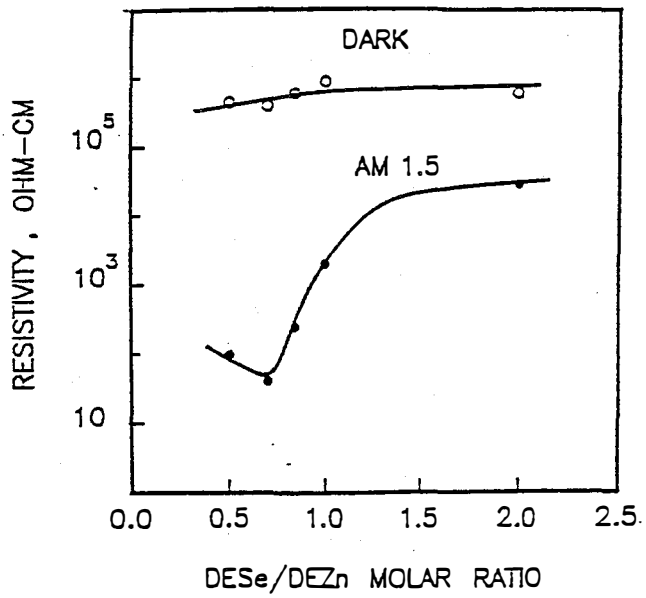

Fig. 2 Resisitivity of Al-doped ZnSe films versus DESe/DEZn ratio, TMAl/DEZn = 0.03

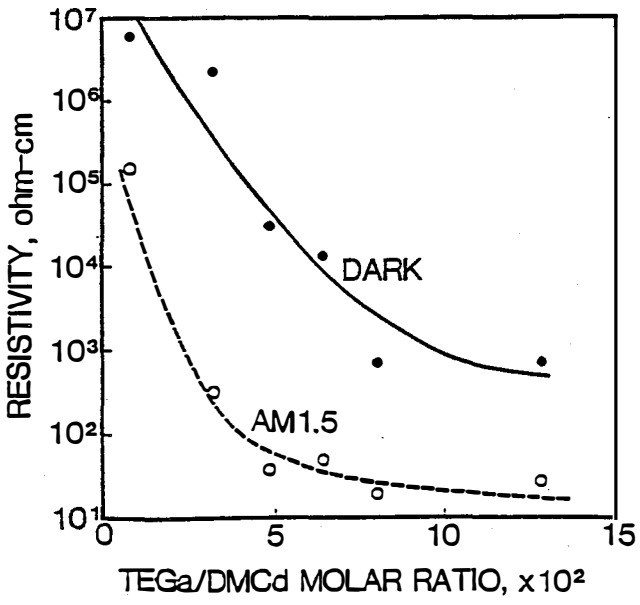

Fig. 3 Resistivity of Ga-doped CdTe films versus TEGa/DMCd ratio

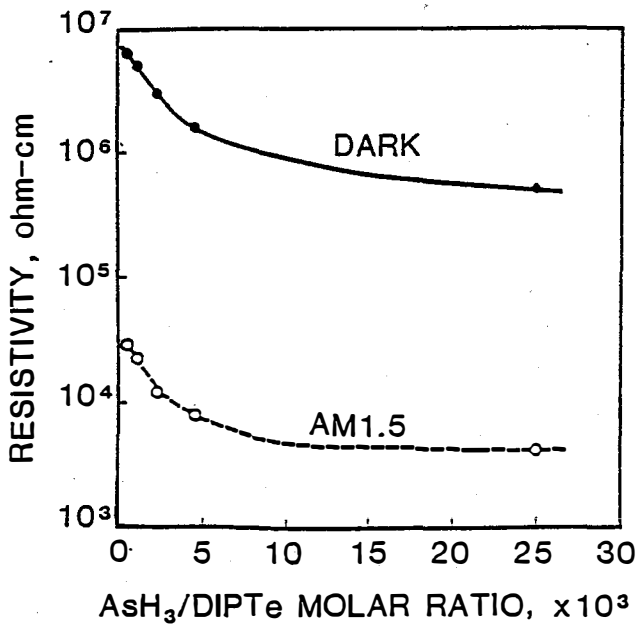

Fig. 4 Resistivity of As-doped CdTe films versus AsH_3/DIPTe ratio

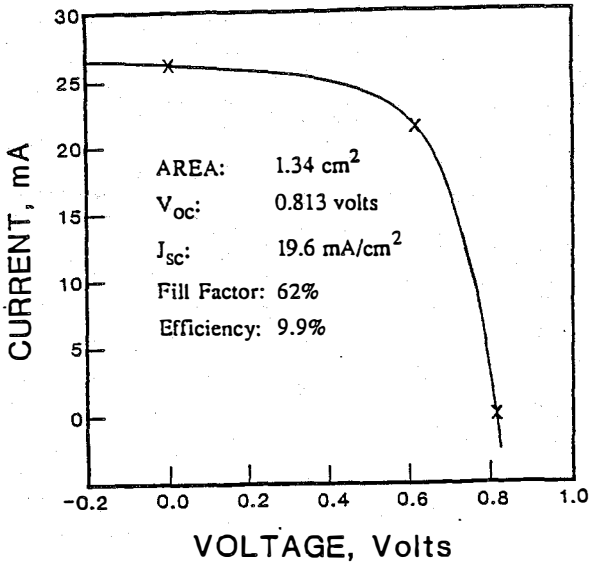

Fig. 5 Current-voltage characteristics of a thin film CdTe (MOCVD) solar cell under global AM1.5 conditions

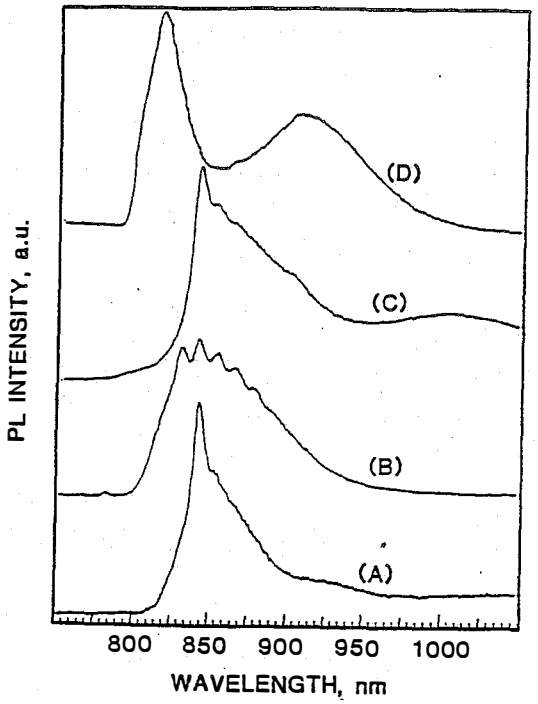

Fig. 6 PL spectra of (1) an as-deposited CdTe/CdS cell illuminated from CdTe (A) and glass (C) surfaces, and (2) a $CdCl_2$ treated cell illuminated from CdTe (B) and glass (D) surfaces

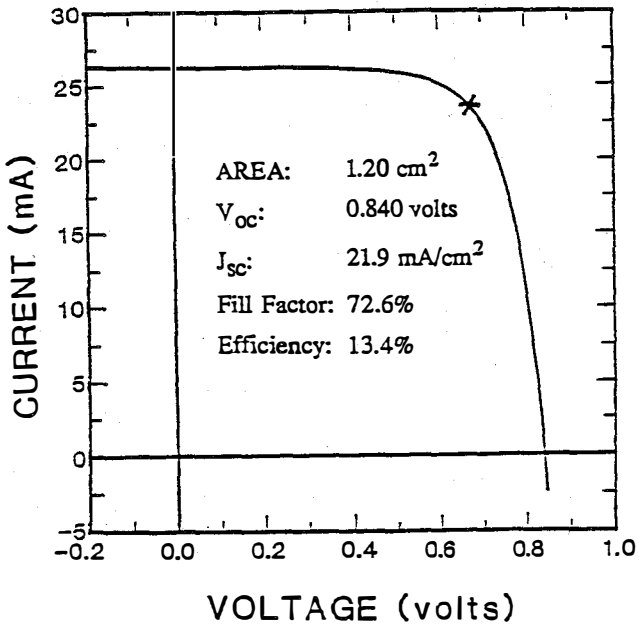

Fig. 7 Current-voltage characteristics of a thin film CdTe (CSS)/CdS solar cell under global AM 1.5 conditions

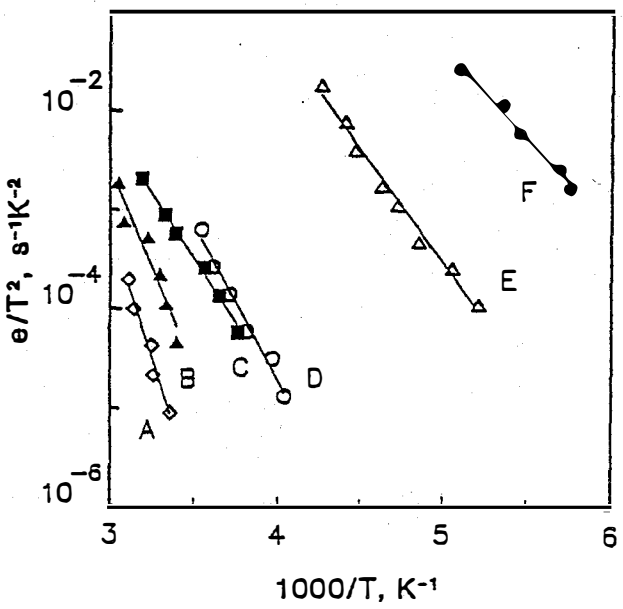

Fig. 8 Emission coefficient versus temperature for CSS CdTe films prepared under various conditions

Title: **Thin Film Cadmium Telluride Photovoltaic Cells**

Organization: Department of Physics and Astronomy
The University of Toledo
Toledo, OH 43606

Contributors: Alvin D. Compaan, principal investigator; Randy G. Bohn, co-investigator; Atilla Aydinli*, Ajit Bhat, Charles N. Tabory, Li-Hua Tsien, Shuzhen Liu, Meilun Shao, Marc E. Savage, and Yuxin Li

Lower-Tier Subcontractor: Solar Cells Inc., Toledo, OH
James F. Nolan

Objectives

This program is focussing on the development of two vacuum-based growth techniques for CdTe thin-film solar cells. Most of the effort during the first year was devoted to the implementaton of laser-driven physical vapor deposition (LDPVD) for CdS, CdTe, ZnTe, and $CdCl_2$ films and their integration into an efficient solar cell structure. The second growth technique used in this project is rf sputtering and was implemented near the end of the first year. The all-LDPVD process followed by heat treatment at 400 °C for 30 minutes has resulted in an 8.7% AM 1.5 solar cell to date.

Technical Approach

The first year of this project was designed to focus on the investigation of two (or more) vacuum-based deposition technologies for polycrystalline CdTe solar cells. The second and third years were originally designed to focus increasingly on the scale-up to submodules and the development of a commercial process. This project began as a collaboration among The University of Toledo, and lower-tier subcontractors Glasstech Solar, Glasstech, and Solar Cells. Glasstech Solar ceased operations in 1990 and was dropped from the contract at the end of calendar year 1990. Meanwhile, Solar Cells' time scale advanced more rapidly than projected and SERI awarded a separate contract with them in the spring of 1991. Thus, this University of Toledo contract was modified to reduce the second and third year emphasis on scale-up to commercialization, but retained the emphasis on basic science and the further development of the LDPVD and sputtering processes. Solar Cells remained a lower-tier subcontractor for the duration of the first contract year.

The University of Toledo is the only research group using LDPVD (also referred to as pulsed laser deposition or laser ablation deposition) for the growth of photovoltaic materials. This growth process was studied intensively during the first contract year. We successfully fabricated by LDPVD complete solar cells with both CdS/CdTe and CdS/CdTe/ZnTe structures. The process included the use of LDPVD for the deposition of $CdCl_2$ prior to a heat treatment at 400 °C. With the departure of Glasstech Solar, the UT group also undertook the development of rf sputtering for CdTe thin-film growth.

A variety of materials characterization and device testing is being performed at UT in support of the fabrication work. These include optical emission spectroscopy of the LDPVD and sputtering processes. Thin films are characterized by optical absorption, x-ray diffraction, scanning electron microscopy with energy dispersive spectroscopy, Raman scattering and photoluminescence, electrical conductivity and Hall effect measurements. Device testing includes current-voltage and spectral quantum efficiency measurements.

Studies of the LDPVD Process

The deposition system we have utilized for LDPVD has been described in an earlier annual report[1] and in ref.2. Important features are that the deposition is driven by an XeCl laser pulse ($\sim$15 nsec, 308 nm, $\sim$3 J/cm^2) from a pressed powder target. The intense laser pulse generates a plume of vapor which rises perpendicular to the target surface in a narrow plume and deposits onto a substrate heated to $\sim$280 °C. The plume consists mostly of uncharged atomic and possibly molecular species. We have used optical spectroscopy of the plume to determine translational velocities and characteristic temperatures in the vapor. Fig. 1 shows a spectral region which has three prominent lines identified with neutral Cd atoms. These data were obtained with an Aries 1/4 meter spectrometer coupled with a PAR OMA-II vidicon. The upper trace was taken at the point of interaction of the laser pulse and the target. The lower trace was obtained from a region $\sim$ 3 mm above the target. The broadening arises from collisions in the dense, hot vapor above the target. The upper state for all three of these lines is the configuration 5s6s ($^3S_1$) which lies 6.38 eV above the ground state of the Cd atom[3]. This implies that a considerable amount of internal excitation occurs in at least some of the vapor constituents.

In addition, we have made time-of-flight measurements by time-resolving the light emission with a photomultiplier and a digitizing oscilloscope. Figure 2 shows two traces obtained with the spectrometer centered on the 480 nm Cd emission line. One may easily convert this temporal trace into a curve of velocity probabilities since the time origin is well defined. (See the top trace in Fig.2.) The resulting velocity probability distribution is plotted in Fig.3. Here the solid curve has the functional form[3]

$$f(v) \doteq (8/3\pi)(m/2kT)^{5/2}\, v^4 \exp(-mv^2/2kT).$$

[The v^4 prefactor arises from a uniformly spatially diverging expansion ($1/r^2$) and from the conversion from temporal to velocity probabilities.] Although there is some discrepancy in the low velocities, the overall fit is quite good for a plume translational temperature of 75,000 K (in the direction perpendicular to the target). This corresponds to typical kinetic temperatures of 5-10 eV in the plume. These conditions are quite different from the temperatures of $<$1000 K which obtain in the case of closed space vapor transport or other near equilibrium evaporative techniques. Spray pyrolysis, electrodeposition, MOCVD utilize temperatures of typically 400 °C or below. On the other hand, sputtering will typically generate kinetic energies of $\sim$ 100 eV or more. Thus LDPVD opens an interesting regime for thin-film growth.

Figure 4 summarizes some of the parameters important for the laser deposition process. The quantity of evaporated or ablated material begins from nearly zero at 0.5 J/cm^2 and rises

approximately linearly with laser power until ~3 J/cm^2 beyond which the material loss saturates. The light intensity monitored at 480 nm rises rapidly with laser power above ~2 J/cm^2, and the neutral atom (Cd) kinetic energy similarly is only measured above 2 J/cm^2, where the emitted light is strong, but then rises with increasing pulse energy. From these data the pulse energy for most efficient target utilization is approximately 3 J/cm^2. Above 3 J/cm^2 additional laser energy simply appears as additional kinetic energy.

RF Sputtering of CdTe

DC and RF sputtering are widely used techniques for the deposition of thin films of insulators, semiconductors, and metals. The physical mechanisms of rf magnetron sputtering of solid targets have some similarity to those of LDPVD except that energetic argon ions, typically, are responsible for the target interactions which generate Cd and Te ions and atoms. The sputtered plume is not as tightly directed normal to the target surface as for LDPVD and the typical kinetic energies expected to be ~ 10^2 eV. Again it is a vacuum-based technique. Near the end of the first year we have implemented an rf sputtering system and produced thin films of CdTe on Corning 7059 glass and have incorporated these films in complete solar cell structures. The investigation and optimization of the sputtering process is still in its early stages at the end of the first contract year.

Studies of Film Properties

As of the end of the first contract year we have found that best cell performance is obtained only after a treatment with $CdCl_2$ followed by annealing at ~400 °C. However, we experienced some difficulty in reproducibly applying a thin film of $CdCl_2$ using standard methanol solutions and consequently developed a method for applying the $CdCl_2$ with laser deposition. Thus we have used LDPVD from a pressed target of anhydrous powdered $CdCl_2$ to apply the film in the same vacuum chamber used for the CdS, CdTe and ZnTe film growth. This has proved to be convenient, reproducible, and advantageous for avoiding water contamination.

Pulsed laser deposition is generally believed to provide a flux of species to the growth surface which closely resembles the target in stoichiometry. This probably accounts for some of its success in the deposition of multicomponent films such as the high temperature superconductors. Of course film stoichiometry also depends on the sticking coefficients of the impinging species. We have examined this behavior in two series of measurements. First, the average sticking coefficient for a plume of Cd and Te was obtained by measuring both the target mass loss and substrate mass increase after a deposition. The sticking coefficients are plotted in Fig. 5 as a function of the substrate temperature. A second set of measurements examined the film stoichiometry of a series of ternary alloys $Cd_xZn_{1-x}Te$. This introduces one constituent which is much lighter in mass than the other two and no constraint on the cation ratio in the film. As-grown films were examined with an electron probe for microanalysis (EPMA) by Alice Mason of NREL. The results showed that the films grown at room temperature showed a considerable excess of elemental tellurium, however, the films grown at 300 °C displayed uniform stoichiometry across the entire film within the errors of the microprobe measurement (2-5%, depending on film thickness) but with a 5 - 35% systematic enrichment of the lighter element Zn over Cd.

The use of pressed powder targets facilitates the preparation of target materials such as the ternary alloys described above but also permits the introduction of dopant materials. Thus we have been able to study the effect of doping of ZnTe with Cu over a wide range of dopant concentrations in the target. Cu-doped ZnTe films have been prepared by LDPVD on alkali-free glass (Corning 7059). Measurements of d.c. electrical conductivity were made at room temperature using a strip line geometry. The data show little sensitivity to copper concentration until about 0.3% atomic fraction. Then the resistivity drops by about five orders of magnitude with an increase of a factor of three in Cu concentration in the target. This behavior is still under investigation.

The surface texture of as-grown and of $CdCl_2$-treated and annealed CdTe films is presented in Fig. 6. Both films were etched for a few seconds in Br-methanol prior to coating with carbon for the SEM. Note that the as-grown LDPVD film on glass is quite smooth on a 1 μm scale but shows some roughness on a scale of 0.1 μm. After annealing at 400 °C for 30 minutes in air, the films develop well defined grains with sizes of ~ 1 μm.

The I-V characteristic of a recently prepared solar cell is shown in Fig. 7. The cell structure was soda-lime glass/SnO_2/CdS/CdTe/Cu/Au. The CdS and CdTe had thicknesses of ~ 0.3 μm and 1.0 μm respectively, grown by LDPVD. A ~ 0.2 μm thick layer of LDPVD $CdCl_2$ covered the CdTe. The structure was then annealing at 400 °C for 30 minutes prior to evaporation of Cu/Au contacts.

Summary

First-order optimization of pulsed laser growth of CdS, CdTe, and ZnTe has been achieved as well as a basic understanding of most of the physical properties of the laser-generated plume. Initial CdTe depositions have been made with rf sputtering. Complete cell structures have been fabricated with an all LDPVD CdS/CdTe cell tested at 8.7%. During the second contract year will concentrate on second order optimization of the LDPVD and sputter deposition processes with considerable efforts on evaluations of materials quality.

References

*Present address: Physics Department, Bilkent U., Ankara, Turkey

1. A. Compaan, et. al., Annual Report, Photovoltaic Program, FY 1990. (March 1991). SERI/TP-211-3643. Available NTIS: Order NO. DE 90000318.
2. A. Compaan, A. Bhat, C. Tabory, S. Liu, M. Nguyen, A. Aydinli, L-H. Tsien, and R.G. Bohn, Solar Cells 30, 79 (1991).
3. A. Bhat, Ph.D. Dissertation, U. of Toledo (1991), unpublished.
4. A. Aydinli, A. Compaan, G. Contreras-Puente, and A. Mason, Sol. State Commun. 80, 465 (1991).
5. A. Compaan, A. Bhat, C. Tabory, S. Liu, Y. Li, M.E. Savage, M. Shao, L. Tsien, and R.G. Bohn, Proc. 22nd IEEE Photovoltaic Specialists Conference, Las Vegas, Oct. 7-11, 1991 (to be published).

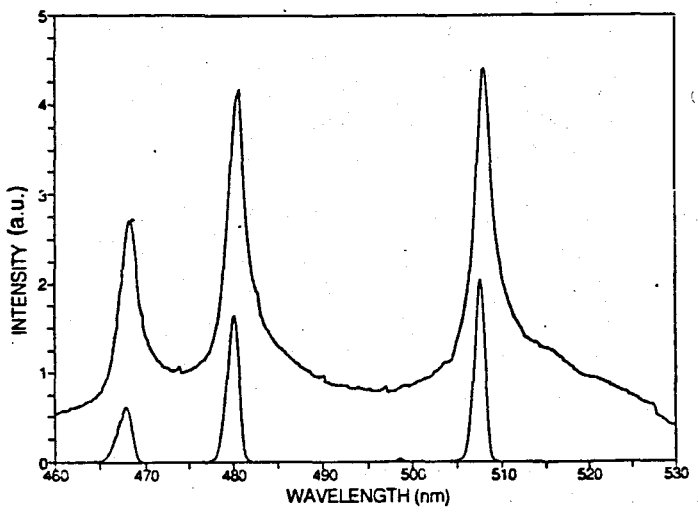

Fig. 1: Spectrum of optical emission from an excimer-laser-irradiated CdS target. The three peaks at λ= 4680, 4800, and 5080 Å have been identified as arising from transitions in neutral cadmium.

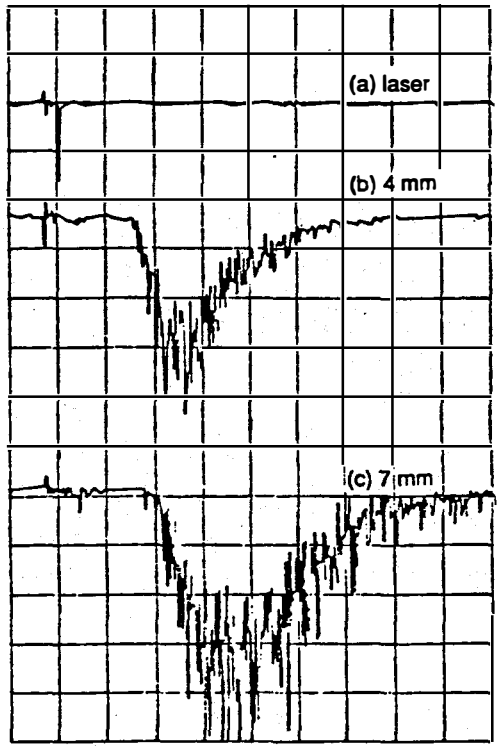

Fig. 2: Time resolved intensity measurement of the λ=4800 Å emission; (a) laser pulse, (b) 4 mm above the laser-target interaction region, (c) 7 mm above. Horizontal axis: 500 nsec/div.

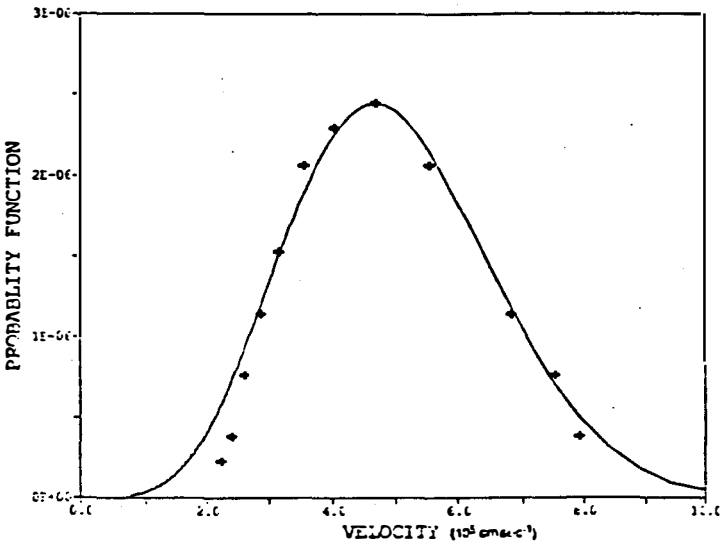

Fig. 3: Distribution of the vertical components of the velocities of neutral cadmium atoms. Solid curve is fit as described in the text.

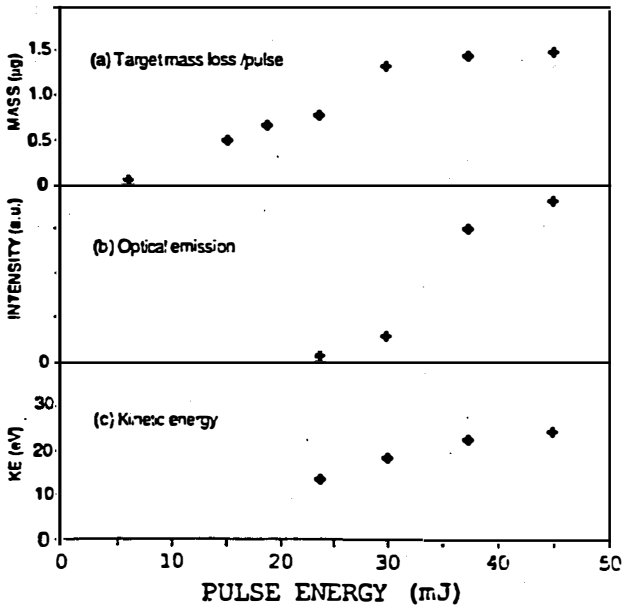

Fig. 4: Dependence on laser pulse energy of (a) target mass loss, (b) peak emission intensity at 480 nm, and (c) Cd atom kinetic energy. Laser spot size on the target was ~ 1 sq. mm.

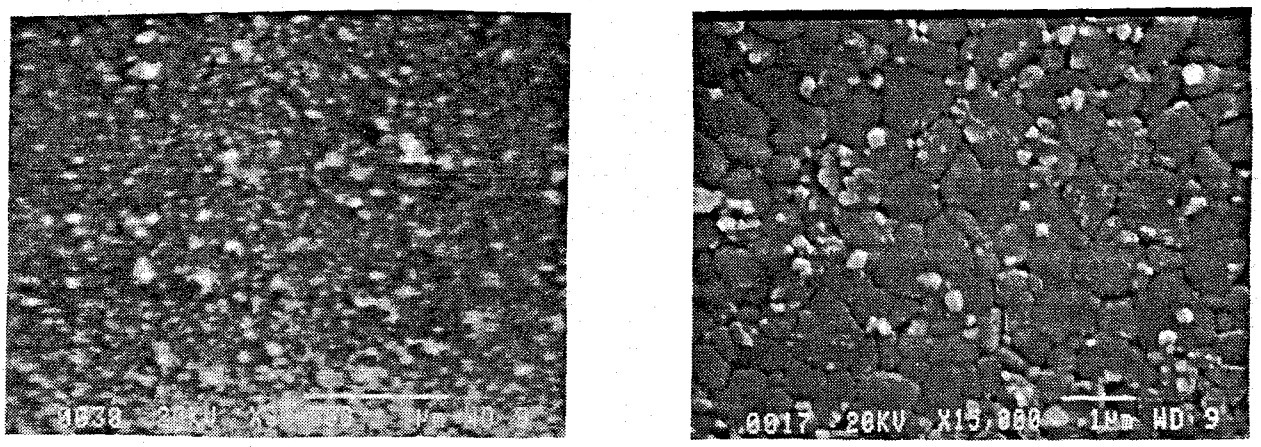

Fig. 6: SEM micrographs of LDPVD CdTe films grown on Corning 7059 glass showing the effects of the $CdCl_2$ layer and annealing. Left: 0.3 μm as-grown film; right: 0.6 μm annealed film.

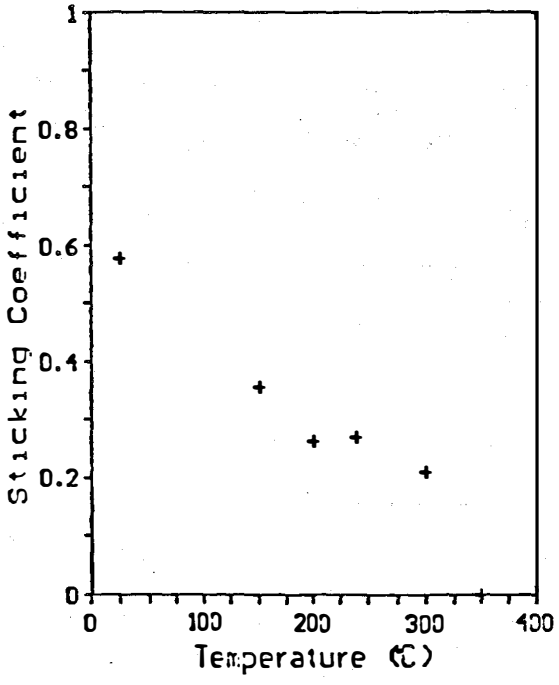

Fig. 5: Average sticking coefficient for LDPVD plume from a CdS target, as a function of substrate temperature.

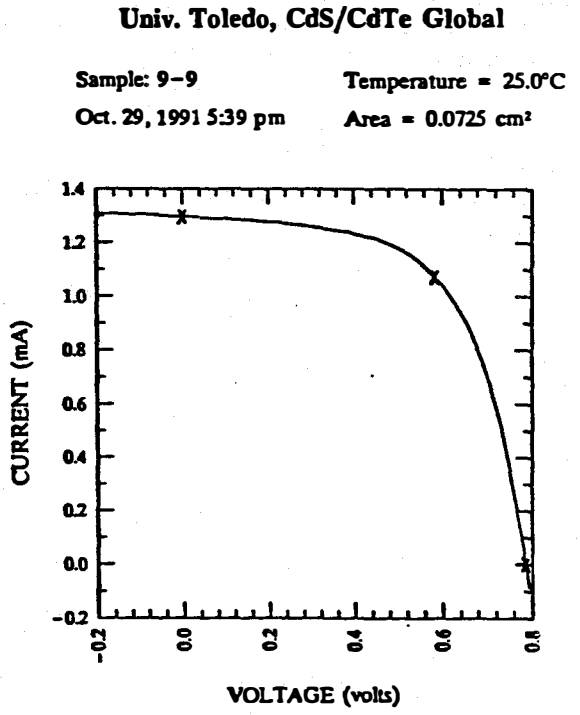

Fig. 7: I-V curve as measured by NREL. Voc = 0.7858 V, J_{sc} = 17.88 mA/cm2, P_{max} = 0.628 mW. Fill factor = 61.64 %, efficiency = 8.7%.

4.0 CRYSTALLINE SILICON MATERIALS RESEARCH

John Benner (Manager), Bhushan Sopori

Although crystalline silicon technologies for material growth and device processing are considered to be mature for a variety of applications, there remain a host of issues about which the current understanding is only marginal. These issues pertain to the role of defects and impurities in altering the properties of silicon and silicon solar cells. It is generally recognized that the presence of impurities/defects in the substrate can degrade the cell performance; however, recent data show that in the presence of crystal defects, the influence of impurities on the cell performance is somewhat mitigated. It is also known that some defects can be passivated by the presence of hydrogen or oxygen, although a detailed knowledge of these effects is certainly lacking. Clearly, these issues are critical to photovoltaic technology based on use of low-cost substrates which contain high concentrations of impurities and/or defects. The current research program was developed in collaboration with industry representatives to ensure that the industry research needs pertaining to basic material issues are adequately addressed. In this coordinated research effort between industry, universities, and NREL, the NREL role is primarily to support the area of test-device fabrication/analysis in order to relate material characteristics directly to solar cell performance.

This research program is designed to develop an understanding of basic mechanisms related to influence of impurities and defects on the important photovoltaic parameters in silicon. In particular, emphasis is toward development of post-growth processes that can be applied to low-cost substrates, preferably as a part of the solar cell fabrication process, in order to improve subcontracts that are supported by NREL in-house research participation. Major areas of research are: (1) mechanisms of hydrogen and oxygen interaction in low-cost silicon; (2) mechanisms of hydrogen passivation and kinetics of hydrogen diffusion; (3) effects of hydrogen on solar cells containing different types of crystal defects; (4) development of techniques for impurity characterization in silicon containing crystal defects; and (5) nondestructive testing of the photovoltaic parameters of commercial material. In the coming year, an effort will be made to develop some low-cost cell processing techniques (that incorporate the knowledge obtained from this research) to fabricate high-efficiency cells on commercial solar cell silicon.

Title: **Basic Studies of Point Defects and Their Influence on Solar Cell Related Electronic Properties of Crystalline Silicon**

Organization: School of Engineering, Duke University, Durham, North Carolina

Contributors: U. M. Goesele, principal investigator; W. J. Taylor, and W.-S. Yang

Introduction

The objective of this work is to increase the understanding of the role of point defects during precipitation processes in solar-grade polycrystalline silicon, and to determine how these point defects affect electrical properties. The thermal history involved in processing of solar cells can induce precipitation of both carbon and oxygen, and these precipitates are suspected to affect the minority carrier diffusion length.[1] (Unsatisfied atomic bonds at the interface between the precipitate and the silicon matrix can act as traps or recombination centers for the carriers.) Strains (volume differences) induced by the precipitate phase can be relieved by absorption/emission of point defects. Since evidence from surface oxide layers [2] indicates that strain influences the electrical behavior of the material, we assume that the strain surrounding a precipitate buried in a matrix can similarly influence the electrical behavior. and that by tailoring the precipitation processes to minimize strain, one can minimize the negative effects of these traps. This year we have been able to determine that the primary point defect involved in strain relief during precipitation is the self-interstitial, we have estimated the diffusivity and solubility of this species, we have generated a computer model for the precipitation process, and have shown a correlation between precipitation and electrical properties.

Determination of the Primary Point Defect in SiO_2 Precipitation [3,4]

As interstitial oxygen atoms leave their sites to precipitate as SiO_2, there is roughly a 100% increase in volume This volume increase (strain) must be relieved if precipitation is to continue, so we consider strain relief via absorption of vacancies or emission of self-interstitials. Since the rate of SiO_2 precipitate growth is dominated by diffusion of oxygen to the preciptate, the point defect species must have a flux into/out of the precipitate at least as large as 1/2 the oxygen in-flux. With the following analysis of the fluxes of the species it is possible to show that, at most temperatures, the vacancy flux is too low to support experimental data. This leads to the conclusion that vacancies are incapable of providing the necessary strain relief. However, self-interstitials *can* provide the necessary flux.

The flux of a species into a spherical sink can be described by

$$J = 4\pi r D C^{eq} \left(\frac{C(\infty)}{C^{eq}} - \frac{C(r)}{C^{eq}}\right) ,$$

where J is the flux, r is the radius of the precipitate, D is the diffusivity, C(r) is the concentration at the edge of the precipitate, $C(\infty)$ is the concentration in the bulk, and C^{eq} is the solubility. Oxygen can be denoted by the subscript Ox, vacancies by V, and self-interstitials by I. The temperature dependence $D_{Ox}C_{Ox}^{eq}$ $D_VC_V^{eq}$, and $D_IC_I^{eq}$ are known, $C_{Ox}(\infty)$ can be measured by FTIR, and $C_V(\infty)$ and $C_I(\infty)$ can be assumed to be near thermal equilibrium. Furthermore, the relationships

$$\frac{C_{ox}(r)}{C_{ox}^{eq}} = \left(\frac{C_V^{eq}}{C_V(r)}\right)^{\frac{1}{2}} \exp\left(\frac{\sigma\Omega_{SiO_2}}{rk_BT}\right) , \quad \text{or for self-interstitials,} \quad \frac{C_{ox}(r)}{C_{ox}^{eq}} = \left(\frac{C_I(r)}{C_I^{eq}}\right)^{\frac{1}{2}} \exp\left(\frac{\sigma\Omega_{SiO_2}}{rk_BT}\right)$$

hold, since precipitation is not reaction-limited. Thus, for the vacancy example, a flux balance

$$\frac{1}{2} D_{ox} C_{ox}^{eq} \left[\frac{C_{ox}(\infty)}{C_{ox}^{eq}} - \left(\frac{C_V^{eq}}{C_V(r)} \right)^{\frac{1}{2}} \exp\left(\frac{\sigma \Omega_{SiO_2}}{r k_B T} \right) \right] = D_V C_V^{eq} \left[\frac{C_V(\infty)}{C_V^{eq}} - \frac{C_V(r)}{C_V^{eq}} \right] .$$

can be solved, resulting in $C_V(r)$ as a function of temperature. Since vacancies and oxygen interact at the precipitate surface, this $C_V(r)$ affects the oxygen flux. The result is an oxygen flux significantly less than that observed experimentally. Experimental data closely matches a model in which point defect interaction is ignored. We make a ratio

$$Q = \frac{\text{Ox Flux Including Pt. Def. Interaction}}{\text{Ox Flux Ignoring Pt. Def. Interaction}} = \frac{\text{Ox Flux Including Pt. Def. Interaction}}{\text{Ox Flux Experimentally Observed}}$$

which is plotted in Figure 1. For the case in which vacancies are the strain relief species, the Q ratio is much less than 1 over most temperatures, indicating that the vacancy model can not match experimental data. However, for the case of self-interstitials as the strain relief species, the Q ratio is always near 1, so the experimental data can be fitted with this model. From this we conclude that at most temperatures, self-interstitials are the dominant point defect for strain relief.

Determination of Self-Interstitial Diffusivity

Since the self-interstitials play such an important role in precipitation processes, knowledge of their diffusivity (D_I) is vital. This will affect how quickly self-interstitial supersaturations can flow to/from the sinks/sources. Unfortunately, D_I is a poorly known quantity at temperatures of 900°C and below, where many cell manufacturing processes occur. Therefore we investigated D_I at these temperatures.

We measured the diffusivity of self-interstitials by generating them at one side of a wafer and observing their arrival at the opposite side via enhanced diffusion of a marker species. The marker species is a boron implant (150keV, 5×10^{14} cm^{-2}) on the front side of a lightly doped p-type silicon wafer, which was then damage-annealed for 30 minutes at 900°C and 30 minutes at 800°C. High concentration ($10^{21} cm^{-3}$) phosphorus spin-on glass was diffused from the back side at 800°C. The in-diffusing phosphorus creates silicon self-interstitials, which subsequently rapidly diffuse across the wafer and assist the boron profile to diffuse. Results showed that, for a sample of thickness 150μm, after only 20 minutes, significant diffusion of the boron profile occurred. This allows a rough lower bound estimate for the diffusivity of the self-interstitials. From $D=x^2/t$ we obtain $D_{I800°C} > 2 \times 10^7 cm^2 s^{-1}$. This estimate is plotted in Figure 2, along with previous estimates. Analysis of the other estimates will be contained in the final report.

Last year's report [5] included a relationship between D_I and the capability of dislocation densities to keep self-interstitial concentrations near thermal equilibrium (they act as sinks). For high D_I, even relatively low dislocation densities are theoretically capable of this. Phosphorus diffusion experiments in dislocated polysilicon corroborate these predictions.

Computer Model for Precipitation

For precipitate modeling, we have generated a computer program which allows input of a given initial precipitate size and number distribution, then observe how these precipitates shrink and grow, based upon variables such as temperature, precipitate/matrix surface energy, and concentrations of the species. The program keeps track of all species, allows for generation of

new point defects, and continually adjusts the critical radius. It is found that a critical factor determining precipitation behavior is the initial size distribution of the precipitate nuclei. This factor is a function of growth conditions, and is still not completely understood.

Correlation of Electrical Properties to Precipitation

Some of our recent experimental work concerns the correlation between precipitates and changes in electrical properties. We expect that, for silicon with high carbon concentration, the interaction of carbon in the precipitation process affects the strain of the system, and that this is reflected in the minority carrier diffusion length (L_D). Using two wafers of similar oxygen concentration and widely different carbon concentrations (Low<$1x10^{16}$ cm^{-3}, High=$3x10^{17}$ cm^{-3}), we performed heat treatments to precipitate out the oxygen. We then measured L_D via surface photo-voltage to discern any differences between the samples. Figure 3 shows results of the study. It is obvious that the effect of precipitation on L_D in the low carbon sample is much more drastic than in the high carbon sample.

In wafers containing large amounts of carbon, the carbon typically precipitates out at a rate of 1/2 that of oxygen. This, along with changes in the FTIR signature of the material, indicate that the carbon is co-precipitating with the oxygen in C-O complexes. This behavior can be understood by noting that carbon is much smaller than silicon, so absorption of a substitutional carbon atom into an oxygen complex reduces the strain associated with precipitation. Combining this reasoning with the results of Figure 3, it seems that strain relief via carbon absorption is preferable to strain relief via self-interstitial emission. Thus, while it is known that oxygen precipitation has negative effects upon electrical properties of silicon, these negative effects may be reduced by providing carbon in concentrations high enough to allow C-O co-precipitation.

Summary

We have concluded that for strain relief during precipitation of oxygen in silicon, the self-intertstitial is the predominant intrinsic point defect used. We have experimentally estimated the diffusivity of the silicon self-interstitial at 800°C (D_I>$2x10^{-7}cm^2s^{-1}$). Computer modeling of the precipitation process shows that a better understanding of the size distribution of nuclei prior to precipitation is necessary. Carbon, since it is smaller than silicon, can also act as a strain relief species, forming C-O complexes. Although oxygen precipitation decreases carrier lifetime, it appears that C-O co-precipitation (which occurs in samples containing large amounts of carbon) has a smaller effect upon the lifetime than O precipitating alone as SiO_2.

References

1. S. Pizzini, A. Sandrinelli, M. Beghi, D. Narducci, F. Allegretti, S. Torchio, G. Fabbri, G.P. Ottaviani, F. Demartin, and A. Fusi, J. Electrochem. Soc., **135**, 155 (1988)
2. C.H. Bjorkman, J.T. Fitch, and G. Lucovsky, Appl. Phys. Lett., **56**, 1983 (1990)
3. W.J. Taylor, T.Y. Tan and U.M. Gösele, Proceedings of the 16th International Conference on Defects in Semiconductors, Bethlehem, PA, July, 1991.
4. W.J. Taylor, T.Y. Tan and U.M. Gösele, Appl. Phys. Lett. **59**, 2007 (1991)
5. Annual Report, Photovoltaic Program FY 1990, (March 1991), SERI/TP-211-3643, 290 pp. Available NTIS: Order No. DE90000318
6. T. Tan and U. Goesele, Appl. Phys. **A37**, 1 (1985)
7. Morehead and Goesele, analysis is unpublished. First used in T. Tan and U. Goesele, Appl. Phys. **A37**, 1 (1985)
8. Griffin, Fahey, Plummer, Dutton 14.34 APL **47**,319(1985)

9. A. Seeger, H. Föll, and W. Frank, in: Radiation Effects in Semiconductors, 1976, N.B. Urli and J.W. Corbett, Eds (Institute of Physics, Bristol and London 1977) Inst. Phys.. Conf. Ser. No. 31, p. 12.
10. G.B. Bronner and J.D. Plummer, J. Appl. Phys. **61**, 5294 (1987)
11. K. Taniguchi, D.A. Antoniadis, and Y. Matsushita, Appl. Phys. Lett. **42**, 961 (1983)
12. K. Wada, N. Inoue, and J. Osaka, in Defects in Semiconductors II S. Mahajan and J. W. Corbett, Eds., (North-Holland, New York, 1983) pg. 125
13. W.B. Rogers, H.A. Massoud, Poroceed. 2nd Int'l Symp. on Process Modeling in Semicond. Tech. G.R. Srinivasan, J.D. Plummer, and S.T. Pantelides, Eds, (The Electrochem. Soc., Pennington, NJ 1991) pg 495
14. H. Yamanaka, Y. Aoki and T. Samizo, Jap. J. Appl. Phys. **29**, 2450 (1990)
15. W. Wijaranakula, J. Appl. Phys. **67**, 7626 (1990)

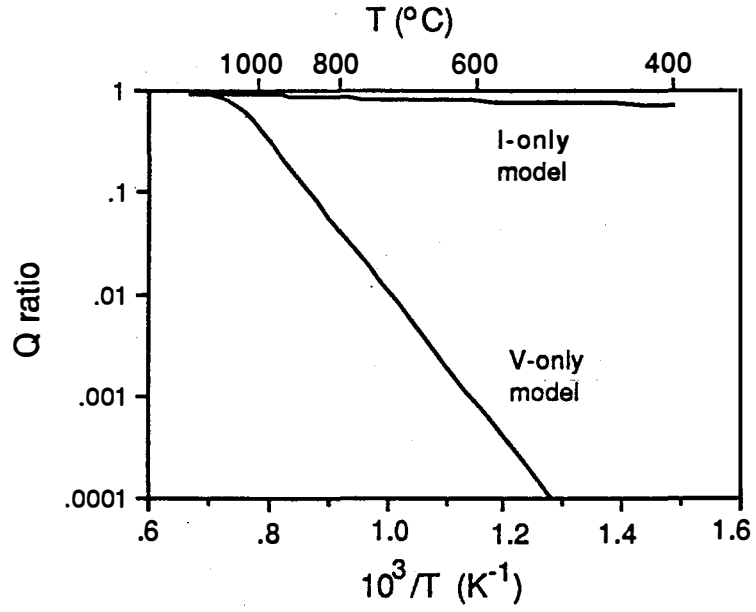

Figure 1: Ratio Q of oxygen flux into precipitate if intrinsic point defects are accounted for, to the case in which point defects are ignored (plotted as a function of inverse absolute temperature). Values of Q significantly less than 1 indicate a model incapable of fitting experimental data.

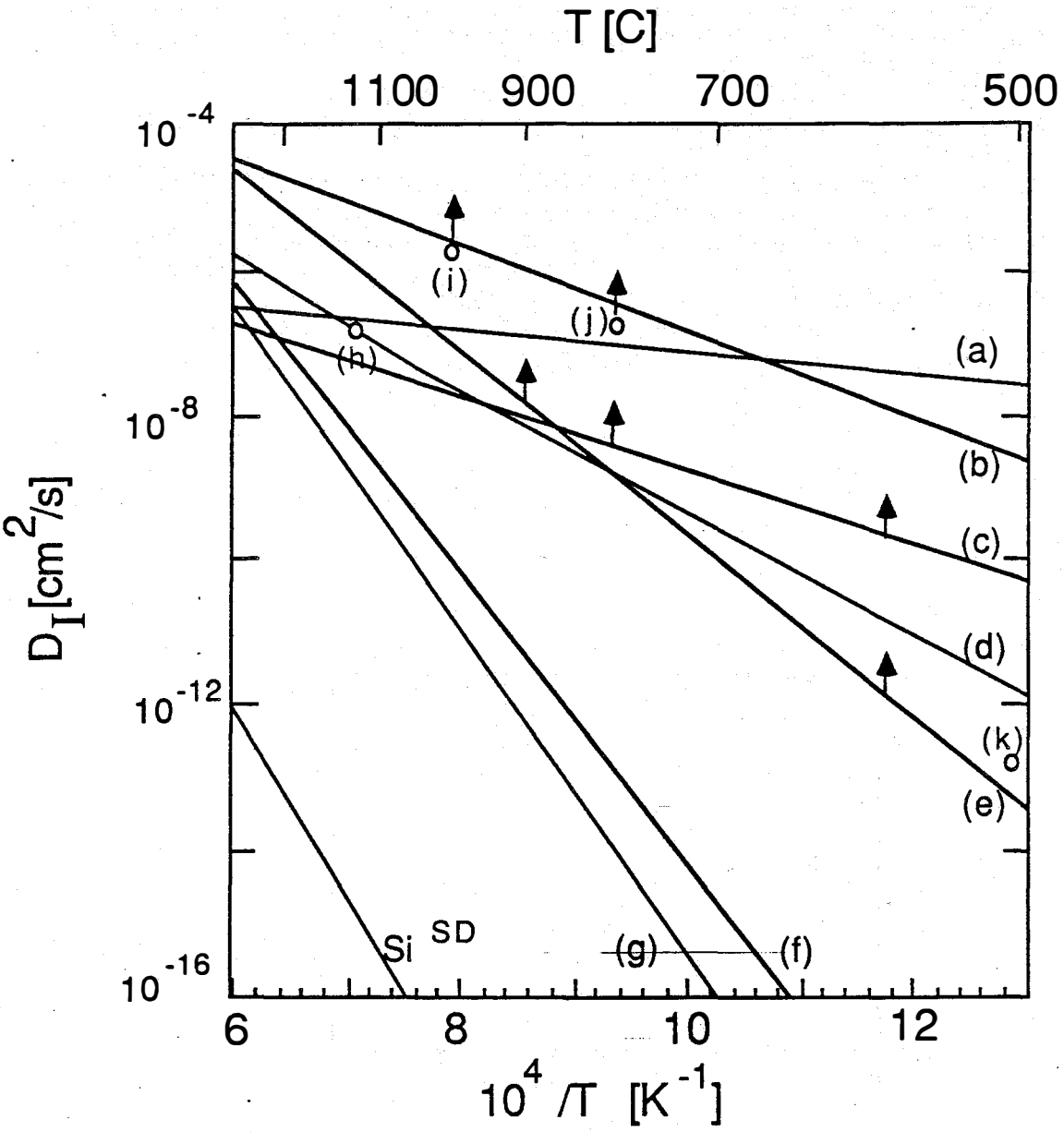

Figure 2: Some of the estimates for D_I presented in the literature, along with the silicon self-diffusion coefficient $D_I C_I^{eq}$ (a) Tan and Gösele [6], (b) Morehead[7], (c) Griffin et al.,[8], (d) Seeger et al.[9],(e) Bronner and Plummer[10], (f) Taniguchi et al.[11], (g) Wada et al.[12], (h) Rogers et al. [13],(i) Yamanaka [14], (j) our work, and (k) Wijaranakula[15].

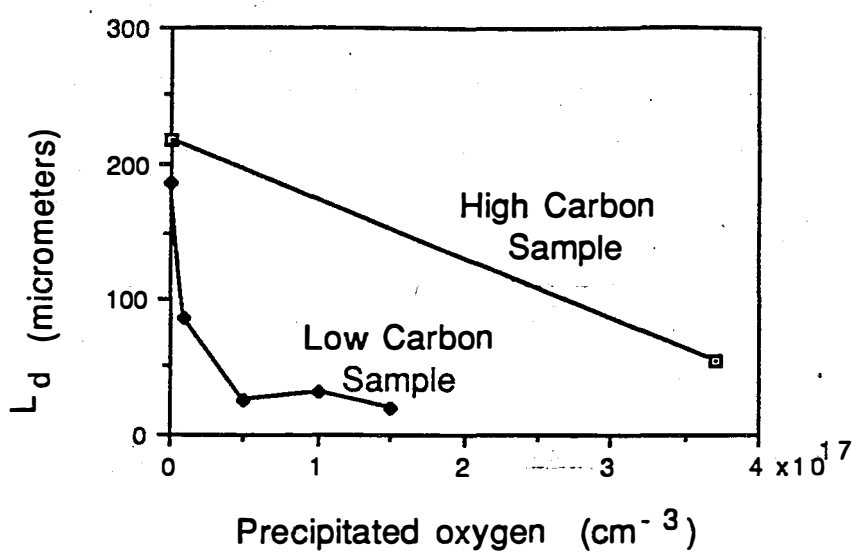

Figure 3: The effect of precipitation upon minority carrier diffusion length (L_D). The sample with an high carbon concentration shows less of an effect than the sample with a low carbon concentration. (Note: for the high carbon wafer, most of the carbon precipitated simultaneously with the oxygen (ΔC_S=1.1x10^{17} cm^{-3})

Title: **Impurity and Defect Characterization in Silicon**

Organization: **Georgia Institute of Technology, Atlanta, Georgia 30332**

Contributors: **A. Rohatgi, W.A. Doolittle, J. Salami, and P. Sana**

Objective

The objective of this program is to understand the role of impurities and defects in polycrystalline silicon and provide silicon solar cells to NREL for optically processed metallization.

Effect of Hydrogen Passivation of Crystal Defects

The effects of hydrogen diffusion and the passivation of crystal defects and impurities were studied on single and polycrystalline silicon obtained from several different vendors. It was found that enhanced diffusion of hydrogen can occur in some of these materials, both in the bulk and along the grain boundaries, with an effective diffusivity of about and order of magnitude higher than previously reported values. Hydrogen incorporated for defect passivation can induce defects in silicon. We have studied these defects and their recombination characteristics, and propose that these defects pose the ultimate limit on the degree of improvement manifested by a cell. The observed behavior of hydrogen plays an important role for defect passivation in solar cells and can be explained on the basis of point defect interactions with hydrogen.

FTIR/etching analysis revealed that optically active hydrogen in Si is confined to the narrow region of the surface damaged during ion implantation. Cross sectional transmission electron microscopy (XTEM) revealed that the surface region (damaged by ion implantation) had several types of defects, dislocations and hydrogen entrapment, stacking faults and platelets. The structure of these platelets was examined and determined (1). Hydrogen was found to segregate at dislocations for hydrogen concentrations greater than $10^{16}cm^3$.

Effect of Illumination Level on the Performance of Polycrystalline Silicon Solar Cells

A combination of grain boundary model (2) and solar cell modelling (3) is used to quantify the effect of illumination level on diffusion length and efficiency of polysilicon cells. It was found that diffusion length is not uniform under illumination for those polysilicon materials in which grain boundaries dominate the recombination. The grain boundary barrier height decreases and diffusion length increases as we approach the illuminated surface (4). The relative improvement in diffusion length and efficiency increases with the concentration level. The illumination level enhanced diffusion length boosts the normal increase in efficiency under concentrated sunlight. It is shown that in a large grain (1mm) polysilicon, an increased illumination level of 50 suns can eliminate the undesirable effects of a grain boundary state density in the range of 10^{11}-$10^{12}cm^{-2}$. The majority of the efficiency improvement due to enhanced diffusion length effect can be realized at ~30 suns, Figure 1.

Model calculations were also performed for small grain thin film polysilicon cells. It was found that the efficiency of a 30 μm grain size polysilicon cells, with $N_{ts}=5x10^{11}cm^{-2}$, can increase from 3.9% at one sun to 11.5% at 50 suns, Figure 1. Reducing the cell thickness to 40μm from 100μm, without any light trapping, raises this length. The illumination level induced diffusion length enhancement effect is more pronounced in polysilicon materials with smaller grain size and higher N_{ts}, Figure 2. Hence, the illumination enhanced diffusion length in polysilicon can

reduce the efficiency gap between the cells made on: a) good and bad polysilicon; b) polysilicon with passivated and non-passivated grain boundaries; c) polysilicon with different grain size, and d) polysilicon and single crystal silicon.

Fabrication of Polycrystalline Silicon Solar Cells

Several solar cell runs were made on different materials with Phosphorus diffusion on the front and Al diffusion on the back after process optimization of each step. The cell configuration for the latest process sequence is shown in Figure 3. The corresponding process sequence summarized below:

1) Wafer Clean
2) Phos. Diffusion
3) Etch Back
4) Al Evaporation on the back side
5) Al Diffusion and Oxidation
6) Lift-Off
7) Annealing
8) Ag Plating
9) Mesa Etch
10) AR Coating

Table 1 shows the data for the polycrystalline cells fabricated on Osaka Titanium poly, Solarex poly, and Wacker cast poly.

Notice that cell efficiencies of the order of 15% were achieved with best results on Osaka Titanium. Figure 4 shows the I-V curve taken at NREL for a 14.9% efficient cell fabricated on Osaka Titanium.

Some single crystal cells were also fabricated for NREL for optically processed metallization. Half of the wafer had conventional Ti-Pd-Ag metallization while the other half was kept bare for aluminum metallization by optical processing, Table 2. We are able to fabricate 18.3% efficient cells on FZ silicon.

References

(1) B.L. Sopori et. al., "Hydrogen in Silicon: Diffusion and Defect Passivation", presented at the **22nd IEEE PVSC**, Las Vegas, NV, October 1992.

(2) Z. Chen, L.C. Burton, "Electrical Properties and Their Depth Variation in Poly-Si under AM1 Illumination", **Phys. Stat. Sol. (a) 122**, p. 361, 1990.

(3) P.A. Basore, D.T. Rover, G.M. Thorson, "Solar Cell Modelling on Personal Computers," **Proc. of 18th IEEE Photovoltaic Specialists Conference**, p. 703-709, 1985.

(4) Z. Chen, A. Rohatgi, and P. Sana, "Effects of Illumination Level on Diffusion Length and Efficiency of Poly-Si Cells", presented at the **22nd IEEE PVSC**, Las Vegas, NV, 1992.

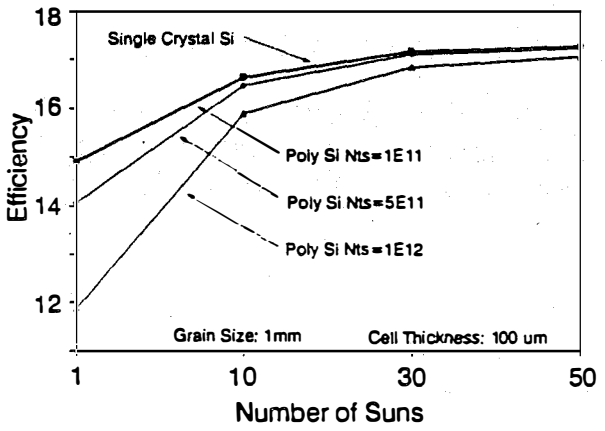

Fig. 1 The effect of concentration level and trap density on the efficiency.

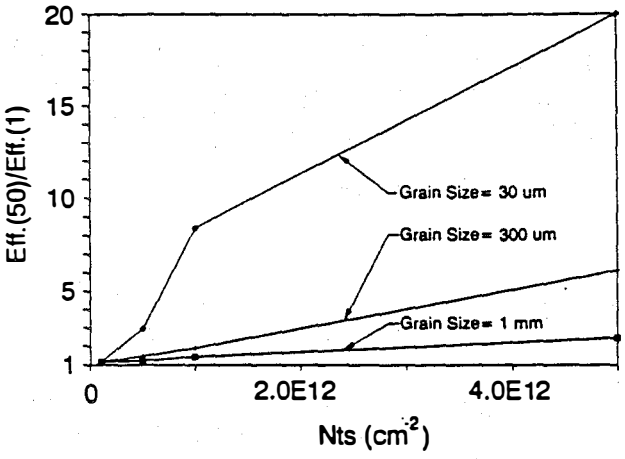

Fig. 2 The effect of trap density and grain size on the efficiency

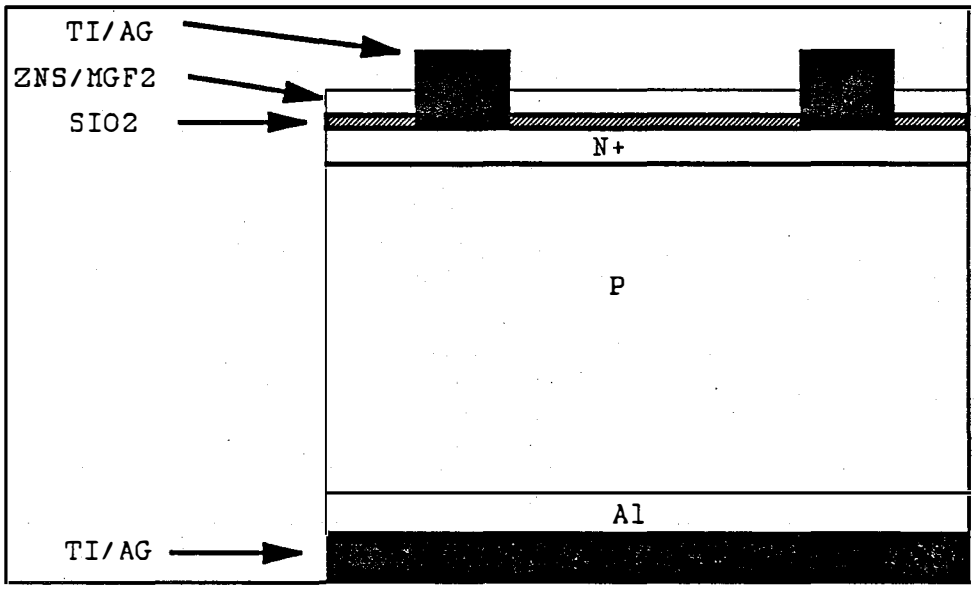

Fig. 3. One Sun Polycrystalline Cell Structure

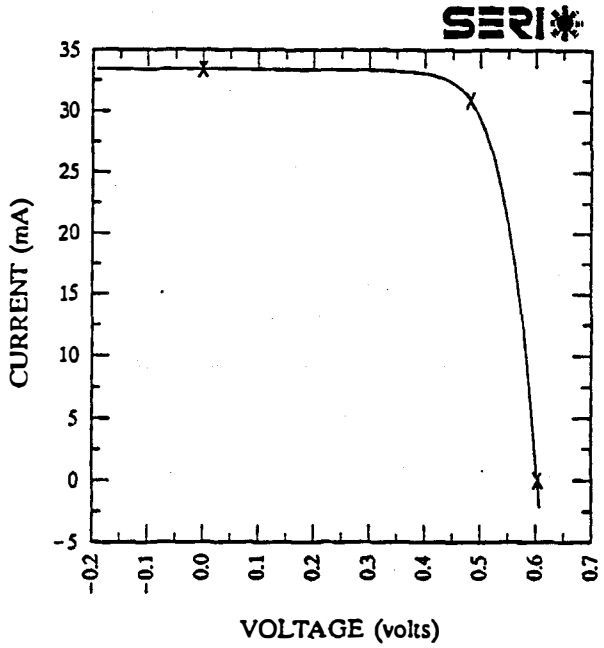

V_{oc} = 0.6044 volts	I_{sc} = 33.42 mA
J_{sc} = 33.42 mA/cm²	P_{max} = 14.92 mW
Fill factor = 73.85 %	I_{max} = 30.93 mA
Efficiency = 14.9 %	V_{max} = 0.4823 V

Fig. 4. I-V curve of the cell tested at NREL

Table I One Sun Polycrystalline Cells

Cell ID	ρ(Ω.cm)	J_{sc}	V_{oc}	FF	EFF
OSAKA					
GT060512*	1.05	33.9	0.616	0.739	15.4
GT060511	1.05	33.8	0.614	0.691	14.4
SOLAREX					
GT060531**	1.00	32.1	0.602	0.752	14.5
GT060523	1.00	32.1	0.599	0.739	14.2
WACKER					
GT060524***	1.23	30.6	0.598	0.764	14.0
GT060532	1.23	30.3	0.593	0.766	13.8

Table II One sun FZ solar cell parameters tested at NREL.

Cell ID	J_{sc}	V_{oc}	FF	EFF%
OP-1-1	37.01	0.650	0.763	18.3
OP-1-2	36.56	0.649	0.764	18.1
OP-1-3	36.13	0.645	0.752	17.5

The Effectiveness and Stability of Impurity/Defect Interactions and Their Impact on Minority Carrier Lifetime

Organization: Materials Science and Engineering Department, North Carolina State University, Raleigh, North Carolina.

Contributors: G.A. Rozgonyi, Program manager; F. Shimura, principal investigator, A. Buczkowski, research associate; T.Q. Zhou, graduate student.

The project is directed towards understanding the chemical and electrical behavior of structural defects and impurities in photovoltaic materials. These impurity/defect complexes usually act as recombination centers, thereby reducing the minority carrier lifetime which generally degrades device efficiency. A central question under investigation is whether extended defects are necessarily lifetime killers or whether they may in some circumstances be electrically inactive. For example, it is known that structural defects getter impurities and that these impurities are generally effective recombination centers because they introduce deep level electron states within the the Si band gap. For this reason it is reasonable to believe that in many practical situations the electrical activity of extended, structural defects are the result of process induced gettering of impurities at structural defects and are not entirely intrinsic characteristics of the structural defects themselves. To evaluate this hypothesis we have sought to study the electrical activity of clean (as-grown) and impurity decorated structural defects. The gettering of impurities and subsequent effects on electrical activity has been observed using scanning electron microscopy in the electron beam induced current mode,SEM/EBIC, transmission electron microscopy, TEM, and other analytical techniques. The minority carrier lifetime dependence on process induced decoration of structural defects has been studied using the LIFETECH-88, laser-microwave system which is a particularly attractive technique because it is a high-throughput, non-destructive device capable of mapping the minority carrier lifetime over entire wafers. Two major advancements in this technology have been achieved recently at NCSU and used extensively in this study. They are the development of an effective algorithm for the separation of the surface and bulk components of the minority carrier lifetime parameter [3] and the subsequent ability to resolve the bulk lifetime dependence on temperature and hence extract the activation energy of impurity states within the Si band gap. The resulting laser-microwave-deep-level-transient-spectroscopy, LMDLTS, is a method of particular importance for testing our central hypothesis that the primary electrical activity of structural defects is largely the result of impurity decoration.

Although it is possible to study extended defects in a number of settings, we have focused our primary efforts on the study of 60 degree interfacial misfit dislocations which form in a relatively controllable fashion when a Si(Ge) alloy layer is grown between a high purity Si capping and buffer layers in heteroepitaxial systems. Specifically for the results herein the capping and buffer layers are nominally 3 μm thick and the Si(2%Ge) alloy layer has a thickness of 2μm. To study the gettering and electrical properties of dislocations the following experiment was conducted. Au, Ni and Cu impurities were intentionally introduced in a heteroepitaxial system containing misfit dislocations from a backside deposited metal film followed by rapid thermal annealing (RTA). Transmission Electron Microscopy (TEM) results indicate that the impurities were gettered along the misfit dislocations in near-surface regions either as Au precipitate colonies, or as $NiSi_2$ and CuSi silicide precipitates[2] SEM/EBIC studies revealed that these precipitates dominate the recombination properties of the initially inactive misfit dislocations. We conclude that the impurity decoration dominated the electrical activity because SEM/EBIC imaging of the as-grown misfit dislocations revealed no discernable localized contrast Fig. [1a] indicating that the undecorated dislocations were not appreciably more effective recombination centers than the high purity epi material which surrounded them. However, surface traces of the misfit dislocations

were visible on the top surface of the same sample using a Nomarski optical microscope, as shown in Fig. 1b, . The dislocations were then decorated with Ni, Au and Cu by diffusion from a back side evaporated layer via rapid thermal annealing for 30 seconds. The temperature range from 400°C to 1200°C was examined in order to achieve different levels of defect decoration. Significant differences in electrical activity of decorated dislocations were observed as a function of the metal and the temperature of annealing. An EBIC image obtained for a Ni sample contaminated at 1000°C is shown in Fig.1c and reveals that: 1) EBIC contrast occurs as dark isolated spots , and 2) dislocation lines are not visible between the spots. Fig. 1d shows a striking TEM image of such a precipitate at a misfit dislocation. The dark EBIC contrast of the Ni contaminated samples and accompanying TEM images indicate that localized recombination centers are now present along the misfit dislocations.

The gold decorated dislocations gave a detectable continuous EBIC contrast after annealing at or above 800°C, whereas no contrast was evident at 600°C. An example of dislocations decorated at 1000°C is given in Fig.1e. At such higher diffusion temperatures the dislocations appear as continuous dark lines indicating that they are active recombination centers along their total length. Fig 1f shows the accompanying TEM image of more or less joined precipitate colonies at the misfit dislocations which are thought to be the source of the SEM/EBIC contrasts.

Comparing the electrical activities of decorated and "clean" misfit dislocations, the as-grown misfit dislocations show no EBIC recombination activity due to their intrinsic structure. One possible explanation is that if the energy level of misfit dislocation is relatively shallower, the recombination activity will not be as efficient as that of the energy level present at the middle of the band gap. Our EBIC study on contaminated samples indicates that the misfit dislocations are electrically activated by gettered impurities and the precipitation is responsible for the strong recombination activity. The EBIC images of decorated MD's with different impurities depend on the distribution of the precipitate at MD interfaces. Therefore, the mechanism of recombination activity related to these precipitates must take into account the following factors: 1) existence of a space-charge region (electrical field) around the precipitates which could increase the effective capture cross section of minority carriers, thus increasing the local recombination activity; 2) deep levels due to the precipitation related defects such as point defects or their aggregates, and secondary dislocation generation as occurs with $NiSi_2$. The most likely mechanism is probably a combination of both factors. The space-charge region increases the captured flux of carriers, and the precipitation related defects introduce deep levels. These are two important parameters affecting the recombination activity and ultimately the EBIC contrast.

As mentioned above, we are also developing a laser / microwave lifetime measurement method using the LIFETECH-88® system. This is a potent method of mapping the minority carrier lifetime parameter over entire wafers in a contactless, high throughput, nondestructive manner in which excess electron-hole-pairs , ehp's, are generated by laser illumination and their subsequent decay is studied by recording the microwave reflectance of the probed wafer as carrier concentrations return to equilibrium. An inherent trait of pulsed laser excitation is that an incident laser pulse creates a distribution of excess electron-hole-pairs, ehp's, which is initially greatest at the illuminated surface and declines exponentially with increasing material depth. Additionally, this depth dependence is a function of laser wave length. Because the surface recombination rate is generally much higher than the bulk rate the distribution of excess ehp's approaches asymptotically with time a condition in which the bulk concentration is greater than the surface concentration as if the excess ehp's had been generated uniformly initially instead of in the manner described above. In this latter condition the log microwave reflectance decreases linearly yielding the time constant of the exponential decay of excess carriers within the material being probed. This time constant τ_{eff} depends both on surface and bulk components according to the relation:

$$1/\tau_{eff} = 1/\tau_{surface} + \tau_{bulk} \qquad \text{eq. [1]}$$

The initial deviation from a pure exponential decay due to the laser excitation function and the dependence of this effect on laser wave length has been exploited to yield a mathematical algorithm for extracting the surface recombination rate from the microwave reflectance data for excitation by two separate laser pulses of unequal wave lengths, subsequently the bulk recombination rate can be extracted using eq.[1]. See ref. [3] for the mathematical details of this analysis. In passing it is worth mentioning that we are currently developing a related technique for deriving the same information using only a single laser. An important example of how the method can be useful is seen in the following experiment.

Clean and decorated interfacial misfit dislocation were created by preparing three wafers identical to those described above except that a 1% rather than a 2% Si(Ge) alloy layer was used in creating misfit dislocations. Two wafers were implanted from the back side with Au and Ni, with dose Cs = $10^{12}/cm^2$ at energy E = 100keV. A third reference wafer was not implanted. Following implantation a cross-grid network of misfit dislocations over the entire wafer was observed nondestructively with large-area XRT topography. Following the implantation process, a cross-grid network of misfit dislocations over the entire wafer was observed nondestructively with large-area XRT topography. A map of the corresponding recombination lifetime was also measured. Then, the wafers were cut into four quarters. Three quarters were annealed with RTA at temperature 400°C, 800°C and 1000°C for 30 seconds, respectively. A fourth reference quarter was not annealed. Because the total wafer thickness is dramatically thicker than the heteroepitaxial layer containing the misfit dislocations, we interpret the minority carrier recombination lifetime due to misfit dislocations as "surface" recombination and that due to bulk defects as "bulk" recombination.

Notice in Fig. 3a that the electrical activity of near surface misfit dislocations and in the bulk were strongly affected by RTA even if there was no metal implanted. The presence of Au and Ni contaminants additionally modify the MD recombination properties where the influence of annealing temperature (metal decoration level) on the bulk and surface component of lifetime is shown, respectively. For metal implanted samples, the bulk lifetime initially slightly increases with temperature within low RTA temperature range (up to 400°C), most likely due to gettering properties of the dislocations. It then decreases within a middle temperature range, when implanted contaminants start to diffuse into semiconductor bulk. At the end, lifetime increases again after impurities are collected at the MD but this increase is not higher than the initial lifetime value. For the reference wafer, lifetime after initial increase decreases monotonically with RTA temperature and reaches the same value as for metal doped samples. It is most likely that lifetime in the bulk of the samples annealed at 1000°C is controlled not by metal contaminants but by defects introduced by the RTA process. The surface lifetime which is indicative of the electrical activity of the misfit dislocations decreases slowly with the RTA temperature up to 800°C. This is associated with a surface recombination velocity increase at the decorated dislocations. However, above 800°C the dislocation activity abruptly decreases again (surface lifetime increases). We believe that this effect is related to the creation of an electric field at the MD which repels minority carriers from the dislocation plane. Notice that, in order to explain this electrical behavior, the formation of $n\text{-}n^+$ (but not a p-n) junction around the dislocation has to be introduced. This is because the electric field associated with a p-n junction attracts minority carriers and increases the observed surface recombination velocity at the junction plane, while a low-high concentration junction repels minority carriers and decreases the "effective" surface recombination.

Additionally, we have developed the capability of determining the activation energy of deep impurity levels in a LM-DLTS system using the LIFETECH-88® system [Ref. 5]. This is done by measuring the lifetime dependence on ambient temperature and evaluating the data mathematically. Fig 3a shows the Shockley-Read-Hall theoretical lifetime calculations for defect states of differing activation energy assuming a trap density of 10^{13}. An example of this technique is shown on the following experiment to evaluate the activation energies of defect related states performed on wafers with known concentrations of Carbon and Oxygen impurities. Silicon samples used for this study were prepared from six CZ silicon ingots (n<100>, 150 mm-diam, 20~30 ohm-cm) with different oxygen and carbon concentrations. The concentrations of interstitial oxygen ([Oi]) and

substitutional carbon ([Cs]) were measured with FT-IR according to the ASTM procedures. The initial oxygen concentration ($[Oi]_O$) was controlled to be in three levels, i.e., L(low), M(middle), and H(high), ranging 13.3~16.4x10^{17} cm^{-3}, while the initial carbon concentration ($[Cs]_O$) was in two levels, i.e., L(low: <1x10^{15} cm^{-3}) and H(high: ~1x10^{16} cm^{-3}), without and with doping carbon powders into the silicon melt, respectively. The results of this analysis are indicated in Fig. 3b.

References

1. *"Electrical Activity of Dislocations: Prospect for Practical Utilization"*, Appl. Physics A, (1991), Z. J. Radzimski, T-Q. Zhou, A. Buczkowski, and G. A. Rozgonyi

2. *"The Gettering and Electrical Activity of Metallic Impurities in Epitaxial Si/Si(Ge) During Rapid Thermal Annealing"*, to be published in **Rapid Thermal and Integrated Processing,** edited by J. Gelpey, M. Green J. Wortman, and R. Singh (MRS, Pittsburgh, PA 1991), MRS Proc. Vol. **224**, T-Q. Zhou, A. Buczkowski, Z.J. Radzimski, and G.A. Rozgonyi

3. *"Bulk and surface component of recombination lifetime based on a two-laser microwave reflection technique"*, J. Appl. Phys. **69**, 6495 (1991), A. Buczkowski, Z. J. Radzimski, G. A. Rozgonyi, and F. Shimura

4 *"Noncontact Analysis for Si (1%Ge)/Si Heterostructure with Laser/ Microwave and X-ray Imaging Techniques"*, to be published in **Defects in Silicon II**, edited by W.M. Bullis, U. Gösele and F. Shimura, ECS Proc. Vol.**91**, (The Electrochemical Society, Pennington, NJ, 1991), A. Buczkowski, Y. Kirino, T-Q. Zhou, Z. J. Radzimski, D. Finn, L. Hellwig, J. Rossi, G. A. Rozgonyi, and F. Shimura

5. *"LM-DLTS Measurements for CZ Silicon Wafers with Different [Oi], [Cs], and Thermal History"*, ibid, K. Katayama and F. Shimura.

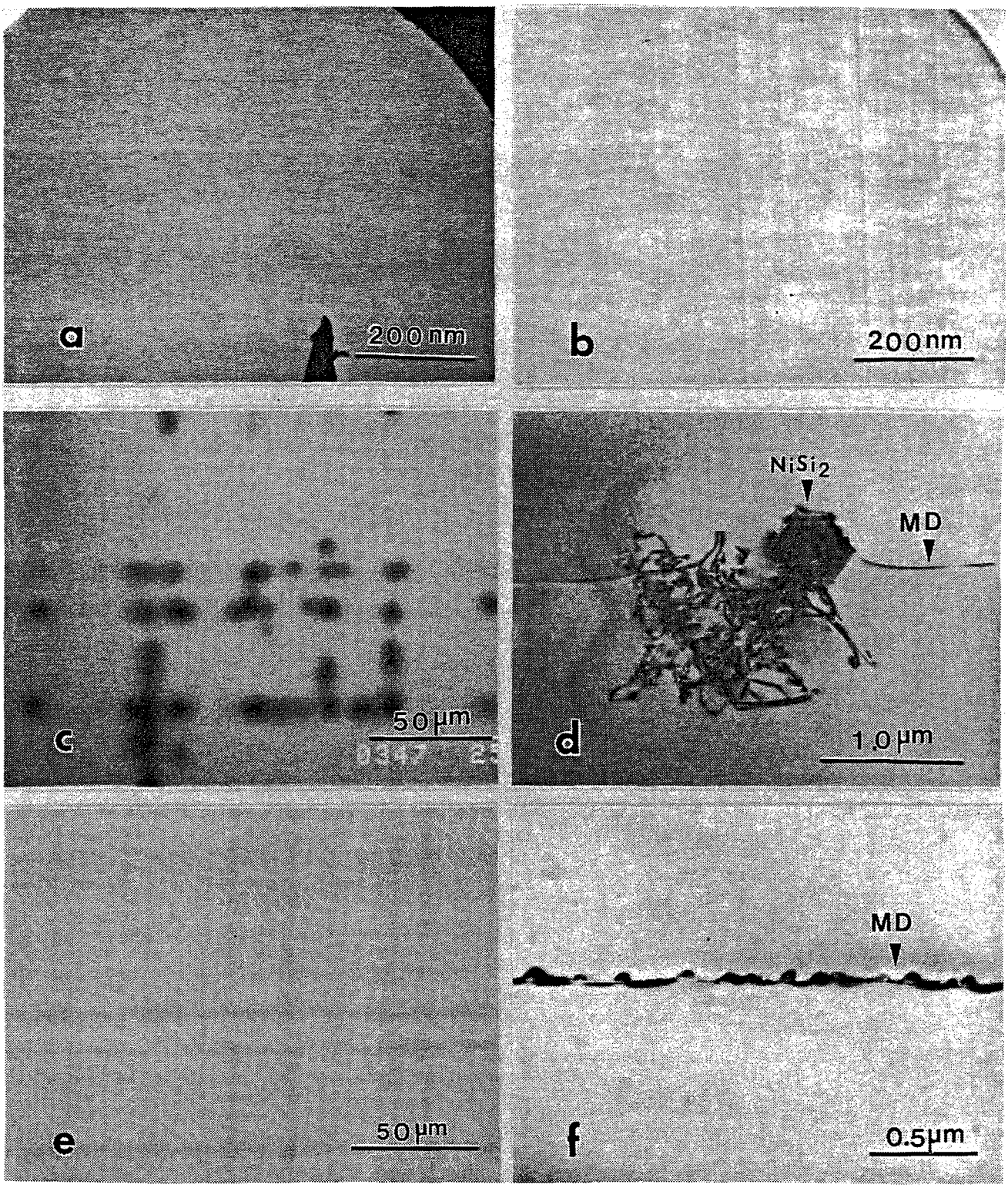

FIG. 1 **a** SEM/EBIC image of an as-grown heteroepitaxial structure showing no contrast from burried interfacial misfit dislocations, **b** Nomarski optical micrograph of the same area. **c** SEM/EBIC image of Ni and **d** Au decorated misfit dislocations. (RTA at 1000°C for 30 seconds)

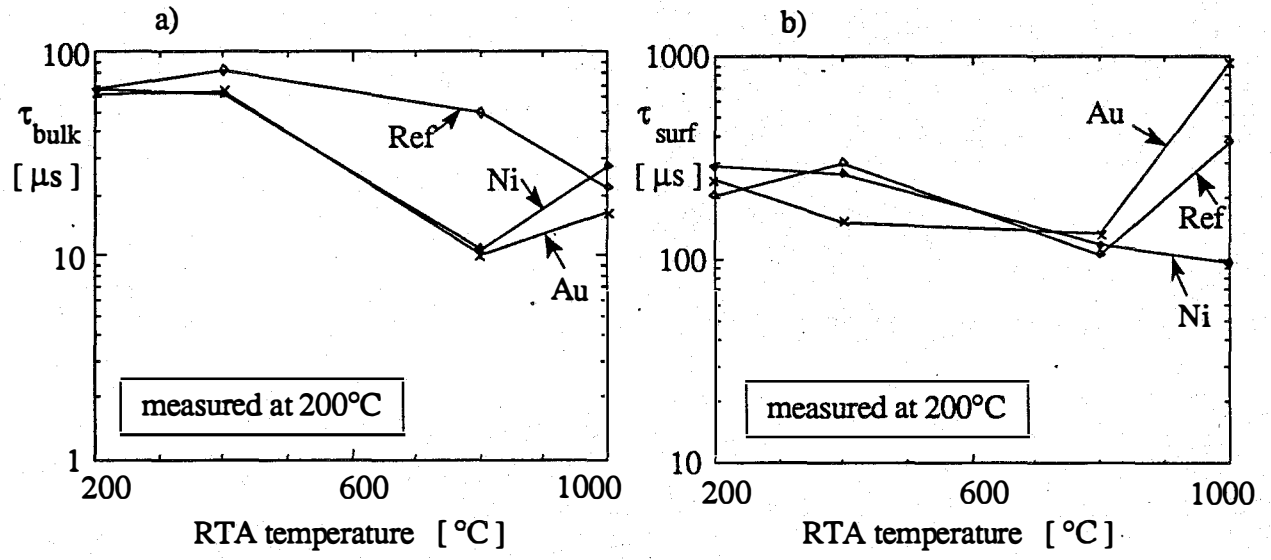

FIG. 2 Influence of TA temperature on **a** bulk and **b** surface component of lifetime measured at 200°C.

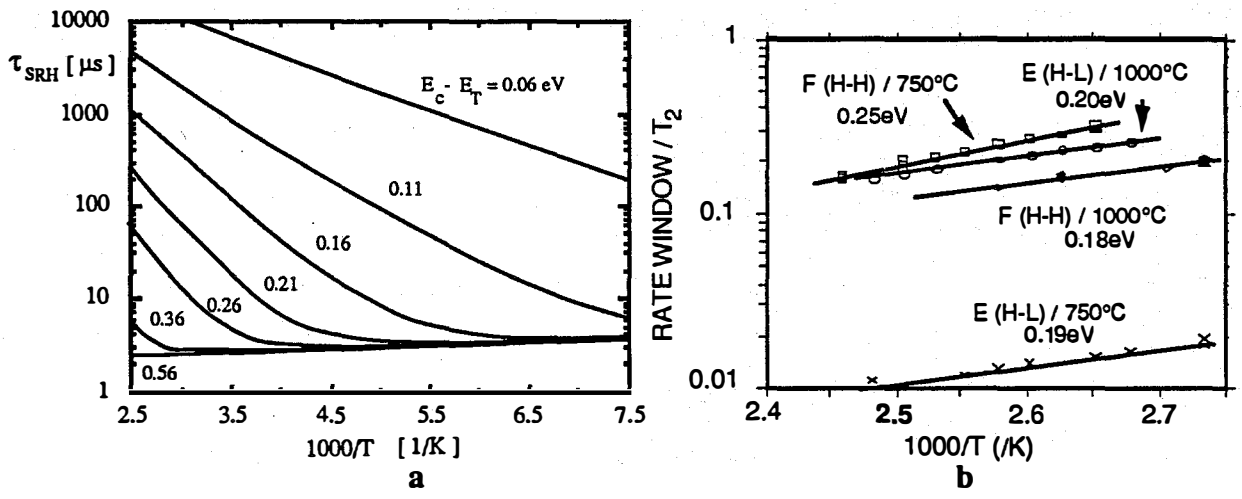

FIG. 3 **a** Theoretical lifetime vs. temperature relationship with activation energy as a parameter. **b.** Arrhenius plots for the recombination centers.

5.0 HIGH-EFFICIENCY CONCEPTS

John Benner, (Manager)

The objective of the High Efficiency Concepts Task is to evaluate and develop advanced photovoltaic technologies capable of energy conversion efficiencies in excess of 20% for flat-plate configurations and 30% in concentrator systems. These goals are discussed in the *Photovoltaics Program Plan FY 1991—FY 1995* as technology targets for the late 1990s. Even on this longer term horizon, it is difficult to envision a technology capable of achieving such high efficiencies without incorporating the demonstrated performance of crystalline III-V semiconductors. Thus, the High Efficiency Concepts task has become synonymous with III-V compound semiconductor research.

NREL's program of research in High-Efficiency Concepts has approached the terrestrial photovoltaic goals from the direction of first demonstrating the feasibility of exceeding the efficiency targets to assure that production engineering trade-offs between performance and cost can be accommodated. Recent advancements by the community researching high efficiency technologies provide a high level of confidence that the efficiency goals can readily be met.

The achievement of 25% efficiency in commercial concentrator modules will likely require production cells having more than 29% efficiency. The system cost target for that efficiency corresponds to cell costs less than $\$10/cm^2$. At least three organizations have demonstrated a single-junction GaAs cell at approximately this efficiency level. Recent successes in multiple-junction technologies show encouraging progress toward fulfilling the theoretical promise of providing commercial cells with more than 35% efficiency. However, a fivefold reduction in processing costs would be needed to meet the cell cost target for concentrator cells. Much of this reduction can be achieved through use of larger wafers and higher through-put deposition systems. Research supported by this program benefits future development efforts by strengthening the understanding of basic mechanisms that affect uniformity of doping, composition, and thickness over large area wafers, from wafer-to-wafer and from run-to-run. Efficient utilization of source materials and evaluation of potentially superior sources (cost, purity, control, safety, and other factors) are also important topics for research. Continued improvement in cell efficiency is also a critical factor in reaching cost-effectiveness for the technology.

Flat-plate technologies have several advantages relative to concentrator technologies because the ability to utilize both the direct and diffuse components of the solar energy resource increases the geographical range of operation, simplifies system design and operation, and opens a variety of market opportunities for small installations. High-efficiency modules can be achieved either through development of multiple junction and/or development of processes for low-cost deposition of single-crystal thin films. Two technologies have already reached performance levels consistent with the efficiency goals. One approach, which produces thin-crystalline-films separated from a reusable substrate in a process called CLEFT, has reached efficiencies of 22.4%. Thin films of GaAs grown on silicon substrates are rapidly closing in on the 20% efficiency target; their efficiency has improved from 11% to 19.9% in the last two years.

Title: **A New Source of Hydrides for Epitaxial Growth**

Organization: Boeing Defense & Space Group, Seattle, WA

Contributors: B. J. Stanbery, program manager and principal investigator

Objectives

The primary objective of this research effort is to evaluate the viability of *in situ* generation of plasma-activated hydride reactants for semiconductor epitaxy through injection of the appropriate elemental species and hydrogen into an Electron Cyclotron Resonance (ECR) plasma source. This provides a safer means of generating activated hydrides for low-temperature epitaxy than current approaches and an additional degree of freedom for the control of the reactant mixture. A secondary objective is to demonstrate the use of this source for the low-temperature growth of single-crystal heteroepitaxial $CuInSe_2$ and ZnSe.

Approach

To achieve these goals we will combine a novel plasma-activated selenium source with conventional evaporation sources for copper and indium or zinc to enable the development of Electron Cyclotron Resonance Plasma-Assisted Epitaxy (ECR-PAE) of $CuInSe_2$ and ZnSe. The selenium source is significantly different than any others yet reported in the scientific literature of the field. It is designed to excite and dissociate the polyatomic elemental vapor exiting from the aperture of an effusion cell, and to combine that flux with a stream of gas at the resonance point. All other ECR sources reported in the literature, to our knowledge, utilize only gas sources. This ECR plasma "cracker" consists of a 2.45 GHz microwave cavity placed within a permanent magnet flux shunt assembly to create a magnetic mirror plasma confinement volume. Microwave power is coupled to the cavity via a high temperature coaxial microwave cable, and coupled within the cavity to the plasma by a special antenna designed to couple efficiently to the "R-wave" eigenmode of the coupled electromagnetic wave and plasma system. The reactants are isolated from the cavity by a sapphire tube in order to prevent unwanted deposition within the source, and insure that all of the escaping reactant flux is directed toward the substrate. The source design utilizes a TE_{111} cavity since that is the lowest resonant mode, and incorporates a gas injector near the resonance point. Thus this ECR source enables the *in situ* generation of hydride precursors for plasma-assisted epitaxial growth utilizing the safer elemental reactants instead of the hydrides (in this case selenium and hydrogen instead of hydrogen selenide).

The ECR-PAE technique for the epitaxial growth of high quality semiconductor epilayers has several advantages when compared with the use of conventional RF plasmas for PAE. They include lower ion energies, higher ionization efficiency, and lower pressure operation.

We will initiate the development of the ECR-PAE process for single crystal $CuInSe_2$ heteroepitaxy on both (111)- and (100)-oriented ZnTe wafers as the starting point of further development. The

proposed technique, utilizing elemental copper, indium, and selenium from independently controllable sources will enable us to investigate various nucleation options and their consequences during the course of this work. Furthermore, the unique ability of this source to introduce to the plasma both chemically active gasses such as hydrogen and inert gasses such as helium will be employed to seek insight into the roles of: physical processes such as intramolecular excitation, molecular dissociation, charge and momentum transfer, and UV irradiation; and chemical processes such as surface hydrogenation and hydride precursor formation.

A second epitaxial growth system will be prepared for the ECR-PAE of ZnSe and MBE growth of ZnTe onto hydrogen plasma-cleaned GaAs wafers. This will enable fabrication of the $CuInSe_2$/ZnTe/ZnSe/GaAs heteroepitaxial structure which we have proposed for the acheivement of a high-efficiency single-crystal $CuInSe_2$-based photovoltaics suitable for incorporation into a cascade cell structure.

Results and Discussion

Our novel ECR plasma reactor has been built and coupled to the exit orifice of a conventional, commercially available MBE effusion cell. The source has been incorporated into a $CuInSe_2$ growth system with a helium gas injection manifold. Source characterization and system calibration experiments have begun. Recently we have undergone a major laboratory renovation to satisfy the Class H-6 occupancy requirements for the safe utilization of hydrogen and generation of hydrogen selenide effluent by both of the growth systems. During that period we have initiated the design of fixturing for the second epitaxial growth system and procurement of its key components. We have also procured relatively high quality (100)- and (111)-oriented single-crystal ZnTe wafers from boules grown by CVD. Though their dislocation densities are high ($2\text{-}4 \times 10^7/cm^2$ as measured by NREL), they are free of inclusions and other macroscopic defects, and should be adequate for process characterization.

Summary and Conclusions

We have constructed an epitaxial growth system for $CuInSe_2$ incorporating a novel Electron Cyclotron Resonance (ECR) plasma source to activate mixtures of an injected gas and the selenium vapor flux of a conventional MBE effusion cell. We will utilize the system during the remainder of this contract phase to develop a unique, low-temperature Plasma-Assisted Epitaxy (ECR-PAE) technique for the growth of high-quality single-crystal semiconductor epilayers for photovoltaic applications. We are not yet able to reach any conclusions with respect to the viability of this approach to the *in situ* generation of hydride precursors for semiconductor epitaxy.

Title: **Arsine and Hydride Radical Generation for MOCVD Growth**

Organization: Electrical Engineering Department, Colorado State University, Fort Collins, Colorado

Contributors: G. J. Collins, principal investigator; B. G. Pihlstrom, L. R. Thompson, T. Sheng, D. Shaw, and A. Simone

The objective of this program is to develop the capability to generate in-situ arsine and hydride radicals from lower toxicity solid precursor sources of arsenic. These techniques are then applied to the deposition of arsenic containing semiconductors. The emphasis is on the toxicity reduction of the starting material as well as the reduced deposition temperature due to the reactivity of the hydride radicals. These hydrogenated species are generated with microwave excited hydrogen plasmas. To date, good quality epitaxial GaAs films have been deposited and characterized, however, the low V-III ratios utilized results in high carbon concentrations (10^{18} to low 10^{20} /cm^3).

Microwave Plasma Source

The in-situ generation of arsenic hydrides is accomplished by reacting an upstream microwave hydrogen plasma with solid arsenic located slightly downstream of the microwave cavity. The arsenic gasification region is intentionally air cooled and measurements of the external temperature shows no increase from room temperature during plasma gasification. The arsine generator employs a 120 W/2.45 GHz microwave hydrogen plasma coupled to a 10 mm diameter, 15 cm long quartz tube via an Evanson microwave cavity[1] and is shown in Figure 1. The hydrogen flow rate through the cavity ranges from 10 to 50 sccm. The arsenic hydrides radicals are generated via surface etching of solid arsenic that is placed approximately 3 cm downstream of the hydrogen plasma. The volatile hydrides are then transported either to a pressure controlled chamber wherein a capillary sampling tube is used for mass spectroscopic diagnostic studies of arsenic hydride generation or to a low pressure deposition reactor, thereby providing arsenic precursors for GaAs homoepitaxy.

The mass spectrum of Figure 2 in the 73-83 AMU range is observed using an Inficon Quadrex 200 mass spectrometer located 20 cm downstream from the solid arsenic source. The spectrum stabilizes a few seconds after plasma ignition and diminishes to zero immediately after plasma cessation. This rapid on-off capability is advantageous for in-situ arsenic hydride generation. The resulting mass spectrum are in good experimental agreement with the dashed vertical line signature pattern for arsine[2]. The diarsine parent peak at 154 AMU is not detected perhaps due to the capillary tube sampling apparatus may have decomposed this fragile specie[3]. The effects of arsine generator ambient pressure and applied discharge power on the intensity of the arsine signal are shown in Figures 3(a) and (b), respectively. The generation rate for the arsenic hydride is calibrated by measuring the total mass of the solid arsenic and the generator apparatus both before and after a one hour deposition via a mass balance accurate to 0.1 mg. The weight difference corresponds to a delivery rate of 95 mg/hr

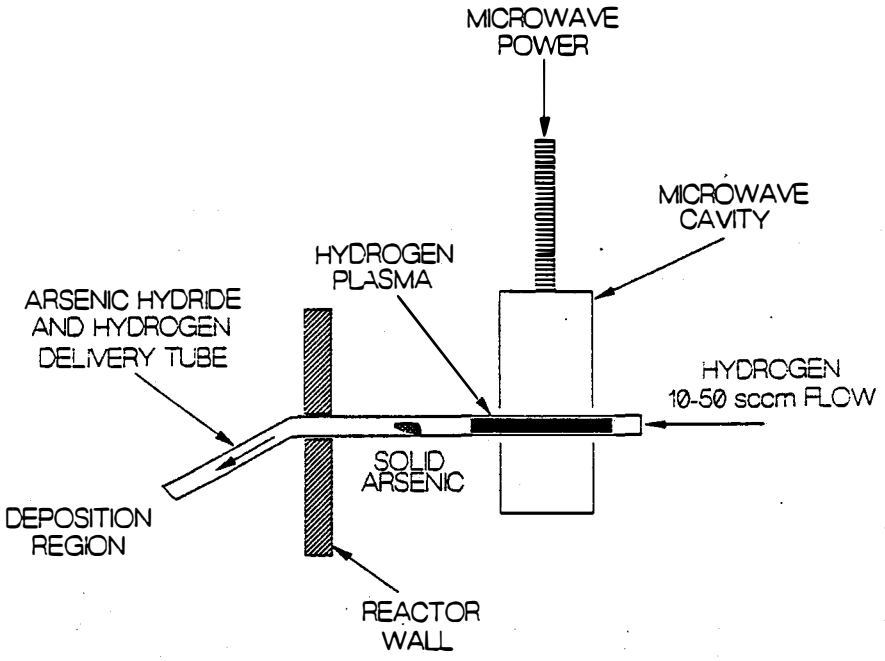

Figure 1. Schematic representation of major elements of the plasma arsine generator.

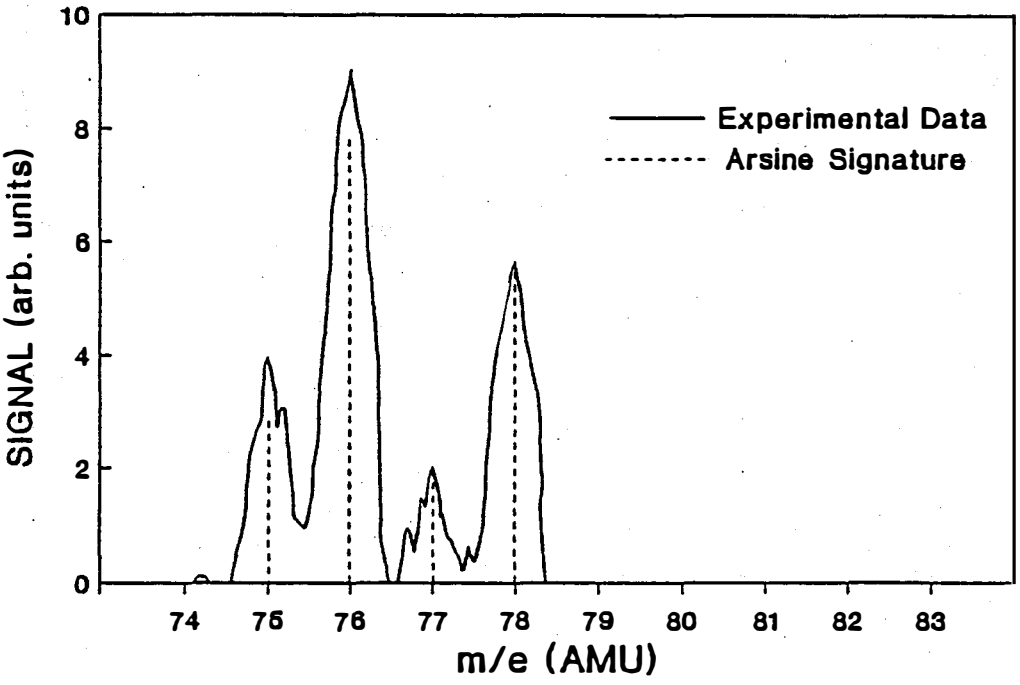

Figure 2. Mass spectrum of arsenic hydrides exiting the arsenic hydride generator.

for the operating conditions of 750 mTorr pressure, 40 Watts microwave power, and 25 sccm of hydrogen flowing through the apparatus. This rate corresponds to generation of 0.5 sccm (21 micromoles/minute) of arsenic hydride. This is used as a calibrated point for the deposition studies discussed herein and Figures 3(a) and (b) are both normalized to this point.

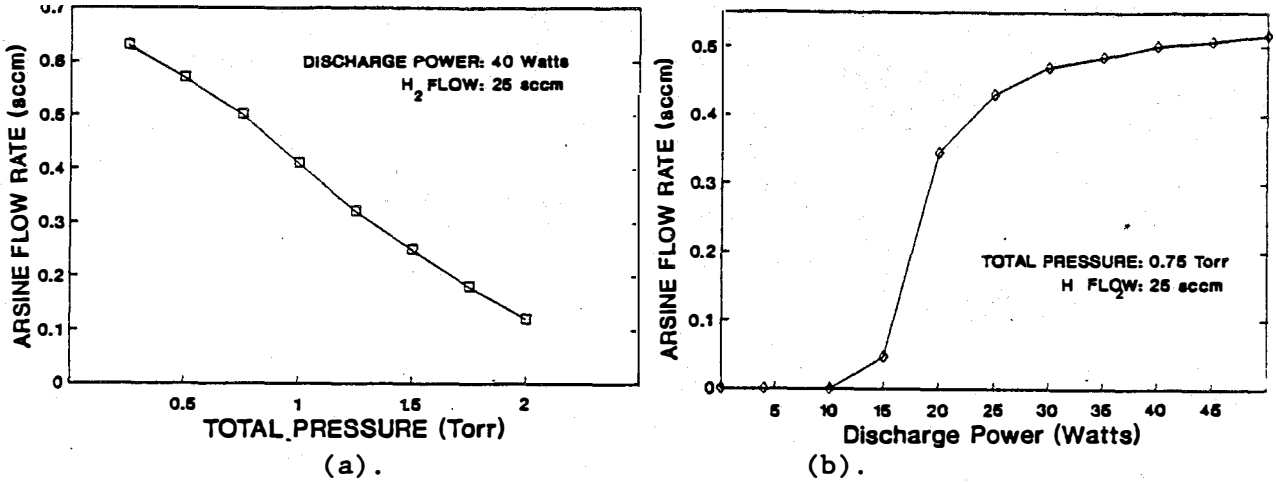

Figure 3. Arsenic hydride generation vs. (a) microwave power and (b) ambient H_2 pressure.

GaAs Film Growth Studies

Substrate samples are loaded into the deposition reactor without any chemical degreasing or polishing, but the samples are heated to 420°C in the reactor for 10 minutes prior to growth in the presence of the generated arsenic hydrides. The reactor substrate heater can rapidly change the deposition temperature at rates greater than 100°C/min. This capability is utilized to change the deposition temperature during growth for the deposition of layered structures, thereby maintaining identical reactor conditions for films grown at varying substrate temperatures. During growth, in addition to the 25 sccm of hydrogen flowing through the arsenic hydride generator, other hydrogen flows into the reactor include 200 sccm from the top of the reactor and 50 sccm through the TMGa bubbler as the carrier gas.

Arsenic hydride generator parameters for film deposition studies include 40 Watts microwave plasma power and 25 sccm hydrogen flow at a total reactor pressure of 750 mTorr. Thus the arsenic hydride mass flow rate into the reactor is fixed at 0.5 sccm during the film deposition studies. The reactor hydrogen flow is 200 sccm. The TMGa flow rate is delivered to the reactor with a controlled flow of hydrogen carrier gas through a typical organometallic bubbler. Bath temperature is held at -9.5°C and the total pressure over the organometallic material is maintained at 450 Torr by a back pressure regulator. An additional carrier gas that does not pass through the bubbler is used such that the total hydrogen flow through the TMGa introduction tube is approximately 50 sccm. The arsenic hydride is introduced though a 10 mm diameter tube with 25 sccm carrier gas that is

directed at the GaAs substrate. Thus the actual gas phase ratio over the growth surface may be slightly higher than the absolute precursor V/III for the GaAs homoepitaxy studies.

Secondary ion mass spectroscopy (SIMS) depth profiling of the sample unambiguously delineates the film/substrate interface via an abrupt decrease in the carbon level of the substrate compared to the film. SIMS depth profile studies of layered structures follow the the change in the carbon levels in films deposited at various substrate temperatures. A stylus profilometer is used to measure the depth of the SIMS sputtered crater and the growth rate is calculated by dividing the film thickness by the growth duration of each layer. The deposited film thickness varies with the substrate temperature as shown in the Arrhenius plot of Figure 4(a). The growth rate activation energy of 54 kcal/mole and 66 kcal/mole at a V/III ratio of 1/1 and 1/4, respectively, is in the range of the homogeneous decomposition of TMGa in the presence of a GaAs surface previously reported as 59 kcal/mole[4]. It is not certain if this activation energy continues to increase at lower V-III ratios or if this is the rate limiting mechanism for the growth of GaAs. This high activation energy is in contrast to values of 16 to 20 kcal/mole measured by others for the deposition of GaAs employing arsine and TMGa with V/III ratios of 9.3 to 36.9 [1]. It is not clear if the activation energy for the deposition is a result of unsaturated arsenic hydrides which may be created in the microwave arsine generator or if it is due to the low quantity of arsenic hydrides available at the surface due to the extremely low V/III ratios employed.

Figure 4(b) displays the carbon concentration in the deposited GaAs films as determined by SIMS analysis (Cs^+ primary ion beam). Carbon concentrations are plotted versus 1/T for the same two V/III ratios (1/1 and 1/4) as in Fig. 4(a). The carbon axis is referenced with respect to the arsenic signal measured in the GaAs films and is calibrated to a C^{12} implant standard in GaAs.

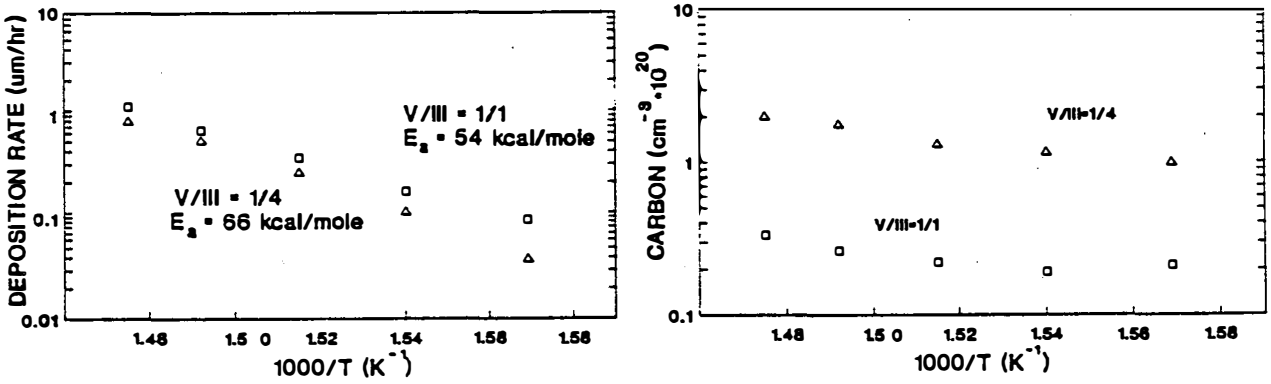

(a). (b).

Figure 4. GaAs film growth rate (a) and carbon content (b) vs. 1/T.

Levels of oxygen on the order of 10^{17} -10^{18} cm^{-3} are also detected in the films via SIMS. The oxygen probably results from hydrogen plasma etching of the quartz tube used in the arsine generator, since close inspection of the quartz tube after use reveals some damage where the plasma contacted it.

Conclusions and Future Work

An in-situ arsenic hydride generator has been developed and successfully utilized to deposit good quality GaAs films . The arsenic hydride generator is advantageous because lower toxicity solid arsenic precursors are used instead of highly toxic high pressure bottled arsine. In addition, the source has the advantage of instant shut down capability in the event of a system failure. Future work on the arsine hydride generator includes investigation of methods to increase the amount of arsine hydrides produced and decrease the amount of oxygen incorporated into the deposited films. The use of other Group III precursors such as triethylgallium (TEGa) will be investigated to lower the carbon level in the deposited GaAs films. Finally, we plan on using the arsine generator to grow AlGaAs films and GaAs/AlGaAs heterostructures.

References

1. K. Evenson, Rev. Sci Instr. **36**, 294 (1965).
2. F. W. Mclafferty and D. B. Stauffer, The Wiley/NBS Registry of Mass Spectral Data, (John Wiley and Sons, New York, NY, 1988) Vol. 1.
3. W. L. Jolly, L. B. Anderson, and R. T. Beltrami, J. Am. Chem. Soc. **79**, 2443 (1957).
4. M. G. Jacko and S. J. W. Price, Can. J. Chem. **41**, 1560 (1963).

Title:	**High-Efficiency Thin-Film Solar Cells**
Organization:	Kopin Corporation Taunton, Massachusetts
Contributors:	R.P. Gale, principal investigator; J.C.C. Fan, J.V. Gormley, R.W. McClelland, B.D. Dingle.

Objectives

The objectives of this research program are to investigate thin-film GaAs/GaInP cells using the CLEFT technique and to determine the process to enable overgrowth of GaAs films using organometallic chemistry.

GaInP Growth and Characterization

The growth and characterization of the ternary compound GaInP for thin-film cells was investigated. Growth experiments were carried out using tertiarybutylphosphine (TBP) as the group 5 source. GaInP layers were grown latticed matched to GaAs. Using double-crystal X-ray diffraction, peak separations of less than 100 arc-sec were reproducibly achieved. This corresponds to lattice mismatch ($\Delta a/a$) of 0.0005 or less. The layers had good surface morphology and exhibited strong room-temperature photoluminescence.

GaInP Cell Performance

Cells were fabricated and measured from GaInP/GaAs structures. Efficiencies reached 14% on both GaInP-window and GaInP-emitter structures, being limited by cell current. Quantum efficiencies showed low response in the blue spectrum, indicating that the GaInP window was not completely effective in passivating the cell surface. Matching of the window lattice constant to GaAs was varied intentionally to produce both compressive and tensile windows, with no effects on cell performance observed. Work on the GaInP/GaAs interface is ongoing.

Organometallic Overgrowth

A second epi system was prepared for DEGaCl installation and overgrowth experiments. GaAs growth using diethylgalliumchloride chemistry was demonstrated with good morphologies and growth rates up to 10 um/hr. Tests of growth on CLEFT masks showed little or no nucleation of polycrystalline material on the mask, indicating initial suitability for the overgrowth process. Overgrowth was observed, but at ratios marginally suited for CLEFT.

The OM overgrowth screening experiment indicated that a higher HCl/Ga ratio was needed, but this could not be achieved using only the DEGaCl chemistry. An external HCl cylinder and line were therefore set up; we could now inject a mixture of 1% HCl in hydrogen along with the DEGaCl and TMGa. HCl/Ga ratios as high as 5 could be achieved with this setup, which produced overgrown films with satisfactory height-to-width ratios. Excellent surfaces were obtained, and the overgrowth mask was maintained clear of polycrystalline nucleation.

Title: **New III-V Cell Design Approaches for Very High Efficiency**

Organization: School of Electrical Engineering, Purdue University
West Lafayette, Indiana 47907-1285

Contributors: M. S. Lundstrom and M. R. Melloch, principal investigators; G. B. Lush, G. J. O'Bradovich M. P. Patkar, and M. P. Young

Objectives and Approach

To realize cost-effective solar cells with efficiencies exceeding 35% is an important objective of the national photovoltaics program. Cell efficiencies are progressing rapidly, but it seems unlikely that the present design approach will produce efficiencies very much above 30% under concentration. Multi-junction cells have already achieved efficiencies well above 30%, but substantial cost reductions are still required. The objective of this project is to examine new *design* approaches for achieving very high conversion efficiencies.

The project is divided into two thrusts with the first centering on exploring new thin-film approaches specifically designed for III-V semiconductors. The second research thrust centers on exploring design approaches for achieving high conversion efficiencies without requiring extremely high-quality material. Basic studies research previously conducted by our group has given us a deep understanding of the loss mechanisms that dominate in present-day cells, and it serves as the foundation for the device design research being proposed. The unconventional design approaches we are exploring also require new basic research on radiative recombination, photon recycling, and AlGaAs loss mechanisms. The research program is, therefore, balanced to increase our basic understanding of III-V cell device physics and to explore the potential of unconventional cell designs.

The project's first thrust is directed at enhancing the already high efficiency of GaAs cells by exploring new, thin-film approaches designed to trap incident light and to take advantage of so-called photon recycling effects. It has long been realized that radiative recombination is not necessarily a loss mechanism; *if* the cell is thick enough and *if* the emitted photons are confined within the cell. By adopting a thin-film cell approach, designed to optically confine the photons emitted by radiative recombination within the cell, lifetimes could be enhanced by an order of magnitude — or even more. Thin-film cells might also benefit from conventional, incident light trapping, which is used with great success for silicon cells. The potential for sizable efficiency gains along with the cell cost advantages make the thin-film approach a promising one that should be broadly applicable to III-V single- and multiple-junction cells.

The second research thrust centers on developing cell designs to maximize conversion efficiencies without requiring extremely high material quality. Success in this phase of the research would benefit multiple-junction cells for which the selection of a component cell often involves a compromise between optimum bandgap and optimum material quality. It could also be a benefit in a manufacturing environment by making the cell's efficiency less dependent on material quality. Our in-house MBE facility with proven capability for producing high-quality GaAs and AlGaAs films will be used to investigate various cell design options. A sound understanding of recombination losses in AlGaAs cells is a prerequisite for selecting an appropriate

design, so basic work to quantify losses in AlGaAs cells is an important part of the research program.

Research Results

During the past year, we initiated a comprehensive study of minority hole recombination in n-type GaAs grown by metalorganic chemical vapor deposition (MOCVD). The objective is to understand the role of radiative, Shockley-Read-Hall, and Auger recombination in solar cells. Another objective is to develop a quantitative understanding of photon recycling. Thirty double heterostructure (DH) films with various active layer thicknesses and six different doping densities were grown by Dr. Hugh MacMillan at Varian and examined by photoluminescence (PL) decay measurements in Dr. Richard Ahrenkiel's laboratory at NREL. The results have provided a wealth of much needed but previously unavailable data for solar cell design (see publications 1-4).

From the measured PL decay, we extract a decay constant, τ_{DH}, and construct a plot of $1/\tau_{DH}$ vs. $2/w$, where w is the thickness of the active layer. Conventional theory,

$$\frac{1}{\tau_{DH}} = \frac{1}{\tau_{bulk}} + \frac{2S}{w}, \qquad (1)$$

states that the plot should be linear with the intercept being the bulk lifetime and the slope being the interface recombination velocity. Typical measured results are displayed in Fig. 1 and show that the characteristics are distinctly nonlinear. These types of characteristics were observed for all samples and suggest that the bulk lifetime varies with w. We find that the nonlinear $1/\tau_{DH}$ vs. $2/w$ characteristics are well-described by photon recycling theory.

Figure 2 displays the measured decay constants for each of the films. At each doping density, the thinnest film displays the shortest decay constant, and the decay constant increases monotonically with DH thickness. All measured lifetimes are well above the radiative estimate evaluated assuming $B = 2 \times 10^{-10}$ cm^3/s. For n-GaAs doped above 10^{18} cm^{-3} we found evidence for SRH recombination, but the lifetimes still exceeded the radiative estimate. These films will also provide the samples for much of the basic studies on photon recycling planned for the next two years.

Because our cell design research will make use of films grown by molecular beam epitaxy (MBE) in our laboratory, we compared the lifetimes of n-type MBE films to n-type MOCVD films. We examined the decay of three MBE films doped at 10^{17} cm^{-3} and three doped at 10^{18} cm^{-3}. The PL lifetimes were found to be quite long, though not as long as those grown by MOCVD at Varian. In comparison to the MOCVD films, the MBE films show stronger evidence of Shockley-Read-Hall (SRH) recombination. At a given film thickness, we find the MBE lifetimes to be roughly 75% of those for Varian's MOCVD films. For the lighter doped films the SRH recombination appears to be due to bulk traps and for the more heavily doped films, to interface traps. Nevertheless, the decay constants for the MBE samples were above the radiative limit (again, assuming $B = 2 \times 10^{-10}$ cm^3/s) which suggests the presence of photon recycling. It appears that although the lifetimes in the MBE films are not quite as long as those in very high quality MOCVD material, they are sufficient for our studies at this point. As the research progresses, however, we shall have to continually work to suppress SRH recombination in the MBE films.

Given the project's emphasis on exploring new cell designs, it is important to have an in-house

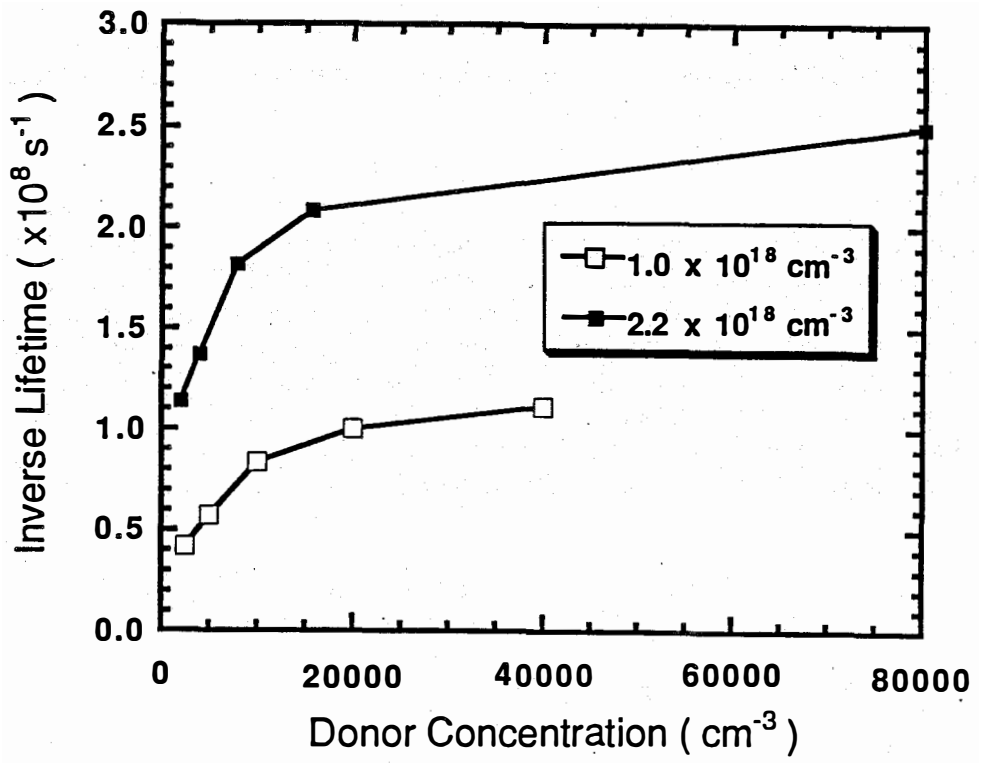

Fig. 1 $1/\tau_{DH}$ vs. $2/w$ for the MOCVD DH films doped at 1.0 and 2.2×10^{18} cm^{-3}.

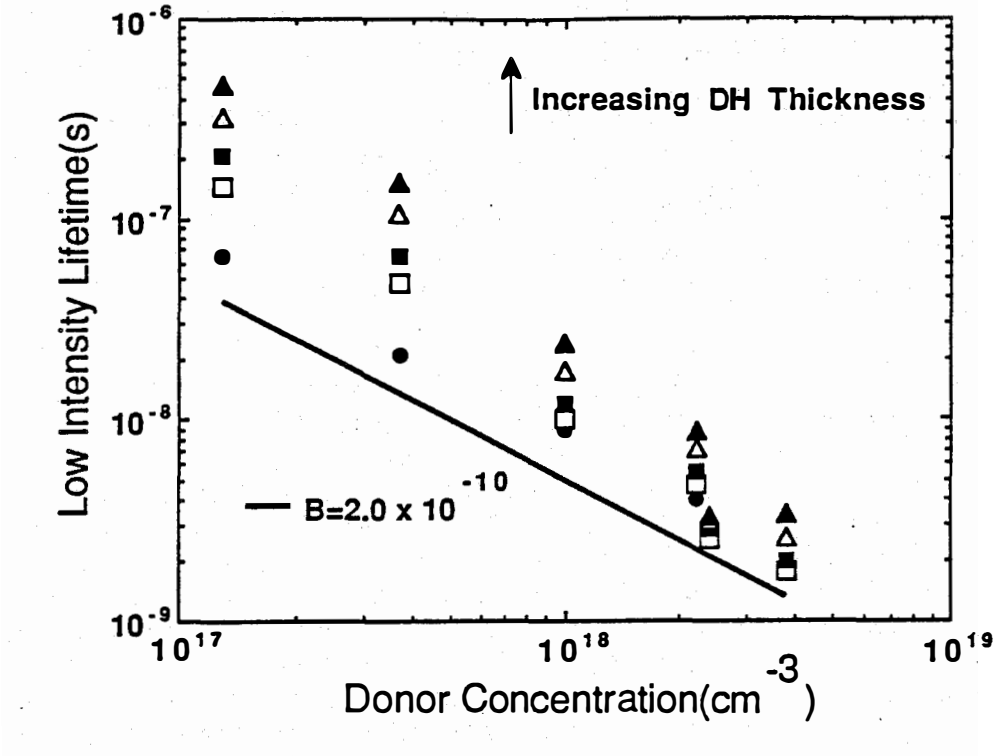

Fig. 2 τ_{DH} vs. doping density for each of the 30 films measured. At each doping density, the shortest lifetime corresponds to the thinnest film, and the lifetime increases monotonically with thickness.

capability for fabricating high-efficiency cells. During the past year, we also spent time implementing a baseline cell fabrication process in our laboratory. For cell metalization, we turned on a new electron beam evaporation system, and for anti-reflection coatings, a new evaporator was designed and constructed. Using p/n MOVCD films supplied by Varian, we constructed and tested solar cells. From the measured internal quantum efficiency and dark current, we projected an efficiency of 22% under 1 sun AM1.5. The cells had no antireflection coating, but dual layer ZnS/MgF_2 coatings have now been deposited and low reflectances have been demonstrated. Having established the cell fabrication capabilities, we are now at work on fabricating AlGaAs solar cells.

Conclusions

This past year was the first of a three-year project. We now have all of the GaAs films that will be needed to conduct the next two year's basic studies, and the information already gained from the PL studies of these films will be of immediate use to the photovoltaic community. Our comprehensive study of recombination in n-type GaAs continues with measurements of the doping-dependent absorption coefficient, the temperature-dependent lifetime, and tests for the presence of Auger recombination. We also plan to examine the lifetime in thin-film DH's with the substrate removed. This information should give us a detailed understanding of radiative recombination and photon recycling. Work to further characterize our MBE films also continues, and techniques to fabricate thin-film cells are being developed. Finally, new designs for AlGaAs cells are being explored.

References

1. G.B. Lush, H.F. MacMillan, B.M. Keyes, R.K. Ahrenkiel, M.R. Melloch, and M.S. Lundstrom, "Photoluminescence Decay Study of Minority Carrier Recombination in n-Type GaAs," presented at the 1991 Electronics Materials Conf., Boulder, Colorado, June, 1991.

2. G.B. Lush, H.F. MacMillan, B.M. Keyes, R.K. Ahrenkiel, M.R. Melloch, and M.S. Lundstrom, "Measurement of Minority Carrier Lifetime in n-Type GaAs and the Implications for Solar Cells," presented at the 22nd IEEE Photovoltaic Spec. Conf., Las Vegas, Nevada, October, 1991.

3. R.K. Ahrenkiel, B.M. Keyes, G.B. Lush, M.R. Melloch, M.S. Lundstrom, and H.F. MacMillan, "Hole Lifetime in GaAs," presented at the 1991 American Vacuum Society Annual Meeting, Seattle, Washington, November, 1991.

4. G.B. Lush, H.F. MacMillan, B.M. Keyes, M.S. Lundstrom, R.K. Ahrenkiel, and M.R. Melloch, "A Study of Minority Carrier Lifetime versus Doping in N-Type GaAs Grown by Metalorganic Chemical Vapor Deposition," submitted for publication.

Title: **Cl-MO and MOCVD Crystal Growth Research**

Organization: Department of Electrical, Computer and Systems Engineering, Rensselaer Polytechnic Institute, Troy, New York

Contributors: J.M. Borrego and S.K. Ghandhi, Co-Principal Investigators

The program objective is to evaluate new reactor designs with minimal convection and high source utilization efficiency, and to characterize the growth of GaAs material using novel metalorganic precursor sources, including chlorinated alkyl sources.

Over the past few years, we have developed an advanced computer program which is directed to OMVPE in practical growth situations. This program has been used to design a novel reactor with a close-spaced vertical structure, in order to eliminate circulation cells in the growth region. Here, an inverted structure has been used since buoyancy-driven recirculation is eliminated by this means.

Simulations of the system show no evidence of recirculation under typical growth conditions (2-6 SLM hydrogen flow, 700°C susceptor, and susceptor-inlet spacings of 0.5 to 5 cm). Simulations for the reactor in a non-inverted configuration, i.e., heater above the susceptor, show that recirculation will occur with spacings in excess of 1.5 cm, but not with lower values. In essence, this means that either the inverted or the more conventional configuration can be used if the spacing is sufficiently small.

The effects of thermal radiation have to be considered, because of the close spacing between the hot susceptor and the water-cooled inlet nozzle. In previous computer programs, this has been estimated, based on experience. In our program, the net radiative heat gain is calculated using an enclosure analysis between six constant radiosity zones along the boundary. Here, an enclosure for a surface is the envelope of other surfaces or open areas surrounding it. The radiosity is the total radiant energy flux leaving the surface, including emitted, reflected and transmitted radiation. By considering radiation going from the surface *to* all parts of the enclosure, and the radiation arriving at the surface *from* all parts of the enclosure, all the various radiation contributions are taken into account.

Six zones were considered for the radiation analysis in order to simplify the calculation of the three-dimensional view factors. The thickness of the susceptor was neglected for the radiation analysis in order to simplify it. The graphite and stainless steel boundary zones were assumed to be gray and opaque respectively, with absorptivities of 0.9 and 0.3 and reflectivities of 0.1 and 0.7 respectively. The net radiative heat gain was used in an energy balance at each boundary control volume. It was combined with the net convective heat gain on the inside, conduction through the wall, and convection and radiation into the ambient.

Figure 1 shows the simulated temperature field for the conditions given above. The isotherms are uniform and parallel in the susceptor-nozzle region and near the top flange, indicating that there is little radial variation of temperature in these regions. However, the isotherms are

relatively non-uniform in the region where there is recirculation. The temperature field is seen to vary rapidly in the susceptor-nozzle region, emphasizing the need for a rigorous thermal analysis for such close-spaced reactors of this type.

A series of growth runs have been made in this reactor. Initially, our work was limited to 1 cm x 1 cm samples because of cost considerations. After sufficient experience was obtained with running the system, work was extended to 2" dia. slices. Initial studies of growth uniformity were carried out on 2" dia. sapphire substrates which could be reused from run to run. Here, layer thickness was measured using Fourier Transform Infrared Spectroscopy (FTIR).

Both undoped as well as n^+-doped layers have been grown on n^+ and SI GaAs substrates respectively. The thickness was determined by FTIR. Under illumination, the difference in refractive indices between epitaxial layer and substrate gives rise to an interference pattern, whose period is directly related to the thickness and refractive index of the epitaxial layer. The refractive index of GaAs was computed as a function of free carrier concentration and wave number from expressions reported by other workers. All measurements carried out in this work were for extrema near the wave number, $\omega = 2000\ cm^{-1}$. The undoped epitaxial layers, which were lightly n-doped, had a refractive index of 3.3; the substrates used in this case were n^+-doped ($10^{18}\ cm^{-3}$) with a refractive of 3.25. The n^+-doped ($5 \times 10^{18}\ cm^{-3}$) epitaxial layers had a refractive index of 3.09 and the substrates used in this case were SI with a refractive index of 3.3. The thickness uniformity over large-area substrates was determined by moving the sample on an x-y stage. Since the wave number in our FTIR equipment can be measured with a least count of $8\ cm^{-1}$, the measurement error is 0.4% for $\omega = 2000\ cm^{-1}$. The extrema are typically measured within a range of $500\ cm^{-1}$ around $\omega = 2000\ cm^{-1}$, which leads to an error in the thickness measurement of 0.2% for undoped samples and 3% for highly doped samples. For the measurement of thickness uniformity, the error in the relative thickness over the wafer should be smaller than these values.

The FTIR technique was also used to measure the free carrier concentration in n^+ layers using the phenomenon of plasma resonance. When the frequency of incident light equals the plasma frequency of the electrons, resonance occurs and leads to a maximum absorption of incident energy. Thus, the reflectance spectrum shows a sharp dip around the plasma frequency. The plasma frequency is directly related to the free carrier concentration in the epitaxial layer. Here, the main source of error in the doping measurement is the difference between the minima in the spectrum and the plasma frequency, and is less than 10% for doping concentrations above $2 \times 10^{18}\ cm^{-3}$. Again, in the measurement of doping uniformity, the error in the relative doping over the wafer should be smaller than this value.

Figure 2 shows the thickness distribution of an undoped GaAs epitaxial layer grown on a 2" diameter GaAs substrate, averaged in the θ-direction, as a function of radial distance from the center. The horizontal dashed lines show the region of $\pm 5\%$ non-uniformity, which in this case is over the central 1.5" diameter region. Outside this region, the growth rate falls rapidly. Thickness uniformity measurements, made on small-area substrates where the lip was located at a distance of 0.5 cm from the center, showed a similar rapid fall in the growth rate near the lip. A new susceptor design, which avoids this lip, is being considered at the present time.

The growth rate distribution in Fig. 2 was integrated over the entire area of the wafer to determine the total moles of Ga deposited per unit time. When this is divided by the total mole flow rate of Ga entering the reactor, it results in a 15.3% Ga deposition efficiency. The efficiency calculated from the weight of the epilayer, as measured by the gravimetric technique, was 15.49%. This provides an independent verification of the thickness measurements using FTIR.

Doping studies with SiH_4 showed that free carrier concentrations up to 7 x 10^{18} cm^{-3} can be achieved with good morphology in this reactor. Figure 3 shows the θ-averaged doping distribution of an n^+- GaAs layer grown on a 2" diameter GaAs substrate, as measured by FTIR. The operating conditions were: d = 1 cm, T_s = 650°C, P = 380 Torr, F = 1 slm, X_{TMGa} = 5.3 x 10^{-4}, AsH_3/TMGa = 22 and X_{SiH_4} = 6 x 10^{-6}. The free carrier concentration is seen to be lower near the center of the sample and higher near the edge.

Again, the horizontal dashed lines show the region of ±5% non-uniformity. The doping non-uniformity over the entire growth region is ±3.3%. The increase in carrier concentration near the sample edge could be due to higher surface temperature near the edge because of better thermal contact with the susceptor and lower heat loss to the gases in this region. SiH_4 doping studies carried out by other workers have shown that the carrier concentration increases by 150% for an increase in susceptor temperature from 650° to 700°C. Interpolating from these results, the doping non-uniformity of ±3.4% would correspond to a temperature variation of 2.2°C over the 2" diameter wafer, which is reasonable for this design. In conventional reactors with no lip effect, increased heat losses near the susceptor edge cause a fall in the doping near the edge. It has also been reported that the use of Si_2H_6 as the dopant source improves the doping uniformity because it has a higher incorporation efficiency, and a weaker temperature dependence of incorporation than SiH_4.

The computer program for calculating lifetime from the transient data obtained by this technique has been upgraded. This upgrade can collect transient data and analyze them for bulk lifetime by regressing the linear portion of the logarithm of the data. The program also has an option to apply a two-layer model to the data, if the front and back surface recombination velocities are significantly factored in data interpretation. This "user friendly" program allows the display of both log and linear graphs at the touch of a button. The user has control over the range of the data displayed as well as the range that is to be regressed for lifetime estimation. The graphs can be overlaid with one or two user selectable lifetime curves for comparison to the regressed curve. These graphs can then be dumped to a HPGL-compatible plotter. There is also an option to round off the axes to convenient steps, to improve the appears of the output data.

The program was written in Turbo C++ for fast execution of the graphics routines and calculations needed for the regression of up to 1000 points. The data is collected via a HPIB bus connected to a Tektronics digital scope. The data file format is very simple with the first three values being the voltage offset (or 1 x 10^{10} in the new format), voltage multiplication factor and a timebase. This is followed by (x,y) integer pairs of data (or just x values in the format). The x value is the voltage digitized to 8 bits or 256 levels and the y value is just a counter value incrementing from 1 to 1024. The y values are totally meaningless and were removed in the new format. For compatibility the program is capable of reading the older file format.

References:

A list of papers written and/or published in FY 1991 now follows.

1. J.M. Borrego and S.K. Ghandhi, Solid State Electron., 33, 733 (1990).

2. H. Bhimnathwala, S. Bothra, S. Tyagi, S.K. Ghandhi and J.M. Borrego, Proc. 21st IEEE Photovoltaic Specialist Conference, p. 394 (1990).

3. S. Bothra, S.D. Tyagi, S.K. Ghandhi and J.M. Borrego, Proc. 21st IEEE Photovoltaic Specialist Conference, p. 404 (1990).

4. M.S. Wang and J.M. Borrego, J. Electrochem. Soc., 137, 3648 (1990).

5. L.M. Smith, D.J. Wolford, R. Venkatasubramanian and S.K. Ghandhi, Appl. Phys. Lett., 57(15), 1572 (1990).

6. P.B. Chinoy and S.K. Ghandhi, J. Crys. Growth, 108, 105 (1991).

7. P.B. Chinoy and S.K. Ghandhi, J. Electrochem. Soc., 135, 1452 (1991).

8. P.B. Chinoy, D.A. Kaminski and S.K. Ghandhi, J. Heat Transfer, Part A, 19 (1991).

9. S. Bothra, S. Tyagi, S.K. Ghandhi and J.M. Borrego, Solid State Electron., 34, 47 (1991).

10. P.B. Chinoy, D.A. Kaminski and S.K. Ghandhi, Solar Cells, 30, 323 (1991).

11. S. Bothra, S. Tyagi, S.K. Ghandhi and J.M. Borrego, Solid State Electron., 34, 47 (1991).

12. S. Bothra and J.M. Borrego, Proc. of 6th Conf. on Semi-Insulating III-V Materials, A.G. Milnes and C.J. Miner, eds., Adams Hilger, England, 209, 523 (1991).

13. M.S. Wang and J.M. Borrego, Proc. Materials Research Symposium, 209, 523 (1991).

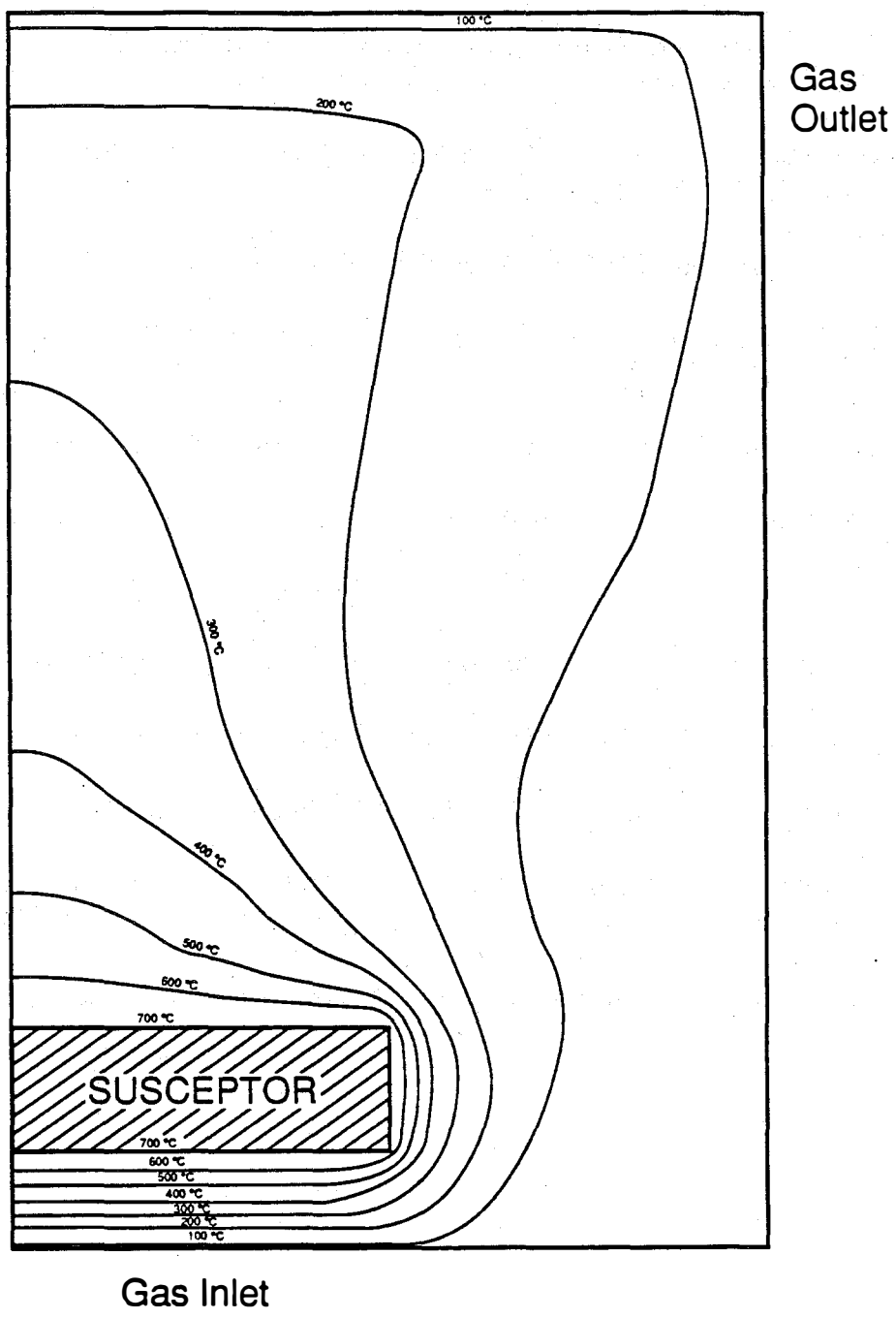

Figure 1. Isotherm for a 700°C susceptor temperature.

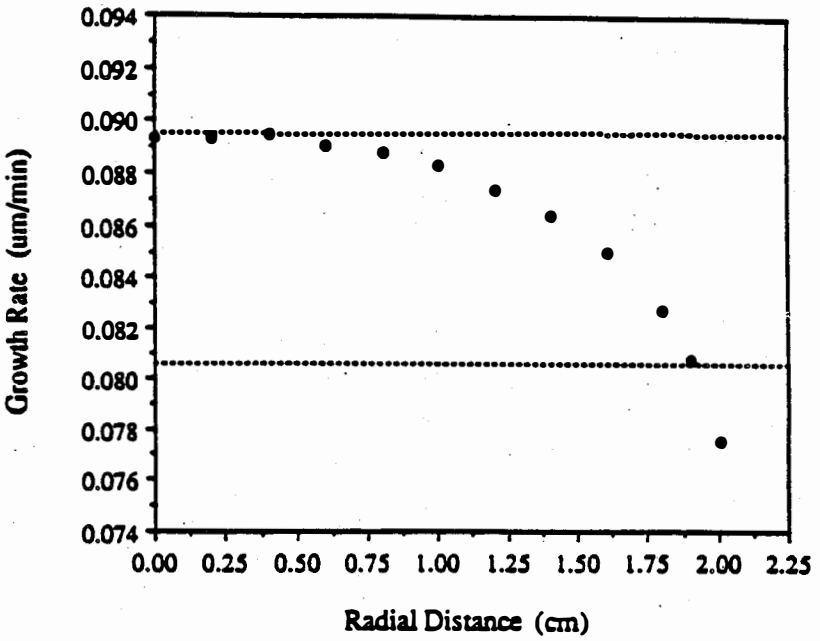

Figure 2. Growth rate vs. radial distance.

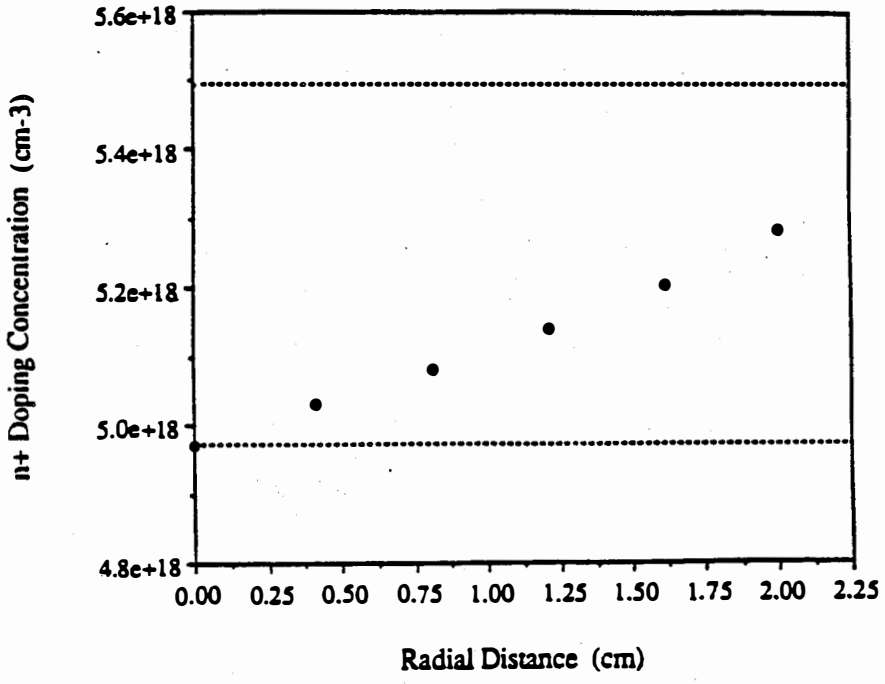

Figure 3. Doping concentration vs. radial distance.

Title: Growth and Development of GaInAsP for Use in High-Efficiency Solar Cells

Organization: Research Triangle Institute, Research Triangle Park, North Carolina

Contributors: P.R. Sharps, principal investigator; M.L. Timmons, R. Venkatasubramanian, T.S. Colpitts, R. Pickett, J.S. Hills, and J. Hancock

Introduction

The quaternary semiconductor compound GaInAsP lattice-matched to GaAs (and hence Ge) is an ideal candidate as a top junction in monolithic cascade cells. With quaternary semiconductors the lattice constant and band gap can be, within limits, varied independently. For GaInAsP lattice-matched to GaAs, the bandgap spans the range from 1.42 to 1.92 eV. Such a range provides great flexibility for current matching with a low band gap junction. For the composition $Ga_{0.83}In_{0.17}As_{0.75}P_{0.25}$, the matching and lattice matching with Ge junctions. Under concentrated sunlight, multiple junction cells using GaInAsP as the top junction project to a theoretical efficiency of about 35% [1].

The overall goals of the present program are:

1. to develop the necessary technology to grow 1.55 eV band gap GaInAsP layers that are lattice-matched to GaAs,
2. to demonstrate high-efficiency GaInAsP single-junction solar cells, and
3. to demonstrate GaInAsP/Ge cascade solar cells suitable for operation under concentrated (500x) sunlight.

Film Growth

The films were grown in a horizontal atmospheric-pressure, organo-metallic vapor phase epitaxy (OMVPE) reactor at 670°C. Many of the details of the growth of the $Ga_{0.83}In_{0.17}As_{0.75}P_{0.25}$ have been presented elsewhere [2,3]. The films were grown using trimethylgallium (TMGa), ethyldiethylindium (EDMIn), 100% arsine, and two different phosphorus precursors, tertiarybutylphosphine (TBP) and phosphine. Initially films were grown with TBP, but more recently phosphine has been used. Intrinsic films are n-type, and those grown with phosphine have a slightly better background carrier density, 8×10^{16} cm^{-3}, as compared to 1.5×10^{17} cm^{-3} for those films grown using TBP. The minority carrier lifetime in the intrinsic films grown using TBP is 35 ns, as measured by time-resolved photoluminescence. H_2Se is used for control of n-type doping, while diethylzinc is used to control the p-type doping.

A key issue in the atmospheric-pressure growth of quaternary materials is uniformity. In our own case, the hydrogen carrier gas flow has been increased to 14 liters/minute to ensure uniform films. The lattice constant varies 0.07% and the band gap varies 0.6% over a 2 cm. distance with the 14 liters/minute carrier flow.

Fig. 1 is a schematic of the solar cells that have been prepared to date. The focus so

far has been on the growth of p-on-n cells. The AlGaAs window and the GaAs cap are grown in a separate reactor.

Cell Results

Results for two different cells are shown in Table I. The active area of the cells is 0.136 cm^2. Cell 945 was grown using TBP, while cell 1314 was grown using phosphine. The cells are virtually identical, except that the emitter doping level in cell 945 was 2×10^{19} cm^{-3}, while that in cell 1314 was 2×10^{18} cm^{-3}. The I-V curve for cell 945, measured at NREL, is shown in Fig. 2, and the spectral response, also measured at NREL, is shown in Fig. 3.

The results for the two cells are nearly identical. The difference in I_{sc} is due to a difference in the light intensity under which the cells were tested. The active area efficiency of 18.8% for cell 945 is encouraging considering that it was the first attempt at making a cell. The spectral response from cell 945 indicates a low "red" response, and is due to a thin base layer. Future cells will incorporate a thicker base layer.

Optimization of the cell is in progress. Other structures are also being considered. A vertical, atmospheric-pressure reactor has recently been installed, and the growth of $GaInP_2$ has been demonstrated. The use of a $GaInP_2$ window grown in the same reactor as the GaInAsP cell will avoid any problems associated with the transfer of the cell from one reactor to another for window growth.

Conclusions

A $Ga_{0.83}In_{0.17}As_{0.67}P_{0.33}$ solar cell lattice-matched to GaAs is described. Initial results are very encouraging, with active area efficiencies greater than 18% reported. Plans are underway to further refine and optimize the cell, including using a $GaInP_2$ window. Plans are also underway to grow optimum cells on Ge substrates, and then eventually grow the full GaInAsP/Ge cascade structure.

References

1. P.J. Faine, S.R. Kurtz, and J.M. Olson, *Proc. 21st IEEE Photovoltaic Specialitst Conf.*, IEEE, NY, 1990, p. 339.
2. P.R. Sharps, M.L. Timmons, T.S. Colpitts, *Appl. Phys. Lett.*, 58 (1991) 2006.
3. P.R. Sharps, J.B. Posthill, and M.L. Timmons, *J. Elect. Mat'ls.*, to be published.

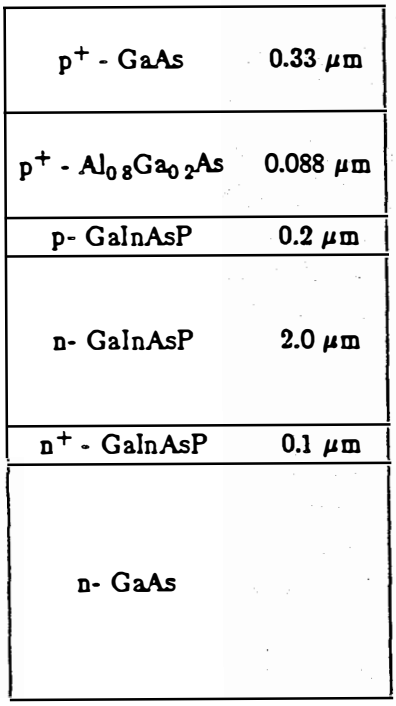

Figure 1. Schematic of the 1.55 eV GaInAsP solar cell.

Table 1
Results for two different cells. The active area of the cells is 0.136 cm^2

Cell	V_{oc}, volts	J_{sc}, mA/cm^2	ff,%	η,%
945	1.07	18.7	80.8	18.8[a]
1314	1.08	20.6	81.7	18.2[b]

[a]For AM1.5 global, intensity 94 mW/cm2
[b]For AM1.5 direct, intensity 100 mW/cm2

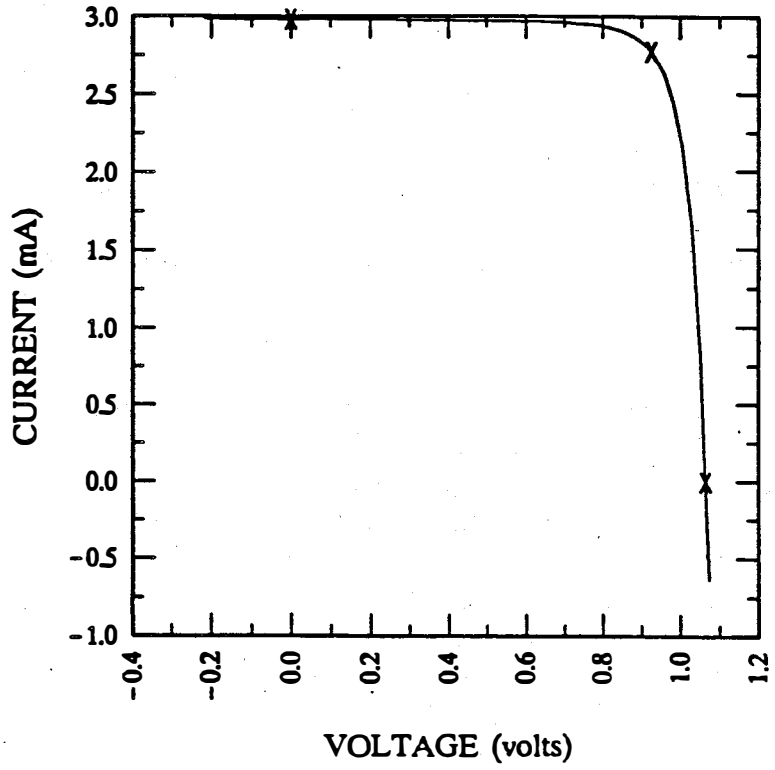

Figure 2. Current-voltage curve for Cell 945.

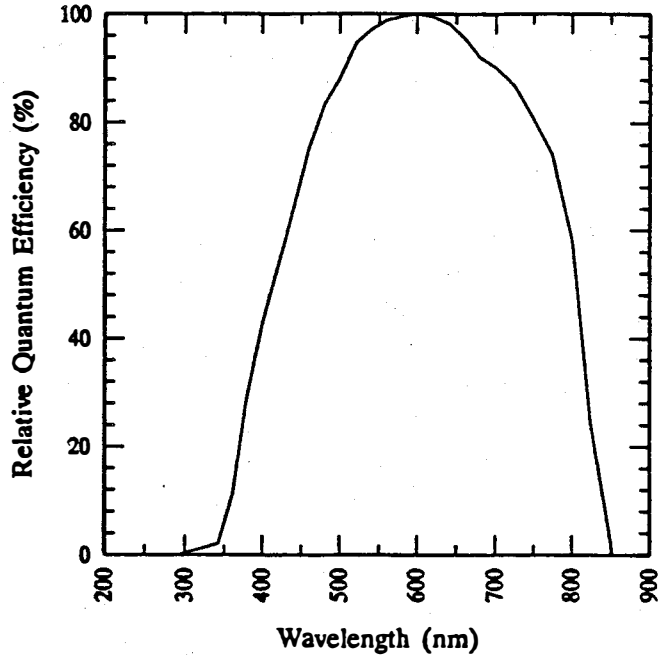

Figure 3. Spectral response measurements for Cell 945. The light bias was 5.4 mA, and there was zero voltage bias.

Title:	**Low-Cost, High-Efficiency Solar Cells Utilizing GaAs-on-Si Technology**
Organization:	Spire Corporation, Bedford, Massachusetts
Contributors:	S. M. Vernon, principal investigator; S. P. Tobin

Introduction

The overall goal of this research is to establish a technology to produce very-high-efficiency solar cells for terrestrial photovoltaic applications, using either multijunction or single-junction concepts. The approach pursued in this program involves the growth of GaAs and/or $GaInP_2$ materials onto Si substrates by the metalorganic chemical vapor deposition (MOCVD) technique. Our efforts this year have been devoted to (a) reducing the defect density in GaAs-on-Si layers by substrate patterning, and (b) developing a technology for producing Bragg-reflector structures for improved-efficiency solar cells having a reduced base thickness. Efforts of our prior NREL contracts have resulted in the achievement of a GaAs-on-Si solar cell having a terrestrial efficiency of ~20% at 200 suns.

Solar Cell Studies Utilizing Bragg Reflectors

Bragg reflector structures (epitaxial multilayer dielectric mirrors, composed of alternating layers of high-and-low composition $Al_xGa_{1-x}As$), as shown in Figure 1, can improve the efficiency of solar cells by reflecting the near-band-gap light back through the cell for a second pass, thus improving the carrier-collection efficiency in materials having fairly short minority-carrier diffusions lengths, such as GaAs on Si. In the previous year, we established the technology for depositing Bragg reflectors by MOCVD; this year we have demonstrated their successful use in GaAs and GaAs-on-Si solar cells.

As the wavelength at which the peak reflectance occurs is very sensitive to the thickness of Bragg reflector period, we first optimized the control of the growth, using low-pressure MOCVD. Our achievements in this area include a run-to-run reproducibility of ~ 1%, and a uniformity of ~ 2%, over a two-inch-diameter wafer. Since the reflectance peak is fairly narrow in wavelength, we have developed a stacked Bragg reflector structure, using twenty periods of a Bragg reflector designed for a peak-reflectance wavelength of 840 nm, followed by twenty periods designed for a peak-reflectance wavelength of 765 nm; this configuration results in a spectral FWHM of the reflectance peak of 154 nm, as compared with only 77 nm for a single stack.

By fabricating solar cells, with and without the use of Bragg reflectors, the results shown in Table I have been obtained. Cells without Bragg reflectors have our standard AlGaAs back-surface field of equivalent thickness. Bragg reflector cells show an increased efficiency over conventional cells, by 0.9 percentage points on Si substrates, and by 0.7 percentage points on GaAs substrates.

The predicted effect of including a Bragg reflector below the base of a homoepitaxial GaAs cell is to increase the quantum efficiency in the wavelength region of ~ 850 nm. This phenomenon has indeed been experimentally confirmed, as is shown in Figure 2.

Concentrator Solar Cell Studies

The basic problem limiting the efficiency in GaAs-on-Si solar cells is the large defect density, which causes increased space-charge recombination and a reduced minority-carrier lifetime. Detailed analyses of current-voltage behavior in GaAs-on-Si cells have shown that the use of concentrated sunlight helps to overcome some of this difficulty by allowing the cell to operate in a regime where the (n = 1) diffusion current dominates, thus leading to higher open-circuit voltages.

Using GaAs-on-Si layers having a dislocation density of ~ 2×10^7 cm^{-2}, and homoepitaxial GaAs, we have made cells with the efficiency values as shown in Table II. These higher efficiencies have resulted from improvements in the deposition, design, and processing of solar-cell structures. Our best previous GaAs-on-Si concentrator cell result is an efficiency of 19.9% at AM1.5D. Dislocation reduction is not a factor in the particular GaAs-on-Si cell advances reported here.

GaAs on Si Material Studies

We have looked at several means of reducing the dislocation density in the GaAs-on-Si layers. One avenue explored involves the use of increased annealing temperatures for the thermal-cycle growth process. We have found that raising the anneal temperature from 900°C to 1000°C does not result in a lower defect level. A more promising, and unique, approach being studied makes use of the concept of restricting the nucleation area for the GaAs on Si. Lithographically patterning the Si substrate with sub-micron dimensions permits the growth of planar GaAs films with greatly reduced dislocation density: preliminary results indicate a value of ~ 10^5 cm^{-2} is achievable.

Future Directions

Our continuing research interests include improving the efficiency of GaAs solar cells as well as reducing the defect level of our GaAs-on-Si "substrates". High-efficiency cell studies will include the development of $GaInP_2$ windows and of GaAs-$GaInP_2$ monolithic tandems, continued optimization of Bragg reflector structures, and combination of Bragg-reflector and concentrator concepts into GaAs-on-Si solar cells. GaAs-on-Si material improvements will be accomplished by continued study of substrate patterning and two-dimensional-nucleation techniques based on the use of atomic-layer epitaxy.

Publications

NREL-funded research has resulted in two articles being published in the scientific literature over the course of this past year. They are listed below:

"Polarized Cathodoluminescence Study of Uniaxial and Biaxial Stress in GaAs on Si," D.H. Rich, A. Ksendov, F.J. Grunthaner, B.A. Wilson, H. Shen, M. Dutta, S.M. Vernon, and T.M. Dixon, Phys. Rev. B 43, 6836 (1991).

"Growth and Characterization of Uniform AlGaAs Bragg Reflectors by LP-MOCVD," S.M. Vernon, S.P. Tobin, M.M. Sanfacon, A.L. Mastrovito, N.H. Karam, and M.M. Al-Jassim, Journal of Electronic Materials, in press (1992).

Table I *Efficiency measurements for GaAs cells on GaAs and on Si substrates, with and without Bragg reflectors. Test conditions: 1 Sun AM1.5 Global, 100 mW/cm², corrected for spectral mismatch, 25°C, 0.25 cm² total area.*

Substrate	Cell Thick. (μm)	Back-Surface Field	V_{oc} (V)	J_{sc} (mA/cm$^{2)}$	FF (%)	Effic. (%)
GaAs	2.0	Bragg	1.062	27.12	85.6	24.7
GaAs	2.0	AlGaAs	1.046	26.77	85.6	24.0
GaAs	4.0	AlGaAs	1.053	26.83	85.6	24.2
GaAs	1.0	AlGaAs	1.063	25.21	85.1	22.8
Si	2.0	Bragg	0.902	24.57	77.4	17.1
Si	2.0	AlGaAs	0.884	23.75	77.2	16.2

Table II *Measured efficiency values for concentrator cells. (Area = 0.126 cm²; all measurements at 25°C).*

Cell Type	Measured At	Spectrum	Suns	Efficiency (%)
GaAs on Si	Sandia	AM1.5D	237	21.3
GaAs on Si	Sandia	AM0	189	19.5
GaAs on Si	Spire	Am1.5G	1	16.1
GaAs on GaAs	Sandia	AM1.5D	180	27.6
GaAs on GaAs	Sandia	AM0	147	24.6
GaAs on GaAs	Sandia	AM1.5G	1	23.7

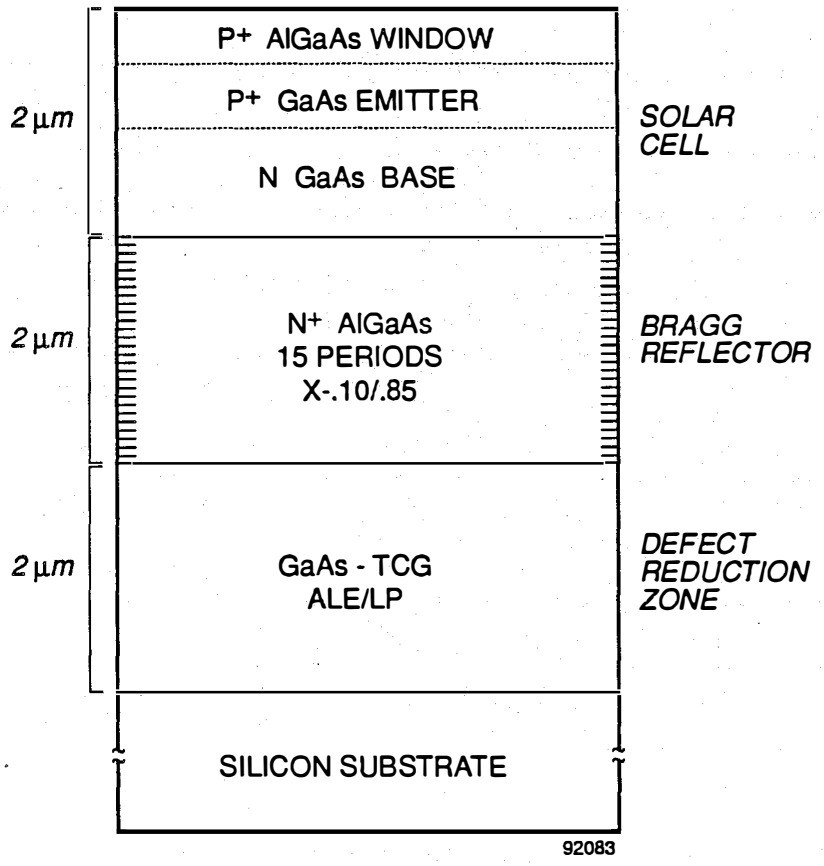

Figure 1 *Structure of a typical GaAs-on-Si solar cell, incorporating a Bragg reflector.*

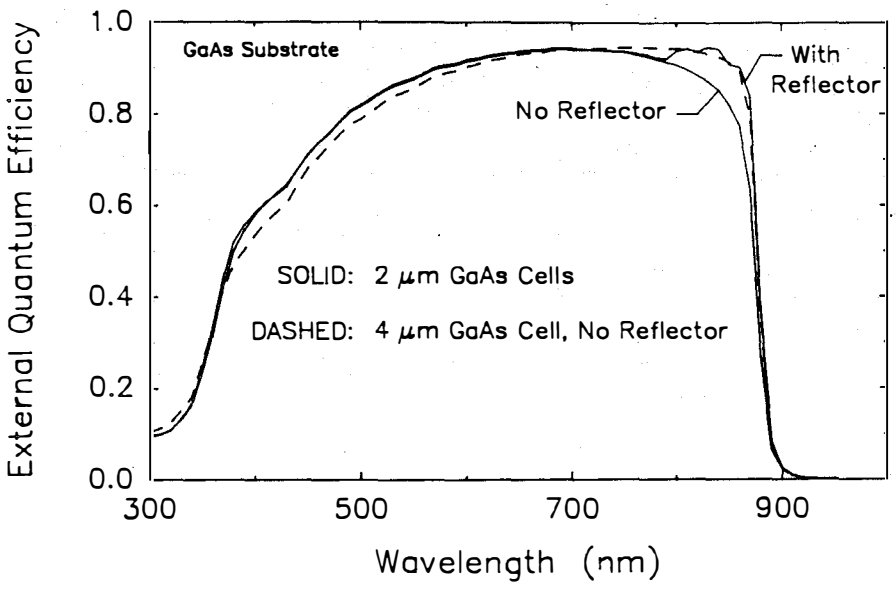

Figure 2 *Measured external quantum efficiency for GaAs cells with and without Bragg reflectors.*

Title: **Atomic Layer Epitaxy for High Efficiency Solar Cells**

Organization: Departments of Electrical Engineering and Materials Science
University of Southern California
Los Angeles, CA

Contributors: P. D. Dapkus, principal investigator, B. Y. Maa, and M. Jow

The objective of this program is to explore and develop a low temperature, large scale epitaxial process for high efficiency solar cells based upon atomic layer epitaxy (ALE). ALE has the potential for high throughput, layer thickness control and uniformity based upon the inherent saturated surface reactions involved in the process. We have previously shown that the growth rate in atmospheric pressure, thermally driven ALE is limited by the maximum temperature attainable before homogeneous gas phase reactions dominate the process and preclude the achievement of saturated monolayer growth. In this program we are exploring the use of photoassisted ALE and vacuum ALE as alternative approaches for achieving usable growth rates and high throughput. The program is structured in two phases. In the first phase, we measured the fundamental thermal and photoassisted surface reaction rates involved in the growth of GaAs using TMGa and a variety of As sources. Based upon these results a decision was made that the the vacuum ALE approach was a viable approach to use for the growth of GaAs and related compounds. The second phase will concentrate upon developing VALE for the growth of high efficiency solar cells. Issues such as materials quality, reactant utilization, and throughput will be examined.

The fundamental surface reactions and reaction rates are being assessed by a combination of tools that allows us to study the surface chemistry that results from reaction of Ga and As sources on the GaAs surface (XPS), the structural properties of the surface (RHEED), and the rates of the surface ordering (reflection difference spectroscopy-RDS). We had previously shown that the end point configuration of the trimethylgallium (TMGa) ALE exposure in vacuum is the 4X6 Ga-stabilized GaAs surface. This was deduced from RHEED and XPS examination of TMGa-saturated GaAs surfaces dosed at elevated temperatures. In this program we have applied RDS techniques to measure the kinetics of the surface reactions of TMGa and tertiarybutylarsine with Ga- and As- stabilized surfaces. RDS is sensitive to both the chemistry and the structure of the surface but by careful choice of the wavelength of light one of these aspects or the other can be emphasized. We choose to emphasize the structural aspects. In RDS the change in the difference of the reflectivities of light polarized along perpendicular <110> directions in the crystal is monitored as a function of time as a surface is exposed to a reactant. Changes in

the atomic arrangement on the surface are monitored by the reflection difference transient.

Typical RDS transients that results when an As-stabilized surface is exposed to TMGa at 500° C are shown in Fig. 1. The transients are labeled to indicate the timing and duration of TMGa and TBAs exposures. Prior to TMGa exposure the surface is a stable 2X4 As-stabilized surface. At the initiation of the TMGa exposure the RDS signal begins to increase as a result of the reaction of TMGa with the surface and the subsequent atomic rearrangement on the surface. The end point RDS signal is reached after the surface reaction is complete. This usually requires a longer time than the TMGa exposure owing to desorption of surface species believed to be CH_3 radicals. If the TMGa exposure is continued beyond an optimum point the RDS transient shows kink indicative of an oversaturated surface. The end point surface is found to be the 4X6 Ga-stabilized surface. The exposure time of TMGa needed to reach the endpoint surface, t_m, is believed to be the TMGa reaction time on an As-stabilized surface. The change in the endpoint reflectance difference is plotted as a function of exposure time for various exposure temperatures in Fig. 2 a) and b). In Table I, the exposure time necessary to reach the saturated endpoint surface configuration, t_m, as measured by RDS and the total time necessary to reach the endpoint are listed for various temperatures. From Fig. 2 and Table I we can conclude that the TMGa surface reaction is not limiting the surface reactions in vacuum ALE. Rather the desorption of species believed to be CH_3 from the surface is believed to limit the total surface reaction rate. More important extrapolation of these data to somewhat higher temperatures suggests that total exposure and surface reaction times leading to monolayer Ga surface saturation of less than one second are possible with TMGa. This has been corroborated by studies of the reaction of TMGa with Ga-stabilized surfaces in which the only surface reaction that occurs is between the As sites on which there are no Ga atoms bonded. The primary reaction here involves the decomposition of TMGa on As sites followed by the desorption of CH_3 and $GaCH_3$. The rates for these desorption processes agree well with the observed times to reaction completion observed for the reaction of TMGa with an As-stabilized surface.

Based on these studies we have developed a model for the VALE reactions of TMGa and GaAs surfaces. The initial As-stabilized surface contains predominantly As atoms on which TMGa reacts rapidly to produce $GaCH_3$ and two CH_3 radicals on the surface. The CH3 radicals desorb from the surface through two channels, one associated with an As bond and one associated with a Ga bond.The latter channel is rate limiting and determines the time to reach the clean Ga-stabilized surface. This surface contains As sites with no Ga bonded to maintain charge neutrality and is reactive to TMGa only through these uncovered As sites. But the surface quickly returns to the As stabilized surface when the TMGa exposure is terminated by the desorption of CH_3 and $GaCH_3$. As a result, the saturation mechanism for ALE are believed fundamentally to be the result of selective adsorption and reaction of

TMGa on As sites, but the rate of the saturation process is controlled by desorption of CH_3.

We have also investigated the surface reactions of tertiarybutylarsine with GaAs Ga-stabilized surfaces. We have found that in the temperature range suitable for rapid TMGa reactions with GaAs surfaces, the reaction of rate of TBAs on a Ga-stabilized surface is fast enough to support a reasonably high throughput ALE process. It now appears certain that self-limited ALE growth of GaAs with ALE cycle times as short as 1-2 seconds are possible. It remains for experimental determination to learn if the materials quality at these growth rates is adequate for high efficiency solar cells.

Tertiarybutylarsine (TBAs) was also successfully used for the first time to grow high quality GaAs by photoassisted ALE and thermal ALE at atmospheric pressure. Its use allowed us to reduce the As exposure by a factor of five over that achievable with As and to achieve an order of magnitude higher PL efficiency for double heterostructure samples. Fig. 3 shows a comparison of PL spectra from two thin layer samples, one grown by photoassisted ALE using TBAs and the other by photoassisted ALE using AsH_3. Note the higher PL efficiency and the narrrower linewidth of the sample grown using TBAs. We believe this observation is a breakthrough in the ALE technology and plan further experiments to examine other materials characteristics.

Experimental samples were also grown for SIMS evaluation of the materials grown with TBAs. The measurements were performed at the University of Illinois and showed a low carbon level compared to layers grown with arsine. GaAs grown with TBAs by ALE shows a similar low background carrier concentration as that grown by LALE. The growth rates are limited at atmospheric pressure by the low temperatures that must be used to avoid unsaturated growth. As a result the layer thicknesses that can be achieved reasonably are limited. To verify the quality of the materials a laser with a GaAs QW active region grown by ALE using TBAs and TMGa. was grown. Devices with threshold current densities as low as 300 A/cm^2 were fabricated. These are the lowest threshold lasers ever constructed by ALE and attest to the improved quality of the materials grown with TMGa and TBAs

Experimental samples grown for C-V evaluation of the background carrier concentration have exhibited background carrier concentrations as low as 3×10^{15} cm^{-3}. This is two orders of magnitude lower than ever observed in materials grown by photoassisted ALE. It may account for the much higher PL efficiency of the samples as well.

A new vacuum ALE reactor has been designed, constructed and is in the final stages of calibration. The reactor is designed based upon the use of a TMGa/TBAs ALE process. The choice of a UHV environment was made to allow the ALE process to be done at temperatures as high as 600°C without the occurrence of homogeneous

reactions that preclude surface controlled saturated growth. The system has been designed to minimize the use of reactants and to provide the minimum cycle time and thus maximum growth rates. A major concern with the choice of reactants and reaction environment is the reduction of carbon in the grown film. Provisions have been made to add an atomic hydrogen source to the system should the optimization of the growth parameters not yield high quality materials. Growth of the first layers are expected in the month of January.

A new analysis chamber has been designed and added to our surface analysis system to allow us to incorporate additional analysis tools, repetitive fast switching of reactants and an atomic hydrogen source to improve the rate of desorption of surface species. The new system will include RHEED and mass spectrometry in addition to RDS to allow us to identify the surface reconstruction corresponding to certain RDS identified states more ambiguously and to allow us to identify desorbing species. This system will provide invaluable information to help the optimization of the VALE process.

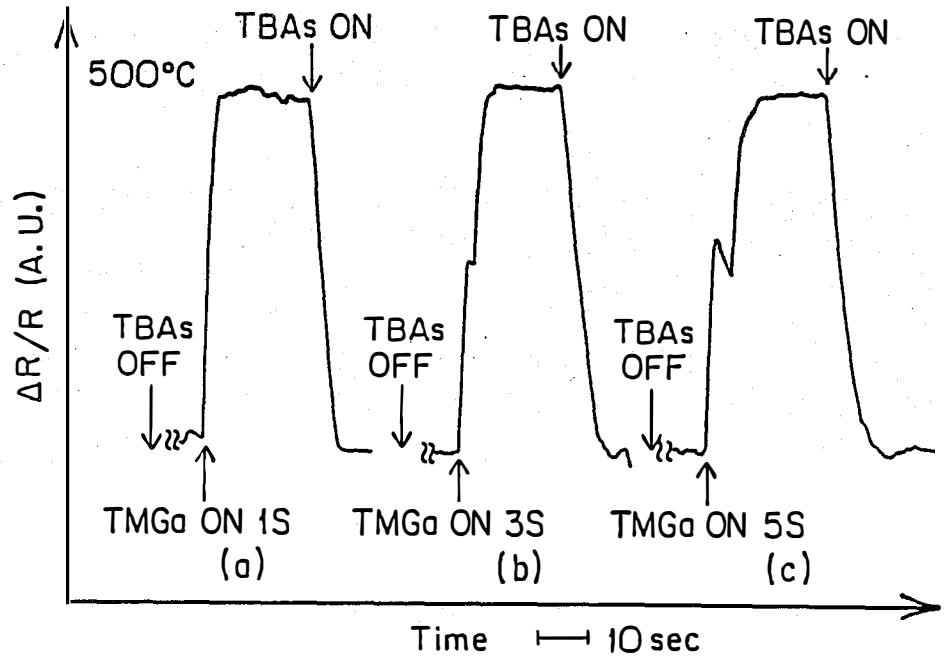

Figure 1 - Reflection Difference Spectroscopy (RDS) transients of an As-stabilized 2X4 GaAs surface exposed alternately to TMGa and TBAs at 500 °C. The transients are illustrated for various TMGa exposure times. Note the occurrence of a "kink" in the transient when the surface is overexposed. Note also that the endpoint RDS level is the same for all exposure times.

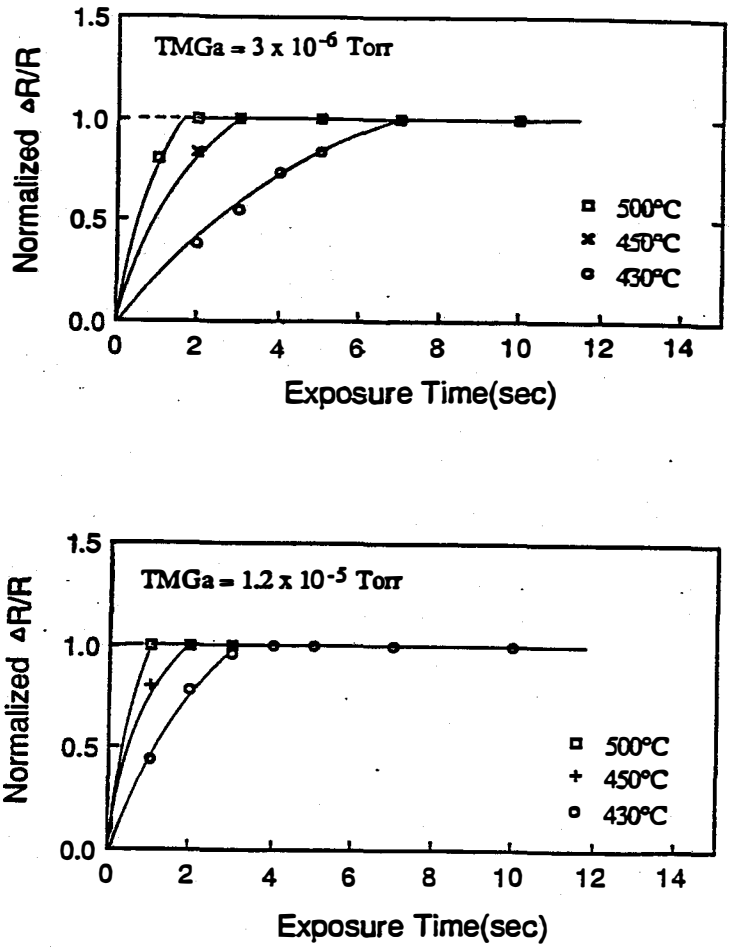

Figure 2 - Endpoint RDS transient signal versus TMGa exposure time, t_m, for various temperatures and two different exposure levels. Note the strong saturation of the RDS endpoint with t_m indicative of a saturated surface reaction. Note also that t_m for saturation decreases strongly with temperature and exposure level.

Table I

Temperature	Exposure Level (Torr)	t_m (sec)	Completion time (sec)
430°C	1.2X10-5	4	25
450°C	1.2X10-5	3	9
500°C	1.2X10-5	2	3

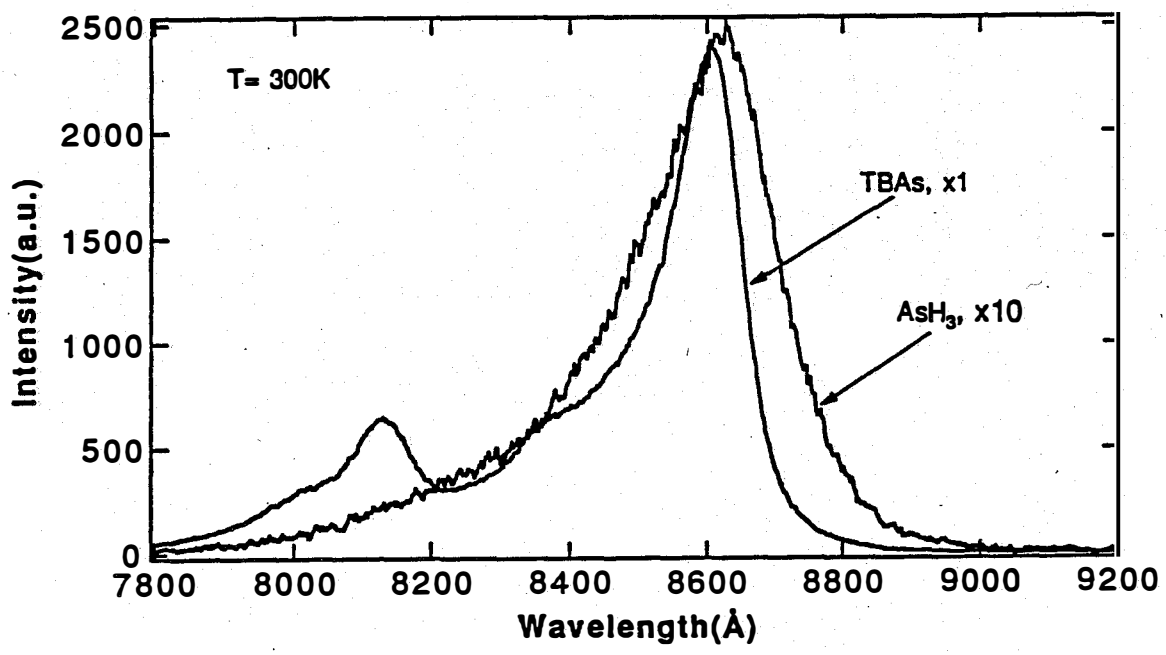

Figure 3 - Photoluminescence spectra of AlGaAs/GaAs double heterostructures in which the central GaAs region is grown by photoassisted ALE at 390°C. The sample of the spectrum labeled as "TBAs" was grown using tertiarybutylarsine and the other sample whose spectrum is shown was grown using arsine. The PL intensity of the TBAs grown sample is 10X greater than the arsine grown sample. The level of carbon incorporation is also decreased by two orders of magnitude in this sample.

6.0 NEW IDEAS FOR PHOTOVOLTAIC CONVERSION PROGRAM

Thomas Basso, (Manager)

The objective of the New Ideas Program is to identify, evaluate, and develop new or innovative materials, device configurations, and concepts for photovoltaics (PV) technology that may be high risk, but that also offer the potential for a major advance of PV understanding and technology development leading to future production of low-cost electricity. The subcontracted research that shows significant potential may be transferred into the appropriate major task area within the DOE National Photovoltaics Program for continuing support.

The New Ideas Program issues public solicitations for new and innovative research ideas that are relevant under DOE program guidelines, including innovative approaches to existing PV technology (e.g., cell and module processing) and innovative new concepts. Responses to these solicitations are submitted by universities, businesses, and nonprofit organizations. Subcontracts are awarded to study the most promising submittals. At the end of 1 year, these subcontracts are reviewed, and successful subcontracts could be renewed for a second year of funding. In late FY 1991, a letter-of-interest (LOI) solicitation was released. More than 100 responses were received. The LOI responses will be reviewed during FY 1992, and those in the competitive range will be invited to submit an expanded proposal for review. Based on FY 1992 funding and the availability of FY 1993 funds, it is likely that subcontract awards will start late in 1992.

During FY 1991 subcontractor progress continued and the subcontracts were renewed on these concepts: novel ways of depositing ZnTe films by solution, researched by the Institute of Energy Conversion at the University of Delaware; development of an inverted AlGaAs/GaAs patterned tunnel junction cascade concentrator cell, at the Research Triangle Institute; and development of high efficiency epitaxial optical reflector cells, at the University of Southern California. These awards started in FY 1990 and were based on the FY 1988 solicitation. That solicitation received nearly 100 responses to the request for LOI. Evaluation of those LOI responses identified several promising ones for further evaluation, and during FY 1989, expanded proposals from 24 LOI finalists were evaluated and the three above awards were funded.

Title: **Novel Ways of Depositing ZnTe Films by a Solution Growth Technique**

Organization: Institute of Energy Conversion
University of Delaware
Newark, Delaware 19716-3820

Contributors: Robert W. Birkmire, Principal Investigator; Anup Mondal, Brian E. McCandless and Tracey I. Yokimcus, Research Contributors

Objectives

The objective of the research is to develop low temperature processes using solution growth techniques to deposit: 1) thin, <50 nm, ZnTe films suitable as a stable transparent ohmic contact for CdTe/CdS solar cells; and 2) thin, <50 nm, ZnSe films as a window/heterojunction for $CuInSe_2$ solar cells.

Technical Approach

ZnTe films were deposited from an aqueous solution by galvanic deposition. The structural, optical and electrical properties of the ZnTe films were characterized using established techniques of x-ray diffraction, four-point probe, and optical reflection and transmission measurements. CdS/CdTe/ZnTe solar cells were fabricated to characterize the contact properties of the ZnTe films on working devices. Properties of devices using the ZnTe contact were compared to devices using Au or Cu/ITO as the CdTe contact.

ZnSe films were deposited from aqueous solutions by electrochemical deposition. The structural and optical properties were characterized using established x-ray diffraction, SEM/EDS and optical reflection and transmission measurements. $CuInSe_2$/ZnSe solar cells were fabricated to characterize the $CuInSe_2$/ZnSe heterojunction. Properties of the devices were compared to standard $CuInSe_2$/CdS devices.

Significant Results

ZnTe

ZnTe films were deposited galvanically, a special case of electrochemical deposition, from an unstirred aqueous bath containing 0.1 M/l $ZnCl_2$ and about 10^{-4} M/l TeO_2 (1,2). Controlling the bath pH between 3 and 4 and temperature between 50°C and 80°C was necessary to deposit uniform, adherent, single phase ZnTe films. The ZnTe films were doped by adding a Cu^{+2} complex to the bath. The galvanic cell was then constructed by placing a glass/ITO/CdS/CdTe substrate externally short-circuited to a zinc counter electrode in the bath. The electrochemical reaction is driven by the potential difference between the substrate and zinc electrode which acts as both a source of electrons for the cathodic reaction and a source of Zn^{+2} ions. The most likely reactions leading to the formation of ZnTe:Cu are:

Anode Reaction

$Zn \rightarrow Zn^{+2} + 2e^-$, $E^\circ_{ox} = +0.76V$

Cathode Reaction

$Zn^{+2} + 2e^- \rightarrow Zn^\circ$, $E^\circ_{red} = -0.76V$

$HTeO_2^+ + 3H^+ + 4e^- \rightarrow Te^\circ + 2H_2O$, $E^\circ_{red} = +0.56V$

$Zn^\circ + Te^\circ \rightarrow ZnTe$

$Cu(TEA)_n^{+2} + 2e^- \rightarrow Cu^\circ + nTEA$

$n=1,2,...$

Figure 1 shows a plot of ZnTe deposition current density with time, having: 1) no Cu; 2) 10^{-5}M/l Cu^{+2}; and 3) 10^{-4} M/l Cu^{+2} ions in solution. A nearly constant current density is obtained after about 4 minutes and is proportional to the growth rate. The growth rate gradually decreases with the depletion of Te ions in solution. The current and thus growth rate were found to be higher when Cu^{+2} was present in solution.

ZnTe films were deposited on CdTe/CdS/ITO/glass substrates suitable for solar cells which were prepared as follows: 1) CdS and CdTe were thermally evaporated onto ITO/glass substrates; 2) the samples were coated with $CdCl_2$ and heat treated at 400°C for 30 minutes in air; and 3) the surface of the CdTe was etched for 5 sec in a Br_2-CH_3OH solution. The ZnTe:Cu was then deposited as a contact to CdTe. To complete the solar cell, a metal contact, either Cu/Au, Ni or ITO, was deposited on the ZnTe:Cu and the cell performance optimized with air heat treatment. Figure 2 shows the AM 1.5 characteristics of a CdS/CdTe/ZnTe:Cu solar cell with a Cu/Au contact, with 8.7% efficiency and a 65.7% fill factor. Using ZnTe:Cu contacts, devices have been fabricated with V_{oc}>750 mV, J_{sc}>20 mA/cm^2, and FF>74%, comparable to results obtained with the Cu/Au contact.

ZnSe

Depositions of ZnSe films were carried out by electrodeposition using either a Na_2SeSO_3 bath or a Na_2SeO_3 bath. Preliminary depositions were made on glass/Mo substrates to characterize the process. Deposition of uniform thin films was self-limiting, yielding films less than 50 nm thick, which limited the extent of physical characterization possible. EDS analysis indicated that the Zn:Se content was 1:1. Beyond this, characterization was limited to analysis of devices made with glass/Mo/$CuInSe_2$ substrates. $CuInSe_2$/ZnSe devices were fabricated using a ZnO transparent contact. Although the devices were of poor quality (efficiency less than 2%), the window layer band edge, estimated from spectral response measurements, was ~2.7 eV indicating the formation of ZnSe.

Conclusions

Cu-doped ZnTe films, 50-300 nm thick, were deposited directly by an electrochemical method for the first time. Single phase films were obtained for bath pH from 3 to 4, [TeO_2] from 10^{-5} to 10^{-4} M/l, and temperature from 50 to 80°C. A copper complex added to the bath allowed controllable p-type doping of the ZnTe films. A CdTe/CdS solar cell using the ZnTe:Cu as the primary contact to the CdTe achieved an efficiency of 8.7% with a FF>65%. The optical transmission of cells using ZnTe:Cu made in this manner is higher than for cells using evaporated ZnTe:Cu (3), making this an attractive contacting method for tandem cells.

Based on EDS analysis and spectral response measurements of devices, we conclude that ZnSe films were electrodeposited onto both glass/Mo and glass/Mo/$CuInSe_2$ substrates. Due to the self-limiting nature of the deposition, the films were very thin, <50 nm. On $CuInSe_2$ substrates, conformal coverage was probably not achieved due to the faceted nature of the $CuInSe_2$ surface. Future work should address these issues and investigate alternative bath chemistries.

References

1. Anup Mondal, Brian E. McCandless, Robert W. Birkmire, "Electrochemical Deposition of Thin ZnTe Films as a Contact for CdTe Solar Cells", Solar Cells, accepted for publication August 16, 1991.

2. Anup Mondal, Robert W. Birkmire, Brian E. McCandless, "A New Method for Forming ZnTe Contacts for CdTe Cells", presented at 22nd IEEE PVSC, Las Vegas, Nevada, October 7-11, 1991.

3. P.V. Meyers, C.H. Liu, L. Russell, V. Ramanathan, R.W. Birkmire, B.E. McCandless and J.E. Phillips, Proc. 20th IEEE PVSC, 1448 (1988).

Figure 1. ZnTe deposition current density and growth rate versus deposition time, a) $[Cu^{+2}]=10^{-4}$ M/l, b) $[Cu^{+2}]=10^{-5}$ M/l, c) $[Cu^{+2}] = 0$.

Figure 2. I-V characteristics at AM1.5 for an ITO/CdS/CdTe/ZnTe:Cu cell measured at SERI. The deposition bath contained $ZnCl_2=10^{-1}$ M/l, TeO2 = 10^{-4} M/l, $Cu(TEA)_n^{+2}$ = 10^{-4} M/l. The deposited ZnTe:Cu film was 50-100 nm thick.

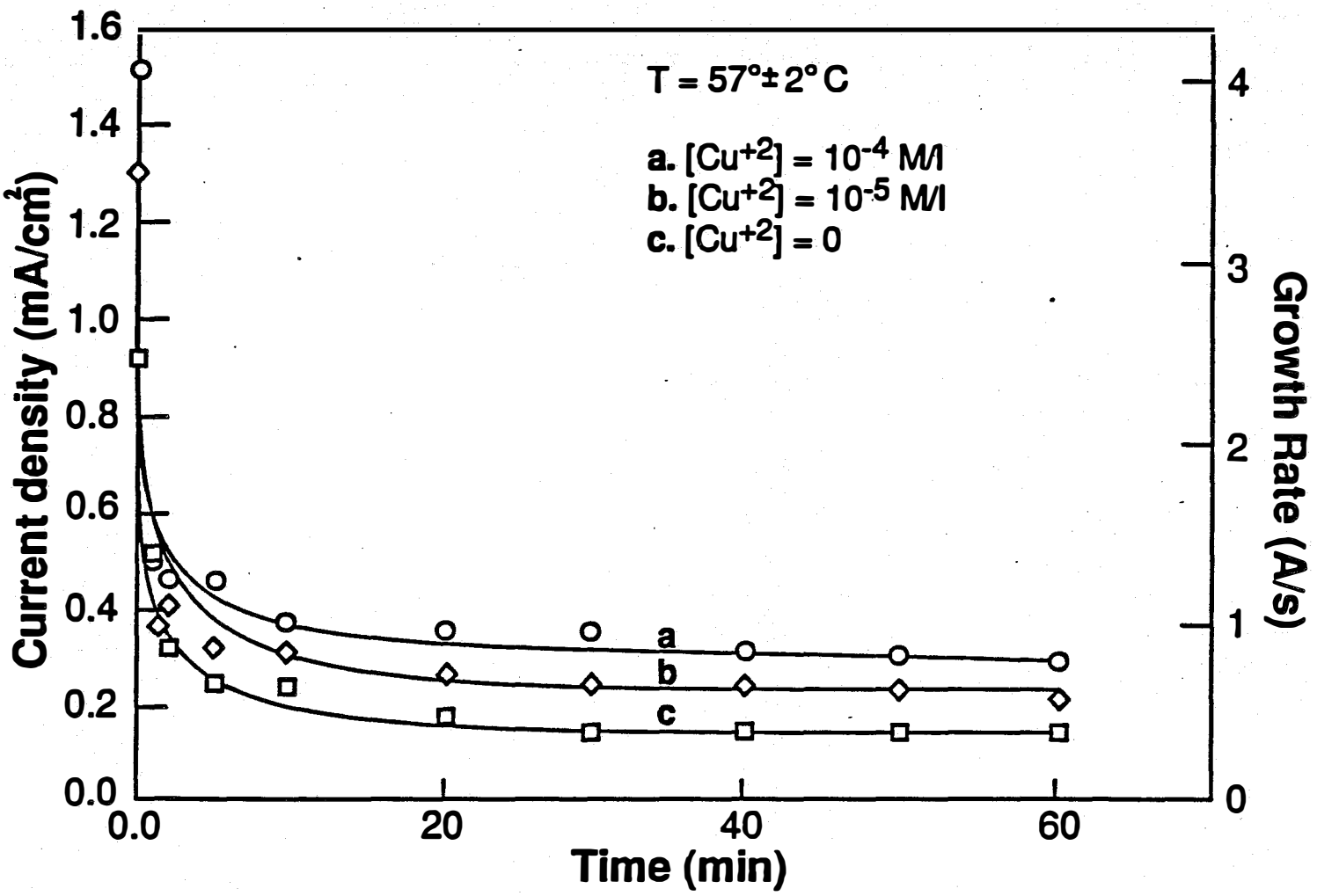

Figure 1. ZnTe deposition current density and growth rate versus deposition time, a) $[Cu^{+2}]=10^{-4}$ M/l, b) $[Cu^{+2}]=10^{-5}$ M/l, c) $[Cu^{+2}] = 0$.

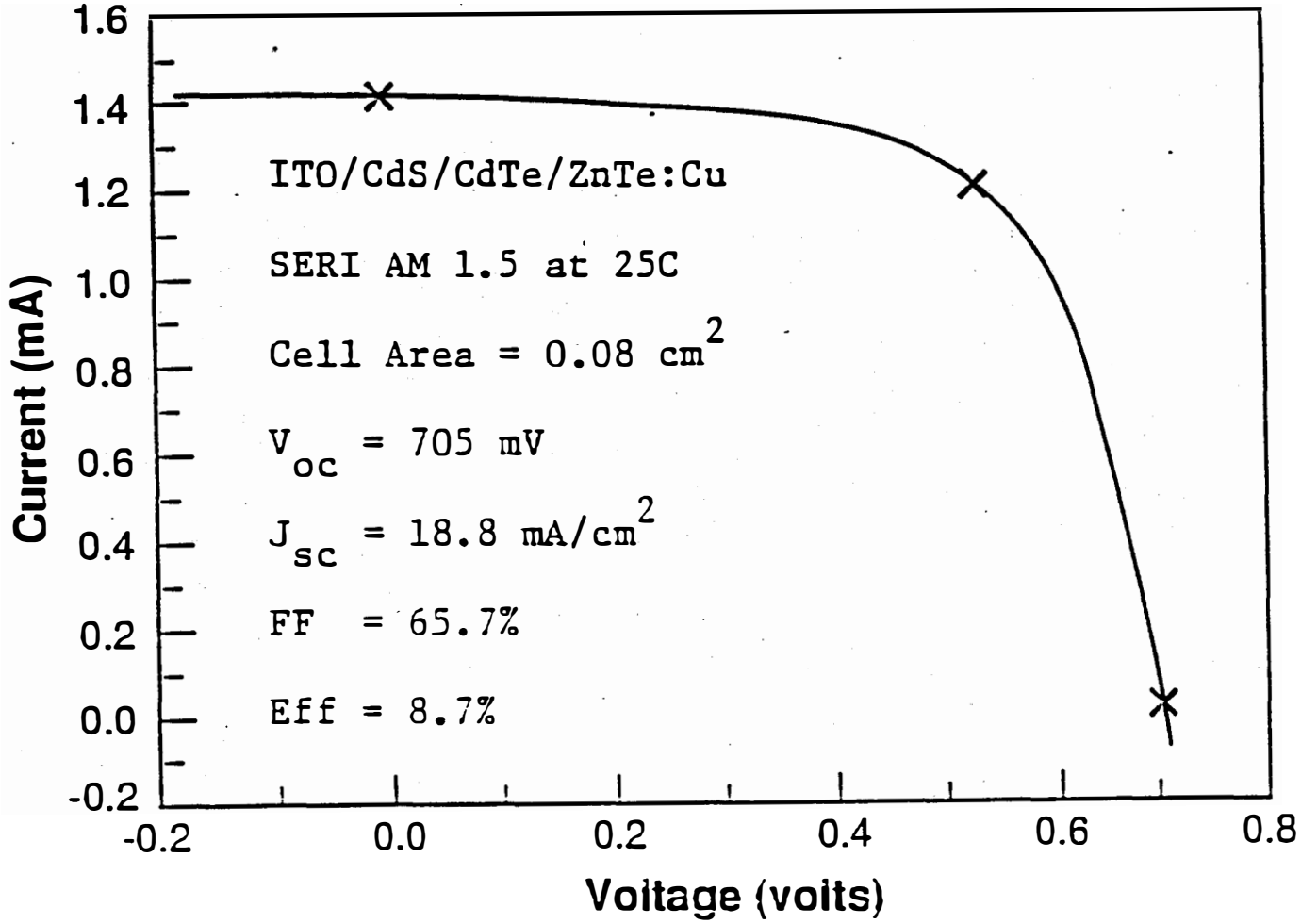

Figure 2. I-V characteristics at AM1.5 for an ITO/CdS/CdTe/ZnTe:Cu cell measured at SERI. The deposition bath contained $ZnCl_2$=10^{-1} M/l, TeO2 = 10^{-4} M/l, $Cu(TEA)_n^{+2}$ = 10^{-4} M/l. The deposited ZnTe:Cu film was 50-100 nm thick.

Title: **An Inverted AlGaAs/GaAs Patterned Tunnel Junction Cascade Concentrator Solar Cell**

Organization: Research Triangle Institute, RTP, NC 27709

Contributors: R. Venkatasubramanian (Principal Investigator)
M.L. Timmons, T.S. Colpitts, J.S. Hills,
J. Hancock, and J.A. Hutchby.

TECHNICAL APPROACH

Inverted growth of III-V solar cells and the development of associated cell processing, including substrate-removal, will offer a significant degree of freedom for improving the performance of many multijunction cascades. This is especially true of the development of high-efficiency $Al_{0.37}Ga_{0.63}As$/GaAs cascades where the high growth temperatures required for the AlGaAs top cell growth can cause the deterioration of the tunnel junction interconnect. Here, we present an approach for inverted-grown AlGaAs/GaAs cascade cells, where the AlGaAs top cell will be grown first at high temperatures, placing the surface to be illuminated nearest to the substrate. Following the growth of the top cell, the GaAs tunnel interconnect and the bottom cell are grown at lower temperatures. After the inverted growth, the AlGaAs/GaAs cascade structure is selectively removed from the parent substrate, Ge in this work.

The development of such a cascade cell has reached these milestones. First, the growth of the top $Al_{0.37}Ga_{0.63}As$ cell was optimized to obtain active-area efficiencies of 13.7% and 14.7% at 1-sun and 100-suns AM1.5D, respectively. Second, a planar GaAs tunnel junction interconnect with a specific resistivity of 3.3×10^{-3} ohm-cm^2 has been developed that is suitable for the AlGaAs/GaAs cascade operating at about 500 AM1.5 suns. Third, a highly selective plasma etching of Ge has been developed to produce thin, free-standing GaAs-AlGaAs structures grown on the Ge. Fourth, a technique called eutectic-metal-bonding (EMB) has been developed for strain-free mounting of thin GaAs-AlGaAs films onto Si carrier substrates. Measured minority-carrier lifetimes in EMB GaAs thin films are as high as 103 ns. Finally, a thin film, inverted-grown, GaAs cell with a 1-sun AM1.5 efficiency of 19.2%, has been demonstrated. These developments suggest that the inverted-growth approach holds considerable promise for obtaining high efficiency AlGaAs/GaAs cascades in the near-term.

$Al_{0.33}Ga_{0.67}As$ TOP CELL DEVELOPMENT

A key to the development of high-efficiency $Al_{0.37}Ga_{0.63}As$ cells is the reduction of moisture and oxygen from source gases and growth ambient. The procedures employed to achieve this are discussed elsewhere [1]. Cell optimization also needs to take into account the increasing near-band-edge absorption in AlGaAs materials with aluminum

content; the absorption coefficient increases from about 1 x 10^{-4} cm^{-1} in GaAs to about 2.3 x 10^{-4} cm^{-1} in $Al_{0.37}Ga_{0.63}As$. This increased optical absorption plus the reduced valence-band offset between $Al_{0.33}Ga_{0.67}As$ and $Al_{0.85}Ga_{0.15}As$, compared to GaAs and $Al_{0.85}Ga_{0.15}As$ in a GaAs cell, make emitter-surface passivation nontrivial. Hence, the role of thin emitters, optimization of the interface between the n-$Al_{0.37}Ga_{0.63}As$ emitter and the n-$Al_{0.85}Ga_{0.15}As$ window, and the use of a multi-layer buffer that acts as a getter[1], can substantially affect the cell performance as indicated by the data of Table 1.

We have measured an efficiency of 13.7% (active-area) at 1-sun AM1.5G on our best $Al_{0.37}Ga_{0.63}As$ cell. The open-circuit voltage of the cell needs to be improved to 1.35 V by developing an optimum technique to dope the emitter region to $\sim$ 2 x 10^{18} cm^{-3} without degradation of J_{sc} and by improved passivation. The efficiency of the cell improves to 14.7% at 100 AM1.5D suns. The use of an Entech coverglass has resulted in J_{sc} improvements of at least 10.5% for the emitter grids [1] employed in the cells.

HIGH CONDUCTANCE GaAs TUNNEL JUNCTIONS

Development of a suitable high-conductance GaAs tunnel interconnect for the AlGaAs/GaAs cascade (indicated in Fig.1) is necessary to reduce the ohmic losses. GaAs p^{++}-n^{++} tunnel diodes have been grown by atmospheric-pressure organometallic vapor phase epitaxy (OMVPE) using zinc as the dopant for the p^{++}-regions and either Se or Si as the dopant for the n^{++}-regions. Growth temperatures between 600-700 °C have been investigated and are compatible with the inverted-growth scheme.

At a growth temperature of 700 °C using a "cycled" growth for the Zn doped p^{++}-GaAs layer, both the conductance and the peak-current of the tunnel diode has been increased by a factor of $\sim$ 65 compared to a tunnel junction with continuous growth for the Zn-doped layer [2]. The conductance of the tunnel diode with cycled growth is apparently maximized at a growth temperature of 650 °C as shown in Table 2. The conductance of the best GaAs tunnel diode is comparable to the reported best values obtained by MBE. Cycled growths for the regions doped heavily with Se are found detrimental for the tunnel-diode performance, manifested by a reduction in conductance of more than two orders of magnitude. However, cycled growth for the n^{+}-GaAs region with Si-doping does not lower the conductance. The OMVPE cycled-growth process and the reasons for the improvement in conductance of the cycled-grown GaAs tunnel junctions are discussed elsewhere [6].

EUTECTIC METAL BONDING AND Ge SUBSTRATE REMOVAL

The inverted growth of $Al_{0.37}Ga_{0.63}As$/GaAs cascade obviously requires the removal of the parent substrate for front-side illumination. Therefore, bonding the thin-film cascade onto a secondary carrier substrate is necessary . The secondary substrate, ideally, should be cheap, rugged, and have good thermal and electrical conduction (if

necessary). Also, the AlGaAs-GaAs thin films should be bonded onto these carrier substrates with very little stress. The stress can interfere with subsequent cell processing.

We have been able to obtain photovoltaic-device-quality GaAs-AlGaAs thin films bonded onto Si substrates, using an approach denoted as eutectic-metal-bonding (EMB). The Si substrate effectively meets the above discussed requirements for the carrier-substrate. EMB involves the growth of GaAs-AlGaAs films (device structures) on lattice-matched Ge substrates. Following this, a film of gold is evaporated onto the face of the epitaxial structure, and a clean Si substrate. The two metal-coated samples are stacked face-to-face in an alloying furnace in intimate physical contact and bonded at $\sim$ 430 °C. The bonding of the GaAs-AlGaAs structure to Si substrate occurs by the formation of low-temperature eutectics of Au-Si and Au-GaAs, as indicated schematically in Fig. 1. The wafer after this step is ready for Ge substrate removal [3].

The material quality of the EMB GaAs-AlGaAs thin films on Si substrates were studied by 300K photoluminescence (PL), transient PL decay for minority carrier lifetime and Raman spectroscopy for the amount of strain in layers. The high quality of the EMB GaAs thin films, using a buffer to control Ge autodoping and subsequently removing the buffer, is evidenced by the demonstration of a minority-carrier lifetime of 103 ns on a EMB GaAs-AlGaAs DH structure (Fig. 2). This is the highest reported lifetime for any freestanding GaAs thin film. Also, the determination of residual elastic strain from Raman spectroscopy indicates that the EMB thin films on Si are strain-free [4].

INVERTED-GROWN GaAs THIN FILM SOLAR CELLS

To demonstrate the feasibility of inverted growth and the associated cell emitter-grid processing in EMB GaAs-AlGaAs thin films on Si (after Ge substrate removal), we present here results on thin film GaAs solar cells. Similar development of inverted-grown AlGaAs/GaAs cascade cells is under investigation.

The use of a 3.5 μm-thick GaAs buffer to reduce Ge autodoping was found to increase the V_{oc} values of thin film GaAs cells from 0.84 V to about 0.94 V under AM0 illumination. Also, the use of buffers was found to be important for improving cell fill factors. The Au-coating (for EMB) on the backside of the thin-film cell has been shown to be a good reflector for incorporating photon-recycling effects. This was evident in the excellent J_{sc} values in the GaAs thin film cells, which are by no means optimized. I-V data for 1-sun AM0 and AM1.5D spectra on our best thin-film GaAs cells are shown in Figure 3a and 3b. The efficiency of these cells are limited by series resistance associated with the non-alloyed contact to the n^+-emitter. The emitter contacts are not alloyed because of the thin-film structure. It is worth noting that Ti/Au metallization has been shown to form low-specific-resistivity non-alloyed ohmic contacts to p^+-GaAs, and therefore, we are investigating the possibility of p^+-n GaAs thin film solar cell structures.

SUMMARY AND CONCLUSIONS

In summary, we have provided the first demonstration of an inverted-grown, thin film, fully processed GaAs solar cell. AM1.5 cell efficiency of $\sim$ 19.2% and AM0 efficiency of $\sim$ 18% for a thin film GaAs cell have been obtained. This suggests that the inverted-growth approach to high-efficiency $Al_{0.37}Ga_{0.63}As$/GaAs cascades is realistically feasible in the near-term. Also, the inverted growth can offer a significant degree of freedom for the complete optimization of many multijunction cascade solar cells. The EMB of GaAs-AlGaAs thin films onto Si substrates, followed by rapid, selective plasma-etch of Ge parent-substrates, was described. This thin-film approach has allowed us to demonstrate a minority-carrier lifetime of 103 ns, the highest for a free-standing GaAs thin film. The development of high-quality $Al_{0.37}Ga_{0.63}As$ top cells and high-conductance GaAs tunnel junctions, discussed here, should enable us to demonstrate resonably high-efficiency inverted-grown AlGaAs/GaAs cascade cells.

In conclusion, the inverted-growth approach also offers other advantages. The Ge substrate removal from the AlGaAs/GaAs cascades, which is a highly production-compatible process, as part of the device fabrication sequence enables a high transmission of photons with energies below the GaAs bandgap. This IR transmission can be used to mechanically stack a moderately high-efficiency Si cell. The EMB scheme described in this effort, can be modified to produce a 3-junction, 2-terminal, current-matched (at AM1.5), monolithic $Al_{0.37}Ga_{0.63}As$/GaAs/Si cascade. Efficiency under concentration for such a cascade, is projected to approach near 40%. Notably, this approach will involve rather inexpensive Si cells, and the OMVPE growth of III-V cascades on potentially cheaper, large-area Ge substrates.

PUBLICATIONS

This NREL-funded research has resulted in the following publications over the past year:

1. R. Venkatasubramanian, M.L. Timmons, T.S. Colpitts and J.S. Hills, Solar Cells, 30, 345 (1991).
2. R. Venkatasubramanian, M.L. Timmons, and T.S. Colpitts, "High Conductance GaAs Tunnel Diodes by OMVPE", Proc. of MRS Symposium on Atomic Layer Growth and Processing, April 1991, Anaheim, CA.
3. R. Venkatasubramanian, M.L. Timmons, and T.S. Colpitts, Appl. Phys. Lett., 59, (1991).
4. R. Venkatasubramanian, M.L. Timmons, T.P. Humphreys, B.M. Keyes, and R.K. Ahrenkiel, "High-Quality Eutectic-Metal-Bonded GaAs-AlGaAs Thin Films on Si Substrates", Accepted for Publication in Appl. Phys. Lett., Dec. 1991.

5. R. Venkatasubramanian, M.L. Timmons, T.S. Colpitts, J.S. Hills, and J.A. Hutchby, "An Inverted-Growth Approach to Development of an IR-Transparent, High-Effficiency, AlGaAs/GaAs Cascade Solar Cell", Proc. of 22nd IEEE Photovoltaic Specialists Conf., Las Vegas, Oct. 1991, in press.

6. R. Venkatasubramanian, M.L. Timmons, T.S. Colpitts, and S. Asher, "Properties and Use of "Cycled" OMVPE GaAs:Zn, GaAs:Si, and GaAs:Se Layers for High-Conductance GaAs Tunnel Junctions", Submitted to Jour. Electronic Materials, Nov. 1991.

Table 1. Effect of surface-passivation and emitter parameters on efficiency of $Al_{0.37}Ga_{0.63}As$ cells.

Sample Number	Emmiter Thickness (μm)	Doping Level in Emitter (cm^{-3})	Multi-Layer Buffer	H_2Se on During Ramp to Window-Growth	1-Sun AM1.5G η(%)
1	0.4	7×10^{17}	No	No	4.2
2	0.2	7×10^{17}	No	No	6.2
3	0.2	7×10^{17}	No	Yes	8.7
4	0.2	7×10^{17}	No	Yes	9.3
5	0.2	7×10^{17}	No	Yes	10.0
6	0.2	7×10^{17}	Yes	Yes	10.8
7	0.2	4×10^{17}	Yes	Yes	13.7

Table 2. Peak tunnel current density of GaAs tunnel junctions at different growth temperatures using continuous and cycled growths for GaAs:Zn.

Growth Temperature ($^\circ$c)	Jp of Tunnel Diode (mA/cm^2) Se:GaAs Continuous	
	Zn: Continuous	Zn: Cycled
700	47	3000
650	256	12800*

* Specific resistivity of 3.3×10^{-3} ohm - cm^2

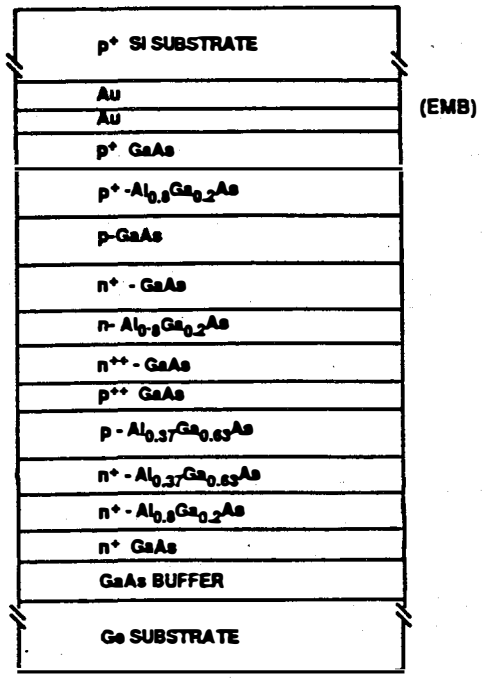

Fig. 1 Schematic of an inverted grown AlGaAs/GaAs cascade with a planar GaAs tunnel junction eutectic-metal-bonded to Si.

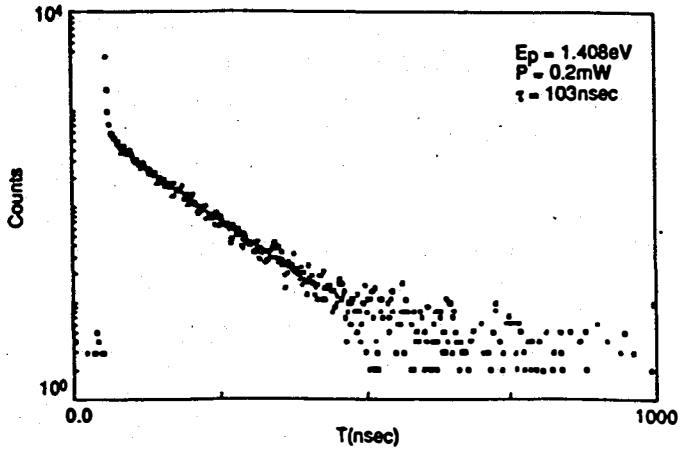

Fig. 2 300K PL-decay of an EMB GaAs AlGaAs DH structure on Si.

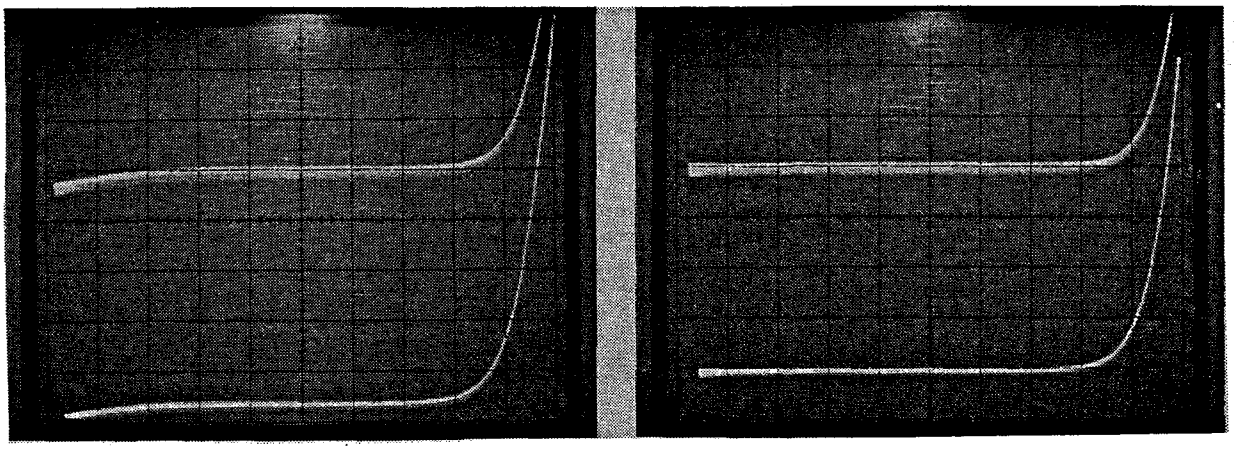

AM0 (XT-10)
V_{oc} = 0.94 V
Active-area J_{sc} = 36 mA/cm^2
FF = 0.72
Active-area Eff. = 18.0%

AM 1.5D
V_{oc} = 0.92 V
Active-area J_{sc} = 28.2 mA/cm^2
FF = 0.74
Active-area Eff. = 19.2%

Fig. 3 a) 1-sun AM0 and b) AM1.5D* solar cell data on a thin film GaAs cell. *Dr. Keith Emery, NREL, Golden, CO, has measured total-area J_{sc} of 20.4 mA/cm^2 in similar, but unoptimized, thin-film GaAs solar cell.

7.0 UNIVERSITY PARTICIPATION PROGRAM

John Benner (Manager)

The objective of this program is to maximize the contribution of universities to the future of photovoltaic (PV) technology by focusing on the traditional needs and strengths of the PV community. Thus, it provides a forum in which the university researchers identify research topics critical to the advancement of PV technology with minimal influence from current programmatic interests. The selected participants are then permitted to pursue the proposed basic and applied research ideas in an environment designed to foster creativity by limiting requirements for delivery of reports, samples and achievement of specific goals. Reporting is limited to annual reports and journal publications. Research Symposia organized by the participants, are held periodically and are open to all students, program participants, and outside researchers. The intent of the initiative is to provide continuity of funding over a minimum three-year period which will allow universities to build and support interdisciplinary teams with specialized expertise which can be applied to furthering the technology base of PV. Such a program is expected to attract the most highly qualified university research teams to the DOE National Photovoltaics Program. The University Participation Program also supports PV industry through the technology transfer which occurs not only by publication of research results in the technical literature, but also through enhanced student awareness of PV technology and education of future professionals.

Title: **New Approaches for High Efficiency Solar Cell**

Organization: Electrical and Computer Engineering Department
North Carolina State University
Raleigh, North Carolina

Contributors: S. M. Bedair and N. A. El-Masry

Objective

The objective of this research program is to address current problems that are hindering progress toward achieving high efficiency cascade solar cell. During the last year our efforts were directed towards the construction of new ALE reactor (production type) that can handle 3, two inch wafers and its use to grow device quality GaAs and AlGaAs. We have also used the ALE approach to achieve carbon doping up to $10^{20}/cm^3$ resulting from the cracking of the TMGa precursors.

A) Atomic layer epitaxy reactor design

A reactor was constructed and was specially designed for ALE growth. The design of this reactor includes two key features: the rapid changing of gases over the substrate and minimal heating of the thermal boundary layer. These two attributes are critical since they determine the maximum temperature at which the ALE process can be effectively used. Rapid switching is necessary because the self-limiting reaction is not stable for long exposure times at high growth temperatures. Rapid alternating gas exposure has been easier to achieve by moving the substrate rather than switching the gas streams as in the vent-run approach. The present reactor design takes advantage of these two concepts, gases are injected with a fairly high speed and the substrate is moved between streams of AsH_3 and trimethylgallium (TMG). The increased gas velocity is achieved by using a small injector aperture and a low reactor pressure. The reactor used is an in house modified Emcore 3200 system operating at 30 Torr. It is designed to operate with the sequential exposure of the substrate to the TMG, H_2, AsH_3, and H_2 gas streams for one complete ALE rotation cycle. The modification necessary to permit this mode of operation, consists of extra injector tubes to purge hydrogen between the TMG and AsH_3 exposures. Also, the reactor chamber is partitioned into six compartments to separate further the reactive gases and also to assist in shearing off the boundary layer. The chamber is divided by 0.010 inch molybdenum sheets (baffles). A topview schematic diagram of the chamber is shown in Fig. 1. Since the surface saturates at one monolayer in ALE conditions, the care needed in tailoring the gas flow dynamics in the conventional metal-organic CVD mode of operation is not necessary. The reactor is capable of growing up to three 2 inch diameter wafers, with a growth rate as high as 0.6 $\mu m\ h^{-1}$. The design does not impose any limitations on

the number and size of wafers and can thus be scaled up to meet large-scale production requirements.

B. Atomic layer epitaxy of GaAs and AlGaAs

The ALE reactor was used for the growth of GaAs with controlled background carbon concentrations in the range 10^{15}-10^{19} cm^{-3}. This was achieved by varying the growth conditions such as the growth temperature, exposure time and reactant flux. SiH_4 was used as the n-type dopant, and carrier concentrations in the range 10^{16}-10^{18} cm^{-3} was achieved.

ALE of $Al_xGa_{1-x}As(0<x<0.4)$ was achieved in the temperature range 550-700°C. A monolayer of AlGaAs was grown per cycle over a fairly narrow range of total column III flux (trimethylaluminum ((TMAI) + TMG). The composition of the AlGaAs films is characterized by 77 K photoluminescence and the background carrier concentration was obtained from Hall measurements. One of the problems we faced in the ALE growth of AlGaAs was the high carbon background doping, probably due to the strong Al-C bond. The background carbon can be reduced by increasing the growth temperature and the V:III ratio. Table 1 summarizes the dependence of the background carbon in ALE growth of $Al_{0.3}Ga_{0.7}As$ on the growth conditions. An order of magnitude reduction in carbon concentration was observed by increasing the growth temperature from 650 to 700°C. Also, a reduction in the value of the total column III flux (TMAI + TMG while maintaining an ALE monolayer growth, resulted in a substantial reduction in carbon doping. The best n-type film had a carrier concentration of $n = 1.6 \times 10^{16}$ cm^{-3} and a room temperature mobility of 2500 $cm^2V^{-1}s^{-1}$ for a film about 1 μm thick. The AlGaAs film could then be doped n-type using silane which was introduced with the AsH_3 flux. N-type films with carrier concentrations in the range 10^{17} - 10^{18} cm^{-3} were achieved. These films showed good optical properties as indicated from photoluminescence measurements and are at least comparable with metal-organic CVD films. Thus, ALE is a suitable candidate for low temperature growth of the top cell in the AlGaAs/GaAs multijunction solar cell structure with silicon and carbon as the n- and p-type dopants respectively.

C) Carbon doping

Carbon is an attractive alternative to the p-type impurities used conventionally in metal-organic CVD such as magnesium and zinc and those used in MBE such as beryllium when high concentrations are desirable. Carbon is a relatively shallow dopant in GaAs and AlGaAs, with ionization energy levels of about 26 meV and 40 meV respectively. Also, carbon has a lower diffusion coefficient in GaAs than the other potential p-type dopants and thus carbon represents the ideal dopant for the heavily doped p^+ layer of the interconnecting junction in the multijunction structures. Also, carbon can be used as a dopant for the contracting layers, thus reducing parasitic and contract resistance. Several approaches

have been employed to achieve high levels of carbon doping in GaAs. They include the use of TMG in metal-organic MBE, trimethylarsenide in metal-organic MOCVD and CCl_4 as an intentional dopant. Recently, CCl_4 has also been used for carbon doping of AlGaAs.

We have found that carbon incorporation in GaAs can be increased by the following: (1) increasing the TMG flux and its exposure time; (2) decreasing the AsH_3 flux and its exposure time; (3) reducing the growth temperature. The same trends are also true for the growth of AlGaAs and here a carrier concentration of about 10^{20} cm^{-3} was achieved. This very high level of p-type doping of GaAs and AlGaAs is attractive for the interconnecting tunnel junction achieved by controlling the above parameters. The mechanism of carbon incorporation can be outlined according to the following process.

Carbon doping of GaAs and AlGaAs by ALE is a direct result of the exposure to TMG or (TMG + TMAl) in the absence of AsH_3 during the ALE cycle. Thus, reaction products such as CH_3 radicals resulting from the cracking of metal-organic molecules are assumed to be adsorbed on the GaAs surface. These CH_3 radicals originating from the gas phase are products of TMG heterogeneous decomposition onto the GaAs surface or homogeneous decomposition in the gas phase. These hydrocarbons are also present in the metal-organic CVD growth of GaAs but the simultaneous presence of atomic hydrogen due to the decomposition of AsH_3 allows the formation of CH_4 and subsequent desorption. In ALE the same process may take place, but with reduced efficiency owing to the time delay between TMG and AsH_3 exposures. The background carbon levels in ALE GaAs film are always higher than those achieved by metal-organic CVD. This may be due to an exchange interaction between the carbon atoms on the surface and the arsenic atoms in the lattice. Once the carbon atoms occupy sites in the bulk lattice, they cannot be easily removed. The probability of such exchange interaction will be enhanced by the time delay between TMG and AsH_3 exposures. Also, the strong Al-C bond for the ALE growth of AlGaAs can impede the desorption of CH_3 and the formation of CH_4 during AsH_3 exposure. These effects can be compensated for by increasing the AsH_3 flux as shown in Fig. 2. More work is needed to optimize the growth conditions of AlGaAs.

D. Conclusion

ALE is a potentially useful technique for the growth of multijunction solar cells. ALE was used to grow device quality GaAs and AlGaAs in a newly designed reactor. Carbon as a p-type dopant can be effectively used for high level doping using the ALE approach. Device quality GaAs and $Al_xGa_{1-x}As$ films were grown with p-type background carbon doping in the ranges 10^{15}-10^{20} cm^{-3} and 10^{16}-10^{20} cm^{-3} respectively. The potential applications of the ALE technique in the photovoltaic field was discussed.

Table 1: Dependence of background doping of $Al_{0.3}Ga_{0.7}As$ on growth conditions

Run #	Growth Temp.C°	V/III	AsH_3 exposure (sec/cycle)	TMG exposure (sec/cycle)	n/p per cm^3	μ cm^2/V sec	ML/ Cycle
E-72	580	161	0.4	0.4	$P=4.68*10^{18}$	77	1.6
E-105	580	227	0.4	0.4	$P=1.5*10^{18}$	91	1.4
E-197	650	232	0.53	0.26	$P=3*10^{16}$	200	0.6
E-203	650	95	0.53	0.26	$P=1.2*10^{19}$	105	1.8
E-222	700	300	0.6	0.26	$N=1.6*10^{16}$	2500	1
E-223	700	150	0.6	0.26	$P=8.3*10^{16}$	109	1
E-223	650	300	0.6	0.26	high resistivity	-	1
E-233	650	150	0.53	0.26	$P=9.9*10^{17}$	103	1
E-262	650		0.53	0.26	$P=0.8 \times 10^{20}$	47	1

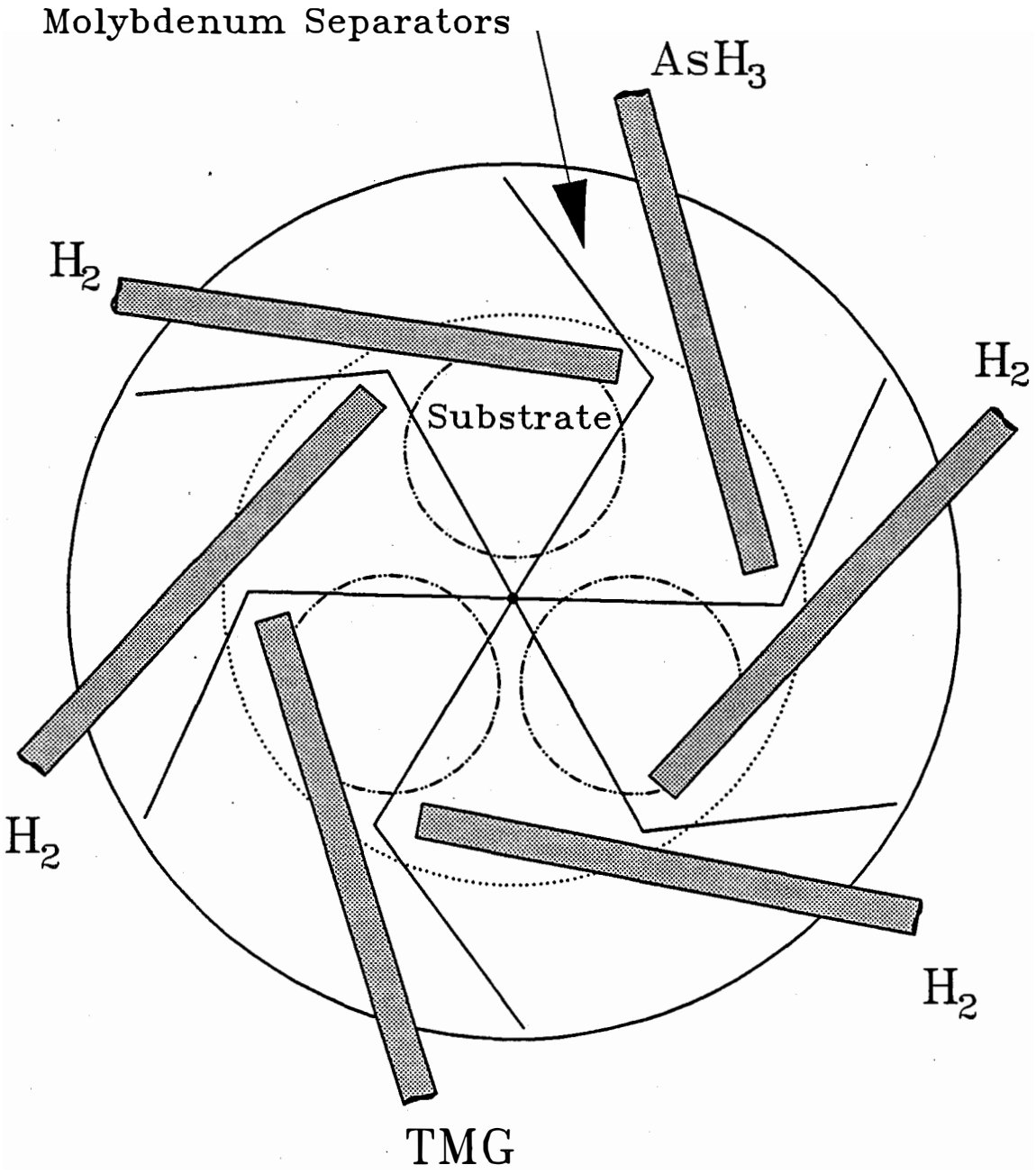

Figure 1: Schematic of the growth chamber

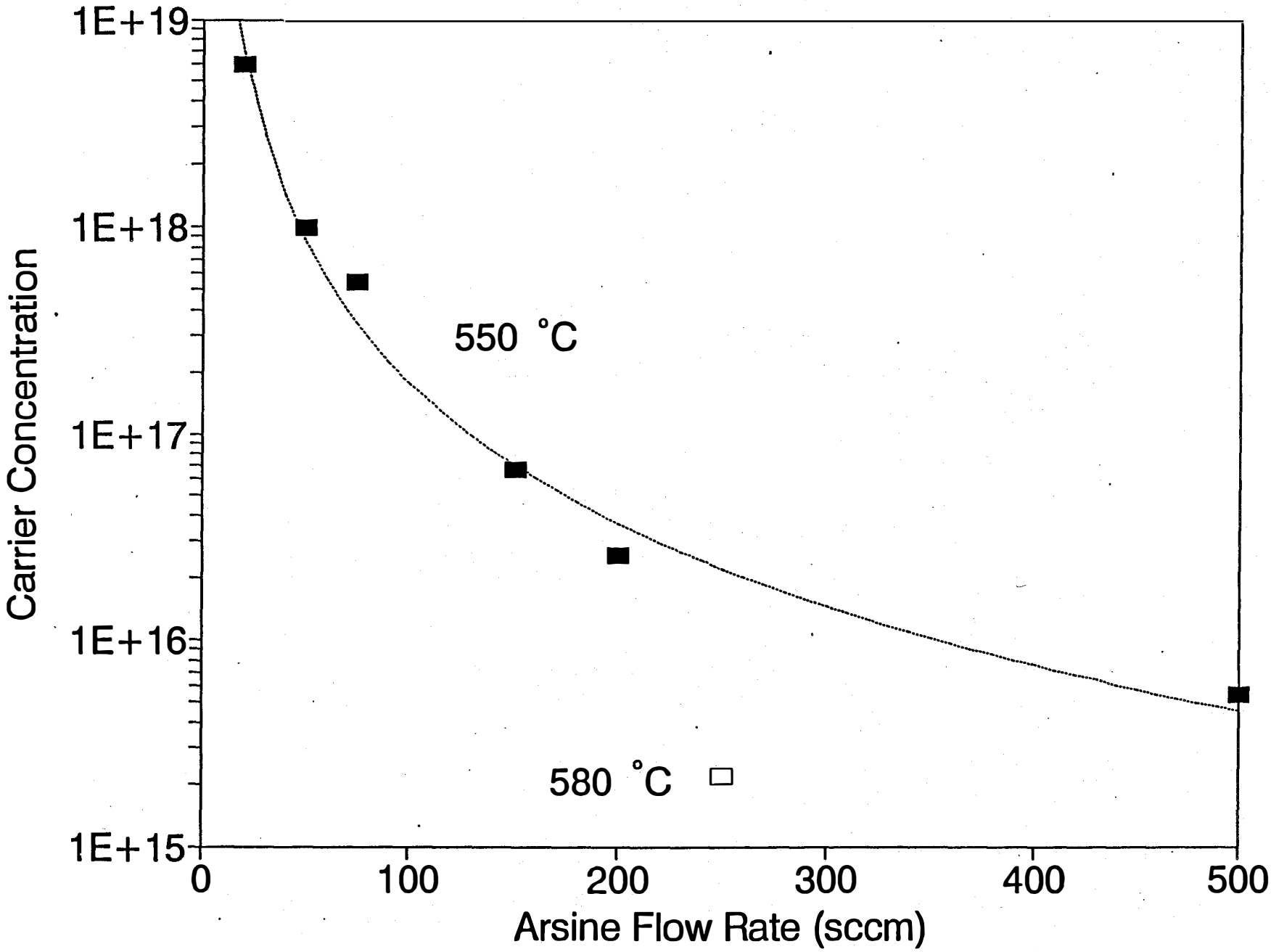

Figure 2: Carbon incorporation vs AsH_3 flux. High resistivity films were obtained at 580°C for an AsH_3 flow of 500 sccm.

Title: **Photon and Ion Assisted Doping and Growth of II-VI Compound Thin Films**

Organization: Department of Materials Science and Engineering,
Stanford University, Stanford, CA 94305-2205

Contributors: R.H.Bube (Principal Investigator), A. L. Fahrenbruch, G. Jensen
D. Kim, J. Mößlein, and A. Lopez-Otero

This is an investigation of the doping and growth of II-VI compound films, especially p-CdTe, by physical vapor deposition with co-evaporation of the dopant. Dopant incorporation by (a) photon-assisted doping (PAD) and (b) ion-assisted doping (IAD), are compared with respect to the growth, structural, and photoelectronic properties of the deposited films.

Methods of Approach

Control of p-type doping in polycrystalline CdTe solar cells is a promising tool for minimizing series resistance loss and maximizing V_{oc} [1]. Our previous work, using IAD [2-7], focused on incorporation of the dopants and yielded carrier densities up to 2×10^{17} cm^{-3} in homoepitaxial films with P as a dopant, but gave films with low minority carrier diffusion length (L_d) (Fig. 1). We have investigated PAD as a gentler alternative that would enable doping, and also yield good L_d [8].

Schetzina *et al.* [9-10] and his students (some of whom have continued to study PAD at other research groups) [11, 12, 13, 14] reported PAD doping of CdTe epitaxial films deposited by MBE to levels up to $p = 6 \times 10^{18}$ cm^{-3} with As. These films also had good crystalline quality, as evidenced by photoluminescence (PL), double-crystal rocking curves (DCRC), and carrier mobility data. Although their data suggest long L_d, it was not measured.

Other workers [15, 16, 17, 18], including ourselves, have not been able to reproduce the PAD results of Schetzina *et al.* However, there is consensus among most, if not all researchers, that illumination during deposition enhances crystalline quality. And, there is also a consensus that using excess Cd flux during deposition increases both doping and crystalline quality. For example, Arias *et al.* [15] found that illumination had little or no effect on doping, but that a Cd/Te flux ratio = 1.1–1.3 was necessary to incorporate and electrically activate As during the MBE growth of p-CdTe—regardless of whether the sample was illuminated or not.

Fig. 1 is is a schematic of our deposition system. Characterization methods include measurements of resistivity, carrier density (by $1/C^2$ vs V), and analysis of In Schottky barriers on the films. SIMS, x ray diffraction rocking curves, and photoluminescence measurements have also been made.

Significant Results

We have grown more than 200 homoepitaxial films using various combinations of illumination (0–100 mW/cm^2), Cd/Te flux ratio (1.0–2.2), dopants (Sb, P, As with $P_{As} = 6 \times 10^{-6}$ to 0.2 Torr, and un-doped), and substrate temperature (140–180°C). (In some cases these parameters were the same as those of Schetzina *et al.* and Arias *et al.*, except for vacuum level.) Using these parameters, we have been unable to reproduce the reported PAD results of Schetzina *et al.* [9–12]. Most of our PAD films appear to be semi-insulating, and, although some films showed measurable conductivity, the effect is modest, and there appears to be little or no correlation between illumination and doping.

However, the use of a Cd/Te flux ratio > 1 shows a strong effect on the electrical properties of In/p-CdTe Schottky diodes (Table 1 and Figs. 3), whether light and/or the dopant (As) are/is present or not. Data are presented in Fig. 4 showing the effects of variation of the growth

parameters on the characteristics of In Schottky barriers on the films. The values of the reverse bias current J(-3V) are assumed to correlate inversely with the crystalline quality (in this case through the density of recombination centers) since the reverse bias current transport is due to recombination in the depletion layer for these devices. The high forward bias voltage current J(+2V) is a measure of the resistivity of the layers.

Proceeding on the assumption that a chemically active As monomer is needed to dope the CdTe we also tried Cd_3As_2 as a dopant source. Preliminary results are very promising, showing hole densities up to $2.5 \times 10^{16}\ cm^{-3}$.

Conclusions and Future Work

We conclude that illumination does not enhance co-evaporation doping, at least under our deposition conditions. However the use of Cd/Te flux ratios > 1 is promising, judging from the large increase in the rectification ratio we observed for In Schottky barriers on the films, and the consensus of results of other workers. The IAD approach remains a fertile ground for research, particularly using Cd/Te flux ratios >1.

We are refocusing our research on two areas. The first is a continuation of the IAD work to include:

(i) The effects of Cd/Te flux ratios > 1 during IAD film growth on doping, self-compensation, crystalline quality, and, especially, L_d.
(ii) N as a dopant.
(iii) Use of un-ionized Cd_3As_2 as a dopant source.
(iv) Post-growth annealing the films in Cd vapor to anneal out ion damage, if present, and to drive the stoichiometry to Cd-rich to determine whether the L_d of IAD samples can be improved.
(v) Extension to polycrystalline thin films.

The second area is the investigation of single-crystal and polycrystalline ZnTe films, grown by CSVT, for low-resistance Ohmic contacts to p-CdTe and as an active component in tandem cells.

Our ultimate goal is to test the most promising technique(s) from the studies above on CdS/CdTe(/ZnTe) heterojunction solar cells based on these IAD doped single-crystal and polycrystalline CdTe films.

References

1. C.M. Fortmann, A.L. Fahrenbruch, and R.H. Bube, J. Appl. Phys. **61**, 2038 (1987).
2. A. Fahrenbruch, A. Lopez-Otero, P. Sharps, and R.H. Bube, Proc. 19th IEEE Photovoltaic Spec. Conf. (1987) p. 1309.
3. P. Sharps, A. Fahrenbruch, A. Lopez-Otero, and R.H. Bube, Proc. 20th IEEE Photovoltaic Spec. Conf. (1988).
4. A.L. Fahrenbruch, K-F. Chien, D. Kim, A. Lopez-Otero, P. Sharps, and R.H. Bube, Solar Cells **27**, 137 (1989).
5. P. Sharps, A. Fahrenbruch, A. Lopez-Otero, and R. H. Bube, Proc. 21st IEEE Photovoltaic Spec. Conf. (1990), p. 493.
6. SERI Final Report, "Ion-Assisted Doping of II-VI Compounds During Physical Vapor Deposition," 9/1/85 to 8/30/89, dated 6/12/90.
7. P. Sharps, A.L. Fahrenbruch, A. Lopez-Otero, and R.H. Bube, J. Appl. Phys. **68**, 6409, 1990.
8. R.H. Bube "Photon and Ion Assisted doping and growth of II-VI Compound Thin Films," NREL Annual Reports I and II, NREL Subcont. XM-0-181-4, 7/1/89-6/31/90 and 7/1/90-6/31/91.

9. R.N. Bicknell, N.C. Giles, and J.F. Schetzina and C. Hitzman, J. Vac. Sci. Technol., **A5**, 3059 (1987).
10. R.L. Harper Jr., S. Hwang, N.C. Giles, and J.F. Schetzina, D.L. Dreifus, and T.H. Myers, Appl. Phys. Lett., **54** (2), 170 (1989).
11. R.N. Bicknell-Tassius *et al.*, J. Cryst. Growth **101**, 33 (1990).
12. K.A. Harris, T.H. Myers, R.W. Yanka, L.M. Mohnkern, and N. Otsuka, Proc. 1990 U.S. Workshop on Phys. and Chem. of HgCdTe and Related II-VI Compounds,J. Vac. Sci. Technol. **B9**, 1752 (1991).
13. Y. S. Wu, et al., J. Appl. Phys. **69**, 268 (1991).
14. K. A. Harris, et al., J. Vac. Sci. Technol. **B9**, 1752 (1991).
15. J.M. Arias et al., Proc. 1989 U.S. Workshop on Phys. and Chem. of HgCdTe and Related II-VI Compounds, 1025 (1989). Also J. Vac. Sci. Technol. **A8**, 1025 (1990).
16. J. Arias, et al., J. Appl. Phys. **69**, 2143 (1991).
17. A. N. Tiwari, et al., J. Cryst. Growth **111**, 730 (1991).
18. C.J. Summers, private communication, 1990 MRS Workshop on Phys. and Chem. of HgCdTe and Related II-IV Compounds, October,1990, San Francisco.

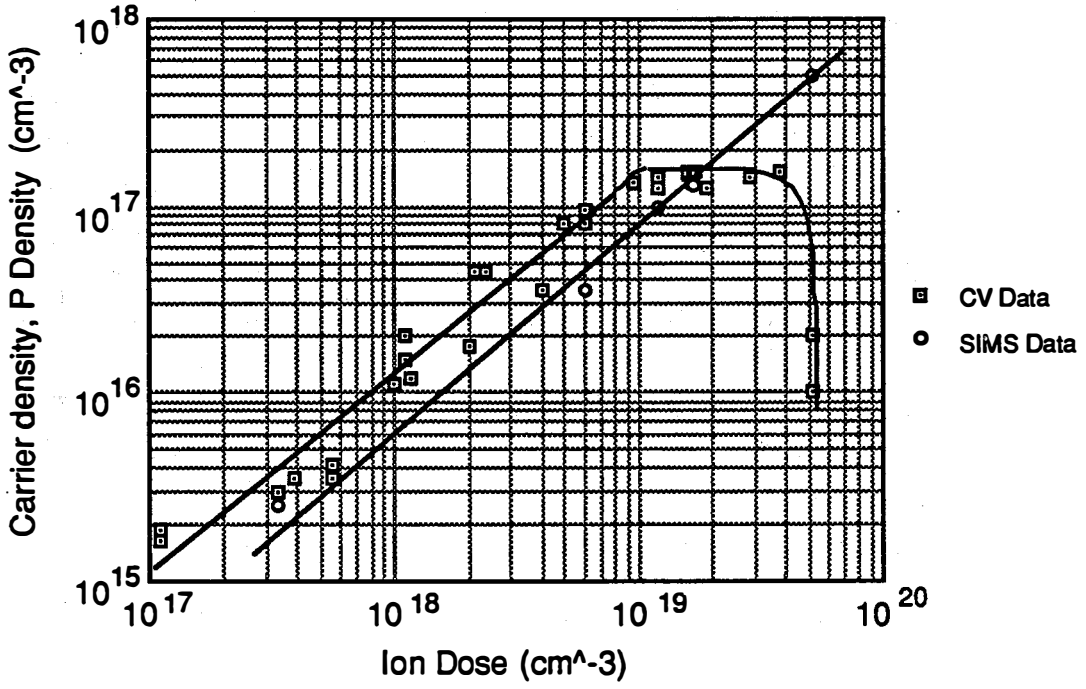

Fig. 1. Carrier density and P density (measured by SIMS) vs. ion dose. Ion dose is the density of P that would be in the layer if all the incident ions were incorporated. Ion energy = 60 eV, T_{sub} = 400°C, growth rate = 10 μm/hr, and film thickness ≈ 10 μm.

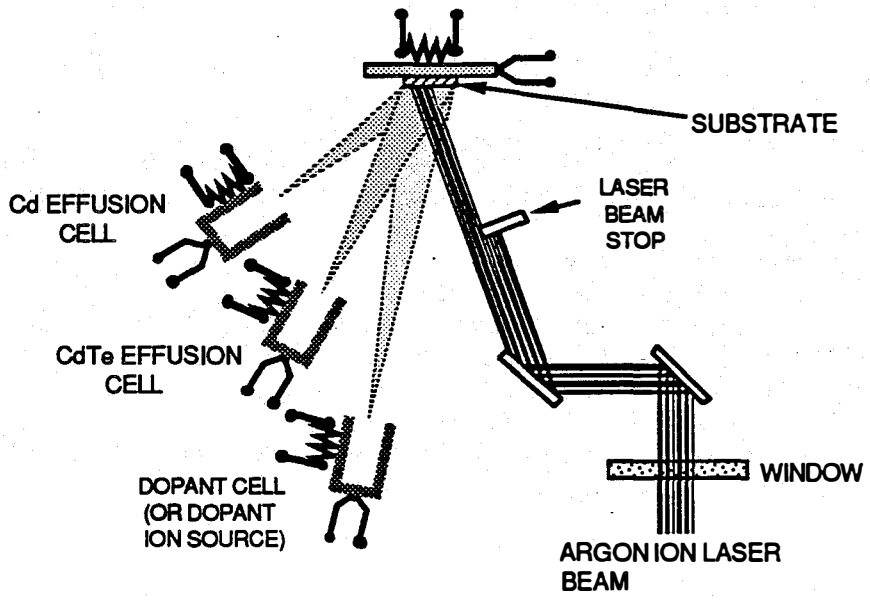

Fig. 2. The experimental setup is capable of deposition in both the IAD and/or PAD modes. Laser beam intensity (blue-green) at substrate is typically 50–100 mW/cm^2.. Depositions are typically homoepitaxial films ≈ 10 μm thick on (100) single crystal p-CdTe substrates.

Table 1. A set of samples showing the effect of illumination, extra Cd flux, and doping on the current densities of In Schottky barriers, used to plot Fig. 3. The table also lists the current densities on these samples after ≈ 2 months storage in the dark at room temperature, as discussed below. Generally, the current densities changed with time so as to reduce the rectification ratio, J_{+2V} / J_{-3V}. $T_s = 180°C$.

		BEFORE and		AFTER DARK STORAGE		BEFORE	AFTER	AFTER/BEFORE	
SAMPLE Ph-	VARIABLE CODE	J(+2V) 10^{-5} A/cm^2	J(-3V) 10^{-5} A/cm^2	J(+2V) 10^{-5} A/cm^2	J(-3V) 10^{-5} A/cm^2	RECTIFICATION RATIO		J(+2V)	J(-3V)
1	D O O	6.1	9.70	5.2	7.50	0.63	0.69	0.85	0.77
2	D O L	2.6	4.00	2.5	3.40	0.65	0.74	0.96	0.85
13	D C L	22	0.07	0.9	0.46	314	1.93	0.04	6.57
16	D C O	1200	0.34	150	0.17	3529	882	0.13	0.50
17	O O O	110	2.10	100	2.00	52	50	0.91	0.95
18	O C O	610	13.0	12	0.14	47	86	0.02	0.01
19	O O L	2.5	1.90	2.6	1.70	1.32	1.53	1.04	0.89
20	O C L	190	0.34	7.1	1.70	559	4.18	0.04	5.00
14	D O L [1]	16000	67	16000	67	250	250	1.0	1.0
22	D O L [1]	190	0.3	700	2	667	350	3.5	6.7

[1] Samples 14 and 22 were grown with incident Cd_3P_2.

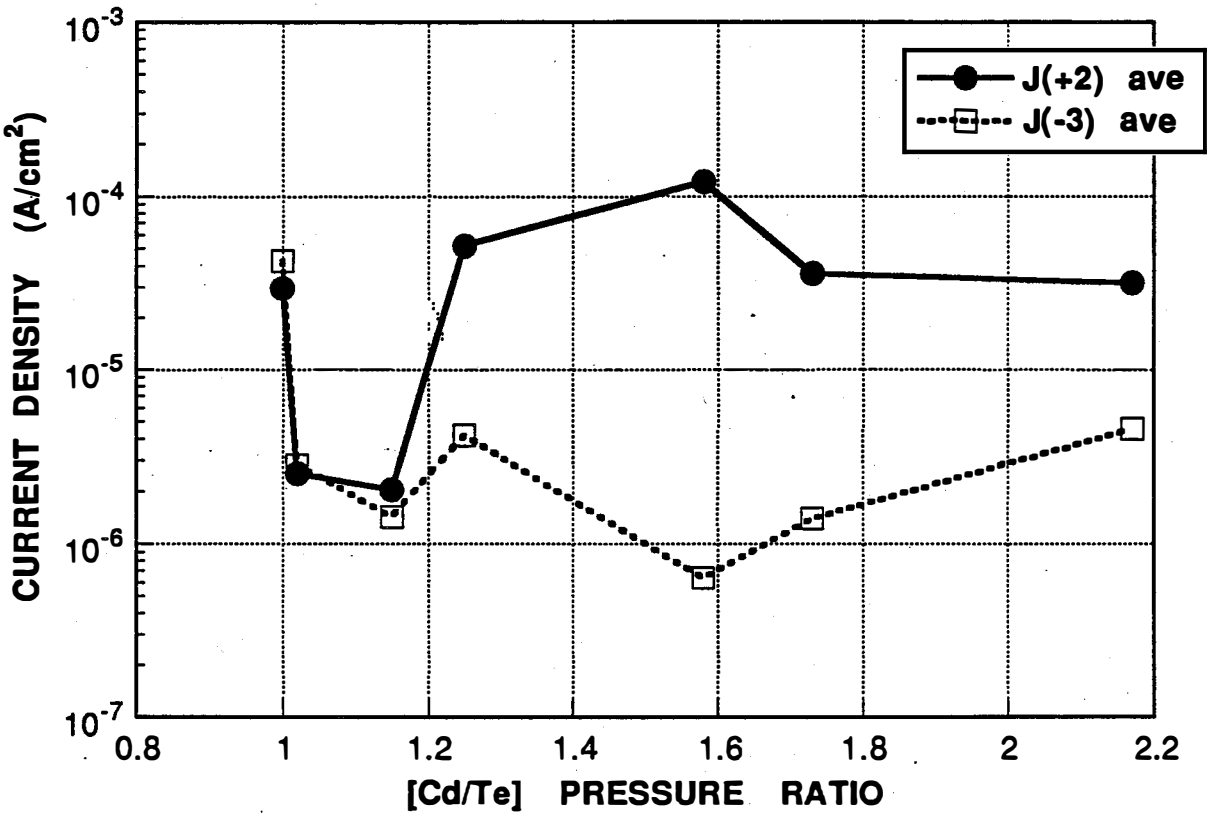

Fig. 3 In Schottky diode current density for +2 V forward bias, J_{+2V}, and -3 V reverse bias, J_{-3V}, as a function of the Cd/Te pressure ratio. Films were grown at 180°C with T_{As} = 200°C and illumination = 80 mW/cm^2. (Values are the average of small and large area contact values.)

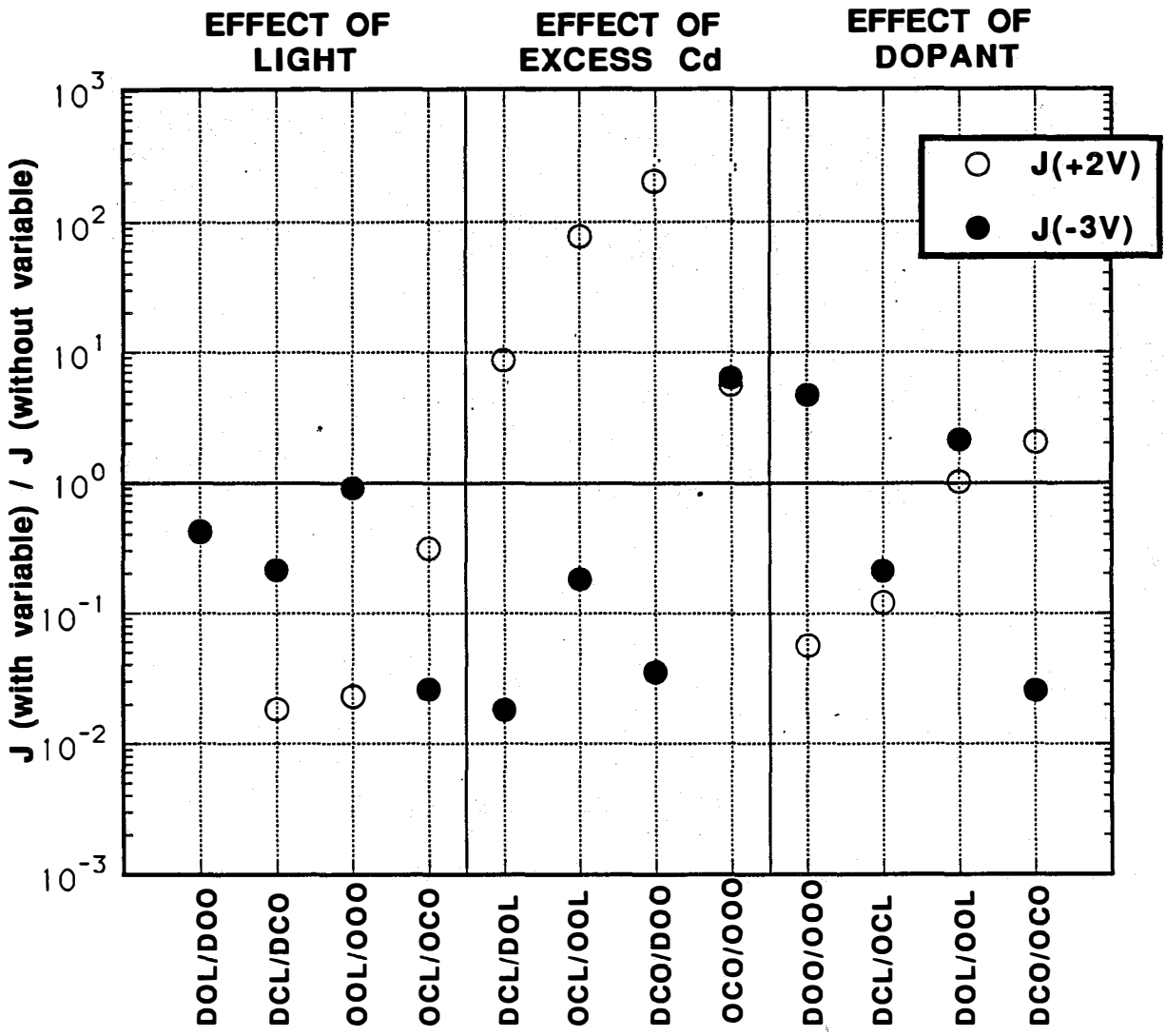

Fig. 4. In Schottky diode current densities J_{+2V} and J_{-3V} for different deposition variables, as abbreviated:

D Dopant
C Excess Cd flux
L Illumination
0 Without the variable in that position.

E.g., DLC means the dopant was present, illumination on, and with excess Cd, while DOC means the same conditions but without illumination. T_s = 180°C for all these depositions. The growth conditions of these samples are listed in Table 2 and the current density data and sample codes are listed in Table 3. The ratio 1.0 means that there is no effect of the particular growth parameter on current density.

Title:	**Electronic Processes in Thin Film PV Materials**
Organization:	Department of Physics, University of Utah, Salt Lake City, Utah
Contributors:	P.C. Taylor, principal investigator; G.A. Williams, W.D. Ohlsen, S. Gu, J.M. Viner, K. Gaughan, S. Hershgold, D. Chen, P. Hari

One important class of materials for PV conversion of solar energy is the group of thin film amorphous semiconductors based on hydrogenated amorphous silicon (a-Si:H). Important alloys include a-Si_xGe_{1-x}:H, a-Si_xC_{1-x}:H and a-Si_xN_{1-x}:H which are used to produce narrower gaps for tandem cells, and wider band gaps for top-surface p-layers, respectively. Also of interest are artificially layered structures, such as a-Si:H/a-Si_xC_{1-x}:H, where the individual layers may be only 10-1000 Å thick.

Defects and impurities in these films create enhanced densities of electronic states in the gap which are deleterious to the performance of PV devices. In addition, both the alloy systems and a-Si:H itself are plagued by electronically- and optically-induced metastabilities (Staebler-Wronski effect) and by metastable departures from equilibrium below a "freezing in" temperature. These metastabilities adversely affect device performance and make projections of useful device lifetimes difficult.

Objectives

The major objectives of this subcontract are (1) to grow and characterize high quality of a-Si:H and related alloys and multilayers using the glow discharge technique, (2) to characterize by optical and magnetic resonance techniques the roles of defects and impurities in amorphous tetrahedrally-coordinated thin films, (3) to determine the quality of the interfaces and junctions which occur in PV devices by employing surface-sensitive optical and magnetic resonance techniques, and (4) to understand the recombination-induced metastabilities (Staebler-Wronski effect) and the frozen-in departures from equilibrium (as mediated by hydrogen diffusion or defect motion) in amorphous tetrahedrally-coordinated thin films. Reviews of these major areas are available elsewhere.[1,2]

Discussion

Several techniques have been employed to accomplish these objectives. Samples are grown in a state-of-the-art glow discharge deposition system and characterized using infrared and Raman spectroscopy, electrical conductivity, electron microprobe, and photothermal deflection spectroscopy (PDS). Other important experimental techniques include nuclear magnetic resonance (NMR), electron spin resonance (ESR), various optical spectroscopies, and double spectroscopies such as optically detected magnetic resonance (ODMR). The subcontract is divided into seven tasks. The first task is the growth and characterization of doped and undoped a-Si:H and related alloys. We have continued our investigations of the use of a liquid organic

source, tertiarybutylphosphine or TBP, to produce n-type doping in a-Si:H.[3,4] The optical and electronic properties of TBP-doped a-Si:H are, in general, very similar to those obtained in phosphine-doped films.[4] Recently we have grown a-Si_xC_{1-x}:H alloys using two liquid organic sources, ditertiarybutylsilane (DTBS) and n-butylsilane (NBS). The band gaps and localized electronic states in the gap have been measured using photothermal deflection spectroscopy (PDS). Figure 1 shows typical data for the absorption coefficient α as a function of photon energy for a-Si_xC_{1-x}:H films produced from mixtures of DTBS and silane. The energy at $\alpha = 0^4$ cm^{-1} can be varied from 1.9 to 3.0 with the incorporation of DTBS during the deposition, but with small amounts of DTBS in the gas mixture the below gap absorption increases by about an order of magnitude over that which occurs in device quality a-Si:H.

Doping is also possible for films made with small admixtures of DTBS in silane[3], but the efficiencies fall rapidly with C incorporation in the films. This situation is demonstrated in Fig. 2 which shows the dark conductivity at 300 K as a function of the gaseous impurity ratio of TBP/SiH_4 with and without the incorporation of DTBS. Undoped samples employing concentrations of 10% DTBS in silane have conductivities on the order of 10^{-10} Ω^{-1} cm^{-1}; however, doping with 1% TBP in the 10% DTBS +90% silane mixture increases the conductivity to 3×10^{-6} Ω^{-1} cm^{-1}. The circles in Fig. 2 correspond to the same composition as the undoped sample designated as curve (c) in Fig. 1.

The second task concerns non-equilibrium phenomena in a-Si:H and related alloys. As part of the TBP doping studies we have examined the thermal stability of n-doped samples of a-Si:H by measuring the temperature dependence of the electrical conductivity as a function of the rates at which the samples are quenched from elevated temperatures (150 °C). A "kink" occurs in the semi-logarithmic plots of the conductivity at a "freeze-in" temperature where at least some of the electronic states in the system fall out of thermal equilibrium. Our measurements on P-doped samples of a-Si:H using both TBP and phosphine have shown that there are differences in the freeze-in temperatures depending on the dopant gas which is used. In particular, samples made with TBP appear to have lower freeze-in temperatures than comparable samples made with phosphine.[4] Recently, we have initiated studies of local diffusion of hydrogen in a-Si:H using NMR techniques. Initial studies are being performed on heavily B-doped a-Si:H where the macroscopic diffusion constants are known to be the greatest.

The third task involves the study of recombination-induced metastabilities in a-Si:H and related alloys. For some time we have used light-induced electron spin resonance (LESR) and below-gap optical absorption as measured by PDS to measure changes in the silicon "dangling bond" densities as a function of optical excitation. Recently we have employed photoluminescence absorption spectroscopy (PLAS) to measure light traveling down the length of a film in a waveguide mode. Details of the PLAS technique are available elsewhere.[5,6] As will be discussed below, the PLAS technique is sensitive to surface effects, so it is important to separate out the surface and bulk contributions. Changes in the below gap absorption have been examined for films of a-Si:H sandwiched between layers of SiO_x or SiN_x. In both cases the metastable increases in below gap absorption are found to be bulk, and not surface, effects.[5]

The investigation of interfacial effects in a-Si:H and related alloys constitutes the fourth task. In PLAS measurements of a-Si:H/SiN_x interfaces we have found a shoulder in the absorption

around 1.2 eV that is probably due to interface states.[6] A detailed interpretation of this feature in the absorption spectrum awaits further measurements.

Previous comparative studies of low-temperature (T ≈ 30 K) optically induced ESR using above gap red (633 nm) and below gap i.r. (1060 nm) light on a-Si:H have shown a suppression of transient optically produced holes with respect to electrons and neutral silicon dangling bonds.[7] These results have suggested the presence of a large density of filled D^- states near the substrate interface perhaps due to band bending. Recently, we have performed experiments as a function of film thickness confirm this interpretation.[8] Using films of 5, 10 and 15 μm thicknesses we have shown unambiguously that the asymmetries in the LESR signals scale with the number of interfaces to within +15%, but when considered as a bulk effect the results vary by more than a factor of three.

The fifth task concerns investigations of defects and impurities in a-Si:H and related alloys. We have been using excitation spectroscopy of PL (PLE), time resolved PL, and PLAS techniques to probe defects which produce absorption below the gap in a-Si:H.[5,9,10] Recently PLE and time resolved PL spectra at 77 K have been measured over the range 1.1 -1.7 eV using the Ti sapphire cw tunable laser as the excitation source.[9] The PLE spectra for PL measured at 1.0 eV and 0.9 eV follow the Urbach tail portion of the absorption. The below gap absorption contributes little to these PLE spectra. This fact means that the contribution to the PL at high energies may be primarily due to an excitation from a bandtail to a band edge followed by recombination between the band tails. On the other hand, the below-gap absorption does contribute to the PLE spectrum when the PL is measured at 0.8 eV. This behavior is consistent with a recombination of carriers through the defect states.

In addition, we have found that the lifetime of the PL decay becomes shorter when the excitation energy is below about 1.66 eV. We have measured the time resolved PL (TRPL) spectra for PL at energies at 1.3 eV, 1.2 eV, 1.1 eV, 1.0 eV, 0.9 eV and 0.8 eV excited at 1.657 eV. When the PL energy is decreased from 1.3 eV down to 0.9 eV, the decay of TRPL spectra becomes monotonically slower. This behavior is consistent with the well known fact that the peak of the PL spectra at high energies shifts to lower energies with time. At 0.8 eV the TRPL spectrum is close to TRPL at 1.3 eV at short times, but close to TRPL at 0.9 eV for longer times. The most reasonable explanation for this behavior is that the PL at 0.8 eV is composed of two recombination processes, i.e., (1) bandtail to bandtail and (2) bandtail to defect states.

We have also measured the PL spectra as a function of excitation energy from above the gap (1.96 eV) down to well below the gap (1.19 eV). In these spectra the peak of the high energy PL band shifts to lower energy when the excitation photon energy decreases. When the excitation energy falls below about 1.45 eV the defect-related PL at 0.8 eV becomes dominant.

In addition to these PLE studies, ^{1}H NMR has been employed to study the local environments of bonded hydrogen and trapped molecular hydrogen (H_2) in a-Si:H films deposited by rf sputtering.[11] All spectra exhibited both broad and narrow components in the ^{1}H NMR free induction decays, that are indicative of clustered and randomly distributed (dilute) hydrogen, respectively. The T_1 of both samples that exhibit long range H diffusion and those that do not exhibits a clear minimum at ≈ 30 K, indicative of relaxation by H_2 trapped in microvoids. After

annealing for 24 hours at 294°C, the ratio of broad-to-narrow components increases to > 10 in all samples, and the magnitudes of the T_1 minima increase to about 1 sec in all samples. This last fact is consistent with the diffusion of molecular hydrogen out of the sample on annealing. Studies of states in the gap constitute the sixth task of this subcontract. We have recently used several sub-gap spectroscopies to study the states in the gap in doped and undoped films of a-Si:H.[5,9] These measurements indicate a sharp rise in the absorption attributed to deep defects (silicon dangling bonds) near 1.3 eV at 77 K. This value is about 0.6 eV less than the value of the optical band gap, and the analog of this behavior has been observed in alloys by other workers.[12]

Task seven is the training of graduate students and postdoctoral research associates. Three students are currently being trained under partial support of this subcontract. In addition, one postdoctoral research associate is benefiting from training received under this program. We currently have active collaborative efforts with Solarex Corp., Xerox PARC, North Carolina State University, University of Delaware, Iowa State University, Gifu University, Kanazawa University and the University of Marburg. All of these institutions have provided well characterized samples to use for various research purposes.

Although they do not fall directly under any of the tasks of the present subcontract, we are continuing to pursue measurements of optical bistability in a-Si:H because of the potential of this material as a bistable optical switch.[13,14]

Conclusions

Major accomplishments of the previous year include (1) the growth of a-Si_xC_{1-x}:H alloys using liquid organic sources (DTBS and NBS) mixed with silane, (2) preliminary doping experiments on a-Si_xC_{1-x}:H films, (3) measurements of the freeze-in temperature in TBP-doped films of a-Si:H, (4) initial feasibility measurements of local diffusion of hydrogen in B-doped a-Si:H using NMR techniques, (5) measurement of optically induced absorption in a-Si:H using PLAS, (6) measurement of a distinct feature in the below-gap optical absorption that is attributable to Si/SiN_x interfaces, (7) confirmation of the role of interfacial regions in below-gap LESR experiments, and (8) the extension of PLE and time-resolved PL spectra in a-Si:H down to 1.1 eV. Future directions for the research include (1) growth of a-Si:H and related alloys using other less toxic, liquid organic sources, (2) continuation of below-gap spectroscopy of a-Si:H using PLE, time resolved PL and PLAS, (3) continuation of the measurements of local hydrogen diffusion in boron-doped a-Si:H using NMR techniques, (4) investigations of the optical properties of a-Si_xGe_{1-x}:H and a-Si_xN_{1-x}:H alloys, and (5) an examination of the correlations between optically induced metastabilities observed in PL, ESR and optical absorption experiments in a-Si:H.

References

1. G. Lucovsky and P.C. Taylor, in *Encyclopedia of Physics*, R.G. Lerner and G.L. Trigg, eds. (VCH Publishers, Inc., New York, 1991), p. 1104.
2. A. Madan and P.C. Taylor, in *The Encyclopedia of Physical Sciences*, (Academic Press, Inc., San Diego, CA), in press.
3. K. Gaughan, S. Hershgold, J.M. Viner and P.C. Taylor, in *Proc. 14th Inter. Conf. on Amorphous Semiconductors (ICAS 14)*, G. Bauer and W. Fuhs, eds. (Elsevier, Amsterdam, 1991), in press.
4. K. Gaughan, S. Hershgold, J.M. Viner and P.C. Taylor, in *Amorphous Silicon Technology - 1991*, A. Madan, Y. Hamakawa, M.J. Thompson, P.C. Taylor and P.G. LeComber, eds. (Materials Research Society, Pittsburgh, 1991), Vol. 219 p. 697.
5. S.Q. Gu and P.C. Taylor, in *Amorphous Silicon Materials and Solar Cells*, AIP Conf. Proc., Vol. 234, B.L. Stafford, ed. (American Institute of Physics, New York, 1991), p. 146.
6. S.Q. Gu, S. Nitta and P.C. Taylor, in *Amorphous Silicon Technology - 1991*, A. Madan, Y. Hamakawa, M.J. Thompson, P.C. Taylor and P.G. LeComber, eds. (Materials Research Society, Pittsburgh, 1991), Vol. 219, p. 843.
7. J. Ristein, J. Hautala and P.C. Taylor, Phys. Rev. B **40**, 88 (1989).
8. J. Hautala and P.C. Taylor, in *Amorphous Silicon Materials and Solar Cells*, AIP Conf. Proc., Vol. 234, B.L. Stafford, ed. (American Institute of Physics, New York, 1991), p. 170.
9. S.Q. Gu and P.C. Taylor in *Proc. 14th Inter. Conf. on Amorphous Semiconductors (ICAS 14)*, G. Bauer and W. Fuhs, eds. (Elsevier, Amsterdam, 1991), in press.
10. S.Q. Gu and P.C. Taylor in *Amorphous Silicon Technology - 1990*, P.C. Taylor, M.J. Thompson, P.G. LeComber, Y. Hamakawa and A. Madan, eds. (Materials Research Society, Pittsburgh, 1990), Vol. 192, p. 107.
11. M. Zheng, E.J. VanderHeiden, P.C. Taylor, R. Shinar, S. Mitra and J. Shinar, in *Amorphous Silicon Technology - 1990*, P.C. Taylor, M.J. Thompson, P.G. LeComber, Y. Hamakawa and A. Madan, eds. (Materials Research Society, Pittsburgh, 1990), Vol. 192, 657.
12. M.S. Bennett, S. Wiedeman and K. Rajan, in *Amorphous Silicon Technology - 1989*, A. Madan, M.L. Thompson, P.C. Taylor, P.G. LeComber and Y. Hamakawa, eds. (Materials Research Society, Pittsburgh, 1989), Vol. 149, p. 577.
13. Z.Y. Xu, J. Tann, M. Gal and P.C. Taylor, Opt. Quantum Electron. (1991), submitted.
14. Z.Y. Xu, J. Tann, M. Gal, K. Gaughan, I. Viohl and P.C. Taylor, Int. J. of Optoelectronics, in press.

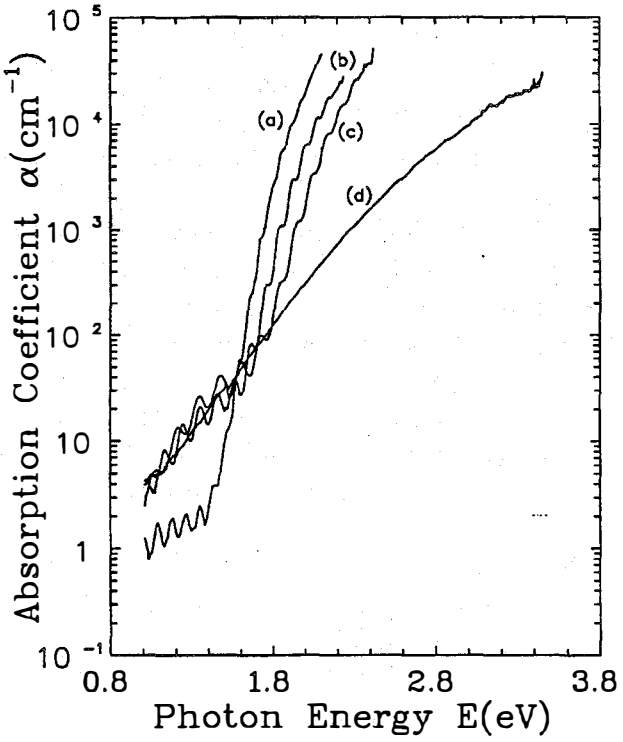

Fig. 1. Absorption coefficient vs. energy for a-SiC:H employing DTBS. (a) 100% SiH_4, (b) DTBS/SiH_4 ≈ 3%, (c) DTBS/SiH_4 ≈ 10%, (d) 100% DTBS.

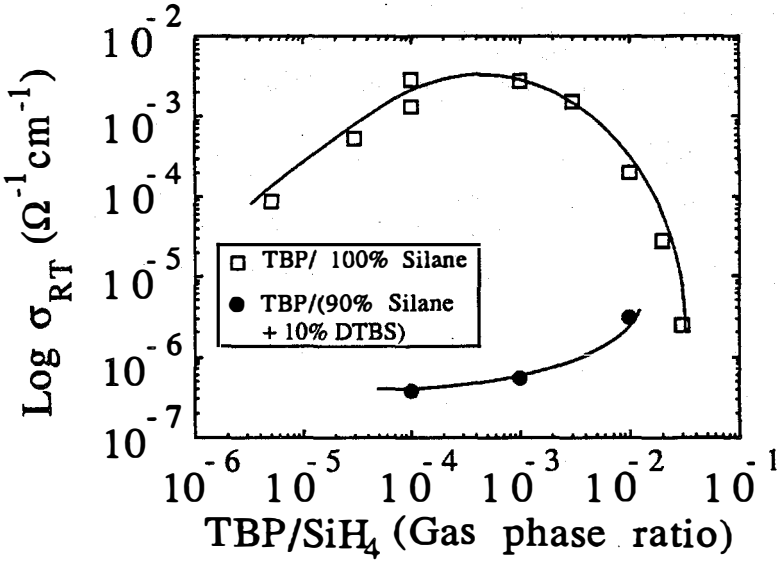

Fig. 2. Electrical conductivity at 300 K of (□) TBP-doped a-Si:H and (•) a-SiC:H produced from ditertiarybutylsilane (DTBS). DTBS/SiH_4 = 10% and E_{04} ≈ 2.3 eV (see Fig. 1, curve c).

8.0 PHOTOVOLTAIC MANUFACTURING TECHNOLOGY (PVMaT) PROJECT

Ed Witt, (Manager), Rick Mitchell, Dave Mooney

The PVMaT Project is a government/industry photovoltaic (PV) manufacturing research and development (R&D) project composed of partnerships between the federal government (through the U.S. Department of Energy) and members of the U.S. PV industry. It is designed to assist the U.S. PV industry in improving manufacturing processes, accelerating manufacturing cost reductions for PV modules, increasing commercial product performance, and generally laying the groundwork for a substantial scale-up of U.S.-based PV manufacturing plant capabilities.

The project is being carried out in 3 separate phases, each focused on a specific approach to solving the problems identified by the industrial participants. These participants are selected through competitive procurements. Furthermore, the PVMaT project has been specifically structured to ensure that these PV manufacturing R&D subcontract awards are selected with no intention to either direct funding toward specific PV technologies (e.g., amorphous silicon, polycrystalline thin films, etc.), or spread the awards among a number of technologies (e.g., only one subcontract in each area). Each associated subcontract under any phase of this project is, and will continue to be, selected for funding on its own technical and cost merits.

The Phase 1 portion of the PVMaT project, the problem identification phase, was completed early in 1991. This effort involved competitive bidding open to any U.S. firm with existing manufacturing capabilities, regardless of material or module design. Early in 1991, the competitive selection process for this phase was completed with the award of 22 subcontracts. Each of these subcontracted efforts was funded at a level of up to $50,000 and involved a duration of 3 months. The problems identified by the research in this phase of the project were process-specific in nature and represented opportunities for individual industrial participants to improve their manufacturing processes, reduce manufacturing costs, increase product performance, and/or support a scale-up of U.S.-based manufacturing plant capabilities. These opportunities have since been detailed in the approaches suggested by these organizations for Phase 2 research. It is not anticipated that another solicitation like Phase 1 will occur. The procurement under this phase was only meant to precede and support the Phase 2A solicitation.

Phase 2 of the PVMaT project is now under way. This is the solution phase of the project and addresses problems of specific manufacturers. The final selection of successful bidders under the first Phase 2 solicitation, called Phase 2A, has been completed. Subcontract negotiations are under way at this time, and the award of research subcontracts is expected in early Fiscal Year 1992. This Phase 2A solicitation was open only to participants in the Phase 1 effort. It is anticipated that as many as six subcontracts will be awarded under this phase, in which successful bidders will be supported for as long as three years as they realize improvements to their manufacturing processes. The envisioned subcontracts under Phase 2 may be up to three years in duration and will be highly cost-shared between the U.S. government and U.S. industrial participants. A second overlapping and similar process-specific solicitation (Phase 2B) is planned to follow soon and will be open to all U.S. PV manufacturing companies.

There are "general" R&D problems in the PV industry that are relatively common problems to the industry as a whole, to a number of companies, or to the design and deployment of PV

systems. Phase 3 of the PVMaT project will address these generic problem areas through a team research approach. A Request for Proposals on this generic manufacturing technology was released in October 1991 (RR-2-11219: Teamed Research and Development on Photovoltaic Manufacturing Technology, Phase 3A - Shared Process Issues), with proposals due in January 1992. Participants for these generic research activities may come from a consortia of industrial companies, individual companies, a university or group of universities, combinations of company and university groups, or other groups with special capabilities for solving a particular problem. These proposed research organizations will focus on module-related R&D problems found to be common to several industrial PV manufacturers. They will also work in tandem with material and component manufacturers to help strengthen the PV industry.

Title: **Photovoltaic Manufacturing Technology Phase - I**

Organization: AstroPower, Inc. Solar Park, Newark, DE 19711

Contributors: W.R. Bottenberg, Principal Investigator; A.M. Barnett, R.H. Hall

The objective of this work was to identify process specific module fabrication problems for the Silicon Film™ manufacturing technology and to identify approaches to solving these problems and the costs to solve these problems. This objective was met by following a four step process: 1) description of the module manufacturing procedure, 2) identification of processes that could lead to improvement, 3) identification of specific problems and 4) description of approaches to achieve the cost reduction and performance goals.

The Silicon-Film™ process is being developed with the objective of achieving a high-performance, low-cost solar cell for terrestrial power applications. The approach is guided by device modeling. A high performance device structure has been designed which can be fabricated from imperfect materials. The technical approach involves development of a technique for preparing crystalline silicon on a low cost substrate. The commercial feasibility of this approach has been demonstrated by the achievement of a 100 cm^2, 10.9% commercial-size solar cell.

There are three primary stages in the manufacture of a module using Silicon-Film™ wafers: wafer formation, solar cell fabrication and module fabrication. The process steps after wafer fabrication are almost identical to those found in the conventional single crystal or polycrystalline silicon technologies.

A three year plan was defined to achieve the following objectives:

1) Improve the productivity of the Silicon-Film™ machine which will lead to reduced wafer costs.
2) Reduce the materials consumption and increase the materials yield in the Silicon-Film™ wafer leading to further reductions in cost.
3) Improve the performance of the solar cells.
4) Decrease the materials consumption in the solar cell fabrication process and increase the mechanization leading to reduced cost.
5) Decrease module cost by integrating and mechanizing the fabrication of modules from solar cells.
6) Increase the size of the solar cell and module to reduce cost.

The ultimate benefit of long-term research on improvement of the Silicon-Film™ wafer manufacturing process and the reduction of manufacturing costs will be the penetration into the utility power markets by these advanced products.

Title:	**Manufacturing Technology Development for $CuInGaSe_2$ Solar Cell Modules**
Organization:	Boeing Defense and Space Group, Seattle, WA
Contributors:	B.J. Stanbery, program manager and principal investigator; R.M Burgess, W.S. Chen, W.E. Devaney, R.A. Mickelsen, and J.M. Stewart
Lower-Tier Subcontractors:	Glasstech Solar Inc, Golden, CO; S. Brown and N.T. Heeke Advanced Technology Materials, Danbury CT; D.C. Gordon

The objective of this study is to identify our current capabilities in manufacturing and process development, and the obstacles to the advancement of manufacturing technology for CIGS solar cell modules; and to develop a plan describing the cot and other requirements to reduce CIGS module production costs, improve their performance, and establish a significant domestic production capacity to enable their cost-effective application to the utility power generation market.

We have developed a two-stage strategy to advance CIGs module manufacturing technology. The Prototype Inline CIGS Production Plant analyzed in the course of this contract is the next logical step in the further development of CIGS module manufacturing technology .

We have developed a preliminary plan to design, build and test a Prototype Inline CIGs Module Production Plant. Our development program scheduling has led us to conclude that this effort can be concluded in three years, and at an estimated expense of about $14M. Completely detailed program cost estimation has not been performed, hence it is important to remember that this cost estimate is tentative. Our determination that this program can be completed in three years is based on our estimates of the time required to complete each task and an analysis of the development activities interrelationships. We assume that this program begins in 1992, and that the second stage project to build the full Scale Inline CIGs module Production Plant begins in 1995 and begins production in 1997.

Calculated direct manufacturing costs have been combined with a technology development plan schedule to project the module peak power production cost in $\$/W_p$ ahead the output capacity in MW_p as a function of time between the years 1994 when the prototype production plant is expected to be first operational and the year 2000 when the first refined, fully developed full-scale production plant achieves its full capacity.

Conclusions:

We have used the method developed by the Electric Power Research Institute (EPRI) for the analysis of the cost of electricity from module cost, BOS cost, technology-specific physical properties, and financial parameters (as updated in the DOE Interlaboratory White Paper of 1991) to calculate the cost of electricity and thereby judge the applicability of CIGS module technology to central utility power generation. The results shown in figure 4 clearly indicate that the further advancement of CIGS module manufacturing technology and scale-up of production has the potential to enable photovoltaics to penetrate this huge market and become a major industry in the United States by the beginning of the 21st century.

Title: **Development of Fixed Abrasive Slicing Technique (FAST) for Reducing Slicing and Silicon Material Costs of Photovoltaic Wafers**

Organization: Crystal Systems, Inc.
27 Congress Street, Salem, MA 01970

Contributors: Frederick Schmid, Principal Investigator; Chandra P. Khattak, Program Manager; Maynard B. Smith, Senior Engineer

Objective

Silicon wafers are a large portion of module cost, and slicing represents nearly half the wafer cost. Current emphasis on production of high-efficiency crystalline silicon photovoltaic modules requires development of effective low-cost slicing technique. The Fixed Abrasive Slicing Technique (FAST) has been proven effective for slicing silicon wafers. Design and fabrication of a high throughput double-headed FAST slicer has been demonstrated as a production technology. Further cost reductions can be achieved by reducing the expendable materials costs, mainly the bladepack. The program addressed degradation mechanism of bladepacks and development to slice multiple bars of silicon.

Results

In FAST a multi-wire bladepack is reciprocated across the silicon workpiece. Slicing is achieved by using fixed diamond on wires as abrasive and water as coolant. Wires equally spaced and tensioned, have diamonds plated on the cutting edge only. Kerf is reduced and diamonds decreased. After slicing through one 10 cm x 10 cm silicon block, the cutting rates degrade. The wire blade development program was initiated to understand the degradation mechanism of the wire packs. Experiments showed a very small number of diamonds on the wire contact the workpiece during FAST slicing and effective feed forces on each diamond tip is high. Under these conditions the diamond tip may form a "wear flat" or may be moved in the nickel setting to a less favorable cutting orientation during the reciprocation action. Since the effective pressure on the diamond tip decreases as the flat increases, diamonds cannot be removed to allow diamonds at lower elevations to surface and restore effective slicing. By choice of diamond type, diamond size and dressing operation, slicing effectiveness of bladepacks is restored. An order of magnitude increase in slicing rates was observed with a three-fold increase in feed force. Under these conditions more diamonds contact the workpiece so that the effective pressure at the diamond tip is not increased and surface damage in the wafer can be kept low.

The results of this investigation show the expendable materials costs can be reduced by minimizing diamond degradation on bladepacks during FAST slicing, maximizing diamond contact on the workpiece, and improving retention of diamonds in the plating matrix.

Future Direction

The expendable materials costs can be reduced by slicing ten silicon bars using the same bladepack. Higher slicing rates with high yields will result in further economies. The material utilization can also be improved by using shaped wires so that the kerf can be reduced significantly.

Title: **Photovoltaic Manufacturing Technology Phase I**

Organization: Energy Conversion Devices, Inc. Troy, MI.

Contributors: Masat Izu, Principal Investigator, Wolodmyr Czubatyj, Herbert Ovshinsky

Objective/Approach -- The object of the program was to identify and describe: 1. capabilities in manufacturing and process development, 2. potential for significantly increased production capacities and reduced manufacturing costs, 3. problems impeding the achievement of those potentials, and 4. cost and other requirements involved in overcoming the problems.

Background and Program Results -- During the past ten years, ECD, has made important progress in the development of PV materials, device design, and manufacturing processes. Among these accomplishments, ECD has pioneered and continues to develop three key proprietary technologies: 1. a low cost, roll-to-roll continuous substrate thin film solar cell manufacturing process, 2. a high efficiency, monolithic, multiple-junction, spectrum splitting thin film amorphous silicon alloy device structure and 3. a high deposition rate, microwave plasma CVD process.

Advantages of ECD's technology include relatively low manufacturing process cost, and lightweight, rugged and flexible modules which result in lowered installed costs. Commercial production of multiple-junction amorphous silicon alloy modules has been underway at ECD for a number of years using the proprietary roll-to-roll process (typically 2,500 ft. long, 14" wide and 5 mil thick stainless steel rolls are processed at approximately 1 ft. per minute). ECD's joint venture United Solar Systems Corp. ("USSC") has a 2MW production plant located in Troy, MI. and modules are currently being manufactured. ECD's ongoing research has produced increases in energy conversion efficiency and manufacturing process throughput. As a result, ECD currently holds the world's record for energy conversion efficiency of an amorphous silicon alloy solar cell device and ECD has also reported on development of a proprietary process for plasma CVD deposition of high quality amorphous silicon alloy films at deposition rates 5 to 10 times greater than those currently employed in the photovoltaic industry. During the program ECD identified recent technological achievements in device design, advanced deposition and module fabrication processes which can bring about substantial cost reductions in future PV module manufacturing.

Conclusions and Future Plans -- In a proposed follow on program (Phase 2A), ECD will develop advanced manufacturing technology with the capability of producing modules with stable 10-11% efficiency at a cost of approximately $1.00 per peak watt. To achieve these goals, we propose a program composed of three tasks: 1. improve module efficiency by developing and demonstrating manufacturing scale technology which can incorporate earlier ECD research advances in device efficiency through the use of multi-junction spectrum splitting and high performance back reflector cell designs, 2. explore opportunities to significantly increase manufacturing throughput by developing and demonstrating high deposition rate silicon alloy solar cell fabrication utilizing proprietary microwave plasma CVD deposition technology and 3. further reduce costs by exploring technologies which lead to reductions in materials and labor cost for mass production. All of these achievements will be transferred to USSC for manufacturing of PV products in the U.S.

Title: Photovoltaic Manufacturing Technology (PVMaT) Improvements for ENTECH's Concentrator Module

Organization: ENTECH, Inc., Dallas-Ft. Worth Airport, Texas

Contributors: M.J. O'Neill, Program Manager, A.J. McDanal and J.L. Perry

Objective: The objective of the Phase 1 program, completed in FY-1991, was to formulate a plan to improve the key manufacturing processes for mass-producing ENTECH's linear Fresnel lens photovoltaic concentrator module. The improved manufacturing processes should simultaneously increase module production rates, enhance module quality, and substantially reduce module costs.

Approach: Our basic approach has been to build on our successful concentrator module technology base, developed over the past dozen years, while evaluating all of our present module manufacturing processes for potential improvements in quality, performance, and cost. Our existing concentrator module manufacturing processes fall into four major categories: (i) photovoltaic cell assembly fabrication; (ii) photovoltaic receiver assembly; (iii) lens lamination; and (iv) module assembly. Working with outside automation experts, we have re-designed the photovoltaic cell assembly for automated soldering, prism covering, and encapsulation, thereby eliminating the bulk of our current module manufacturing labor content. The new cell assembly approach also dramatically simplifies the receiver assembly process, improving yields and quality. Working with 3M, we have re-designed the Fresnel lens for automated in-line lamination at 3M's plant, eliminating labor, yield, and facility costs associated with our previous in-house lamination process. Working with our metal parts suppliers, we have enlarged our module and expanded allowable tolerances to facilitate rapid field assembly at low cost.

Key Results: We have defined a significantly improved manufacturing approach for our concentrator modules. We have assembled a team of organizations (including 3M, Texas Instruments, Integrated Production Systems, and Consumers, Inc.) and prepared a detailed plan to design and implement a modern factory capable of producing more than 10 MW/year of our concentrator modules at prices meeting the near-term goal of the U.S. Department of Energy. We are currently negotiating a Phase 2A contract with the Department of Energy, National Renewable Energy Laboratory, and Sandia National Laboratories team to develop and install this new factory at our present facility.

Conclusion: The key conclusion drawn from the Phase 1 program is that our simple, efficient, error-tolerant 21X linear Fresnel lens concentrator module can realistically meet the near-term Department of Energy goal of 12 cents/kWh levelized electricity cost with the new production approach discussed above, without further breakthroughs in materials, efficiency levels, device stability, or basic manufacturing approaches. Thus, our concentrator approach represents a very low-risk path to meet the near-term Department of Energy goal.

Reference

1. M.J. O'Neill et al, "Photovoltaic Manufacturing Technology Improvements for ENTECH's Concentrator Module," Phase 1 Final Report for NREL Subcontract No. XC-1-10057-13, DFW Airport, TX, June 1991.

Title: Monolithic Amorphous Silicon Modules on Continuous Polymer Substrate

Organization: Iowa Thin Film Technologies, Inc.
Suite 607, ISIS
ISU Research Park
Ames, IA 50010

Contributor: D.P. Grimmer, principal investigator; F.R. Jeffrey; S.A. Martens; L. Geier; J. Jackman

Objective:

The objective of this PVMat Phase I study was to examine various competing processes for the manufacture of monolithic amorphous silicon PV modules on continuous polymer substrates. From this study, the module manufacturing process with the lowest cost per watt was to be determined.

Approaches:

The basic approach was to identify process bottlenecks and large capital equipment costs. A thorough search was conducted for vendors of necessary manufacturing equipment applicable to the proposed processes. In addition to the vendor/equipment search, some experimental work was done to insure feasibility of certain process improvements. A manufacturing simulation program ran continuing validation studies on the manufacturing processes used in the a-Si PV module pilot-plant. Economic models were used in tandem with the manufacturing simulation model, to obtain the lowest cost per watt. Hence, another use of these models is to decide where to allocate future capital resources in the production process.

Results:

Three scenarios were examined: a baseline, roll-to-roll processing without print-etching steps; roll-to-roll deposition with sheet module processing using automatic feed and a print-etch step; and roll-to-roll deposition with roll-to-roll module processing and a print-etch step. Assuming a 6 W_p one ft^2 module, the cases for the baseline roll-to-roll, print-etch/sheet, and print-etch/roll-to-roll configurations yielded a manufacturing cost of \$0.95/W_p, \$0.97/W_p, and \$0.94/W_p, respectively.

Conclusions:

From an industrial engineering perspective, methods that do all deposition processes first will be favored, because the process station scheduling will be easier. Because the a-Si and ZnO deposition appear to be the bottleneck steps, adding one each additional a-Si and ZnO machines could double production output without increasing labor costs.

References:

1. "Monolithic Amorphous Silicon Modules on Continuous Polymer Substrate," Final Technical Report (March 1991) for NREL PVMat, Phase I, under subcontract SERI/XC-1-10057-18. Available from NREL: Document No. SERI/TP-214-4488.

Title: Manufacturing of Ultra-high Efficiency Thin-film Concentrator Cells

Organization: Kopin Corporation
Taunton, Massachusetts

Contributors: R.P. Gale, principal investigator; J.C.C. Fan, M. Spitzer, R.W. McClelland.

Objectives

This project was part of the Photovoltaic Manufacturing Technology Phase I Program. The program purposes were to advance photovoltaic manufacturing technologies, reduce module production costs, increase module performance, and expand U.S. production capability. We have investigated the application of advanced concentrator cell and module technology for these purposes.

Approach

The use of a concentrator approach has the potential to satisfy DOE cost requirements, provided that the module is highly efficient and that the cost of the solar cell is low. We found that these goals can be met, provided the following improvements and advances are made: (1) use of CLEFT III-V multi-junction cells for lowest cost and highest possible efficiency, (2) use of low-loss optics for up to 1000 sun concentration, (3) simplified module design for automated assembly, (4) superior environmental endurance for 30 year lifetime, and (5) multi-megawatt manufacturing capacity for necessary economies of scale. The passively cooled VS 1000 sun module is the ideal baseline module for this effort, since it has been proven to work well with highly efficient cells. Phase 1 consisted of an examination of the development required to expedite the commercialization of the above technology.

Phase 1 Results

The plan developed is as follows. We baseline the GaAs concentrator cell and 1000X module design into pilot operation at Kopin. In order to attain the above improvements, we will use Kopin's existing pilot line for production of CLEFT GaAs solar cells; these cells already exhibit efficiency of about 24% AM1.5. We will modify the CLEFT cell to form concentrators that perform well at 500 to 1000 suns. The know-how for this modification will derive from an integration of Kopin and VS technologies. The pilot line will be broadened to include cell receiver and module assembly, using VS technology obtained from Varian as a baseline. A second generation design will be formulated to address improvements in the module and these will be incorporated into the pilot line, along with the CLEFT concentrator cell. In parallel, we integrate Kopin's CLEFT GaAs cell technology with the advanced AlGaAs and InGaAs material technology obtained by VS from Varian to develop a near-term two-junction mechanical stack with an efficiency of 35%. The receiver thus developed will be compatible with a three-junction approach.

Title: **Thin EFG Octagons**

Organization: Mobil Solar Energy Corporation
4 Suburban Park Drive, Billerica MA 01821

Contributor: Juris P. Kalejs, Principal Investigator

Objective:

The objective was to identify and characterize as part of Phase 1 of the US DOE PVMaT Initiative: 1) current capabilities in Mobil Solar octagon manufacturing technology for 10 cm x 10 cm crystalline silicon wafers, produced using the Edge-defined Film-fed Growth (EFG) technique, and for laser cutting of octagons into wafers; 2) potential manufacturing improvements due to the decrease of the thickness and to the increase in laser cut edge quality and in cutting speed that lead to significantly reduced manufacturing costs, improved performance and increased production capacities; 3) problems impeding the achievement of these potentials; and 4) costs and other requirements involved in overcoming the problems.

Results

A program was formulated and time and cost estimates made for commercial development of an EFG technology for production (growth and cutting) of 200 micron thick 10 cm x 10 cm area crystalline silicon wafers. The EFG process would produce hollow octagonal polygons of sheet silicon, with each octagonal face having a 10 cm width, grown to a length of 5 m with continuous melt replenishment. Octagons are cut into wafers using high speed lasers. The program objectives targeted for crystal growth and cutting, when implemented, clearly advance Mobil Solar's competitive position by reducing the cost of the wafer. The PV industry at large will benefit from an additional source of high quality polycrystalline silicon wafers.

The technical objectives that were set required programs to: reduce EFG wafer thickness from the current 400 microns to a target of 200 microns, and improve thickness uniformity and flatness (i.e., reduce stress acting during growth); decrease the laser cutting damage and increase the edge strength of the thinner wafers by a factor of three to improve the mechanical yield, while at the same time increasing wafering rates by a factor of three; improve process control and wafer productivity by implementing advanced intelligent processing strategies and on-line material property monitoring techniques during crystal growth.

The main problems to be solved in achieving these objectives were identified as: improvement in thickness uniformity across the octagon face (wafer) through implementation of new process control concepts and furnace designs; improved control of thermoelastic stresses in order to increase flatness and reduce residual wafer stress; and reduction in edge damage and possibly elimination of edge microcracks produced in laser cutting with a new generation of lasers capable of cutting silicon at much higher rates.

If these technical objectives were to be met in EFG technology development, this would result in lower costs in three integral parts of the Mobil Solar silicon wafer and module production - silicon material cost (direct materials), wafer mechanical integrity (yield) and laser cutting (throughput) - and lead to reductions in wafer production costs to more than a factor of two below existing polycrystalline wafer costs.

Details appear in the Phase 1 Final Report submitted to NREL.

Title: **Photovoltaic Manufacturing Technology: Phase I**

Organization: Photon Energy, Inc., El Paso, Texas

Contributors: S.P. Albright, R.R. Chamberlin, J.F. Jordan

Introduction and Objectives

Photon Energy Inc.(PEI) has been involved with the development of CdS/CdTe devices and modules since 1984. PEI is presently under subcontract to NREL to further the technological developments already existing at PEI. The PVMAT concept was designed to aid in the solution of manufacturing-related issues. PEI was awarded a Phase I subcontract.

Specific Goals For The PVMAT Subcontract

The Photovoltaic Manufacturing Technology Initiative is designed to help accelerate the early stages of this sizable engineering project. Phase I of the PVMAT subcontract was designed to smooth the Phase 2 proposal-writing requirements by providing a means for problem identification regarding manufacturing. The objectives under this Phase I subcontract were four-fold:

* Identification of the current capabilities in manufacturing and process development,

* Identification of manufacturing potentials envisioned to lead to significantly increased production capacities and reduced manufacturing costs,

* Identification of problems likely to impede the achievement of those potentials,

* Cost and other requirements involved in overcoming the problems in manufacturing technology.

Each of the above objectives under this Phase I subcontract have been explored and studied.

Results

The process steps which can result in the largest labor cost reduction through automation, have been identified. Technological advancements, engineering and automation efforts, and improved step-to-step material and module handling can result in large labor reductions. Effort relating to improvement of the safe handling and recycling of industrial materials is important to PEI's commitment to remain an environmentally friendly industry.

Summary

The ability to subsidize the engineering efforts required for low-cost processing through the Photovoltaic Manufacturing Initiative could allow a significant acceleration toward the achievement of low-cost, high-performance photovoltaic products at PEI.

Title: **Cost Effective Manufacturing of the SEA 10X Concentrator Array**

Organization: SEA Corporation
2010 Fortune Drive, Suite 102
San Jose, California 95131

Contributors: Neil Kaminar, principal investigator
John McEntee and Don Curchod

David G. Vanecek and Mick Fitzgerald
of Automation & Robotics Research Institute

SEA is developing commercial PV systems with the goal of reducing non-polluting electricity costs to below polluting sources of energy. Under the effort described here, we identified changes to our SEA 10X concentrator manufacturing techniques that will allow production at a selling price of 71 ¢/W and that will produce AC bus bar electricity at 4 ¢/KW-hr.[1]

The SEA PV concentrator system differs from other PV concentrator systems in a number of important ways: It was designed from the inception as a commercial product using cost-effective, currently available components and manufacturing processes. It uses "one-sun" solar cells in conjunction with an inexpensive extruded plastic lens. Production costs have been minimized through the use of a simple design with a minimum number of parts and manufacturing steps.

The SEA 10X concentrator consists of an extruded, linear-focus Fresnel lens which focuses on a string of one-sun cells. The cells are bonded to a sheet aluminum heat sink with an electrically insulating adhesive. The anodization and adhesive provide the necessary electrical standoff. The module sides are planned to be molded along with the lens. They are made reflective over their entire internal surface by a thin aluminum film which acts as a secondary optical element, providing improved on- and off-track performance. End caps with molded-in bearing shafts complete the module assembly. Tracking is along a single axis in the east-west direction. Because of the wide acceptance angle, only a simple, low precision tracker drive is needed. The arrays are shipped completely assembled and require only setting on a flat surface, installating four fasteners, and connecting the wires.

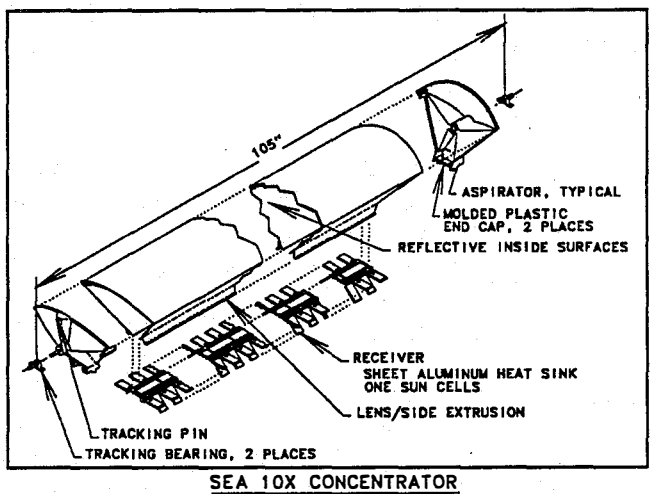

SEA 10X CONCENTRATOR

[1]Kaminar, McEntee, Curchod, Cost Effective Manufacturing of the SEA 10X Concentrator Array, SERI/TP-214-4479, publication in process.

Title: **Research on Advanced Photovoltaic Manufacturing Technology**

Organization: Siemens Solar Industries
Camarillo, California

Contributors: C. Eberspacher, principal investigator; A.J. Anderson, T. Jester, K.E. Knapp, R. Probst, and S.A. Vasquez

Phase 1 focused on identifying and quantifying the opportunities for significant advancement in the scale and economy of high-volume manufacturing of high-efficiency photovoltaic modules. Concurrent programs to advance existing commercial-scale crystalline silicon module manufacturing technology and to implement pilot-scale thin film $CuInSe_2$ (CIS) module manufacturing were defined.

The program for advancing crystalline silicon technology is targeted at expanding U.S. commercial production capacity, increasing module performance, and decreasing module manufacturing costs. U.S. module manufacturing capacity expansion requires the improvement of silicon crystal ingot yields and growth rates, and the development of thin wafer sawing and thin cell processing technologies. Module performance increases require improvements in silicon crystal quality, in impurity gettering and junction diffusion processes, in contacting techniques, and in antireflection coatings and surface passivation processes. Module manufacturing cost reductions require cell processing and module assembly automation, module design and materials improvements, and waste reductions.

The program for implementing thin film CIS module manufacturing focuses on establishing U.S. pilot production capacity and on realizing the low manufacturing costs possible with thin film processing. U.S. manufacturing capacity requires the development of deposition and patterning processes suitable for high-volume production of large-area modules, and the integration of module processing, handling, and transport to minimize labor costs and maximize productivity. Low manufacturing costs require fully automated substrate-to-module processing, high materials use efficiency, and a better understanding of the source materials specifications needed for high-efficiency module performance.

The implementation of the improvements identified in crystalline silicon modules technology could halve module cost and double Siemens Solar's U.S. manufacturing capacity. The implementation of the opportunities identified in thin film CIS module technology could create a module technology with high-volume manufacturing costs substantially below those of any competing solar technology. Phase 2 will focus on exploring and implementing the opportunities identified in Phase 1.

Title: **High Throughput Manufacturing of Thin Film CdTe Photovoltaic Modules**

Organization: Solar Cells, Inc., Toledo, Ohio

Contributors: J.F. Nolan, Principal Investigator; S.A. Kaake, P.V. Meyers, and R.D. Nicholson

Objective: The objective of the program was to identify the primary problems standing in the way of low cost manufacture of photovoltaic modules and to propose solutions to these problems.

Approach: The SCI approach is to construct an automated continuous manufacturing line for thin film PV modules with glass substrates fed in the beginning of the line and finished PV modules flowing out the end of the line. The thin film approach keeps the materials cost and cell interconnection cost low and the automated continuous line keeps the labor cost low. The higher the throughput, the lower the capital, labor and overhead cost per unit.

After an evaluation of the advantages and limitations of competing thin film technologies, SCI chose CdTe as the semiconducting material, primarily to obtain high efficiency, good stability and the freedom to choose a deposition technique compatible with a high throughput continuous PV manufacturing line. The deposition technique chosen was Close Spaced Sublimation (CSS), primarily because it has a very high deposition rate (4μm/min) compared to other thin film deposition processes. This reduces cost further by increasing the throughput of the line.

A feature of the SCI approach is that tempering of the glass substrate is included as an integral part of the PV production line. This reduces the total installed PV system cost since it eliminates the need to laminate the modules to a second piece of tempered glass to obtain the strength required to withstand hail impact and strong winds in field installations.

Results: A number of problems were identified which must be solved to achieve low cost manufacture of PV modules. These include:

1. Throughput must be increased to reduce capital, labor and overhead cost per unit. This can be done with CSS deposition of thin film CdTe, but the process must be scaled up to large area modules (60cmx120cm) at production speeds.
2. Equipment for high throughput deposition of large area thin film CdTe modules is not available. Equipment to do this must be designed, built, de-bugged and operated to prove reliability.
3. The requirement to laminate the PV module to a second piece of glass must be eliminated to obtain low cost modules. This means that the module substrate must be tempered to obtain strength and a low cost encapsulant must be found that is both effective and compatible with a high throughput continuous PV module manufacturing line.

Conclusion: It appears feasible to reduce the manufacturing cost of PV modules to $1.00 per Watt in four years by constructing an automated continuous manufacturing line to produce 60cmx120cm thin film CdTe modules using the CSS deposition process.

Title: **Photovoltaic Manufacturing Technology - Phase 1**

Organization: Solarex Corporation, Crystalline Division, Frederick, MD & Solarex Corporation, Thin Film Division, Newtown, PA

Contributors: J. H. Wohlgemuth, Principle Investigator; D. Whitehouse, S. Wiedeman, A. W. Catalano and R. Oswald

OBJECTIVES

In this first phase of the Photovoltaic Manufacturing Technology Program, the objectives were: 1) to prepare a description of the processes and procedures involved in Solarex's manufacture of crystalline silicon cells and modules and in Solarex's manufacture of amorphous silicon modules, 2) to identify the potential changes in module and cell manufacturing processes that can lead to improved performance, reduced manufacturing costs and significantly increased production volume, 3) to identify potential problems that might impede the achievement of the expected benefits from the identified changes to the process sequences and 4) to describe how Solarex would attempt to solve these problems.

RESULTS

A detailed description was prepared for the two Solarex process sequences used to manufacture PV modules, cast polycrystalline silicon and amorphous silicon. These two processes were analyzed using an IPEG based costing model [1] to determine what the major cost drivers are in the present process sequences and to serve as a baseline for determining what changes can lead to lower cost. The second step was to evaluate the potential cost savings of a large number of possible changes to the baseline sequences. The cost modelling lead to selection of specific changes for each of the two process sequences. For cast polycrystalline silicon the proposed changes included use of the advanced casting system, wire saw wafering, automated cell manufacture, lower cost backsheet and frameless mounting designs. The proposed thin film technology utilizes a triple junction amorphous silicon based process and frameless mounting designs.

Process specific problems identified during the program included the economic use of wire saws, achievement of higher cell efficiencies, implementation of a triple junction amorphous silicon process and more efficient use of materials during the thin film deposition processes. Generic issues included handling of cells and glass plates, frameless mounting of modules and scale-up/automation of processes.

CONCLUSIONS

Both of the process sequences evaluated, cast polycrystalline silicon and amorphous silicon triple junctions, have potential for significant cost reduction if a number of specifically defined technical problems can be solved.

REFERENCES

[1] R.G. Chamberlain, Proceedings of 13th IEEE PV Specialist Conf. p. 904, 1978.

Title: **Low-Cost Manufacturing of Point-Focus Concentrating Modules and Its Key Component, the Fresnel Lens.**

Organization: Solar Kinetics, Inc.
10635 King William Dr.
Dallas, TX 75220

Contributors: Shabbar T. Saifee, Principal Investigator and Andrew Konnerth III.

The objective of this work was to review the current status of photovoltaic module fabrication at Solar Kinetics, Inc. (SKI) and specify the approach required to achieve high- volume manufacturing capability. Low-cost manufacturing of a key component, the Fresnel lens was also reviewed.

We have developed a 300 sun concentrating point-focus photovoltaic module. Currently, we are packaging these modules for independent 2 kW systems. These modules are being fabricated by a combination of manual and semi-automated processes. One of the key factors that is incorporated in the design of the modules is lowering the component and module fabrication costs. This effort also reviews the major manufacturing costs and identifies components and processes whose improvements would significantly reduce manufacturing cost. The Fresnel lens is one key component. Investigation of specific alternative manufacturing methods and sources has substantially reduced the lens costs and can exceed the DOE cost reduction goals.

The approach that SKI proposes is to injection mold small lens parquets (14"x14") to minimize the cumulative distortions due to humidity and temperature effects as seen in all acrylic lens. Injection molding seems to be the lowest cost approach for fabrication of such high-efficiency acrylic lenses.

During this investigation, the importance of two philosophies became clear. One is the concept of concurrent engineering. The second is flexible manufacturing. All components and assemblies must be designed for automation. To ensure this, the developers of the manufacturing and automation processes must constantly work with the component designers to achieve the most cost-effective final design. The concept of flexible manufacturing is important for this product because it is an immature technology; it will require high investment in fixed tooling; it will aid in the prototype stage and during production.

References

1. Saifee, S. T., and A. Konnerth III. "Low-Cost Manufacturing of Point-Focus Concentrating Modules and Its Key Component, the Fresnel Lens." SERI Subcontract No. XC-1-10057-15. Golden: Solar Energy Research Institute, 1991.

Title: **Photovoltaic Manufacturing Technology, Phase I Dendritic Web Photovoltaics**

Organization: Solar Web, Inc.
Pittsburgh, PA
(Subcontractor to Westinghouse Electric Corp.)

Contributors: J. Easoz, Principal Investigator; R. Herlocher, D. Kulik, R. Rosey, R. Sprecace, C. Quinter

Objective

The objective of this program was to identify current manufacturing capabilities, and potentials for significantly increasing production capacities and reduced manufacturing costs for single crystal silicon dendritic web based photovoltaic modules. In addition, the work scope included identification of problems impeding the achievement of the those potentials, and an assessment of cost and other requirements involved in overcoming those problems.

Approach

The approach for this program started with the documentation of the current manufacturing process on a step by step basis. Each process step was then evaluated for potentials improvements which could reduce labor, and increase module efficiency, production yield, silicon utilization, and capital expenditures. The capital savings, labor savings and production yield improvements were calculated based on a constant 4.1 MW/yr plant output. The cost of product was then generated based on the resulting lower cost of production for a constant factory capacity. Once these potential improvement areas had been identified, key problem areas were defined and development programs were formulated, costed, and scheduled.

Results and Conclusions

The program efforts resulted in a document[1] which describes in detail the process, potential process improvements, impact of the improvements on product cost and production levels, and recommends a program designed to effect these process improvements. A total of thirteen major task elements were identified. Each of the individual tasks were detailed in terms of content, cost, and schedule over a three year period. Four of these task elements deal with crystal growth throughput improvements (full width seedings, oxide control, high velocity growth, and web width development), while most of the others deal with cell efficiency, process yield, and silicon utilization. Other task areas address process control, automation, and module efficiency. The report concludes that there is a potential to reduce product costs by a factor of between 4.5 and 7.5 within 4 years depending on whether additional line capacity is installed, and bifacial modules are produced.

References

1. Final Technical Report, Photovoltaic Manufacturing Technology Program - Phase I, J.R. Easoz, R.H. Herlocher, April 1991, SERI/TP-214-4487.

Photovoltaic Manufacturing Technology - Phase I

Spectrolab Inc., Sylmar, CA 91342

D.R. Lillington, program manager; A.V. Mason, principal investigator

The objective of Spectrolab's work under Phase I of the PVMat contract was to describe current capabilities and to identify key approaches to reduce the cost and improve the performance of photovoltaic modules and cells.

The approach was to determine needed improvements in cell design and material quality for Si, GaAs and GaAs/Ge cells and receivers to obtain the desired cost and performance objectives. The simplest cell discussed was a silicon concentrator cell; modeled at 22% 200X AM1.5, this cell can be fabricated for less then $.12/kWh. Another candidate solar cell is the GaAs/Ge concentrator cell, which is anticipated to have a 28% 400X AM1.5 efficiency. The introduction of large area germanium wafers, uniform MOCVD growths and batch processing should make this cell cost effective. A new planer MOCVD reactor, anticipated on line in 1992, will reduce costs by improving uniformity, cycle time and material utilization. Two specific multijunction concentrator designs were also discussed, they are based on discrete GaAs and Ge cells and are capable of achieving over 30% AM1.5D efficiency at 300X.

A technology roadmap was developed to achieve the performance and cost objectives for candidate cells and receivers. Of the cell designs considered, the silicon concentrator cell requires the least development. The manufacturing capability exits today to meet the short term cost goals, additional work will bring the cost down to $.06/kWh. Modules that utilize GaAs solar cells require an extensive development program to meet cost goals. Both process development and cells design would be part of this plan. Cost goals would be obtained through the use of large area germanium substrates and uniform MOCVD GaAs growths. The programs specified on the roadmap will bring us closer to making photovoltaic concentrator power generation a viable economic energy source.

Organization:

Objectives:

Approach:

Title: **Phase 1 - PV Manufacturing Technology Project**

Organization: Utility Power Group, Chatsworth, CA

Contributors: M.J. Stern, principal investigator; G. Duran, K.K. Mackamul, and D.D. Metcalf

OBJECTIVE

The objective of this Phase 1 subcontract was to identify technical obstacles to reducing the manufacturing cost of PV modules.

APPROACH

UPG analyzed its current manufacturing process for specific areas in which improvement would yield substantial benefits. Assuming a specific degree of improvement in the identified areas, a future manufacturing process was described and evaluated.

RESULTS

The primary obstacles to manufacturing cost reduction were the lack of a reliable and low cost substitute material for glass as a rear surface in the encapsulation process, and the lack of commercially available high volume termination and module packaging equipment. Although raw materials utilization was found to be a critical area, reduction in labor was by far the controlling factor.

CONCLUSIONS

Elimination of the identified obstacles will result in a 26% reduction in the per watt manufacturing cost of PV modules produced in UPG's existing production facility, and an 81% reduction to $1.24 per watt for PV modules produced in a future production facility optimized in terms of production economies-of-scale.

9.0 PHOTOVOLTAIC (PV) MODULE AND SYSTEM PERFORMANCE AND ENGINEERING PROJECT

Richard DeBlasio (Manager)

The PV Module and System Performance and Engineering Project is structured to conduct state-of-the-art PV module, system, and application research, engineering, testing, evaluation, and analysis tasks, to provide technical results and solutions to technical issues, and to develop PV applications and application opportunities. The project is also designed to maintain and enhance supporting facilities and capabilities that are consistent with DOE's new *Photovoltaics Program Plan FY 1991–FY 1995*, are complementary to other DOE PV projects, and will ensure that project capabilities and facilities are available resources for cooperative research and utilization by the PV research and development community.

Project activities are managed through the module and systems performance and engineering project management task and organized to address project objectives through the following five primary tasks: (1) Cell and Module Standardized Characterization Performance; (2) Module and System Performance Testing; (3) Module Reliability Research: (4) Solar Radiation Research; and (5) System and Utility Applications.

The following subcontract activities represent support for industry/utility PV power projects, domestic and international standards development, PV systems applications including demand-side management, assessment of and effects on roof-mounted modules, and solar resource utility load matching assessment.

Title: **Evaluation of Roof-Integrated PV Module Designs and Systems**

Organization: Florida Solar Energy Center

Contributors: Kirk Collier

Objectives

- To evaluate the present state-of-the-art of roof-integrated PV modules,
- To identify the pros and cons of roof-integrated thin film and crystalline silicon PV modules,
- To provide recommendations for further development of roof-integrated concepts including building changes and module changes (if any) required to facilitate implementation of roof-integrated concepts, and
- To outline a research plan for proof-of-concept implementation.

Approach

The subcontractor will perform a technology assessment of the present state-of-the-art of roof-integrated PV modules. This assessment will include a literature review of past work in PV and low temperature solar thermal collectors, telephone discussions with manufacturers of residential skylights and commercial architectural glass, and a visit to the (former) Southwest RES and the Los Alamos National Laboratory to discuss and learn from their roof-integrated projects.

The subcontractor will evaluate the information gathered and provide a detailed list of the pros and cons of roof-integrating PV modules. To the extent that inconsistencies are identified regarding the advisability of roof-integration between thin film and crystalline silicon modules, these variations will be highlighted and discussed. Through the discussions with the residential skylight and commercial architectural glass manufacturers, opportunities for synergistic use of existing building technologies will be identified and discussed.

The subcontractor will outline a research and development program based on the information and insights developed. This R&D program should be designed to resolve PV module and building system uncertainties, and provide proof-of-concept validations. To the maximum extent possible the R&D program outline should include the participation of representatives from the building, skylight, and architectural glass industries, as well as the PV industry.

Results

This 6 month project was started in November 1991 and is expected to be completed in May 1992. As of December 1991, the initial literature review efforts had begun.

Title: **Management and Administration of the IEC/PV/TC-82 Secretariat and U.S. Participation in International Standards Development**

Organization: Solar Energy Industries Association (SEIA), 777 North Capitol Street, N.E., Suite 805, Washington, D.C. 20002-4226

Contributors: R. Klein, Principal Investigator

This contract is for Management and Administration of the International Electrotechnical Commission (IEC) PV/Technical Committee (TC)82, Solar Photovoltaic Energy Systems, Secretariat and U.S. Industrial Participation in both domestic and international PV standards development.

The contract also provides some supporting funds for the Photovoltaic standards development activities for IEEE Standards Coordinating Committee 21. TC82 has 4 functioning working groups: WG1, Glossary; WG2, Modules; WG3, Systems; and WG4, Storage. The Secretariat coordinates all TC-82 meetings and IEEE SCC21 PV Standards meetings.

FY '91 Accomplishments:

International PV Standards:

Nine (9) Secretariat documents for circulation as Draft International Standards (DIS) were prepared during FY'91. Each of these documents comprise one segment of a comprehensive International Standard that will be incorporated in the "Design Qualification and Type Approval of Terrestrial Photovoltaic (PV) Modules" document.

Final manuscripts are being readied for printing of: (1) Salt mist corrosion of PV modules, (2) General classification and description of terrestrial photovoltaic (PV) modules. (3) Rating of direct coupled photovoltaic pumping systems, and (4) Design qualification and type approval of terrestrial photovoltaic modules. A Strategic Policy Statement was prepared to define the mission of the IEC Photovoltaic Standards Technical Committee 82.

U.S. (Domestic) PV Standards:

Three IEEE/SCC 21 meetings were held during the year to deliberate on various PV standards being discussed by the committee. IEEE PV Standards 928 "IEEE Recommended Criteria for Terrestrial Photovoltaic Power Systems" and IEEE PV Standard 929 "IEEE Recommended Practice for Utility Interface of Residential and Intermediate Photovoltaic (PV) Systems" were reaffirmed.

IEEE approved a "Project Authorization Request (PAR)" to commence work on development of a comprehensive Module Qualification Test document. The objective of the Qualification Test document is to develop a comprehensive procedure for testing thin-film and crystalline silicon flat-plate PV modules.

Title: **Long Term Environmental Effects on Roof-Mounted Photovoltaic Modules**

Organization: Southwest Technology Development Institute
Contributors: Robert Hammond

Objectives

The long term degradation of modules fabricated with EVA has become a concern to the DOE PV Program and to PV manufacturers. Evidence indicates that the rate of EVA degradation is related to module operating temperature, which raises concerns about roof-mounted modules since they operate hotter than ground- or rack-mounted modules.

The objectives of this effort are: to conduct a methodical evaluation of module degradation, and to document module operating temperatures as a function of roof-mount design.

Approach

In coordination with NREL staff, the Southwest Technology Development Institute (SWTDI) will select 12 modules of a specific design from each of 4 to 6 manufacturers that will be dedicated to this long term evaluation effort. Modules with a significant exposure history (installed prior to 1985) will be selected where available. Both crystalline and thin film modules will be evaluated. For the modules selected, SWTDI records will be reviewed to retrieve available data on the "as delivered" module efficiencies. Manufacturers will also be contacted to determine if records of individual module IV curves are available. If individual module efficiencies cannot be obtained, measured array efficiencies will be used to estimate individual module efficiencies.

All of the modules available for this project are currently mounted on the rooftops of prototype buildings at the SWTDI. Selected modules on each prototype building will be rewired so that each module is electrically terminated at a terminal strip to facilitate taking individual module IV curves. Each of these modules will have a thermocouple bonded to its back surface and terminated at the terminal strip. For the selected modules, SWTDI will measure the present individual module efficiencies, and obtain both light and dark IV curves at a measured module temperature. SWTDI will develop a detailed measurement protocol that will be reviewed and approved by NREL prior to beginning the measurements. SWTDI will take these measurements according to the approved protocol at 3-month intervals for two full years. Following baseline efficiency measurements, one module of each type will be packaged and shipped to NREL for destructive analysis. The remaining modules will continue exposure testing with quarterly performance measurements. At 6-month intervals, one module of each type will be removed, packaged, and shipped to NREL for analysis (a total of 4 shipments).

SWTDI will prepare a summary report documenting all module mounting designs installed at SWTDI along with an evaluation of module operating temperatures. The summary report will include a commentary on the various mounting methods that discusses the design tradeoffs such as ease of installation, ease of maintenance, water tightness, and the design impact on module operating temperature. Results of a 1985 SWRES study of module temperature vs. module

spacing above the roof will also be included.

Results

This 24 month effort is scheduled to start in January 1992 and will run through December 1993.

Title:	**Solar Resource, Utility Load Matching Assessment**
Organization:	Atmospheric Sciences Research Center, State University of New York at Albany
Contributors:	Richard Perez

Objectives

The objective of this study is to apply the techniques demonstrated in New York to a broad cross section of utilities located in various regions of the U.S. Participating utilities will receive a preliminary evaluation of PV's potential for contributing to meeting their load requirements and will be better informed about how to pursue an interest in PV development. Future activities could include deployment of solar resource measuring equipment, high value systems, and/or demonstration systems.

Approach

The subcontractor will work with NREL and EPRI personnel to establish a working relationship with up to 25 utilities. NREL and EPRI will have the primary responsibility for utility identification and coordination. The subcontractor will prepare a formal presentation to be given at a kickoff meeting at NREL on a mutually agreeable date. The presentation will include a thorough review of the work conducted for the NYPA and plans for this project.

The subcontractor will perform selected satellite/ground truth correlations for the years 1987 and/or 1988 depending upon the availability and quality of ground measurement records available from the utilities and NREL. The subcontractor will work with NREL personnel to identify when satellite/ground measurements are well correlated and when they are not. The contractor will provide each participating utility with an estimate of the quantity and quality of the available solar resource for its service territory. For utilities with large service territories covering many climatic zones, the contractor will attempt to provide an indication of areas of high and low resource potential.

The subcontractor will perform PV output versus utility load correlations for the utility loads provided by NREL (up to 25 loads). These loads will include a variety of actual utility system load profiles, distribution system load profiles, power pool load profiles and artificial system load profiles. The criteria used to quantify the load matching will include: PV effective load carrying capability, PV energy versus load distributions, and minimum buffer storage requirements.

Results

This 18 month subcontact was started in September 1991 and runs through March 1993. A project kickoff meeting was held in October where the outline of the project was reviewed and support from the utilities attending the meeting was solicited. As of December 1991, the satellite data base has been assembled and data are being collected from the participating utilities.

Title: Amorphous Silicon Utility/Industry Photovoltaic Power Project

Subcontractor: to be determined

On March 29, 1991, the solicitation RF-1-11061 entitled "**Amorphous Silicon Utility/Industry Photovoltaic Power Project**" was released to the general public. The objectives of the project are 1) to assist in the development and qualification of utility-scale monolithic multijunction amorphous silicon photovoltaic modules, 2) to improve the reliability of utility-scale amorphous silicon mondules and utility grid-connected systems, 3) to demonstrate potential markets for amorphous silicon photovoltaic modules and systems, and 4) to form utility/manufacturer/user teams to promote photovoltaics within the utility sector. Responses were received on June 3, 1991 and currently are under evaluation.

Title: **Evaluation of DSM Incentive Opportunities for Photovoltaics**

Organization: Center for Energy and Urban Policy Research, University of Delaware

Contributors: John Byrne

Objectives

- To evaluate existing residential, commercial and industrial DSM incentive programs with regard to incentive levels and utility avoided costs,
- To analyze the interactions between incentive programs, avoided costs, and regulatory influences, and
- To describe the role PV could play in residential and commercial DSM programs including the likely incentive levels and the leading utilities and states that could be approached for implementation.

Approach

Task 1 of the project is directed at identifying existing DSM incentive programs. In this task the subcontractor will develop a data base of electric utility DSM incentive programs. The data base will include incentive programs offered to all customer sectors including residential, commercial, industrial and agricultural. The data collected will include a description of the incentive program, the associated rates and rate structures, and avoided cost information if available. The contractor will also characterize the regulatory environment in the states where incentive programs are identified.

In Task 2 the subcontractor will analyze the data collected in Task 1 to understand the interactions and relationships between incentive programs, rate structures, avoided costs, and the local regulatory climate. Both quantitative (statistical) and qualitative analysis techniques will be used to interpret and summarize the data.

In Task 3 the subcontractor will evaluate the opportunities and limitations of photovoltaics as a demand-side management option. Incentives and policies that could promote PV as a DSM option will be identified. Any technical obstacles identified during the project that would hinder realizing the PV-DSM opportunity will be identified. Based on existing DSM incentive programs, likely incentive levels for PV-DSM will be determined for key states. For these key states, pilot programs for PV-DSM will be designed that are consistent with the structure of existing DSM incentive programs. These program designs will be discussed with the relevant utilities and feedback will be sought that further fine-tunes the designs.

Results

This 14 month subcontact was started in October 1991 and runs through December 1992. A project kickoff meeting was held in October where the outline of the project was reviewed and support from the utilities attending the meeting was solicited. As of December 1991, data collection is well underway from secondary and primary data sources. Analysis will begin during the first quarter of CY 1992.

10.0 LIST OF ACTIVE SUBCONTRACTS

Active Contract List

Contractor, Principal Investigator, Address	Work Title (Research Activity)	Contract Number	Total Funding ($K)	FY 1991 Funding ($K)	Start/ End Dates
AMORPHOUS SILICON FY1991					
APS C. Sherring Princeton, NJ 08542	Stable Hi-Eff. Large Area a-Si Based Submodules	06003-1	1000.0	1000.0	1/91 2/94
Harvard R. Gordon Cambridge, MA 02138	Optimization of Transparent & Reflecting Films for a-Si Solar Cells	1912101	300.0	100.0	5/91 2/92
Harvard W. Paul 1350 Mass. Ave. Cambridge, MA 02138	Structural & Electronic a-SiGe:H Alloys	81813101	504.5	130.0	5/91 4/92
NASA/JPL Y. Shing Pasadena, CA 91109	Electron Cyclotron Resonance Deposition of a-Si:H and its Alloys	11100101	325.0	325.0	1/91 1/94
National Institute of Standards & Tech. 11/90 A. Gallagher Boulder, CO 80303	Diagnostics/Glow Discharges Used for a-SiGe:H Alloy Deposition	404078	631.7	99.9	4/88
Solarex Corp. A. Catalano Newtown, PA 18940	Stable Hi-Eff. a-Si Multijunction Modules	01903301	1099.5	2099.4	5/90 6/93
Univ. of Delaware J. Meaken Newark, DE 19716	Photo-CVD of a-Si Alloy Materials & Devices	81809201	1046.9	32.0	5/88 3/91
North Carolina Univ. M. Silver Chapel Hill, NC 27599	Recombination & Metastability in a-Si & Si Ge Alloys	110063-5	91.7	91.7	2/91 1/92
Univ. of Oregon J. Cohen Eugene, OR 97403	Origin of Metastable Light-Induced Changes in a-Si:H	110063	106.3	106.3	4/89 5/91

Contractor, Principal Investigator, Address	Work Title (Research Activity)	Contract Number	Total Funding ($K)	FY 1991 Funding ($K)	Start/ End Dates
AMORPHOUS SILICON FY1991					
USSS S. Guha Troy, MI 48084	Hi-Eff. Multigap Multijunction a-Si Based Submodules	119033	1000.0	1000.0	1/91 2/94
Washington University R. Norberg St. Louis, MO 63130	Research into the Structures of a-Si Alloy Films	06055-1	224.8	60.0	1/87 3/91
Xerox Corporation R. Street 3333 Coyote Hill Rd. Palo Alto, CA 94304	Research on Electronic & Structural Properties of a-Si Silicon Alloys	11006309	200.0	200.0	11/86 8/90
POLYCRYSTALLINE THIN FILMS FY1991					
Astropower, Inc. J. Rand Newark, DE 19711	Dev. of Large-Area Monolithically Integrated Si-Film PV Devices	1106401	485.7	485.7	5/91 2/94
Boeing Defense A. Witzel Seattle, WA 98124	Poly $CuGaInSe_2$ Thin Films Solar Cells	11901906	150.0	150.0	5/91 5/92
CA Inst. of Technology M. Nicolet Pasadena, CA 91025	Stable Contacts to a-Si Thin Film Contacts $CuInSe_2$ Thin Film Contacts	80713301	149.0	45.0	9/87 1/91
Colorado State Univ. J. Sites Fort Collins, CO 80523	Role of Polycrystallinity in CdTe & $CuInSe_2$	01004601	160.0	80.0	4/90 5/93
Georgia Tech. A. Rohatgi Atlanta, GA 30332	Hi-Eff. CdTe & ZnTe Thin Film Cells	70603101	757.6	149.9	6/87 3/93
ISET V. Kapur Inglewood, CA 90301	Hi-Eff. $CuInSe_2$ & $CuInSe_2$-Alloy Films	01901902	623.4	623.4	7/90 9/93

Contractor, Principal Investigator, Address	Work Title (Research Activity)	Contract Number	Total Funding ($K)	FY 1991 Funding ($K)	Start/ End Dates
POLYCRYSTALLINE THIN FILMS FY1991					
Martin Marietta M. Misra Denver, CO 80201	Sputtering Techniques for CIS and CdTe Modules	11107001	395.6	395.6	9/91 11/93
Photon Energy S. Albright El Paso, TX 79924	Hi-Eff. Large Area CdTe & CdHgTe Panels	01901901	1360.3	699.9	6/90 8/93
Univ. Colorado A. Hermann Boulder, CO 80309	Novel Thin Film $CuInSe_2$ Fabrication	01001201	50.4	14.9	3/90 4/91
Univ. Delaware R. Birkmire Newark, DE 19716	Fundamentals Polycrystalline Thin Film Materials & Devices	01002301	601.4	601.4	1/90 3/93
Univ. of Illinois A. Rockett 809 S. Wright St. Champaign, IL 61820	Alternate Fabrication Techniques for Hi-Eff. $CuInSe_2$ & $CuInSe_2$	01001701	99.5	40.0	3/90 5/92
Univ. of S. Florida T. & S. Chu Tampa, FL 33620	Thin Film CdTe, ZnTe, & $Hg_{1-x}Zn_xTe$ Solar Cells	81809101	824.6	199.9	7/88 5/92
Purdue Univ. R. Schwartz W. Lafayette, IN 47907	Dev. of Computer Model For Poly Thin-Film $CuInSe_2$ & CdTe Solar Cells	01001301	50.0	50.0	1/90 10/90
Siemens Solar K. Mitchell Camarillo, CA 903011	$CuInSe_2$ Modules	11901905	700.0	700.0	5/91 5/92
Solarex R. Arya Newtown, PA 18940	Poly Submodules Based on $CuInSe_2$ Materials	11901904	600.0	600.0	11/90 12/93
Univ. of Toledo A. Compaan Toledo, OH 43606	CdTe PV Cells and Module Fabrication	01901903	285.4	285.4	7/90 9/93

Contractor, Principal Investigator, Address	Work Title (Research Activity)	Contract Number	Total Funding ($K)	FY 1991 Funding ($K)	Start/ End Dates
CRYSTALLINE SILICON MATERIALS RESEARCH FY1991					
Duke Univ. U. Göesele Dept. of Mech. Engin. Durham, NC 27706	Point Defects & Their Influence on Solar Cell Related Elec. Properties of Crystalline Silicon	81809701	288.6	44.9	7/88 9/90
Georgia Tech A. Rohatgi Atlanta, GA 30332	Impurity Characterization Support for Silicon	01914501	174.8	30.0	10/89 10/91
N. Carolina St. Univ. G. Rozgonyi Box 7214 Raleigh, NC 27695	Effectiveness & Stability of Impurity/Defect Interactions & Their Impact on Minority Carrier Lifetime	81809702	420.0	70.0	6/88 7/91
Suny/Albany J. Corbett Albany, NY 12201	Passivation & Gettering in Solar Cell Silicon	8189703	363.3	57.4	7/88 10/91
Univ. of Southern CA S. Forrest University Park Los Angeles, CA 90089	Electric Characterization Support for Crystalline Silicon	81815401	45.3	19.6	10/88 11/91
ADVANCED HIGH EFFICIENCY FY1991					
Boeing Aerospace B. Stanberry Seattle, WA 98124	New Plasma Source of Hydrides for Epitaxial Growth	11914208	138.1	138.1	4/91 10/92
Colo. State Univ. G. Collins Ft. Collins, CO 80523	Arsine & Hydride Radical Generation for MOCVD Growth	01914209	145.5	78.0	7/90 2/93
Kopin Corp. J. Fan Taunton, MA 02980	Hi-Eff. Thin-Film GaAs & Ternary III-V Solar Cells	01914204	597.5	298.9	7/90 8/93
Purdue Res found M. Lundstrom W. Lafayette, IN 47907	New III-V Cell Design Approaches for Very High Eff. Cells	01914201	398.7	199.9	8/90 9/93

Contractor, Principal Investigator, Address	Work Title (Research Activity)	Contract Number	Total Funding ($K)	FY 1991 Funding ($K)	Start/ End Dates
ADVANCED HIGH EFFICIENCY FY1991					
Rensselaer Ghandhi/Borrego Troy, NY 12180	MOCVD Crystal Growth	01914210	150.8	100.1	6/90 8/93
R.T.I S. Ghandhi Troy, NY 12180	Materials & Structure for Ultra-High-Efficiency Solar Cells	01914203	198.5	99.1	7/90 2/93
Spire Corp. S. Vernon Bedford, MA 01730	GaAs Based Ternary Compounds & Multibandgap Solar Cell Research	01914207	5.6	5.6	8/90 10/93
Univ. So. Cal P. Dapkus Los Angeles, CA	Atomic Layer Epitaxy for Low Temperature Growth of PV Materials	01914206	306.7	207.0	6/90 7/93
VS Corp. J. Werthan Palo Alto, CA 94303	Metalorganic Vapor Phase Epitaxial Growth of AlCaAs/CaAs CaSCa	196393	196.3	196.3	5/91 6/93
NEW IDEAS FY1991					
Res. Triangle Instit. M. Timmons R.T.I.	An Inverted AlGaAs/GaAs Patterned Tunnel Junction Cascade Concentrator Cell	01811002	198.1	98.1	1/90 2/92
Univ. of Delaware R. Birkmire Newark, DE 19716	Novel Ways of Depositing ZnTe Films by a Solution Growth Technique	18110-1	100.0	100.0	1/90 1/91
Univ. of S. California D. Dapkus Los Angeles, CA 90089	High Efficiency Epitaxial Optical Reflector Cells	01811003	92.8	92.8	1/90 2/91

Contractor, Principal Investigator, Address	Work Title (Research Activity)	Contract Number	Total Funding ($K)	FY 1991 Funding ($K)	Start/ End Dates
UNIVERSITY PARTICIPATION PROGRAM FY1991					
No. Carolina St. Univ. S. Bedair Box 7003 Raleigh, NC 27695	New Approaches to Hi-Eff. Solar Cells by MOCVD	91814101	318.4	79.5	7/89 8/92
No. Carolina St. Univ. G. Lucovsky Raleigh, NC 27695	Fundamental Studies of Defect Generation in a-Si Alloy Grown by Remote Plasma Enhanced CVD	91814102	252.0	63.7	7/89 8/92
Stanford University R. Bube 660 Arguello Way Stanford, CA 94305	Ion Beam & Photo-Assisted Growth & Doping of II-VI Compounds	91814104	341.9	86.9	7/89 8/92
Univ. of Utah C. Taylor 309 Park Bldg. Salt Lake City, UT 84112	Electronic Processes in Thin Film PV Materials	91814103	338.3	83.9	7/89 8/92
PHOTOVOLTAIC MANUFACTURING TECHNOLOGY 1991					
Spire Corp Patriots Park Bedford, MD	PV Manfg. Technology Phase I	10057-1	49.8	49.8	1/91 3/91
Astropower, Inc. 30 Lovette Ave. Newark, DE 19711	PV Manfg. Technology Phase I	10057-2	50.0	50.0	1/91 3/91
Solarex Corp. 1335 Piccard Dr. Rockville, MD 20850	PV Manfg. Technology Phase I	10057-3	49.9	49.9	1/91 3/91
Siemens Solar Indust. P.O. Box 6032 Camarillo, CA 936011	PV Manfg. Technology Phase I	10057-4	46.2	46.2	3/91 5/91
Westinghouse Elec. P.O. Box 10864 Pittsburgh, PA 15236	PV Manfg. Technology Phase I	10057-5	49.9	49.9	1/91 3/91

Contractor, Principal Investigator, Address	Work Title (Research Activity)	Contract Number	Total Funding ($K)	FY 1991 Funding ($K)	Start/ End Dates
PHOTOVOLTAIC MANUFACTURING TECHNOLOGY 1991					
Utility Power Group 9410 DeSoto Ave. Chatsworth, CA 91311	PV Manfg. Technology Phase I	10057-6	49.6	49.6	1/91 3/91
GlassTech Solar 6900 Joyce St. Golden, CO 80403	PV Manfg. Technology Phase I	10057-7	49.9	49.9	1/91 3/91
Global PV Specialist 21525 Parthenia St. Conoga Park, CA 91304	PV Manfg. Technology Phase I	10057-8	47.8	47.8	1/91 3/91
Alpha Solarco Inc. 11534 Gondola Dr. Cincinnati, OH 45241	PV Manfg. Technology Phase I	10057-9	48.4	48.4	1/91 3/91
Photon Energy, Inc. 9650A Railroad Dr. El Paso, TX 79924	PV Manfg. Technology Phase I	10057-10	49.5	49.5	1/91 3/91
E.C.D. 1675 West Maple Rd. Troy, MI 48084	PV Manfg. Technology Phase I	10057-11	50.0	50.0	1/91 3/91
Mobil Solar 4 Suburban Park Dr. Billerica, MA 01821	PV Manfg. Technology Phase I	10057-12	50.0	50.0	1/91 3/91
Entech Inc. 1015 Royal Lane Dallas/Ft. Worth Airport, TX 75261	PV Manfg. Technology Phase I	10057-13	49.9	49.9	1/91 3/91
Boeing Co. P.O. Box 3999 Seattle, WA 98124	PV Manfg. Technology Phase I	10057-14	49.8	49.8	1/91 3/91
Solar Kinetics 10635 King Wilms Dr. Dallas, TX 75220	PV Manfg. Technology Phase I	10057-15	48.3	48.3	1/91 3/91

Contractor, Principal Investigator, Address	Work Title (Research Activity)	Contract Number	Total Funding ($K)	FY 1991 Funding ($K)	Start/ End Dates
PHOTOVOLTAIC MANUFACTURING TECHNOLOGY 1991					
Chronar Corp. 195 Clarksville Rd. Lawrenceville, NJ 08648	PV Manfg. Technology Phase I	10057-16	49.0	49.0	1/91 3/91
Crystal Systems 27 Congress St. Salem, MA 01970	PV Manfg. Technology Phase I	10057-17	50.0	50.0	1/91 3/91
Iowa TF Tech. Inc. Suite 607, ISU Ames, IA 50010	PV Manfg. Technology Phase I	10057-18	47.8	47.8	1/91 3/91
Solar Cells Inc. 2650 N. Reynold Rd. Toledo, OH 43615	PV Manfg. Technology Phase I	10057-19	38.0	38.0	1/91 3/91
Kopin Corp. 695 Myles Stndish Blvd Taunton, MA 02780	PV Manfg. Technology Phase I	10057-20	50.0	50.0	1/91 3/91
Solar Energy App. 2010 Fortune Dr. San Jose, CA 95131	PV Manfg. Technology Phase I	10057-21	50.0	50.0	1/91 3/91
Spectrolab, Inc. 12500 Gladstone Ave. Sylmar, CA 91342	PV Manfg. Technology Phase I	10057-22	35.1	35.1	1/91 3/91
MODULE AND SYSTEM PERFORMANCE TESTING AND ENGINEERING					
Univ. of Delaware J. Byrne Newark, DE 19716	Eval of DSM Incentive Opportunities for PV	XR211248-1	96.9	96.9	10/91 12/92
Atmos. Sci. Rsch. Cntr Richard Perez State Univ. of NY Albany, NY 12222	Solar Resource, Utility Load Matching Assessment	XR111168-1	106.3	106.3	9/91 9/93

Contractor, Principal Investigator, Address	Work Title (Research Activity)	Contract Number	Total Funding ($K)	FY 1991 Funding ($K)	Start/ End Dates
MODULE AND SYSTEM PERFORMANCE TESTING AND ENGINEERING					
Florida Solar Energy Kirk Collier Univ./Central FL Orlando, FL 32816	Evaluation of Roof-Integrated PV Module	HR21202-1	49.9	49.9	11/91 5/92
Solar Energy Industries (SEIA) P. Klein Washington, DC 20002	Management & Administration Secretariat & U.S. Parti./ International Standards Dev.	1C010083-1	70.0	26.8	5/90 4/30

11.0 PV SUBCONTRACTED RESEARCH
FY 1991 BIBLIOGRAPHY

Subcontractor Reports and Publications

Abou-Elfotouh, F. A.; Kazmerski, L. L.; Bakry, A. M.; Al-Douri, A. (1990). "Correlations of Single-Crystal $CuInSe_2$ Surface Processing with Defect Levels and Cell Performance." *Conference Record of the Twenty First IEEE Photovoltaic Specialists Conference - 1990; Kissimmee, Florida; May 21-25, 1990.* New York: The Institute of Electrical and Electronics Engineers, Inc.; pp. 541-545.

Ahrenkiel, R. K.; Keyes, B. M.; Shen, T. C.; Chyi, J. I.; Morkoc, H. (1 March, 1991). "Minority-Carrier Lifetime in $Al_xGa_{1-x}As$ Grown by Molecular-Beam Epitaxy." *Journal of Applied Physics* (69:5); pp. 3094-3096. Work performed by Solar Energy Research Institute, Golden, Colorado, and Coordinated Science Laboratory, University of Illinois at Urbana-Champaign, Urbana, Illinois.

Ahrenkiel, R. K.; Dunlavy, D. J.; Keyes, B.; Vernon, S. M.; Tobin, S. P.; Dixon, T. M. (1990). "Design of High Efficiency Solar Cells by Photoluminescence Studies." *Conference Record of the Twenty First IEEE Photovoltaic Specialists Conference - 1990; Kissimmee, Florida; May 21-25, 1990.* New York: The Institute of Electrical and Electronics Engineers, Inc.; pp. 432-436. Work performed by Solar Energy Research Institute, Golden, Colorado, and Spire Corporation, Bedford, Massachusetts.

Albright, S. P.; Chamberlin, R. R.; Jordan, J. F. (November 1990). *High-Efficiency Large-Area CdTe Panels, Final Subcontract Report, June 1887 - July 1990.* SERI/TP-211-4034. 46 pp. Work performed by Photon Energy, Inc., El Paso, Texas. Available NTIS: Order No. DE91002117.

Baron, B. N.; Birkmire, R. W.; Phillips, J. E.; Shafarman, W. N.; Hegedus, S. S.; McCandless, B. E. (January 1991). *Fundamentals of Polycrystalline Thin Film Materials and Devices, Final Subcontract Report, 16 January 1989 - 15 January 1990.* SERI/TP-211-4133. 97 pp. Work performed by the Institute of Energy Conversion, University of Delaware, Newark, Delaware. Available NTIS: Order No. DE91002130.

Baron, B. N.; Birkmire, R. W.; Phillips, J. E.; Shafarman, W. N.; Hegedus, S. S.; McCandless, B. E. (1991). *Fundamentals of Polycrystalline Thin Film Materials and Devices, Final Subcontract Report, 16 January 1989 - 15 January 1990.* SERI/TP-211-4133. 97 pp. Work performed by the Institute of Energy Conversion, University of Delaware, Newark, Delaware. Available NTIS: Order No. DE91002130.

Baron, B. H.; Birkmire, R. W.; McCandless, B. E.; Roy, M.; Phillips, J. E.; Shafarman, W. N. (July 1990). *Materials Analysis and Device Optimization of $CuInSe_2$ Solar Cells, Final Subcontract Report, 16 January 1987 - 15 January 1989.* SERI/TP-211-3896. 56 pp. Work performed by Institute of Energy Conversion, University of Delaware, Newark, Delaware. Available NTIS: Order No. DE90000365.

Baron, B. N.; Birkmire, R. W.; McCandless, B. E.; Phillips, J. E. (July 1990). *Two Terminal $CuInSe_2$ Based Cascade Cells, Final Subcontract Report, 16 January 1987 - 15 January 1989.* SERI/TP-211-3914. 32 pp. Work performed by Institute of Energy Conversion, University of Delaware, Newark, Delaware. Available NTIS: Order No. DE90000363.

Basol, B. M.; Kapur, V. K.; Mitchell, R. L. (1990). "$Cd_{1-x}Zn_xTe$ Films Obtained by the Solid-State Reaction of Elemental Layers." *Conference Record of the Twenty First IEEE Photovoltaic Specialists Conference - 1990; Kissimmee, Florida; May 21-25, 1990.* New York: The Institute of Electrical and Electronics Engineers, Inc.; pp. 509-513. Work performed by International Solar Electric Technology, Inglewood, California, and Solar Energy Research Institute, Golden, Colorado.

Basol, B. M.; Kapur, V. K. (1990). "$CuInSe_2$ Thin Films and High-Efficiency Solar Cells Obtained by Selenization of Metallic Layers." *Conference Record of the Twenty First IEEE Photovoltaic Specialists Conference - 1990; Kissimmee, Florida; May 21-25, 1990.* New York: The Institute of Electrical and Electronics Engineers, Inc.; pp. 546-549. Work performed by International Solar Electric Technology, Inglewood, California.

Basol, B. M.; Kapur, V. K. (November 1990). *Low-Cost CdZnTe Devices for Cascade Cell Application, Final Subcontract Report, 15 May 1989 - 15 May 1990.* SERI/TP-211-4033. 27 pp. Work performed by International Solar Electric Technology, Inglewood, California. Available NTIS: Order No. 91002116.

Bennett, M.; Podlesny, R. (1990). "Two Source Simulator for Improved Solar Simulation." *Conference Record of the Twenty First IEEE Photovoltaic Specialists Conference - 1990; Kissimmee, Florida; May 21-25, 1990.* New York: The Institute of Electrical and Electronics Engineers, Inc.; pp. 1438-1442. Work performed by Solarex Corporation, Thin Film Division, Newtown, Pennsylvania.

Bennett, M. S.; Catalano, A.; Rajan, K.; Arya, R. R. (1990). "Improved Stability in Amorphous Silicon Germanium Solar Cells Made from Hydrogen-Diluted Silane and Germane." *Conference Record of the Twenty First IEEE Photovoltaic Specialists Conference - 1990; Kissimmee, Florida; May 21-25, 1990.* New York: The Institute of Electrical and Electronics Engineers, Inc.; pp. 1653-1655. Work performed by Solarex Corporation, Thin Film Division, Newtown, Pennsylvania.

Bhimnathwala, H. G.; Tyagi, S. D.; Bothra, S.; Ghandhi, S. K.; Borrego, J. M. (1990). "Lifetime Measurements by Open Circuit Voltage Decay in GaAs and InP Diodes." *Conference Record of the Twenty First IEEE Photovoltaic Specialists Conference - 1990; Kissimmee, Florida; May 21-25, 1990.* New York: The Institute of Electrical and Electronics Engineers, Inc.; pp. 394-398. Work performed by Electrical, Computer and Systems Engineering Department, Rensselaer Polytechnic Institute, Troy, New York.

Birkmire, R. W.; Shafarman, W. N.; Varrin, Jr., R. D. (1990). "Options for Fabrication and Design of $CuInSe_2$ Based Solar Cells." *Conference Record of the Twenty First IEEE Photovoltaic Specialists Conference - 1990; Kissimmee, Florida; May 21-25, 1990.* New York: The Institute of Electrical and Electronics Engineers, Inc.; pp. 550-555. Work performed by Institute of Energy Conversion, University of Delaware, Newark, Delaware.

Book of Abstracts; SERI Workshop in the Role of Point Defects/Defect Complexes in Silicon Device Fabrication, (August 1990). SERI/CP-211-3976. 67 pp. Conference held 30-31 August 1990, Keystone, Colorado. Available NTIS: Order No. DE90000377.

Bothra, S.; Tyagi, S. D.; Ghandhi, S. K.; Borrego, J. M. (1990). "Surface Recombination Velocity and Lifetime in InP Measured by Transient Microwave Reflectance." *Conference Record of the Twenty First IEEE Photovoltaic Specialists Conference - 1990; Kissimmee, Florida; May 21-25, 1990.* New York: The Institute of Electrical and Electronics Engineers, Inc.; pp. 404-408. Work performed by Electrical, Computer and Systems Engineering Department, Rensselaer Polytechnic Institute, Troy, New York.

Branz, H. M.; Silver, M. (15 October 1990). "Potential Fluctuations Due to Inhomogeneity in Hydrogenated Amorphous Silicon and the Resulting Charged Dangling-Bond Defects." *Physical Review. B, Condensed Matter* (42:12); pp. 7420-7428. Work performed by Solar Energy Research Institute, Golden, Colorado, and University of North Carolina, Chapel Hill, North Carolina.

Bube, R. H.; Fahrenbruch, A. L.; Lopez-Otero, A.; Chien, K.-F.; Grimbergen, M.; Kim, D.; Sharps, P. (July 1990). *Ion-Assisted Doping of II-VI Compounds During Physical Vapor Deposition, Final Subcontract Report, 1 September 1985 - 30 August 1989.* SERI/TP-211-3907. 89 pp. Work performed by Department of Materials Science and Engineering, Stanford University, Stanford, California. Available NTIS: Order No. DE90000358.

Burdick, J.; Glatfelter, T. (1990). "Outdoor Performance Studies of a-Si Alloy Multi-Junction Solar Cells Using Simulated Solar Illumination." *Conference Record of the Twenty First IEEE Photovoltaic Specialists Conference - 1990; Kissimmee, Florida; May 21-25, 1990.* New York: The Institute of Electrical and Electronics Engineers, Inc.; pp. 1403-1408. Work performed by Energy Conversion Devices, Inc., Troy, Michigan.

Catalano, A.; Arya, R. R.; Bennett, M.; Fieselmann, B.; Morris, J.; Newtown, J.; Podlesny, R.; Tawseme, E.; Wiedeman, S.; Yang, L.; Rothwarf, A.; Shapiro, F. (September 1990). *Research on High-Efficiency, Large-Area, Amorphous Silicon Based Solar Cells, Final Subcontract Report, 1 February 1989 - 28 February 1990.* SERI/TP-211-3906. 82 pp. Work performed by Solarex Thin Film Division, Newtown, Pennsylvania and Drexel University, Philadelphia, Pennsylvania. Available NTIS: Order No. DE90000356.

Catalano, A. (1990). "Advances in a-Si:H Alloys for High Efficiency Devices." *Conference Record of the Twenty First IEEE Photovoltaic Specialists Conference - 1990; Kissimmee, Florida; May 21-25, 1990.* New York: The Institute of Electrical and Electronics Engineers, Inc.; pp. 36-40. Work performed by Solarex Thin Film Division, Newtown, Pennsylvania.

Catalano, A.; Arya, R. R.; Bennett, M.; Fieselmann, B.; Goldstein, B.; Morris, J.; Newton, J.; O'Dowd, J.; Oswald, R. S.; Podlesny, R.; Wiedeman, S.; Yang, L. (July 1990). *Research on Stable, Large-Area Amorphous Silicon Based Submodules, Phase III, Semi-Annual Subcontract Report, 1 February 1989 - 31 July 1989.* SERI/TP-211-3805. 94 pp. Work performed by Solarex Thin Film Division, Newtown, Pennsylvania. Available NTIS: Order No. DE90000339.

Crandall, R. S.; Balberg, I. (4 February 1991). "Mobility-Lifetime Products in Hydrogenated Amorphous Silicon." *Applied Physics Letters* (58:5); pp. 508-510. Work performed by Solar Energy Research Institute, Golden, Colorado, and The Racah Institute of Physics, The Hebrew University, Jerusalem, Israel.

D'Aiello, R; Czanderna, A. W. "PV Modules-Reliability, Qualification Testing, Materials Durability, Structure, and Life Prediction." Prepared for a tutorial offering at the 22nd IEEE PV Specialist Conference (October 7-11, .1991).

Delong, M. C.; Taylor, P. C.; Olson, J. M. (6 August 1990). "Excitation Intensity Dependence of Photoluminescence in $Ga_{0.52}In_{0.48}P$." *Applied Physics Letters* (57:6); pp. 620-622. Work performed by Department of Physics, University of Utah, Salt Lake City, Utah; and Solar Energy Research Institute, Golden, Colorado.

DeLong, M. C.; Viohl, I.; Ohlsen, W. D.; Taylor, P. C.; Olson, J. M. (15 January 1991). "Microwave Thermal Modulation of Photoluminescence in III-V Semiconductors." *Physical Review. B, Condensed Matter* (43:2); pp. 1510-1519. Work performed by Department of Physics, University of Utah, Salt Lake City, Utah, and Solar Energy Research Institute, Golden, Colorado.

DeLong, M. C.; Taylor, P. C.; Olson, J. M. (July/August 1990). "Growth Temperature and Substrate Orientation Dependences of Moving Emission and Ordering in $Ga_{0.52}In_{0.48}P$." *Journal of Vacuum Science and Technology. B, Microelectronics, Processing and Phenomena* (8:4); pp. 948-954. Work performed by Department of Physics, University of Utah, Salt Lake City, Utah; and Solar Energy Research Institute, Golden, Colorado.

Deng, X. J.; Tsuo, Y. S.; Trefny, J. U. (1990). "Ion-Beam Hydrogenation of Sputter-Deposited Amorphous Silicon and Amorphous Silicon-Germanium Alloys." *Conference Record of the Twenty First IEEE Photovoltaic Specialists Conference - 1990; Kissimmee, Florida; May 21-25, 1990.* New York: The Institute of Electrical and Electronics Engineers, Inc.; pp. 1591-1594. Work performed by Colorado School of Mines, Golden, Colorado and Solar Energy Research Institute, Golden, Colorado.

Devaney, W. E.; Chen, W. S.; Stewart, J. M.; Gillette, R. B. (July 1990). *High Efficiency $CuInSe_2$* and $CuInGaSe_2$ Cells and Materials Research, Final Subcontract Report, 1 November 1987 - 31 October 1989. SERI/TP-211-3909. 73 pp. Work performed by Boeing Electronics High Technology Center, Seattle, Washington. Available NTIS: Order No. DE90000362.

Doolittle, W. A.; Rohatgi, A.; Brenneman, R. (1990). "Correlation Between Impurities, Defects and Cell Performance in Semicrystalline Silicon." *Conference Record of the Twenty First IEEE Photovoltaic Specialists Conference - 1990; Kissimmee, Florida; May 21-25, 1990.* New York: The Institute of Electrical and Electronics Engineers, Inc.; pp. 681-686. Work performed by School of Electrical Engineering, Georgia Institute of Technology, Atlanta, Georgia, and Solarex Corporation, Frederick, Maryland.

Fortmann, C. M. (1990). "a-SiGe:H Alloy Material Limitations and Device Considerations." *Conference Record of the Twenty First IEEE Photovoltaic Specialists Conference - 1990; Kissimmee, Florida; May 21-25, 1990.* New York: The Institute of Electrical and Electronics Engineers, Inc.; pp. 1493-1500. Work performed by Institute of Energy Conversion, University of Delaware, Newark, Delaware.

Fortmann, C. M.; Zhou, T.; Malone, C.; Gunes, M.; Wronski, C. R. (1990). "Deposition Conditions, Hydrogen Content, and the Staebler-Wronski Effect in Amorphous Silicon." *Conference Record of the Twenty First IEEE Photovoltaic Specialists Conference - 1990; Kissimmee, Florida; May 21-25, 1990.* New York: The Institute of Electrical and Electronics Engineers, Inc.; pp. 1648-1652. Work performed at Institute of Energy Conversion, University of Delaware, Newark, Delaware and Center for Materials and Processing, Pennsylvania State University, University Park, Pennsylvania.

Fraas, L. M.; Avery, J. E.; Sundaram, V. S.; Dinh, V. T.; Davenport, T. M.; Yerkes, J. W.; Gee, J. M.; Emery, K. A. (1990). "Over 35% Efficient GaAs/GaSb Stacked Concentrator Cell Assemblies for Terrestrial Applications." *Conference Record of the Twenty First IEEE Photovoltaic Specialists Conference - 1990; Kissimmee, Florida; May 21-25, 1990.* New York: The Institute of Electrical and Electronics Engineers, Inc.; pp. 190-195. Work performed by Boeing High Technology Center, Seattle, Washington; Sandia National Laboratories, Albuquerque, New Mexico; and Solar Energy Research Institute, Golden, Colorado.

Gillette, R. B.; Devaney, W. E.; Chen, W. S.; Stewart, J. M. (July 1990). *High Efficiency $CuInSe_2$ and $CuInGaSe_2$ Cells and Materials Research, Final Subcontract Report, 1 November 1987 - 31 October 1989.* Work performed by Boeing Electronics High Technology Center, Seattle, Washington. Available NTIS: Order No. DE90000362.

Gordon, R. G.; Hu, J.; Musher, J.; Giunta, C. (February 1991). *Optimization of Transparent and Reflecting Electrodes for Amorphous Silicon Solar Cells, Annual Subcontract Report, 1 October 1989 - 30 September 1990.* SERI/TP-214-4141. 43 pp. Work performed by Department of Chemistry, Harvard University, Cambridge, Massachusetts. Available NTIS: Order No. DE91002132.

Guha, S. (August 1990). *Research on High-Efficiency, Multiple-Gap, Multi-Junction Amorphous Silicon-Based Alloy Thin-Film Solar Cells, Final Subcontract Report, 1 March 1987 - 28 February 1990.* SERI/TP-211-3918. 157 pp. Work performed by Energy Conversion Devices, Inc., Troy, Michigan. Available NTIS: Order No. DE90000364.

Hahn, M. J.; Berry, W. B.; Mrig, L. (1990). "Comparative Short Term/Long Term Field Test Performance and Stability of Tandem and Single Junction a-Si Modules." *Conference Record of the Twenty First IEEE Photovoltaic Specialists Conference - 1990; Kissimmee, Florida; May 21-25, 1990.* New York: The Institute of Electrical and Electronics Engineers, Inc.; pp. 1057-1061. Work performed at University of Notre Dame, Notre Dame, Indiana and Solar Energy Research Institute, Golden, Colorado.

Hanak, T. R.; Bakry, A. M.; Ahrenkiel, R. K.; Timmons, M. L. (1990). "DX-Center in Se-Doped $Al_xGa_{1-x}As$." *Impurities, Defects and Diffusion in Semiconductors: Bulk and Layered Structures, Materials Research Society Symposium Proceedings, Volume 163*, Wolford, D. J.; Bernholc, J.; and Haller, E. E. Pittsburgh, PA: Materials Research Society; pp. 781-784. Presented at the MSR Fall Meeting, November 27 - December 1, 1989, Boston, Massachusetts. Work performed by Department of Physics, University of Denver, Denver, Colorado; Solar Energy Research Institute, Golden, Colorado; Research Triangle Institute, Research Triangle Park, North Carolina.

Hass, K. C.; Davis, L. C.; Zunger, A. (15 August 1990). "Electronic Structure of Random $Al_{0.5}Ga_{0.5}As$ Alloys: Test of the "Special-Quasirandom-Structures" Description." *Physical Review. B, Condensed Matter* (42:6); pp. 3757-3760. Work performed by Research Staff, Ford Motor Company, Dearborn, Michigan, and Solar Energy Research Institute, Golden, Colorado.

Hegedus, S. S. (1990). "Capacitance Studies of a-SiGe:H p-i-n Solar Cells." *Conference Record of the Twenty First IEEE Photovoltaic Specialists Conference - 1990; Kissimmee, Florida; May 21-25, 1990.* New York: The Institute of Electrical and Electronics Engineers, Inc.; pp. 1544-1549. Work performed by the Institute of Energy Conversion, University of Delaware, Newark, Delaware.

Luft, W. (1990). "Research in the U.S. on High-Efficiency Amorphous Silicon Photovoltaic Devices." *International Journal of Solar Energy*, (8:3); pp. 155-160.

Lundstrom, M. S.; Melloch, M. R.; Pierret, R. F.; Carpenter, M. S.; Chuang, H. L.; Keshavarzl, A.; Klausmeier-Brown, M. E.; Lush, G. B.; Morgan, J. M.; Stellwag, T. B. (July 1990). *Basic Studies of III-V High Efficiency Cell Components, Annual Subcontract Report, 15 August 1988 - 14 August 1989.* SERI/TP-211-3904. 120 pp. Available NTIS: Order No. DE90000360.

Materials Science and Engineering Division Technical Summary Report, January, 1991. (January 1991). SERI/MP-210-4206. 24 pp.

Melloch, M. R.; Tobin, S. P.; Bajgar, C.; Keshavarzi, A.; Stellwag, T. B.; Lush, G. B.; Lundstrom, M. S.; Emery, K. (2 July 1990). "High Efficiency $Al_{0.22}Ga_{0.78}As$ Solar Cells Grown by Molecular Beam Epitaxy." *Applied Physics Letters* (57:1); pp. 52-54. Work performed by School of Electrical Engineering, Purdue University, West Lafayette, Indiana; Spire Corporation, Bedford, Massachusetts; and Solar Energy Research Institute, Golden, Colorado.

Melloch, M. R.; Tobin, S. P.; Bajgar, C.; Stellwag, T. B.; Keshavarzi, A.; Lundstrom, M. S.; Emery, K. (1990). "High-Efficiency GaAs and AlGaAs Solar Cells Grown by Molecular Beam Epitaxy." *Conference Record of the Twenty First IEEE Photovoltaic Specialists Conference - 1990; Kissimmee, Florida; May 21-25, 1990.* New York: The Institute of Electrical and Electronics Engineers, Inc.; pp. 163-167. Work performed by School of Electrical Engineering, Purdue University, West Lafayette, Indiana; Spire Corporation, Bedford, Massachusetts; and Solar Energy Research Institute, Golden, Colorado.

Melloch M. R.; Harmon, E. S.; Emery, K. A. (March 1991). "Large-Area, 8cm^2 GaAs Solar Cells Fabricated from MBE Material." *IEEE Electron Device Letters*, Vol. 12, No. 3, pp. 137-139.

Metzdorf, J.; Wittchen, T.; Heidler, K.; Dehne, K.; Shimokawa, R.; Nagamine, F.; Ossenbrink, H.; Fornarini, L.; Goodbody, C.; Davies, M.; Emery, K.; DeBlasio, R. (1990). "Objectives and Results of the PEP '87 Round-Robin Calibration of Reference Solar Cells and Modules." *Conference Record of the Twenty First IEEE Photovoltaic Specialists Conference - 1990; Kissimmee, Florida; May 21-25, 1990.* New York: The Institute of Electrical and Electronics Engineers, Inc.; pp. 952-959. Work performed by PTB, Federal Republic of Germany; ISE, Federal Republic of Germany; DWD-MOH, Federal Republic of Germany; ETL, Japan; JMI, Japan; JRC, C.E.C.; ENEA, Italy; RAE, United Kingdom; Solar Energy Research Institute, Golden, Colorado.

Mitchell, K. W.; Willet, D. R. (October 1990). *Research on Stable, High-Efficiency, Large-Area Amorphous Silicon Based Modules - Task B, Final Subcontract Report, 1 March 1989 - 28 February 1990.* SERI/TP-211-3967. 39 pp. Work performed by Siemens Solar Industries, Camarillo, California. Available NTIS: Order No. DE91002115.

Mitchell, R. L.; Zweibel, K.; Ullal, H. S. (November 1990). *Research on Polycrystalline Thin-Film Materials, Cells, and Modules.* SERI/TP-211-4061. 7 pp. Prepared for the ASME/JSME/JSES Joint Thermal Engineering and Solar Energy Conference, 17-22 March 1991, Reno, Nevada. Available NTIS: Order No. DE91002124.

Mooney, G. D.; Hermann, A. M. (September 1990). *Novel Thin-Film $CuInSe_2$ Fabrication, Final Subcontract Report.* SERI/TP-211-3864. Work performed by University of Arkansas, Fayetteville, Arkansas, and University of Colorado, Boulder, Colorado. Available NTIS: Order No. DE90000345.

Morris, J.; Arya, R. R.; Poplawski, C.; Catalano, A.; Podlesny, R.; Newton, J. L.; Wilczynski, A.; Lommasson, T. (1990). "High Performance Interconnected Amorphous Silicon Based Modules." *Conference Record of the Twenty First IEEE Photovoltaic Specialists Conference - 1990; Kissimmee, Florida; May 21-25, 1990.* New York: The Institute of Electrical and Electronics Engineers, Inc.; pp. 1455-1458. Work performed by Solarex Corporation, Thin Film Division, Newtown, Pennsylvania.

Moskowitz, P. D.; Fthenakis, V. M.; Zweibel, K. (1990). "Health and Safety Issues Related to the Production, Use and Disposal of Cadmium-Based Photovoltaic Modules." *Conference Record of the Twenty First IEEE Photovoltaic Specialists Conference - 1990; Kissimmee, Florida; May 21-25, 1990.* New York: The Institute of Electrical and Electronics Engineers, Inc.; pp. 1040-1042. Work performed by Biomedical and Environmental Assessment Group, Brookhaven National Laboratory, Upton, New York and Solar Energy Research Institute, Golden, Colorado.

Nann, S.; Emery, K. (1991). "New Proposals for Energy Rating of Photovoltaic Devices." *1991 World Congress, Proceedings of the Biennial Congress of the International Solar Energy Society; Denver, Colorado; 19-23 August 1991.* Arden, M. E.; Burley, S. M. A.; Coleman, M., eds. New York: Pergamon Press; Vol. 1, Part 1, pp. 75-80.

Nann, S.; Riordan, C. (1990). "Solar Spectral Irradiance Under Overcast Skies." *Conference Record of the Twenty First IEEE Photovoltaic Specialists Conference - 1990; Kissimmee, Florida; May 21-25, 1990.* New York: The Institute of Electrical and Electronics Engineers, Inc.; pp. 1110-1115. Work performed by Centre for Solar Energy and Hydrogen Research, Federal Republic of Germany and Solar Energy Research Institute, Golden, Colorado.

Nelson, A. J.; Gebhard, S.; Rockett, A.; Colavita, E.; Englehardt, M.; Hochst, H. (15 October 1990). "Synchrotron-Radiation Photoemission Study of CdS/$CuInSe_2$ Heterojunction Formation." *Physical Review. B, Condensed Matter* (42:12); pp. 7518-7523. Work performed by Solar Energy Research Institute, Golden, Colorado; Department of Materials Science and Engineering, University of Illinois at Urbana-Champaign, Urbana, Illinois; Department of Physics, University of Calabria, Cosenza, Italy; and Synchrotron Radiation Center, University of Wisconsin-Madison, Stoughton, Wisconsin.

Nelson, A. J.; Engelhardt, M.; Hochst, H. (1990). "Synchrotron Radiation Photoemission Study of the Electronic Structure of the Filled Tetrahedral Semiconductors LiZnAs and LiZnP." *Journal of Electron Spectroscopy and Related Phenomena* (51); pp. 623-628. Presented at the Fourth International Conference on Electron Spectroscopy, University of Hawaii, July 10-14, 1989. Work performed by Solar Energy Research Institute, Golden, Colorado, and Synchrotron Radiation Center, University of Wisconsin-Madison, Stoughton, Wisconsin.

Nelson, A. J.; Gebhard, S.; Kazmerski, L. L.; Colavita, E.; Engelhard, M.; Hochst, H. (1 October 1990). "Characterization of Native Oxide of $CuInSe_2$ using Synchrotron Radiation Photoemission." *Applied Physics Letters* (57:14); pp. 1428-1430. Work performed by Solar Energy Research Institute, Golden, Colorado; Physics Department, University of Calabria, Cosenza, Italy; Synchrotron Radiation Center, University of Wisconsin-Madison, Stoughton, Wisconsin.

Newton, J. L.; Kritikson, K. (1990). "Electrical and Structural Properties of a-Ge:H Alloys." *Conference Record of the Twenty First IEEE Photovoltaic Specialists Conference - 1990; Kissimmee, Florida; May 21-25, 1990.* New York: The Institute of Electrical and Electronics Engineers, Inc.; pp. 1662-1666. Work performed by Solarex Corporation, Thin Film Division, Newtown, Pennsylvania.

Norberg, R. E.; Fedders, P. A. (August 1990). *Structure of Amorphous Silicon and Germanium Alloy Films, Annual Subcontract Report, 15 January 1989 - 14 January 1990.* SERI/TP-211-3908. 31 pp. Work performed by Department of Physics, Washington University, St. Louis, Missouri. Available NTIS: Order No. DE9000355.

Osterwald, C. R.; Emery, K. A.; Myers, D. R.; Hart, R. E. (1990). "Primary Reference Cell Calibrations at SERI: History and Methods." *Conference Record of the Twenty First IEEE Photovoltaic Specialists Conference - 1990; Kissimmee, Florida; May 21-25, 1990.* New York: The Institute of Electrical and Electronics Engineers, Inc.; pp. 1062-1067. Work performed at Solar Energy Research Institute, Golden, Colorado and NASA Lewis Research Center, Cleveland, Ohio.

Partain, L. D.; Chung, B-C.; Virshup, G. F.; Schultz, J. C.; MacMillan, H. F.; Ristow, M. L.; Kuryla, M. S.; Bertness, K. A.; Klausmeier-Brown, M. E.; Wanlass, M. W.; Coutts, T. J. (1990). "Progress Toward a 30%-Efficient, Monolithic, Three-Junction, Two-Terminal Concentrator Solar Cell for Space Applications." *Conference Record of the Twenty First IEEE Photovoltaic Specialists Conference - 1990; Kissimmee, Florida; May 21-25, 1990.* New York: The Institute of Electrical and Electronics Engineers, Inc.; pp. 184-189. Work performed by Varian Research Center, Palo Alto, California, and Solar Energy Research Institute, Golden, Colorado.

Phillips, J. E. (1990). "Determination of Diffusion Length with Bi-Facial Spectral Response." *Conference Record of the Twenty First IEEE Photovoltaic Specialists Conference - 1990; Kissimmee, Florida; May 21-25, 1990.* New York: The Institute of Electrical and Electronics Engineers, Inc.; pp. 782-786. Work performed by Institute of Energy Conversion, University of Delaware, Newark, Delaware.

Research on High-Efficiency, Multiple-Gap, Multi-Junction Amorphous Silicon-Based Alloy Thin-Film Solar Cells, Phase III, Semi-Annual Subcontract Report, 1 March 1989 - 31 August 1989. (July 1990). SERI/TP-211-3804. 53 pp. Work performed by Energy Conversion Devices, Inc., Troy, Michigan. Available NTIS: Order No. DE90000338.

Rohatgi, A.; Summers, C. J.; Erbil, A.; Sudharsanan, R.; Ringel, S. (October 1990). *High Efficiency Cadmium and Zinc Telluride-Based Thin Film Solar Cells, Final Subcontract Report, 1 March 1989 - 28 February 1990.* SERI/TP-211-3952. 86 pp. Work performed by School of Electrical Engineering, Georgia Institute of Technology, Atlanta, Georgia. Available NTIS: Order No. DE91002112.

Roy, M.; Phillips, J. E. (1990). "Effect of Oxidation-Reduction Heat Treatments on $CuInSe_2$/CdS Device Behavior." *Conference Record of the Twenty First IEEE Photovoltaic Specialists Conference - 1990; Kissimmee, Florida; May 21-25, 1990.* New York: The Institute of Electrical and Electronics Engineers, Inc.; pp. 743-747. Work performed by Institute of Energy Conversion, University of Delaware, Newark, Delaware.

Schultz, J. C.; Klausmeier-Brown, M. E.; Ristow, M. L.; Al-Jassim, M. M. (1990). "High Efficiency 1.0-eV GaInAs Bottom Solar Cell for 3-Junction Monolithic Stack." *Conference Record of the Twenty First IEEE Photovoltaic Specialists Conference - 1990; Kissimmee, Florida; May 21-25, 1990.* New York: The Institute of Electrical and Electronics Engineers, Inc.; pp. 148-152. Work performed by Device Laboratory, Varian Research Center, Palo Alto, California, and Solar Energy Research Institute, Golden, Colorado.

Schwartz, R. J.; Gray, J. L. (1990). "Use of $CuIn_{1-x}Ga_xSe_2$ Layers to Improve the Performance of $CuInSe_2$ Cells." *Conference Record of the Twenty First IEEE Photovoltaic Specialists Conference - 1990; Kissimmee, Florida; May 21-25, 1990.* New York: The Institute of Electrical and Electronics Engineers, Inc.; pp. 570-574. Work performed by School of Electrical Engineering, Purdue University, West Lafayette, Indiana.

SERI Photovoltaic Subcontract Reports: Abstracts and Document Control Information, 1 January - 31 July 1990. (October 1990). SERI/TP-211-3934. 21 pp. Available NTIS: Order No. DE90000378.

Shen, D. S.; Schropp, R. E. I.; Chatham, H.; Hollingsworth, R. E.; Xi, J.; Bhat, P. K. (1990). "High Efficiency a-Si/a-Si Tandem Solar Cells." *Conference Record of the Twenty First IEEE Photovoltaic Specialists Conference - 1990; Kissimmee, Florida; May 21-25, 1990.* New York: The Institute of Electrical and Electronics Engineers, Inc.; pp. 1471-1474. Work performed at Glasstech Solar, Inc., Golden, Colorado.

Shen, D. S.; Bhat, P. K. (August 1990). *Amorphous Silicon Solar Cells Prepared at High Deposition Rates, Annual Subcontract Report, 1 July 1989 - 30 June 1990.* SERI/TP-211-3949. 30 pp. Work performed by Glasstech Solar, Inc., Golden, Colorado. Available NTIS: Order No. DE90000371.

Singh, R.; Thakur, R. P. S.; Katz, A.; Nelson, A. J.; Gebhard, S. C.; Swartzlander, A. B. (17 September 1990). "Relationship between Thermal Stress and Structural Properties of SrF_2 Films on (100)InP." *Applied Physics Letters* (57:12); pp. 1239-1241. Work performed by School of Electrical Engineering and Computer Science, University of Oklahoma, Norman, Oklahoma; AT&T Bell Laboratories, Murray Hill, New Jersey; and Solar Energy Research Institute, Golden, Colorado.

Sites, J. R. (August 1990). *Analysis of Loss Mechanisms in Polycrystalline Thin Film Solar Cells, Final Subcontract Report, 1 April 1988 - 31 March 1990.* SERI/TP-211-3950. 39 pp. Work performed at Colorado State University, Fort Collins, Colorado. Available NTIS: Order No. DE90000372.

Sopori, B. L.; Zhou, T-Q.; Rozgonyi, G. A. (1990). "Defect Generation/Passivation by Low Energy Hydrogen Implant for Silicon Solar Cells." *Conference Record of the Twenty First IEEE Photovoltaic Specialists Conference - 1990; Kissimmee, Florida; May 21-25, 1990.* New York: The Institute of Electrical and Electronics Engineers, Inc.; pp. 644-649. Work performed by Solar Energy Research Institute, Golden, Colorado, and Department of Materials Science and Engineering, North Carolina State University, Raleigh, North Carolina.

Sopori, B. L.; Benner, J.; McBrayer, J. D. (1990). "One Sun Crystalline Silicon Materials Research: Current Direction and Future Needs." *Conference Record of the Twenty First IEEE Photovoltaic Specialists Conference - 1990; Kissimmee, Florida; May 21-25, 1990.* New York: The Institute of Electrical and Electronics Engineers, Inc.; pp. 653-658. Work performed by Solar Energy Research Institute, Golden, Colorado, and Sandia National Laboratories, Albuquerque, New Mexico.

Stafford, B. L.; Dalal, V. L.; Baron, B. N.; Silver, M. (1990). "a-(Si,Ge):H Alloys: Status and Issues." *Conference Record of the Twenty First IEEE Photovoltaic Specialists Conference - 1990; Kissimmee, Florida; May 21-25, 1990.* New York: The Institute of Electrical and Electronics Engineers, Inc.; pp. 1619-1623.

Sudharsanan, R.; Rohatgi, A. (1990). "Effects of Pre-Heat Treatment of CDS on MOCVD CdTe/CdS Solar Cell Performance." *Conference Record of the Twenty First IEEE Photovoltaic Specialists Conference - 1990; Kissimmee, Florida; May 21-25, 1990.* New York: The Institute of Electrical and Electronics Engineers, Inc.; pp. 504-508. Work performed by School of Electrical Engineering, Georgia Institute of Technology, Atlanta, Georgia.

Tavakolian, H.; Sites, J. R. (1990). "Individual Losses in Thin-Film CdTe Solar Cells." *Conference Record of the Twenty First IEEE Photovoltaic Specialists Conference - 1990; Kissimmee, Florida; May 21-25, 1990.* New York: The Institute of Electrical and Electronics Engineers, Inc.; pp. 556-561. Work performed by Department of Physics, Colorado State University, Fort Collins, Colorado.

Taylor, P. C.; Williams, G. A.; Ohlsen, W. D. (August 1990). *Electronic Processes in Thin Film PV Materials, Final Report, 1 September 1986 - 31 May 1989.* SERI/TP-211-3905. 40 pp. Work performed by Department of Physics, University of Utah, Salt Lake City, Utah. Available NTIS: Order No. DE90000359.

Thakur, R. P. S.; Singh, R.; Nelson, A. J.; Ullal, H. S.; Chaudhuri, J.; Gondhalekar, V. (1 January 1991). "Comparative Study of Phosphosilicate Glass on (100) Silicon by Furnace and Rapid Isothermal Annealing." *Journal of Applied Physics* (69:1); pp. 367-371. Work performed by School of Electrical Engineering and Computer Science, University of Oklahoma, Norman, Oklahoma; Solar Energy Research Institute, Golden, Colorado; and Department of Mechanical Engineering, Wichita State University, Wichita, Kansas.

Tsuo, Y. S.; Xu, Y.; Crandall, R. S.; Han, D.; Qui, C.; Pankove, J. I. (1990). "Hydrogen-Plasma Reactive Flush for a-Si:H and a-SiGe:H Solar Cell Fabrication." *Conference Record of the Twenty First IEEE Photovoltaic Specialists Conference - 1990; Kissimmee, Florida; May 21-25, 1990.* New York: The Institute of Electrical and Electronics Engineers, Inc.; pp. 1416-1419. Work performed at Solar Energy Research Institute, Golden, Colorado and University of Colorado, Boulder, Colorado.

Turner, W. A.; Jones, S. J.; Pang, D.; Bateman, B. F.; Chen, J. H.; Li, Y.-M.; Marques, F. C.; Wetsel, A. E.; Wickboldt, P.; Paul, W.; Bodart, J.; Norberg, R. E.; El Zawawi, I.; Theye, M. L. (1990). "Structural, Optical, and Electrical Characterization of Improved Amorphous Hydrogenated Germanium." *Journal of Applied Physics* (67:12); p. 7430. Work performed by Harvard University, Cambridge, Massachusetts; Washington University, St. Louis, Missouri; and Universite P. et M. Curie, Paris, France.

Ullal, H. S.; Zweibel, K.; Mitchell, R. (1990). "U.S. Polycrystalline Thin Film Solar Cells Program." *Properties of II-VI Semiconductors: Bulk Crystals, Epitaxial Films, Quantum Well Structures, and Dilute Magnetic Systems.* Materials Research Society Symposium Proceedings, Vol. 161, Bartoli, F. J., Jr.; Schaake, H. F.; and Schetzina, J. F., eds., Pittsburgh, PA: Materials Research Society; pp. 193-198. Presented at the MRS Fall Meeting, November 27 - December 2, 1989, Boston, Massachusetts.

Varrin, Jr., R. D.; Verma, S.; Birkmire, R. W.; McCandless, B. E.; Russell, T. W. F. (1990). "Reactor Analysis of Copper Indium Selenization." *Conference Record of the Twenty First IEEE Photovoltaic Specialists Conference - 1990; Kissimmee, Florida; May 21-25, 1990.* New York: The Institute of Electrical and Electronics Engineers, Inc.; pp. 529-534. Work performed by Institute of Energy Conversion, University of Delaware, Newark, Delaware.

Vernon, S. M.; Tobin, S. P.; Al-Jassim, M. M.; Ahrenkiel, R. K.; Jones, K. M.; Keyes, B. M. (1990). "Experimental Study of Solar Cell Performance Versus Dislocation Density." *Conference Record of the Twenty First IEEE Photovoltaic Specialists Conference - 1990; Kissimmee, Florida; May 21-25, 1990.* New York: The Institute of Electrical and Electronics Engineers, Inc.; pp. 211-216. Work performed by Spire Corporation, Bedford, Massachusetts, and Solar Energy Research Institute, Golden, Colorado.

Wang, T. H.; Ciszek, T. F.; Schuyler, T. (February 1991). "Charge Carrier Recombination Centers in High-Purity, Dislocation-Free, Float-Zoned Silicon due to Growth-Induced Microdefects." *Journal of Crystal Growth, American Crystal Growth 1990: Proceedings of the Eighth American Conference on Crystal Growth, Vail, CO, 15-20 July 1990* (109:1-4); pp. 155-161.

Wanlass, M. W.; Ward, J. S.; Gessert, T. A.; Emery, K. A.; Horner, G. S; Coutts, T. J.; Virshup, G. F.; Ristow, M. L. (1990). "Development of High-Performance GaInAsP Solar Cells for Tandem Solar Cell Applications." *Conference Record of the Twenty First IEEE Photovoltaic Specialists Conference - 1990; Kissimmee, Florida; May 21-25, 1990.* New York: The Institute of Electrical and Electronics Engineers, Inc.; pp. 172-178. Work performed by Solar Energy Research Institute, Golden, Colorado, and Varian Associates, Palo Alto, California.

Wiedeman, S.; Morris, J.; Yang, L. (1990). "Optical Losses In Multi-Junction a-Si:H Based Solar Cells and Modules." *Conference Record of the Twenty First IEEE Photovoltaic Specialists Conference - 1990; Kissimmee, Florida; May 21-25, 1990.* New York: The Institute of Electrical and Electronics Engineers, Inc.; pp. 1529-1534. Work performed by Solarex Corporation, Thin Film Division, Newtown, Pennsylvania.

Willing, F.; Wiedeman, S.; Newton, J.; O'Dowd, J.; Jansen, K. (1990). "Power Optimization for Large-Area a-Si Solar Modules." *Conference Record of the Twenty First IEEE Photovoltaic Specialists Conference - 1990; Kissimmee, Florida; May 21-25, 1990.* New York: The Institute of Electrical and Electronics Engineers, Inc.; pp. 1432-1437. Work performed by Solarex Thin Film Division, Newtown, Pennsylvania.

Wong, D.; Kim, H. K.; Li, A.-Z.; Schlesinger, T. E.; Miles, A. G. (November 1990). *Improvement of Bulk and Epitaxial III-V Semiconductors for Solar Cells by Creation of Denuded Recombination Zones, Final Subcontract Report, 1 September 1986 - 30 June 1990.* SERI/TP-211-3990. 151 pp. Work performed by Carnegie Mellon University, Pittsburgh, Pennsylvania. Available NTIS: Order No. DE90000387

Zweibel, K. (1990). *Harnessing Solar Power: the Photovoltaics Challenge.* New York: Plenum Press; 330 pp.

Document Control Page	1. SERI Report No. NREL/TP-410-4724	2. NTIS Accession No. DE92001248	3. Recipient's Accession No.

4. Title and Subtitle	5. Publication Date
Annual Report, Photovoltaic Subcontract Program, FY 1991	March 1992
	6.

7. Author(s)	8. Performing Organization Rept. No.
Photovoltaics Program Branch, NREL	

9. Performing Organization Name and Address	10. Project/Task/Work Unit No.
National Renewable Energy Laboratory 1617 Cole Boulevard Golden, Colorado 80401-3393	PV211101
	11. Contract (C) or Grant (G) No. (C) (G)

12. Sponsoring Organization Name and Address	13. Type of Report & Period Covered
	Annual Progress Report
	14.

15. Supplementary Notes

16. Abstract (Limit: 200 words)
This report summarizes the fiscal year (FY) 1991 (October 1, 1990, through September 30, 1991) progress of the subcontracted photovoltaic (PV) research and development (R&D) performed under the Photovoltaic Advanced Research and Development Project at the National Renewable Energy Laboratory (NREL)—formerly the Solar Energy Research Institute (SERI). The mission of the national PV program is to develop PV technology for large-scale generation of economically competitive electric power in the United States. The technical sections of the report cover the main areas of the subcontract program: the Amorphous Silicon Research Project, Polycrystalline Thin Films, Crystalline Silicon Materials Research, High-Efficiency Concepts, the New Ideas Program, the University Participation Program, and the Photovoltaic Manufacturing Technology (PVMaT) project. Technical summaries of each of the subcontracted programs provide a discussion of approaches, major accomplishments in FY 1991, and future research directions.

17. Document Analysis
a. Descriptors
photovoltaic cells ; amorphous materials ; silicon ; thin films ; deposition ; copper selenide ; cadmium telluride ; gallium arsenide ; efficiency ; semiconductor materials ; solar cells

b. Identifiers/Open-Ended Terms
National Renewable Energy Laboratory

c. UC Categories
270

18. Availability Statement	19. No. of Pages
National Technical Information Service U.S. Department of Commerce 5285 Port Royal Road Springfield, VA 22161	323
	20. Price A14